MEMBRANE ACTION IN SIMPLY SUPPORTED SLABS

By

MOHAMMED F ALMOGRABI
BSc.(CIVL), MSc.

Thesis submitted for the Degree of
Doctor of Philosophy
To the Department of Civil and Offshore Engineering,
Heriot-Watt University, Edinburgh

DEPARTMENT OF CIVIL AND OFFSHORE ENGINEERING,
HERIOT-WATT UNIVERSITY, EDINBURGH

June 1999

COPYRIGHT STATEMENT

TABLE OF CONTENTS

LIST OF TABLES

LIST OF FIGURES

NOTATION

General symbols

$\{\}, \{\}^T$	Vector.
$[\], [\]^T, [\]^{-1}$	Rectangular matrix.
	T denoted transpose of the vectors and matrices.
	-1 denoted inverse of the matrix.
$\| \|$	Euclidean norm of a vector.

Scalars

A	Area.
A_s	Area of steel.
a	Depth of compressive block of concrete.
B	Tension stiffening parameter.
C_c	Compressive force in concrete.
D	Flexural rigidity of plate.
d	Depth of the lever arm.
d_n	Depth of the neutral axis.
E_c	Initial modulus of elasticity of concrete.
E_s	Secant modulus.
E_{sh}	Modulus of strain hardening of steel.
E_{st}	Initial modulus of elasticity of steel.
f	Yield function.
$f_c^{'}$	Compressive strength of concrete.
f_t	Tensile strength of concrete.
f_y	Yield strength of steel.
h	Depth of the slab section.
K	Constant of a slab section.
k	Shear correction factor.
k_r, k_θ	Radial and circumferential curvatures.
L	Differential matrix operator.
L_1, L_2	Short and long sides for rectangular slab.
M, M_0	Moment with and without in-plane axial force.
M_n, M_{nu}	Applied moments and Moment capacity of the slab section.
M_x, M_y, M_{xy}	Applied bending and twisting moments.
M_x^*, M_y^*	Design moments in x and y-direction.
M_r, M_θ	Radial and circumferential moments of a circular slab.
N	Isoparametric shape function.

P	Lagrange shape function.
P_x, P_y, P_{xy}	In-plane axial and in-plane shear forces in rectangular slab.
P_r, P_θ	Radial and circumferential membrane force in circular slab.
Q	Radial shear force.
q	Uniformly distributed load.
R	Radius of a circular slab.
r, r_1	Total radius of plastic tensile membrane and radius of pure tensile plastic membrane in radial slab.
S	Ratio of the uniaxial ultimate compressive to tensile strength of concrete.
T_0	Total tensile force in steel.
T_{st}, T_{sb}	Total tension in top and bottom steel.
u, v	In-plane displacements at the plate middle surface.
u', v'	In-plane displacements at and arbitrary point located at a distance from the plate middle surface.
V	Volume.
w, w'	Lateral displacements.
w_0	Lateral displacement of the slab centre.
w_i	Weight function.
x, y, z	Cartesian co-ordinate.
z_1, z_2	Co-ordinate of the top and bottom of the slab.
α	Discontinuity factor for the pre and post cracking response of concrete in tension.
α_D, α_E	Displacement and energy convergence tolerance.
β	Compression softening parameter.
ε_i, σ_i	Strain and stress in principle direction i.
$\varepsilon_{pi}, \sigma_{pi}$	Peak stain and stress in principal direction i.
$\varepsilon_{cu}, \varepsilon_{su}$	Crushing and ultimate strain in concrete and steel respectively.
ε_y	Yield strain in steel.
$\varepsilon_1, \varepsilon_2$	Real strains in principle direction 1 and 2.
$\varepsilon_{e1}, \varepsilon_{e2}$	Modified strains in principal directions 1 and 2.
$\varepsilon_{p1}, \varepsilon_{p2}$	Real peak strains in principle direction 1 and 2.
$\varepsilon_{ep1}, \varepsilon_{ep2}$	Modified peak strains in principal directions 1 and 2
σ_1, σ_2	Principle stresses in directions 1 and 2.
K	Biaxial principle stress ratio.
η, ξ	Local co-ordinates.
μ_0, μ_θ	Depth of the neutral axis in the centre and in the circumferential direction for a circular slab.
ν	Poisson's ratio.
$\sum$	Summation.

λ	Rate of straining.
θ_x, θ_y	Rotations of the normals to the un-deformed middle surface in xz and yz planes respectively.
ϕ_x, ϕ_y	Average transverse shear deformations.
$\Delta\delta_i$	Specified incremental displacement component.

Vectors.

$\{F\}$	Internal forces.
$\{f\}$	Internal forces for an element.
$\{\overline{f}\}$	Body force.
$\{P\}$	Applied load.
$\{p\}$	Surface traction
$\{\sigma\}, \{\varepsilon\}$	Stress and strain vectors.
$\{\overline{\sigma}\}, \{\overline{\varepsilon}\}$	Stress resultant and associated strain vector.
$\{\varepsilon^L\}$	Linear strain.
$\{\varepsilon^{NL}\}$	Non-linear strain.
$\{\delta\}$	Nodal displacements.
$\{\psi\}$	Residual force.

Matrices.

$[B]$	Strain-displacements.
$[B_L]$	Linear strain-displacement.
$[B_{NL}]$	Non-linear strain displacements.
$[K_T]$	Tangent stiffness matrix.
$[K_0]$	Small displacements stiffness matrix.
$[K]$	Small displacements stiffness matrix with the length of the mid-surface assumed to remain constant.
$[K_\sigma]$	Geometric stiffness matrix.
$[K_L]$	Large displacement stiffness matrix.
$[K_P]$	In-plane stiffness matrix.
$[\hat{\sigma}]$	Stress matrix.
$[D]$	Material matrix.
$[\overline{D}]$	Material matrix associated with the stress resultant.
$[J]$	Jacobian matrix.

Subscripts

b	Flexural.

p	In-plane.
s	Shear.
e	Element.
i	Iteration number.
n	Incremental number.

ACKNOWLEDGEMENTS

I am grateful to my supervisor Professor I M May for his supervision. The work described in this thesis would have not been possible without the ideas, advice, encouragement and support I received from him.

I am also grateful to my wife and my children for their support and encouragement during the period of my study.

I would like to express my sincere thanks to my friend Mr. S H Lodi for his support and encouragement.

DECLARATION

The work embodied in this theses is a result of the author's own investigation except where due references are made. It has been submitted, and is not being concurrently presented in candidature for any other degree.

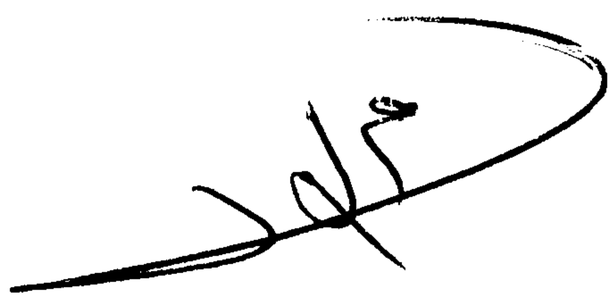

(Mohammed Almograbi)

DEDICATION

Dedicated to my parents, wife and my children

MEMBRANE ACTION IN SIMPLY SUPPORTED SLABS

Mohammed Almograbi

(ABSTRACT)

In the design of reinforced concrete slabs, design methods based on the assumption of linear elastic behaviour or using empirical formulas can give very conservative estimates of the load-carrying capacity of such slabs. Methods of analysis based on plasticity theory, for example limit analysis theory, have been developed to provide more realistic tools. The upper bound solution and the lower bound solution predicted using the limit analysis cannot be determined in a straightforward way. Moreover, the membrane action is usually ignored in the methods of design mentioned above. Experimental tests carried out on simply supported slabs indicated collapse loads higher than those predicted by the various analytical methods as a result of the development of the tensile membrane action in the plane of the slab with increasing deflections. Several plastic methods have been derived to include this phenomenon in the analysis of simply supported slabs; however, many contain shortcomings in their treatment of this important effect.

A non-linear finite element program, which can predict such membrane action, has been modified and validated against results from laboratory tests up to failure and used to study the behaviour of the slabs throughout the different stages of loading. The steel is modelled as smeared and assumed to be elastic perfectly plastic or with allowance for strain hardening. The material model for concrete includes phenomena such as tension stiffening, compression softening and cracking model.

The computer program has been employed subsequently to investigate the membrane action and the various parameters influencing it. The membrane action is found to develop at a load between the onset of cracking and the yield line theory load and increases with increasing deflections. The distribution of the membrane action is found to be a zone of circumferential and radial tensile forces in the centre of the slab surrounded by a zone of circumferential compressive forces in the outer region. A comparison between the available plastic methods, which include the membrane action effect, and the finite element method, is also carried out. The load-deflection curves predicted using such plastic methods were found to be different from the actual load-deflection curves of simply supported slabs. This is due to the rigid-plastic assumption of the plastic methods, where the elastic deflections are neglected. The enhancement of the load-carrying capacity of the slabs resulting from membrane action with reinforcement designed using the Wood and Armer rules and yield line theory has been also investigated. The increase was found to be significant in both cases for square slender slabs with low reinforcement ratio with a larger increase for slabs designed using yield line theory.

Design guidelines have been developed for rectangular slabs by including the effect of tensile membrane action for slabs with reinforcement designed using the Wood and Armer rules. The developed design method could lead to economies in the amount of reinforcement required in some slabs by including the effect of membrane action.

CHAPTER 1

INTRODUCTION

In 1955, Ockleston [1] carried out a test up to failure on the dental hospital building in Johannesburg in which it was observed that the interior panels of the floor system carried considerably more loads than that predicted by yield line theory [2]. Ockleston [3] identified the phenomena as membrane action, which can develop in the plane of the slab, but made no attempt to calculate the membrane forces. The first attempt to analyse a reinforced concrete slab for membrane action appears to have been made by Wood [4]. On the basis of equilibrium equations and the collapse mechanism Wood [4] determined the load-deflection relationship for a restrained isotropic circular slab subjected to uniformly distributed load Fig. 1.1. Since then the effect of membrane forces on the load-carrying capacity of reinforced concrete slabs has become an active field of research [5,6,7,8,9,10,11,12,13]

There are two types of membrane action. The first one is compressive membrane action which can develop at small deflections in restrained slabs, and the second one is tensile membrane action which develops simultaneously with compressive membrane action but at large deflections in both simply supported and restrained slabs.

An example to show the development of membrane action is a one way spanning slab strip subjected to a uniformly distributed load of magnitude, q, per unit length and restrained against lateral movement. Under increasing load the change in geometry resulting from slab deflections causes the neutral axis of the slab segment to move towards the upper surface. A failure mechanism is formed by the development of yield lines or hinges at the supports and at mid-span Fig. 1.2a. If the slab is under reinforced, the neutral axis at failure is very close to the upper surface of the slab [14]. Thus pure bending is accompanied by extensions and rotations at the supports δ_a and θ_a and at the mid-span, δ_b and θ_b Fig.1.2b. If horizontal spreading of the supports is restrained by stiff boundary elements or beams, the increase in the span due to the change in geometry will be opposed by the stiff boundary elements, thus generating in-plane forces Fig. 1.3. The compressive membrane forces so induced tend to increase the flexural strength of the slab section, resulting in an ultimate load in excess of that calculated using yield line theory.

A load-deflection curve of a uniformly loaded two-way spanning rectangular reinforced concrete slab having laterally restrained edges is shown in Fig. 1.4, as curve 1. For small deflections the load increases as membrane forces are built up. At the peak load, point A, the neutral axes are close to mid-depth [14]. With the formation of a mechanism, an unstable failure occurs and the slab snaps through. The load drops as the neutral axis moves towards the upper surface of the slab, and the compressive membrane forces decrease [14]. At point B, the slab may be cracked through in the centre and a tensile membrane starts to form in the central region. At this point central

deflection is either equal to or a little more than the thickness of slab [5]. If the reinforcement is sufficiently ductile, the full depth cracking of concrete over the central region of slab as a result of the large stretch of the slab surface transforms the reinforcement to plastic tensile membrane and the load may then increases until fracture occurs at point *C*. The part *OA* of the load-deflection curve is referred to as the part under increasing compressive action, part *AB* under decreasing compressive membrane action, and the part beyond point *B* is under tensile membrane action [4,5,6,7,8,12,13,14].

Enhancement of the load carrying capacity of a slab by tensile membrane action can also develop in a slab simply supported along its edges. However, in simply supported slabs the tensile membrane action develops after cracking at loads lower than yield line theory load; thereafter enhancing the load-carrying capacity of the slab significantly at large deflections. The change in the slab geometry as a result of increasing deflections at mid-span causes the central regions of the supported edges to tend to move inwards but they are restrained from doing so by the adjacent outer regions. This creates a central area of tensile membrane stresses within the slab together with a surrounding ring of compression, Fig.1.5. Tension may develop throughout the depth of the slab in the central area; this may result in the penetration of tensile cracks into the top face of the slab and any further load is carried mainly by the reinforcing bars acting as a tensile plastic membrane [4,5,6,8,9,10,12].

A typical load-deflection curve of a uniformly loaded two-way spanning rectangular reinforced concrete slab on simply supports is shown in Fig. 1.4. If the slab is

unrestrained, then point A on curve 1 tends to move downward and coincide with point B, and the load-deflection curve for the complete unrestrained slab changes from curve 1 to curve 2 Fig.1.4. In the initial stages of loading, the slab is uncracked so that its stiffness is very high Part OA'. After cracking, the slab is less stiff $A'B$, and in this stage the tensile membrane forces start to develop. As yielding of the reinforcement becomes general, deflections increase rapidly with an increase in load until fracture occurs at point C. The enhancement of the ultimate load at part BC is result of tensile membrane action [4,9].

The objectives of this research are to investigate the membrane action in reinforced concrete slab on simple supports and to develop guidelines for the design of rectangular, simply supported slabs including the effect of tensile membrane action.

In order to carry out this investigation a computer program for non-linear finite element analysis for reinforced concrete slab developed by Ganaba [13] has been modified, tested and used in this study.

In Chapter 2, a review of the available literature on the ultimate load analysis of simply supported reinforced concrete two-way slabs, with particular reference to those including membrane action, is first presented, followed by a review of the methods available for analysis and design of slab without membrane action. Results of some ultimate load tests of simply supported slabs which have been conducted in the past are also summarised.

In Chapter 3, A brief description of the computer program and the solution techniques employed in this study are presented.

In Chapter 4, a review of the available models for the concrete and reinforced concrete is presented. Discussion of the material model used for concrete under biaxial state of stress is given. The modelling of compression softening, tension stiffening and cracking are also discussed and the model for reinforcing steel is introduced.

In Chapter 5, results from the computer analyses are presented and compared with experimental results to demonstrate the validity and applicability of the analysis.

In Chapter 6, an investigation of membrane action in simply supported slabs using the finite element analysis is described. Comparison between the results of the finite element analysis and some plastic methods, which include membrane action, i.e. Wood's [4] method for circular slab and Kemp's [15] method for square slab is also presented. Study of the membrane action effect on the ultimate load for slabs on different simply supports and designed using Wood and Armer [16,17] rules and yield line theory [18] is also presented.

In Chapter 7, guidelines for the design of rectangular simply supported slabs by including the membrane action effect are presented.

Chapter 8 gives the summary of, and conclusions from the present research. Recommendations and suggestions for further work are also given.

1.1 REFERENCES

1. Ockleston A. J., "Load test on three storey reinforced concrete building in Johannesburg", Structural Engineer, Vol., 33, No. 10, October 1955, pp. 304-322.

2. Johansen K. W., Brudlinieteorir, Gjellerup, Copenhagen, Denmark 1943, English edition., "Yield line theory", Cement and Concrete Association, London 1962, 181p.

3. Ockleston A. J., "Arching action in reinforced concrete slabs", Structural Engineer,Vol. 36, No. 6, June 1958, pp. 197-201.

4. Wood R. H., "Plastic and elastic design of slabs and plates", Thames and Hudson. 1961.

5. Park R., Gample, W. L. "Reinforced concrete slabs", A Wiley-Interscience Publication, John Wiley & Son, USA, 1980.

6. Wood R. H., "How slabs design has developed in the past, and what the indications are for future development", Cracking, Deflection and Ultimate Load of Concrete Slab System, SP-30, ACI. Detroit, 1971, pp. 203-221.

7. Park R., "Ultimate strength of rectangular concrete slabs under short-term uniform loading with edges restrained against lateral movement", Proceeding of the Institute of Civil Engineers. Vol. 28. June 1964.pp 125-150.

8. Taylor R. and Hayes B., "Some tests on the effect of edge restraint on punching shear in reinforced concrete slabs", Magazine of Concrete Research. Vol. 17, No 50. March 1965. Pp 39-44.

9. Taylor R., "A note on a possible basis for a new method of ultimate load design of reinforced concrete slabs", Magazine of Concrete Research. Vol. 17, No 53. December 1965. pp 183-186.

10. Taylor R., Maher D. R. H. and Hayes B., "Effect of the arrangement of reinforcement on the behaviour of reinforced concrete slabs", Magazine of Concrete Research. Vol. 18, No 55. June 1966. pp 85-94.

11. Park R., "The ultimate strength and long-term behaviour of uniformly loaded two-way concrete slabs with partial lateral restraint at all edges", Magazine of Concrete Research. Vol. 16, No 48. September 1964. pp 139-152.

12. Park R., "Tensile membrane behaviour of uniformly loaded rectangular reinforced concrete slabs with fully restrained edges", Magazine of Concrete Research. Vol. 16, No 46. March 1964. pp 39-44.

13. Ganaba T. H., "Finite element analysis of plates and slabs", PhD. Theses, Department of Engineering Science, University of Warwick, August 1985.

14. Braestrup M. W., "Dome effect in reinforced concrete slabs: rigid plastic analysis", Journal of the Structural Division, ASCE, Vol.106, No. ST6, June 1980, pp. 1237-1253.

15. Kemp K. O., "Yield of square reinforced concrete slab on simply supports allowing for membrane action", Structural Engineer. Vol. 7, July 1967. Pp. 235-240.

16. Wood R. H, "The reinforcement of slabs in according with a predetermined field of moments", Concrete, London, Vol. 2, February 1968, pp 69-76.

17. Armer G. S. T., "Discussion on 'The reinforcement of slabs in accordance with a predetermined field of moments", Concrete, London, Vol. 8, August 1968, pp 319-321.

18. Johansen K. W., Brudlinieteorir, Gjellerup, Copenhagen, Denmark 1943, English edition. "Yield line theory", Cement and Concrete Association, London 1962, 181p.

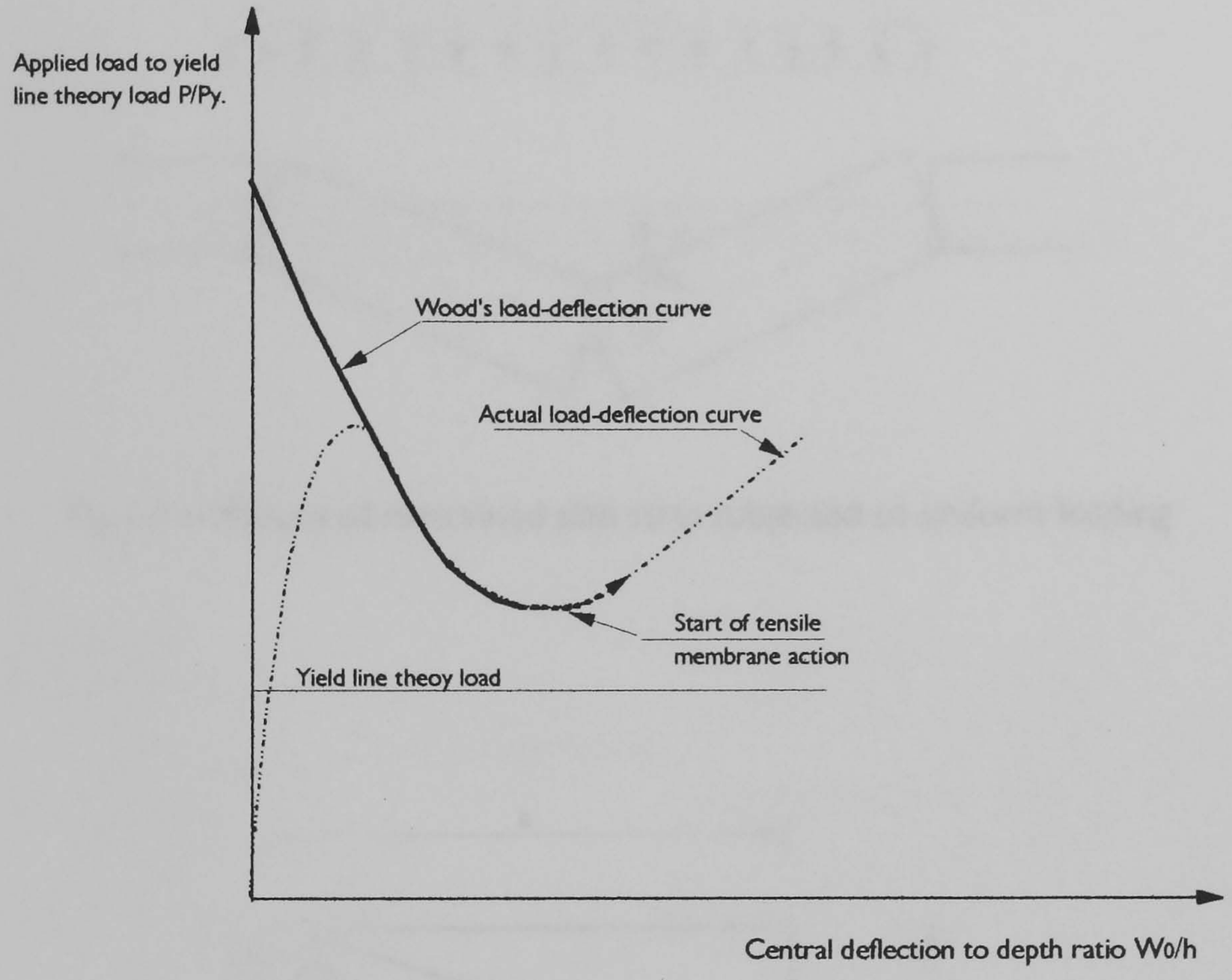

Fig. 1.1- Load-deflection curve for restrained slab

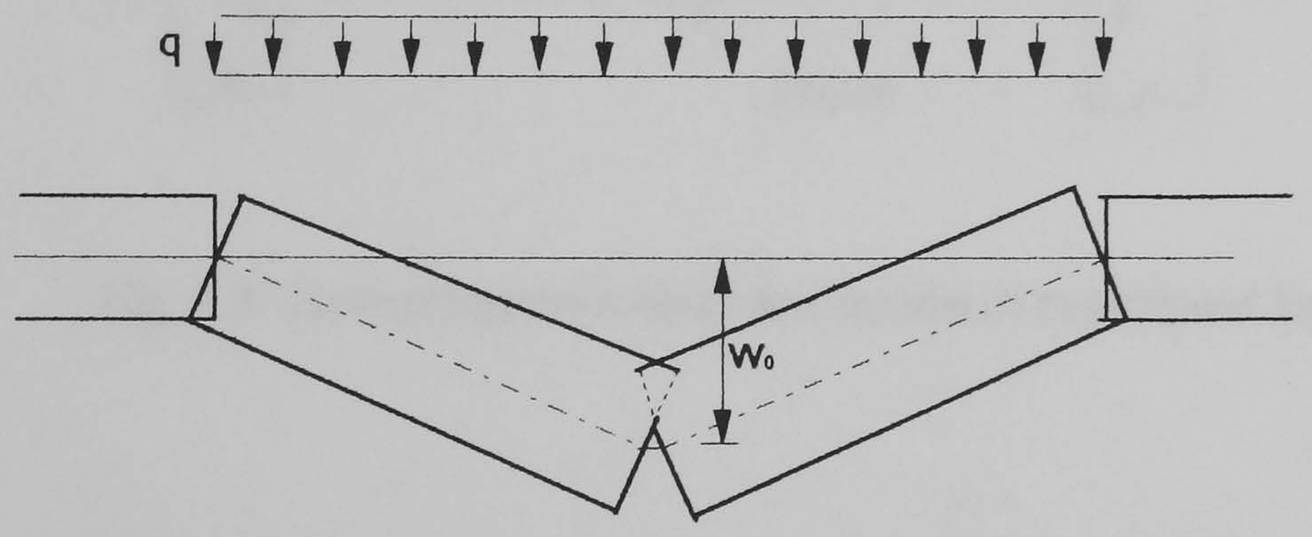

Fig.1.2 a- Failure of restrained slab strip subjected to uniform loading

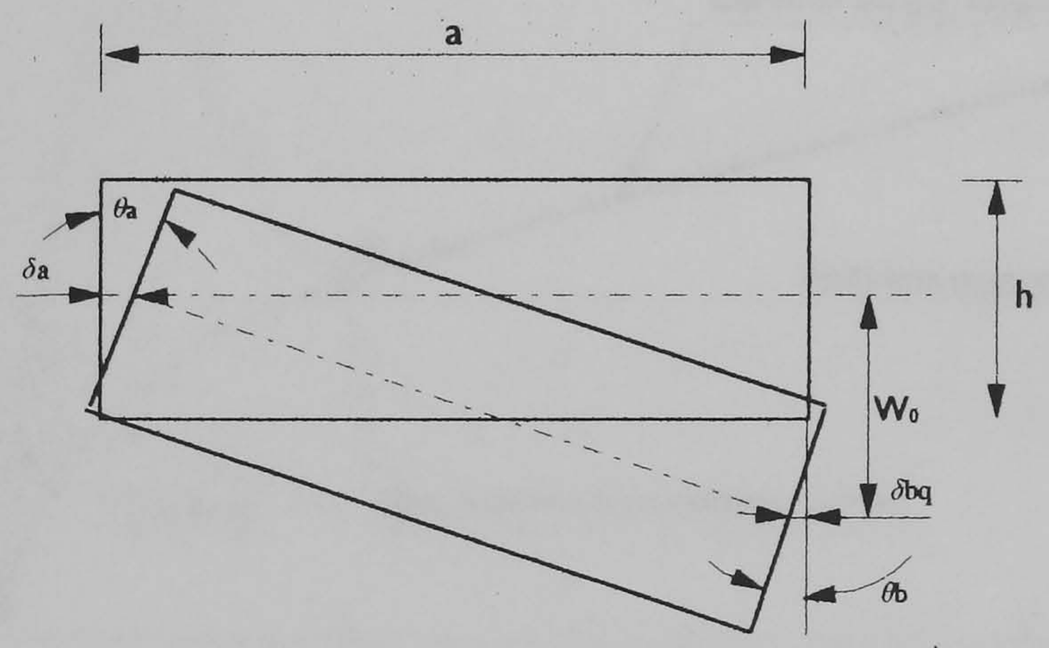

Fig.1.2 b- Deformation of one half of the slab strip.

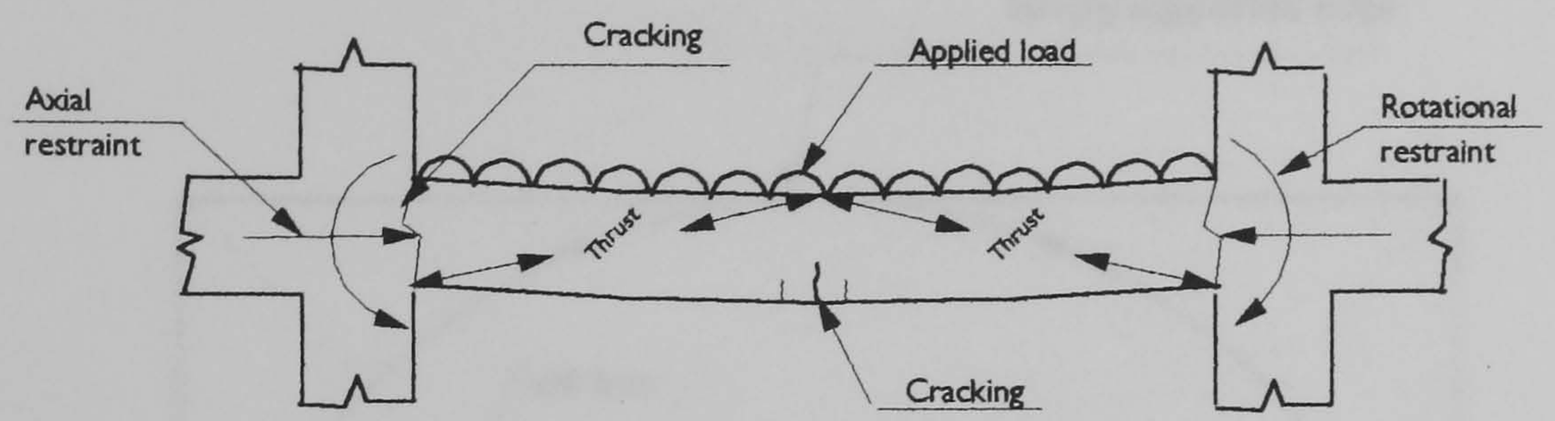

Fig. 1.3- Compression membrane action in restrained slab.

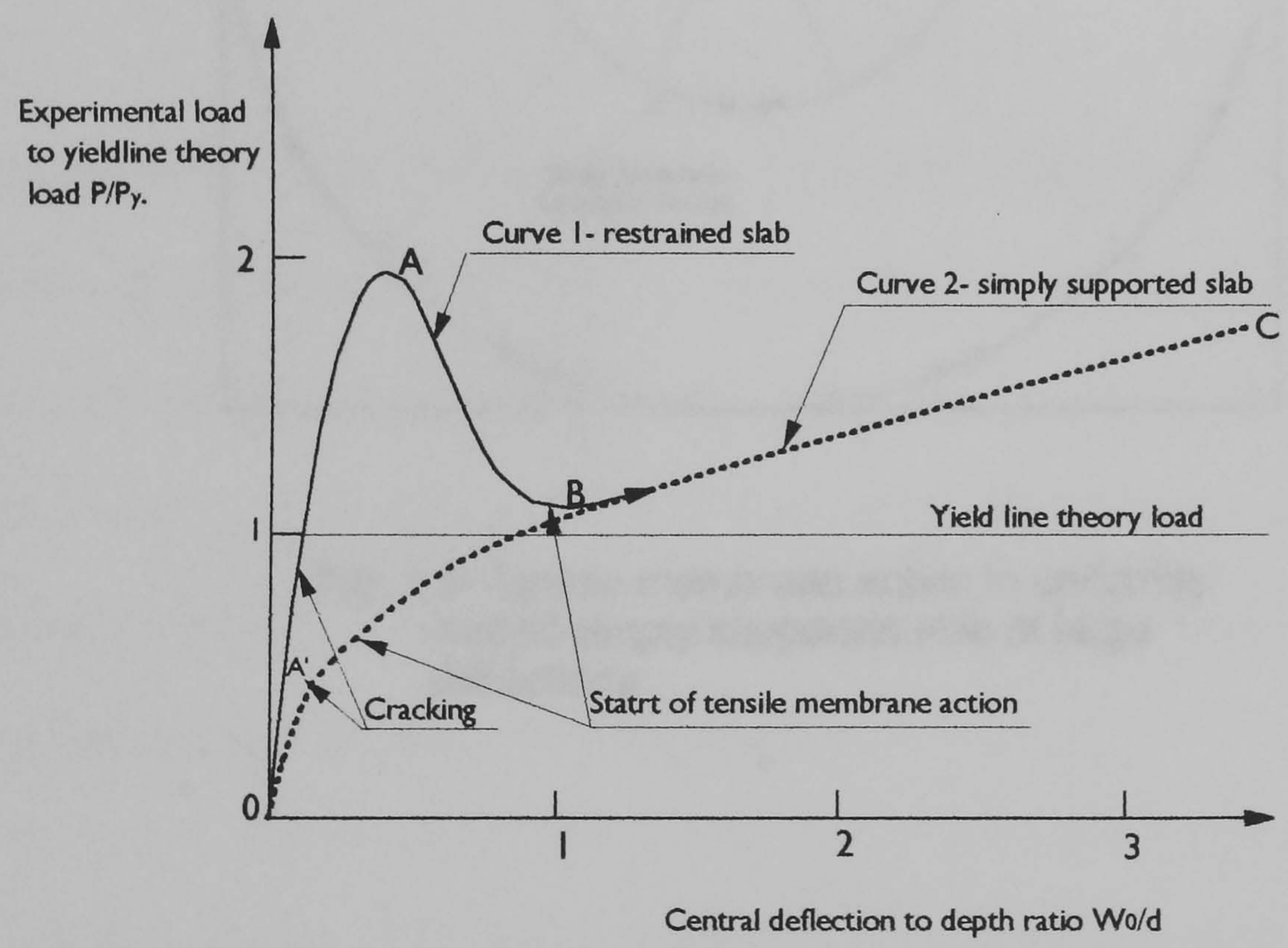

Fig. 1.4- Load-deflection curves for reinforced concrete slab

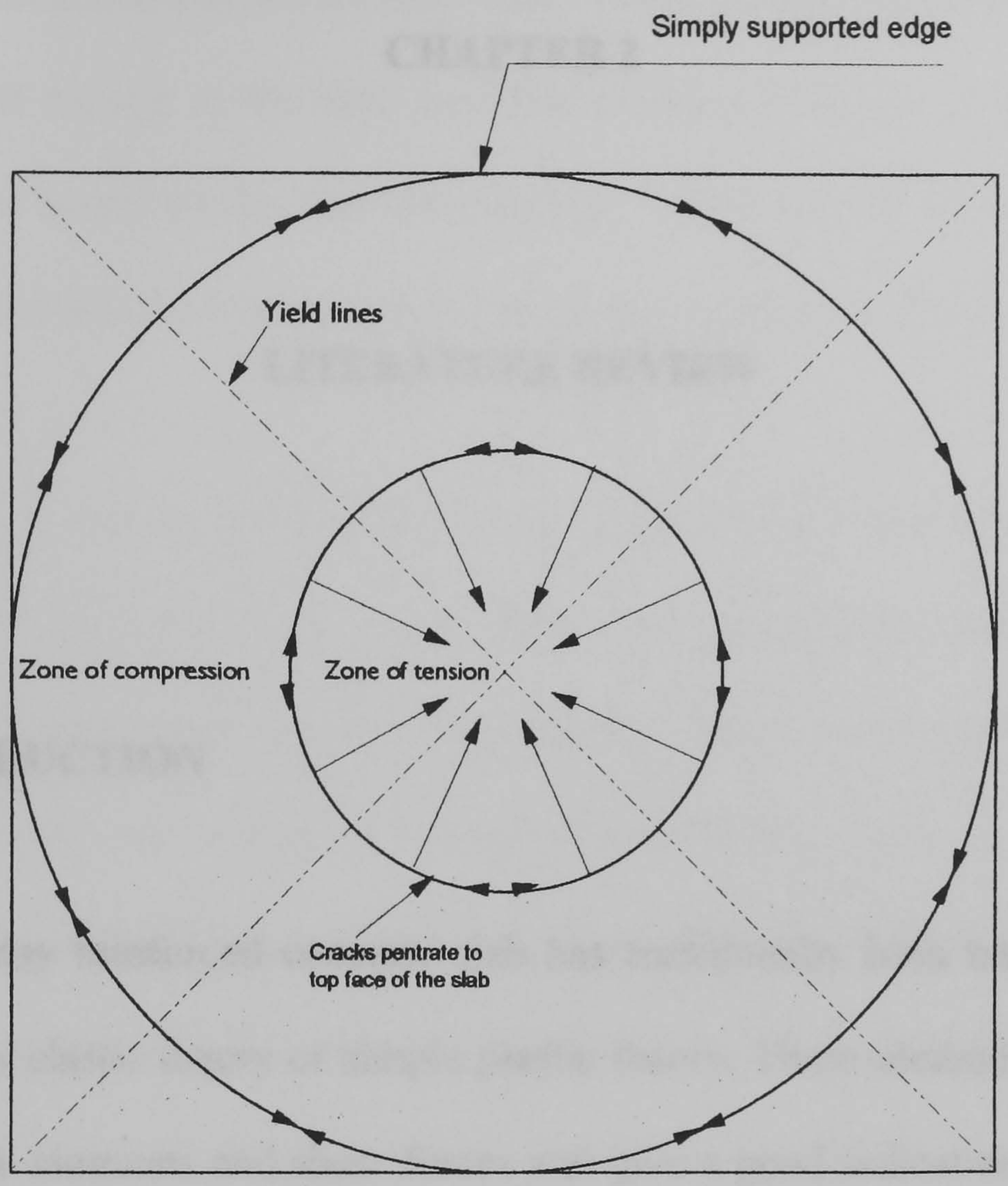

Fig. 1.5- Tensile membrane action in uniformly loaded simply supported slab at large deflections

CHAPTER 2

LITERATURE REVIEW

2.1 INTRODUCTION

The design of any reinforced concrete slab has traditionally been based on classical methods such as elastic theory or simple plastic theory. These methods considered the presence of only moments and shear forces and give a good indication of the ultimate load that would occur without membrane forces in the slab. However, membrane forces are often present in reinforced concrete slabs as a result of the boundary conditions and the geometry of the deformations of the slab.

For example, the yield line theory developed by Johansen [12] has been widely adopted for the calculation of the ultimate loads of two-way reinforced concrete slabs. This theory is based on the premise that a certain characteristic pattern of plastic hinges (yield lines) is formed which leads to failure. Along these plastic hinges, the plastic moment capacity of the slab cross section is assumed to have been reached and these plastic hinges turn the slab into a mechanism. The deformation of the slab takes place as

a result of the rotation along the yield lines, and the portions of the slab between the yield lines are assumed to remain rigid. Since the theory, based on the assumption of the formation of mechanism and the collapse load, is estimated by equating the internal rate of dissipation of energy to the rate at which external loads do work, it provides a theoretical upper bound on the true ultimate load. However, this solution is still small compared with the other solutions which include the membrane action effects.

Several studies of membrane action in simply supported reinforced concrete slabs have been conducted. However, only approximate ultimate strength theories have been developed at present and, further, the studies have pointed to difficulties in incorporating membrane action in design. Nevertheless, there is no doubt that membrane action will increase the ultimate load of many reinforced concrete slabs significantly compared with that predicted if membrane action has not been considered.

In this Chapter a review is made of the literature available on the ultimate load analysis of simply supported reinforced concrete two-way slabs, with particular reference to those including membrane action, followed by the available methods for analysis and design of slabs without membrane action. The results of load tests of simply supported slabs which have been conducted in the past are also summarised and discussed.

2.2 REVIEW OF MEMBRANE ACTION IN SIMPLY SUPPORTED SLABS

Compared with compressive membrane action in restrained reinforced concrete slabs very little theoretical work on the effect of membrane action in simply supported slabs has been reported. A major contribution was made by Wood [1] who developed a solution for a simply supported circular slab allowing for the effect of the membrane action. The loading on the slab considered was a uniformly distributed load. The concrete slab was assumed to be iso-tropically reinforced at the bottom face only and it was assumed to have rigid perfectly plastic properties and to yield under the action of bending moment M and in-plane axial force P, taken to act at mid-depth. The yield criterion was derived from the stress distribution shown in Fig. 2.1. The moment M and the in-plane compressive force P per unit width of the slab are

$$M = A_s f_y \left(d - \frac{h}{2} \right) + \frac{2}{3} f_c^{'} \left(0.85 d_n \left(\frac{h}{2} - 0.425 d_n \right) \right) \qquad 2.1$$

$$P = \frac{2}{3} f_c^{'} (0.85 d_n) - A_s f_y \qquad 2.2$$

where A_s, is the area of the steel, $f_c^{'}$ is the concrete cube strength and f_y is the yield strength of the reinforcement.

The moment corresponding to $P = 0$ is

$$M_0 = A_s f_y \left(d - 0.75 \frac{\rho f_y}{f_c^{'}} \right) \qquad 2.3$$

An important quantity in membrane analysis is the ratio of maximum tensile strength to maximum crushing strength of the section t, where, $t = \frac{\rho f_y}{f_c^{'}} = \frac{A_s f_y}{f_c^{'} d}$, and ρ, is the percentage of the reinforcement.

Substitution of the neutral axis depth d_n obtained from equation 2.2 into equation 2.1 and divide by M_0 leads to the yield criterion in non-dimensional form

$$\frac{M}{M_0}=1+\alpha\left(\frac{P}{T_0}\right)-\beta\left(\frac{P}{T_0}\right)^2 \qquad 2.4$$

where $T_0=A_s f_y$, $\alpha=\dfrac{\left(0.5\dfrac{h}{d}-\dfrac{3}{2}t\right)}{\left(1-\dfrac{3}{4}t\right)}$ and $\beta=\dfrac{\left(\dfrac{3}{4}t\right)}{\left(1-\dfrac{3}{4}t\right)}$

The yield criterion for a slab section with $\frac{h}{d}=1.2$ and $t=0.04$ using the above expression is shown in Fig. 2.2.

It was assumed that the membrane forces become significant only after the formation of the yield mechanism. Thus a conical collapse mechanism was assumed to develop in the first instance before any tensile membrane action comes into play, and when at the centre of the slab the neutral axis reaches the top fibre of concrete, a pure tensile membrane action develops. Conditions at the centre of a slab with a conical collapse mode are shown in Fig.2.3. It was further assumed that the plastic potential coincides with the yield surface, i.e., the plastic strains with component k in the direction of the moment, M and ε in the direction of tensile in-plane force, T may be represented by a vector, Fig. 2.2. Generally if the yield criterion is

$$f(M,T)=0 \qquad 2.5$$

then the plastic flow will have related components such that

$$\text{extension strain} = \varepsilon = \lambda \frac{\partial f}{\partial T}$$

$$\text{curvature strain} = k = \lambda \frac{\partial f}{\partial M}$$

where λ is an arbitrary rate of straining.

The plastic strains ε_r and k_r in the radial direction and ε_θ and k_θ in the circumferential direction were determined as a function of deflection from the strain rates imposed by the collapse mechanism shown in Fig.2.4 thus

$$\varepsilon_r = \frac{du}{dr} + \frac{1}{2}\left(\frac{dw}{dr}\right)^2 = 0 \qquad 2.6$$

$$k_r = \frac{d^2 w}{dr^2} \qquad 2.7$$

$$\varepsilon_\theta = \frac{u}{r} \qquad 2.8$$

$$k_\theta = -\frac{1}{r}.\frac{dw}{dr} \qquad 2.9$$

Since the ratio of $\frac{\varepsilon_\theta}{k_\theta}$ is equal to the depth of the neutral axis μ_θ in the circumferential direction and $T = -P$, then from the yield criterion, the non-dimensional membrane force in the circumferential direction, $\frac{P_\theta}{T_0}$ can be determined such that

$$\frac{\varepsilon_\theta}{k_\theta} = \mu_\theta = \frac{-\frac{\partial f}{\partial T}}{\frac{\partial f}{\partial M}} = \frac{\frac{\alpha}{T_0} - \frac{2\beta P_\theta}{T_0}}{\frac{1}{M_0}}$$

and thus

$$\frac{P_\theta}{T_0}=\frac{\alpha}{2\beta}-\frac{\mu_\theta T_0}{2\beta M_0} \qquad 2.10$$

Provided the slab is not cracked throughout its depth there is some compressive stress in the concrete cross section. In this case the value of μ_θ was determined directly from the geometry of the collapse mechanism Figs.2.3-2.4 [1], as a function in the depth of the neutral axes at the centre, μ_0, and the central deflection, w_0. When the slab cracked through its full depth, the pure plastic membrane was assumed to be developed (the term pure membrane action means $T_\theta = T_0$) and to have a spherical surface, i.e. the curvature strains k_r and k_θ must be the same. In this case the radial extension u, was determined by equating the radial strain, ε_r and the circumferential strain, ε_θ and used in the equation 2.10 rather than μ_θ to calculate the circumferential membrane force.

Equilibrium equations including membrane action were derived for a circular slab carrying a uniformly distributed load q Fig.2.5 under radially symmetrical loading such that,

The vertical forces,

$$\frac{d}{dr}(rQ_r)+\frac{d}{dr}\left(rT_r\frac{dw}{dr}\right)=-qr \qquad 2.11$$

Radial horizontal force

$$\frac{d}{dr}(rT_r)-T_\theta=0 \qquad 2.12$$

Radial moments

$$\frac{d}{dr}(rM_r)-M_\theta-rQ_r=0 \qquad 2.13$$

By combining equation 2.11 and 2.13

$$\frac{d^2}{dr^2}(r M_r) - \frac{dM_\theta}{dr} + \frac{d}{dr}\left(r T_r \frac{dw}{dr}\right) = -qr \qquad 2.14$$

where Q_r is the radial shear force, T_r is the radial membrane force and M_θ and M_r are the circumferential and radial moments.

The radial membrane force was determined by substituting the circumferential membrane force, equation 2.10 into equation 2.12. The circumferential and the radial moments were determined by substituting the corresponding membrane forces in to the yield criterion equation 2.4. The increase in the load-carrying capacity was determined by substituting the membrane forces and the corresponding moments in to equation 2.14.

A typical load-deflection curve O`AC, normalised with respect to the yield line theory load, obtained from the analysis, is shown in Fig. 2.6. The experimental behaviour of a simply supported slab OAE is shown also. The discrepancy in the initial portions of these two curves is the result of the assumption of rigid behaviour up to the yield line theory load. The theoretical load-deflection diagram shows an increase in the load with deflection without any limit, while in practice the failure of the reinforcement or the crushing of the concrete will limit the load-carrying capacity of the slab.

Kemp [2] presented an upper bound solution for a simply supported square slab allowing for the effect of membrane action, assuming the slab to be made up of rigid

plastic material, and reinforced at the bottom face only. The square yield criterion was used and the plastic strain rate resultants corresponding to this yield criterion were assumed to be consistent with the plastic potential. A collapse mechanism of diagonal yield lines was assumed. The triangular portions of the slab between the yield lines were assumed to be rigid with plastic deformations, axial and bending, only possible at the yield lines. The plastic potential function was assumed to be equal to the yield criterion and equated with the ratio of the plastic axial strain to the curvature strain rates. The plastic strain rates and consequently the depth of the neutral axis at the centre of the slab were determined as a function of deflection from the geometry of the yield mechanism shown in Fig.2.7, and from the horizontal equilibrium of the triangular elements, shown in Fig.2.8. The depth of the neutral axis being known, the magnitude of the membrane forces and the corresponding moments were obtained from the yield criterion as a function of the central deflection of the slab. The corresponding load at any central deflection was found by considering the equilibrium of one of the four rigid triangular quarters of the slab, by taking the moments about the mid-depth of the simply supported edge, Fig. 2.9. The expression developed showed that the theoretical collapse load was dependent on the ratio of the central deflection to the effective depth and the parameter, $t=\frac{\rho f_y}{f_c'}$. A typical load–deflection curves obtained from the analysis and normalised with respect to yield line theory load are shown in Fig.2.10. It was concluded that for a low percentage of reinforcement the enhancement in the load carrying capacity was pronounced. If a maximum deflection could be specified on the basis of satisfactory service behaviour, a saving in the reinforcement from 10% to 20 % could be achieved by allowing for membrane action in simply supported slabs depending on the

percentage of reinforcement. The method in essence follows the analysis proposed by Wood [1] for a circular isotropic slab.

From the observation of the behaviour of test slabs, Taylor [3] suggested that the load-carrying capacity of simply supported square slabs could be determined from the change of geometry resulting from deflections which results in a continual increase in the effective lever arm of the internal forces, Fig.2.11. For square slab of side L carrying a uniformly distributed load q, if the equilibrium of segment A is considered by taking moment about the support line, the following equations can be written for a slab at a particular deflection,

$$\frac{qL^2}{24} = g\sum T \qquad 2.15$$

where $\sum T$ is the total tensile force in reinforcing steel and g is the distance from centroid of steel to centroid of concrete compression. The load-deflection curve determined from such calculations agrees fairly well, with actual load-deflection curves for loads greater than the yield line theory collapse load as shown in Fig.2.12. It was concluded that, from the experimental data available, such a design procedure could lead to economies in the amount of reinforcement required in some slabs; such economies would probably only be significant in thin slabs.

The analysis developed by Park [4] for rectangular restrained slabs at large deflections can also be used, with some modifications, for simply supported slabs. The reinforcement was assumed to act as a plastic membrane at large deflections when the concrete has cracked through the slab. The reinforcement was assumed to have no strain

hardening. Equilibrium equations for the plastic membrane were derived and solved using the standard membrane theory [25], to obtain the load-deflection curve. The load deflection curve obtained was linear. A typical load-deflection curve for restrained slab is shown in Fig.2.13; for this slab the top reinforcement existed only around the edges and the top reinforcement has not been included in the assumed plastic membrane. Comparison of this theoretical curve with the experimental curves shows the theory to be conservative. It appears that such an analysis would be valid at very large deflections when the slab really behaves as a plastic net whereas, at moderately large deflections, the load will be carried both by bending and membrane action.

The conventional yield line theory for two-way reinforced concrete slabs was extended by Morley [5] to allow for membrane action. The membrane forces acting on the yield lines are calculated from a consideration of the displacement rates for the assumed collapse mechanism and the in-plane equilibrium of the membrane forces Fig. 2.14. The membrane forces being known, the moments on the yield lines are obtained from the yield criterion. The load deflection relationship was established using the principle of virtual work. This general extension of the yield line method for moderately large deflections is for restrained slabs but can also be applicable for simply supported slabs. However, this analysis is for isotropic slabs and cannot be directly applicable to orthotropic slabs. Results for a simply supported circular slab under uniformly distributed load predicted using this method were compared with the results of Wood [1] for a circular slab as shown in Fig. 2.15. The curves remain remarkably close to deflection of 0.4d. For deflections greater than the slab depth Wood predicted loads progressively greater than Morley's results as has been mentioned by Morley [5]. The

method also compared with theoretical and experimental results of Taylor [3] for square simply supported slab Fig.2.16 good agreement was obtained.

Sawczuk [6] presented a kinematical approach for the analysis of membrane action in simply supported slabs. The slab was assumed to be made up of rigid plastic material and iso-tropically reinforced at top and bottom. Based on kinetically admissible collapse modes, dissipation functions were derived and the load-deflection relationships were established. The axial forces and moments at the yield sections were dependent on deflections. The load-deflection curve obtained was linear elastic up to the yield line theory load; after that the response is purely plastic. In the calculation of the theoretical collapse load, the ultimate strength of the reinforcement rather than the yield strength was taken. Three simply supported slabs were tested and the results of the theoretical analysis and the experimental results were compared. Comparison between the experimental and theoretical results is shown in Fig.2.17. Since the experimental deflection represents the total deflection, that is elastic and plastic, the elastic deflections were added to those of post-yield deflection. However, it may be not correct to obtain the total deflection of the slab by simple addition for elastic and plastic deflections of post-yield deflections involves some approximation.

Hayes [7] extended the method of Sawczuk [6], by using an equilibrium approach instead of the kinematical approach. The type of collapse mechanism assumed is shown in Fig2.18a. The in-plane axial and shear forces were assumed to exist along these yield lines and the in-plane plastic hinges were assumed to form at section X-X on the long side of the slab, Fig.2.18b. The magnitude of the axial forces and the shear force were

calculated by using the in-plane equilibrium of the rigid portions between the yield lines and taking moments of the forces about the in-plane plastic hinges. Experiments were also carried out to verify the analysis. The load deflection relationship obtained from the analysis was linear. A comparison between the analytical and experimental results is shown in Fig.2.19, but the experimental and analytical results are not in good agreement. A comparison between this method and the other methods for Sawczuk[6] and Kemp[2] is presented in Fig.2.20. Hayes [7] concluded that the difference between the developed method and Kemp's analysis becomes only of significance for very small percentages of reinforcement.

Desayi [8] developed a method to determine the complete load-deflection curve behaviour of simply supported rectangular reinforced concrete slabs subjected to uniformly distributed load. The procedure in general followed the approach of Kemp [2] for square slabs, but was extended to include rectangular orthotopic slabs. The analysis was carried out in two stages. In the first stage the deflections up to the yield line theory load were calculated using the results for elastic theory of plates [10]. The cracking of concrete and the reduction in the modules of elasticity of concrete under higher stresses were accounted for by modifying the flexural rigidity of the slab section. In the second stage the load-deflection behaviour beyond the yield line theory load was determined by a procedure which incorporated the effect of membrane action on the load-carrying capacity. A simple yield line collapse mechanism was assumed to develop and the in-plane forces and moments were assumed to exist along these yield lines Fig.2.21. The depth of the neutral axis in x and y-directions was determined separately from the geometry of the mechanism and from the equilibrium of the membrane forces. The

value of the depth of the neutral axis in x and y-directions being known, the membrane forces and the corresponding moments were calculated from the yield criterion. The collapse load was calculated by considering the equilibrium of the moments and the membrane forces on the yield lines and taking the moment of the forces about the edge. Experiments were also carried out on twelve slabs to verify the analysis. Comparison between the theoretical and experimental results is shown in Fig. 2.22. Desayi [8] concluded that theoretical load-deflection curve is in satisfactory agreement with the test results if the ultimate strength of the steel is to be used in the expression, and is underestimates the experimental load-deflection curve of the slabs if yield strength is used in the expression.

Desayi [10] extended the above method [8] to cover skew simply supported reinforced concrete slabs subjected to uniformly distributed load. Twenty-three simply supported skew slabs were tested to verify the results of the analysis. Good agreement between the theoretical and experimental load-deflection curves was obtained as shown in Fig.2.23.

Following the same approach of Kemp [2] Verreyya [11] obtained an upper bound solution for a simply supported square slab with a central circular opening. Experiments were carried out for six slabs with central circular opening. Comparison between the theoretical and experimental load-deflection curves is shown in Fig.2.24; the load-deflection curves are in agreement with each other. It was concluded that the enhancement of the load-carrying capacity for square slabs with a central circular opening depends upon the ratio of deflection at a point where the diagonal meets the free edge of the circular opening to the effective depth of the slab and the parameter t.

2.3 ANALYSIS AND DESIGN OF REINFORCED CONCRETE SLABS WITHOUT INCLUDING MEMBRANE ACTION.

There are two possible approaches to the analysis and design of reinforced concrete slab systems. The approaches available are elastic theory and plastic theory. Such methods can be used to analyse a given slab system to determine either the stresses in the slabs and the supporting system or the load-carrying capacity. Alternatively, the methods can be used to determine the distribution of moments and shears to allow the reinforcing steel and concrete section to be designed. In the following sections, methods of analysis and design for reinforced concrete slabs based on elastic and plastic theory are discussed.

2.3.1 ELASTIC ANALYSIS OF SLABS

Classical elastic theory applies to isotropic slabs, which are sufficiently thin for shear deformations to be insignificant and sufficiently thick for in-plane forces to be unimportant. The distribution of moments and shear forces found by elastic theory is such that:

1. The equilibrium and boundary conditions are satisfied at every point in the slab.
2. Stress is proportional to strain; that is, bending moments are proportional to curvatures.

The behaviour of linear elastic thin plates loaded normal to their plane are governed by the fourth-order differential equation in terms of deflection of the slab at general point (x, y)on the slab, the loading on the slab and the flexural rigidity of the slab section as given below

$$\frac{\partial^4 w}{\partial x^4} + 2\frac{\partial^4 w}{\partial x^2 \partial y^2} + \frac{\partial^4 w}{\partial y^4} = \frac{q}{D} \qquad 2.16$$

Where

w is the deflection of the plate in direction of loading at point (x, y).

q is the loading imposed on the plate per unit area a function of x and y.

D is the flexural rigidity of the plate = $\frac{Eh^3}{12(1-\nu^2)}$

E is the Young's modules of plate material.

h is the plate thickness.

ν is the Poisson's ratio.

Equation 2.16 is difficult to solve in many realistic cases, particularly when the effects of deformations of the supporting system are to be taken into account. However, many analytical techniques have been developed to obtain solutions. In particular, the use of computers and finite difference or finite element methods enable elastic theory solutions to be obtained for slab systems with any loading or boundary conditions. Standard computer programs and charts and tables are available to assist the designer. The solution gives the distributions of bending and torsional moments and shear forces

throughout the slab. The action in the supporting system can also be determined. Timoshenko [9] gives a thorough treatment of elastic theory.

2.3.2 PLASTIC ANALYSIS AND DESIGN OF SLABS

The yield line theory [12] described in section 2.1 is one of the plastic methods used to analyse a given slab system. The upper bound solution estimated using the theory gives an ultimate load, which is either correct or too high, but if all the possible collapse mechanisms for the slab system are examined, the mechanism giving the lowest ultimate load is the correct one. The main advantage of the yield line theory is that it requires only relatively simple calculations and can be applied to any shape of slab. The method does not give any information on the best steel distribution, load distribution to supports and stress distribution inside rigid regions.

For a proper estimation of the ultimate load, an upper bound solution itself is not sufficient and a corresponding lower bound solution should be available. Lower bound solutions are those which satisfy equilibrium and boundary conditions and provide a statically admissible moment field which does not violate the yield condition anywhere in the slab. In the case of reinforced slabs, to obtain a statically admissible moment field for predicting the lower bound on ultimate load is difficult and very few solutions are available at present. For simply supported and fixed circular slabs with isotropic reinforcement lower bound solutions are given by Wood[1] which coincide with the upper bound solutions, and thus unique solutions are known. Some lower bound

solutions are given by Wood [1] and Kemp [24] for simply supported rectangular slabs with either isotropic or orthtropic reinforcement, but they do not coincide exactly with the upper bound solutions. However, a satisfactory value of ultimate load is assumed to have been obtained.

An interesting design procedure based on the lower bound approach has been suggested by Hillerborg [13]. Usually, a slab is designed to have reinforcement in orthogonal x and y-directions, so Hillerborg thought it proper to eliminate torsional moment M_{xy} from the differential equation of the equilibrium of the slab which is given by

$$\frac{\partial^2 M_x}{\partial x^2} + 2\frac{\partial^2 M_{xy}}{\partial x \partial y} + \frac{\partial^2 M_y}{\partial y^2} = -q \qquad 2.17$$

Thus equation 2.17 reduces to

$$\frac{\partial^2 M_x}{\partial x^2} + \frac{\partial^2 M_y}{\partial y^2} = -q \qquad 2.18$$

And the total load carried by the slab is split up into two parts, one part of the load αq being carried by strip in x-direction and the remaining load, $(1-\alpha)q$ carried by strip in the y-direction, thus

$$\frac{\partial^2 M_x}{\partial^2 x^2} = -\alpha q$$
$$\frac{\partial^2 M_y}{\partial^2 y^2} = -(1-\alpha)q \qquad 2.19$$

The above approach appears to provide a simple and powerful technique for the design of two-way slabs. Wood and Armer [14] extended and examined Hillerborg's strip method in great detail from the lower bounds approach and tested some typical reinforced concrete slabs designed by using the above method. It was concluded that the strip method provides a safe method of design for ultimate load and that at working load the slabs behaviour in terms of deflections and cracking was satisfactory.

2.3.3 DESIGN OF SLABS IN PRE DETERMINED MOMENT FIELDS.

Hillerborg[15] proposed a method for the reinforcement of slabs and shells in mixed moment fields without including membrane forces. The work was based on normal moment yield criterion approach, i.e. the moment capacity of the section must be greater than or equal to the applied moments in the direction normal to the yield line. The applied bending and twisting moments, Fig.2.25,were transformed into a direction normal to the failure direction and the difference between the moment capacity and the applied moments was then minimised. The capacity of the section was defined using Johansen's yield criterion [12].

If the moment capacity of the section must be greater than or equal to the applied moments, thus

$$M_{nu} \geq M_n \qquad 2.20$$

where, M_{nu} = capacity of the section normal to the failure direction.

M_n = applied moments transformed in the failure direction.

The moment capacity, M_{nu}, using Johansen's yield criterion [12] is given by

$$M_{mu}=M_x^*\cos^2\theta+M_y^*\sin^2\theta \qquad 2.21$$

And the applied moments, M_n, transformed normal to failure direction are

$$M_n= M_x\cos^2\theta+M_y\sin^2\theta+2M_{xy}\sin\theta\cos\theta \qquad 2.22$$

Where, θ is the direction of failure.

Substituting the value of, M_{nu}, and, M_n, from equations 2.21 and 2.22 into equation 2.20, dividing by, $\cos^2\theta$, and introducing

$$\tan\theta = k \qquad 2.23$$

to obtain the following formulation.

$$f(k)=M_x^*+k^2M_y^*-M_x-k^2M_y-2kM_{xy}\geq 0 \qquad 2.24$$

Equation 2.24 must hold good for all values of k. The greater the value of $f(k)$, the greater will be the margin of safety. The most critical direction, k_1, can therefore be obtained by finding the minimum of $f(k)$ at given value of M and M_u.

$$\frac{df(k)}{dk}=2k_1M_y^*-2k_1M_y-2M_{xy}=0 \qquad 2.25$$

$$\frac{d^2(k)}{dk^2}=2M_y^*-2M_y>0 \qquad 2.26$$

From equation 2.25 the value of M_y^* can be obtained.

$$M_y^*=M_y+\frac{1}{k}|M_{xy}| \qquad 2.27$$

and from equation 2.25 and 2.26 the following condition is obtained

$$\frac{M_{xy}}{k_1} > 0 \qquad 2.28$$

Similarly the design moments M_x^* and M_y^* in x and y directions can be obtained as follows.

Positive moments, Fig.2.25.

$$M_x^* = M_x + k_1 \left| M_{xy} \right| \qquad 2.29a$$

$$M_y^* = M_y + \frac{1}{k_1} \left| M_{xy} \right| \qquad 2.29b$$

Negative moments, Fig.2.25.

$$M_x^* = M_x - k_2 \left| M_{xy} \right| \qquad 2.30a$$

$$M_y^* = M_y - \frac{1}{k_2} \left| M_{xy} \right| \qquad 2.30\,b$$

Where

M_x, M_y, M_{xy} = applied bending and twisting moments.

M_x^*, M_y^* = design moments in orthogonal reinforcement directions.

In the above expressions k_1 and k_2 are arbitrary positive factors; for economical reasons, these factors should as a rule be close to unity, and should be chosen so that the condition,

$$M_x^* . M_y^* \geq 0 \qquad 2.31$$

The above expressions may also be used for designing the reinforcement of slabs and shells if M_x and M_y are placed by the corresponding perpendicular stresses and M_{xy} by the shearing stress.

Wood [16] developed rules for reinforcement arranged at right angle for slab element subjected to mixed moment fields using Hillerborg's [15] approach. The work was based on the normal moment yield criterion, i.e. the moment capacity of the section must be greater than or equal to the applied moments in the direction normal to the yield line. The moment capacity of the section was defined using Johansen's yield criterion [12]. The applied moments were transformed in the direction normal to the failure direction and then the difference between the capacity and the applied moments was minimised using the concept that in the failure direction the curve representing the strength must be tangential to the applied moments curve. Wood [16] has also shown that the failure directions, k_1 and k_2 in equation 2.29 and equation 2.30 is equal to 1, i.e. the failure direction is 45°. Therefore, equations 2.29 and 2.30 can be written as follows.

For bottom steel

$$M_x^* = M_x + |M_{xy}| \qquad 2.32a$$

$$M_y^* = M_y + |M_{xy}| \qquad 2.32\ b$$

and if $M_x^* < 0$ then

$$M_x^* = 0 \qquad 2.32\ c$$

$$M_y^* = M_y - \frac{|M_{xy}^2|}{M_x} \qquad 2.32\ d$$

Similarly if $M_y^* < 0$ then

$$M_y^* = 0 \qquad 2.32\ e$$

$$M_x^* = M_x \frac{\left|M_{xy}^2\right|}{M_y} \qquad 2.32\ \text{f}$$

For top steel

$$M_x^* = M_x - \left|M_{xy}\right| \qquad 2.33\ \text{a}$$

$$M_y^* = M_y - \left|M_{xy}\right| \qquad 2.33\ \text{b}$$

and if $M_x^* > 0$ then

$$M_x^* = 0 \qquad 2.33\ \text{c}$$

$$M_y^* = M_y - \frac{\left|M_{xy}^2\right|}{M_x} \qquad 2.33\ \text{d}$$

Similarly if $M_y^* > 0$ then

$$M_y^* = 0 \qquad 2.33\ \text{e}$$

$$M_x^* = M_x - \frac{\left|M_{xy}^2\right|}{M_x} \qquad 2.33\ \text{f}$$

Where

M_x^* and M_y^* = design moments in reinforcement direction x and y-directions respectively.

M_x, M_y, M_{xy} = applied bending and twisting moments.

Armer[17] extended the equations developed by Wood [16], to cover skew reinforcement the equations are known as the Wood and Armer rule.

2.4 ULTIMATE LOAD TESTS OF SIMPLY SUPPORTED SLABS

Taylor [18] tested 10 uniformly loaded square slabs simply supported at all edges over 1.83 m spans. The span/thickness ratios were 41, 36 or 24. The slabs were designed either by the strip method or analysed using yield line theory. Uniformly spaced bars at right angles parallel to the supports, bars 45° to the supports, bars with different spacing, and bars curtailed before reaching the supports were the variables studied. The design ultimate load of the slabs was 22.9 to 23.8 kN/m^2. The maximum loads reached in the tests were 1.26 to 1.8 times the design ultimate loads. This large enhancement of the strength was attributed to tensile membrane action, which can develop at large deflections. At large deflections loads are no longer carried to the supports by ordinary bending action, as is evident from the penetration of cracking to the top surface in the central region of the slab, and from the change of the slab geometry. For the slabs with curtailed bars the ultimate load was not enhanced to the same extent. From these test results it was concluded that for the simple case of slabs tested, the strip method and yield line theory design method resulted in slabs with safe predictions of ultimate loads and satisfactory service loads.

Seven rectangular slabs of spans 3.66 m by 1.83 m were tested by Armer [19] under uniform loading. The slabs were 57 mm thick. The slabs were designated T1 to T7. Slabs T1,T2 and T3 were cast with integral edge beams and supported simply at corners. Slabs T4 to T7 were not cast with edge beams and were simply supported along all edges. Slabs T3 to T7 were also supported on a column at the slab centre. Slab T2 had a 1.37m by 0.91m rectangular opening near the slab centre. Slab T1 was designed

by the simple strip method. Slab T2 was designed by the simple strip method with strong bands in the slab around the opening. Slabs T3 to T4 were designed by Hillerborg's advanced strip method. Slabs T5 and T6 were designed by the modified version of the advanced strip method suggested by Wood and Armer [19]. Slab T7 was designed by the simple strip method with strong bands within the slab passing each way over the central column. The design ultimate loads of the slabs varied between 20.1 and 40.2 kN/m^2. The actual ultimate loads reached were 1.3 to 2.22 times the design loads. These very large enhancements of slab strength were evidently the result of the assumption that the load is carried by flexure only. In fact, during the test membrane action within the slab was very apparent, particularly around the columns. Therefore, there is no doubt for the safety of the design method because of the development of the membrane action.

Ghoneim and MacGregor [20,21] tested nineteen large-scale square and rectangular slabs simply supported on four sides. The slabs were subjected to various combinations of in-plane compressive and lateral loads (load perpendicular to the plate). The test slabs were divided into four series. All the slabs in a given series had the same concrete strength, side dimensions, and slenderness ratio. Series A consisted of four rectangular slabs with side dimensions of 1.829 m by 4.267 m. Three of these were tested under combined in-plane and lateral loads with the in-plane loads applied along the short edge, and one was tested under lateral load only. Series B consisted of four rectangular slabs of side dimensions of 1.829 m by 2.745 m. Two of these were tested under combined loads with the in-plane loads applied along the short edge, one was tested under combined loads with in-plane load applied along the longer edge and one was

tested under lateral load only. Series C consisted of nine square slabs of side dimensions of 1.829 m. Six of these were tested under combined uniaxial compression and lateral loads, two were tested under combined biaxial compression and lateral loads, and one was tested under lateral load only. Series D consisted of two square slabs having the same side dimensions as series C. One of these was tested under combined in-plane uniaxial compression and lateral loads, while the other was tested under lateral load only. The slabs tested under lateral load only in each series were for comparison with those tested under combined loads. The uniformly distributed load was simulated by the application of 18 concentrated loads to the rectangular slabs of series A and 12 concentrated loads to the rectangular slabs of series B and 9 concentrated loads to the square slabs. The reinforcement for all slabs consisted of equal reinforcement at top and bottom. Each layer comprised steel running in both orthognal directions. The behaviour of the tested slabs indicated that the slabs tested under lateral loads only carried loads much higher than those predicted by the yield-line theory. The actual ultimate loads reached were 1.23 to 1.72 times the design loads; this is attributed to the tensile membrane action, which developed at large deflection. The failure of plates tested under combined loads was caused by either compressive crushing of concrete, before or after the yielding of the tension steel, or by instability of the plate. The effect of the in-plane load on the lateral load capacity of the tested plates was found to be dependent mainly on the slenderness of the slab and on the reinforcement ratio. For moderate values of in-plane load levels, increasing the in-plane loads level may result in an increase or a decrease of the lateral load capacity of plates carrying combined loads. This depends on several factors, such as the aspect ratio of the plate, its slenderness, and whither the in-plane load is applied uniaxially or biaxially. The lateral load was found to be varied

between 62% for rectangular slender slabs tested under combined loads with in-plane load applied uniaxially along the longer edge to 37% for square stocky slabs with in-plane load applied biaxially.

Desayi [10] tested 23 skew slabs under uniformly distributed load to investigate the effect of tensile membrane action on simply supported skew slabs. The slabs were with aspect ratio of 1.5 and covered skew angles of 15°, 30° and 45°. All slabs were 50 mm deep and had span in one direction of 1.5 m and perpendicular distance between the two parallel sides of 1.0 m. The slabs were extended 15 cm beyond the supports for necessary anchorage of reinforcement. The slabs were divided into four groups. Groups 1, 2 and 3 were designated S1 to S6 each, and the skew angles were 15° for group 1, 30° for group 2 and 45° for group 3. Group 4 was designated S1 to S5, S1and S5 were with skew angle of 15°, S3and S4 were with skew angle of 30° and S2 was with skew angle of 45°. Group 4 was tested with corners held down. The uniformly distributed load was simulated by 16 point loads on each slab element. The slabs were with a different percentage of reinforcement in each direction. The reinforcement ratio in the short span and long span respectively were 0.53 and 0.7 for S1, 0.42 and 0.7 for S2, 0.315 and 0.7 for S3, 0.42 and 0.467 for S4, 0.315 and 0.467 for S5 and 0.315 and 0.35 for S6. The steel was mild steel bars of 4 mm diameter with yield strength of 566 N/mm^2 and ultimate strength of 650 N/mm^2. In all the tested slabs there was enhancement in the ultimate load above the yield line theory load; the enhancement was found to be dependent up on the skew angle and the percentage of the reinforcement. The ratio of the experimental ultimate load to yield line theory load was found to vary

between 1.08 in the case of S1 with skew angle of 15° and high reinforcement ratio and 1.61 in the case of S6 with skew angle of 45° and small reinforcement ratios.

Hago and Bhatt [22] tested five rectangular reinforced concrete slabs designed using the Wood and Armer rules [16,17] by using elastic stress fields at ultimate load in conjunction with a yield criterion based on the normal moment criterion as given by Johansen [12]. Slabs designated 1A, 1B, 2 and 3 were simply supported along all edges. Slab 4 was simply supported on two adjacent sides while the opposite corner was on a spherical support. All the slabs were 100 mm deep and tested under concentrated loads applied using hydraulic jacks. Slabs 1A and 1B were rectangular slabs with aspect ratios of 1.5 and 1.3 respectively and were designed for ultimate loads of 415 and 216 *kN* equally distributed on eight point loads. Slab 2 was a rectangular slab with aspect ratio of 1.3 and designed for ultimate load of 213 *kN* equally distributed as four point loads. Slab 3 was a square slab designed for ultimate load of 210 *kN* equally distributed as two point loads along the diagonal. Slab 4 was a square slab designed for an ultimate load of 90 *kN* equally distributed as two point loads along the diagonal. The behaviour of the slabs was found to be satisfactory both at working and at ultimate load. The ratio of the ultimate load to the design load was found to vary between 0.8 for the rectangular slab A1 which failed prematurely in shear during the test to 1.31 for the rectangular slab 2. The average experimental and ultimate design load was 1.17 times the ultimate load for which the slabs were designed. Hago and Bhatt [22] concluded that the direct design method is simple and direct and the variable moment fields can be easily handled.

Bensalem [23] tested six simply supported slabs to study the service and ultimate load behaviour of reinforced concrete slabs. The slabs were designed using Wood and Armer rules [16,17] and non-elastic stress fields. The non-elastic stress fields at ultimate load were determined using a finite element procedure. The slabs were simply supported on four edges. Slabs designated S1, S2 and S3 were square slabs with 2 m length and 100 mm deep; the slabs were designed for an ultimate load of 210 kN distributed to four point loads but with different levels. Slabs S4 and S6 were square slabs with 2 m length and depth of 100 and 150 mm respectively; the slabs were supported on a column support at the middle and designed for of 320 kN distributed equally at four point loads. Slab S5 was a rectangular slab of overall dimensions of 3 m by 2 m and 100 mm deep. The slab was designed for a total load of 210 kN equally distributed at eight point loads. The ratio of the experimental to design load was found to vary between 1.15 for S1 to 1.61 for S2. The average actual ultimate load for the tested slabs was found to be 1.20 times the design load. Bensalem [23] concluded that the use of non-elastic stress fields in direct design of reinforced concrete slabs leads to satisfactory behaviour both at service and ultimate loads.

2.5 CONCLUSIONS

The review of literature available for ultimate load tests [8,18,19,20,21,22,23] of simply supported slabs designed using the classical elastic and plastic design methods [12,15,16,17] without including the membrane action effect, shows that the tested slabs

sustained loads much higher than the loads for which they are designed. This is attributed to membrane action effect which become significant at large deflections.

The available methods for the analysis of simply supported slabs, which includes the membrane action resulting from the change of geometry [1,2,3,4,5,6,7,8,10,11] are based on the rigid-plastic approach. The load-deflection curves predicted using these methods are different from the experimental load-deflection curves; this is result of the assumption of rigid behaviour up to the yield line theory load. Therefore it seems necessary to use the finite element method which represents the experimental behaviour more closely and to study the development of membrane action prior to and post yield line theory load.

2.6 REFERENCES

1. Wood R. H., "Plastic and elastic design of slabs and plates", Thames and Hudson. 1961.

2. Kemp K. O., "Yield of square reinforced concrete slab on simply supports allowing for membrane action", Structural Engineer. Vol. 7, July 1967. Pp. 235-240.

3. Taylor R., "A note on a possible basis for a new method of ultimate load design of reinforced concrete slabs", Magazine of Concrete Research. Vol. 17, No 53, December 1965, pp. 183-186.

4. Park R., "Tensile membrane behaviour of uniformly loaded rectangular reinforced concrete slabs with fully restrained edges", Magazine of Concrete Research, Vol. 16, No 46. March 1964. pp 39-44.

5. Morley C. T., "Yield line theory for reinforced concrete slabs at moderately large deflection", Magazine of Concrete Research, Vol. 19, No 61. December 1967, pp. 211-221.

6. Sawczuk A. and Winnick L., "Plastic behaviour of simply supported plates at large deflections", International Journal of Solids and Structures", Vol. 1. No. 1. February 1965, pp 97-111.

7. Hayes B., "Allowing of membrane action in the plastic analysis of rectangular reinforced concrete slabs", Magazine of Concrete Research, Vol. 20, No 65, December 1968., pp. 205-211.

8. Desayi P. and Kulkarni A. B., "Load deflection behaviour of simply supported rectangular reinforced concrete slabs", Procedure of International Association of Bridge and Structural Engineers 1, P-11/78, February 1978, pp. 1-16.

9. Timoshenko S. P. and Krieger W., "Theory of plates and shells", Second edition, McGraw Hill, Kogakusha, 1959.

10. Desayi P., "Simply supported RC skew slabs", International Journal of Structures, Vol. 7. No 79. July-December 1987. pp. 119-139.

11. Verreyya V., "Effect of membrane action on yield load of simply supported square slabs with central circular opening", Journal of Institute of Engineers (India), Part CI: Civil Engineers Division, November 1984, Vol. 65, pp. 139-146.

12. Johansen K. W., Brudlinieteorir, Gjellerup, Copenhagen, Denmark 1943, English edition. "Yield line theory", Cement and Concrete Association, London 1962, 181p.

13. Hillerborg A., "Strip method of design", A View Point Publication, Slough, 1975.

14. Wood R. H. and Armer G. S. T., "Theory of the strip method for the design of slabs", Procedure of the Institute of Civil Engineers (London), Vol. 41, October 1968, pp. 285-311.

15. Hillerborg A., "Reinforcement for slabs and shells designed according to the theory of elasticity", Betong 1953, Vol. 38, No. 2, pp 101-109. Translated by GN Gibson, Graston, building research station, January 1962, 7p Library communication No. 1081.

16. Wood R. H, "The reinforcement of slabs in according with a predetermined field of moments", Concrete, London, Vol. 2, February 1968, pp 69-76.

17. Armer G. S. T., "Discussion on 'The reinforcement of slabs in accordance with a predetermined field of moments", Concrete, London, Vol. 8, August 1968, pp 319-321.

18. Taylor R., Maher. D. R. H. and Hayes B. "Effect of arrangement of reinforcement on the behaviour of reinforced concrete slabs", Magazine of Concrete Research, Vol. 18, No. 55, June 1966.

19. Armer G. S. T., "Ultimate load test for slabs designed by the strip method", Procedure of Institute of Civil Engineering, Vol. 41, October 1968, pp. 313-331.

20. Ghoneim M. G. and MacGregor J. G., "Tests of reinforced concrete plates under combined in-plane and lateral loads", ACI. Structural Journal, January-February 1994.

21. Ghoneim M. G. and MacGregor J. G., "Behaviour of reinforced concrete plates under combined in-plane and lateral loads", ACI. Structural Journal, March-April 1994.

22. Hago A. and Bhatt P., "Tests on reinforced concrete slabs designed by direct design procedure", ACI. Structural. Journal, November-December 1986.

23. Bensalem A. "Direct design of reinforced concrete structures using non-elastic stress fields", PhD. Theses Department of Civil Engineering University of Glasgow, 1993.

24. Kemp K. O., "A lower pound solution to the collapse of an orthogonally reinforced slab on simply supports", Magazine of Concrete Research. Vol. 14, No. 41, July 1962, pp 79-84.

25. Timoshenko S. and Goodir J. N., "Theory of Elasticity", 2nd Edition, McGraw Hill, New York, 1951, 506 pp.

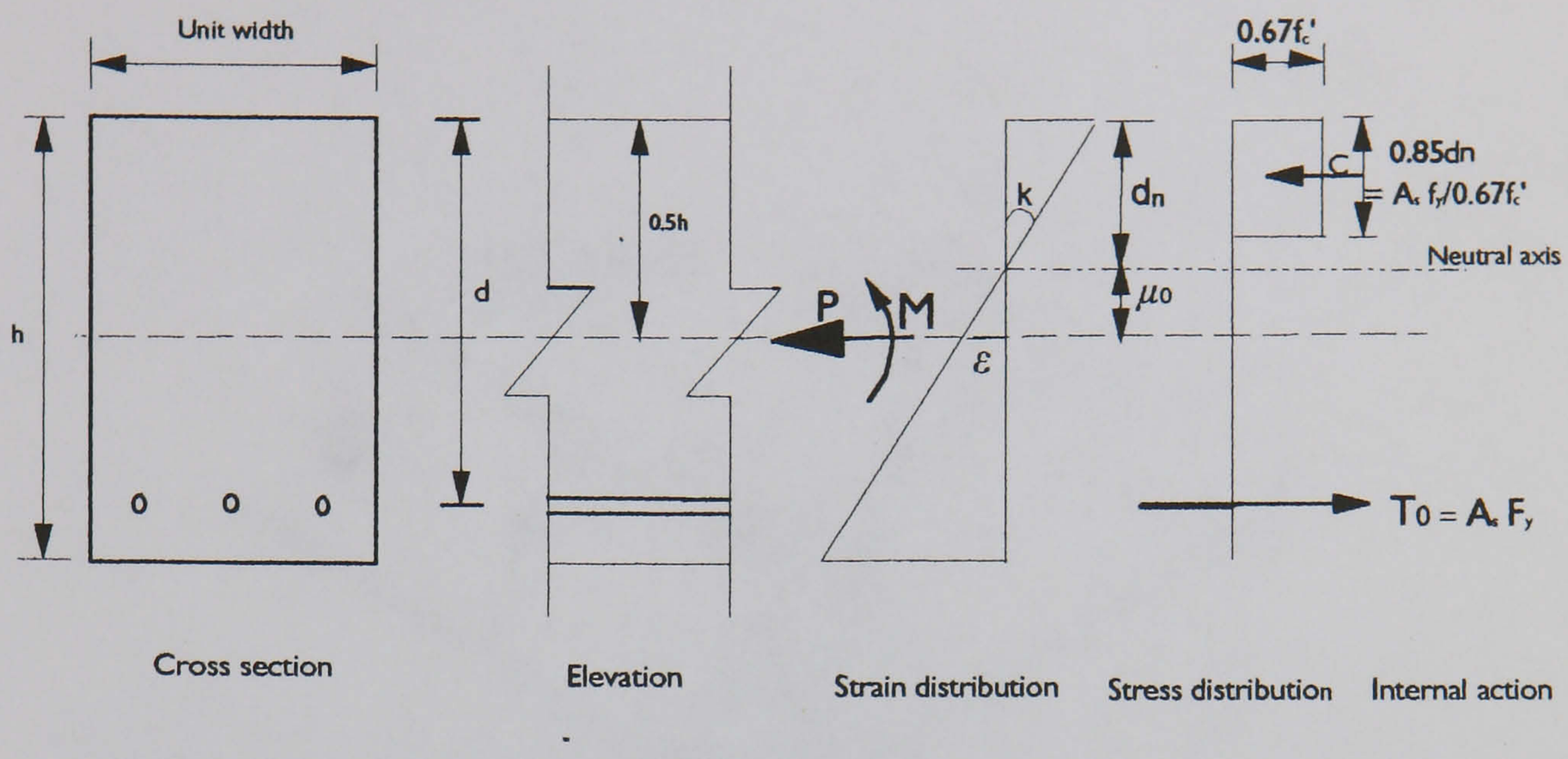

Fig.2.1- Stress distribution on the slab section

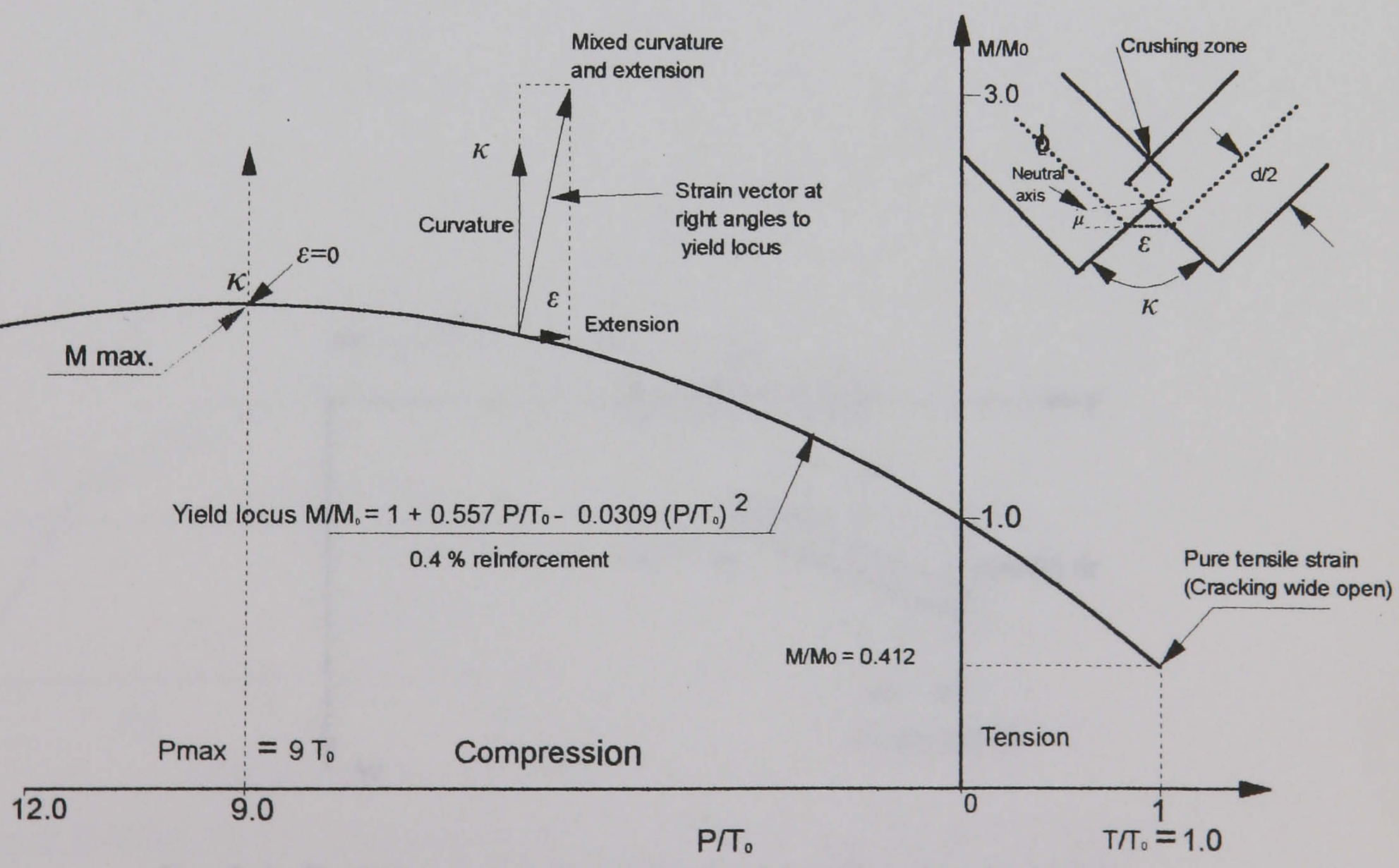

Fig. 2.2 Yield criterion for a typical slab section

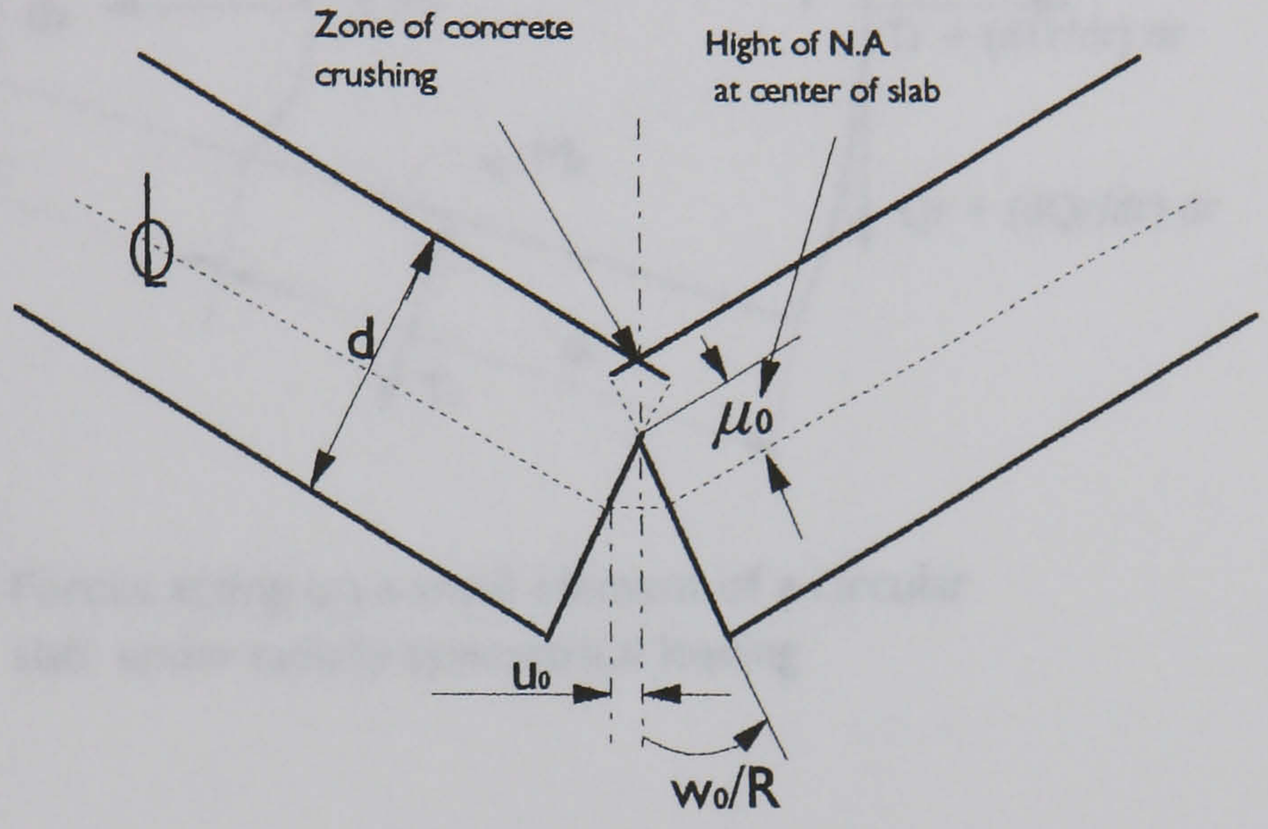

Fig. 2.3- Conditions at the centre of a slab with a conical collapse mode

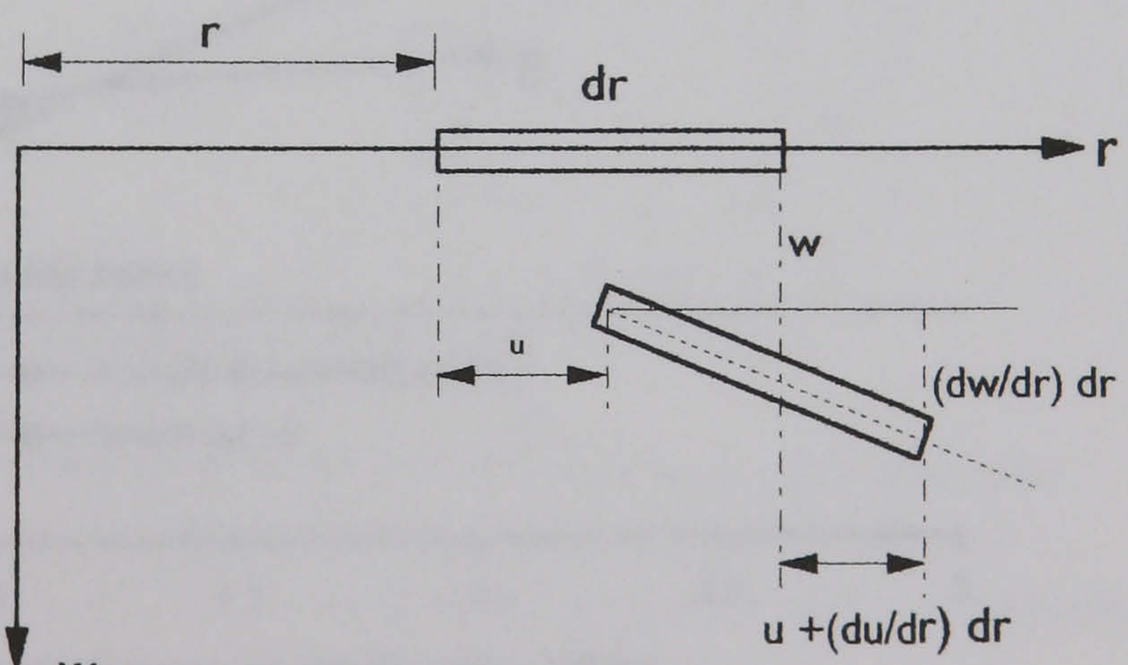

Fig. 2.4- Radial extension and vertical deflection in a slab element

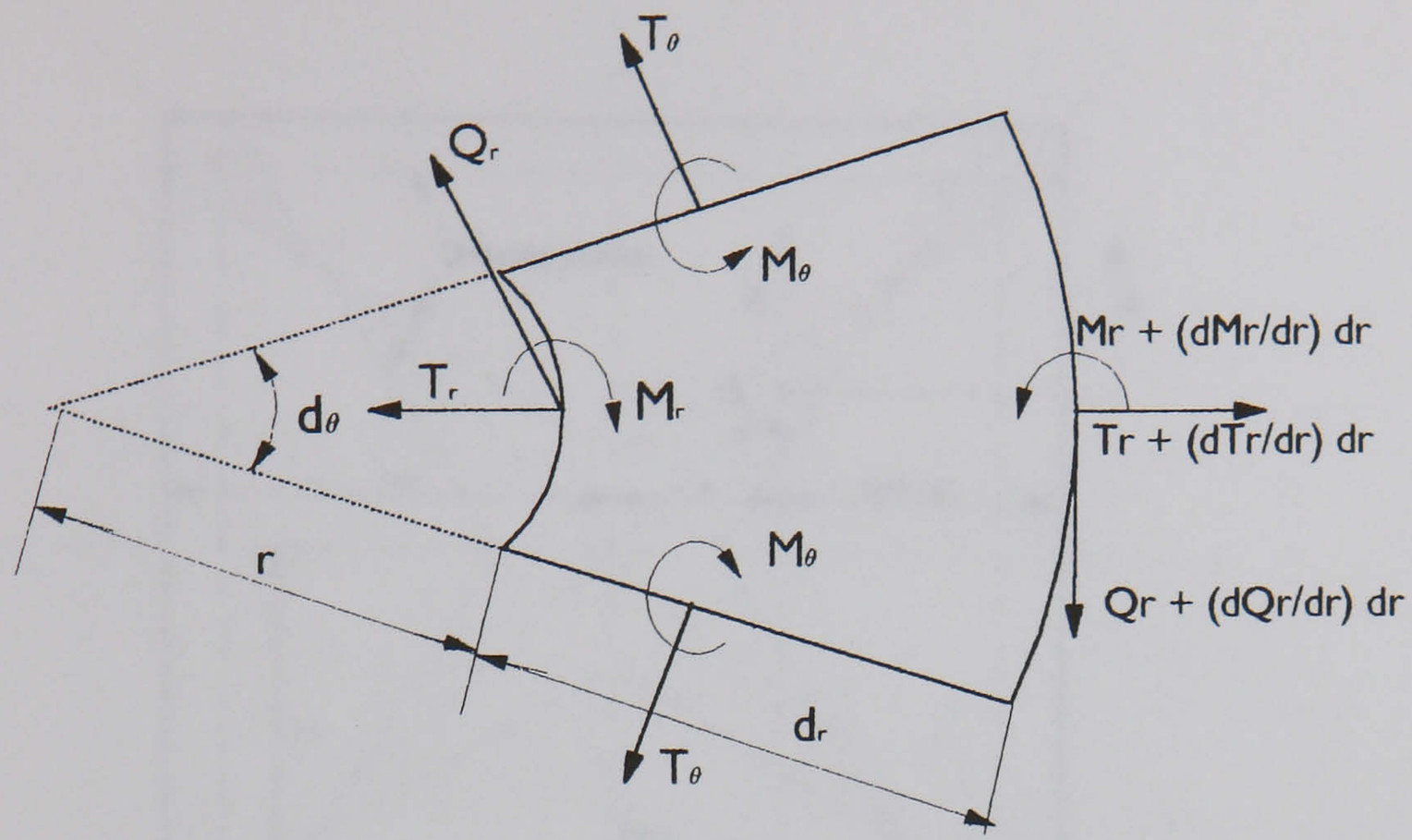

Fig. 2.5- Forces acting on a small element of a circular slab under radially symmetrical loading

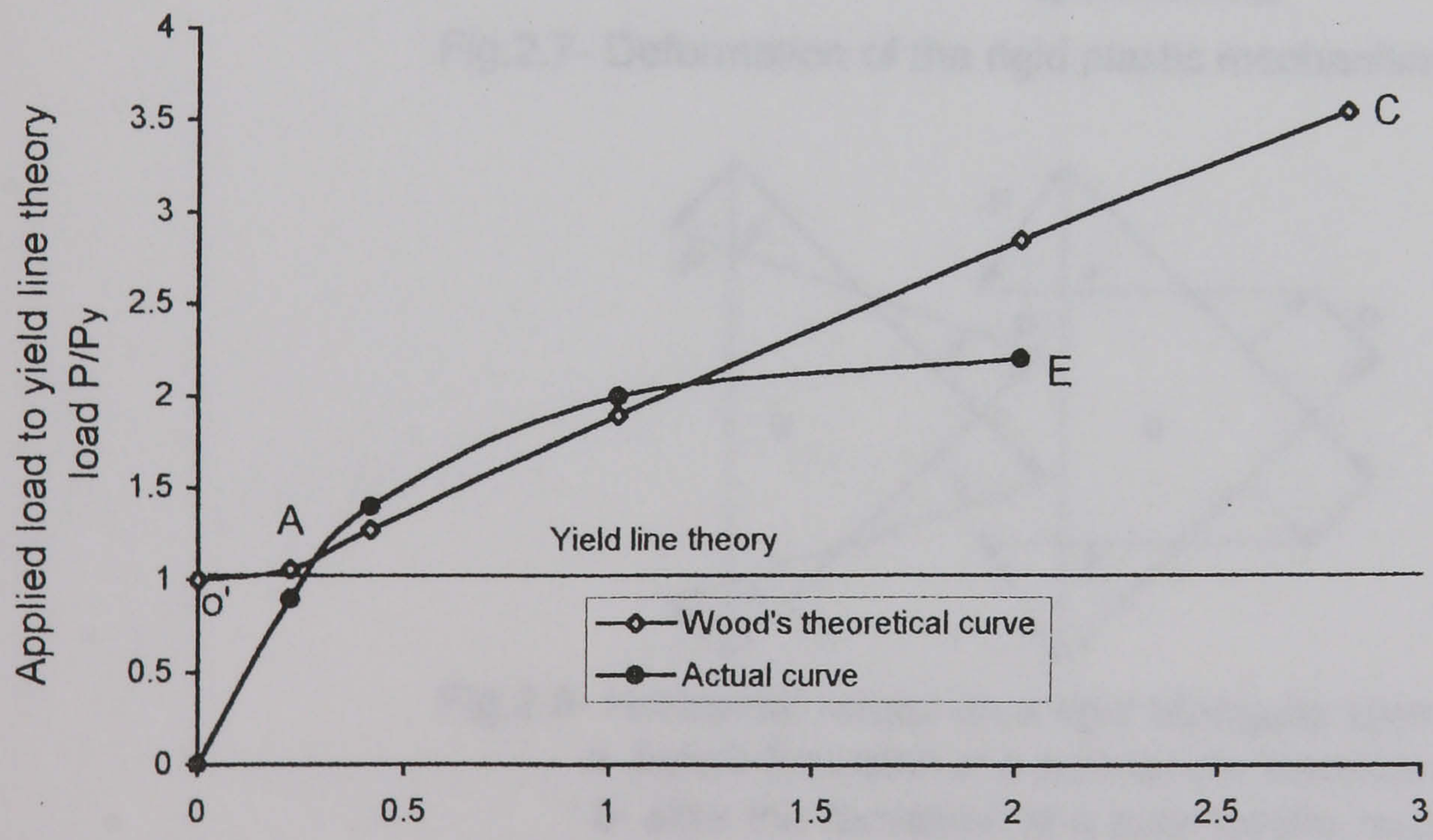

Fig.2.6-Wood's [1] theoretical results for simply supported circular slab with t=0.04

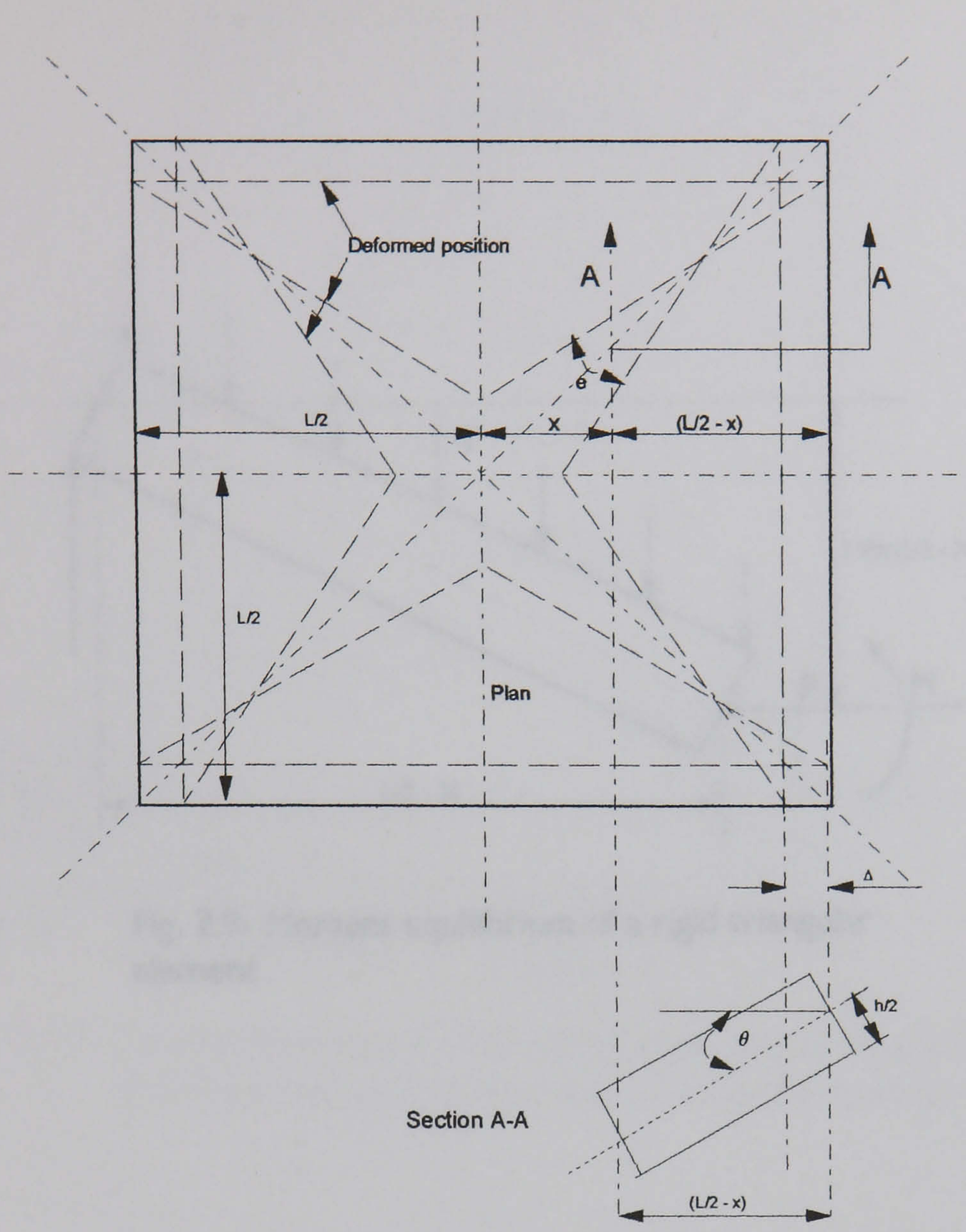

Fig.2.7- Deformation of the rigid plastic mechanism

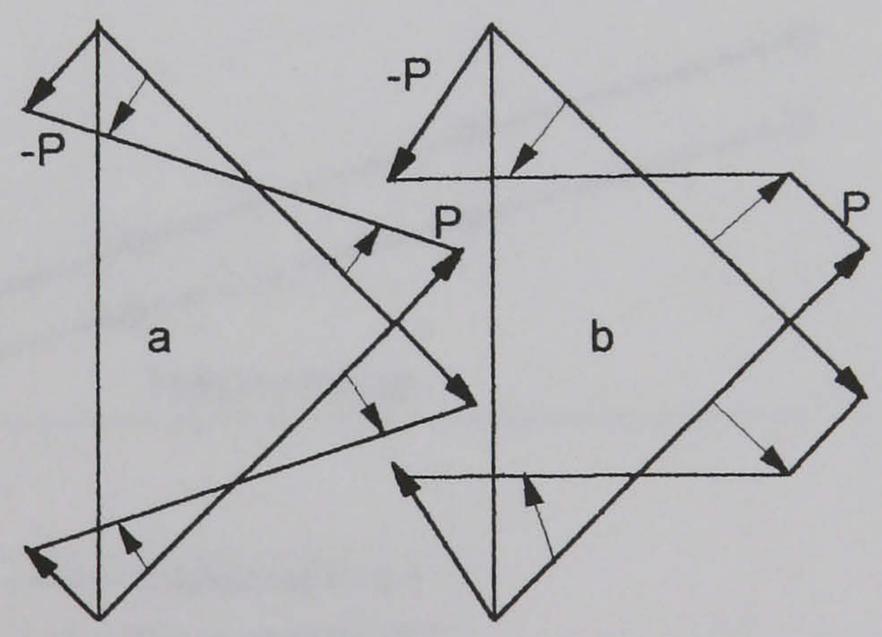

Fig.2.8- Horizontal forces on a rigid triangular element
a- before formation of a pure tensile membrane.
b- after the formation of a pure tensile membrane.

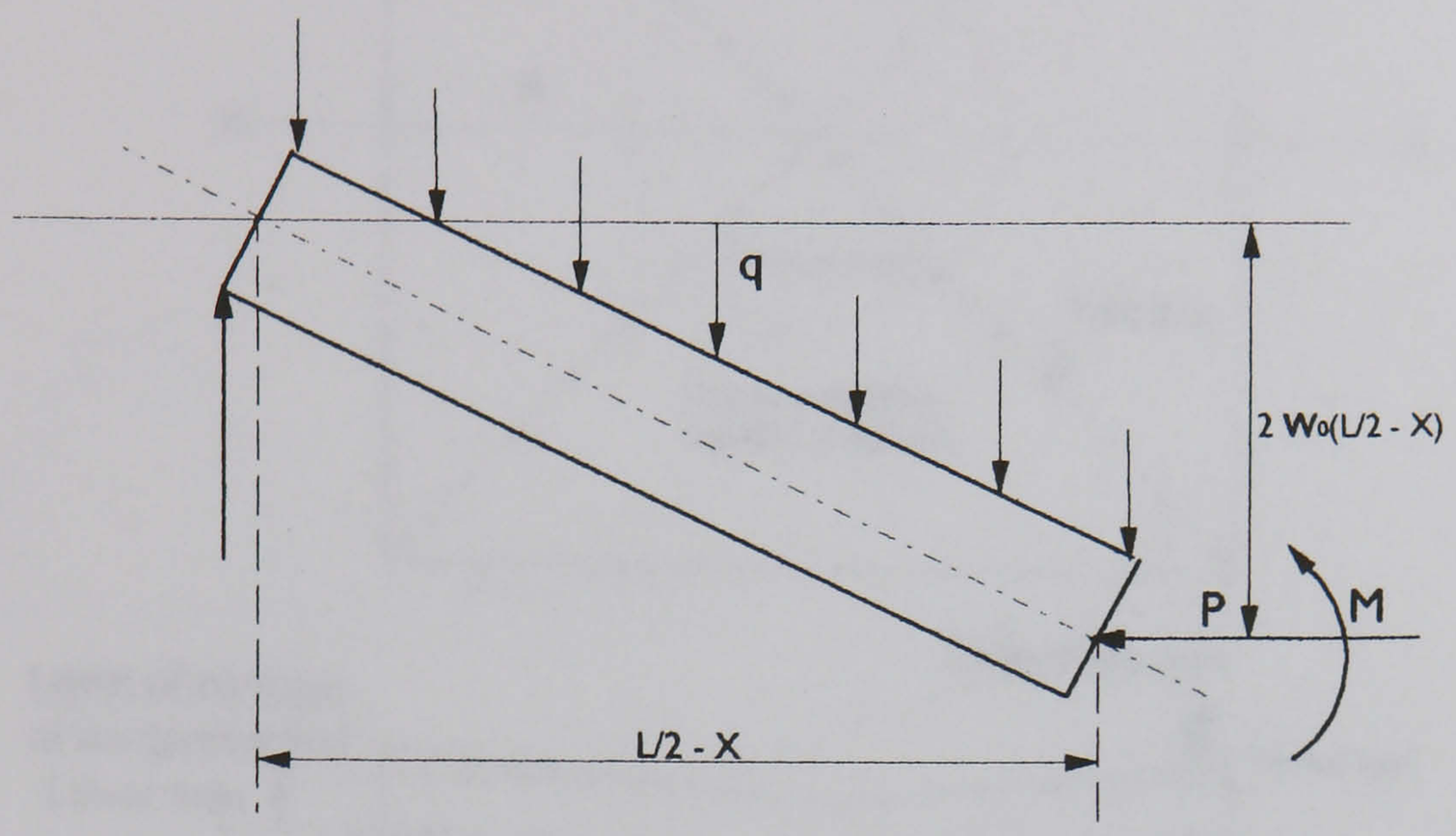

Fig. 2.9- Moment equilibrium of a rigid triangular element

Fig 2.10- Kemp's [2] theoretical results for square slab with different *t* parameters

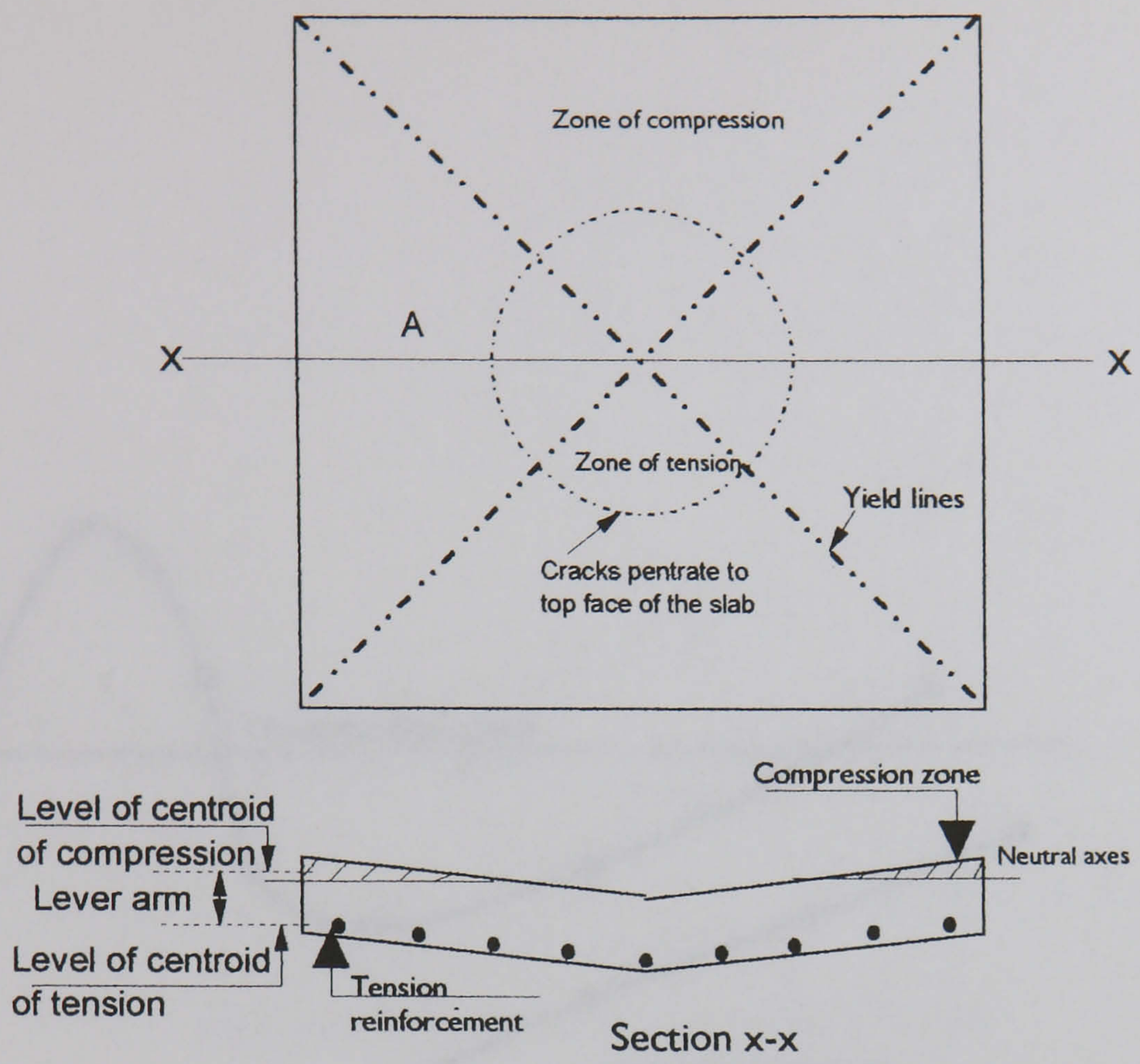

Fig. 2.11- Development of tensile membrane action in uniformly loaded simply supported slab at large deflections

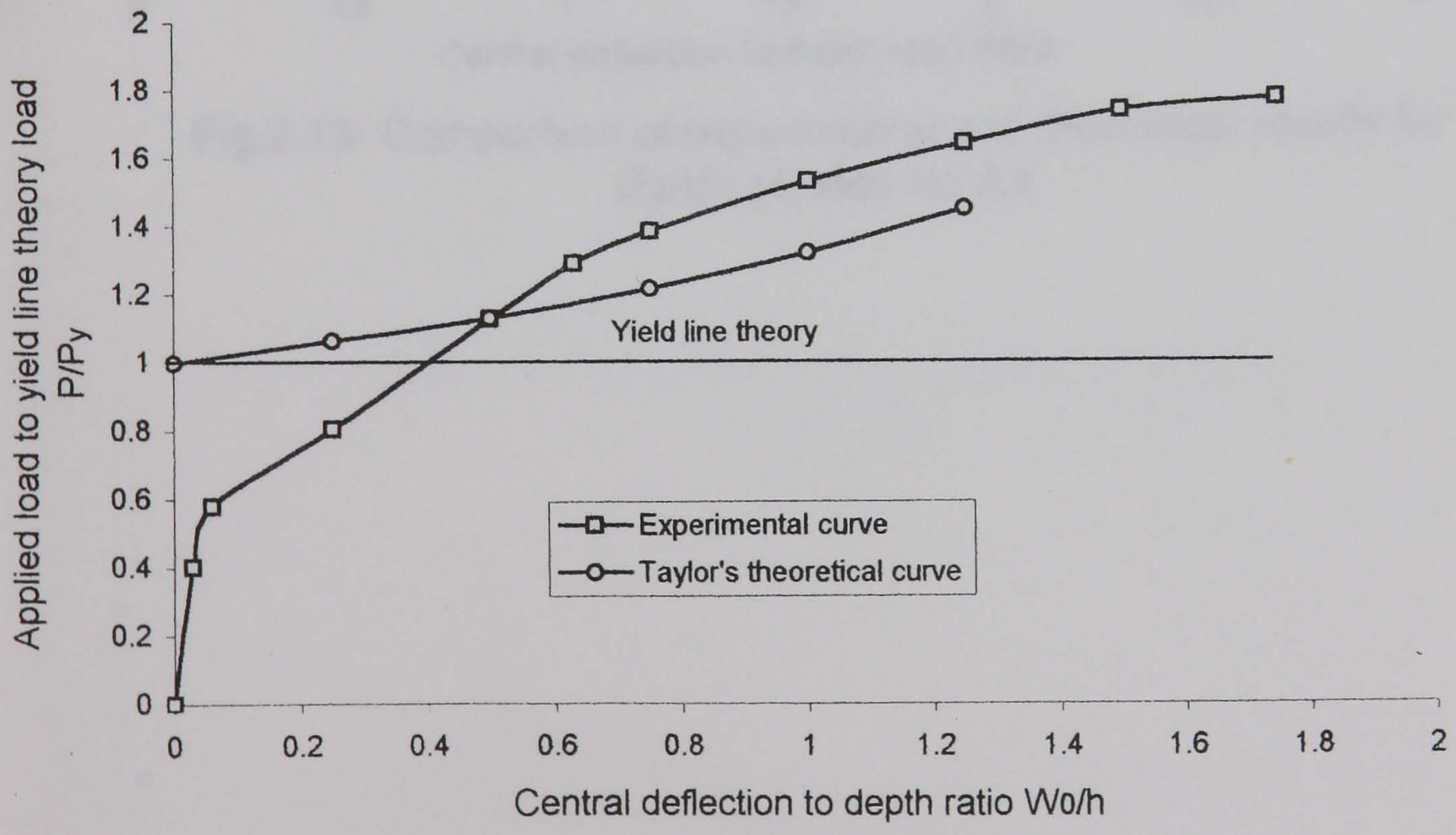

Fig. 2.12-Comparison of experimental and analytical results for Maher's [3] slab No. S2

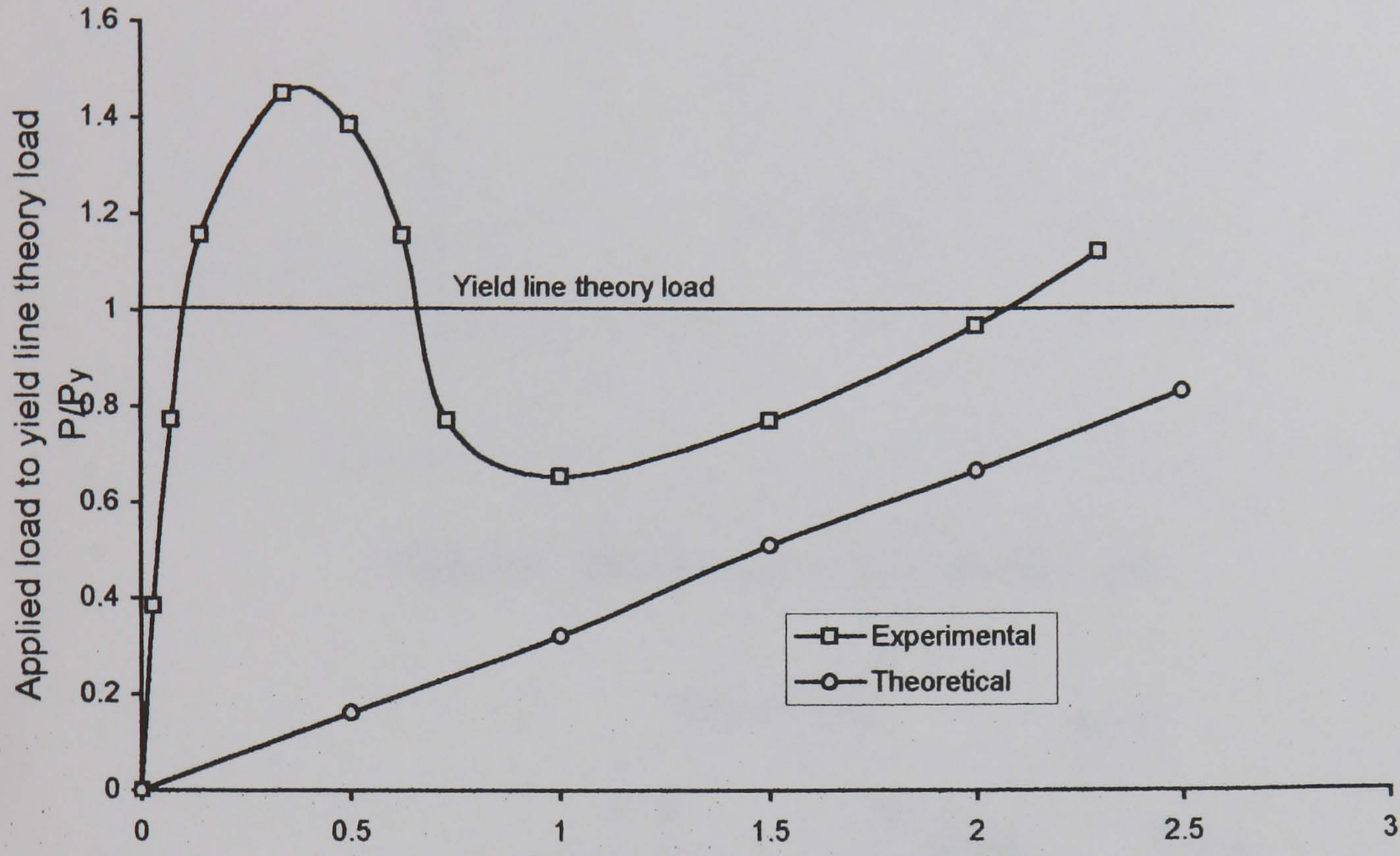

Fig.2.13- Comparison of experimental and theoretical results for Park's [4] slab No.A4

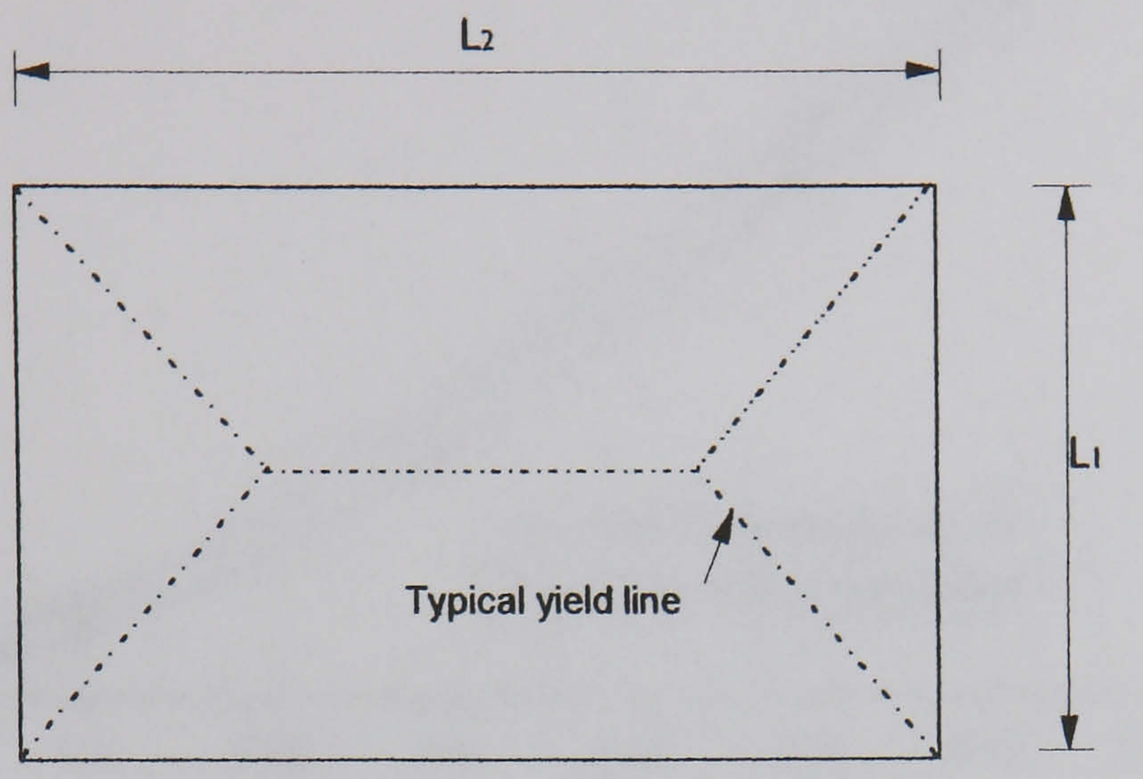

Fig.2.14 a- Yield line pattern in a rectangular slab.

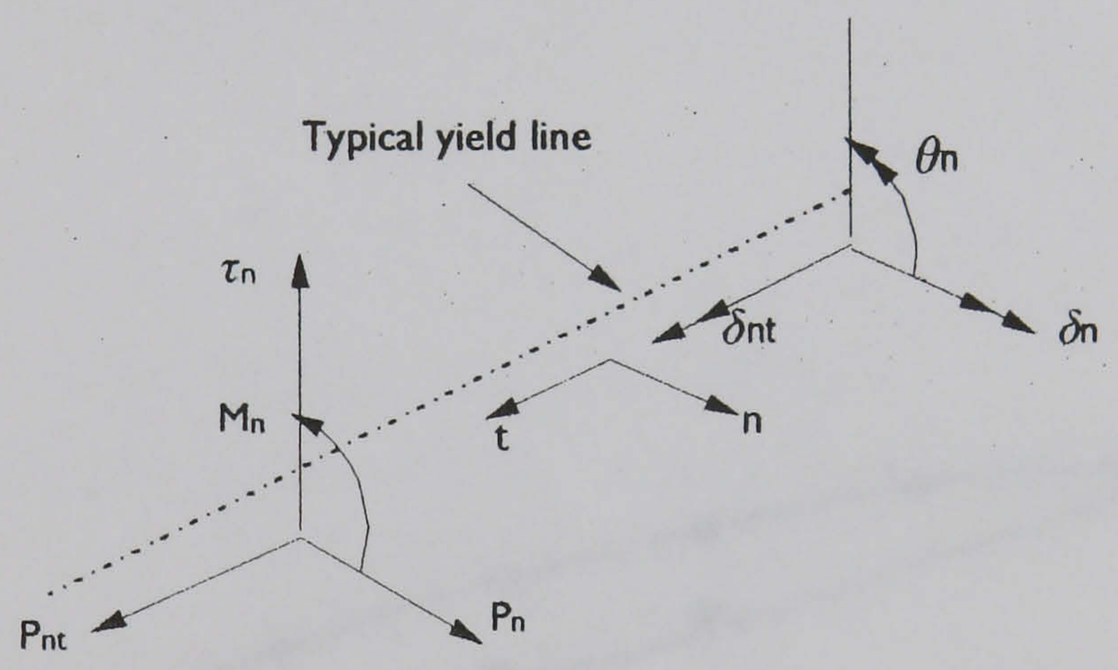

Fig.2.14 b- Displacement rates and stresses resultant on a yield line.

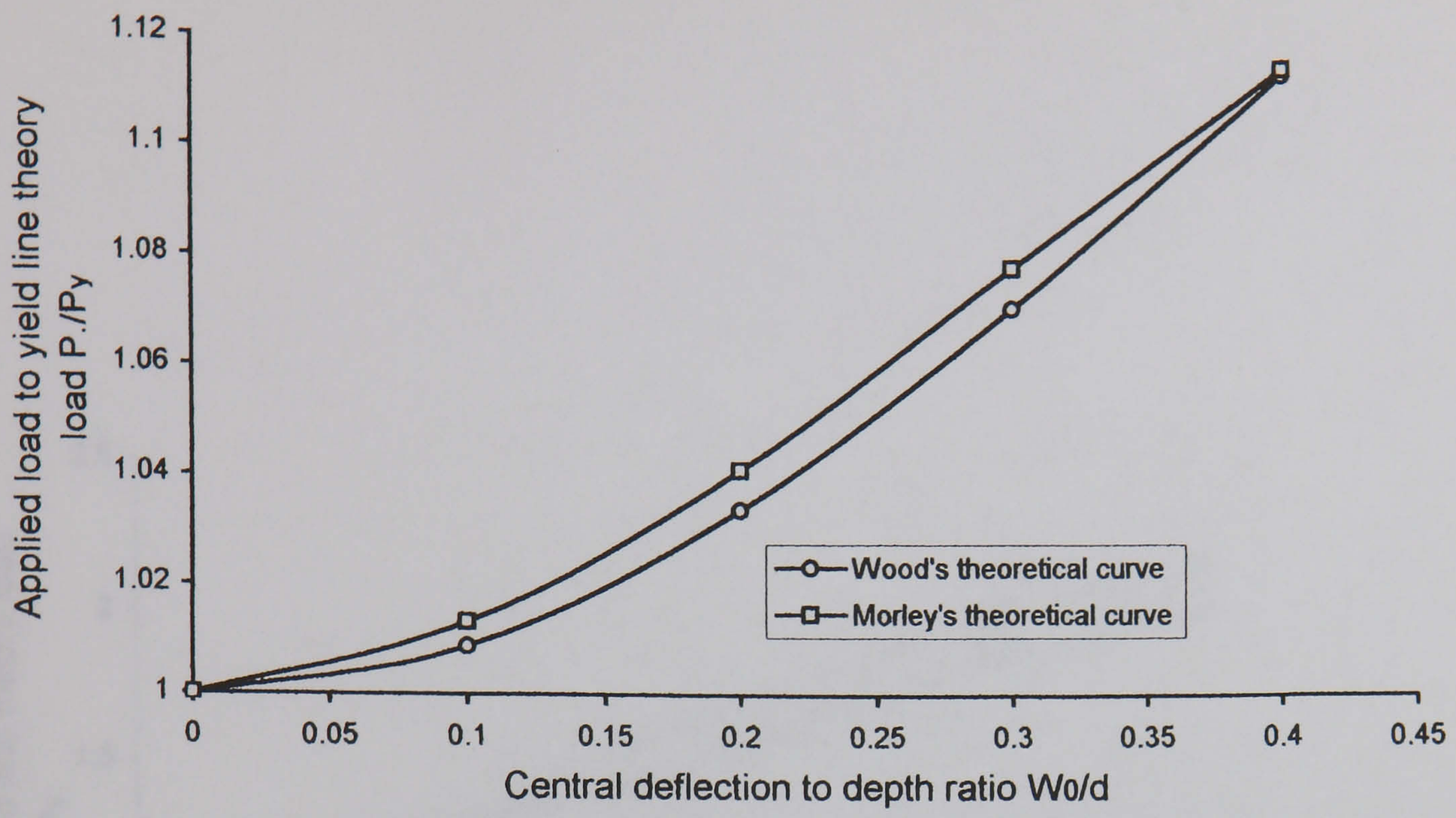

Fig.2.15-Comparison of results for a simply supported circular slab under uniform load [5].

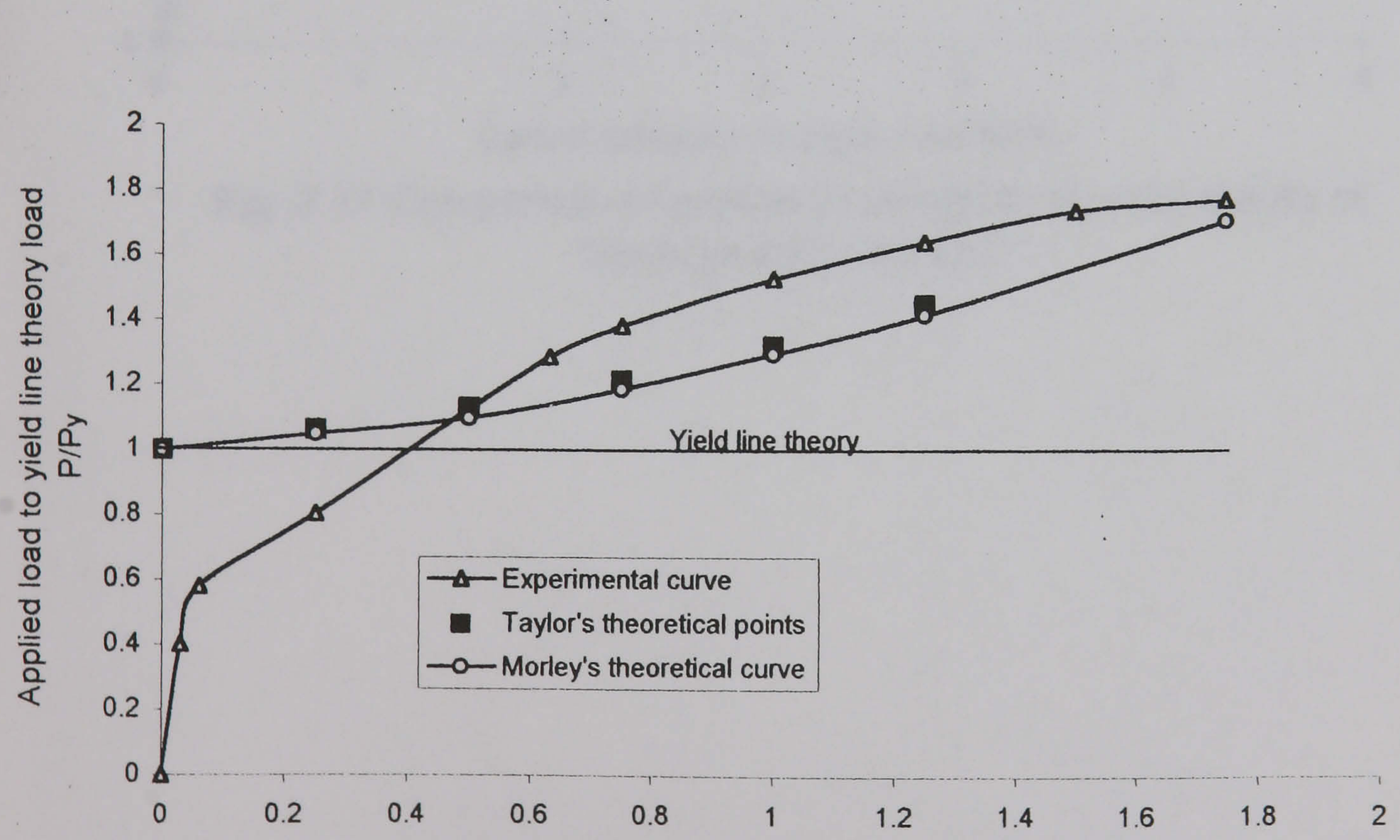

Fig. 2.16-Comparison of the theoretical and experimental results for Maher's Slab [5]

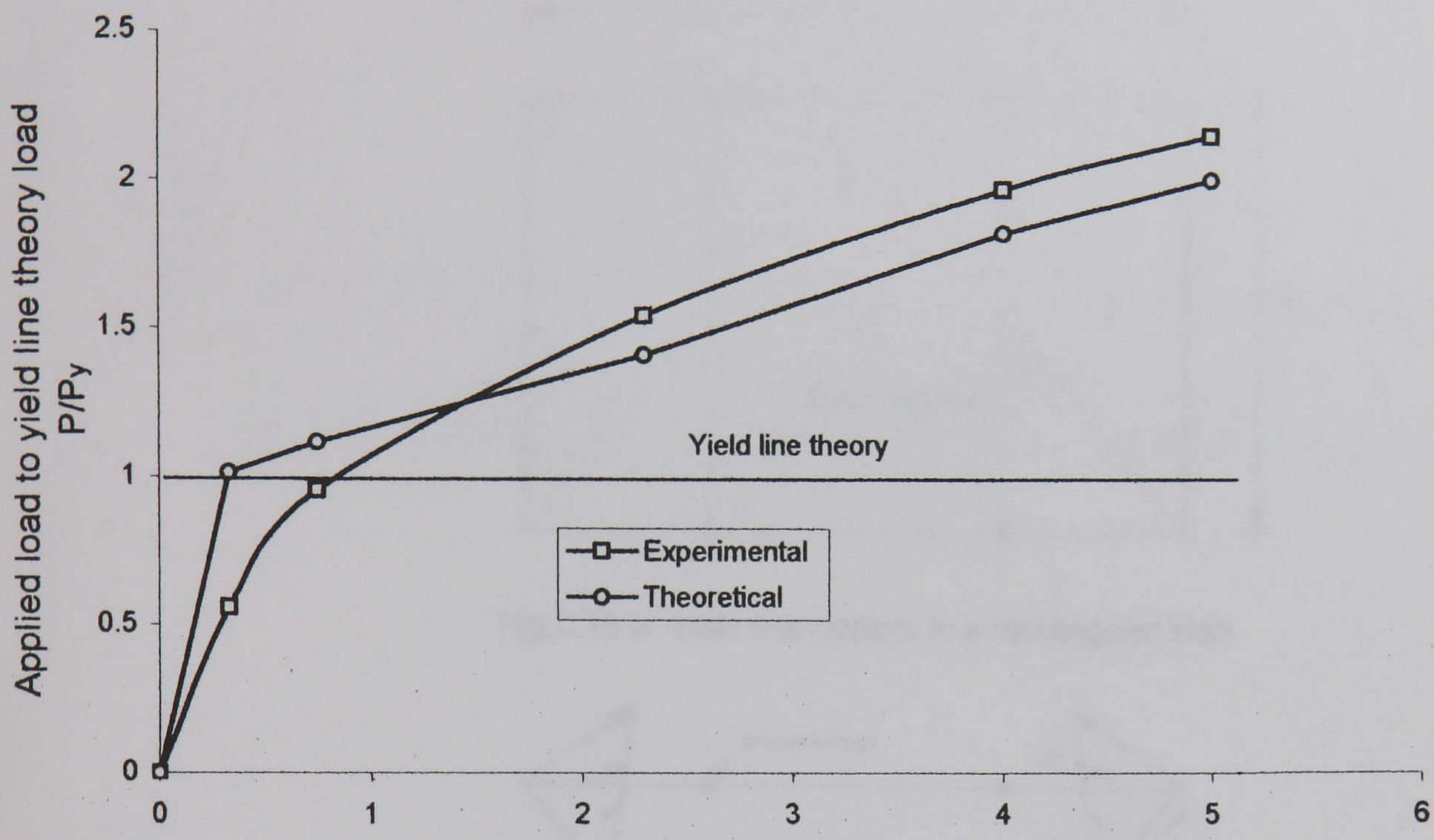

Fig. 2.17-Comparison of experimental and theoretical results of Sawczuk's [6] slab No.I

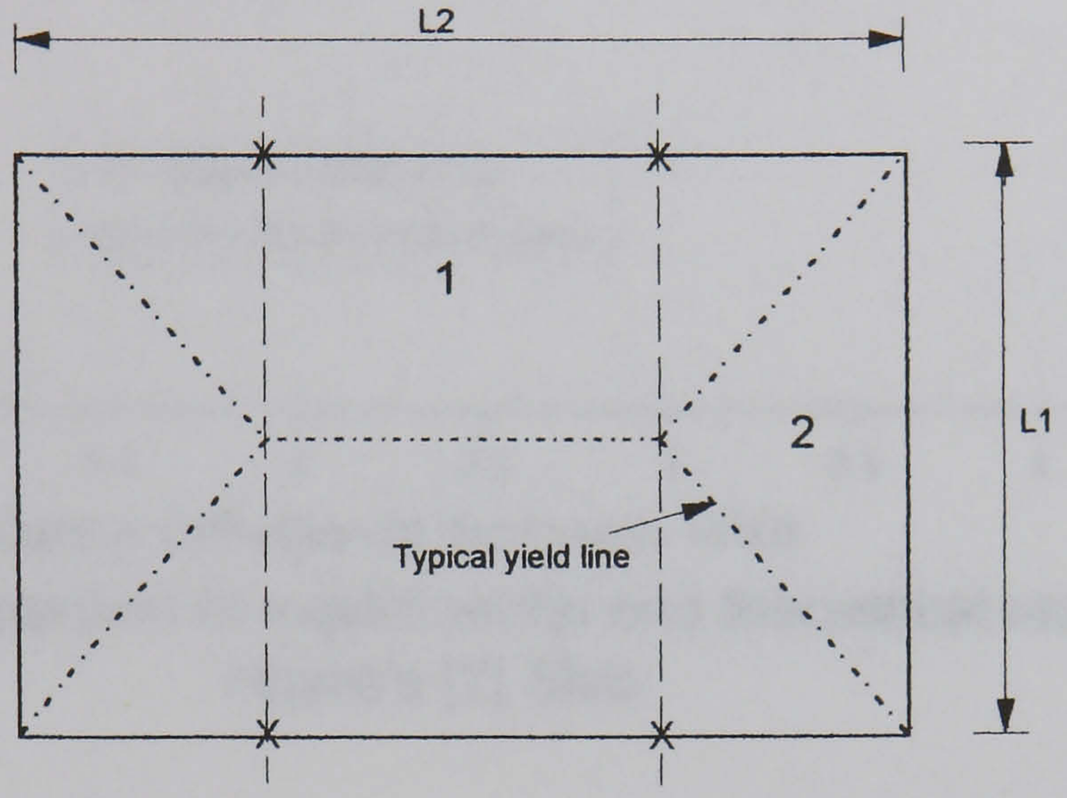

Fig.2.18 a- Yield line pattern in a rectangular slab

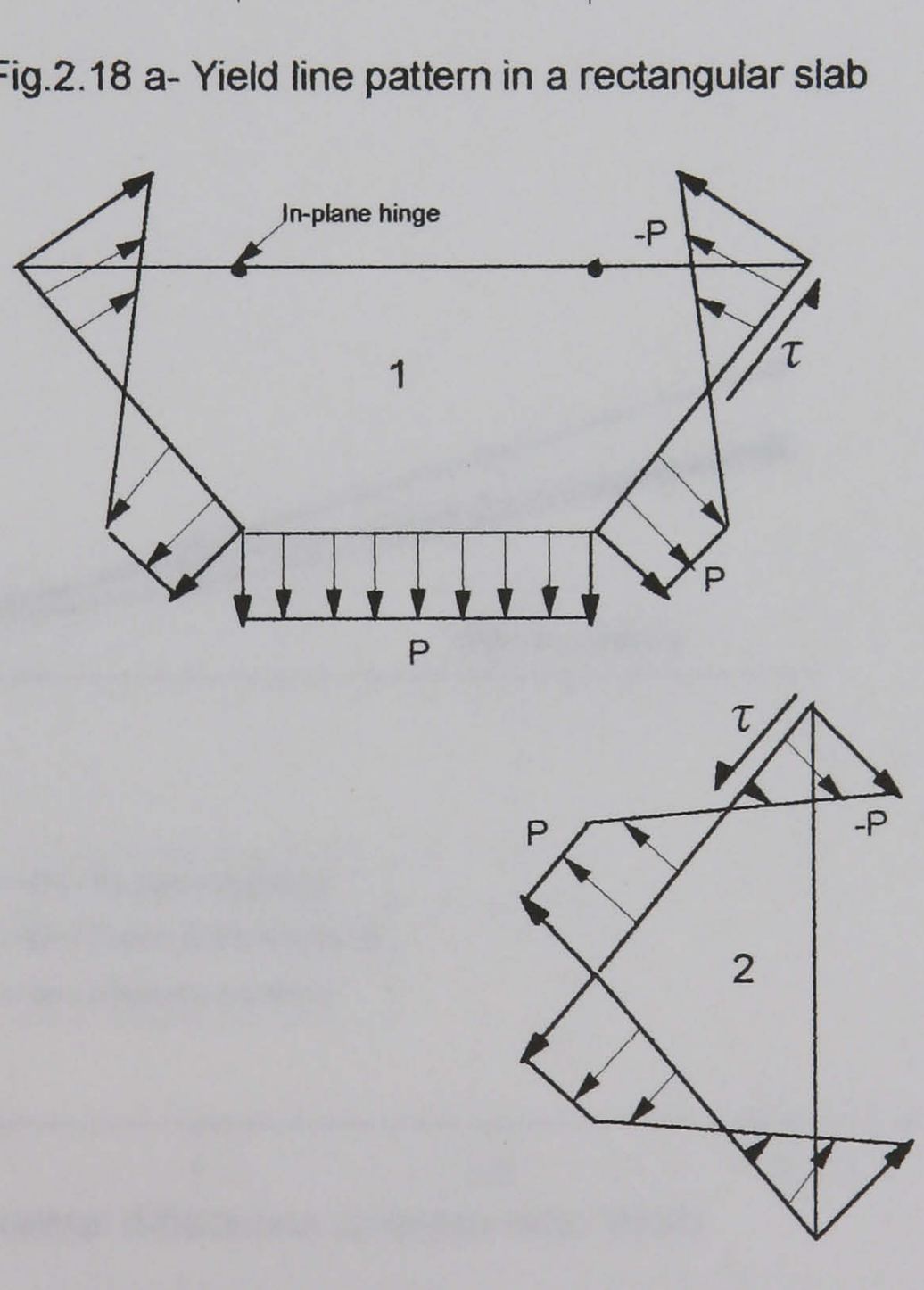

Fig.2.18 b- In-plane stress distribution for the equilibrium method

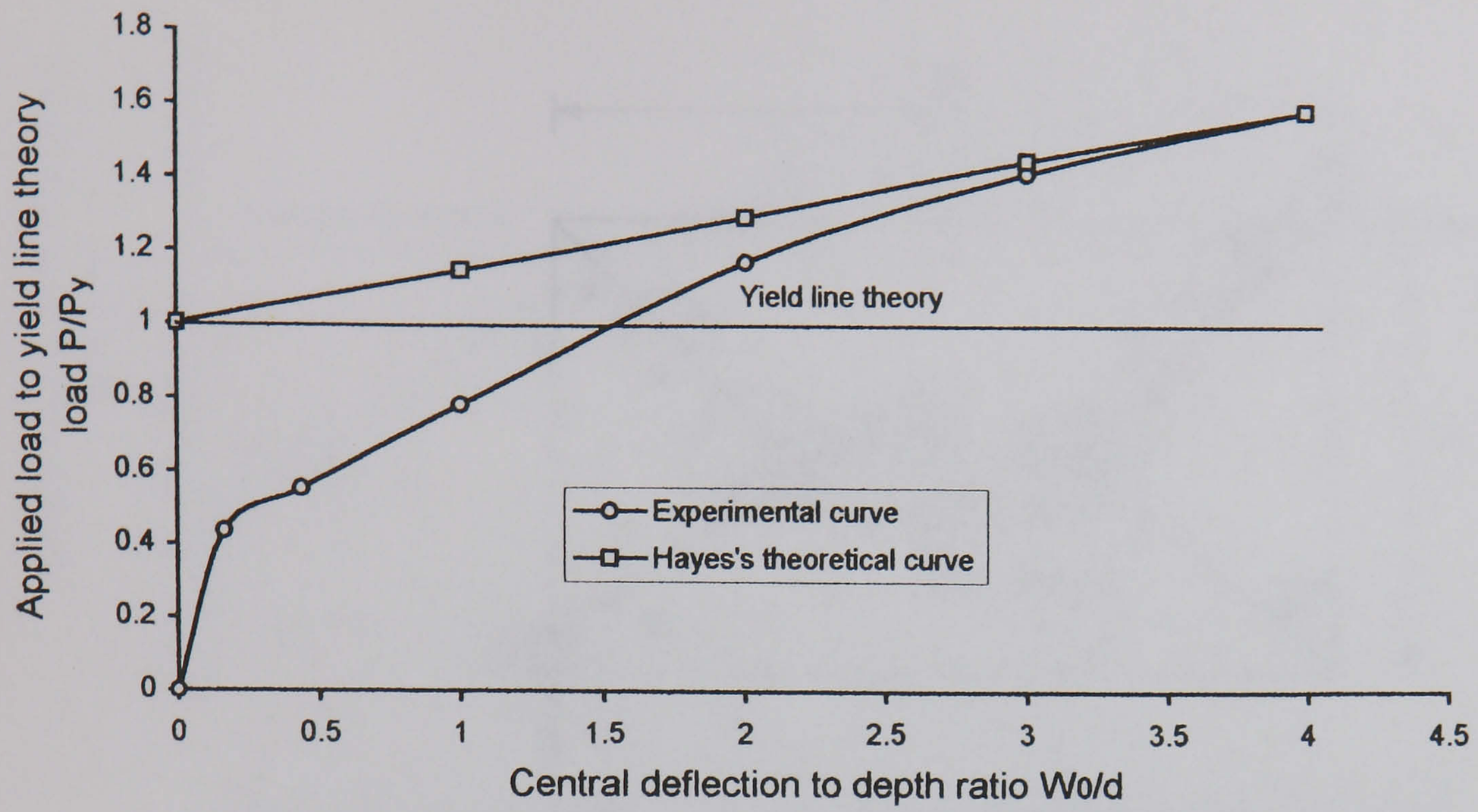

Fig.2.19- Comparison of experimental and theoretical results of Hayes's [7] Slab

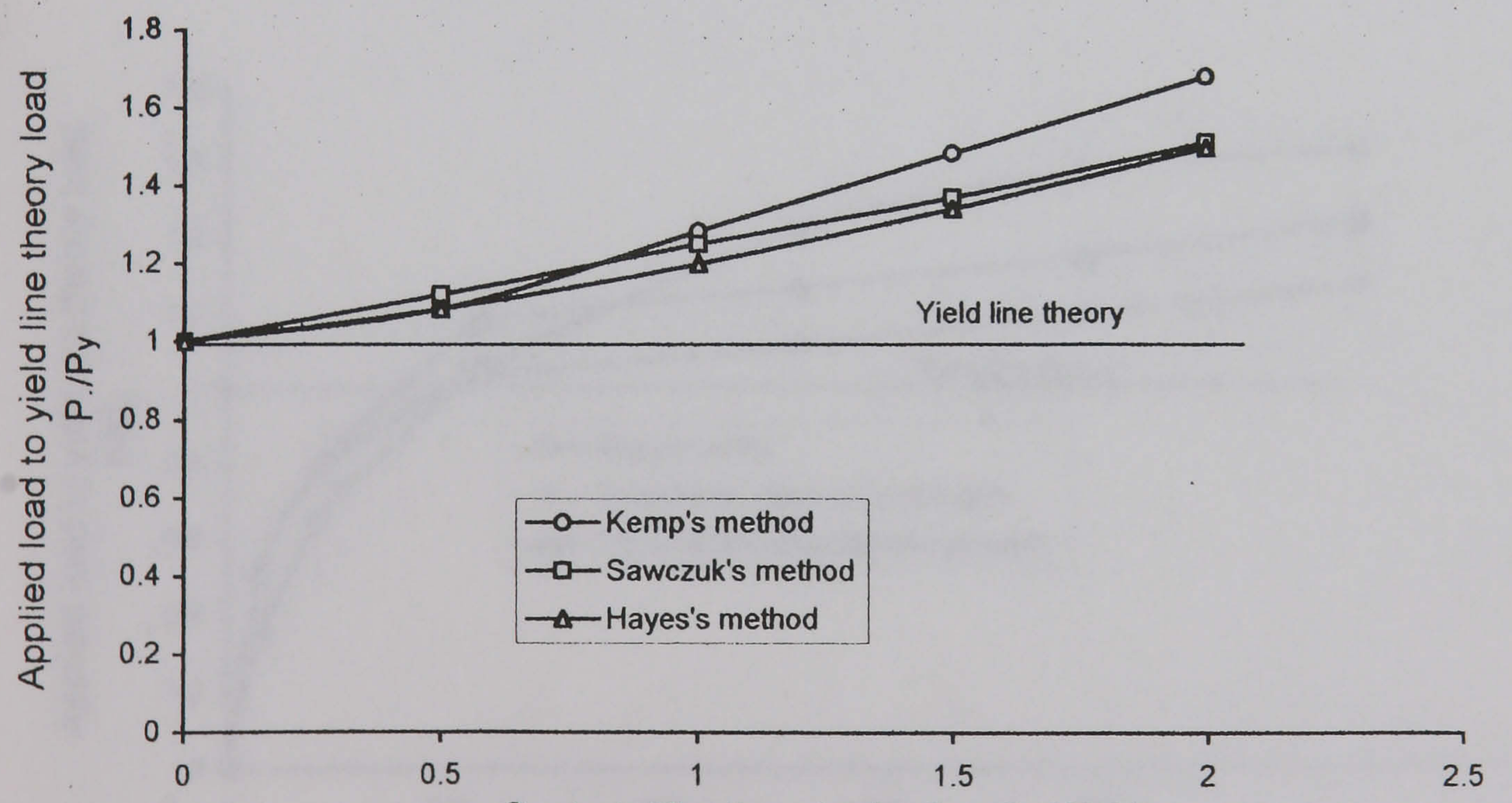

Fig. 2.20-Comparison of analysis for square slab with t= 0.04, [7].

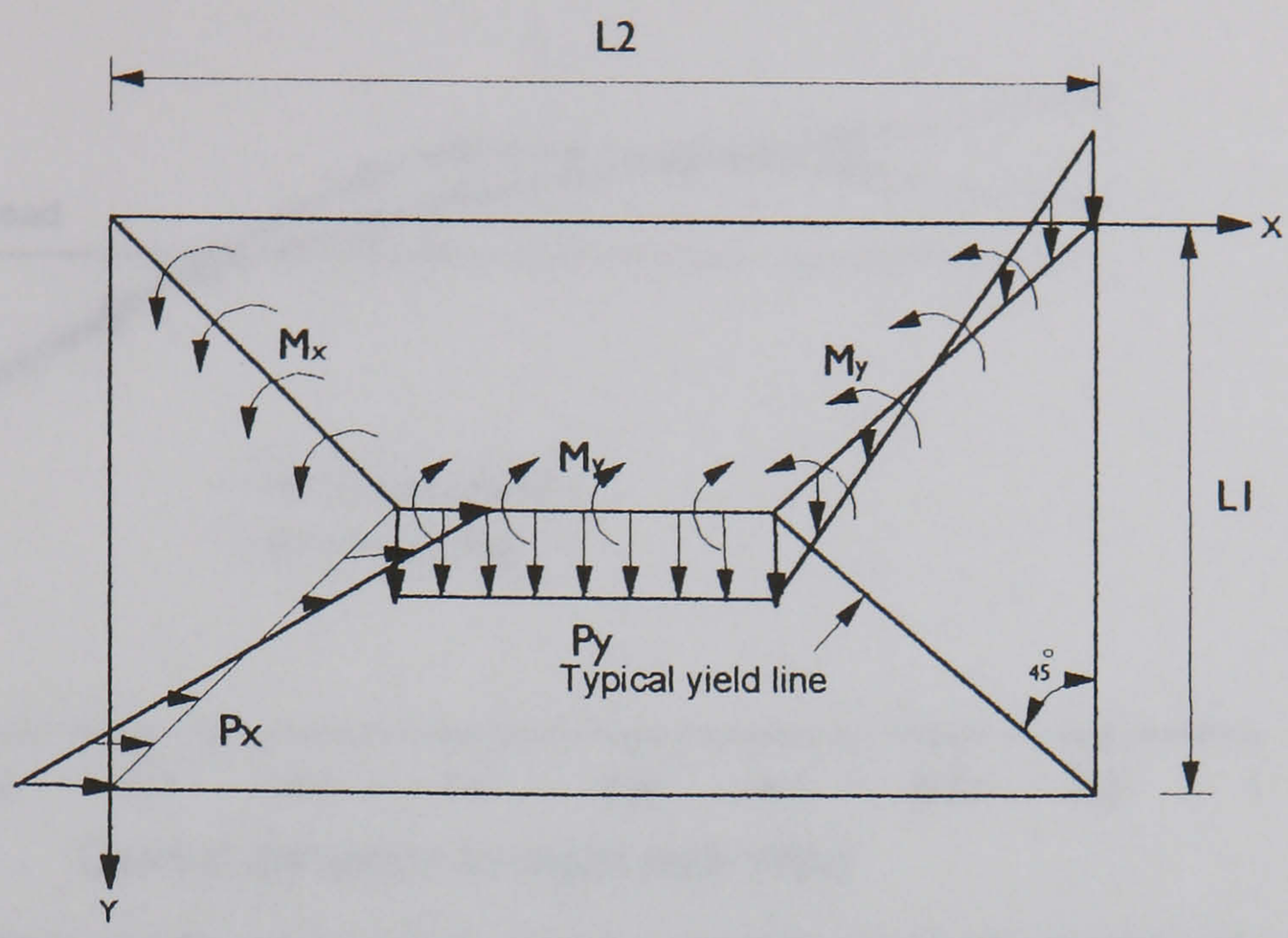

Fig.2.21- Forces and moments on yield lines

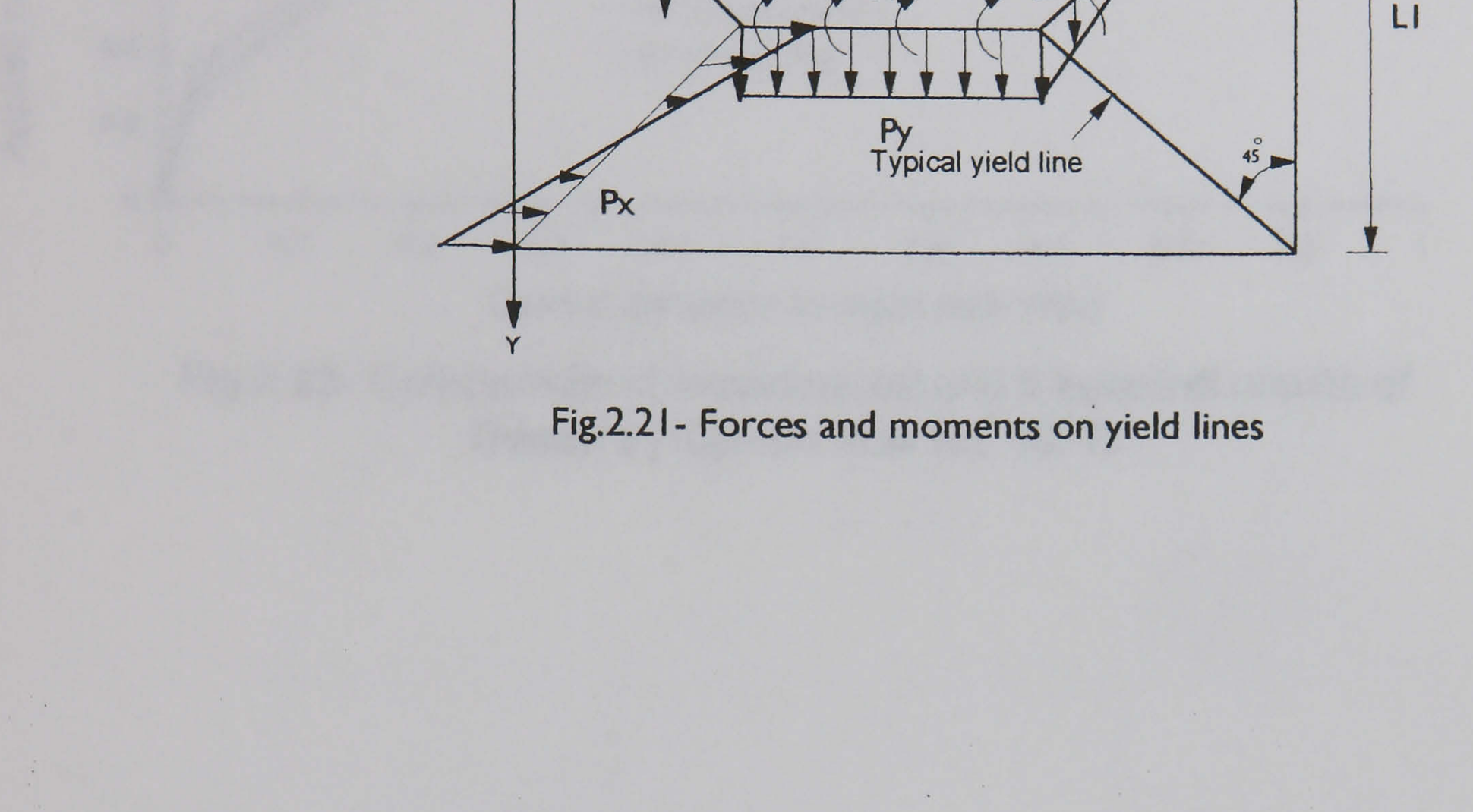

Fig. 2.22- Comparison of experimental and analytical results of Desayi's [8] slab No. T4

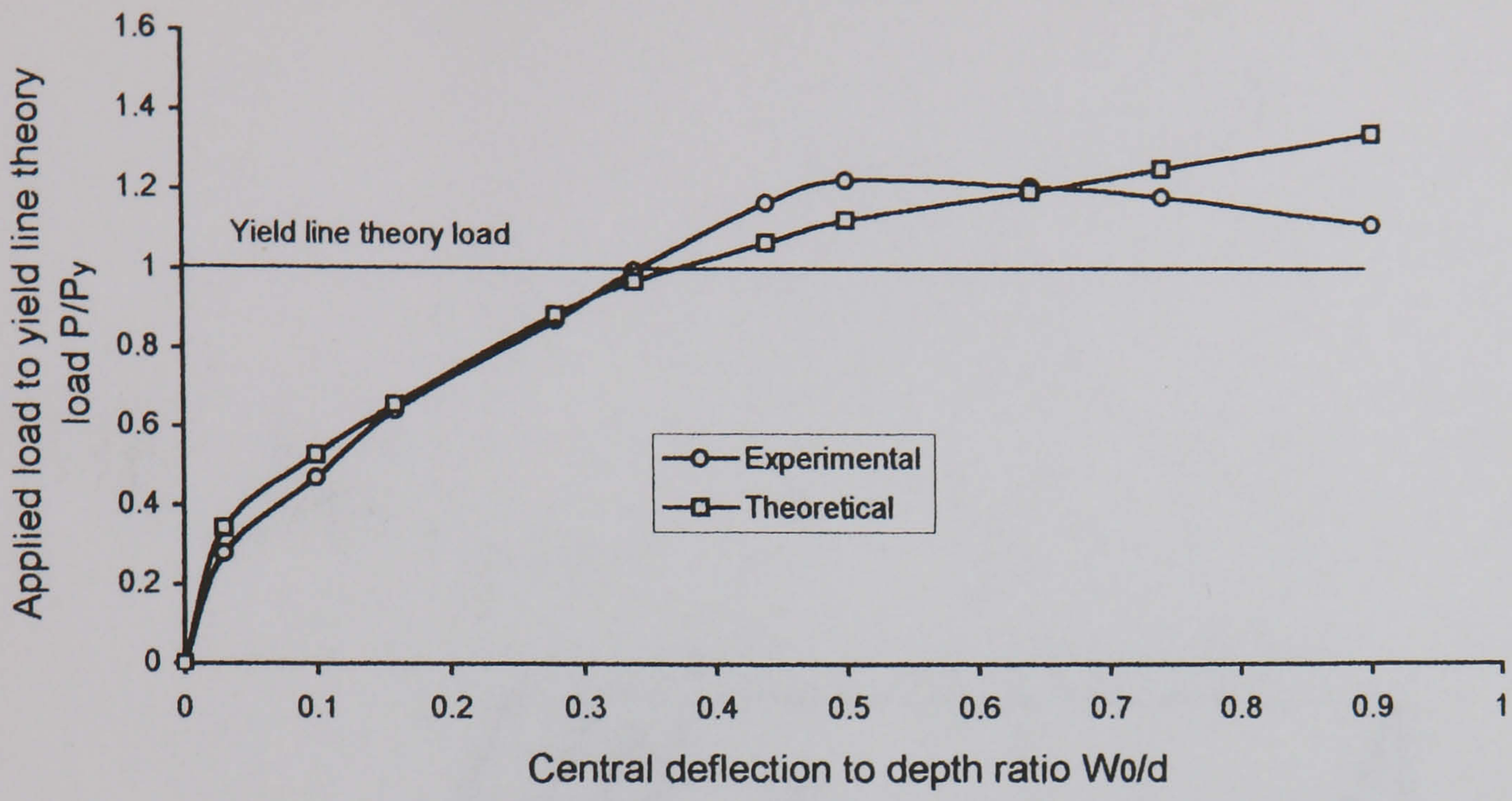

Fig.2.23- Comparison of experimental and theoretical results of Desayi's [10]skew slab No. S2-15

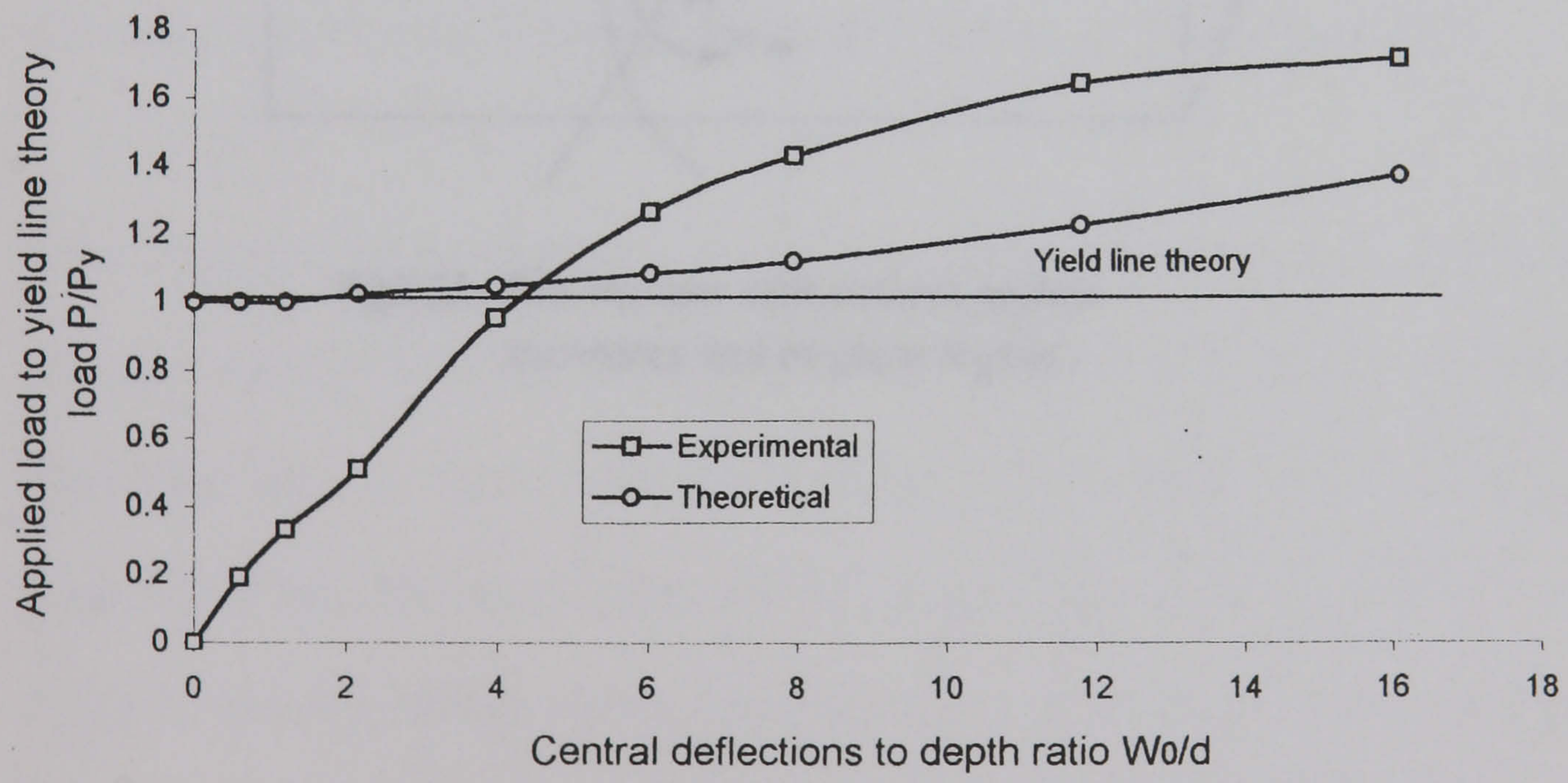

Fig.2.24-Comparision of experimental and theoretical results of Vreeryya's [11] slab No. SL2

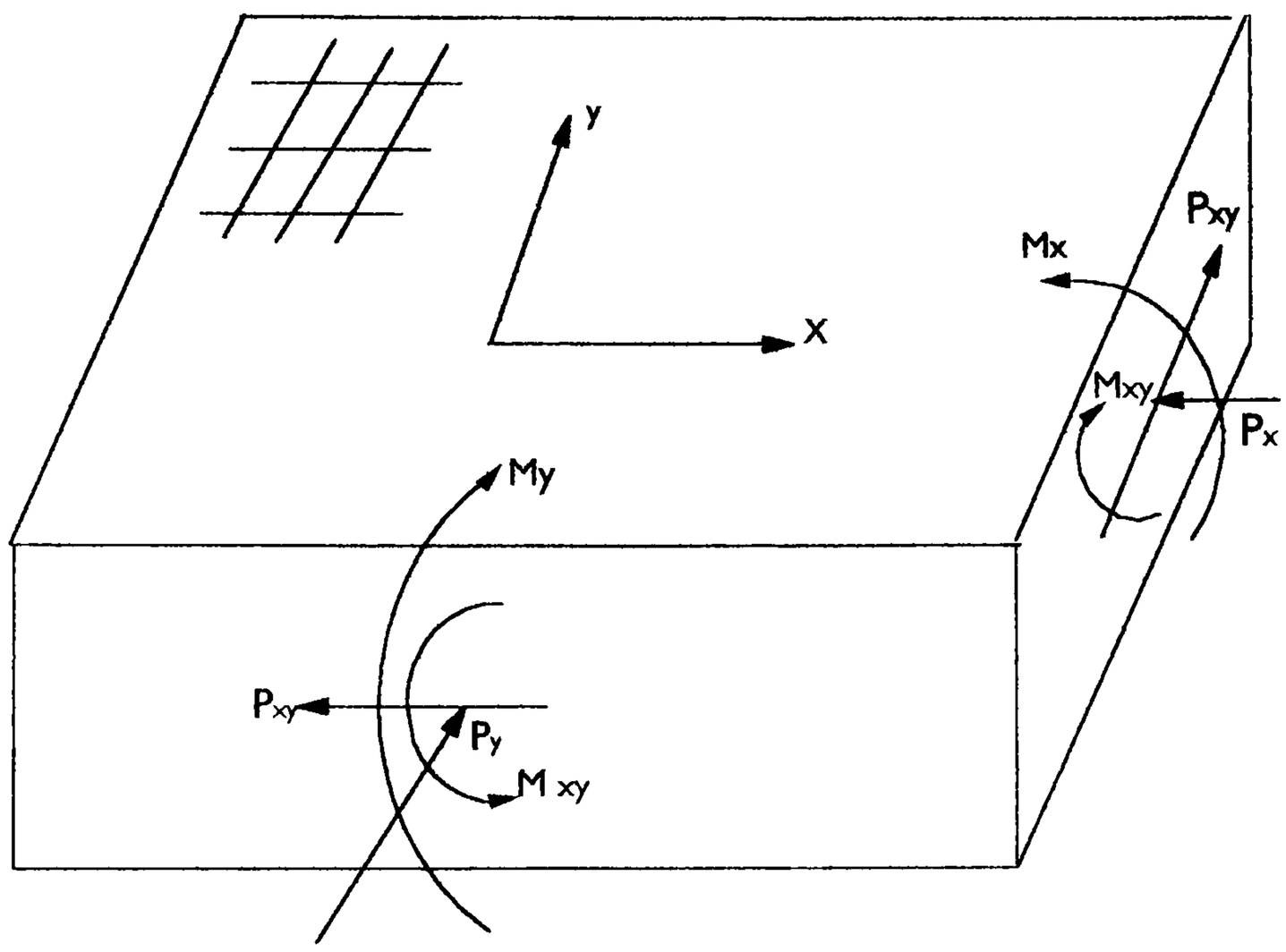

Fig.2.25- Slab element with positive applied moments and in-plane forces

CHAPTER 3

FINITE ELEMENT FORMULATION AND NON-LINEAR SOLUTION TECHNIQUE

3.1 INTRODUCTION

The finite element method has been described extensively in the literature. A comprehensive discussion of the method and its application is given in several texts [1-5] amongst which may be mentioned particularly that of Zienkiewicz [2].

This Chapter deals with the theory of the finite element program used in this study. The program was developed by Ganaba[6] and comprises both geometric and material non-linearities, both the load control and the displacement control can be used to trace the response of the slab up to collapse. The program makes use of some of the standard NAGFE level 0 [15] subroutines. The program has been modified by the author in order to predict a better response for the analysed slabs. The major modification where the inclusion of a new material model, which will be described in detail in Chapter 4.

A brief description of the program is given in this Chapter; a full description can be found in [6].

A brief description of the finite element concepts is given in Section 3.2 and the assumptions that are generally made to derive the equations of plate theory which are used in the finite element formulation will be discussed in section 3.3.

In section 3.4 the various sets of elasticity equations, namely those of strain-displacement, stress-strain and equilibrium equations are presented.

In section 3.5 the use of virtual work to establish the incremental equilibrium equation for use in finite element formulation is discussed and the finite element formulation is presented in section 3.6.

The elements used in the study are presented in section 3.7 and the finite element representation is given in section 3.8.

The stiffness matrices and the numerical evaluation of such matrices are presented in sections 3.9. The numerical integration and the integration rule implemented in this study are presented in section 3.10.

Section 3.11 deals with the solution of the non-linear equation. The convergence tolerance used in this study is presented in Section 3.12. The solution strategy is given in Section 3.13.

3.2 THE FINITE ELEMENT CONCEPT

In the finite element displacement method, a continuum with an infinite number of degrees of freedom is represented by a discrete model, which has a finite number of degrees of freedom. The discrete model is composed of sub-regions, or elements, of finite size which have a simpler geometry than that of the continuum. A finite number of points, or nodes, are identified on the element, where the finite elements are to be joined and conditions of equilibrium and compatibility are to be enforced. Displacement functions within each element are assumed so that the displacements at each point within the element are dependent upon the nodal values. An important aspect of the finite element concept is that an individual element may be considered in isolation from the assemblage of elements. Therefore the displacement functions over the element in terms of the nodal values can be approximated independently of the ultimate location of the element within the discrete model. Thus, it is possible to develop an assemblage of various finite elements in which the nodal values of the assumed local displacement functions are left arbitrary [4,5].

3.3 BASIC ASSUMPTION

The analysis of plates using the finite element displacement method may be formulated using either Kirchhoff [2] or Mindlin [7] plate theory. In the Kirchhoff theory shear deformation is ignored, that is normals to the mid-surface remain normal after deformation. Alternatively, in Mindlin plate theory, which allows for shear deformation,

normals remain straight, but not necessarily normal to the mid-surface after deformation. In both formulations stresses in the direction normal to the plate middle surface are neglected.

In order to determine the displacements u', v' and w' for an arbitrary point p' located at z from the middle surface, Fig. 3.1, the displacements can be expressed in terms of the displacements at the middle surface such that.

$$\begin{aligned} u' &= u - z\theta_x \\ v' &= v - z\theta_y \\ w' &= w \end{aligned} \qquad 3.1$$

where u, v and w are the displacements at the plate middle surface and θ_x and θ_y are the rotations of the normals to the undeformed middle surface in the xz and yz planes respectively. These rotations are given by

$$\begin{aligned} \theta_x &= \frac{\partial w}{\partial x} + \phi_x \\ \theta_y &= \frac{\partial w}{\partial y} + \phi_y \end{aligned} \qquad 3.2$$

where ϕ_x and ϕ_y are the average transverse shear deformations.

3.4 BASIC RELATIONSHIPS

The behaviour of a solid body subjected to external forces is governed by three fundamental equations, namely strain-displacement, stress-strain and equilibrium equations. These relationships will be presented in this section with reference to a Mindlin plate formulation.

3.4.1 STRAIN-DISPLACEMENT RELATIONSHIP

For a Mindlin plate the relevant Green's strain vector $\varepsilon^{'}$ is given by [8] as

$$\left\{\varepsilon^{'}\right\}=\begin{bmatrix}\varepsilon_x^{'}\\ \varepsilon_y^{'}\\ \gamma_{xy}^{'}\\ \gamma_{xz}^{'}\\ \gamma_{yz}^{'}\end{bmatrix}=\begin{bmatrix}\dfrac{\partial u^{'}}{\partial x}+\dfrac{1}{2}\left(\dfrac{\partial u^{'}}{\partial x}\right)^2+\dfrac{1}{2}\left(\dfrac{\partial v^{'}}{\partial x}\right)^2+\dfrac{1}{2}\left(\dfrac{\partial w^{'}}{\partial x}\right)^2\\ \dfrac{\partial v^{'}}{\partial y}+\dfrac{1}{2}\left(\dfrac{\partial u^{'}}{\partial y}\right)^2+\dfrac{1}{2}\left(\dfrac{\partial v^{'}}{\partial y}\right)^2+\dfrac{1}{2}\left(\dfrac{\partial w^{'}}{\partial y}\right)^2\\ \dfrac{\partial u^{'}}{\partial y}+\dfrac{\partial v^{'}}{\partial x}+\dfrac{\partial u^{'}}{\partial x}\dfrac{\partial u^{'}}{\partial y}+\dfrac{\partial v^{'}}{\partial x}\dfrac{\partial v^{'}}{\partial y}+\dfrac{\partial w^{'}}{\partial x}\dfrac{\partial w^{'}}{\partial y}\\ \dfrac{\partial u^{'}}{\partial z}+\dfrac{\partial w^{'}}{\partial x}+\dfrac{\partial u^{'}}{\partial x}\dfrac{\partial u^{'}}{\partial z}+\dfrac{\partial v^{'}}{\partial x}\dfrac{\partial v^{'}}{\partial z}+\dfrac{\partial w^{'}}{\partial x}\dfrac{\partial w^{'}}{\partial z}\\ \dfrac{\partial v^{'}}{\partial z}+\dfrac{\partial w^{'}}{\partial y}+\dfrac{\partial u^{'}}{\partial y}\dfrac{\partial u^{'}}{\partial z}+\dfrac{\partial v^{'}}{\partial y}\dfrac{\partial v^{'}}{\partial z}+\dfrac{\partial w^{'}}{\partial y}\dfrac{\partial w^{'}}{\partial z}\end{bmatrix} \qquad 3.3$$

Introducing the Von Karman assumption [9], implies that derivatives of $u^{'}$ and $v^{'}$ with respect to x, y and z are small therefore multiples of such derivatives can be neglected.

The strain-displacement equation, equation 3.3, can be expressed in terms of the deformations of the plate middle surface, equation 3.1, such that

$$\{\varepsilon\} = \begin{Bmatrix} \varepsilon_x \\ \varepsilon_y \\ \gamma_{xy} \\ \gamma_{xz} \\ \gamma_{yz} \end{Bmatrix} = \begin{Bmatrix} \varepsilon_p^l \\ 0 \end{Bmatrix} + \begin{Bmatrix} z\varepsilon_b^l \\ \varepsilon_s^l \end{Bmatrix} + \begin{Bmatrix} \varepsilon_p^{nl} \\ 0 \end{Bmatrix} \qquad 3.4$$

where the linear in-plane strains are given by

$$\{\varepsilon_p^l\} = \begin{Bmatrix} \dfrac{\partial u}{\partial x} \\ \dfrac{\partial v}{\partial y} \\ \dfrac{\partial u}{\partial y} + \dfrac{\partial v}{\partial x} \end{Bmatrix} \qquad 3.5a$$

the flexural strain is given by

$$\{\varepsilon_b^l\} = \begin{Bmatrix} -\dfrac{\partial \theta_x}{\partial x} \\ -\dfrac{\partial \theta_y}{\partial y} \\ -\dfrac{\partial \theta_x}{\partial y} - \dfrac{\partial \theta_y}{\partial_x} \end{Bmatrix} \qquad 3.5b$$

the linear transverse shear strains are given by

$$\{\varepsilon_s^l\} = \begin{Bmatrix} \dfrac{\partial w}{\partial x} - \theta_x \\ \dfrac{\partial w}{\partial y} - \theta_y \end{Bmatrix} \qquad 3.5c$$

and the non-linear in-plane strains are given by

$$\left\{\varepsilon_p^{nl}\right\}=\begin{Bmatrix}\frac{1}{2}\left(\frac{\partial w}{\partial x}\right)^2\\ \frac{1}{2}\left(\frac{\partial w}{\partial y}\right)^2\\ \frac{\partial w}{\partial x}\frac{\partial w}{\partial y}\end{Bmatrix} \qquad 3.5d$$

3.4.2 STRESS-STRAIN RELATIONSHIP

For a linear elastic isotropic material, Green's strain vector $\{\varepsilon\}$ is related to the Piola-Kirchhoff stress vector $\{\sigma\}$ by the following constitutive relationship:

$$\{\sigma\}=[D]\{\varepsilon\} \qquad 3.6$$

where the Piola-Kirchhoff stress vector $\{\sigma\}$is given by

$$\{\sigma\}=\{\sigma_x \quad \sigma_y \quad \tau_{xy} \quad \tau_{xz} \quad \tau_{yx}\}^T \qquad 3.7a$$

the elastic material matrix $[D]$ is given by:

$$[D]=\frac{E}{(1-\nu^2)}\begin{bmatrix}1 & \nu & 0 & 0 & 0\\ \nu & 1 & 0 & 0 & 0\\ 0 & 0 & \frac{1-\nu}{2} & 0 & 0\\ 0 & 0 & 0 & \frac{1-\nu}{2} & 0\\ 0 & 0 & 0 & 0 & \frac{1-\nu}{2}\end{bmatrix} \qquad 3.7b$$

where E and ν are Young's modulus and Poisson's ratio respectively.

The plate formulation can be reduced to a two-dimensional form by virtue of the Mindlin assumptions that normals to the middle surface remain straight during deformation. The strains can be expressed in terms of the deformations at the plate middle surface and the stresses in terms of their resultants. The stress resultants, $\{\bar{\sigma}\}$, can be obtained by integrating the stress distribution throughout the plate thickness. For an elastic material the integration can be carried out explicitly such that:

$$\{\bar{\sigma}\}=\int_{z_2}^{z_1}\begin{Bmatrix}\sigma_x\\ \sigma_y\\ \tau_{xy}\\ z\sigma_x\\ z\sigma_y\\ z\tau_{xy}\\ \tau_{xz}\\ \tau_{yz}\end{Bmatrix}.dz=\begin{Bmatrix}\bar{\sigma}_p\\ \bar{\sigma}_b\\ \bar{\sigma}_s\end{Bmatrix} \qquad 3.8$$

where z_1 and z_2 are the co-ordinates of the top and bottom of the plate respectively, with the Z-direction being the normal to the plate surface. The stress resultant components acting per unit width of the plate, $\{\bar{\sigma}_p\}$, $\{\bar{\sigma}_b\}$ and $\{\bar{\sigma}_s\}$ are the in-plane forces, moments and transverse shear forces respectively.

The strain vector associated with the stress resultants given in equation 3.8 may be expressed in terms of a linear and a non-linear strain parts such that

$$\{\bar{\varepsilon}\}=\{\bar{\varepsilon}^{l}\}+\{\bar{\varepsilon}^{nl}\}=\begin{Bmatrix}\varepsilon_p^l\\ \varepsilon_b^l\\ \varepsilon_s^l\end{Bmatrix}+\begin{Bmatrix}\varepsilon_p^{nl}\\ 0\\ 0\end{Bmatrix} \qquad 3.9$$

The constitutive relationship, equation 3.6, can be written in terms of the stress resultant vector, equation 3.8, and the associated total strain vector, equation 3.9, such that

$$\{\bar{\sigma}\}=[\bar{D}]\{\bar{\varepsilon}\} \qquad 3.10$$

Rewriting equation 3.10 in terms of stress resultant components the constitutive relationship is given by

$$\begin{Bmatrix}\bar{\sigma}_p\\ \bar{\sigma}_b\\ \bar{\sigma}_s\end{Bmatrix}=\begin{bmatrix}\bar{D}_p & 0 & 0\\ 0 & \bar{D}_b & 0\\ 0 & 0 & \bar{D}_s\end{bmatrix}\left[\begin{Bmatrix}\varepsilon_p^l\\ \varepsilon_b^l\\ \varepsilon_s^l\end{Bmatrix}+\begin{Bmatrix}\varepsilon_p^{nl}\\ 0\\ 0\end{Bmatrix}\right] \qquad 3.11a$$

where the in-plane material matrix $[\bar{D}_p]$ is given by

$$[\bar{D}_p]=\frac{Eh}{(1-\nu^2)}\begin{bmatrix}1 & \nu & 0\\ \nu & 1 & 0\\ 0 & 0 & \frac{1-\nu}{2}\end{bmatrix} \qquad 3.11b$$

the flexural material matrix $[\bar{D}_b]$ is given by

$$[\overline{D}_p]=\frac{Eh^3}{12(1-\nu^2)}\begin{bmatrix}1 & \nu & 0\\ \nu & 1 & 0\\ 0 & 0 & \frac{1-\nu}{2}\end{bmatrix} \qquad 3.11c$$

and the transverse shear material matrix $[\overline{D}_s]$ is given by

$$[\overline{D}_s]=\frac{Ehk}{(1-\nu^2)}\begin{bmatrix}\frac{1-\nu}{2} & 0\\ 0 & \frac{1-\nu}{2}\end{bmatrix} \qquad 3.11d$$

where h is the plate thickness, and k is a transverse shear correction factor which is necessary to account for assumption of constant transverse shear strains.

3.4.3 EQUILIBRIUM EQUATION

The equilibrium equations for a three-dimensional solid body can be written as Timoshenko et al [11].

$$\begin{aligned}\frac{\partial\sigma_x}{\partial x}+\frac{\partial\tau_{xy}}{\partial y}+\frac{\partial\tau_{xz}}{\partial z}&=f_x\\ \frac{\partial\sigma_y}{\partial y}+\frac{\partial\tau_{xy}}{\partial x}+\frac{\partial\tau_{xz}}{\partial z}&=f_y\\ \frac{\partial\sigma_z}{\partial z}+\frac{\partial\tau_{xz}}{\partial x}+\frac{\partial\tau_{yz}}{\partial y}&=f_z\end{aligned} \qquad 3.12$$

where f_x, f_y and f_z are body forces acting per unit volume.

3.5 VIRTUAL WORK EQUATION

The principle of virtual work has been used to determine the governing equilibrium equations for use in the finite element formulation. Symbolically the principle is expressed as

$$dW_{\text{int}} - dW_{ext} = 0 \qquad 3.13$$

The external work can be expressed as the work done in moving the body force f and the surface tractions p through a virtual displacement du, as

$$dW_{ext} = \int_V du^T f \, dV + \int_S du^T p \, ds \qquad 3.14$$

where V is the volume of the body and S is that part of the surface of the body where the external tractions are prescribed. The change in the strain energy, internal work, resulting from a set of virtual strains $d\varepsilon$, corresponding to the virtual displacements is

$$dW_{\text{int}} = \int_V d\varepsilon^T \sigma \, dv \qquad 3.15$$

and by making use of equation 3.14 and 3.15 equation 3.13 may be expressed as

$$\int_V d\varepsilon^T \sigma \, dV - \int_V du^T f \, dV - \int_S du^T p \, ds = 0 \qquad 3.16$$

where $d\varepsilon$ is the virtual Green's strain vector because of the virtual displacement field du given in equation 3.3, and σ and f are the stresses and body forces respectively given in equations 3.7 and 3.12. Equation 3.16 satisfies the equilibrium and compatibility conditions but no assumptions have been made about the material

properties and the size of the deformations. Therefore it can be used for solution of problems involving geometric and material non-linearities.

The virtual work equation, equation 3.16, can be expressed in terms of "mid-plane" quantities in terms of the stress resultants obtained by integrating the stress distribution through the plate thickness and the associated strains such that

$$\int_A d\bar{\varepsilon}^T \bar{\sigma}\, dA - \int_A du^T \bar{f}\, dA - \int_S d\bar{u}^T p\, ds = 0 \qquad 3.17$$

where $d\bar{\varepsilon}$ is the virtual strain vector because of the virtual displacement at the plate middle surface du given in equation 3.9, $\bar{\sigma}$ is the stress resultant given in equation 3.8 and $\bar{f}$ is the body forces resultant per unit area.

Section 3.6 will show how equation 3.17 is used to obtain an incremental finite element formulation.

3.6 FINITE ELEMENT FORMULATION

In finite element analysis, the general body is approximated as an assemblage of an arbitrary number of finite elements, n, with the elements being interconnected at nodal points on the element boundaries. In the displacement formulation for the finite element, e, the displacement field u^e is expressed in terms of the nodal value δ^e and a set of interpolation functions N such that,

$$u^e = N\,\delta^e \qquad 3.18$$

Strains are related to the nodal values by the following relations

$$\varepsilon^e = L.u^e \qquad 3.19a$$

$$\varepsilon^e = B.\delta^e \qquad 3.19b$$

where L is a differential matrix operator and B is a strain-displacement matrix.

The virtual work equation 3.17 contains the variation of the strain vector $d\bar{\varepsilon}^e$ resulting from the virtual displacement du^e. The variation of the displacement field, equation 3.18 is given by

$$du^e = N.d\delta^e \qquad 3.20$$

The variation of the strain vector, equation 3.9, can be expressed in terms of the linear and non-linear components such that

$$d\bar{\varepsilon}^e = d\bar{\varepsilon}^{e\,l} + d\bar{\varepsilon}^{e\,nl} \qquad 3.21$$

The variation of the strain vector, equation 3.21, may be written in terms of the variation of the nodal displacements δ such that

$$d\overline{\varepsilon^e} = [B_l + B_{nl}].d\delta^e \qquad 3.22$$

where B_l and B_{nl} are linear and non-linear strain-displacement matrices.

In the application of the finite element method to non-linear problems, equilibrium is established by calculating the internal resistance forces in the structure resulting from the deformation and comparing these forces with the externally applied loads. When the difference, which can be considered as unbalanced forces, is within an acceptable tolerance, equilibrium is assumed to have occurred. The equilibrium equation for internal and external forces can be obtained by substituting equations 3.20 and 3.21 into the virtual work equation, equation 3.17, such that

$$\psi(\delta) = F - P \qquad 3.23$$

where the internal force vector F is given by

$$F = \sum_n \int_{A^e} [B_l + B_{nl}]^T \{\overline{\sigma}\} dA^e \qquad 3.24a$$

the applied load vector P is given by

$$P = \sum_n \int_{A^e} N^T \overline{f}\, dA^e + \int_S N^T p\, ds \qquad 3.24b$$

where $\psi(\delta)$ is the unbalanced force and $\sum_n$ and A^e denotes the summations over all elements and the area of an element respectively.

Taking variations of equation 3.23 with respect to the nodal displacements δ, the tangent stiffness matrix can be obtained such that

$$\frac{d\psi}{d\delta} = K_T \qquad 3.25$$

where K_T is the tangent stiffness matrix and is given by [2,8].

$$K_T = K_0 + K_\sigma + K_L \qquad 3.26$$

where K_0 represents the usual, small displacement stiffness matrix and given by

$$[K_0] = \sum_n \int_{A^e} [B_l]^T \left[\overline{D}\right][B_l] dA^e \qquad 3.27a$$

K_σ is the geometric stiffness matrix which depends on the stress level and is given by

$$[K_\sigma] d\delta = \sum_n \int_{A^e} d[B_{nl}]^T \left\{\overline{\sigma}\right\} dA^e \qquad 3.27b$$

K_L ,is the large displacement matrix which depends on the current displacements and is given by

$$[K_L]=\sum_n\left[\int_{A^e}[B_l]^T[\overline{D}][B_{nl}]dA^e+\int_{A^e}[B_{nl}]^T[\overline{D}][B_l]dA^e+\int_{A^e}[B_{nl}]^T[\overline{D}][B_{nl}]dA^e\right] \quad 3.27c$$

3.7 ELEMENTS USED IN THE STUDY

The flat shell element has been used throughout the present study. The element comprises two elements. The first one is the Heterosis plate bending element and the second one is the 8-node membrane element.

The Heterosis element is a 9-node quadrilateral with 8-nodes lying on the element boundary, Fig. 3.2, which have w,θ_x and θ_y degrees of freedom and a node at the mid point which has θ_x and θ_y only. The element employs serendipity shape functions for the lateral displacement w, and Lagrangian shape functions for the rotations θ_x and θ_y. The Heterosis element, the local numbering system and the local co-ordinates of the element are shown in Fig. 3.2.

The isoparametric membrane element with 8-nodes lying on the element boundary which have u and v degree of freedom Fig. 3.3. The element employs the serendipity shape functions to represent the in-plane displacement fields u and v. The element, the local numbering system and the local co-ordinates are shown in Fig. 3.3.

3.7.1 SHAPE FUNCTIONS

For an element, the natural local co-ordinate system (ξ,η) is usually used to express the displacement components. The origin of the local co-ordinate system is the centre of the element Figs. 3.2-3.3.

The serendipity shape functions $N_i(\xi,\eta)$ for node i in terms of the local co-ordinates ξ,η are:

For the corner nodes $i = 1,3,5,7$

$$N_i(\xi,\eta)=\frac{1}{4}(1+\xi\xi_i)(1+\eta\eta_i)(\xi\xi_i+\eta\eta_i-1) \qquad 3.28$$

for the mid-side nodes $i = 4,8$

$$N_i(\xi,\eta)=\frac{1}{2}(1-\xi^2)(1+\eta\eta_i) \qquad 3.29$$

for the mid-side nodes $i = 2,6$

$$N_i(\xi,\eta)=\frac{1}{2}(1-\eta^2)(1+\xi\xi_i) \qquad 3.30$$

The Lagrangian shape functions $P_i(\xi,\eta)$ for node i in terms of the local co-ordinates ξ,η are:

For nodes $i = 1,2,3$

$$P_i(\xi,\eta)=\overline{N}_1(\xi).\overline{N}_j(\eta) \qquad j=1,2,3 \qquad 3.31$$

for nodes $i=4,8,9$

$$P_i(\xi,\eta)=\overline{N}_2(\xi).\overline{N}_j(\eta) \qquad j=3,1,2 \qquad 3.32$$

for nodes $i=5,6,7$

$$P_i(\xi,\eta)=\overline{N}_3(\xi).\overline{N}_j(\eta) \qquad j=3,2,1 \qquad 3.33$$

where

$$\begin{aligned}\overline{N}_1(\xi)&=\xi(\xi-1)/2\\ \overline{N}_2(\xi)&=(1+\xi)(1-\xi)\\ \overline{N}_3(\xi)&=\xi(\xi+1)/2\end{aligned} \qquad 3.34$$

3.8 FINITE ELEMENT REPRESENTATION

The displacement field within an element is assumed to be functions of discrete nodal values and the shape functions. The in-plane displacement components u and v are approximated by

$$\begin{Bmatrix} u \\ v \end{Bmatrix} = \sum_{i=1}^{8} N_i \begin{Bmatrix} u_i \\ v_i \end{Bmatrix} \qquad 3.35$$

where N_i are the serendipity shape functions.

The lateral displacement w and the rotations θ_x and θ_y are approximated by

$$w = \sum_{i=1}^{8} N_i \, w_i \qquad 3.36a$$

$$\begin{Bmatrix} \theta_x \\ \theta_y \end{Bmatrix} = \sum_{i=1}^{9} P_i \begin{Bmatrix} \theta_{xi} \\ \theta_{yi} \end{Bmatrix} \qquad 3.36b$$

where P_i are Lagrangian shape functions.

3.9 STIFFNESS MATRICES

The stiffness matrices used in the various analyses to be carried out will be formulated in this section using the finite element approximation given in equations 3.35 and 3.36.

The small displacement stiffness matrix k_0, equation 3.27a, is given by

$$k_0 = \sum_n \left[\int_{A^e} \begin{bmatrix} B_p^T \, \overline{D}_p \, B_p & 0 \\ 0 & B_b^T \, \overline{D}_b \, B_b \end{bmatrix} dA^e + \int_{A^e} \begin{bmatrix} 0 & 0 \\ 0 & B_s^T \, \overline{D}_s \, B_s \end{bmatrix} dA^e \right] \qquad 3.37$$

where the first term of equation 3.37 is the in-plane and flexural parts and the second term is the transverse shear part. The in-plane strain displacement matrix $\lfloor B_p \rfloor$ is given by

$$[B_p]=\begin{bmatrix} \frac{\partial N_i}{\partial x} & 0 \\ 0 & \frac{\partial N_i}{\partial y} \\ \frac{\partial N_i}{\partial y} & \frac{\partial N_i}{\partial x} \end{bmatrix} \qquad 3.38a$$

the flexural strain-displacement matrix $[B_b]$ is given by

$$[B_b]=\begin{bmatrix} 0 & -\frac{\partial P_i}{\partial x} & 0 \\ 0 & 0 & -\frac{\partial P_i}{\partial y} \\ 0 & -\frac{\partial P_i}{\partial y} & -\frac{\partial P_i}{\partial x} \end{bmatrix} \qquad 3.38b$$

and the transverse shear strain-displacement matrix $[B_s]$ is given by

$$[B_s]=\begin{bmatrix} \frac{\partial N_i}{\partial x} & -P_i & 0 \\ \frac{\partial N_i}{\partial y} & 0 & -P_i \end{bmatrix} \qquad 3.38c$$

If the length of the mid-surface of the plate is assumed to remain constant, equation 3.37 can be expressed by

$$[k_0]=\sum_n\left[\int_{A^e} B_b^T\,\overline{D}_b\,B_b\,dA^e+\int_{A_e} B_s^T\,\overline{D}_s\,B_s\,dA^e\right] \qquad 3.39$$

The geometric stiffness matrix $[k_\sigma]$, equation 2.27b, can be expressed in terms of a flexural and a transverse shear parts such that [12,13].

$$[k_\sigma]=\sum_n\left[\int_{A_e} G_b^T\,\hat{\sigma}\,G_b\,.t\,dA_e+\int_{A_e} G_s^T\,\hat{\sigma}\,G_s\,\frac{h^3}{12}dA_e\right] \qquad 3.40$$

in which

$$[G_b]=\begin{bmatrix}0 & 0 & \dfrac{\partial N_i}{\partial x} & 0 & 0\\ 0 & 0 & \dfrac{\partial N_i}{\partial y} & 0 & 0\end{bmatrix} \qquad 3.41a$$

$$[G_s]=\begin{bmatrix}0 & 0 & 0 & \dfrac{\partial N_i}{\partial x} & \dfrac{\partial N_i}{\partial x}\\ 0 & 0 & 0 & \dfrac{\partial N_i}{\partial y} & \dfrac{\partial N_i}{\partial y}\end{bmatrix} \qquad 3.41b$$

$$[\hat{\sigma}]=\begin{bmatrix}\sigma_x & \tau_{xy}\\ \tau_{xy} & \sigma_y\end{bmatrix} \qquad 3.41c$$

where h is the plate thickness.

The large displacement stiffness matrix $[K_L]$, equation 2.27c, is given by

$$[K_L]=\sum_{ele}\int_{A_e}\begin{bmatrix} 0 & B_p^T\,\overline{D}_p\,B_{nl} \\ B_{nl}^T\,\overline{D}_p\,B_p^T & B_{nl}^T\,\overline{D}_p\,B_{nl}\end{bmatrix}dA_e \qquad 3.42$$

where the non-linear strain-displacement matrix $[B_{nl}]$ is a function of the lateral displacement w and is given by

$$[B_{nl}]=\begin{bmatrix} \frac{\partial w}{\partial x} & 0 \\ 0 & \frac{\partial w}{\partial y} \\ \frac{\partial w}{\partial y} & \frac{\partial w}{\partial x}\end{bmatrix}\begin{bmatrix} \frac{\partial N_i}{\partial x} & 0 & 0 \\ \frac{\partial N_i}{\partial y} & 0 & 0\end{bmatrix} \qquad 3.43$$

The total stiffness matrix for in-plane behaviour of a plate loaded in its plane is given by

$$[K_p]=\sum_{ele}\int_{A_e}B_p^T\,\overline{D}_p\,B_p\,dA_e \qquad 3.44$$

3.10 EVALUATION OF THE STIFFNESS MATRICES

In general it is not possible to perform analytically the integration required to set up the stiffness matrices and the equivalent nodal loads for the elements used. Therefore, resort has to be made to some suitable scheme of numerical integration.

In the layered approach, the plate thickness is divided into a finite number of layers parallel to the middle plane of the plate or by the introduction of numerical integration

points through the thickness. The stress resultants, the in-plane forces and moments, are determined by integrating the stress at the various layers or sampling points through the thickness. The function to be integrated is replaced by the sum of a series such that

$$\int_a^b f(x)dx = \sum_{i=1}^{n} W_i \, f_i \qquad 3.45$$

where W_i are the weights, n is the number of the sampling points and f_i is $f(x)$ evaluated at the ith sampling points.

In this study, the various stiffness matrices have been evaluated numerically with a selective integration scheme using Gauss quadrature. The 3x3 rule for the in-plane and flexural components and the 2x2 rule for the transverse shear components have been used Fig. 3.4. The derivative of the shape function is determined at the Gauss quadrature points in the local co-ordinate system (ξ, η). The inverse of the Jacobian matrix is used to convert the derivative from the local co-ordinate system to the global co-ordinate system (x, y), such that

$$\begin{bmatrix} \frac{\partial N}{\partial x} \\ \frac{\partial N}{\partial y} \end{bmatrix} = [J]^{-1} \begin{bmatrix} \frac{\partial N}{\partial \xi} \\ \frac{\partial N}{\partial \eta} \end{bmatrix} \qquad 3.46$$

The integration is carried out in the local co-ordinate system using the following transformation

$$\int\int f(x,y)dx\,dy = \sum_{i=1}^{m} f(\xi,\eta)|J|.w_i \qquad 3.47$$

where m is the number of Gauss points and w_i is the weight at ith Gauss point and $|J|$ is the determinate of the Jacobian matrix.

The Labatto rule has been used in this work for the determination of the in-plane and flexural stresses resultants through the depth. The abscissas and weights for the Labatto rule are listed in Table 3.1. Further details about the Labatto integration rule can be found in [14].

3.11 SOLUTION OF THE NON-LINEAR EQUATION

Most non-linear solution methods are based on the assumption that the non-linear response can be approximated by a series of linear solutions. The equilibrium equation for internal and external forces, equation 3.23 can be rewritten as

$$\{\psi(\delta)\}^n = \{F\}^n - \{P\}^n \qquad 3.48$$

where ψ is the out of balance or residual force vector, δ is the vector of the nodal displacement, F is the internal force vector and P is the applied load vector.

Solution of the governing equations, equation 3.48, can be carried out using either incremental or iterative methods of solutions.

3.11.1 INCREMENTAL METHODS

In these methods, the solution of equation 3.48, is usually carried out by applying the external loads as a sequence of sufficiently small increments, so that the structure can be assumed to respond linearly within each increment. This method can lead to deviation from the true response, Fig. 3.5.

More efficient incremental schemes can be obtained by combining the pure incremental method with a single equilibrium correction. A better approximation of the true response can be obtained using this technique, Fig.3.6.

The accuracy of the solution using either the pure incremental or the corrected incremental methods depends on the size of the load increment. The increments need to be small enough in order to obtain a good approximation of the true response since the accumulating errors are carried from one increment to the next throughout the solution process.

3.11.2 ITERATIVE METHODS

In this method the load is applied incrementally and a series of iterations is carried out within each increment to eliminate the cumulative errors inherent in the previous method.

If an approximate solution to $(\delta)^n$, to equation 3.48 is reached, an improved solution can be achieved using a truncated Taylor series of the form

$$\{\psi(\delta)\}_{i+1}^n = \{\psi(\delta)\}_i^n + \frac{d\psi}{d\delta}]_{\delta_i^n} \{\Delta\delta\}_i^n \qquad 3.49$$

where

$$\frac{d\psi}{d\delta}]_{\delta_i^n} = [K_T]_i^n \qquad 3.50$$

Equation 3.50 represents the tangential stiffness matrix at iteration *i* of increment *n*.

An improved value of the displacement $\{\delta\}_{i+1}^n$ can be obtained by computing

$$\{\delta\}_{i+1}^n = \{\delta\}_i^n + \{\Delta\delta\}_i^n \qquad 3.51$$

The incremental displacements $\{\Delta\delta\}_i^n$ can be determined from equations 3.49 and 3.50 such that

$$\{\Delta\delta\}_i^n = -[K_T]_i^{n^{-1}} \{\psi\}_i^n \qquad 3.52$$

The solution is carried out by solving a new set of linearized equations, equation 3.52. Displacements are then updated using equations 3.51 and the residual forces are calculated from equation 3.48. The process is repeated until the solution converges.

Various methods can be classified based on the manner in which the stiffness matrix is formed.

3.11.2.1 NEWTON-RAPHSON METHOD

In this method the tangential stiffness matrix is formed and decomposed at the beginning of every iteration. The solution process is illustrated diagrammatically in Fig. 3.7, for a one-degree of freedom. The major drawback of this method is the high cost of it. The repeated formations and decomposition of the stiffness matrices require much more time than that required for the solution of the system of equations.

3.11.2.2 MODIFIED NEWTON-RAPHSON METHOD

In this method the tangential stiffness matrix is updated and held constant for a number of iterations, after which it is again updated. The solution process is illustrated diagrammatically in Fig. 3.8, for a one degree of freedom. This method is more economical than the Newton-Raphson method since it involves fewer expensive reformations and decompositions of the stiffness matrix; however, it may require more iterations than those required using the standard Newton-Raphson method.

3.12 CONVERGENCE CRITERIA

Generally in a non-linear analysis convergence is assumed to occur when the difference between the applied loads and the internal forces reached an acceptably small value. The criteria used are set so that the iterative process is terminated when it is considered that additional iterations would not significantly improve the accuracy of the solution.

Two convergence criteria, based on displacements and energy respectively, were used in this study to check for convergence. The displacement criterion is that

$$\frac{\|\Delta\delta\|_i}{\|\delta\|_{i+1}} \leq \alpha_D \qquad 3.53$$

where $\| \ \|_i$ is the euclidean norm at iteration i

$$\|\Delta\delta\|_i = \sqrt{\sum_{i=1}^{n} \{\Delta\delta\}_i^2}$$

α_D is the displacement convergence tolerance.

The energy criterion used in the analysis is based on the energy released during an iteration by the residual forces and the iterative displacements are compared with the maximum energy released in a previous iteration of that particular increment. Thus convergence is assumed when

$$\frac{\{\psi\}^T \{\Delta\delta\}_i}{\{\psi\}_1^T \{\Delta\delta\}_1} \leq \alpha_E \qquad 3.54$$

where α_E is the energy convergence tolerance.

3.13 DESCRIPTION OF THE TECHNIQUES USED IN THE SOLUTION OF THE GOVERNING EQUATIONS

Load control and displacement control techniques can be used to solve the non-linear equations in this study. The load control technique obviously fails to trace the falling part of the response, indicated by points 1-2-3, shown in Fig. 3.9; it can only trace point 3 after tracing point 1; displacement control can easily do so and has proved to be suitable and efficient. The displacement control solution algorithm proposed by Stricklen [16] and implemented by [6] has been used in this study.

The concept of the displacement control technique is based on selecting a single incremental nodal displacement component and specified as a controlling parameter while the corresponding load value is considered to be one of the unknowns. The non-linear equation, equation 3.48, can be rewritten as

$$[K]\{\Delta\delta\}-\{P\}=\{\psi\} \qquad 3.55$$

where the incremental generalised force vector $\{P\}$ can be expressed in terms of an incremental load factor $\Delta\lambda$ and a generalised force vector $\{P^*\}$ resulting from unit load, such that

$$\{P\}=\Delta\lambda\{P^*\} \qquad 3.56$$

Using equation 3.56, equation 3.55 can be rewritten as

$$[K]\{\Delta\delta\}-\Delta\lambda\{P^*\}=\{\psi\} \qquad 3.57$$

Assume that the i^{th} incremental displacement component $\Delta\delta_i$ is specified and, for simplicity, assume that equation 3.57 is reordered such that the specified displacement is the final term in the vector $\Delta\delta$. The later assumption enables the theoretical derivation to be simplified; in practice it is not necessary that the specified displacement component should be the final term. Equation 3.57 can be rewritten as

$$\begin{bmatrix}[K_{11}] & -\{P_1^*\}\\ [K_{21}] & -P_1^*\end{bmatrix}\begin{bmatrix}\{\Delta\delta_1\}\\ \Delta\lambda\end{bmatrix}=\begin{bmatrix}\{\psi_1\}\\ \psi_i\end{bmatrix}-\Delta\delta_i\begin{bmatrix}\{K_{12}\}\\ K_{22}\end{bmatrix} \qquad 3.58$$

where K_{22}, $\Delta\delta_i$, P_1^* and ψ_i are scalars, $[K_{12}]$ is a column vector and $[K_{21}]$ is a row vector.

The matrix on the left-hand side of equation 3.58 is a non-symmetric matrix; however, the sub-matrix $[K_{11}]$ is symmetric if the original stiffness matrix $[K]$ is symmetric. To avoid solving a non-symmetric system of equations the unknown incremental displacement components and the incremental load factor can be obtained by expanding equation 3.58, such that

$$[K_{11}]\{\Delta\delta_1\}=\Delta\lambda\{P_1^*\}+\{\psi_1\}-\Delta\delta_i\{K_{12}\} \qquad 3.59$$

$$\{K_{21}\}\{\Delta\delta_1\}=\Delta\lambda.P_i^* +\psi_i-\Delta\delta_i K_{22} \qquad 3.60$$

where $\Delta\delta_1$ can be obtained from equation 3.59, such that

$$\{\Delta\delta_1\}=[K_{11}]^{-1}\left[\Delta\lambda.\{P_1^*\}+\{\psi_1\}-\Delta\delta_i\{K_{12}\}\right] \qquad 3.61$$

and the incremental load factor can be obtained from equation 3.60 and 3.61, such that

$$\Delta\lambda=\frac{\psi_i-\{K_{21}\}[K_{11}]^{-1}\{\psi_1\}+\left|\{K_{21}\}[K_{11}]^{-1}\{K_{12}\}-K_{22}\right|\Delta\delta_i}{\{K_{21}\}[K_{11}]^{-1}\{P_1^*\}-P_i^*} \qquad 3.62$$

The solution of the non-linear system of equations, equation 3.58, is found by solving equation 3.62 followed by equation 3.61. The main operations performed in the displacement control method are shown in Fig. 3.10. At the beginning of each increment a load factor λ is set equal to zero and the incremental displacement component is assigned a present value. The incremental load factor was obtained from equation 3.62 and hence the incremental displacements $\{\Delta\delta_1\}$ were determined from equation 3.61.

Since the specified incremental displacement component was specified at the beginning of the increment, it must be held constant during the iterative process, therefore it was set at equal zero after the first iteration.

At the end of each iteration the load factor λ was updated such that

$$\lambda = \lambda + \Delta\lambda \qquad 3.63$$

The nodal displacements were then updated using equation 3.51 and the process was repeated until convergence occurred.

3.14 SOLUTION STRATEGY

The modified Newton-Raphson method was used to trace the non-linear response. Solution of the governing equations was carried out by incrementing the applied load or a specified displacement component. The main operations in the analysis are shown in Fig.3.11. At the beginning of each increment the iterative nodal displacements were calculated by solving the governing equations using load control or displacement control. The nodal displacements were then updated to obtain the total nodal displacements using equation 3.51. Using the nodal displacements, the strains at the Gauss quadrature points of each element were then determined. The transverse shear resultants were determined in direct manner since the transverse shear stress was assumed to vary linearly throughout the thickness.

The in-plane and flexural stresses were determined from the strains at the sampling points through the cross-section using the material models described in Chapter 4. The in-plane and the flexural stresses resultants were determined numerically by integration of the corresponding stresses through the thickness.

The internal forces were then determined for each element using

$$\begin{Bmatrix} f_p \\ f_b \end{Bmatrix} = \int_{A^e} \begin{bmatrix} B_P & B_{nl} \\ 0 & B_b \end{bmatrix}^T \begin{Bmatrix} \overline{\sigma_p} \\ \overline{\sigma_b} \end{Bmatrix} dA^e \qquad 3.55$$

$$\{f_s\} = \int_{A^e} [B_s]^T \{\overline{\sigma_s}\} dA^e \qquad 3.56$$

where the subscripts p, b and s refer to the in-plane, flexural and transverse shear components respectively.

The internal forces of all elements were added together to obtain an internal forces vector $\{F\}$, for all the structure.

The internal force vector $\{F\}$ was then subtracted from the applied load vector $\{P\}$ to obtain a vector of residual forces $\{\psi\}$. If the applied load vector and the internal force vector are in equilibrium then, $\{\psi\} = 0$. Generally this is not true, so $\{\psi\}$has to be reapplied around the structures again and the nodal displacements updated.

As the analysis is repeated, the terms in $\{\psi\}$become smaller if the analysis converges. When an iteration has converged, the incremental process is repeated until the analysis is terminated.

3.15 REFERENCES

1. Zienkiewicz O. C. and Cheung Y. K., " Finite elements in the solution of field problems", Engineer, Vol. 220, 1965.

2. Zienkiewicz O. C., " The finite element method", 3rd Edition, McGraw-Hill, New York, 1977.

3. Crisfield M. A., "Finite elements and solution procedures for structural analysis", Prentice-Hall, Swansea, 1986.

4. Oden J. T., "Finite elements of non-linear continua", McGraw-Hill, New York, 1972.

5. Cook R.D., " Concept and application of finite element analysis" , 2nd Edition, John-Wiely and Sons, New York, 1981.

6. Ganaba T. H., "Non-linear finite element analysis of plates and slabs", PhD. Thesis, University of Warwick 1985.

7. Midlin R. D., "Influence of rotatory inertia and shear on flexural motions of isotropic, elastic plates", Journal of Applied Mechanics, ASME., Vol. 18, 1951, pp. 31-38.

8. Pica A., Wood R. D. and Hinton E., "Finite element analysis of geometrically non-linear plate behaviour using a Mindlin formulation", Computers and Structures, Vol. 11, 1980, pp. 203-215.

9. Fung Y. C., "Foundations of solid mechanics", Prentice-Hall, Englewood Cliffs, New Jersey, 1965.

10. Owen D. R. J. and Figueiras J. A., "An isotropic elastic-plastic finite analysis of thick and thin plates and shells", International Journal for Numerical Methods in Engineering, Vol. 19, pp. 1983, pp. 541-566.

11. Timoshenko S. and Goodier J. N., "Theory of elasticity", McGraw-Hill, London, 1951.

12. Timoshenko S. P. and Woinowsky-Krieger S., "Theory of plates and shells", McGraw-Hill, New York, 1959.

13. Hinton E. and Bicanic N., "A Comparison of Lagrangian and Serendipity Mindlin plate elements for free vibration analysis", Computer and Structures, Vol. 10, 1979, pp. 483-493.

14. Abramowitz, "Handbook of mathematical functions", Davies Publications, New York, 1965.

15. NAGFE Library level 0,"The science and engineering Council", Documentation, 1980.

16. Haisler W.E., Stricklin J.A. and Key J.E., "Displacement incrementation in non-linear structural analysis by self-correcting methods", International Journal for Numerical methods in Engineering, Vol. 11, 1977, pp.3-10.

Table 3.1- Weights and abscissas for Labatto rule

Sampling point number	Abscissas = $\pm x_i$	Weight factor = w_i
7	1.00000 000	0.04761 904
	0.83002 390	0.27682 604
	0.46884 879	0.43174 538
	0.0000 000	0.48761 904
9	1.00000 00000	0.02777 77778
	0.89975 79954	0.16549 53616
	0.67718 62795	0.27453 87126
	0.36311 74638	0.34642 85110
	0.00000 00000	0.37151 92744

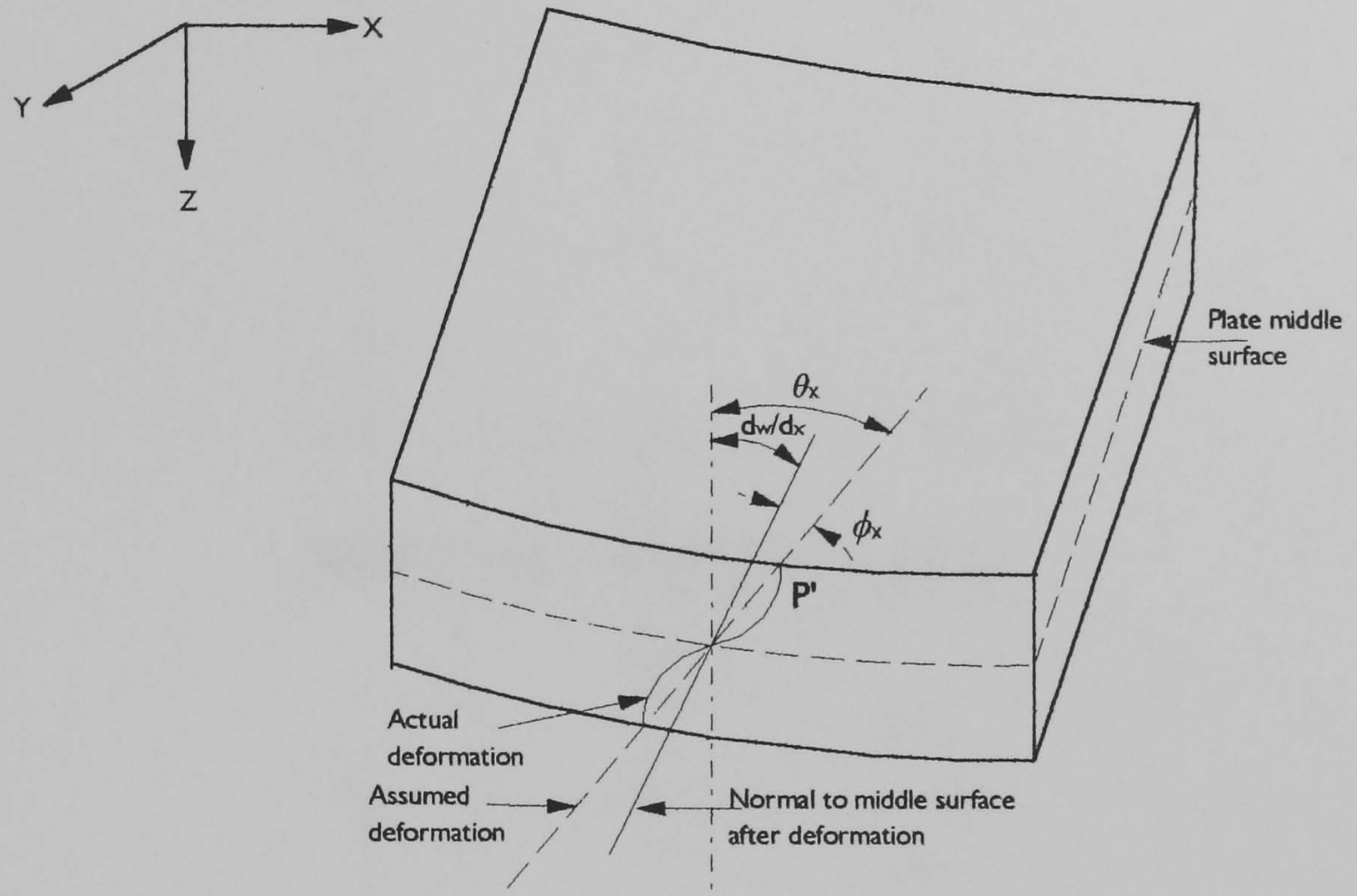

Fig.3.1- Deformation at cross-section of plate

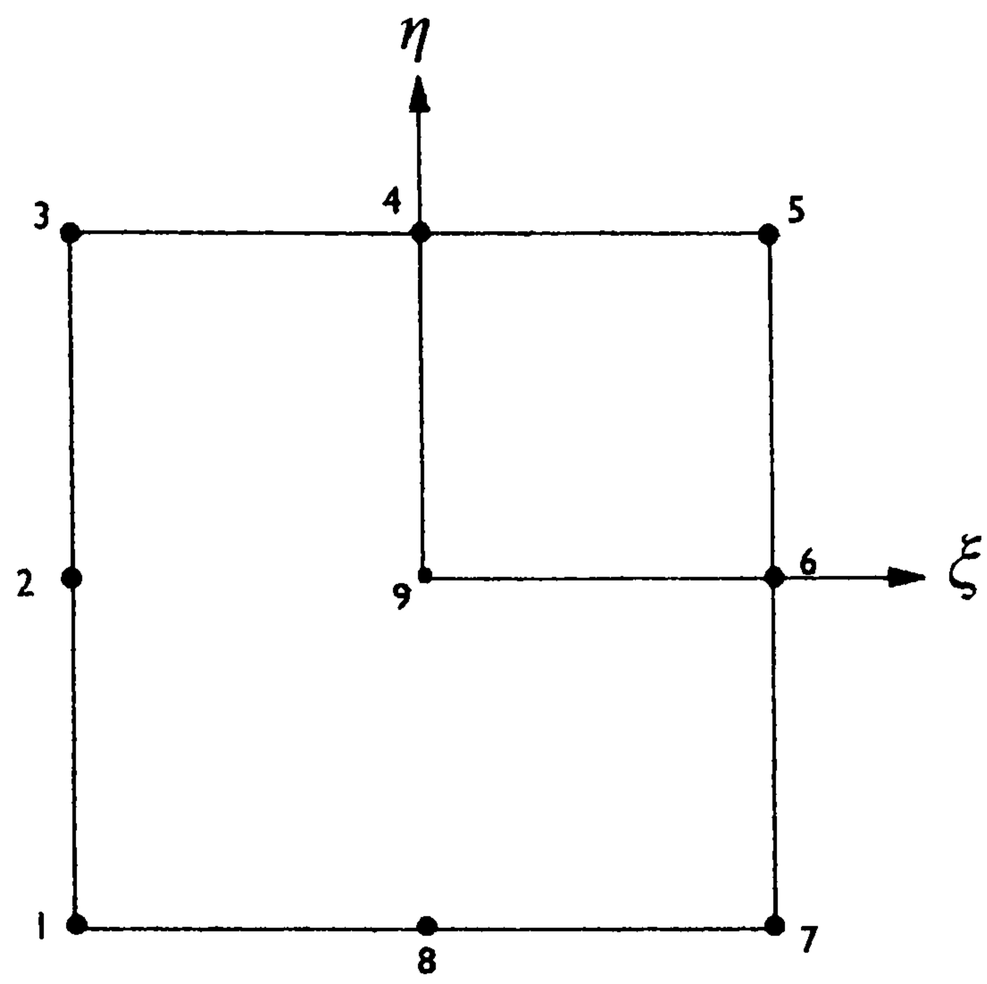

Fig.3.2- Heterosis plate bending element

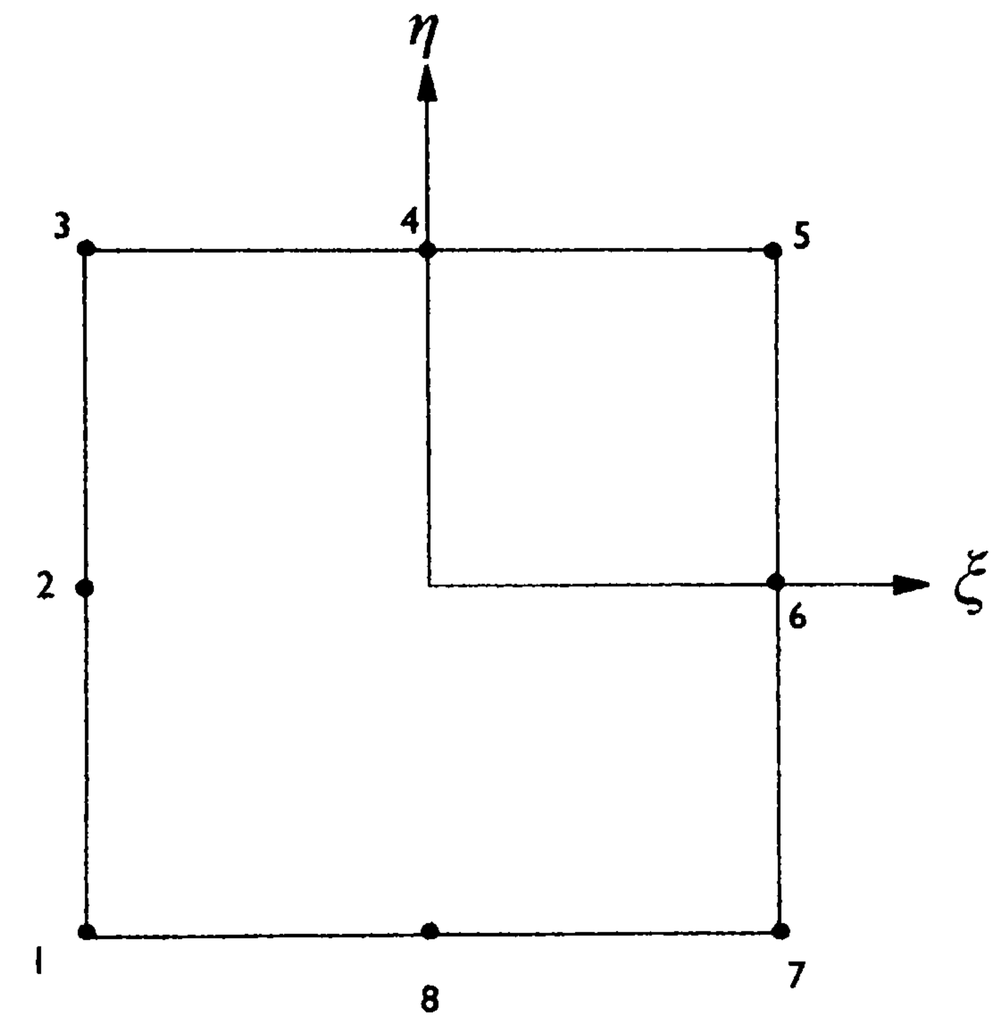

Fig.3.3- Serendipity membrane element

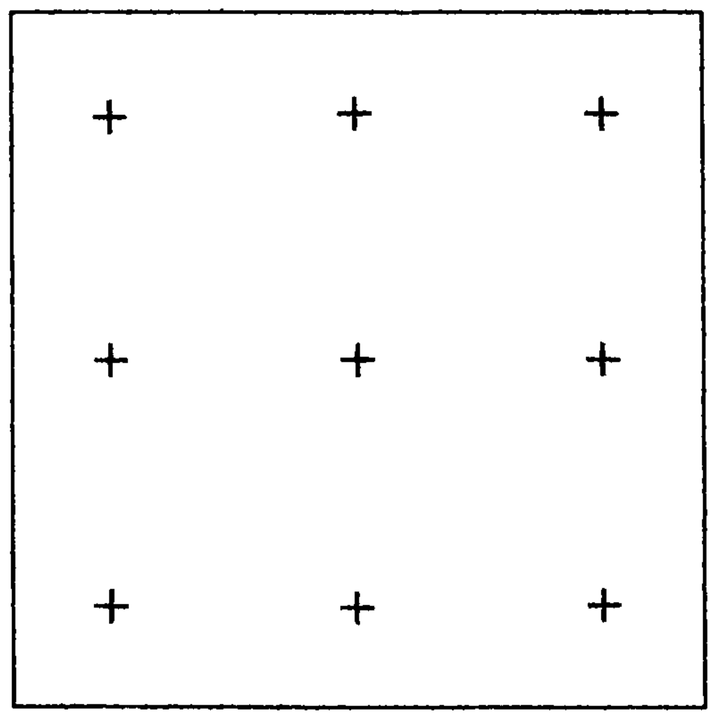

a-3x3 Gauss quadrature rule for flexural and in-plane stress components

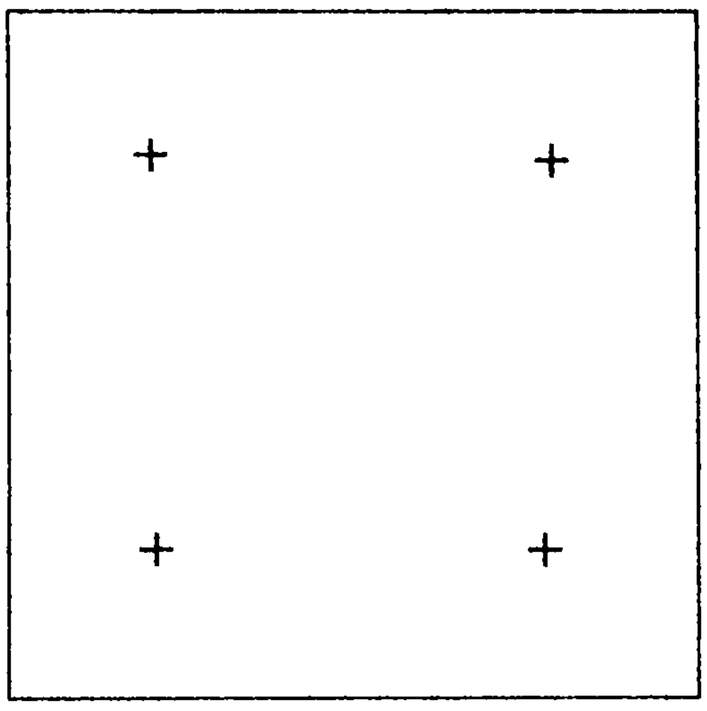

b-2x2 Gauss quadrature rule for transverse shear stress component

Fig.3.4- Integration rules used in the analysis

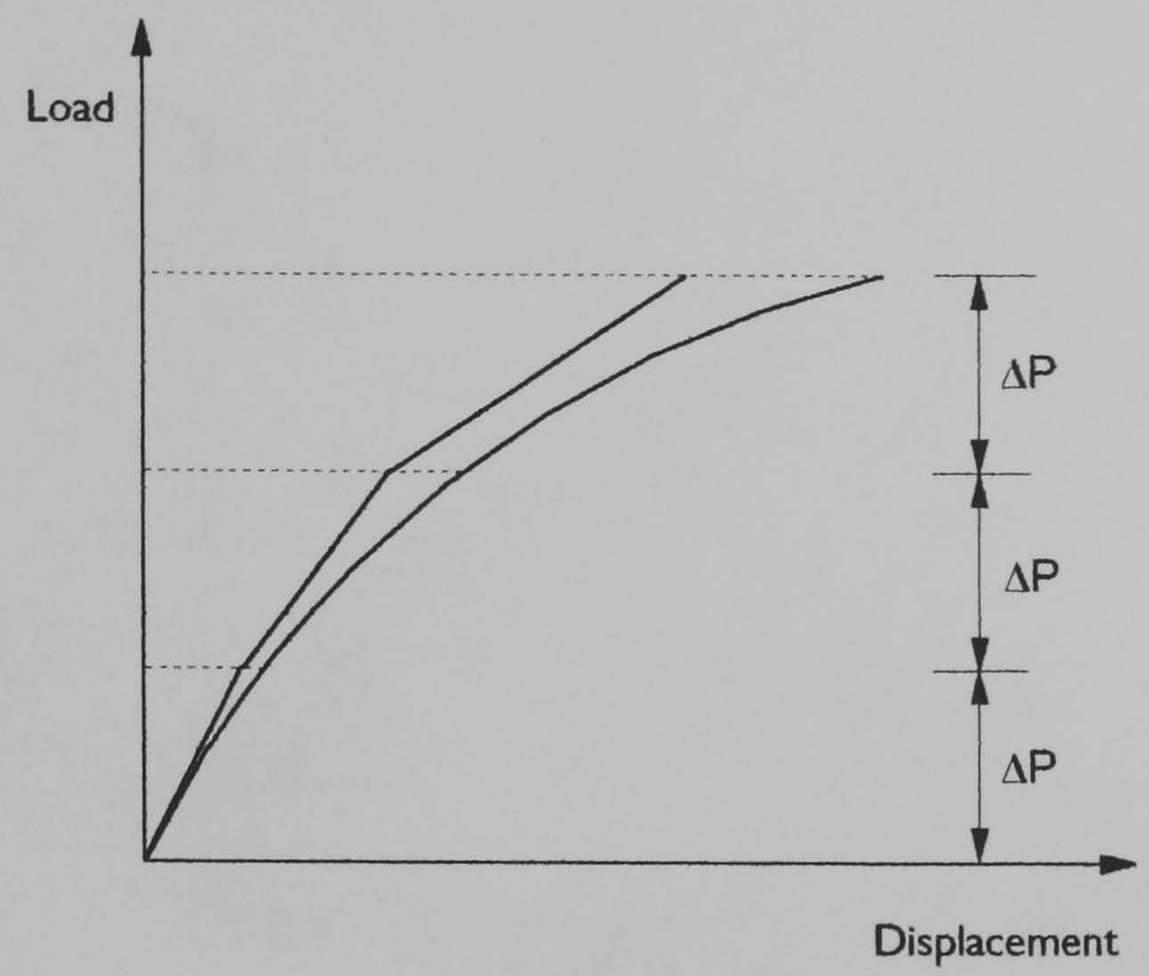

Fig.3.5- Incremental load method without corrections

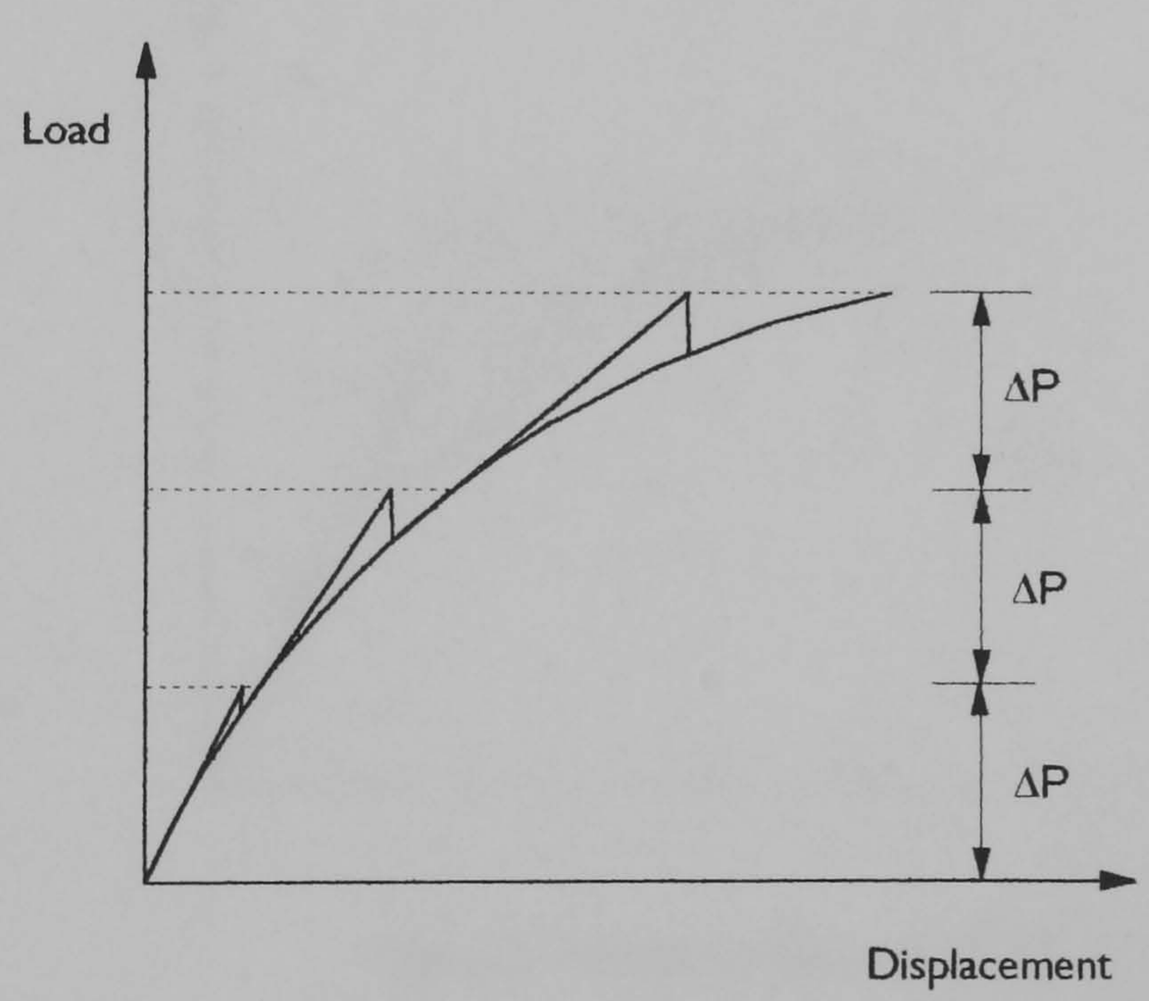

Fig.3.6- Incremental load method with equilibrium corrections

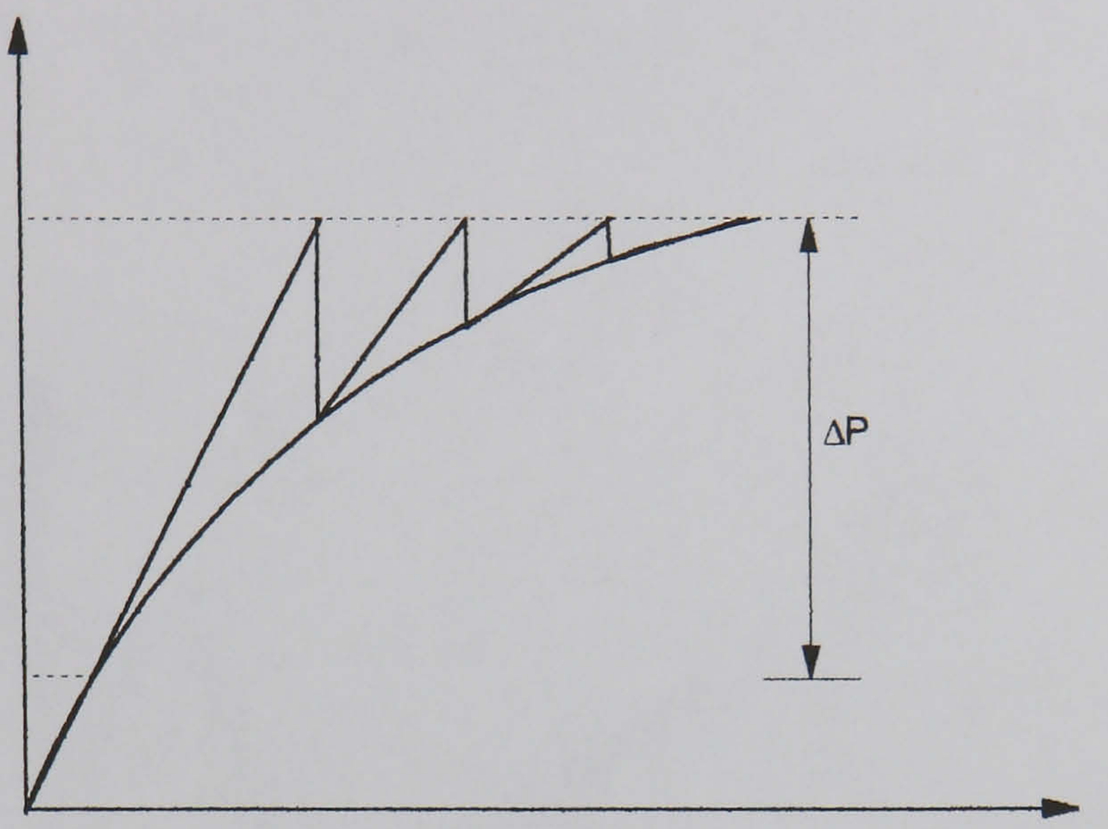

Fig. 3.7- Newton-Raphson method

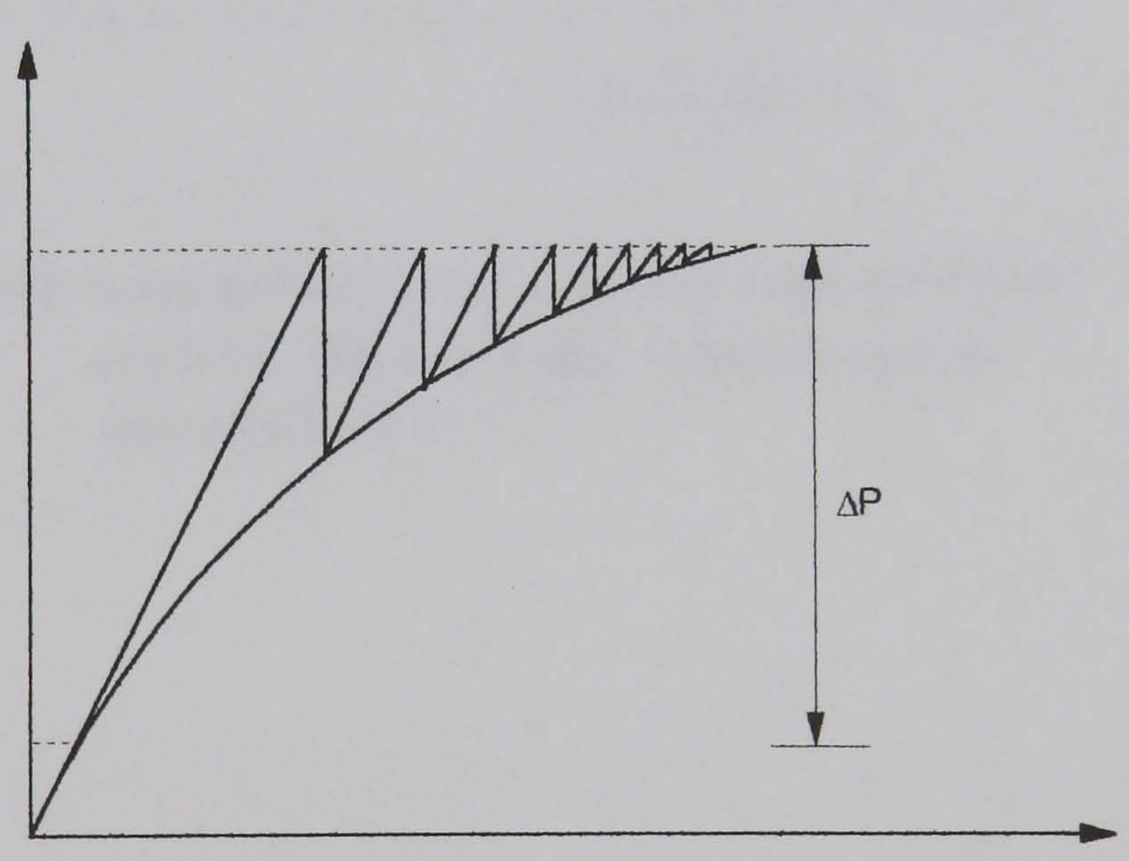

Fig. 3.8- Modified Newton-Raphson method

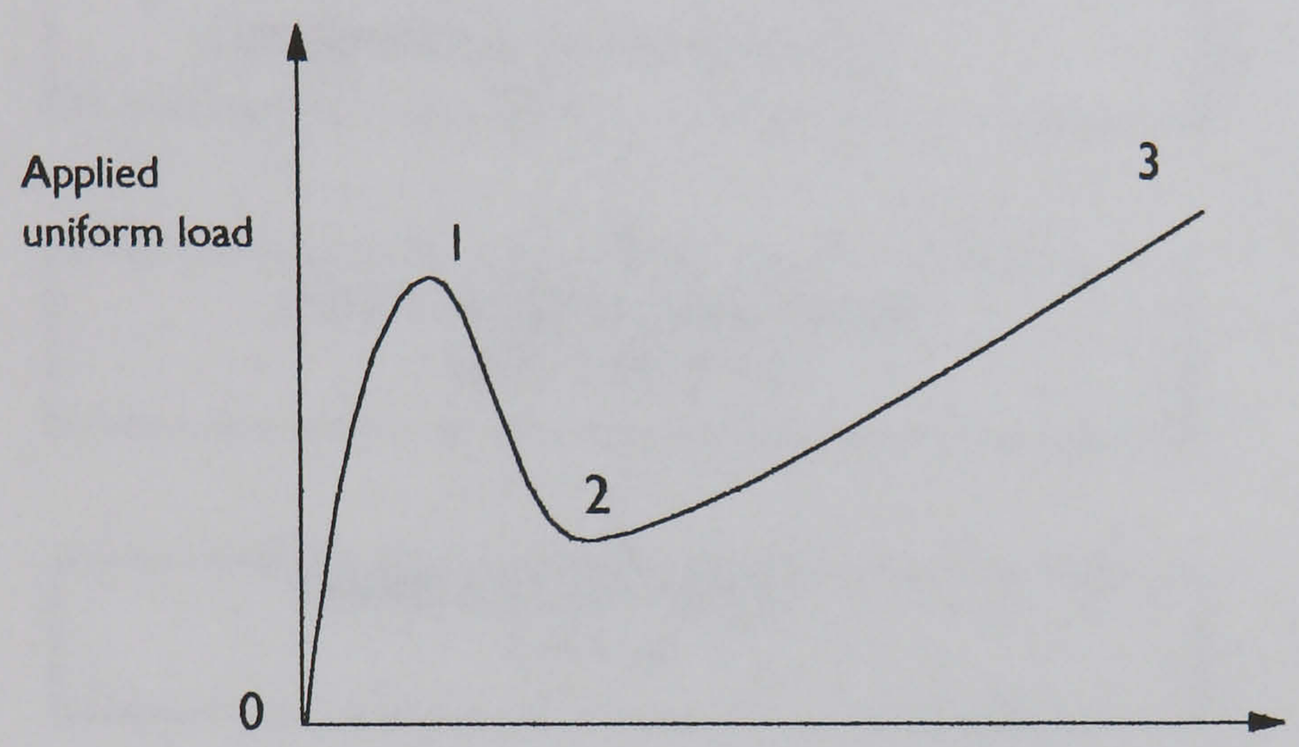

Fig.3.9- Load-deflection curve for two-way reinforced concrete slab with edges restraind againest lateral movement.

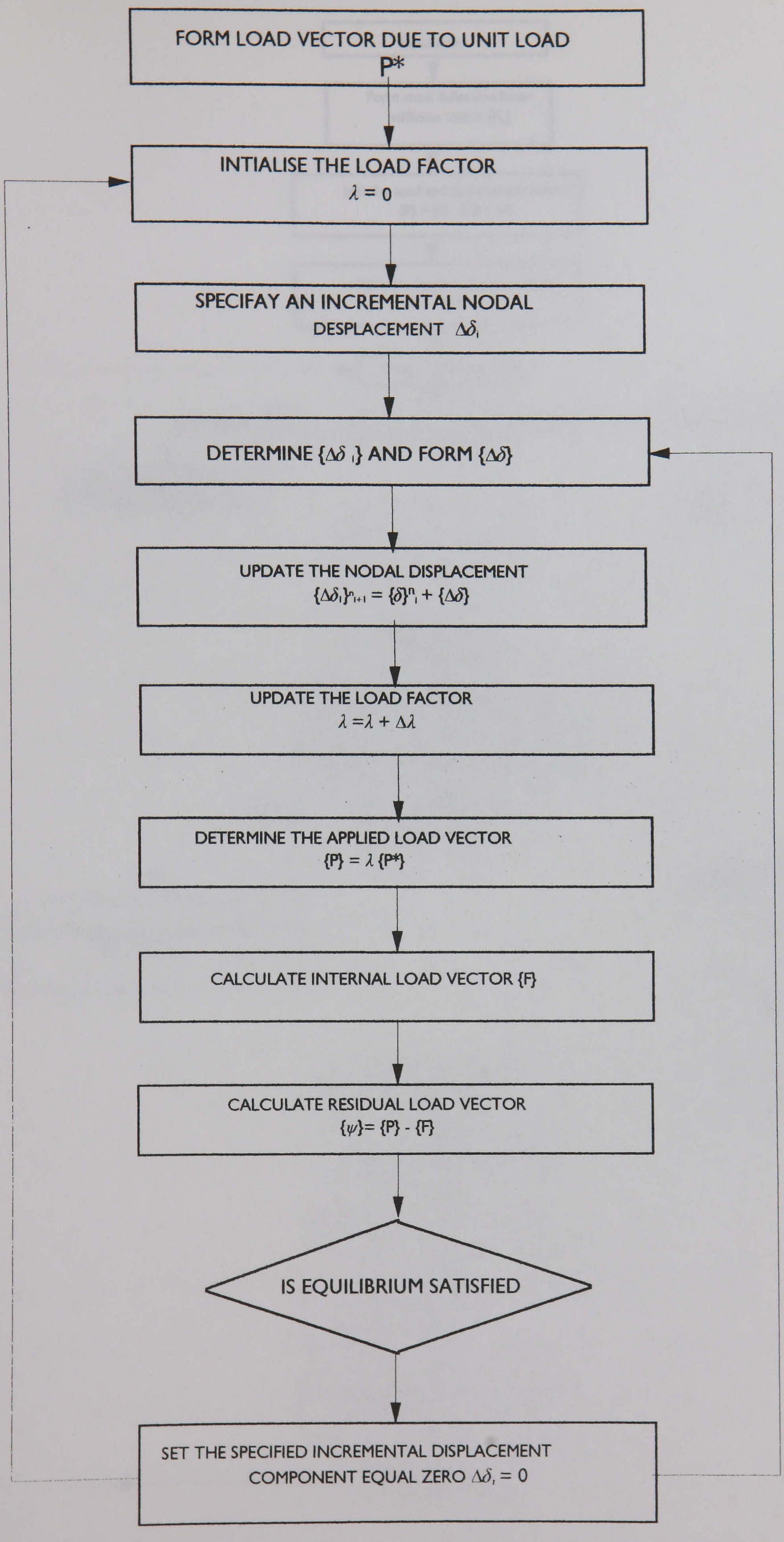

Fig. 3.10- Main operations used in the displacement control

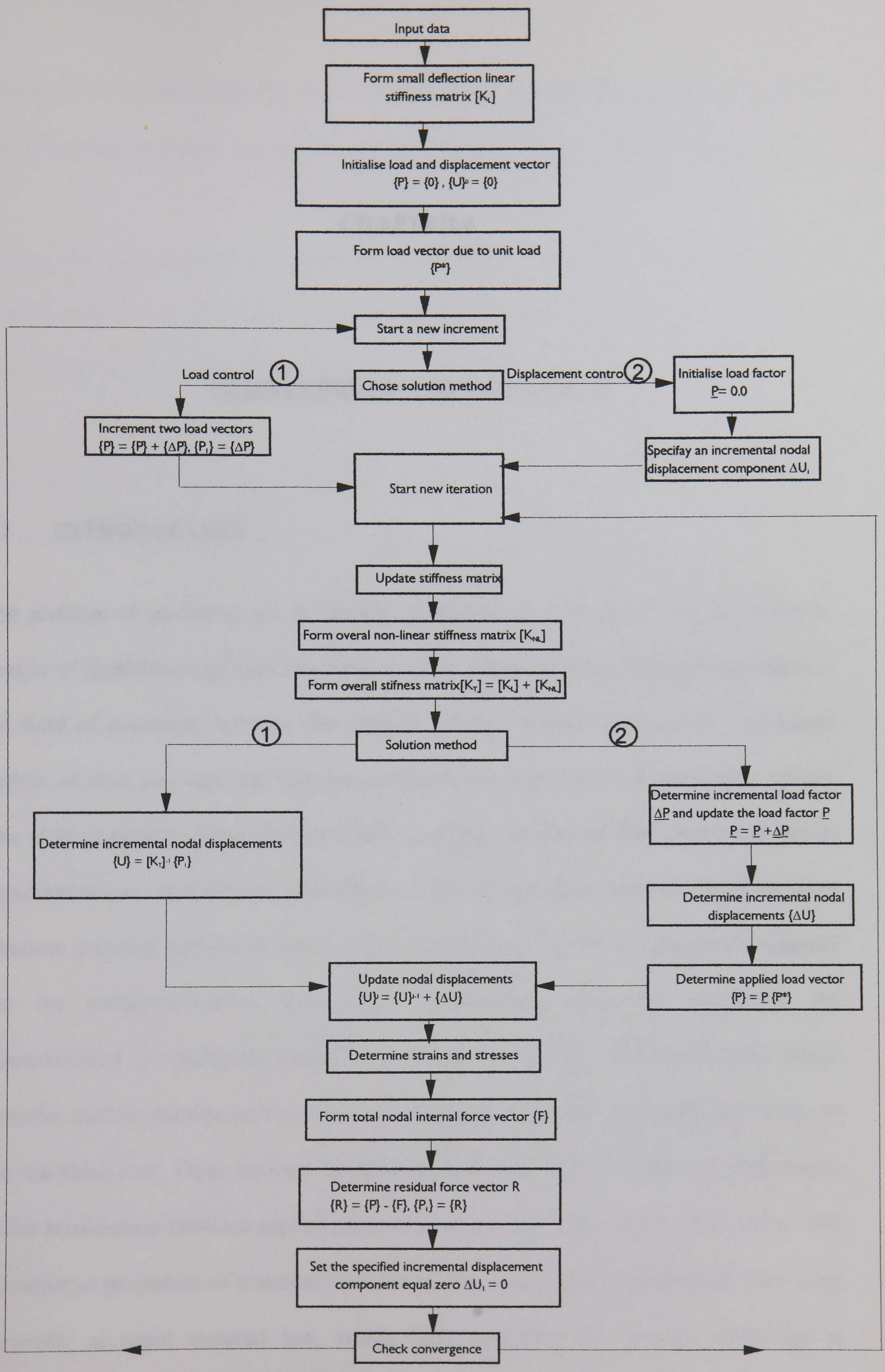

Fig.3.11- Main operations performed in the analysis

CHAPTER 4

MODELLING OF THE MATERIALS

4.1 INTRODUCTION

The problem of modelling the mechanical behaviour of concrete for use for analytical studies of reinforced concrete structures remains one of the most difficult challenges in the field of structural concrete. The analysis of the complete response of a structural system of steel and concrete requires consideration of a number of non-linear effects. The most important effects include tensile cracking, yielding of steel, non-linear stress-strain behaviour, compressive crushing of concrete, aggregate interlock, bond between concrete and steel and dowel action of reinforcing bars. The basic information required are the multidimensional stress-strain relationships describing adequately the characteristics of reinforced concrete. These are called the constitutive laws, which describe mathematically the behaviour of constituent materials approximating closely to the real behaviour. These laws are based on experimental data and allow the formulation of the relationship between applied multi-axial stress state and the resulting strains. The constitutive properties of concrete have not yet been universally defined and there is no generally accepted material law, which fully describes the concrete behaviour in

combined stress conditions [1]. The scatter of the results can be attributed to variations in three principal factors, namely the material, the test method and the loading system.

In the following sections a review of the different numerical models that can be employed for concrete for use in a finite element analysis are presented and the models adopted in the analysis are discussed.

Generally, there are two approaches for defining the complicated stress-strain behaviour of concrete under the various stress states. They can be classified into.

1. Elastic based models.
2. Plastic based models.

Detailed discussions of these approaches are given in [2,3]. In the following sections, the basic concepts and the limitations of these approaches will briefly discussed.

4.2 ELASTICITY BASED MODELS.

During the last three decades, a relatively large number of elasticity based constitutive models has been developed to represent the behaviour of concrete under general type of loading. In this model the stress strain behaviour can be expressed as

$$\{d\sigma\}=[D]\{d\varepsilon\} \qquad 4.1$$

where $[D]$ represents either the secant or tangential constitutive matrix. $\{\sigma\}$ and $\{\varepsilon\}$are the stress and strain vectors respectively.

In general two different approaches have been employed in the formulation of the non-linear elastic based constitutive relations. These are the total and the incremental stress-strain formulations. In the total, stress-strain models, the current state of stress is assumed to be uniquely expressed as a function of the current state of strain. This type of formulation is reversible and path-independent and thus is suitable for concrete structures under short term monotonic loading. In spite of this shortcoming the total stress-strain models have been used, mainly because of their simplicity, to predict the non-linear behaviour of concrete under biaxial and triaxial stress states.

The incremental, hypoelastic, stress-strain models are used to describe the behaviour of materials in which the state of stress depends on the current state of strain and the stress path followed to reach that state. This type of formulation is incrementally reversible and path dependent and, therefore provides a good representation of concrete behaviour under non-monotonic and non-proportional loading regimes.Several incremental models have been developed for isotropic and orthotropic stress-strain relationships under biaxial and triaxial stress states. [4,5,6,7,8].

4.3 PLASTICITY BASED MODELS.

For concrete under compression, non-linear deformations occur when it is stressed beyond the limit of elasticity. These deformations are basically inelastic since upon

unloading only a portion of the total strain can be recovered. Therefore, the total strain in concrete may be separated into recoverable and irrecoverable components. The recoverable part is treated within the framework of elasticity, while the irrecoverable part can be treated on the basis of the theory of plasticity.

Four fundamental assumptions are required to formulate the constitutive relations for plasticity models for concrete. They are

1. The shape of initial yield surface and subsequent loading surfaces.

2. The evolution of subsequent loading surfaces.

3. The formulation of an appropriate flow rule that specifies the stress-strain relation in plastic range.

4. A crushing surface expressed in terms of strains.

Plasticity based models have been extensively used to describe the behaviour of concrete [9,10,11,12,13]. In general models based on the theory of plasticity assume an elastic plastic hardening behaviour of concrete up to the ultimate strength followed by a rigid plastic response until the crushing surface is reached. After crushing, the concrete is assumed to lose completely its resistance against further deformation.

Approaches based on plastic-fracturing theory have been developed and used in modelling the post failure, softening of concrete[14,15,16]. The fracturing phenomena are better described in terms of loading surfaces that depend on strains rather than stresses since micro-fracturing can lead to a decrease in stress at constant strain. Therefore, two loading surfaces are required in the plastic-fracturing theory to account for the strain hardening behaviour. In addition to strain decomposition, the stress increment is also decomposed into an elastic stress increment and a fracture stress decrement.

4.4 MATERIAL MODELS FOR PLAIN CONCRETE UNDER BIAXIAL STRESS.

The elastic and plastic models described above have been used successfully in the analysis of reinforced concrete structures. Several attempts have been made to explain and quantify the ultimate stress state of the concrete under bi-axial stresses. The work carried out for non-linear models of concrete is reviewed in this section.

Liu [17] developed a stress-strain relationship for concrete under compression with any stress ratio, taking into account the Poisson's ratio effect. A failure envelope in bi-axial compression was proposed and the stress-strain equation for the representation of the behaviour of concrete was also developed. The expressions were based on the experimental data of Liu [18]. The work was, however, limited to biaxial compression-compression state.

Kupfer [19], proposed a failure surface based on tests carried out for the full range of biaxial loading. Expressions were proposed for the ultimate stress, bulk modulus and shear modulus.

Tasuji[20] developed expressions for the ultimate strengths of concrete under bi-axial stress combinations. The expressions were based on test results for concrete specimens of dimensions of 127 mm x 127 mm x 12.5 mm loaded for different biaxial stress combinations. The average uniaxial strength used for the concrete was 31.1 MPa. for compression and 2.7 Mpa for tension. The stress ratios used were of 0, 0.2 and 0.5 for the compression-compression region, –0.05, -.01 and –0.25 for the tension-compression region and 0, 1.0 and 2.0 for tension-tension region. The specimens with uniaxial and biaxial compression were applied with a constant stress rate of 2.52 MPa./min and 0.9 MPa./min for tests in tension.

Tasuji[21] modified and extended the proposed expressions in [17] for biaxial stress states compression to a general stress-strain relationship that described the behaviour of concrete in biaxial compression-tension, tension-tension and compression-compression. The proposed model was compared with other models [17,19,20] and the experimental data of Kupfer [19]. Tasuji[21] concluded that the model give a better representation of ultimate stress state, Fig.4.1.

Ganaba[22] identified that Tasuji's model [21] had some deficiencies because of the empirical nature of the developed expressions. It was found that the values of the peak

strains corresponding to the peak stresses showed inconsistencies at the boundaries of the different bi-axial stress regions. Using the experimental data of Tasuji[20], Ganaba[22] proposed expressions for the strains corresponding to the peak stresses, which satisfy the boundary conditions at the intersections of the different bi-axial stress regions.

Lodi[23] showed that the model developed by Tasuji[21], and modified by Ganaba[22] had some deficiencies in the biaxial compression state of stress as a result of the imperical nature of the expression. It was found that the stress-strain curve defined using the expression developed by Liu [17] and extended by Tasuji[21] is stiffened up in the minor principal direction with the decreasing in the stress ratio, and the strain corresponding to the peak stress becomes tensile for stress ratio less than the Poisson's ratio. Lodi [23] developed a non-linear elastic model to determine the ultimate stresses for biaxial compression state of stress. Modified strains, to take into account the Poisson's ratio effect at any stress level, are used in the model. The proposed model is discussed in more detail in Section 4.6.1.1.

4.5 MATERIAL MODELS FOR REINFORCED CONCRETE.

Figs.4.2a and 4.2b, show reinforced concrete panels loaded in uni-axial tension and in pure shear respectively. To predict the behaviour of such panels, cracking of the concrete must be considered. Prior to cracking, the behaviour can be predicted by superposition of the concrete and steel responses by the standard procedures of

elasticity. Predicting the post-cracking behaviour of reinforced concrete in compression tension, (tension stiffening and compression softening) has proved to be difficult. Tension stiffening and compression softening phenomena must be modelled adequately to study the response of reinforced concrete. The following sections provide an overview of the work done to model such phenomena.

4.5.1 TENSION STIFFENING MODELS.

When reinforced concrete reaches its ultimate tensile strength, primary cracks will form. At these primary cracks the stress carried by concrete drops to zero and the steel carries the load; however, the concrete between the cracks is still capable of carrying some tensile stresses. This is referred to as the tension stiffening effect. As the load increases secondary cracks will form resulting in a decrease in the average stress carried by the concrete. Eventually a secondary system of internal cracks develops around the reinforcing steel resulting in a breakdown of the bond between the concrete and the reinforcing steel. At this stage the concrete carries no load [25], Fig.4.3. Tension stiffening affects the service behaviour of reinforced concrete members by significantly increasing the stiffness of the reinforced concrete element in the post cracking range as compared with the element in which tension stiffening is not considered. Various models have been proposed for tension stiffening relating the resulting average tensile stress in concrete to the average tensile strains [28,41] Fig. 4.4. A review of the work to model tension stiffening is given in this section.

Clark [26,27] tested 14 beams and 9 slabs under two point loading with various steel areas and bar arrangements. It was concluded that the tension stiffening could be calculated on the basis of an average tensile stress expressed as a function of the tensile strength of concrete, acting over an effective area of concrete surrounding the bars in the tension zone. The value of the average tensile stresses and the effective zones over which tension stiffening acts were proposed for beams and slabs. Clark's tests show that the bar spacing has negligible effect on tension stiffening provided that it is not greater than about 1.5 times the slab depth.

Gilbert [28] used a layered discrete element method to investigate the behaviour of reinforced concrete slabs under short term loading. In this method the concrete is ignored after cracking and the post cracking response was modelled by increasing the reinforcing steel stiffness fictitiously. This approach implies that the tension stiffening effect is concentrated at the reinforcing steel level, whereas experimental observations show that this effect is distributed through the depth of the tension zone.

Link [29] proposed a model for tension stiffening for generally oriented cracks. As the cracks are not usually normal to the reinforcement, tension stiffening was quantified using an equivalent steel ratio normal to the crack orientation. The proposed model consisted of a linear ascending branch up to cracking followed by a non-linear descending curve up to the yielding of steel. The model was implemented into a finite element program and compared with the tests conducted by Vecchio and Collin [30]. A good agreement was found with the experiments.

4.5.2 COMPRESSION SOFTENING MODELS.

Cracked reinforced concrete in compression has been observed to exhibit a lower strength and stiffness than uni-axially compressed concrete. The so-called compression softening effect responsible is thought to be related to the degree of transverse cracking and straining present Fig. 4.5. It significantly influences the strength, ductility and load-deflection response of a concrete element. Several of experimental investigations have been undertaken to determine the degree of softening that occurs, and the factors that influence it [30,32,36]. At the same time several of analytical models have been proposed aimed at modelling this behaviour [30,31,32,35,37,38]. In this section, a review is made of the experimental data available and the various analytical models proposed for compression softening.

30 square reinforced concrete slabs were tested at the University of Toronto [30]. The slabs were loaded by different combinations of in-plane stress. These tests were carried out in a specially designed test rig. The panels had varying amounts of reinforcement in the two orthogonal directions. The test results revealed that the principal compressive stress in the concrete was a function not only of the principal compressive strain, but also of the principal tensile strain. It was observed that, as the tensile strain in the orthogonal direction increased the compressive strength of concrete was significantly reduced compared with the uniaxial compressive strength. A stress-strain curve was proposed to define the response of the concrete in the presence of orthogonal cracking. It was proposed that both the peak compressive stress and the corresponding strain

should be reduced by the same amount. The reduction factor was dependent on the ratio of principal tensile and compressive strains Fig.4.6.

Vecchio and Collins [31] modified the compression softening model, which was proposed in reference [30]. A reduction factor for the concrete strength based on orthogonal cracking was proposed to model the softened response. The reduction factor was a function of the principal tensile strain corresponding to the maximum uni-axial compressive strength of concrete and was applied to the compressive strength only Fig.4.7. The model was compared with the experimental results for the reinforced concrete panels [30] and good agreement was obtained.

Vecchio and Collins [32] subsequently proposed two further models for compression softening based on the results of 116 specimens tested at the University of Toronto. Parabolic curves were used to define the stress-strain response of softened concrete. Model A was based on the equation proposed by Theronfeldt [33] and Model B was based on Hognested'equation [34]. A reduction factor was applied to the uniaxial compressive strength and corresponding strain of concrete to model the softened response for Model A but for Model B it was applied to the uniaxial compressive strength of the concrete only. The reduction factor was found to be a function of the principal tensile and compressive strains and the uni-axial compressive strength of concrete Fig.4.8. Model A predicted a better response than Model B. The two models were compared with the other models [30,31,35,36,37,38] and it was found that both models predicted the softening better than the others. However, Model A gave a better

response than Model B. Model A has been adopted to model the softened compressive strength in this study and is discussed in more detail in Section 4.6.1.2.

4.6 MATERIAL MODEL USED IN THE ANALYSIS

A non-linear elasticity model based on the total stress-strain formulation has been utilised for the representation of the concrete behaviour in the analysis. The concrete was assumed to be an orthotropic material in the two principal directions and the behaviour in each direction depends on the stress in the other direction.

4.6.1 MODELLING OF CONCRETE.

In order to determine the behaviour of the reinforced concrete in different stress states, the concrete can be considered to be subjected to one of the three bi-axial stresses states named compression-compression, compression-tension and tension-tension. Modelling of the different bi-axial stresses states is given in the following sections.

4.6.1.1 RESPONSE IN COMPRESSION-COMPRESSION

The parabolic equation developed by Hognestad [34] has been used to model the response of concrete in compression in the principal directions up to the peak stress, followed by a linear falling branch. The stress at which the concrete has been assumed to crush has been taken as 0.85 of the peak stress, σ_p, Fig. 4.9. The concrete has been

assumed to carry zero stress beyond the crushing strain, ε_{cu}, which corresponds to a stress of $0.85\sigma_p$ on the linear falling branch. The formulations used are:

For $\varepsilon_i \leq \varepsilon_{pi}$ (up to peak stress)

$$\sigma_i = \frac{\sigma_{pi}}{\varepsilon_{pi}} \varepsilon_i \left(2 - \frac{\varepsilon_i}{\varepsilon_{pi}} \right) \qquad 4.2a$$

For $\varepsilon_i > \varepsilon_{pi}$ (post peak stress)

$$\sigma_i = \sigma_{pi} - \frac{0.85\sigma_{pi}}{\varepsilon_{cu} - \varepsilon_{pi}} \left(\varepsilon_i - \varepsilon_{pi} \right) \qquad 4.2b$$

where, σ_i stress in principal direction i.

ε_i strain in principal direction i.

σ_{pi} peak stress in principal direction i.

ε_{pi} strain corresponding to peak stress in principal direction i.

ε_{cu} crushing strain.

In order to determine the stresses for given strains, the peak compressive stress and corresponding strain must be known. The model developed by Lodi [23] is employed in this study to determine the peak compressive stresses and corresponding strains.

The model developed by Lodi[23] was a non-linear elastic isotropic model. Modified strains, to take into account the Poisson's ratio effect at any stress level, as proposed by Cope[39], are used. The Poisson's ratio was assumed to be constant throughout an analysis for the compression-compression stress state.

The modified strains are given by

$$\begin{Bmatrix} \varepsilon_{e1} \\ \varepsilon_{e2} \end{Bmatrix} = \frac{1}{1-\nu^2} \begin{bmatrix} 1 & \nu \\ \nu & 1 \end{bmatrix} \begin{Bmatrix} \varepsilon_1 \\ \varepsilon_2 \end{Bmatrix} \qquad 4.3$$

where, ε_{e1} and ε_{e2} are modified elastic strains which account for the Poisson's ratio effect, ν is the Poisson's ratio and ε_1 and ε_2 are the real strains in the principal directions 1-1 and 2-2 respectively.

The linearized strength envelope proposed by Tasuji [21] Fig. 4.10. has been used but the strains corresponding to peak stress have been changed. The expression for the strains corresponding to the peak stresses has been obtained by rearranging equation 4.3.

$$\begin{Bmatrix} \varepsilon_{p1} \\ \varepsilon_{p2} \end{Bmatrix} = \begin{bmatrix} 1 & -\nu \\ -\nu & 1 \end{bmatrix} \begin{Bmatrix} \varepsilon_{ep1} \\ \mathrm{K}\,\varepsilon_{ep1} \end{Bmatrix} \qquad 4.4$$

where K stress ratio $= \frac{\sigma_2}{\sigma_1}$, where $\sigma_2 \geq \sigma_1$ algebraically.

σ_1, σ_2 stress in principal direction 1 and 2.

$\varepsilon_{p1}, \varepsilon_{p2}$ measured strains corresponding to peak stresses in principal directions 1-1 and 2-2 respectively for any stress ratio k.

ε_{ep1} modified strain corresponding to peak stress in principal direction 1-1.

Since the model is based on the theory of elasticity the peak stress and corresponding strain in the minor principal direction will be proportional to the peak stress and corresponding strain in the major principal direction, Fig. 4.11. The above expression yields a relationship between the modified and measured strains corresponding to peak stresses.

$$\varepsilon_{ep1} = \frac{\varepsilon_{p1}}{1 - \nu K} \qquad 4.5$$

since, $$\varepsilon_{ep2} = K\, \varepsilon_{ep1} \qquad 4.6$$

where, ε_{ep2} is the modified strain corresponding to the peak stress in principal direction 2-2.

Substituting the value of ε_{ep1} from equation 4.5 into equation 4.6 to obtain,

$$\varepsilon_{ep2} = \frac{K_{p1}}{(1 - \nu K)} \qquad 4.7$$

letting,

$$c = \frac{\sigma_{p1}}{f_c'} \qquad 4.8$$

where, $f_c^{'}$ is the uniaxial compressive strength of concrete. The peak stress in principal direction 1-1, equation 4.2, will be

$$\sigma_{p1} = c\, f_c^{'} = E_s\, \varepsilon_{ep1}\left(2 - \frac{\varepsilon_{ep1}}{\varepsilon_{ep1}}\right) = E_s\, \varepsilon_{ep1} \qquad 4.9$$

where E_s = secant modulus at peak stress = $\dfrac{f_c^{'}}{\varepsilon_p}$

ε_p = strain corresponding to the uniaxial compressive strength of concrete.

or, $$\frac{\varepsilon_{ep1}}{c} = \frac{f_c^{'}}{E_s} \qquad 4.10$$

Substituting the value of E_s into equation 4.10 and simplifying to obtain the expression for strain corresponding to the peak stress in the principal direction 1-1,

$$\varepsilon_{ep1} = c\, \varepsilon_p \qquad 4.11$$

Using equation 4.6, the modified strains corresponding to peak stress in principal direction 2-2 will then be

$$\varepsilon_{ep2} = \mathrm{K}\, c\, \varepsilon_p \qquad 4.12$$

Equations 4.11 and 4.12 are the expressions representing the strains corresponding to the peak stresses in the major and the minor principal stress direction.

The expression for c varies with the stress ratio, K . The expressions for the peak stresses and corresponding strains are summarised below for the various stress ratios.

For $0 \leq K \leq 0.2$

$$\sigma_{p1} = \left(1 + \frac{K}{1.2 - K}\right) f_c' \qquad 4.13a$$

$$\varepsilon_{ep1} = c\,\varepsilon_p = \left(1 + \frac{K}{1.2 - K}\right) \varepsilon_p \qquad 4.14a$$

For $0.2 \leq K \leq 1.0$

$$\sigma_{p1} = 1.2\, f_c' \qquad 4.13b$$

$$\varepsilon_{ep1} = 1.2\, \varepsilon_p \qquad 4.14b$$

For $0 \leq K \leq 1.0$

$$\sigma_{p2} = K\, \sigma_{p1} \qquad 4.13c$$

$$\varepsilon_{ep2} = K\, c\, \varepsilon_p \qquad 4.14c$$

4.6.1.2 RESPONSE IN COMPRESSION-TENSION

It has been mentioned in section 4.5.2 that the compressive response of concrete under compression-tension stress state has been modelled using Model A proposed by Vecchio and Collins [32]. The model consists of three distinct stages: an ascending parabolic branch, a constant stress region and a linear falling branch, Fig.4.12. Equation 4.2a has been used to predict the ascending part of the compressive response to ensure compatibility with the compression-compression stress-state.

Model A is based on a statistical analysis of the experimental data. The softening has been incorporated through a softening factor, β, which is given by

$$\beta = \frac{1}{1 + k_c + k_f} \qquad 4.15$$

where
$$k_c = 0.35\left(-\frac{\varepsilon_1}{\varepsilon_2} - 0.28\right)^{0.8} \geq 1, \ \varepsilon_1 \leq \varepsilon_y \qquad 4.16$$

$$k_f = 0.1825\sqrt{f_c'} \geq 1.0 \qquad 4.17$$

where $\varepsilon_1, \varepsilon_2, \varepsilon_y$ are the principal tensile strain, principal compressive strain and the yield strain of the reinforcement in tension respectively. The softening factor, β, is applied to both the uniaxial compressive strength and the corresponding strain to obtain the softened response.

For the falling branch equation 4.2b is used. The maximum stress and corresponding strain of concrete in compression when in a state of compression-tension are summarised below.

For region I, $\varepsilon_1 \leq \beta\varepsilon_p$

$$\sigma_{p1} = \beta f_c^{'} \qquad 4.18a$$

$$\varepsilon_{p1} = \beta \varepsilon_0 \qquad 4.19a$$

For region II, $\varepsilon_p \leq \varepsilon_1 \leq \varepsilon_p$

$$\sigma_{p1} = \beta f_c^{'} \qquad 4.18b$$

$$\varepsilon_{p1} = \beta \varepsilon_0 \text{ to } \varepsilon_0 \qquad 4.19b$$

For region III, $\varepsilon_p \geq \varepsilon_1 \geq \varepsilon_p$

$$\sigma_{p1} = \beta f_c^{'} \qquad 4.18c$$

$$\varepsilon_{p1} = \varepsilon_0 \text{ to } \varepsilon_{cu} \qquad 4.19c$$

where ε_{cu} is the crushing strength of the concrete.

The tensile response of concrete under compression-tension stress state has been modelled as a linear elastic material prior to cracking. This approach has been generally adopted to model the pre-cracked tensile response of concrete [30,33].

$$\sigma_2 = E_c \varepsilon_2 \qquad 4.20a$$

where E_c is the modules of elasticity of the concrete.

After cracking occurs the response has been modelled by a linear descending branch which ends at the yielding of the reinforcement, $B\varepsilon_t$. The strain at which descending branch ends has been defined in terms of the cracking strain, ε_t. The post cracking response is usually termed as tension stiffening and discussed in detail in section 4.5.1. Tension stiffening can play a significant role in the overall response of reinforced concrete. This effect becomes evident after cracking and it influences the response prior to the yielding of reinforcement.

The governing equation used in this study to model tension stiffening is given below.

$$\sigma_2 = \alpha\left(\sigma_{p2} - \frac{\sigma_{p2}}{(\xi - 1)\varepsilon_{ep2}}\right)(\varepsilon_{e2} - \varepsilon_{ep2}) \qquad 4.20b$$

where α, is a factor defining the discontinuity between the pre and post cracking response. For $\alpha = 1$ there is no discontinuity and for $\alpha = 0$ there is no tension stiffening. Fig. 4.13.

In order to determine the cracking stress and strain the model proposed by Tasuji[21] has been used. The expressions used are

$$\sigma_{p2} = f_c^{'}\left(1+\frac{\mathrm{K}}{1+\mathrm{K}\,s}\right) \qquad 4.21$$

where $s=\frac{f_c^{'}}{f_t}$ = ratio of the uniaxial compressive strength to the uniaxial tensile strength, and

$$\varepsilon_{ep2} = \frac{\sigma_{p2}}{E_c} \qquad 4.22$$

After cracking Poisson's ratio was assumed to be zero.

4.6.1.3 RESPONSE IN TENSION -TENSION

In biaxial tension the ultimate stress state is modelled using a square failure surface [21]. The expression for ultimate biaxial tension stress state is

$$\sigma_{p1} = \sigma_{p2} = f_t \qquad 4.23$$

The expression for cracking strains is

$$\varepsilon_{ep1} = \varepsilon_{ep2} = \frac{f_t}{E_c} \qquad 4.24$$

After cracking the response has been modelled using the same model as for the response in compression tension stress state.

4.6.2 MODELLING OF THE CRACKING.

Several models for cracking have been developed for use in a finite element analysis. Most models rely on a strength criterion for crack initiation.

Cracking in concrete may be represented using discrete or smeared models, Fig. 4.14. In the discrete model, cracks are allowed to develop along the element boundaries. The nodal points are separated when cracks occur. This approach has a disadvantage in that it involves changes in the topology of the finite element mesh following the formation of a crack and the lack of generality in possible crack direction.

In the smeared crack modelling, local discontinuities resulting from cracking are represented in a distributed manner. This type of crack model, which has been adopted in the analysis, fits the finite element displacement method, since the continuity of the displacement field remains intact.

The main criticism of the smeared crack model is that it is not capable of predicting local fracture.

After a crack has formed its direction can be taken as fixed or it can be free to rotate. In the fixed crack approach the crack direction is defined by the orientation of the initial

crack and is then fixed regardless of the change in the principal direction as the load is changed.

The rotating crack approach, which has been adopted in the analysis, was originally proposed by Cope [40]. This model is based on the assumption that the crack direction is always normal to the direction of the maximum tensile principal stress.

4.6.3 MODELLING OF THE REINFORCEMENT.

Reinforcing steel has been assumed to be capable of carrying axial forces only. The reinforcing steel bars at specific depth have been smeared into a steel layer with the same area as the original reinforcement. Each steel layer has the same orientation and has its centre at the same position as the original reinforcing steel bars.

To model the stress-strain relationship of the reinforcing steel layer a bi-linear model was used in the analysis. As shown in Fig. 4.15, the following properties were required to construct the stress-strain curve.

E_{st} = initial modulus of elasticity of steel.

E_{sh} = modulus of strain hardening of steel.

σ_0 = yield stress.

ε_{su} = ultimate strain.

The strain hardening effect could be included in the representation of the reinforcing steel; however, if the modulus of the strain hardening, E_{sh}, was set at zero the stress-strain relationship become an elasto-plastic one. Loading in tension and compression has been assumed to be elastic until the stress reaches the yield stress, σ_0; beyond that yielding was assumed to have occurred. Failure has been assumed to occur when the strain reached the ultimate strain, ε_{su}. The reinforcing steel has been then assumed to rupture and carry zero stress.

The elastic constitutive relationship for a reinforced steel layer oriented in the X-direction is given by

$$\begin{Bmatrix} \sigma_x \\ \sigma_y \\ \tau_{xy} \end{Bmatrix} = \begin{bmatrix} E_{st} & 0 & 0 \\ 0 & 0 & 0 \\ 0 & 0 & 0 \end{bmatrix} \begin{Bmatrix} \varepsilon_x \\ \varepsilon_y \\ \varepsilon_{xy} \end{Bmatrix} \qquad 4.25$$

4.7 PROCEDURE ADOPTED TO DETERMINE STRESSES.

Six material properties for concrete are required in order to construct the stress-strain relationship. These properties are the uniaxial compressive strength, f_c', the corresponding strain, ε_0, Poisson's ratio, ν, the uniaxial tensile strength, f_t, the corresponding cracking strain, ε_t, and the crushing strain, ε_{cu}. All six material properties of concrete can be determined experimentally. The procedure adopted for the

evaluation of the stress in the concrete at any particular load increment is summarised as follows:

1. The principal strain, ε_i, and the angle between the Cartesian and the principal direction, θ, are determined from

$$\varepsilon_{1,2} = \frac{\varepsilon_x + \varepsilon_y}{2} \pm \sqrt{\left(\frac{\varepsilon_x + \varepsilon_y}{2}\right)^2 + \left(\frac{\gamma_{xy}}{2}\right)^2} \qquad 4.26$$

and

$$\theta = \frac{1}{2}\tan^{-1}\left(\frac{\gamma_{xy}}{\varepsilon_x - \varepsilon_y}\right) \qquad 4.27$$

2 An initial estimate for the stress ratio, K_{ini}, for the first load increment is made by using the linear elastic relationship between the principal stress and strain.

$$K_{ini} = \frac{\sigma_2}{\sigma_1} = \frac{\varepsilon_2 + \nu\varepsilon_1}{\varepsilon_1 + \nu\varepsilon_2} \qquad 4.28$$

For subsequent load increments a value of stress ratio, K, from the previously converged load increment is used.

3. The modified strains are determined using equation 4.3.

4. For the given stress ratio, the peak stresses, σ_{pi}, and the corresponding modified strains, ε_{epi}, are calculated using equations 4.13 and 4.14 or 4.18 and 4.19 or 4.23 and 4.24.

5. The principal stresses, σ_i, are determined using equations 4.2 and 4.20.

6. The stress ratio, k, is recalculated using principal stresses, σ_i.

7. Steps 4 to 6 are repeated until the stress ratio, K, becomes acceptably small (1% difference between two successive iterations). Investigation of the convergence of biaxial principal stress ratio indicated that convergence occurred within three iterations.

8. The principal stresses are then resolved into the Cartesian direction using the following relationship:

$$\begin{Bmatrix} \sigma_x \\ \sigma_y \\ \tau_{xy} \end{Bmatrix} = \begin{bmatrix} \cos^2\theta & \sin^2\theta & 2\sin\theta\cos\theta \\ \sin^2\theta & \cos^2\theta & -2\sin\theta\cos\theta \\ -\sin\theta\cos\theta & \sin\theta\cos\theta & \cos^2\theta-\sin^2\theta \end{bmatrix} \begin{Bmatrix} \varepsilon_1 \\ \varepsilon_2 \\ 0 \end{Bmatrix} \qquad 4.29$$

4.8 REFERENCES:

1. Buyukozturk O. and Shareef S. S., " Constitutive modelling of concrete in finite element analysis", Computer and Structures, Vol. 21, No. 3, pp. 581-610, 1985

2. Chen W. F., " Plasticity in reinforced concrete", McGraw-Hill, 1982

3. Chen W. F. and Saleeb, A F., " Constitutive equation for engineering materials", Vol. 1, Elasticity and modelling, 1981, Vol. 2, Plasticity and modelling, 1982, John Willey and Sons, New York.

4. Gerstle K. H., " Simple formulation of biaxial concrete behaviour", ACI Journal, Vol. 78, No. 1, September 1981, pp 62-68.

5. Drawin D. and Peckhold D. A., "Analysis of RC shear panels under cyclic loading", Journal of Structural Division. ASCE, Vol. 102, ST2, February 1976, pp 355-369.

6. Drawin D. and Pecknold D. A., "Non-linear biaxial stress-strain law for concrete". Journal of Engineering Mechanics Division, ASCE, Vol. 103, EM2, April 1977, pp 229-241.

7. Elwi A. A. and Murray D. W., "A 3D hypoelastic concrete constitutive relationship", Journal of Engineering Mechanics Division, ASCE, Vol. 105, EM4, August 1979, pp 623-641.

8. Bathe K. J. and Sundberg J. A., "Computational modelling of reinforced concrete structures (Chapter 4)", edited by Hinton, E and Owen, R. Pineridge press, Swansea, 1986, pp 101-121.

9. Buyukozturk O., "Non-linear analysis of reinforced concrete structures", Computer and Structures, Vol. 7, 1977, pp 149-159.

10. Chen A. C. T. and Chen W. F., "Constitutive relations for concrete", Journal of Engineering Mechanics, ASCE, Vol. 101, EM4, August 1975, pp 465-581.

11. Owen D. J. R. and Figrueiras J. A., "Ultimate load analysis of reinforced concrete plate and shell including geometric non-linear effects", Finite element software for plates and shells, Edited by Hinton E and Owen D. R. J., Pineridge press Swansea, 1984.

12. Imbabi M. S. and Cope R. J., "An equivalent elasto-plastic constitutive model for biaxially loaded concrete", Proceeding of International Conference on Computer Aided Analysis and Design of Concrete Structures, edited by Damjanic et al., Vol. 1, Split, Yugoslavia, September 1984, pp 275-288.

13. Cervera M. and Hinton E., "Computational modelling of reinforced concrete structures (Chapter 12)", edited by Hinton E, and Owen R., Pineridge Press Swansea, 1986, pp 327-370.

14. Bazant Z. P. and Kim S. S., "Plastic-fracturing theory for concrete", Journal of Engineering Mechanics, ASCE, Vol. 105, June 1979, pp 407-428 with errata in Vol. 106.

15. Hsieh S. S., Ting E. C. and Chen W. F., " A plastic-fracture model for concrete" Journal of solid and Structures, Vol. 18, No. 3, 1982, pp 181-197.

16. Glemberg R. and Samuelsson A., "A general constitutive model for concrete structures", Procedings of International Conference on Computer Aided Analysis and Design of Structures. Edited by Damjanic et al., Vol. 1, Split, Yugoslavia, September 1984, pp 119-132.

17. Liu T. C. Y., Nilson A. H. and Slate F. O., "Biaxial stress-strain relationship for concrete", Journal of Structural Division, Proceeding ASCE, Vol. 98, ST5, May 1972, pp 1025-1034.

18. Liu T. C. Y., "Stress-strain response and fracture of concrete in uniaxial and biaxial compression", Research report No. 339, Department of Structural Engineering, Cornell University, New York, February 1971.

19. Kupfer H. B. and Gerstle K. H., "Behaviour of concrete under biaxial stresses", Journal of ACI, Vol. 66, No.8, August 1969, pp 656-666.

20. Tasuji M. E., Salte F. O. and Nilson A. H., "Stress-strain response and fracture of concrete in biaxial loading", Journal of ACI, Proceeding, Vol. 75, No. 7, July 1978, pp 306-312.

21. Tasuji M. E., Nilson A. H., and Slate F. O., "Biaxial stress-strain relationships for concrete", Magazine of Concrete Research, Vol. 31, No, 109, December 1979, pp 217-224.

22. Ganaba T. H., "Nonlinear finite element analysis of plates and slabs". PhD. Theses, University of Warwick, August 1985, 215p.

23. Lodi S.H.,"Reinforced concrete slab elements under bending and twisting moments", PhD. Thesis, Department of Civil and Offshore Engineering, University of Heriot-Watt, December 1997. 228p.

24. Liu T. H., Nilson A. H., and Slat F. O., " Biaxial stress-strain relationship for concrete", Proceedings of ASCE, Vol. 98, ST5, May 1972, pp 1025-1034.

25. Goto Y., "Cracks formed in concrete around deformed tension deformed bars", ACI. Journal Proceedings, Vol. 668, No. 4, 1971, pp 244-251.

26. Clark L. A., and Sperias D. M., "Tension stiffening of reinforced concrete beams under short term load", Cement and concrete association, Technical report, No. 42.521, July 1978, 20p.

27. Clark L. A., and Cranston W. B., "The influence of bar spacing on tension stiffening in reinforced concrete slabs", Proceeding of the international conference on concrete slabs, Advances in slabs technology, Dundee, April 1979, pp 118-128.

28. Gilbart R. I., and Warner R. F., "Tension stiffening in reinforced concrete slabs", Journal of Structural Division, ASCE Proceedings. Vol. 4, ST12, December 1978, pp 1885-1900.

29. Link R. A., Elwi A. E., and Scanlon A., "Biaxial tension stiffening due to generally oriented reinforcing layers", Journal of Engineering Mechanics, Vol. 115, No. 8, August 1989, pp 1647-1662.

30. Vecchio F. and Collins M. P., " The response of reinforced concrete panels to in-plane shear and normal stress", Publication No. 82-03, Department of Civil Engineering University of Toronto, March 1982,332p.

31. Vecchio F. J. and Collins M. P., "The modified compression-field theory for reinforced concrete elements subjected to shear", ACI, Structural Journal, Vol. 83, No. 2 , March-April 1986, pp 219-231.

32. Vecchio F. J. and Collins M. P., "Compression response of cracked reinforced concrete", Journal of Structural Engineering, Vol. 119, No. 12, December 1993, pp 3590-3610.

33. Wu Z. Yoshikawa H. and Tanaba T., "Tension stiffness model for cracked concrete", Journal of Structural Engineer. ASCE, Vol. 117, No. 3. March 1991, pp 715-732.

34. Hognestad E. Hanson N. W. and McHenry D., "Concrete stress distribution in ultimate strength design", Journal of ACI. Vol. 52, No. 6, December 1955, pp 445-479.

35. Belarbi A. and Hsu T. T. C., "Constitutive laws of reinforced concrete in biaxial compression-tension", Research Report UHCEE 91-2, University of Houston, USA, 1991.

36. Kollegger J. and Melhorn G. "Experimentalle untersuchungen zur Bestimmung der Druckfestigkeit des gerissnen bej einer Querzugbeanspruchung", Report 413, Deutscher Ausschuss *Für* Stahlbeton, Berlin Germany, 1990.

37. Miyahara T. Kawakami T. and Meakawa K.. "Nonlinear behaviour of cracked reinforced concrete plate element under uniaxial compression", Concrete Library International, Japan Socity of Civil Engineering. JSCE. Vol. 11, 1988, pp 306-319.

38. Shirai S. and Noguchi H., "Compressive deterioration of cracked concrete", proceedings of ASCE Structures, Congress 1989, Design, Analysis and Testing, ASCE, New York, 1989, pp 1-10.

39. Cope R. J., "Computational modelling of reinforced concrete structure (Chapter 1)", edited by Hinton E. and Owen R., Pineridge press, 1986, pp 3-43.

40. Cope R. J. Rao P. V. Clark L. A. and Norris P., "Modelling of reinforced concrete behaviour for finite element analysis of bridge slabs", Numerical

methods for Non-linear Problems, Prineridge press, Swansea, 1980, pp. 457-470.

41. Lin C. S. and Scordelis A. C., "Non-linear analysis of reinforced concrete shells of general form", Journal of the Structural Division, ASCE Vol. 101, No. EM4, 1975, pp. 149-156.

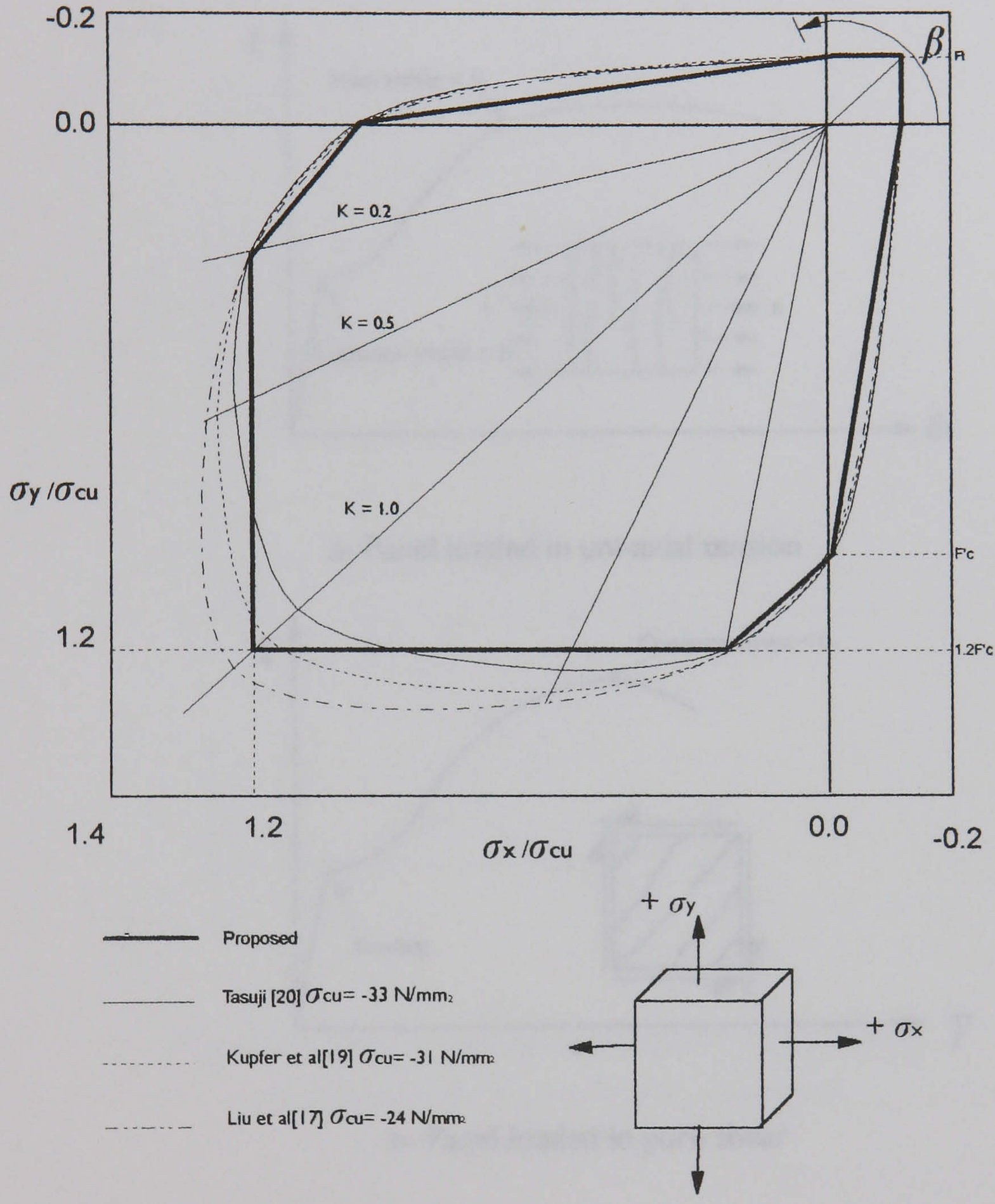

Fig. 4.1- Comparison of models representing the ultimate biaxial stress state of concrete Tasuji et al [21]

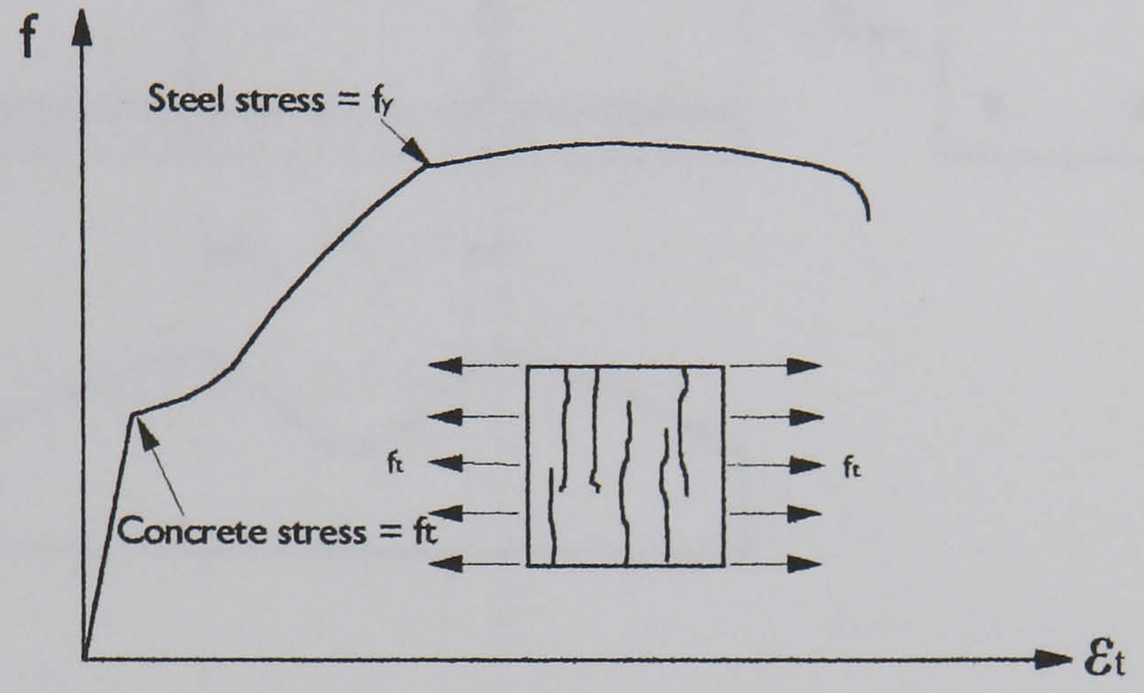

a- Panel loaded in uni-axial tension

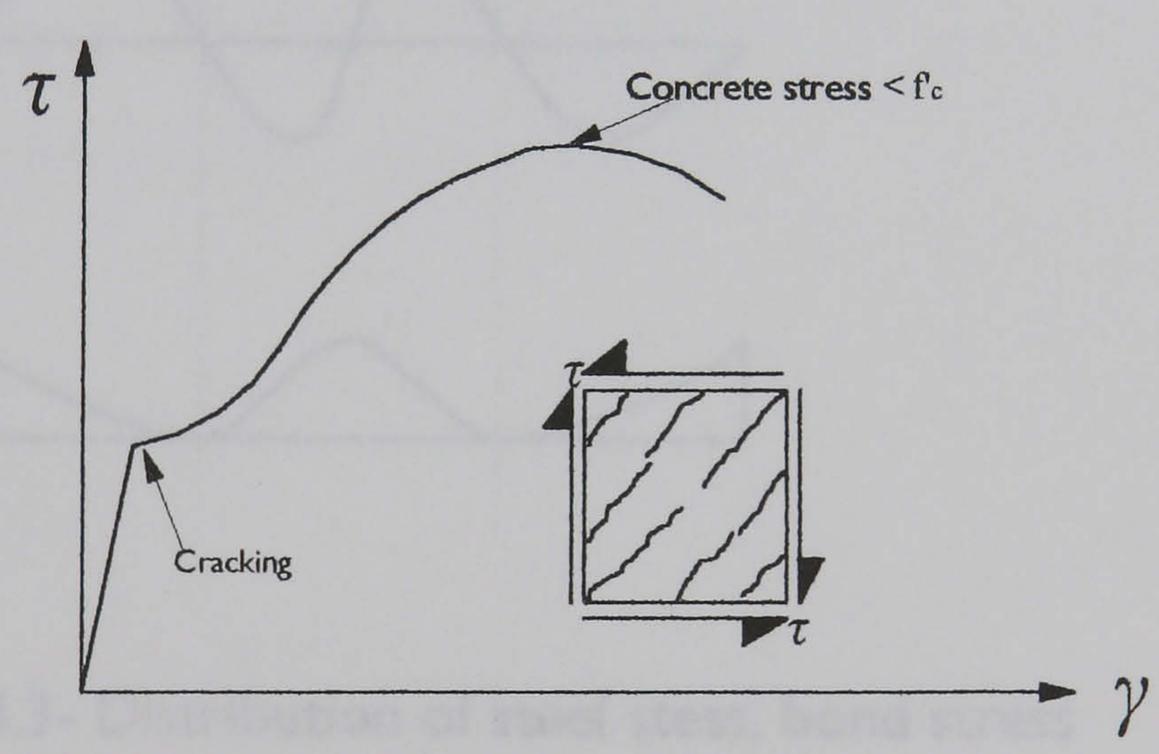

b- Panel loaded in pure shear

Fig.4.2- Reinforced concrete panels loaded in uniaxial tension and pure shear [30]

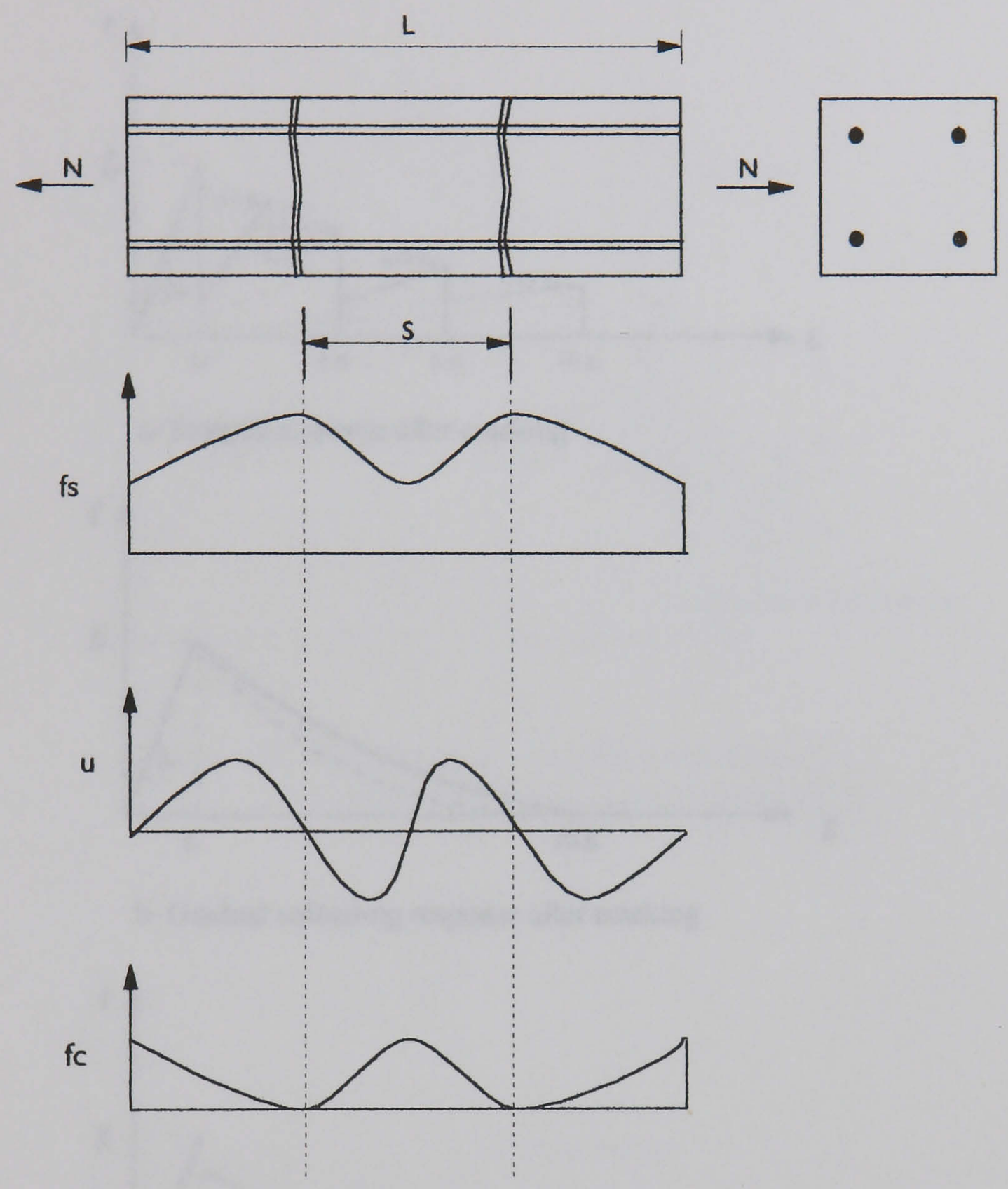

Fig.4.3- Distribution of steel stess, bond stress and concrete stress in tension specimen.

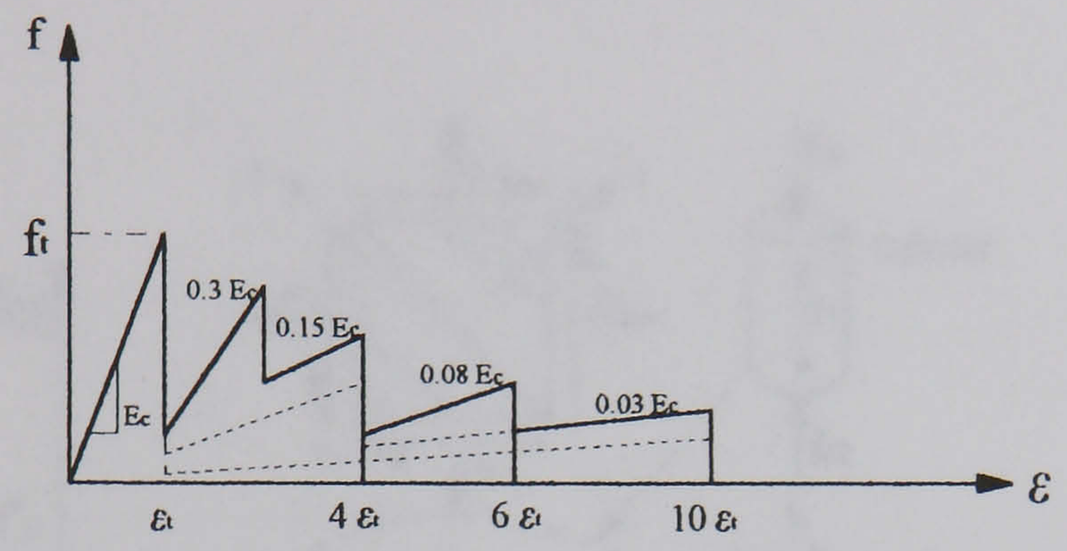

a- Stepped response after cracking

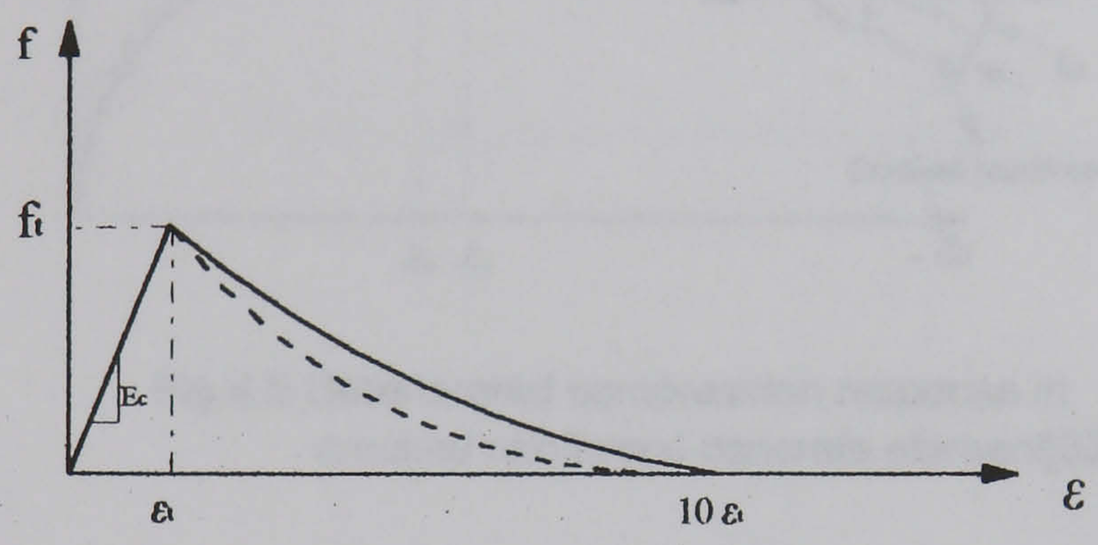

b- Gradual unloading response after cracking

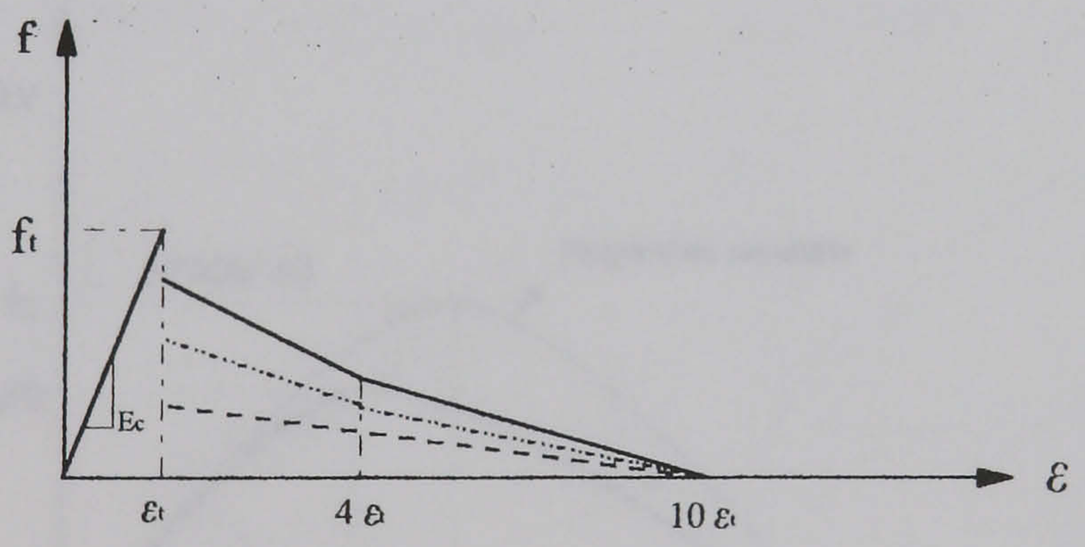

c- Discontinuous response after cracking

Fig.4.4- Tension stiffening models [28,41]

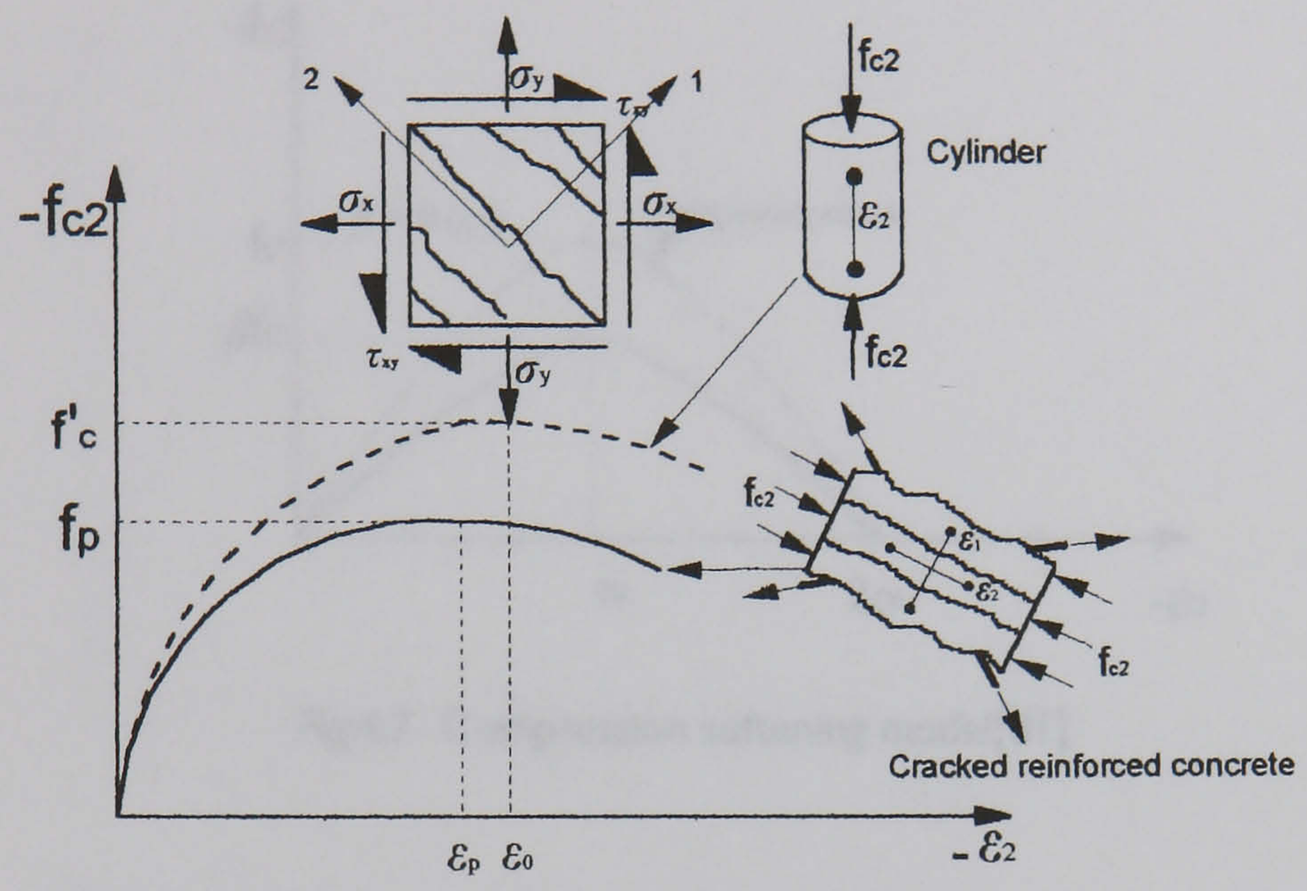

Fig.4.5-Deteriorated compression response in cracked reinforced concrete element[32]

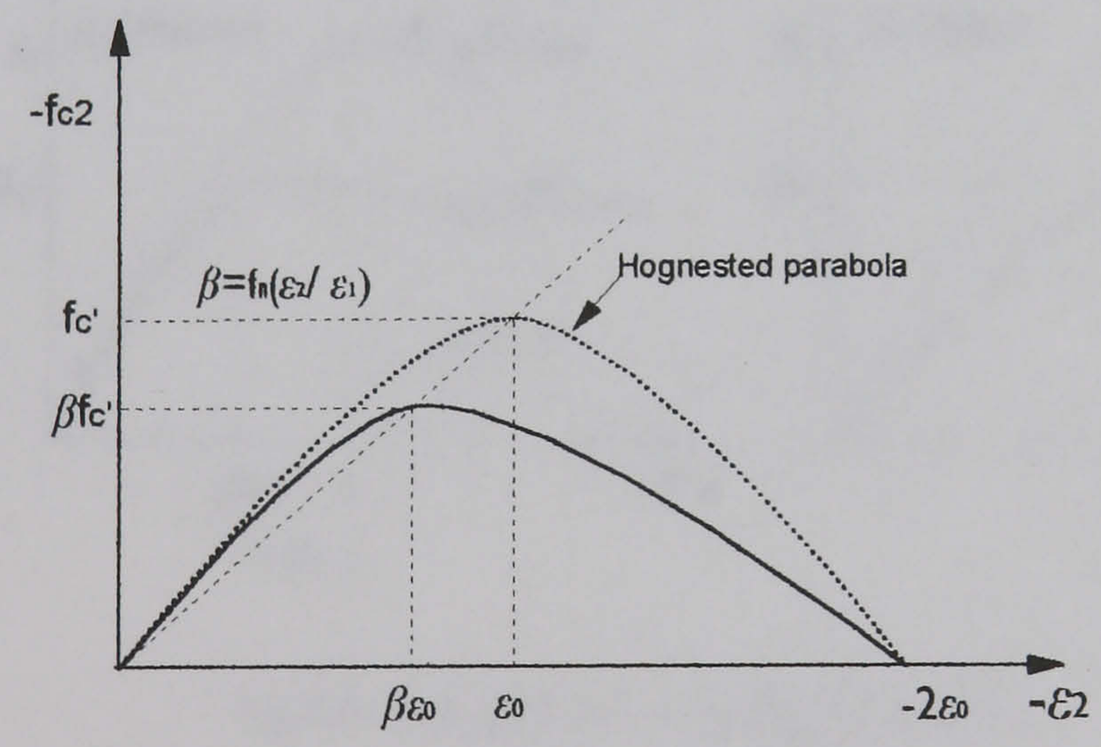

Fig.4.6- Compression softening model [30]

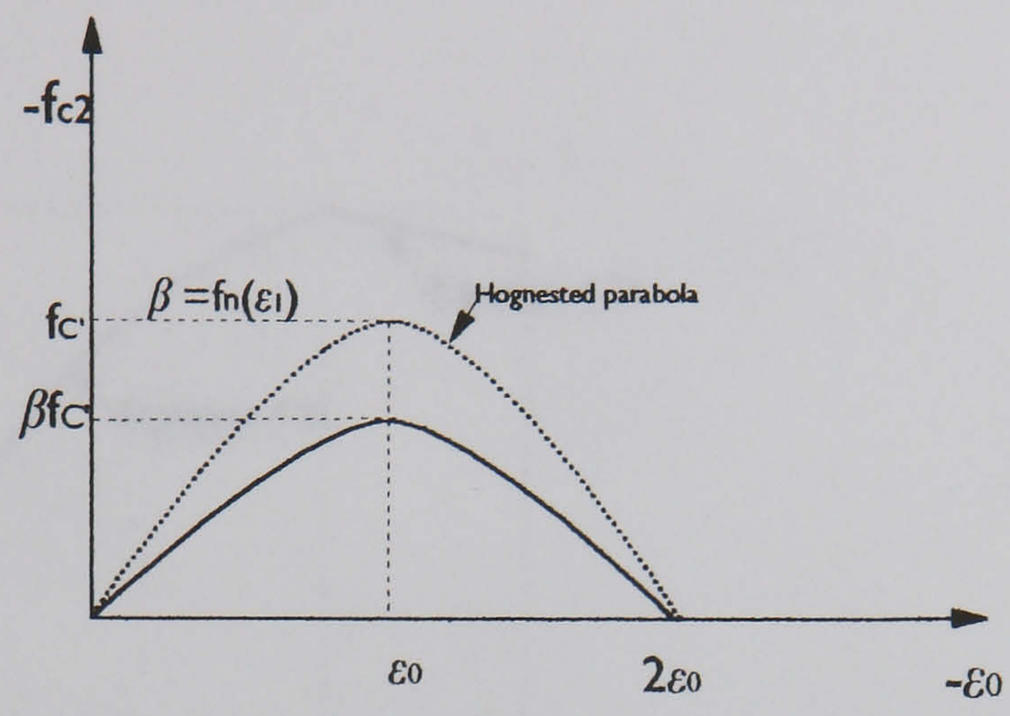

Fig.4.7- Compression softening model[31]

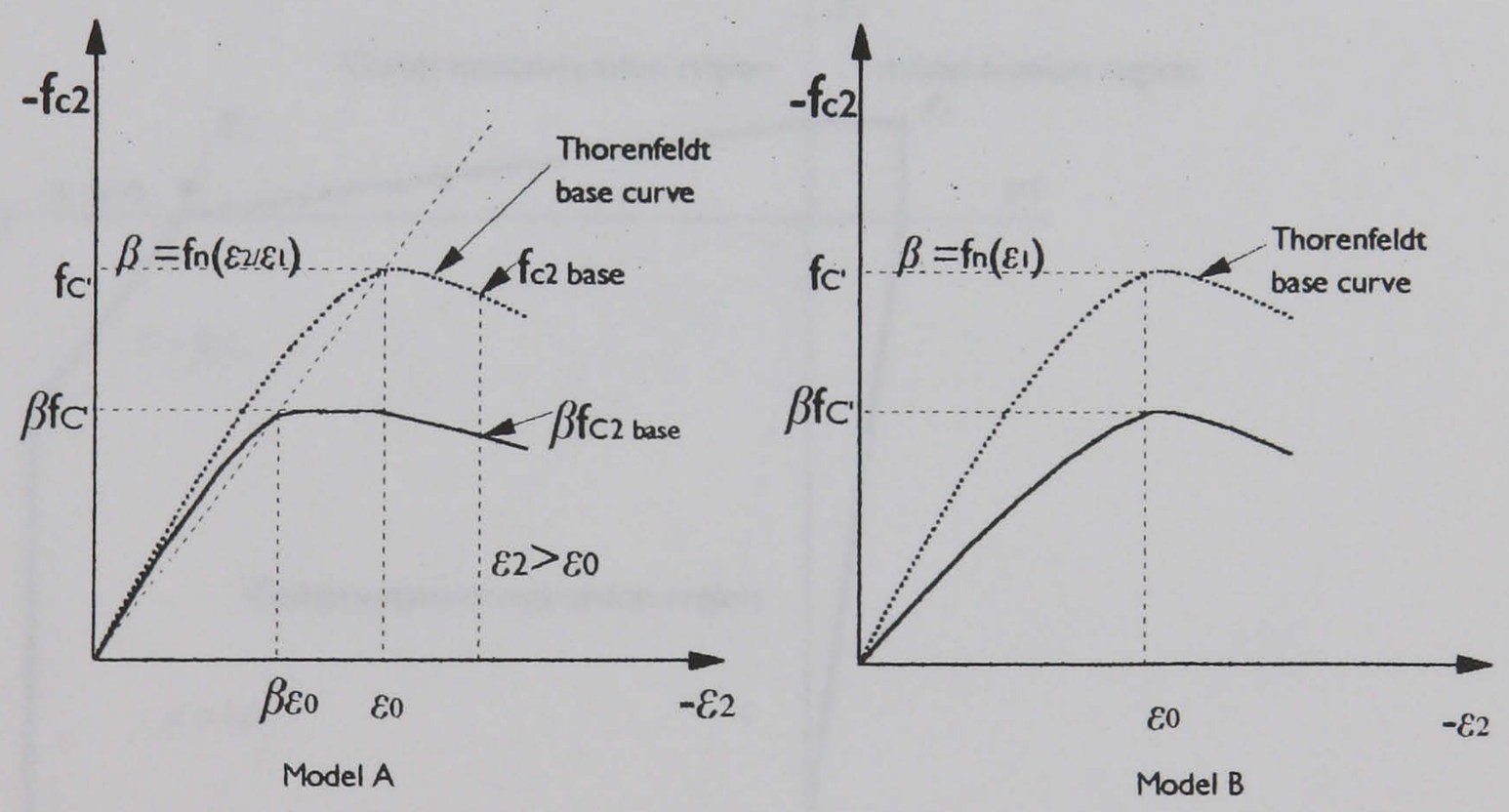

Fig.4.8- Compression softening model [32]

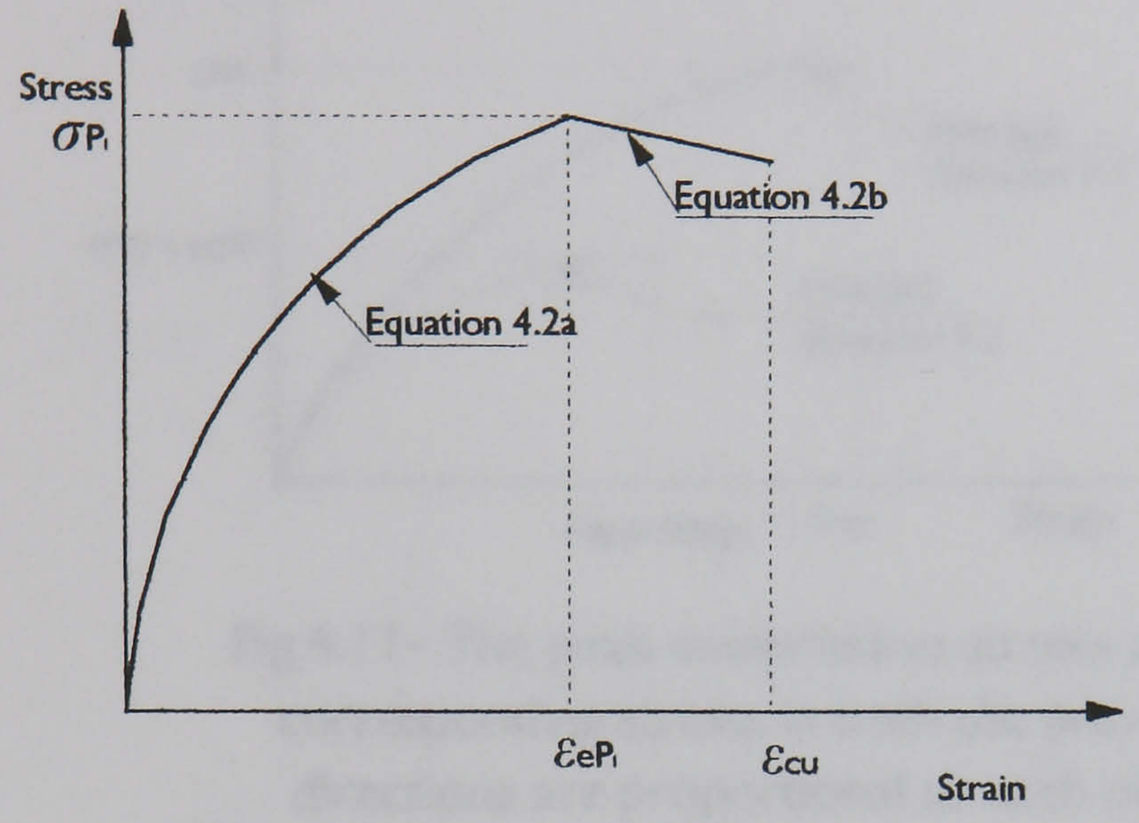

Fig.4.9- Stress-strain response of concrete in compression

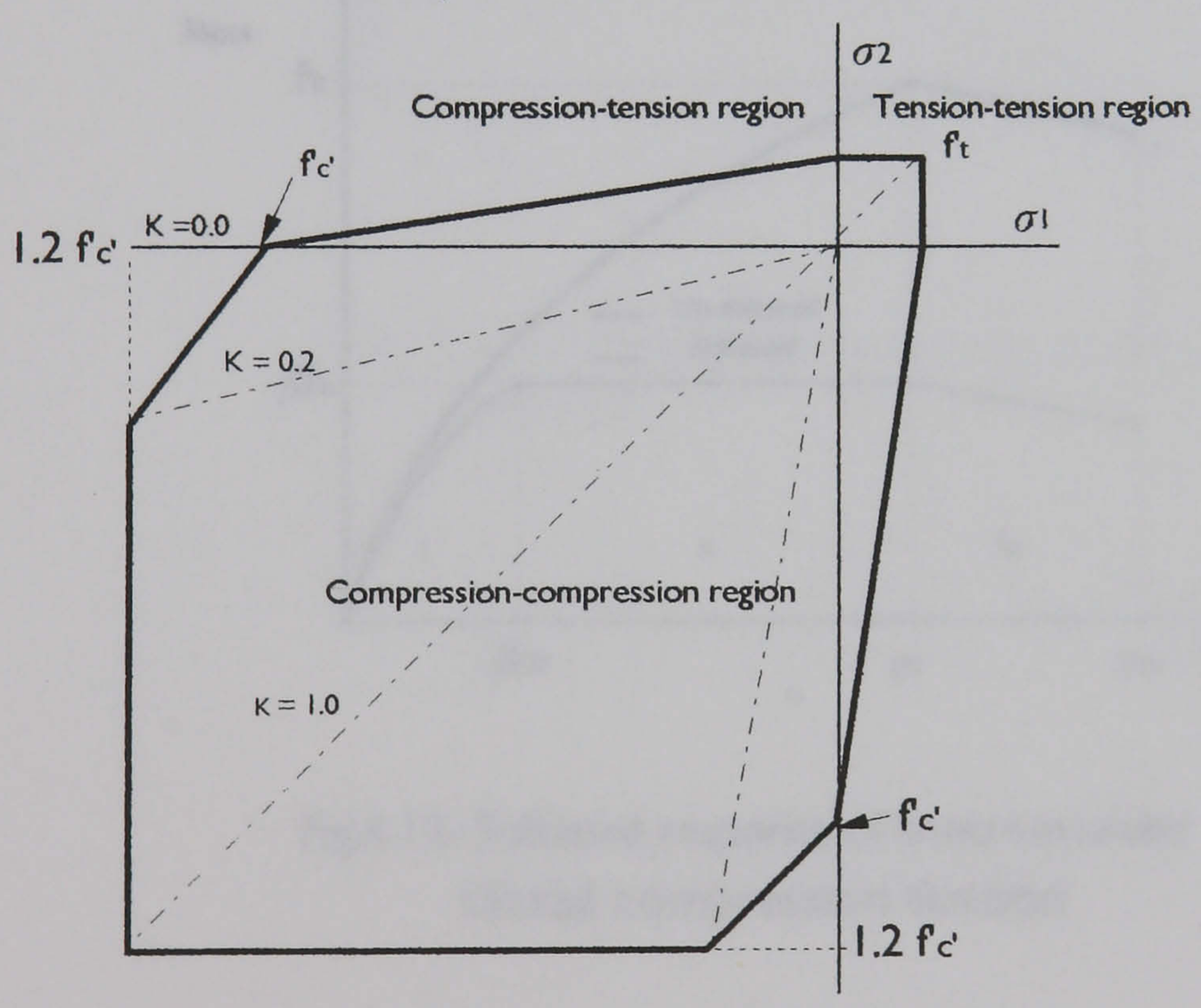

Fig. 4.10- Biaxial strength envelop used in the present study

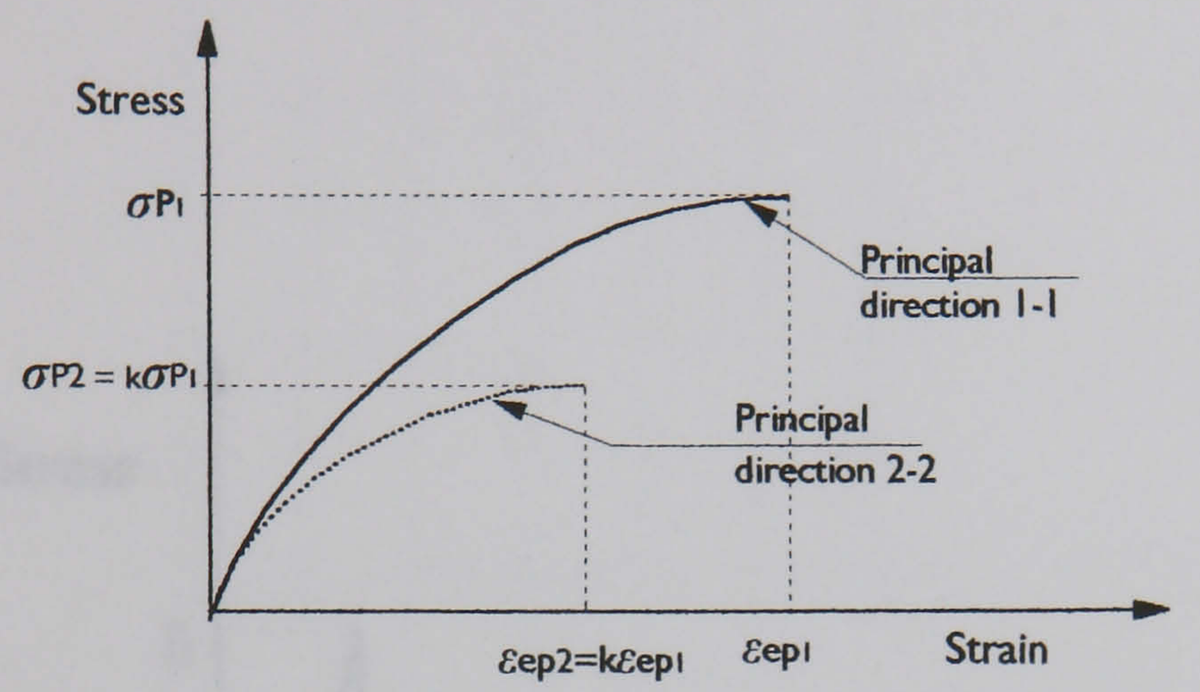

Fig.4.11- The peak compressive strsses and corresponding strains in both the principal directions are proportional to each other

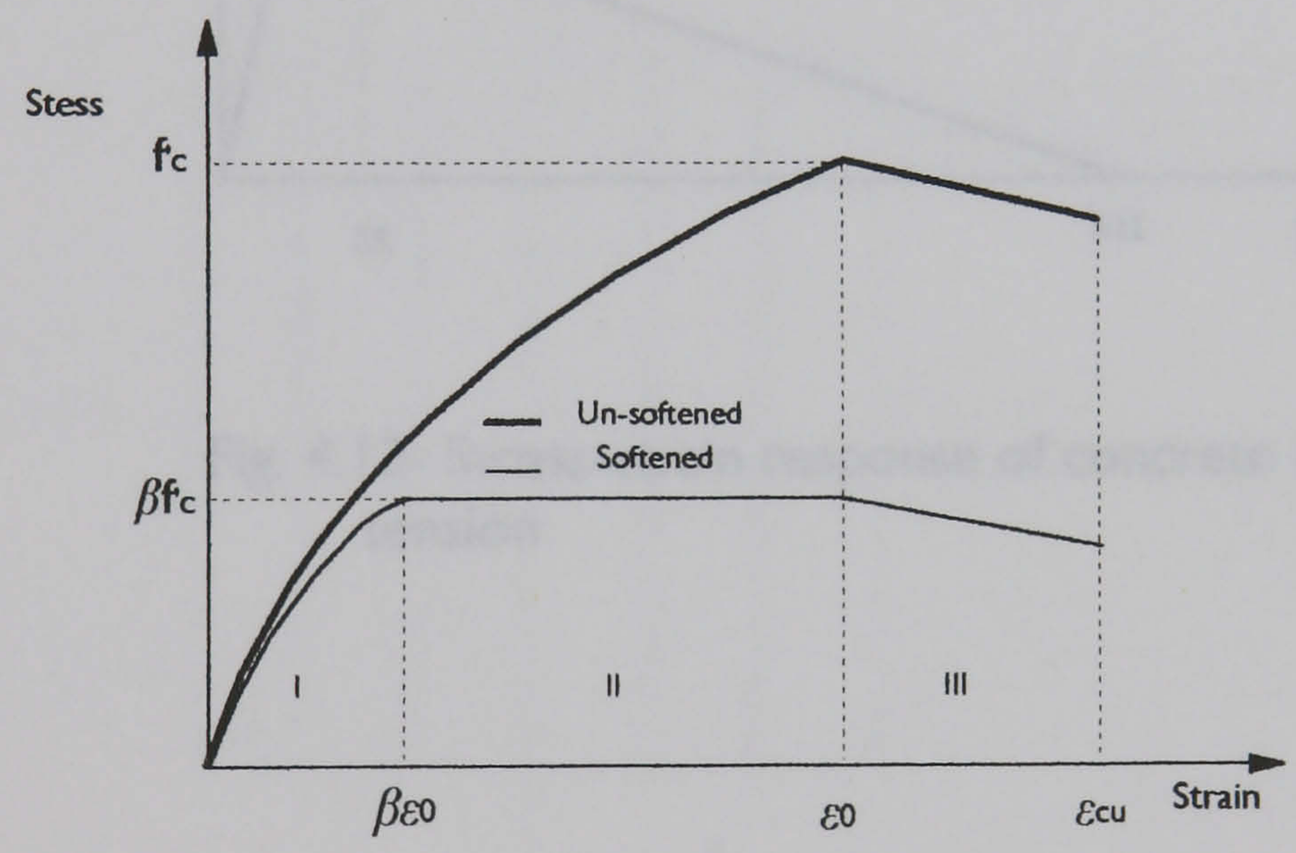

Fig.4.12- Softened response of concrete under biaxial compression tension

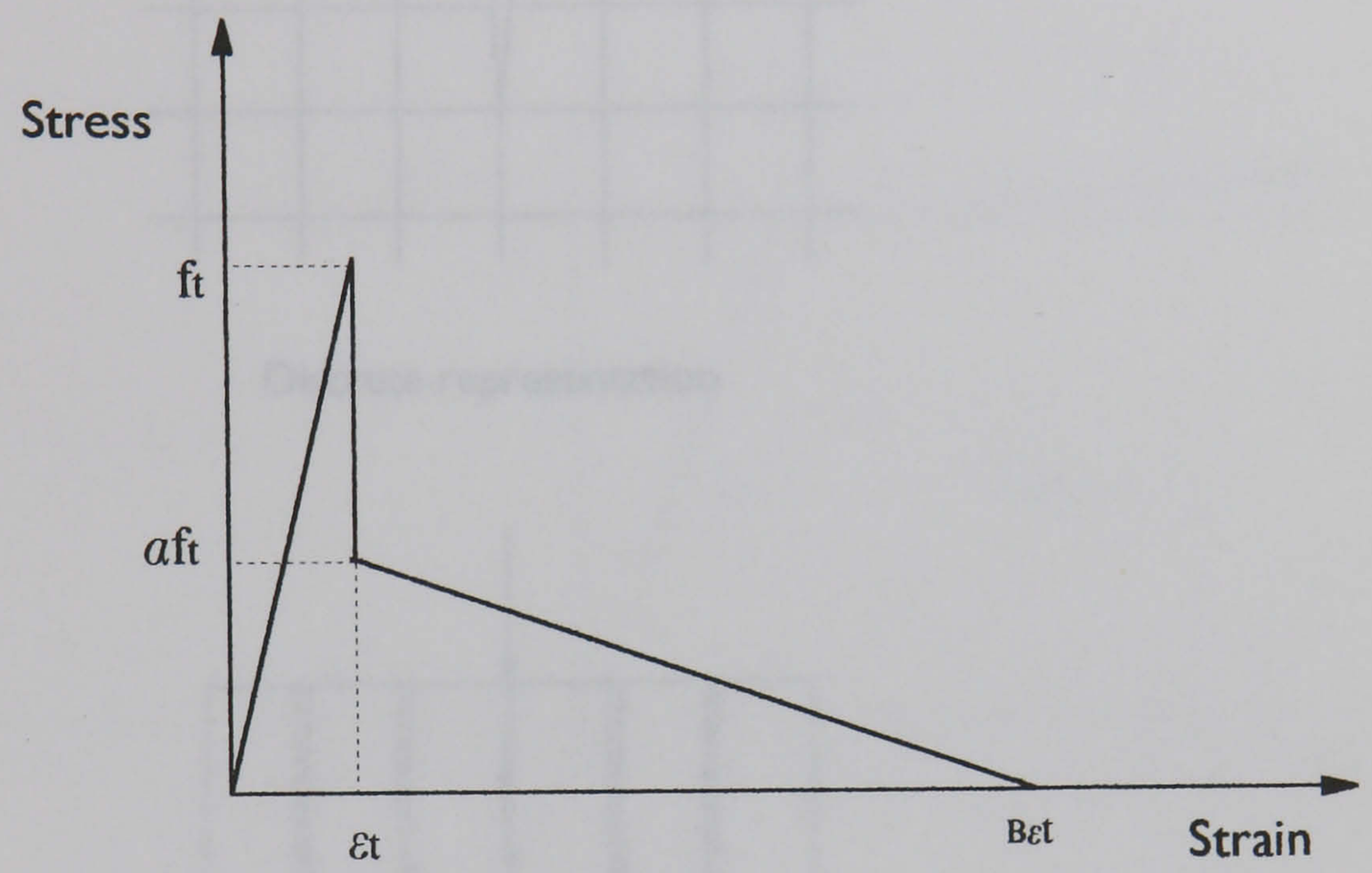

Fig. 4.13- Stress-strain response of concrete in tension

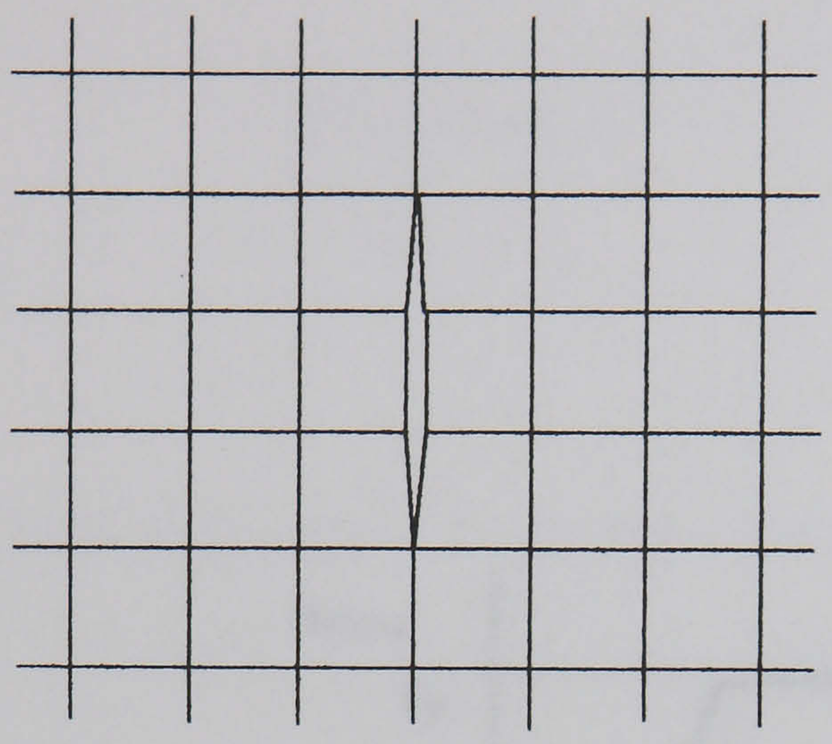

Discrete representation

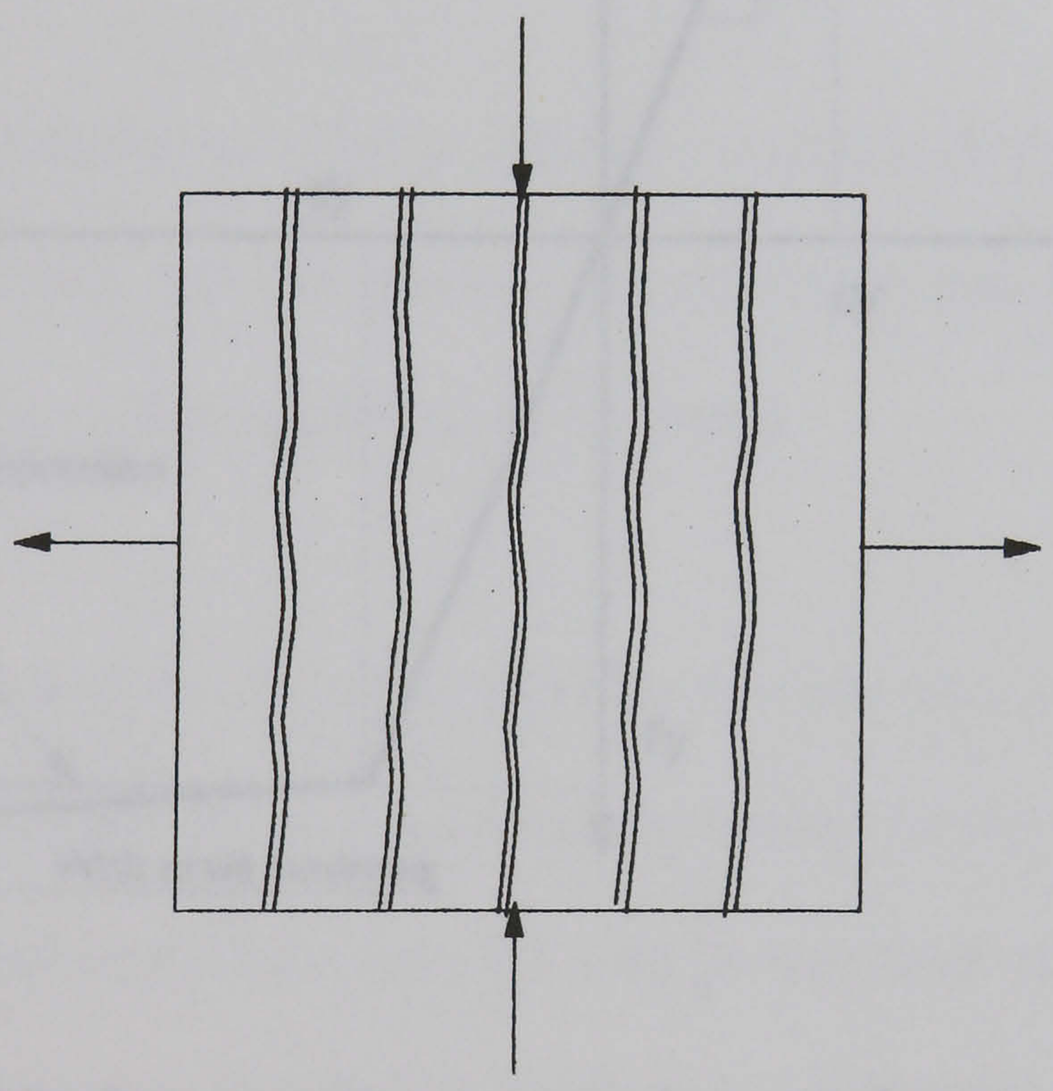

Smeared representation

Fig. 4.14- Discrete and smeared representation of a single crack

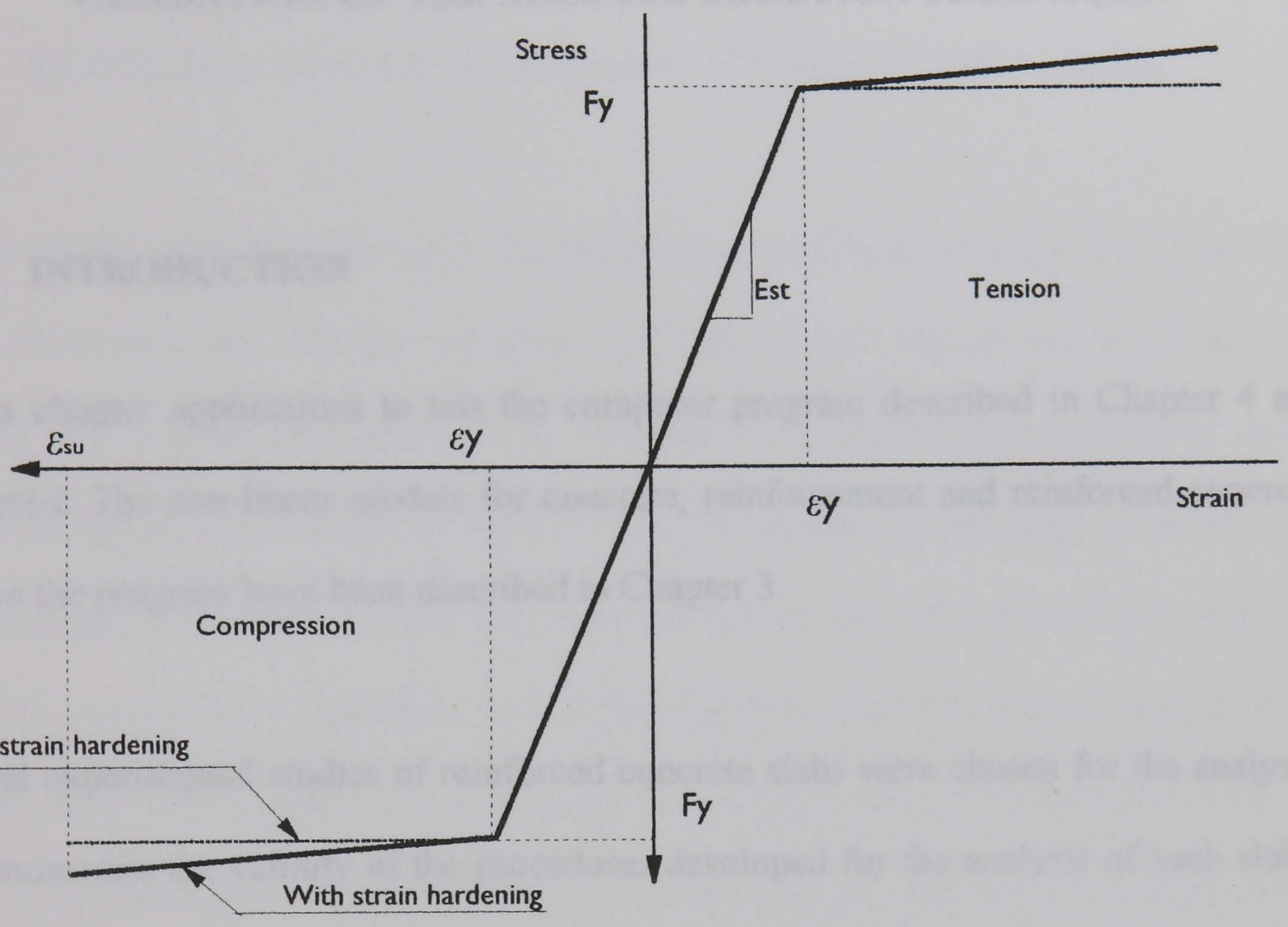

Fig.4.15- Stress-strain curve for reinforcing steel

CHAPTER 5

VALIDATION OF THE ADOPTED SOLUTION TECHNIQUE

5.1 INTRODUCTION

In this chapter applications to test the computer program described in Chapter 4 are presented. The non-linear models for concrete, reinforcement and reinforced concrete used in the program have been described in Chapter 3.

Several experimental studies of reinforced concrete slabs were chosen for the analyses to demonstrate the validity of the procedures developed for the analysis of such slabs. The first set of experimental data were for simply supported slabs under out-of-plane concentrated or uniformly distributed loads or combined out-of-plane uniformly distributed load and in-plane compressive load, and were taken from the tests carried out by various authors [1,2,3,5,6,7,8,9,10,11]. The second set of experimental works was conducted at the University of Toronto by Vecchio and Collins [12] and was concerned with the testing of concrete panels under in-plane shear and normal stress. The third set was chosen from the experiments carried out at the University of Toronto, by Marti et al.[13] and was concerned with the testing of slabs under pure twisting.

The load-deflection curve, cracking history, reinforcement yielding, ultimate load and mode of failure were recorded for the analysed slabs. A convergence tolerance between 0.003 and 0.005 for the displacements and 0.01 to 0.03 for the energy has been used for the different numerical examples in this Chapter.

5.2 REINFORCED CONCRETE SLABS ON SIMPLEY SUPPORTS.

A total of 100 experimental results for simply supported reinforced concrete slabs have been tabulated from different authors [1,2,3,5,6,7,8,9,10,11]. In order to test the program and to study the increase in the ultimate load resulting from membrane action effect and the parameters influencing it for simply supported slabs, eighteen slabs have been selected for the analysis from the above references. The selection has been made in order to ensure that the variables include loading type, slab slenderness, aspect ratio, reinforcement ratios in the two orthogonal directions, arrangement of reinforcement, design rule and type of simply support conditions. The material and section properties of the selected slabs are given in Table 5.1.

5.2.1 McNeice's slab.

A 914 mm x 914 mm x 44.5 mm square slab simply supported on four corners loaded with a central point load has been tested by McNeice [1]. The slab was symmetrically reinforced at the bottom only with a reinforcement ratio of 0.85% in both directions. The reinforcement was placed at 11.2 mm from the slab bottom. Because of symmetry

only a quarter of the slab has been considered for the analyses. The analysis was carried out for different meshes, different tension stiffness parameters and for different numbers of integration points through the depth. The experimental results and the analytical results using 3x3, 4x4, 5x5 and 6x6 meshes are shown in Fig. 5.1. The load-deflection curve obtained using 4x4 mesh was in good agreement with the experimental results through out the full response. 3x3, 5x5 and 6x6 meshes give good agreement up to 75% of the experimental ultimate load. However, at ultimate 3x3-mesh over-estimates the ultimate load by 11%, and 5x5 and 6x6 meshes are under-estimate the ultimate load by 8% and 8.5% respectively. The response of the slab has been found unchanged for a number of elements greater than 6x6, so the converged theoretical solution is assumed to be predicted by using 6x6 mesh. The cost of the computational time for 6x6 mesh was found to be increased by three times the computational time for 4x4 mesh.

Because 4x4 mesh is predicted close response to the experimental one at reasonable time and the difference between the response of a 4x4 mesh and 6x6 mesh is only 9.7% which is acceptably different. Then a 4x4 mesh was used to study the effect of the tension stiffening model and the number of integration points through the depth for the above slab. The experimental and the analytical results for different tension stiffening parameters and 9 integration points are shown in Fig. 5.2. The assumption of brittle failure for the concrete, B= 0, results in deflections being over-estimated with an average of 23 iterations per load increment. Improvement in the correlation of the experimental and analytical results can be seen when allowance is made for tension stiffening. The results obtained with the tension stiffening parameter, B= 20 and 9 integration points, gave acceptable agreement with the experimental results with

convergence obtained in an average of 16 iteration per load increment; however, when B=30 the load-deflection curve was too stiff in the post-cracking range.

The effect of the number of the integration points on the slab behaviour is illustrated in Fig.5.3. The greater the number of integration points, the more accurate the analysis, but an increase in the number of integration points means an increase in the computation time. Thus an optimum number of integration points is of vital importance. It can be observed from the figure that the load-deflection curve and the ultimate loads predicted using 9 and 15 integration points through the depth of the slab are almost the same. However, the ultimate load predicted using 9 and 15 integration points was 4% less than that with 7 integration points. Thus an optimum number of integration points through the depth of 9 has been chosen through out this study.

5.2.2 Hago's slabs.

Two square slabs with different simple support conditions and different steel arrangements were chosen from the six slabs tested by Hago [2,3]. The slabs were designed for point loads using the Wood and Armer rules [4], and the elastic stress distribution at ultimate load. The design moments used are given in table 5.2.

5.2.2.1 Slab No. 3.

Slab 3 was 2000 mm x 2000 mm x100 mm square, simply supported on four edges and designed for a total load of 210 kN., equally applied as four point loads. The loading system and the arrangement of the top and bottom reinforcement are shown in Fig. 5.4.

Because of the symmetry of the loads, a quarter of the slab was analysed using different meshes. The analytical result for different mesh sizes is shown in Fig.5.5. The number of elements used significantly influenced the time taken for the analysis. Comparison of the experimental and analytical results indicated that a 3x3 mesh gives a very stiff response. A 4x4 mesh gives an acceptable solution at a reasonable cost in computational time. The computational time increased by almost three times when a 6x6 mesh was used compared with a 4x4 mesh.

A displacement increment of 0.5 mm was adopted for the analysis. A maximum of 18 iterations was recorded during the analysis at the early stage of cracking, which took place at 0.34 of the design load. The bottom reinforcement yielded at 0.93 of the design load, whereas experimentally the reinforcement yielded at the design load. A ductile flexural failure occurred in both the test and the analysis. The loads from the test and the analysis using 4x4 mesh were 13% larger than the Wood and Armer load. This was probably caused by membrane action.

5.2.2.2 Slab No. 4.

Slab No. 4 was 2000 mm x 2000 mm x 100 mm square, with two adjacent edges simply supported and the opposite corner carried on a spherical support to achieve a point

support. The slab was designed for a total load of 90 kN., applied as two equal point loads. The arrangement of the reinforcement and the applied loads is shown in Fig. 5.6. Since the slab was not symmetrical a 6x6 finite element mesh was used over the entire slab.

A reasonably good agreement was obtained between the experimental and the analytical results as shown in Fig. 5.7. A displacement increment of 0.5 mm was fixed for the analysis and a maximum of 21 iterations was recorded in the increment in which cracking occurred, which took place at 0.19 of the Wood and Armer load. Yielding of the reinforcement started at approximately 90% of the Wood and Armer load. The mode of failure predicted was a ductile flexural failure. The numerical failure of the slab took place at approximately 98% of the experimental load. The increase in the ultimate load above the Wood and Armer load from the test and from the analysis was 12.5% and 3% respectively.

5.2.3 Bensalem's slabs.

Bensalem[5] tested six simply supported slabs. The slabs were designed for point loads using the Wood and Armer rules [4], with a non-elastic stress distribution at ultimate load to determine the area of the reinforcement required. The design moments used are given in table 5.2. Two slabs with different support conditions, aspect ratio, loading arrangement and different reinforcement were chosen for the analysis.

5.2.3.1 Slab S4.

Slab No. S4 was 2000 mm x 2000 mm x 100 mm square, simply supported on four edges and with a column support in the centre of the slab. The slab was designed for a total load of 320 kN, equally applied as four point loads. The arrangement of the reinforcement and the applied loads is shown in Fig. 5.8. Because of the symmetry only quarter of the slab was analysed using a 4x4 mesh.

Good agreement was obtained between the experimental and the analytical results prior to cracking which occurred at 0.26 of design load and at post cracking as shown in Fig. 5.9. The behaviour of the slab near to ultimate load was ductile as a result of yielding of the reinforcement, which took place at 0.98 of Wood and Armer load. The slab failed in flexure at about 1.42 of Wood and Armer load; however, experimentally the slab failed by punching shear at 1.48 of the Wood and Armer load. The increase in the ultimate load above the Wood and Armer load from the test and from the analysis was 40% and 36% respectively.

5.2.3.2 Slab S5.

This was a rectangular slab with clear dimensions of 3000 mm x 2000 mm x 100mm. The slab was designed for a total load of 210 kN, applied as eight equal point loads. The arrangement of the reinforcement and the applied loads is shown in Fig. 5.10. Since the slab was symmetrical only a quarter of the slab was analysed using a 4x4 finite element mesh.

Reasonably good agreement was obtained between the experimental and the analytical results, as shown in Fig. 5.11. The slab failed flexurally in a ductile manner. The experimental and the analytical failure of the slab took place at about 1.43 of the Wood and Armer load; however, near failure the analytical result was less stiff than the experimental one. The increase in the ultimate load above the Wood and Armer load from the test and from the analysis was 42% and 41% respectively.

5.2.4 Ghoneim's slabs.

An extensive experimental study of the behaviour of reinforced concrete slabs simply supported on four edges has been carried out by Ghoneim et al [6,7] at the University of Alberta. The slabs were subjected to out-of-plane uniformly distributed load only or combined in-plane compressive and out-of-plane uniformly distributed load. Three slabs subjected to combined in-plane compressive and out-of-plane uniformly distributed loads, and two slabs subjected to out-of-plane uniformly distributed load only were analysed. Table 5.3 gives the ratio of the applied in-plane load per unit width to the uni-axial strength of the concrete multiplied by the panel thickness for the analysed slabs. Also included in table 5.3 are the ratios of the applied in-plane load to the balanced load for the analysed specimen.

5.2.4.1 Slabs No. C1,C2 and C6.

Slabs C1,C2 and C6 were square slender slabs with clear dimensions of 1829 mm x 1829 mm x 67.8 mm; they were symmetrically reinforced at top and bottom with

0.383% of reinforcement in both directions. Slab C1 was tested under out-of-plane load only, slab C2, was tested under uniaxial compressive in-plane load and out-of-plane uniformly distributed load, and C6 was tested under biaxial in-plane compressive load and out-of-plane uniformly distributed load. Because of symmetry a 4x4 finite element mesh was used to model a quarter of the slabs.

Reasonably good agreement was obtained between the experimental and the analytical results as shown in Fig. 5.12. From the figure it is clear that in slab C1 there is a significant change in stiffness upon first cracking, which occurs at a load of 11.5 kPa.. The cause of such behaviour is associated with the sudden transfer of the force carried by concrete at the crack to the reinforcing bars. In slabs C2 and C6 cracks occur at loads of 22 kPa. and 30 kPa. respectively and there is no such significant change in stiffness; this is because the slabs are subjected to in-plane compressive loads over the whole depth, which delayed the formation of cracking. At ultimate, the failure of slab C1 was ductile failure as a result of yielding of the reinforcement which occur at a load of 65 kPa., while the failure of slabs C2 and C6 was caused either by compressive crushing of the concrete or by instability of the slabs. The increase in the ultimate load above the yield line theory load for the slab C1 from the test and from the analysis was 63%.

5.2.4.2 Slab model No. D1 and D2.

Slabs D1 and D2 were stocky square slabs with a clear dimension of 1829 mm x 1829 mm x 92.8 mm symmetrically reinforced at the top and bottom with 0.392% of steel in both directions. Slab D1 was tested under out-of-plane load only and D2 was tested

under combined uni-axial in-plane and out-of-plane loads. A 4x4 finite element mesh was used to model a quarter of the slab.

Reasonably good agreement was obtained between the experimental and the analytical results, as shown in Fig. 5.13. The initial responses up to cracking for the two slabs were similar. However, after cracking the load-deflection curve of slab D1 became progressively less stiff and exhibited progressively more ductile behaviour as a result of the extensive yielding of the reinforcement. Slab D2, conversely, demonstrated a stiffer response in the beginning but at ultimate the theoretical behaviour was ductile as a result of yielding of the reinforcement which occurred at load about 110 kPa.; however, experimentally, the slab failed by brittle failure caused by crushing of the concrete. The increase in the ultimate load above the yield line theory load for the slab D1 from the test and from the analysis was 20% and 18% respectively.

5.2.5 Taylor's slabs.

Tests on 10 two-way spanning, simply supported slabs subjected to uniformly distributed load have been reported by Taylor et al.[8]. The slabs were designed with using either the strip method or yield line theory for similar ultimate loads of 8 tons. Different arrangements of the reinforcement were adopted. The slab slenderness was also varied. Two slabs were chosen for analysis from this group.

5.2.5.1 Slab No.S1.

Slab S1 was a 1981 mm x 1981 mm x 50.8 mm square slab reinforced at the bottom only with a reinforcement ratio of 0.46% in the *x*-direction and 0.394% in the *y*-direction, arranged as shown in Fig. 5.14a. A 4x4 finite element mesh was used to model a quarter of the slab.

The experimental and analytical results are shown in Fig. 5.14b. The experimental and the analytical results are in good agreement prior to cracking which occurs at load of 42 kN and up to ultimate load At ultimate load the slab behaviour was ductile as a result of yielding of the reinforcement which occurred at 119 kN. The increase in the ultimate load above the design load from the test and from the analysis was 66%.

5.2.5.2 Slab No.S8.

Slab No. S8 was a 1981mm x 1981mm x 44.45mm slab designed using the strip method and reinforced at the bottom only. The reinforcement was 4.77 mm diameter arranged as shown in Fig.5.15a. A 4x4 finite element mesh was used to model a quarter of the slab.

Reasonably good agreement was obtained between the experimental and the analytical results through out the load-deflection curve, as shown in Fig. 5.15b. The percentage increase in the ultimate load above the design load caused by membrane action from the test and from the analysis was 57%.

5.2.6 Brotchie's slabs.

Forty five slabs were tested by Brotchie et al. [9]; four of them were simply supported on four edges and the rest were restrained slabs. All slabs carried uniformly distributed loads and were either unreinforced or reinforced at the bottom only with smooth steel wire uniformly and equally distributed in each direction. The tests were mainly to investigate the increase in the ultimate load capacity resulting from either compressive or tensile membrane action. The parameters varied in the tests were reinforcement ratio and slenderness ratio. Two of the simply supported slabs were chosen to be analysed.

5.2.6.1 Slab No. 8.

Slab S8 was a 400 mm x 400 mm x 19 mm symmetrically reinforced at the bottom only, with 1% of steel in both directions. The reinforcement was placed at 4.8 mm from the bottom of the slab. A 4x4 finite element mesh was used to model a quarter of the slab.

Good agreement was obtained between the analytical and the experimental load-deflection curve, Fig.5.16. The behaviour of the slab near collapse was ductile caused by yielding of the reinforcement which occurred at a load of about 0.2 MPa. The increase in the ultimate load above the yield line theory load from the test and from the analysis was 7%.

5.2.6.2 Slab No. 12.

Slab 12 was a 400 mm x 400 mm x 38.1 mm, symmetrically reinforced at the bottom only with 1% of reinforcement at both directions. The reinforcement was placed at 5

mm from the bottom of the slab. A 4x4 finite element mesh was used to model a quarter of the slab.

Reasonably good agreement of the experimental and the analytical load-deflection curve was obtained, Fig. 5.17. The failure mode of both numerically and experimentally was a brittle failure caused by crashing of the concrete at a load equal to the yield line theory load. There was no increase in the ultimate load above the yield line theory load for this slab.

5.2.7 Sawczuk's slabs.

Three rectangular slabs were tested by Sawczuk et al.[10], under a uniformly distributed load, in order to investigate the post yield behaviour for a simply supported rectangular slabs. Two slab with different steel ratios were analysed

5.2.7.1 Slab No.1.

Slab No.1 was a rectangular slab with clear dimensions 2000 mm x 1000 mm x 30 mm reinforced at bottom only with reinforcement ratio of 0.907% in both directions placed at 4 mm from the bottom of the slab. A 4x4 finite element mesh was used to model a quarter of the slab.

A reasonably good agreement was obtained between the experimental and the analytical results as shown in Fig. 5.18. The slab behaviour was ductile and failed in flexure as a

result of yielding of the reinforcement at an ultimate load 10% less than the experimental ultimate load. The increase in the ultimate load above the yield line theory load from the test and from the analysis was 24% and 14% respectively.

5.2.7.2 Slab No.2

Slab No.2 was the same as slab No.1 except that the percentage of reinforcement was 0.453% in both directions. A 4x4 finite element mesh was used to model quarter of the slab.

The behaviour of the slab was similar to slab No.1. A reasonably good agreement was obtained between the experimental and the analytical results, Fig. 5.19. The slab failed at a load 10% less than the experimental ultimate load. The increase in the ultimate load above the yield line theory load from the test and from the analysis was 51% and 41% respectively.

5.2.8 Desayi's slabs.

Twelve rectangular slabs were tested by Desayi et al. [11] under uniformly distributed load. The variables in the tests were the slab slenderness, aspect ratio and steel ratio. The object of the tests was the study of the complete load-deflection behaviour of simply supported rectangular reinforced concrete slabs. Two slabs from this group were analysed.

5.2.8.1 Slab S4.

Slab S4 was a rectangular slab with clear dimensions of 1270 mm x 1020 mm x 50.8 mm reinforced at the bottom only with steel ratio of 0.25% in both directions. Because of the symmetry a 4x4 finite element mesh was used to model quarter of the slab.

Reasonably good agreement was obtained between the experimental and the analytical load-deflection results, Fig. 5.20. The increase in the ultimate load above the yield line theory load caused by membrane action from the test and from the analysis was 61%.

5.2.8.2 Slab T4.

Slab T4 was a rectangular slab with clear dimensions of 1270 mm x 1020 mm x 38.2 mm reinforced at bottom only with steel ratio of 0.33% in both directions. Because of the symmetry a 4x4 finite element mesh was used to model quarter of the slab.

Reasonably good agreement was obtained between the experimental and the analytical results as shown in Fig. 5.21. The increase in the ultimate load above the design load from the test and from the analysis was 62% and 56% respectively.

5.3 REINFORCED CONCRETE PANELS UNDER PURE SHEAR.

An extensive experimental study of the behaviour of reinforced concrete panels under in-plane shear and normal stresses has been carried out by Vecchio and Collins [12].

Results of this study revealed that a reduction of the concrete compressive strength, dependent on the transverse tensile strain after cracking, occurs. These findings can be used to improve substantially the capability of finite element models to predict the ultimate load of reinforced concrete members, which fail in compression-tension as a result of, for example, shear and torsion.

The panels were tested in a specially designed loading rig capable of applying in-plane shear and direct tension or compression loading Fig. 5.22. The specimens were loaded by forces applied to shear keys uniformly distributed around the perimeter of the panel. If the applied forces were slightly inclined to the plane of the rig, they would have tended to push the panel out of the testing plane. Hence, a lateral support frame was provided to resist any out-of-plane forces and therefore the displacement perpendicular to the plane of the rig was restrained along the perimeter of the panel.

The panels were 890 mm x 890 mm x 70 mm symmetrically reinforced with two layers of wire mesh typically at 50 mm centres, of various diameters. The steel wires were aligned parallel to the sides of the panel. A clear cover of 6mm was provided between faces of the panel and the outer layer of the reinforcement.

Five panels were analysed. The selection of the panels has been made in order to ensure different loading cases including pure shear, combined shear and biaxial tension and combined shear and biaxial compression, and to ensure different areas of reinforcement in the longitudinal and transverse directions in case of pure shear. Table 5.4 gives the material and section properties and the loading of such panels.

The finite element model used one element, because the stresses are uniformly distributed throughout the panel. The finite element mesh, boundary conditions and loading arrangement used in the analysis are shown in Figs. 5.23a and 5.23b.

Figs. 5.24-5.28 show the comparison between the experimental and analytical results. The analytical and the experimental results of such slabs agreed well in terms of ultimate load, failure mode, pre-cracking stiffness and post cracking deformation. Generally the panels failed in a ductile shear failure, caused by the yielding of either the longitudinal or transverse reinforcement prior to failure.

5.4 REINFORCED CONCRETE PANELS UNDER PURE TWISTING.

Nine square slabs with clear dimensions of 1700 mm x 1700 mm x 200 mm were tested by Marti et al [13] at the University of Toronto, under pure torsion with varying amounts of steel in the two orthogonal directions. A summary of the material and section properties is given in Table 5.5.

The loading arrangement to apply torsion was that the three corners of the slab were on supports which gave restraint against translation in the vertical direction but were free to rotate. A downward load was applied to the fourth corner. This set-up led to a loading condition in which two sets of equal and opposite vertical forces, P, were applied at the two corners of the panel as shown in Fig. 5.29. The forces were transferred through hanger roads and spherical bearing to the centre of 25 mm x 150 mm x 150 mm, with steel plates clamped to the corners of the panel. The weight of the panel, *W*, was

supported at corners A and C. It was assumed that this type of loading would produce uniform twisting through out the slab.

The self-weight of the panel is considered in the finite element analysis and only quarter of the panel has been modelled using 4x4 elements. The finite element mesh and boundary conditions used in the analysis are shown in Fig. 5.30.

Figs. 5.31-5.38 shows the comparison between the experimental and analytical results for eight of the nine slabs. Slab No.1 failed abruptly at corner and repeated under No.7 by using a supplementary reinforcement in the z-direction along the edges of the specimen. A reasonably good agreement was obtained between the experimental and the analytical results prior to cracking post cracking and at ultimate. Panels 2,4, and 7, shown in Figs.5.32, 5.34 and 5.37, failed abruptly because of brittle corner failure close to ultimate load during the tests.

5.5 CONCLUSION

The computer program described in Chapter 3 has been used to simulate the behaviour of simply supported reinforced concrete slabs subjected to out-of-plane, point load or uniformly distributed loads only or combined out-of-plane uniformly distributed load and in-plane uniaxial or biaxial compression. The analytical results from the program have been compared with experimental results from the tests on slabs loaded as described above and good agreement has been obtained throughout the full load deflection of the slabs.

Slabs subjected to out-of-plane point loads or uniformly distributed loads carried loads much higher than those predicted by the methods used for the design, such as the Wood and Armer rules, the strip method or yield line theory. This is attributed to the tensile membrane action effect, which develops with increasing deflection. The increase of the ultimate load was found to be dependent on slenderness of the slab, aspect ratio of the slab and the area of the reinforcement. The variation of the ultimate load above the design load was found to vary between 66% for square slender slab with $\frac{L}{d}$ = 36 and reinforcement ratio of 0.46 in x-direction and 0.394% in y-direction to zero for stocky square slab with $\frac{L}{d}$=15 and 1% of reinforcement in both directions.

The effect of the in-plane compressive load on the lateral load capacity is found to be dependent on the slenderness of the slab. For stocky square slabs, the presence of the in-plane load increased the lateral load capacity, while it results in a substantial reduction in the lateral load capacity of slender slabs.

The program has also been used to analyse reinforced concrete slabs subjected to in-plane shear, combined in-plane shear and bi-axial tension, combined in-plane shear and bi-axial compression and torsion. The analytical results were also in good agreement with the experimental results obtained from slabs under such loading conditions.

5.6 REFERENCES

1. McNeice G. M. and Kemp K. O., "Comparison of finite element and unique limit analysis solution for certain reinforced concrete slabs", Proceedings of the Institute of Civil Engineers, Vol. 43, 1969, pp.629-640.

2. Hago A W., "Direct design of reinforced concrete slabs", PhD Thesis, Glasgow University, 1982.

3. Hago A. W. and Bhatt P., "Tests on reinforced concrete slabs designed by direct design procedure", ACI Journal, November-December 1986, pp 916-924.

4. Wood R. H., "The reinforcement of slabs in according with a predetermined field of moments", Concrete, London, Vol. 2, February 1968, pp 69-76.

5. Bensalem A., "Direct design of reinforced concrete structures using non-elastic stress fields", PhD Thesis Glasgow University, 1993.

6. Ghoneim M. G. and MacGregor J. G., "Test of reinforced concrete plates under combined in-plane and lateral loads", ACI Structural Journal. January-February 1994, pp 19-30.

7. Ghoneim M. G. and MacGregor J. G., "Behaviour of reinforced concrete plates under combined in-plane and lateral loads", ACI Structural Journal. March-April 1994, pp 188-197.

8. Taylor R., Maher D. R. H. and Hayes B., "Effect of arrangement of reinforcement on the behaviour of reinforced concrete slabs", Magazine of Concrete Research, Vol. 98, 1966, pp.85-94.

9. Brotchie J. F. and Holley M. J., "Membrane action in slabs", Cracking, Deflection and Ultimate Load of Concrete Slab Systems, SP-30, ACI, Detroit, 1971, pp. 345-377.

10. Sawzuck A. and Winnick L., "Plastic behaviour of simply supported plates at moderately large deflections", International Journal of Solids and Structures. Vol. 1, No. 1, February 1965, pp. 97-111.

11. Desay P. and Kulkarni A. B., "Load deflection behaviour of simply supported rectangular reinforced concrete slabs", Proc. Int. Asso. Bridge and Structural Engg. 1, P-11/78, February 1978, p.1-16.

12. Vecchio F. and Collins M. P., "The response of reinforced concrete panels to in-plane shear and normal stress", Publication No. 82-03, Department of Civil Engineering, University of Toronto, March 1982. 332p.

13. Marti P., Leesti P. and Khalifa W.U., "Torsion test on reinforced concrete slab elements", Jnl. of St. Eng., ASCE, Vol. 113, No. 5, May 1987, pp 994-1010.

Table 5.1 Section and material properties of simply supported slabs.

Reference	$L_x\ mm$	$L_y\ mm$	$h\ mm$	$f_c^{'}\ MPa.$	$f_y\ MPa.$
McNeice [1]	914	914	44.5	32.4	345
Hago [2,3] S3	2000	2000	100	44.2	460
Hago [2,3] S4	2000	2000	100	37.3	473
Bensalem [5] S4	2000	2000	100	58.77	477
Bensalem [5] S5	2000	3000	100	59.26	477
Ghoenim [6,7] C1,C2 and C6	1829	1829	67.8	25.21	450
Ghoenim [6,7] D1 and D2	1829	1829	92.8	26.12	450
Taylor [8] S1	1981.2	1981.2	50.8	35.5	381.6
Taylor [8] S8	1981.2	1981.2	44.45	38.5	381.6
Brothie [9] S8	400	400	19.05	30.9	421.8
Brothie [9] S9	400	400	38.1	29.5	386.7
Sawczuk [10] S1	1000	2000	30	17.5	269
Sawczuk [10] S2	1000	2000	30	17.5	269
Desayi [11] S4	1020	1270	50.8	24	555
Desayi [11] T4	1020	1270	50.8	24	555

Table 5.2- Wood and Armer [1,2] design moments

Moment at bottom	Moment at top
$M_x^* = M_x + \lvert M_{xy} \rvert$ and $M_y^* = M_y + \lvert M_{xy} \rvert$	$M_x^* = M_x - \lvert M_{xy} \rvert$ and $M_y^* = M_y - \lvert M_{xy} \rvert$
if $M_x^* < 0$,then $M_x^* = 0$ and $M_y^* = M_y + \left\lvert \frac{M_{xy}^2}{M_x} \right\rvert$	if $M_x^* > 0$,then $M_x^* = 0$ and $M_y^* = M_y - \left\lvert \frac{M_{xy}^2}{M_x} \right\rvert$
if $M_y^* < 0$ then, $M_y^* = 0$ and $M_x^* = M_x + \left\lvert \frac{M_{xy}^2}{M_y} \right\rvert$	if $M_y^* > 0$,then $M_y^* = 0$ $M_x^* = M_x - \left\lvert \frac{M_{xy}^2}{M_x} \right\rvert$

Table 5.3- Levels of applied in-plane loads for Ghoneim et. al.[6,7]

Specimen	$\frac{N_x}{f_c' h}$	$\frac{N_y}{f_c' h}$	$\frac{N_x}{N_x\, balanced}$	$\frac{N_y}{N_y\, balanced}$
C1	0.0	0.0	0.0	0.0
C2	0.0	0.383	0.0	1.089
C6	0.384	0.383	1.096	1.164
D1	0.0	0.0	0.0	0.0
D2	0.0	0.365	0.0	1.04

Table 5.4- Material properties and loading ratio of Vecchio and Collins [12] panels.

No.	PV.9	PV.22	PV.26	PV.27	PV.28
$F_x : F_y : F_{xy}$	0:0:1	0:0:1	0:0:1	0.83 :0.83 :1	-0.32: -0.32:1
$A_{sx}\ mm^2/mm$	0.625	0.625	0.625	0.625	0.625
$A'_{sx}\ mm^2/mm$	0.625	0.625	0.625	0.625	0.625
$A_{sy}\ mm^2/mm$	0.625	0.532	0.355	0.625	0.625
$A'_{sy}\ mm^2/mm$	0.625	0.532	0.532	0.625	0.625
$f'_c\ MPa.$	11.6	19.6	21.3	20.5	19.0
$f_t\ MPa.$	1.38	2.42	2.0	2.04	1.66
$f_y\ MPa.$	455	458	456	442	483

Table 5.5- Material properties of Marti et al. [13] panels.

No.	2	3	4	5	6	7	8	9
$A_{sx}\ mm^2/mm$	1	2	1	2	2	0.5	2	2
$A'_{sx}\ mm^2/mm$	1	2	0.5	0.5	1	0.5	0.5	2
$A_{sy}\ mm^2/mm$	1	2	0.5	0.5	1	0.5	0.5	2
$A'_{sy}\ mm^2/mm$	1	2	0.5	0.5	1	0.5	0.5	2
$f'_c\ MPa.$	36.2	37.5	44.7	35.6	23.3	44.4	49.1	44.4
$f_t\ MPa.$	3.72	3.35	4.65	3.38	2.78	4.39	4.51	3.9
$f_y\ MPa.$	551	481	551	516	516	479	446	412

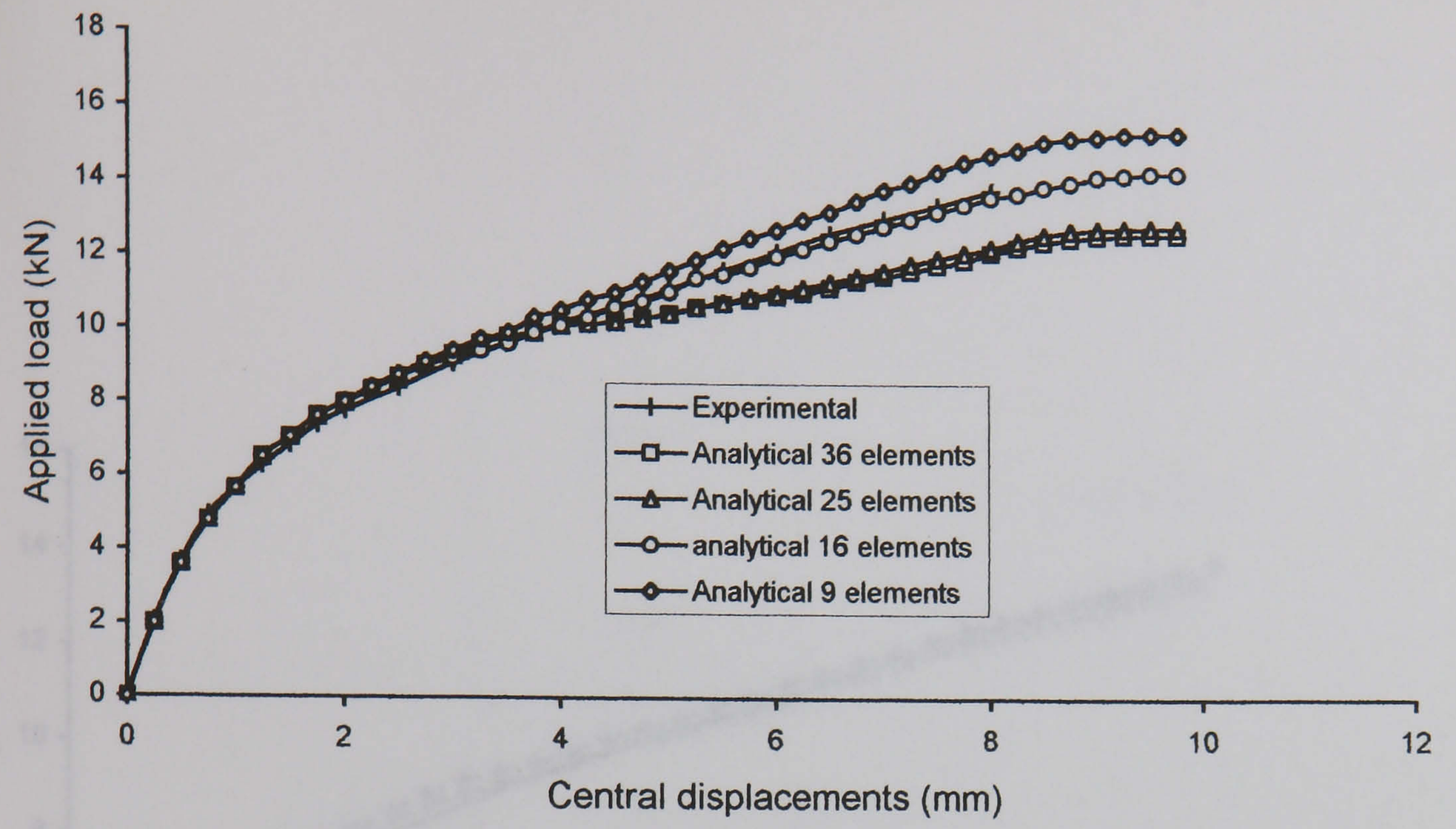

Fig. 5.1-Comparison of experimental and analytical results of McNeice slab [1] for different mesh size

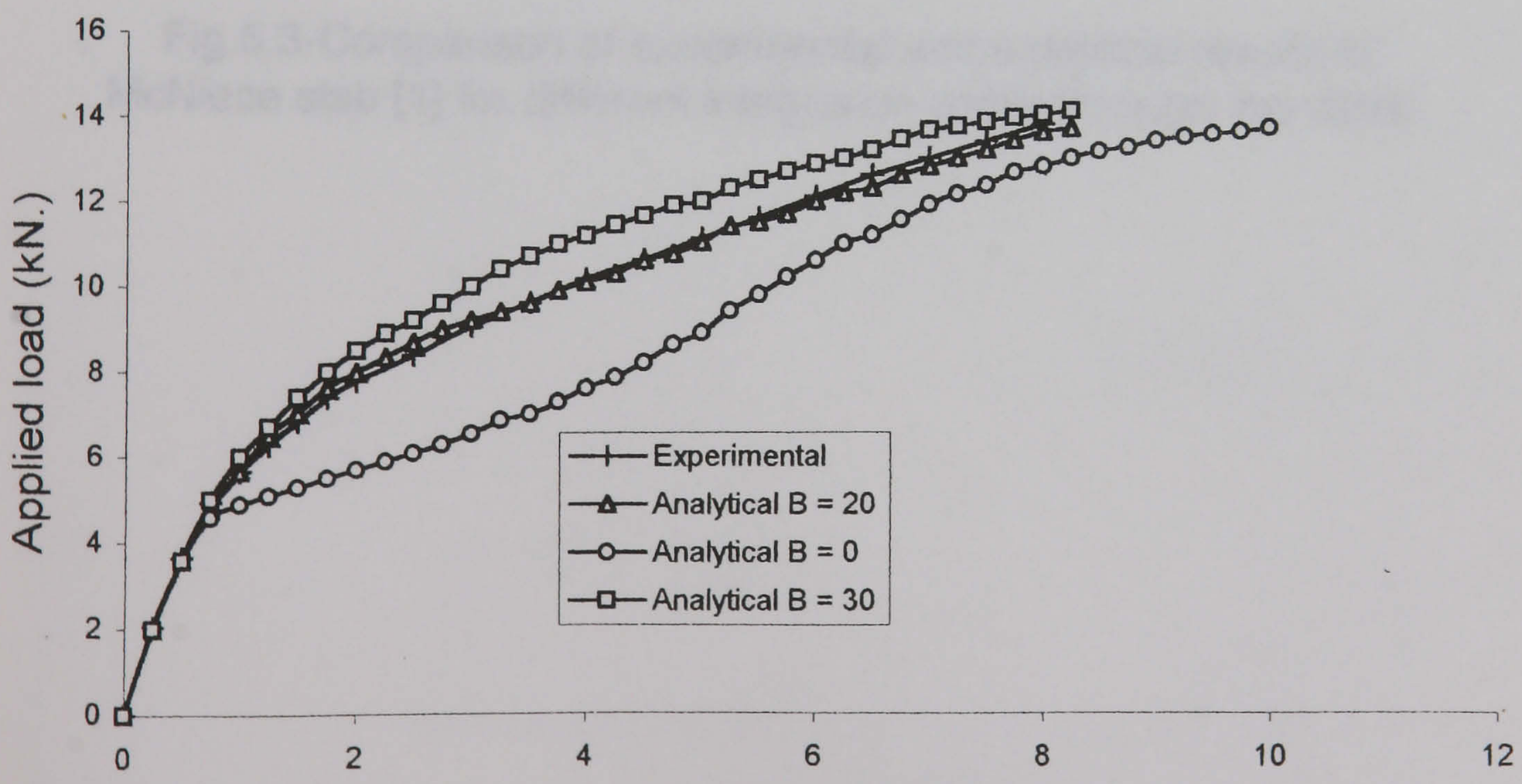

Fig.5.2-Comparison of analytical and experimental results of McNeice slab [1] for different tension stiffness

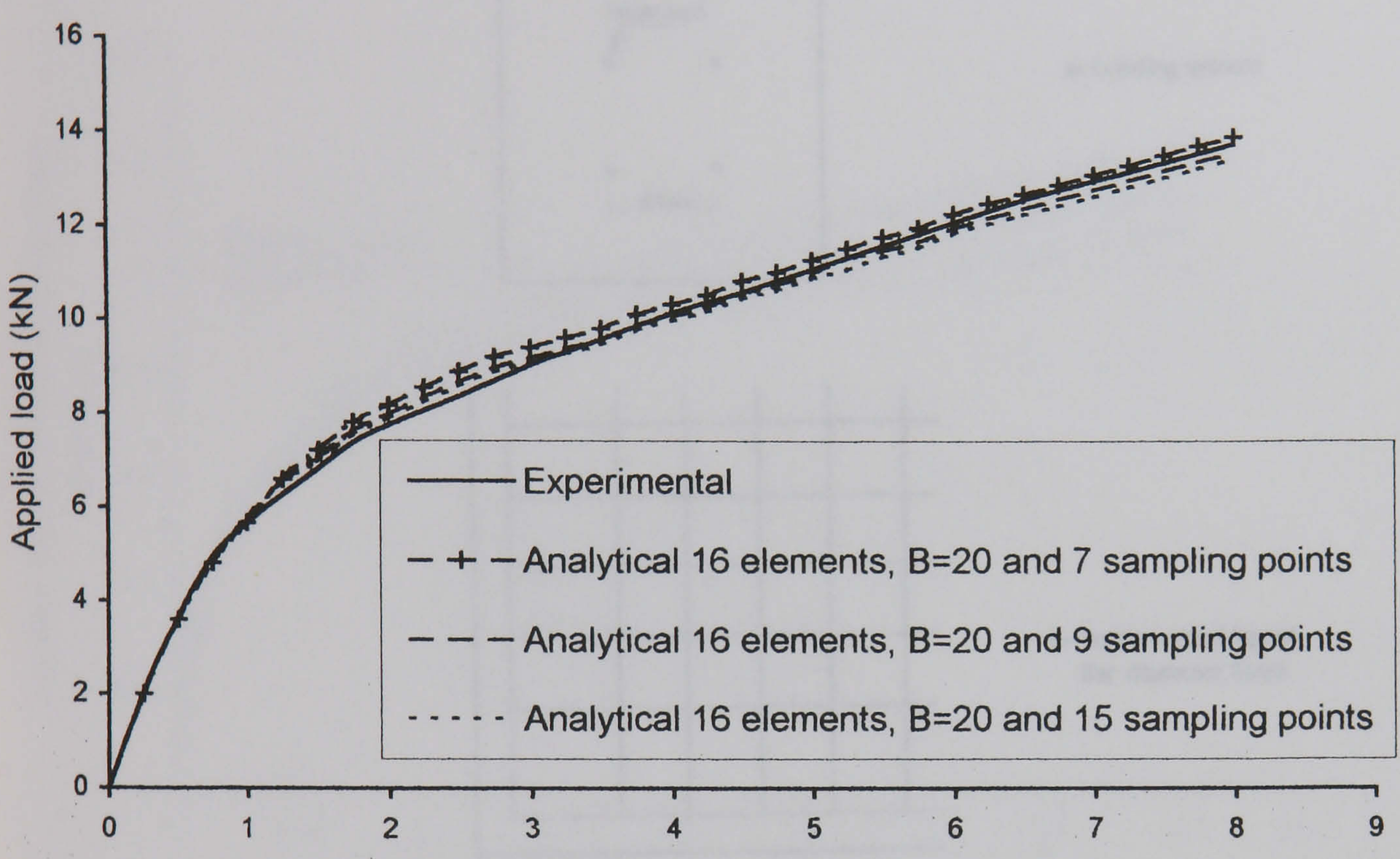

Fig.5.3-Comparison of experimental and analytical results of McNiece slab [1] for different integration points through the depth.

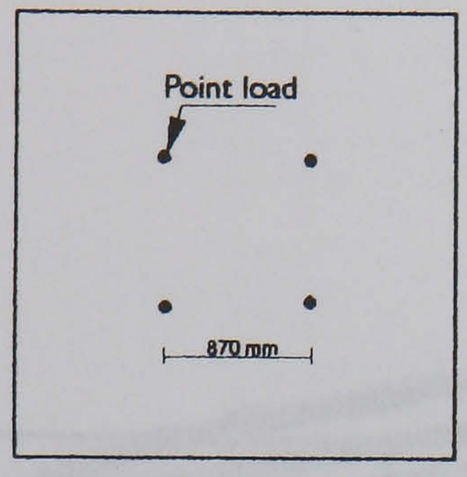

a- Loading system

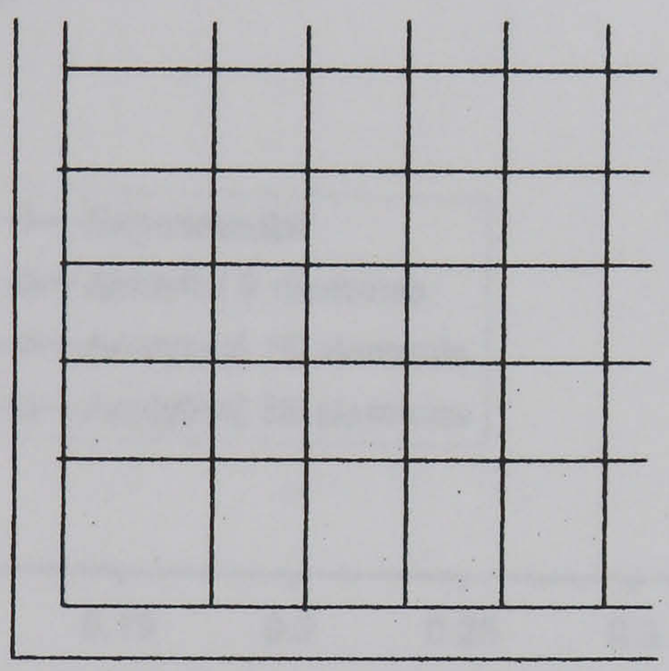

b- Bottom steel layout
Bar diameter 8mm

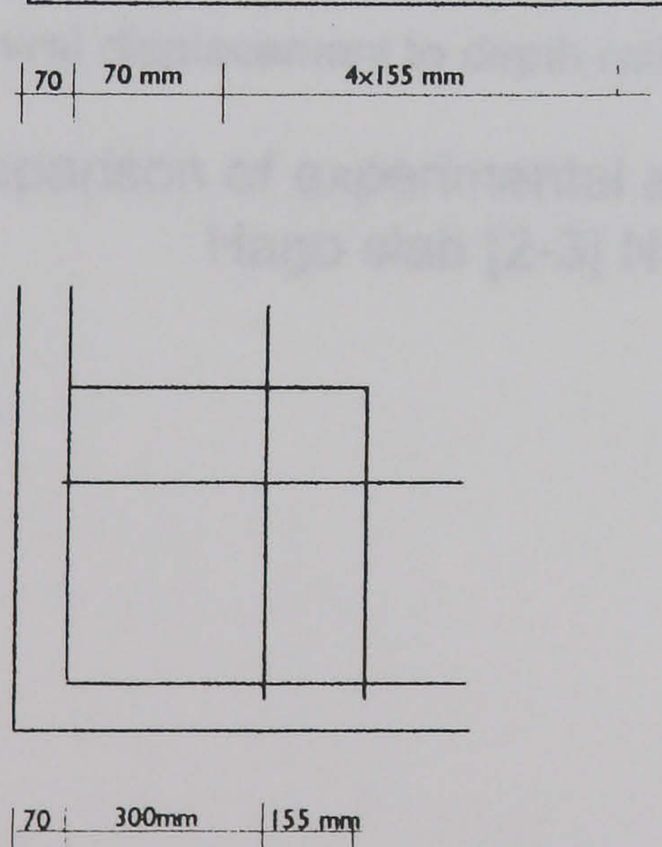

c- Top steel layout
Bar diameter 8mm

Fig.5.4- Loading conditions and steel layout for Hago's [3] slab No.S3

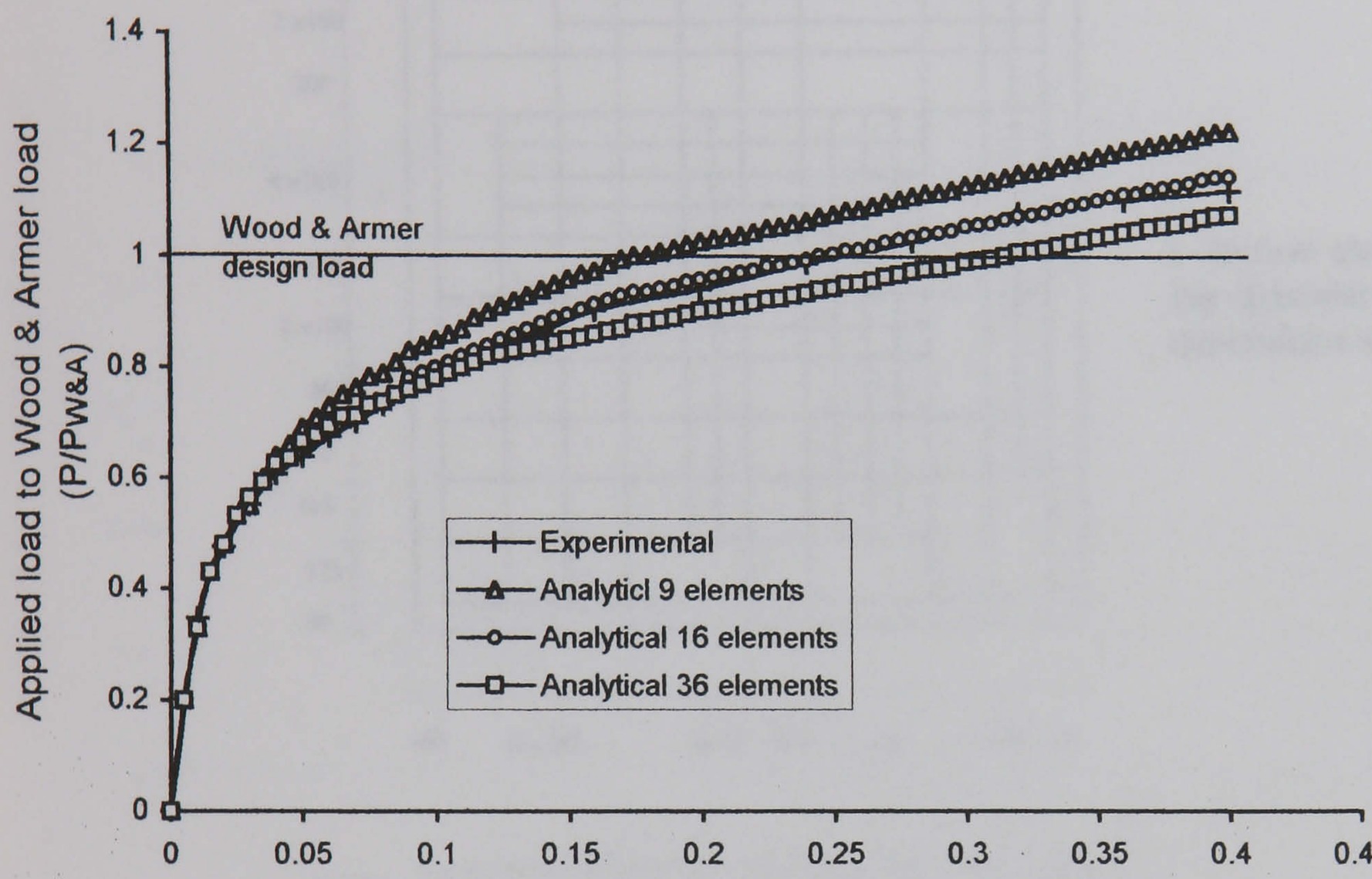

Fig.5.5-Comparison of experimental and analytical results of Hago slab [2-3] No. 3

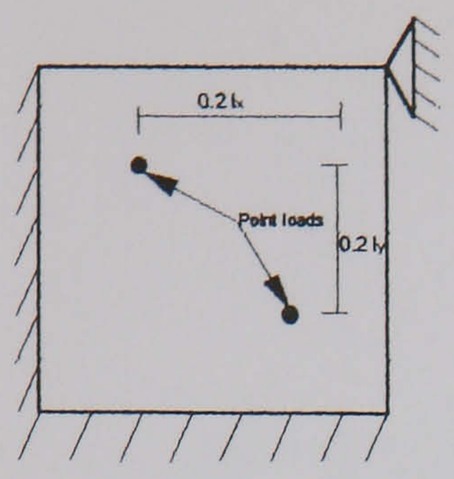

a- Loading conditions

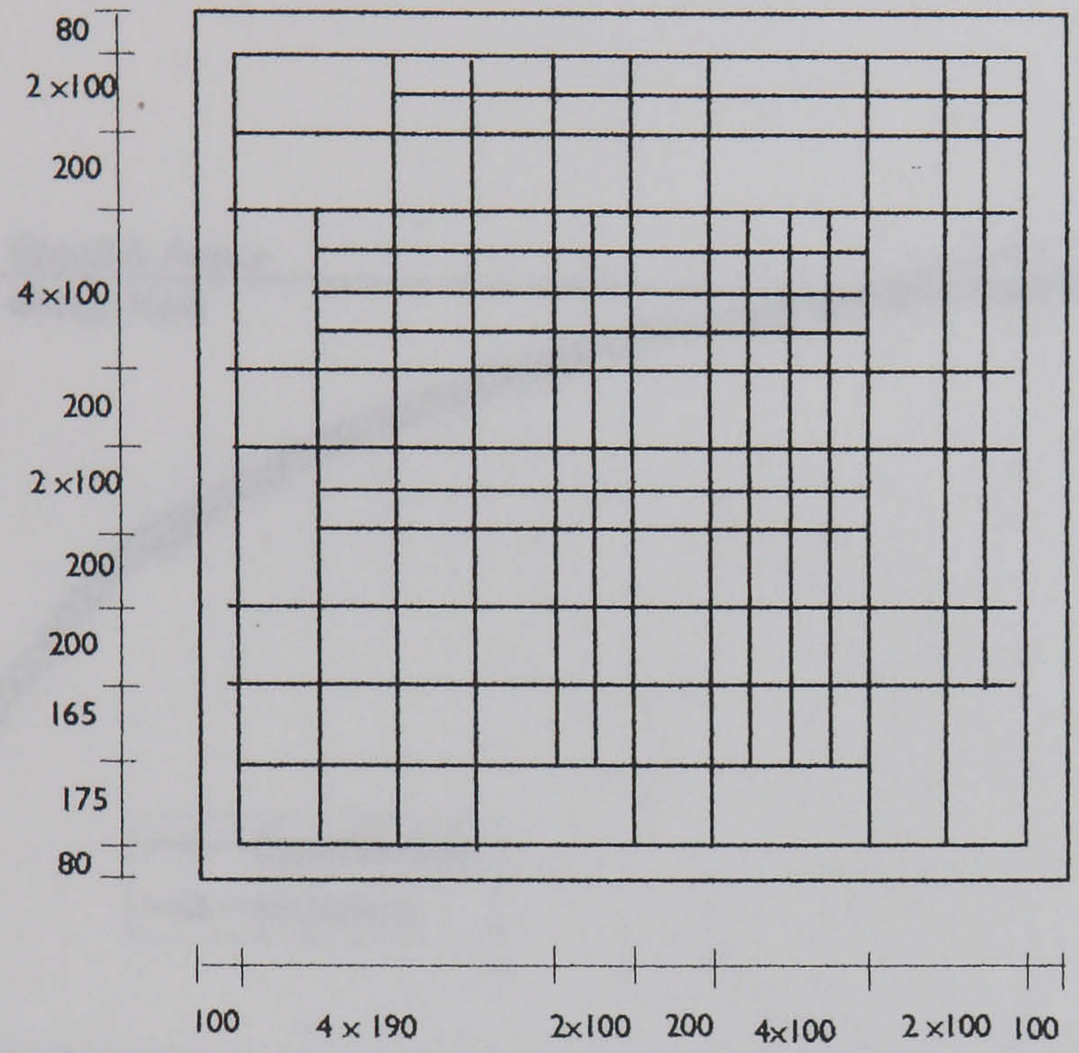

b- Bottom steel layout
Bar diameter 8 mm all
dimensions in mm

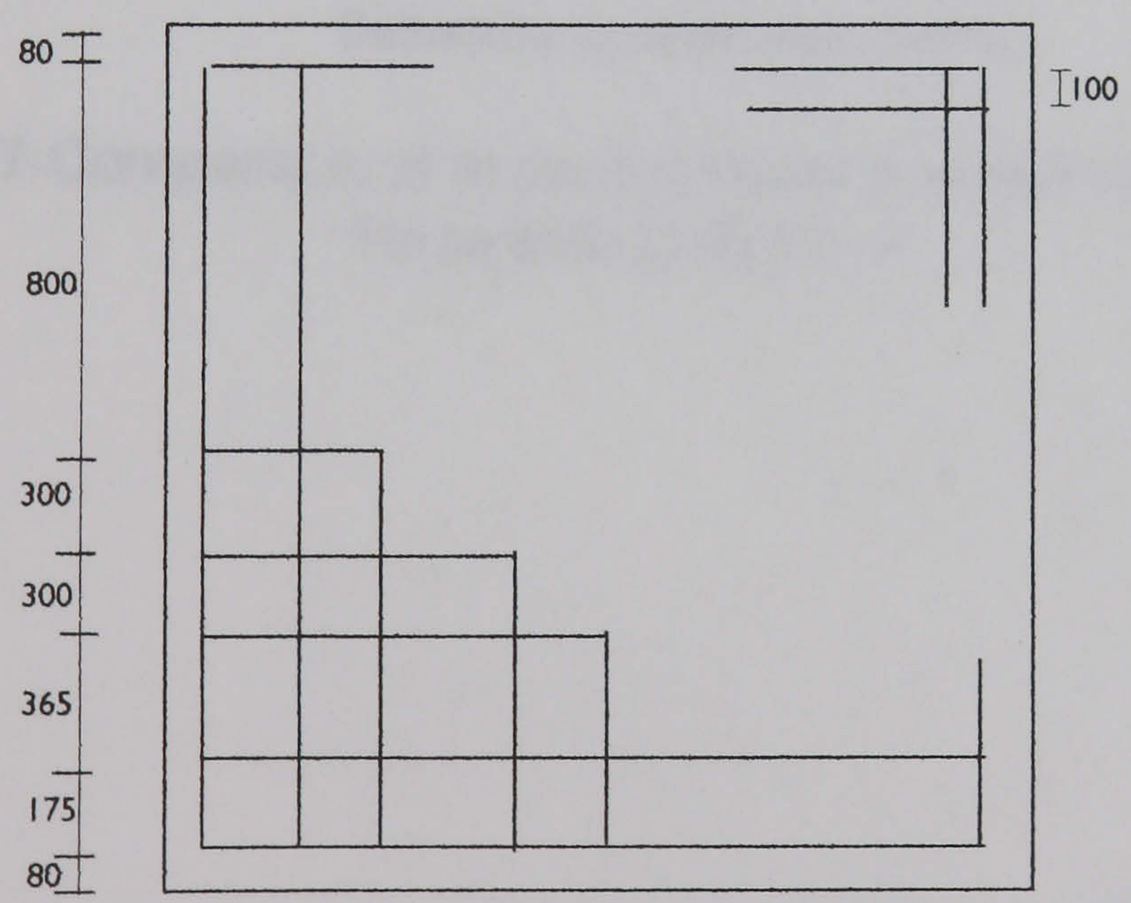

c- Top steel layout
Bar diameter 8 mm
all dimensions in mm

Fig. 5.6-Loading conditions and steel layout of Hago's [3] slab No.4.

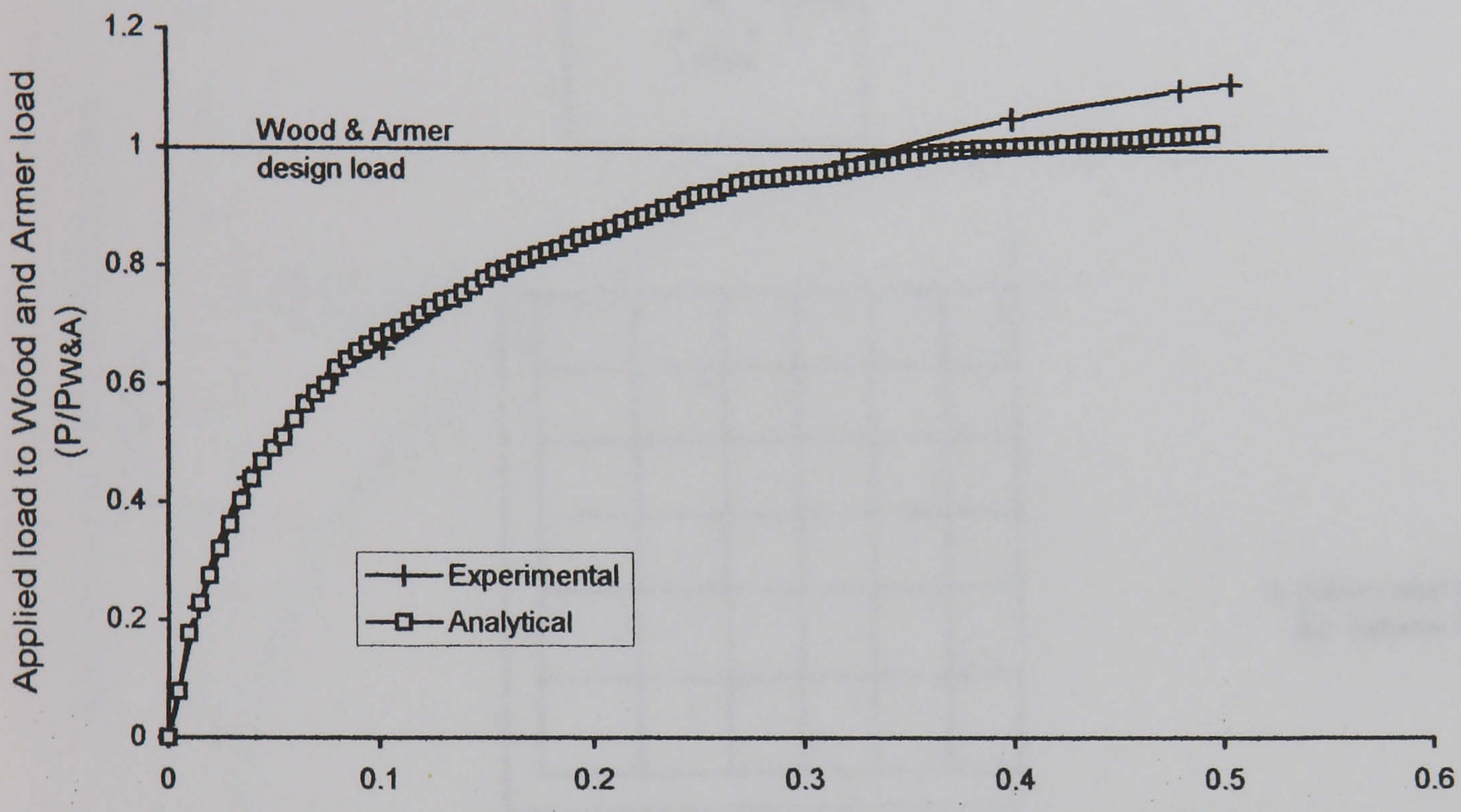

Fig.5.7-Comparison of experimental and analytical results of Hago slab [2-3] No. 4.

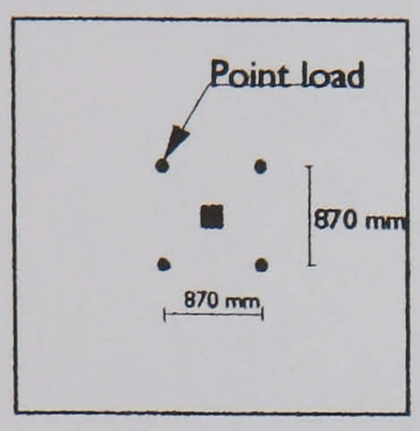

a- Loading conditions

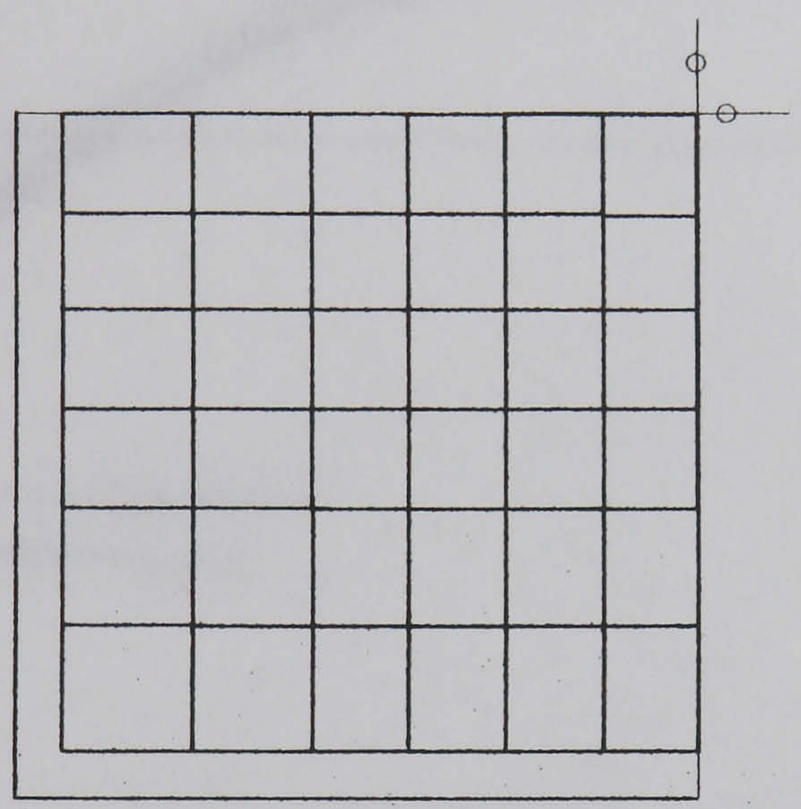

b- Bottom steel layout
Bar diameter 8mm

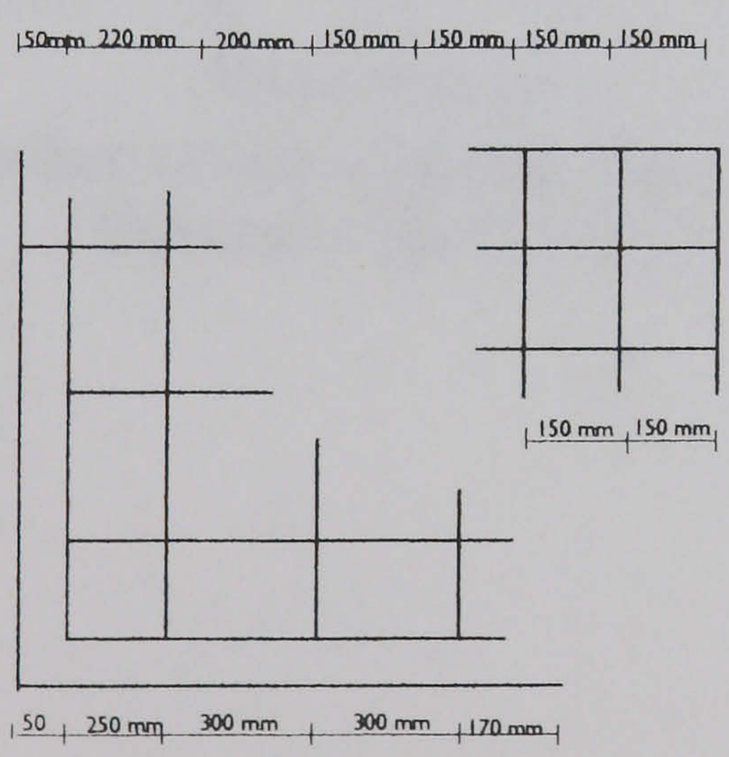

c- Top steel layout
Bar diametre 6mm

Fig.5.8- Loading conditions and steel layout for
Bensalem's [5] slab model S4.

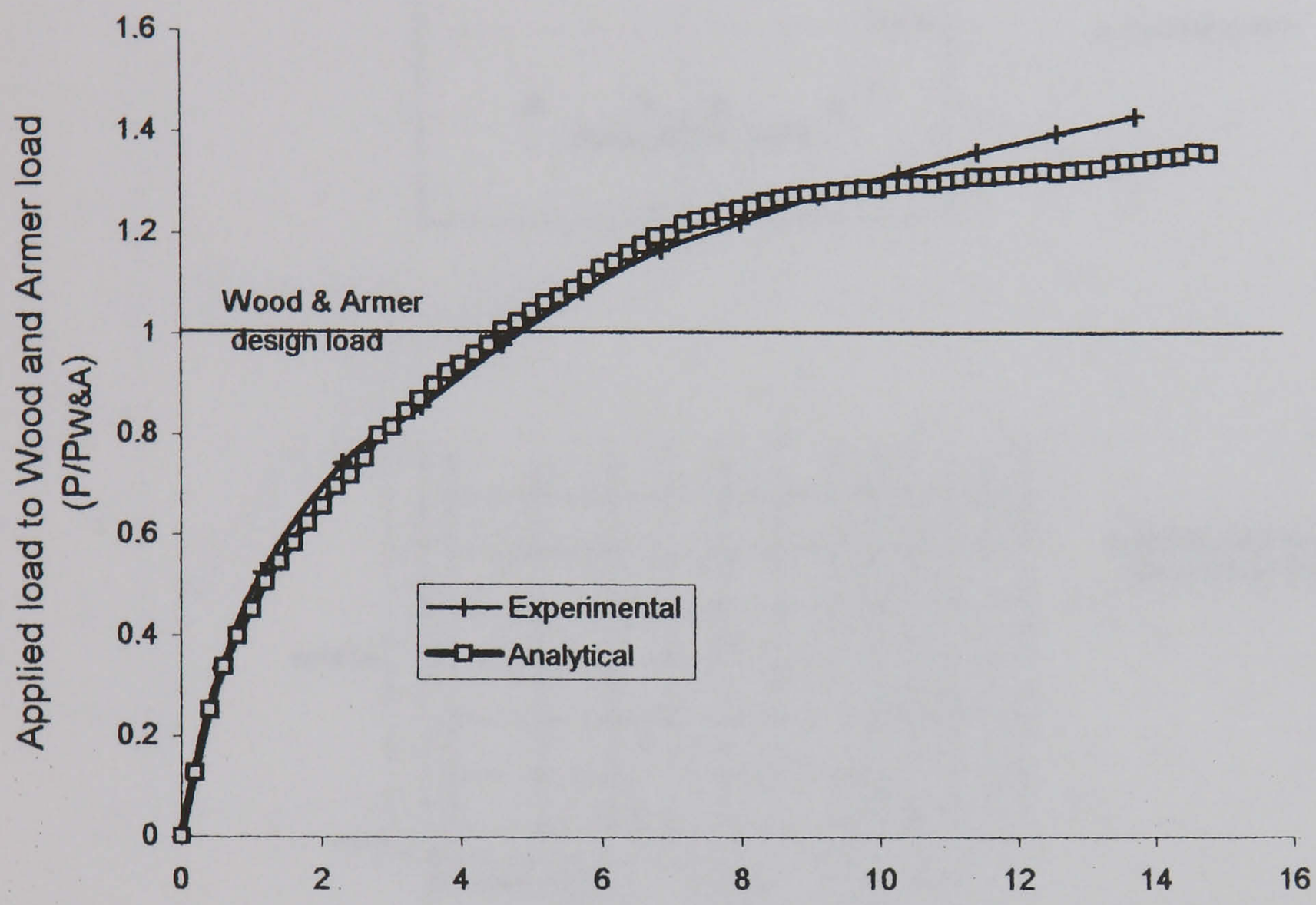

Fig.5.9-Comparison of experimental and analytical results of Bensalem slab [5] No. 4.

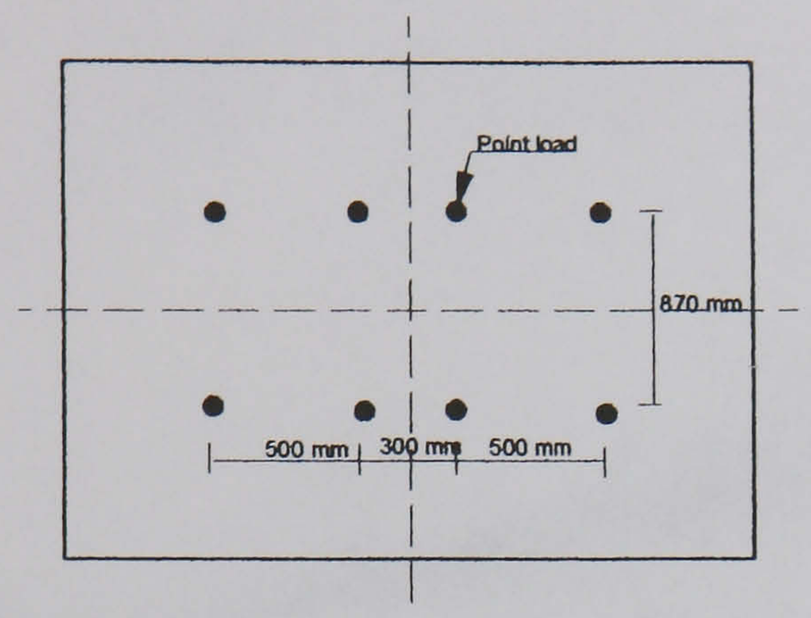

a- Loading system

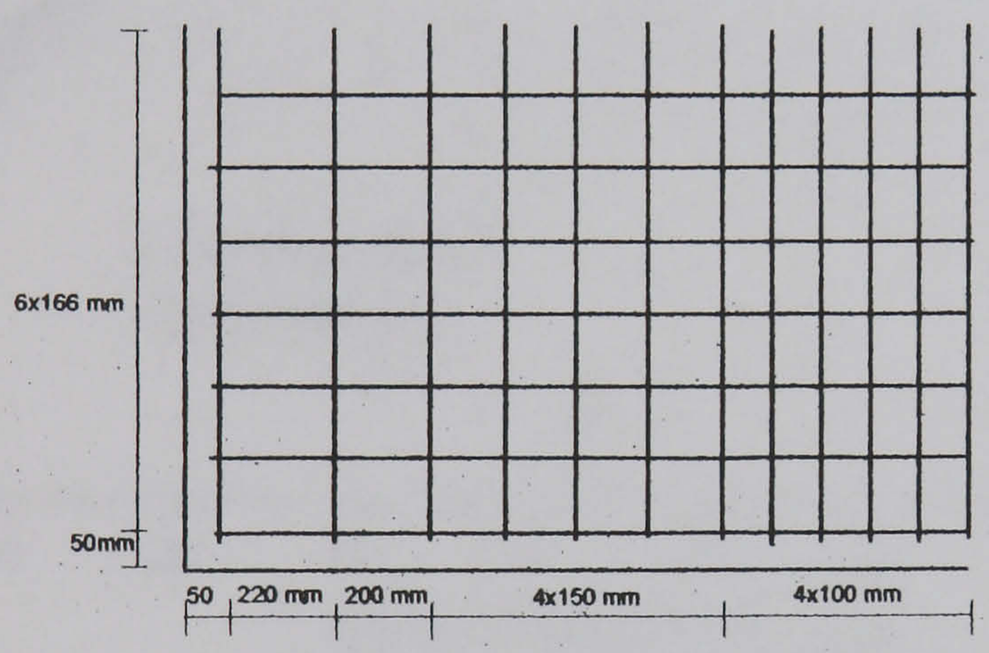

a- Bottom steel layout
Bar diameter 8mm

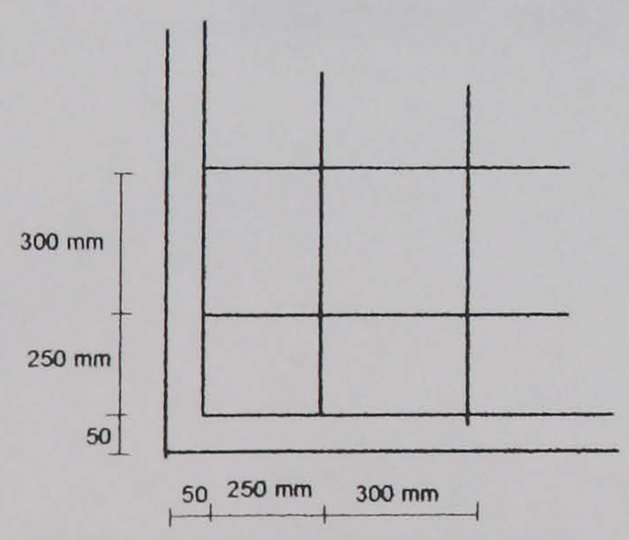

a- Top steel layout
Bar diameter 8mm

Fig.5.10- Loading conditions and steel layout for Bensalem's [5] slab No.S5

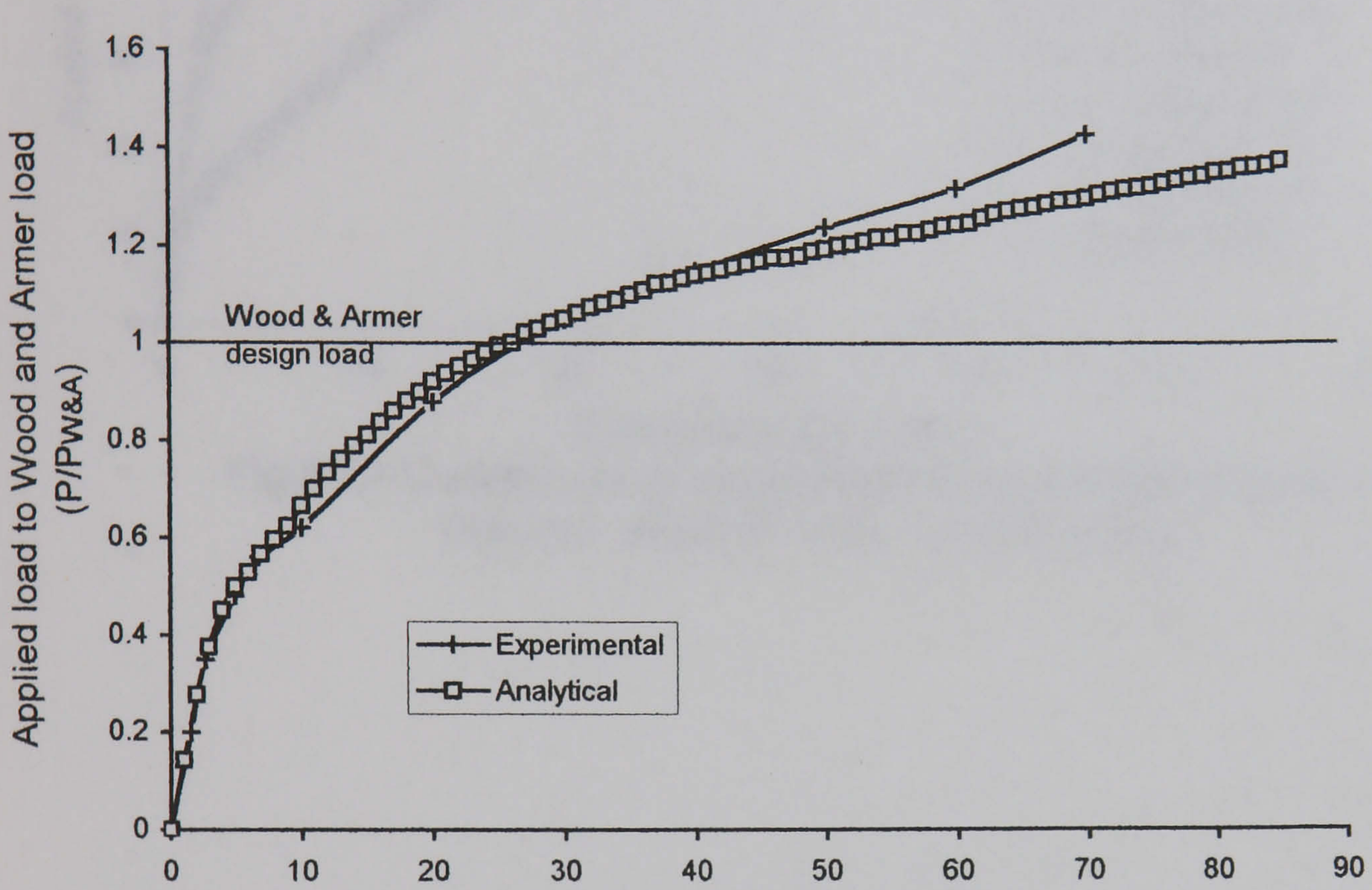

Fig.5.11-Comparison of experimental and analytical results of Bensalem slab [5] No. 5.

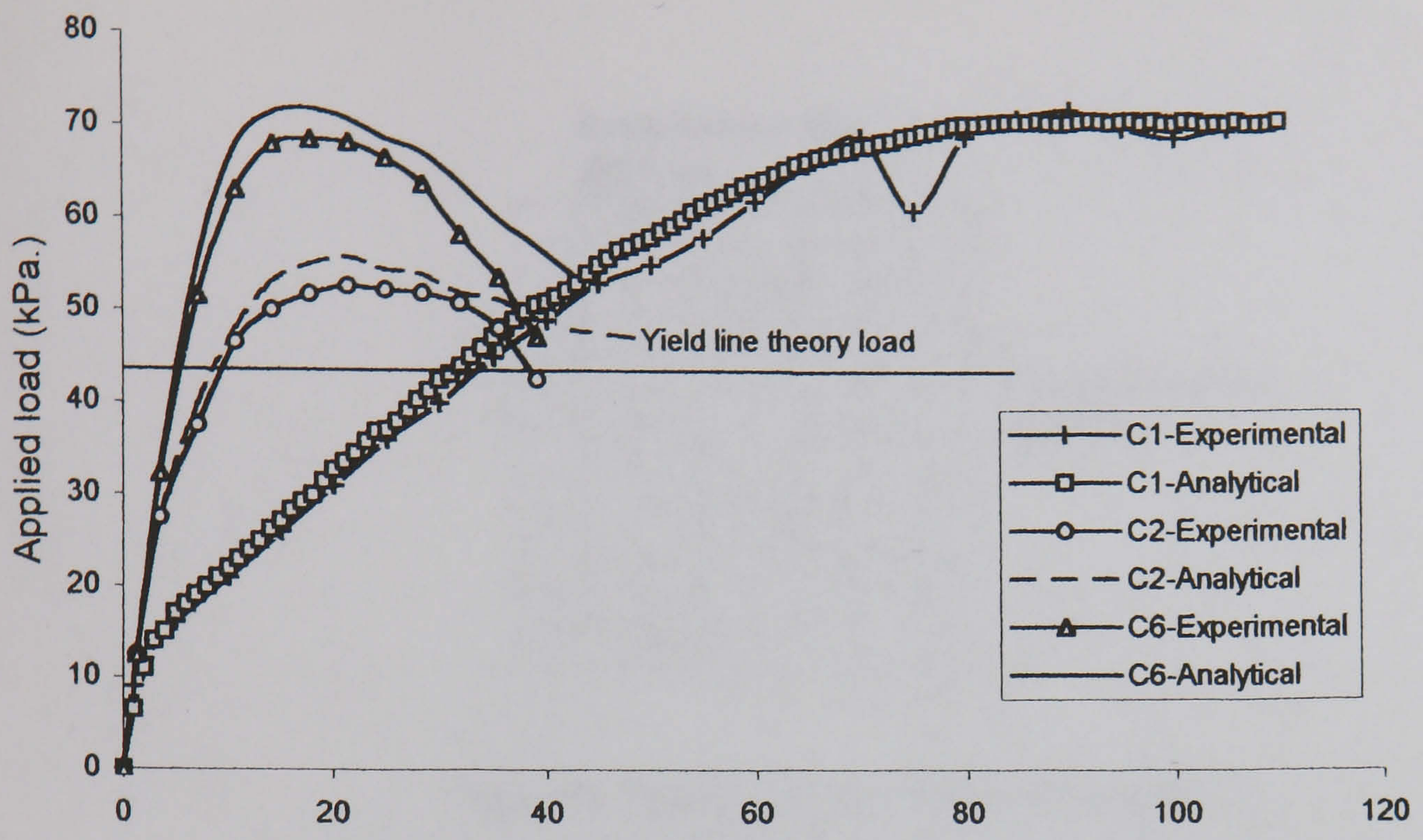

Fig.5.12-Comparison of experimental and analytical results of Ghonem slabs [6-7] No. C1,C2, and C6

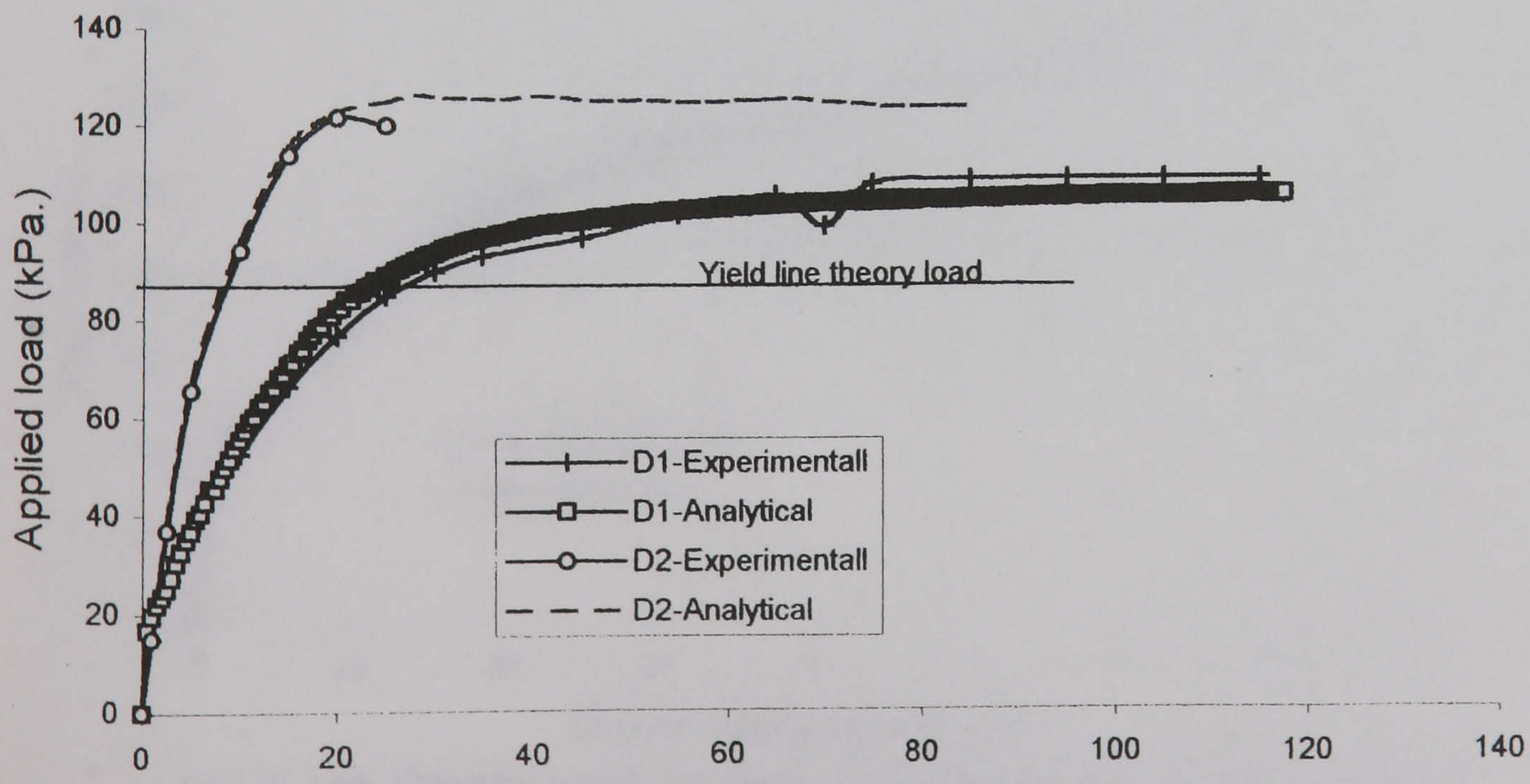

Fig.5.13-Comparison of Experimental and Analytical results of Ghonem slabs [6-7] No. D1 and D2

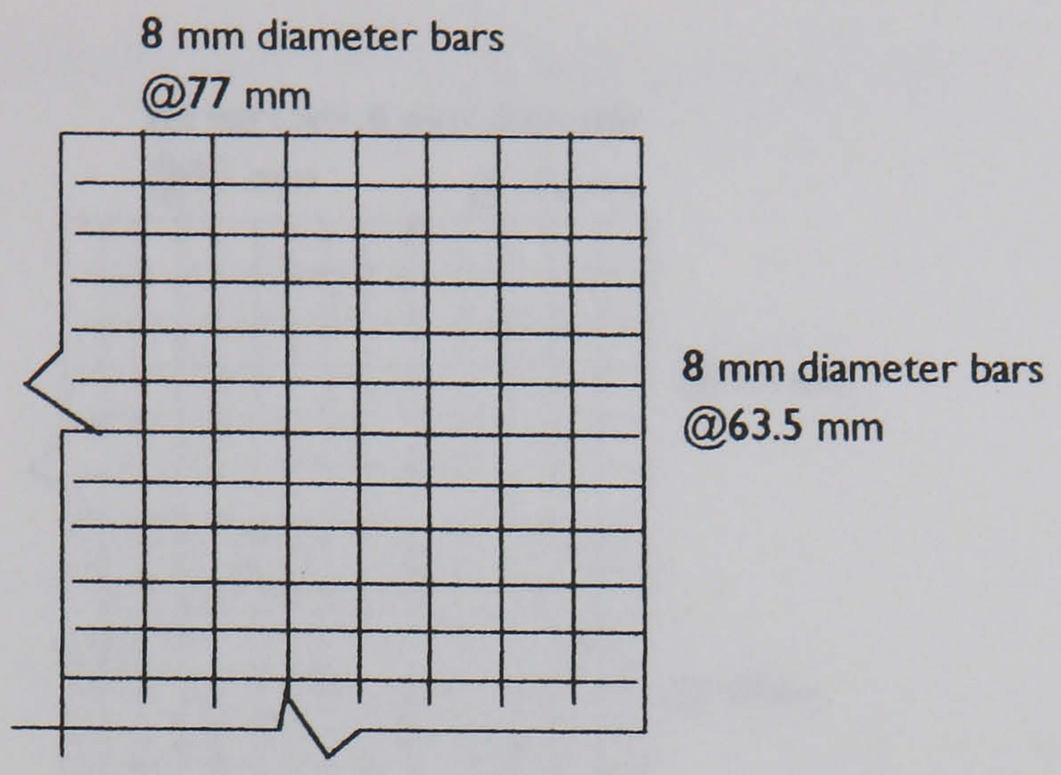

Fig.5.14a- Steel layout for Taylor's [8] slab No.1.

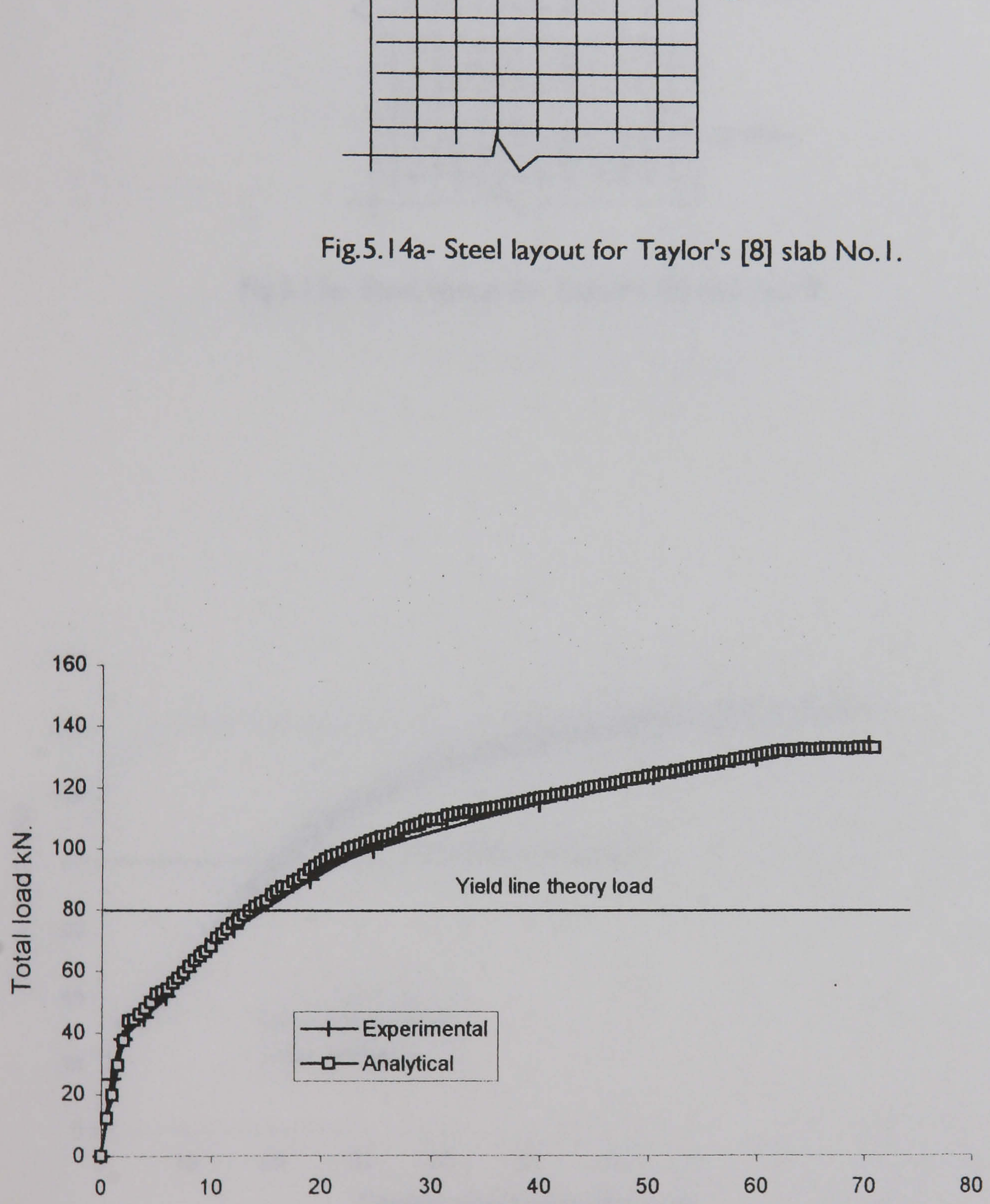

Fig.5.14b-Comparison of experimental and analytical results of Taylor slab [8] No. 1.

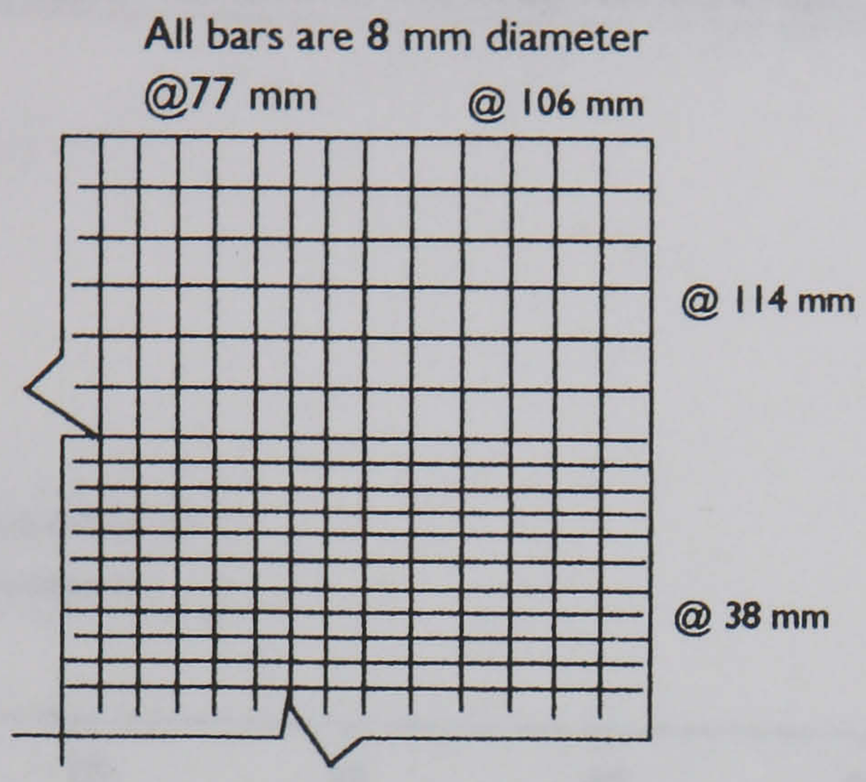

Fig.5.15a- Steel layout for Taylor's [8] slab No. 8.

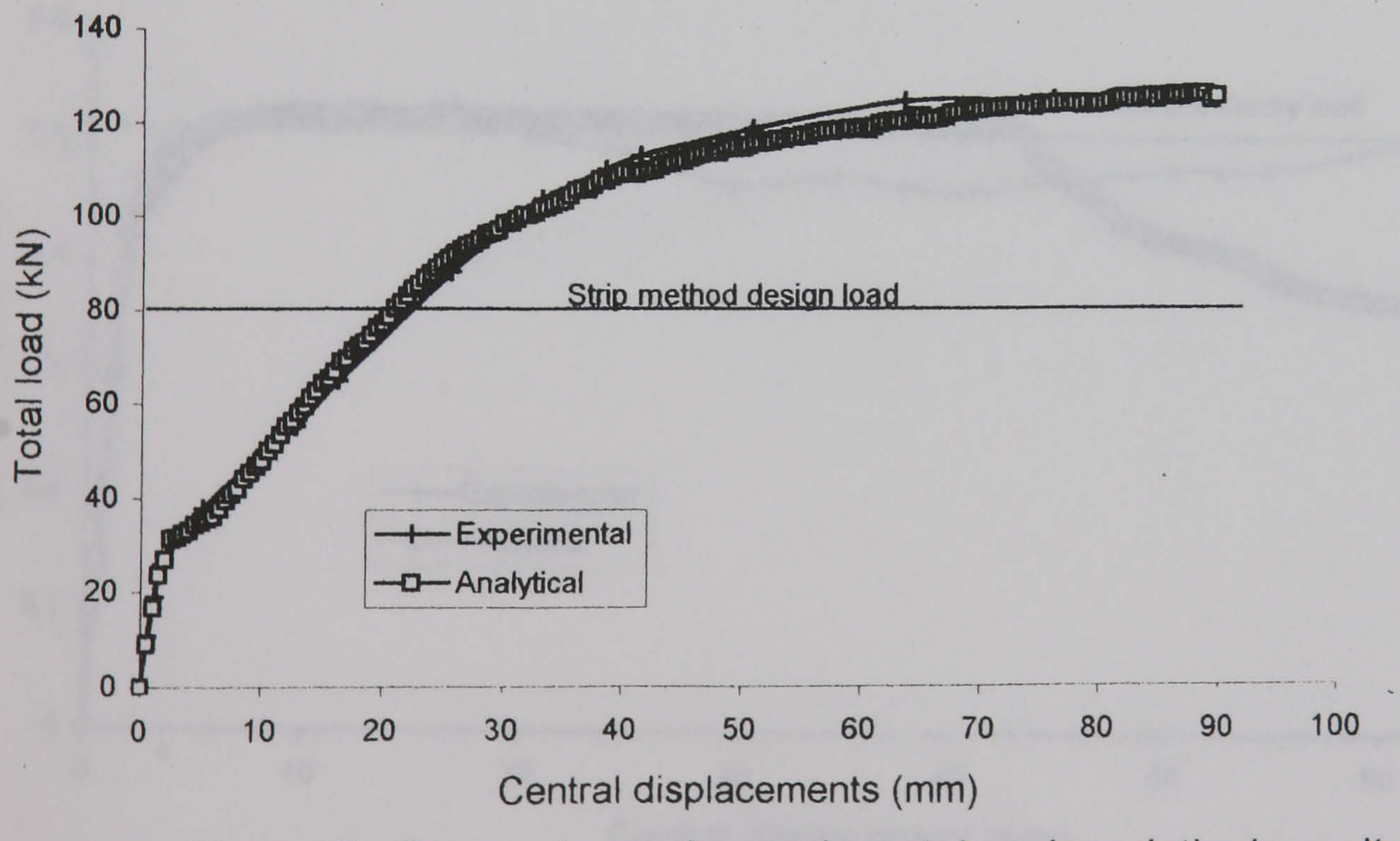

Fig.5.15b-Comparison of experimental and analytical results of Taylor slab [8] No. 8.

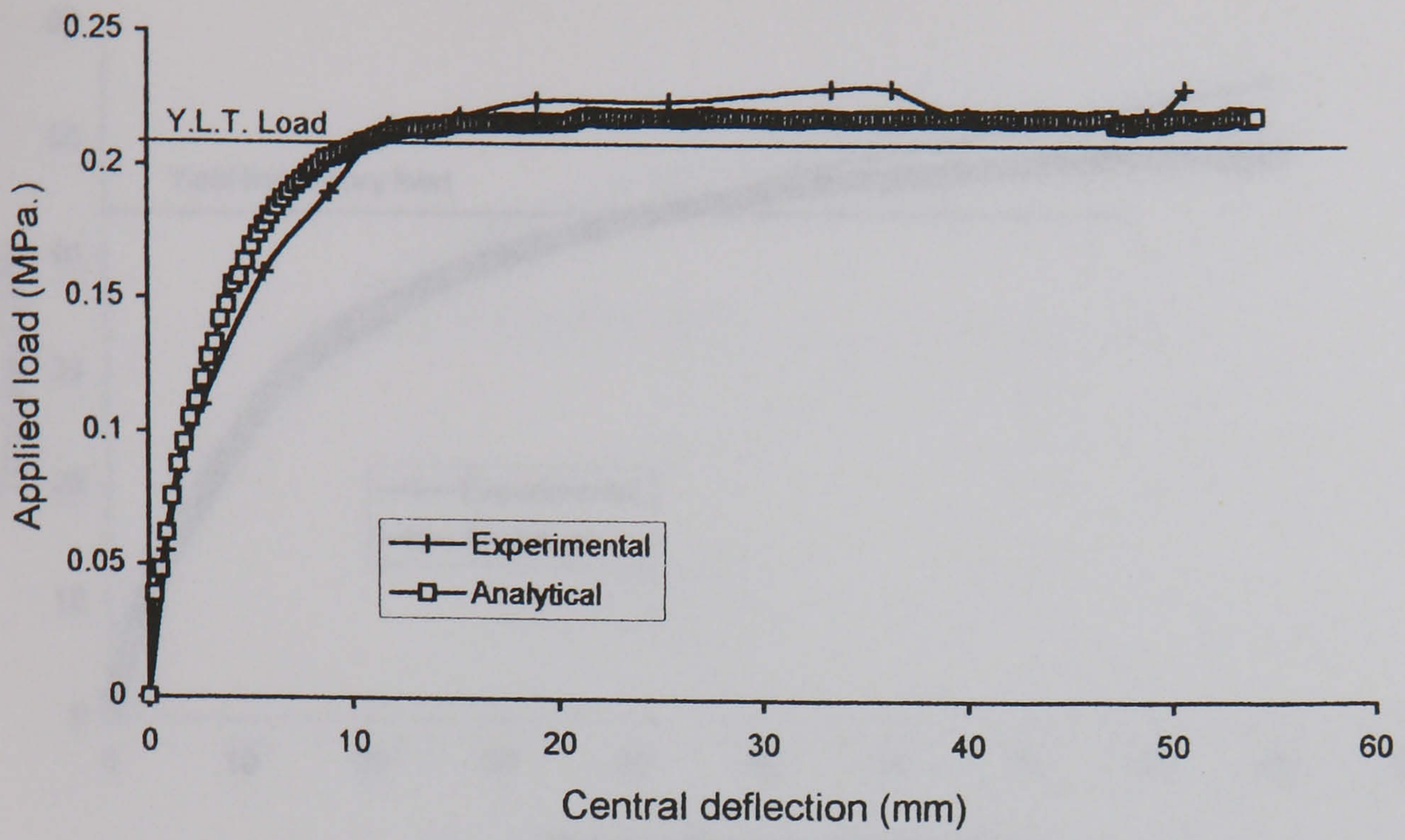

Fig.5.16-Comparison of experimental and analytical results of Brotchie slab [9] No. 8.

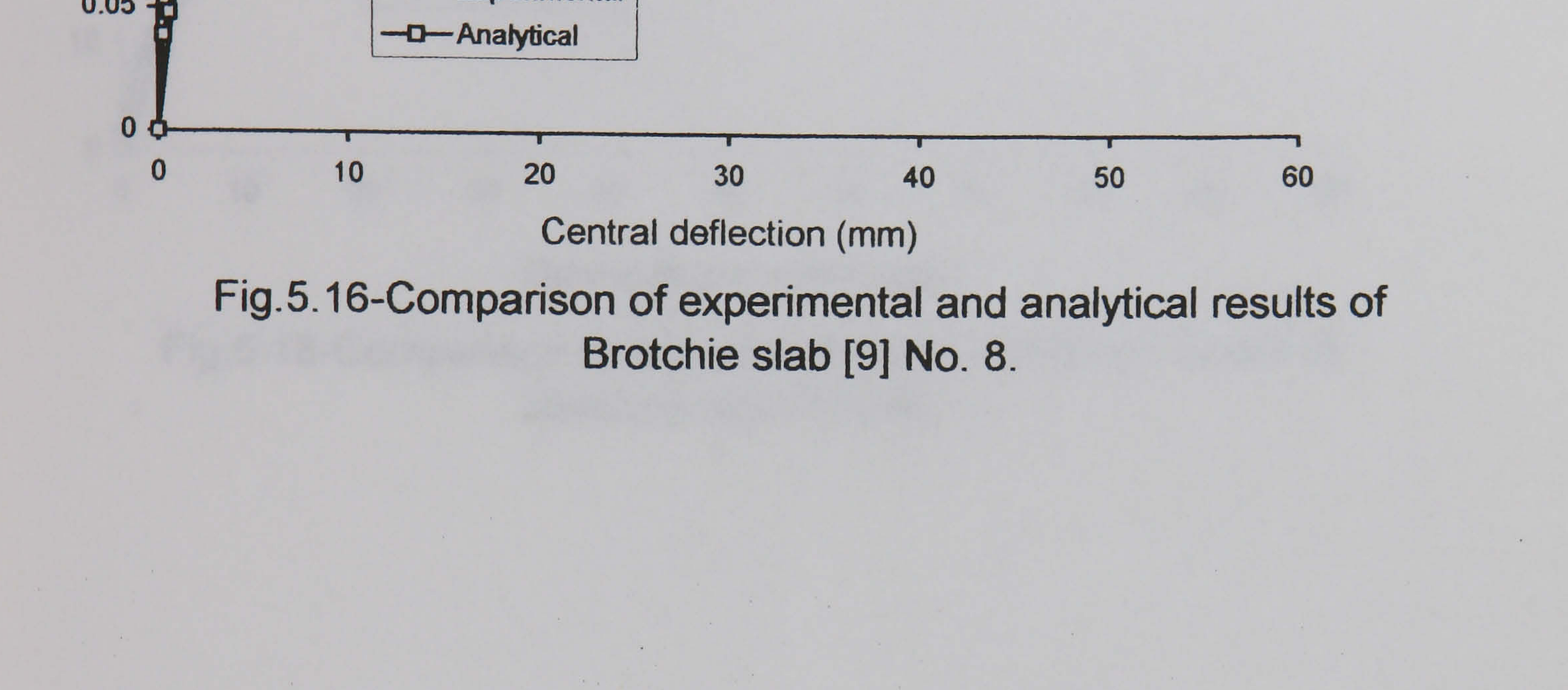

Fig.5.17-Comparison of experimental and analytical results of Brotchie slab [9] No. 12.

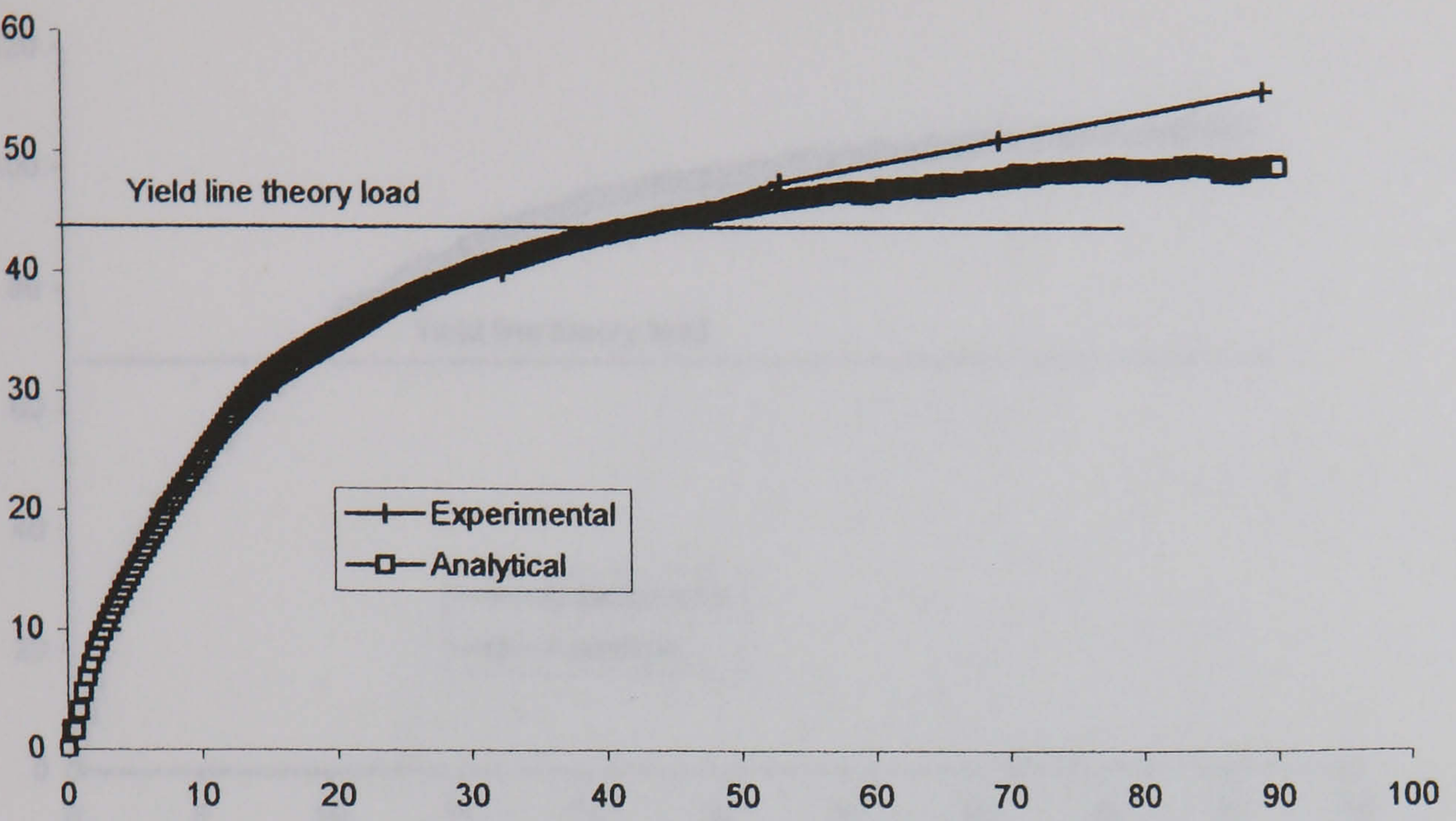

Fig.5.18-Comparison of experimental and analytical results of Sawczuk slab [10] No. 1.

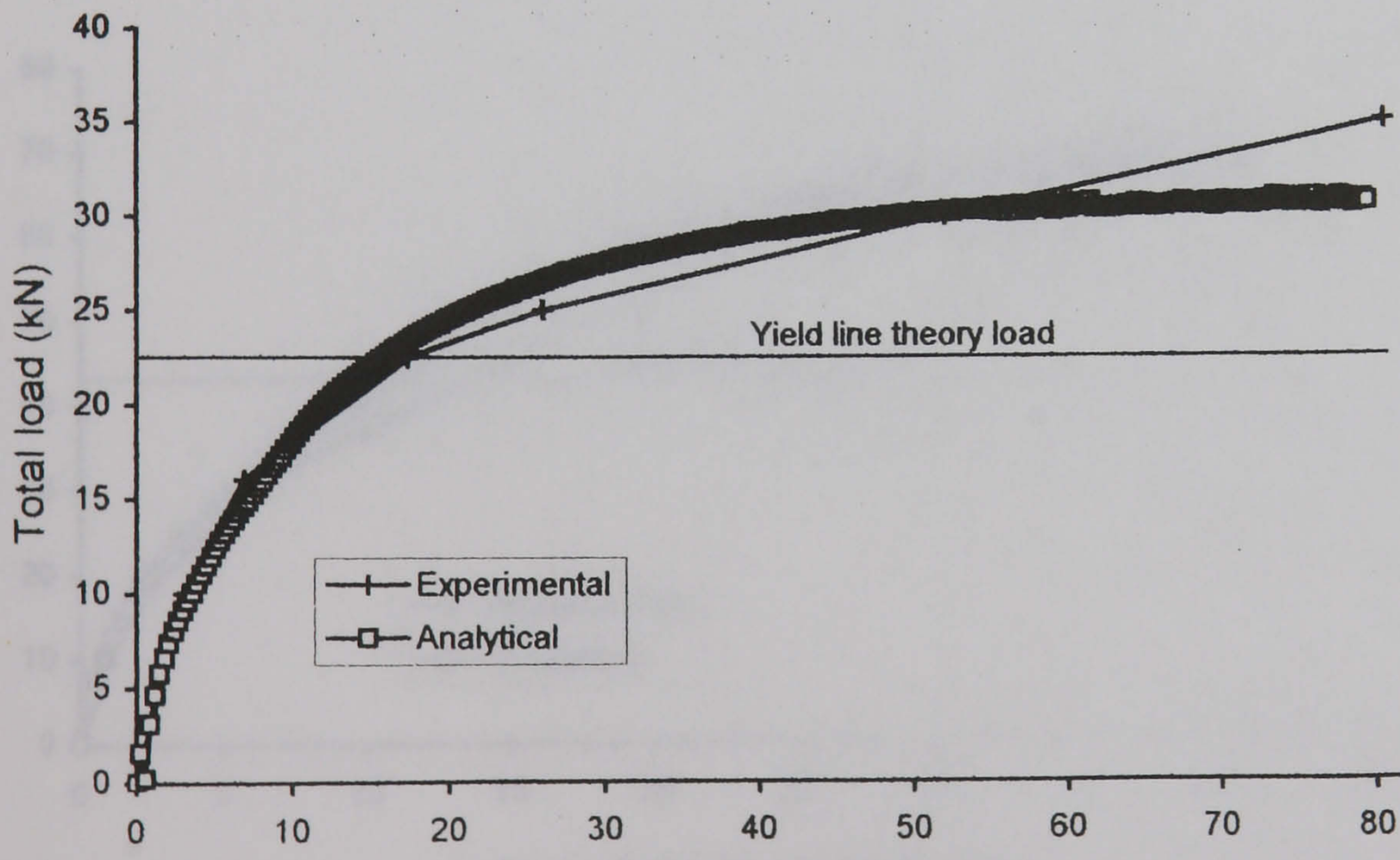

Fig.5.19-Comparison of experimental and analytical results of Sawczuk slab [10] No. 2.

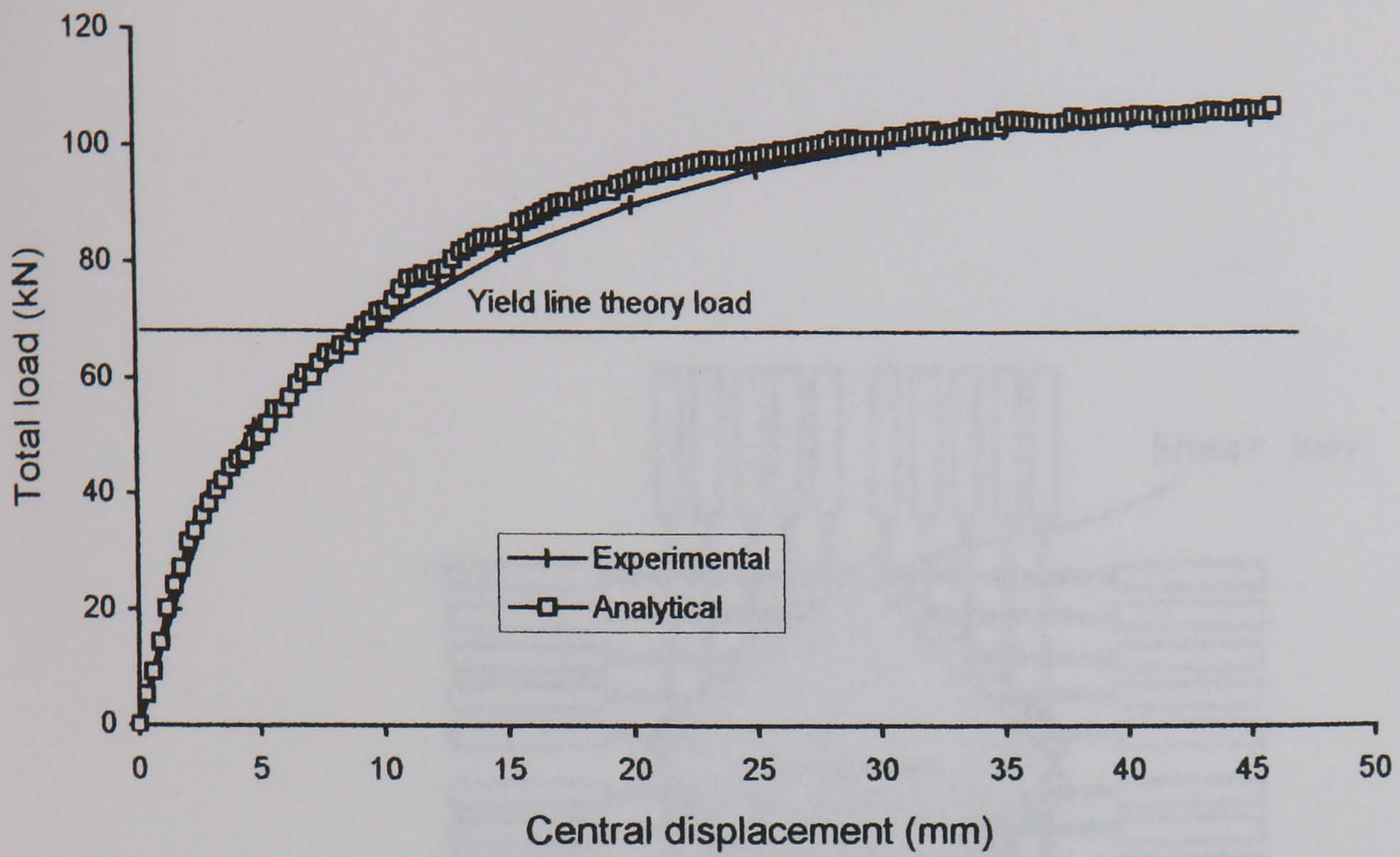

Fig.5.20-Comparison of experimental and analytical results of Desayi slab [11] No. S4.

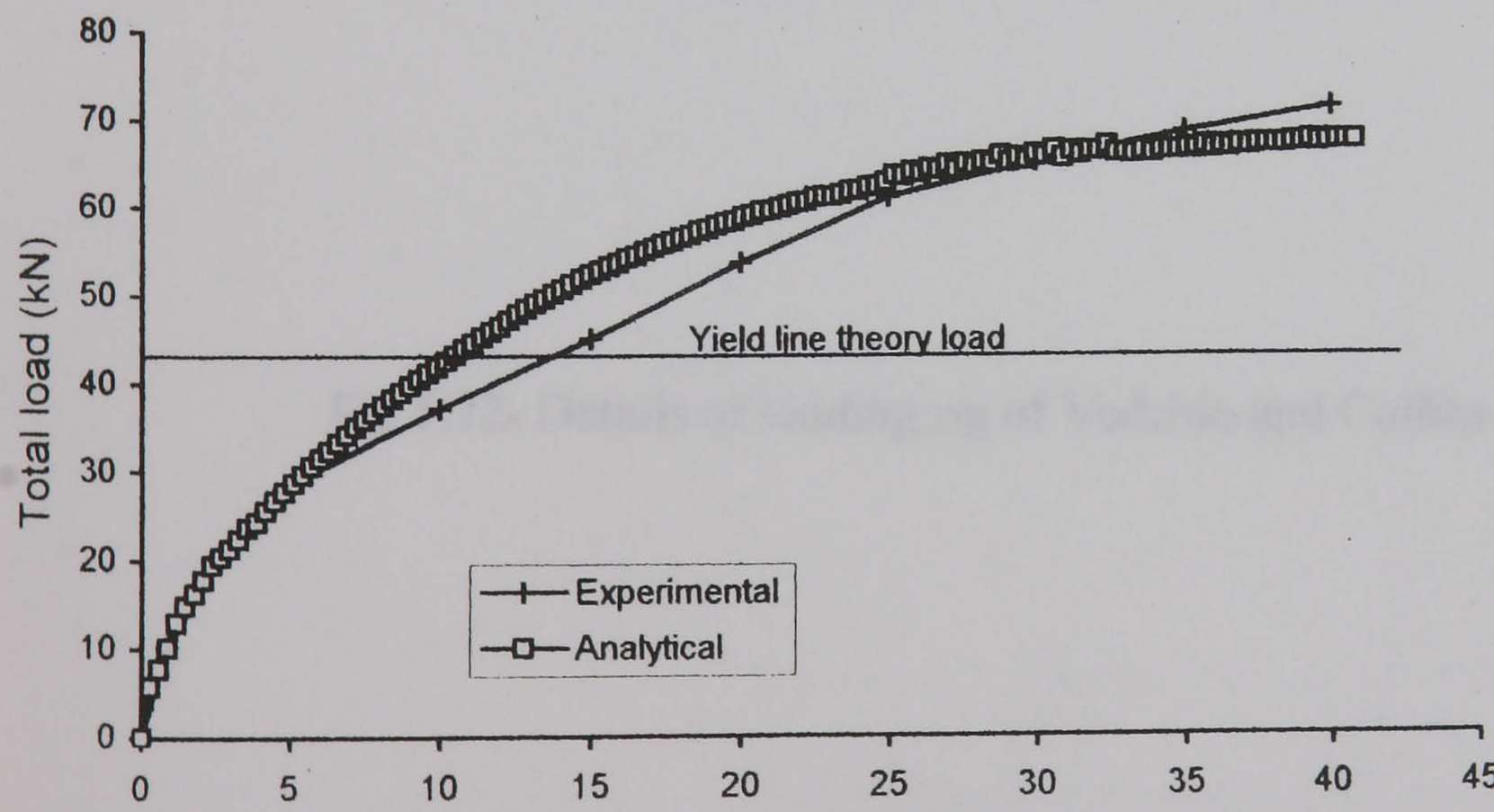

Fig.5.21-Comparison of experimental and analytical results of Desayi slab [11] No. T4.

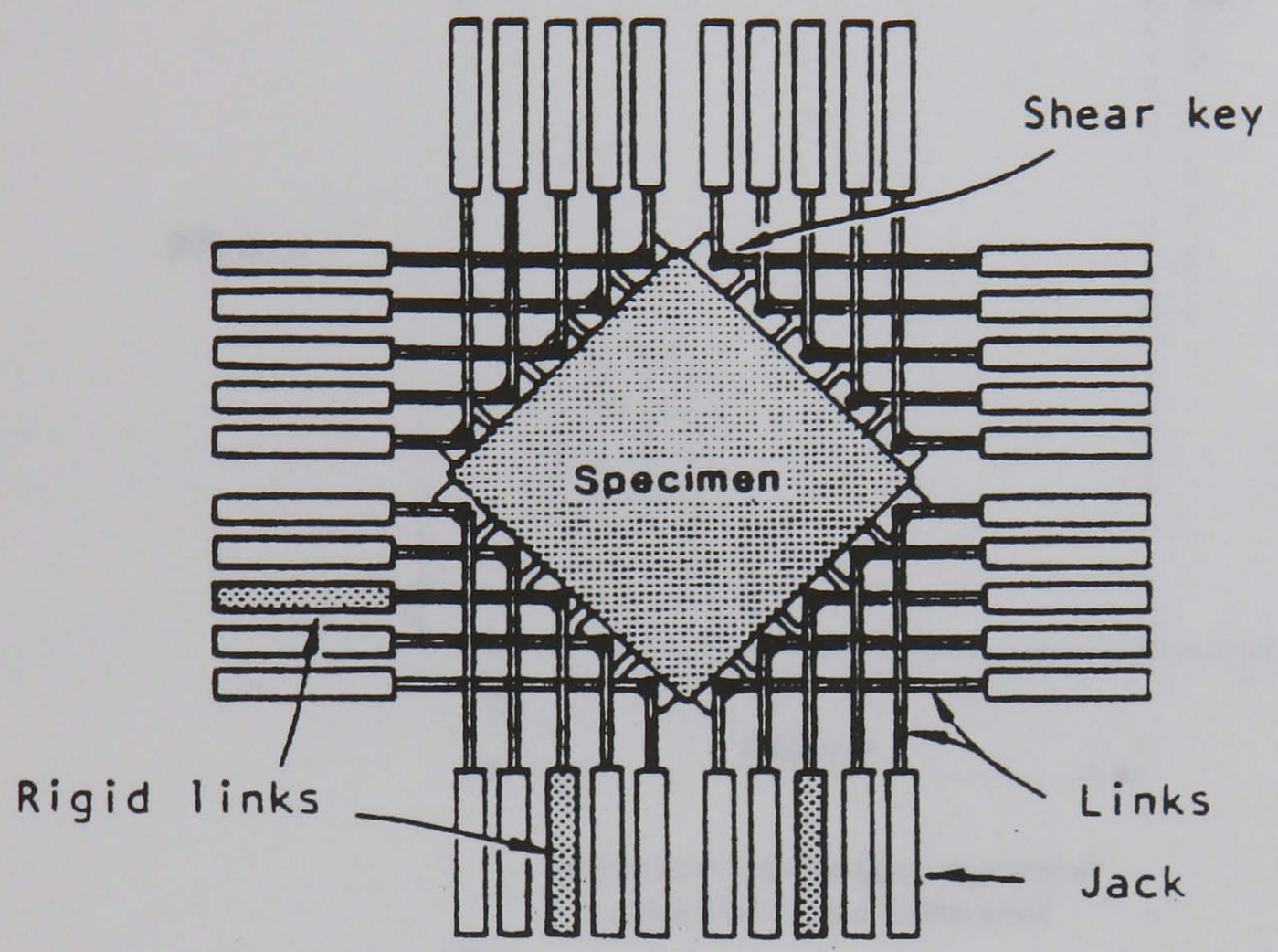

Fig.5.22- Details of loading rig of Vecchio and Collins [12].

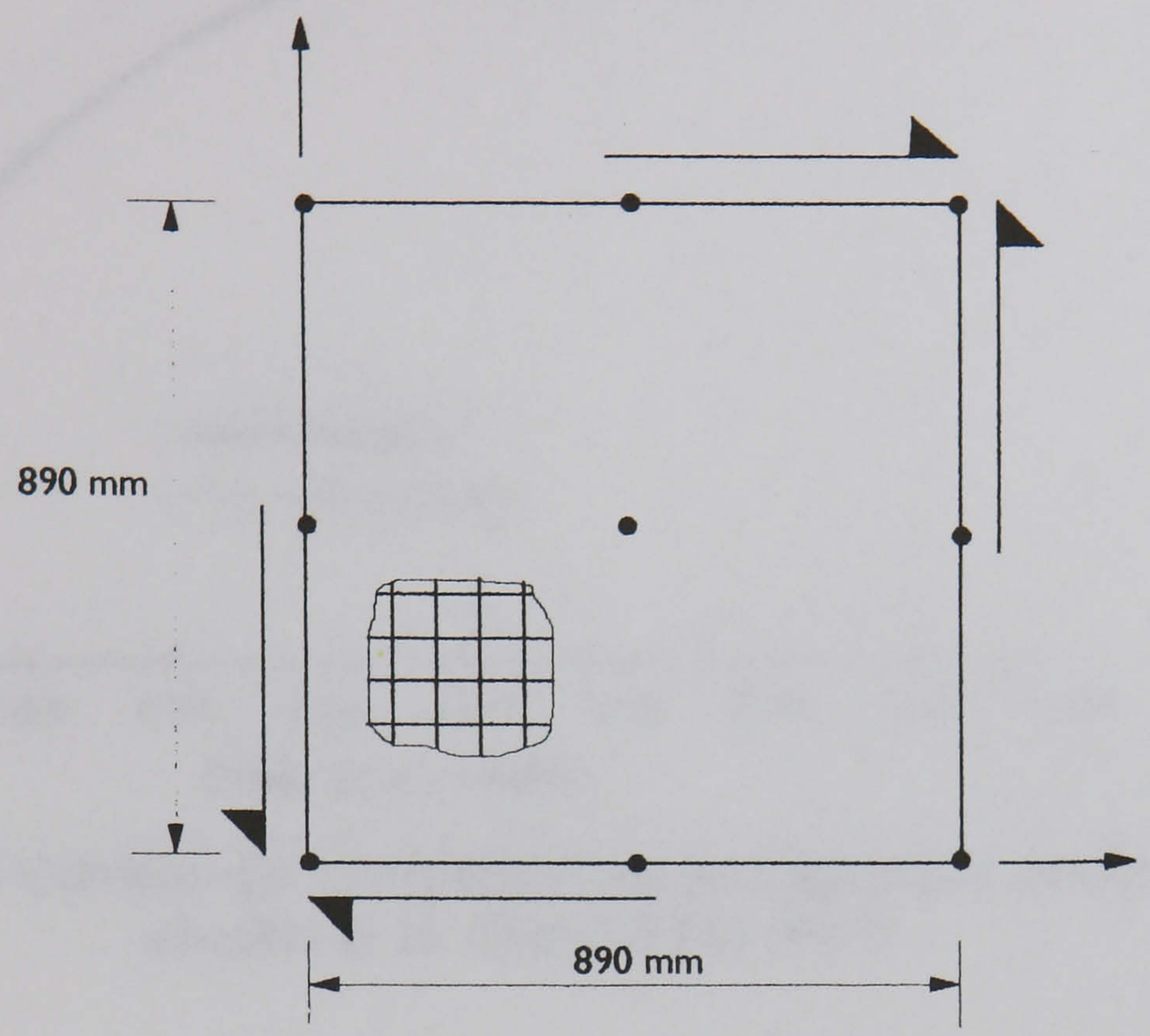

a-Dimensions and loading arrangement of
a typical Vecchio and Collins panel

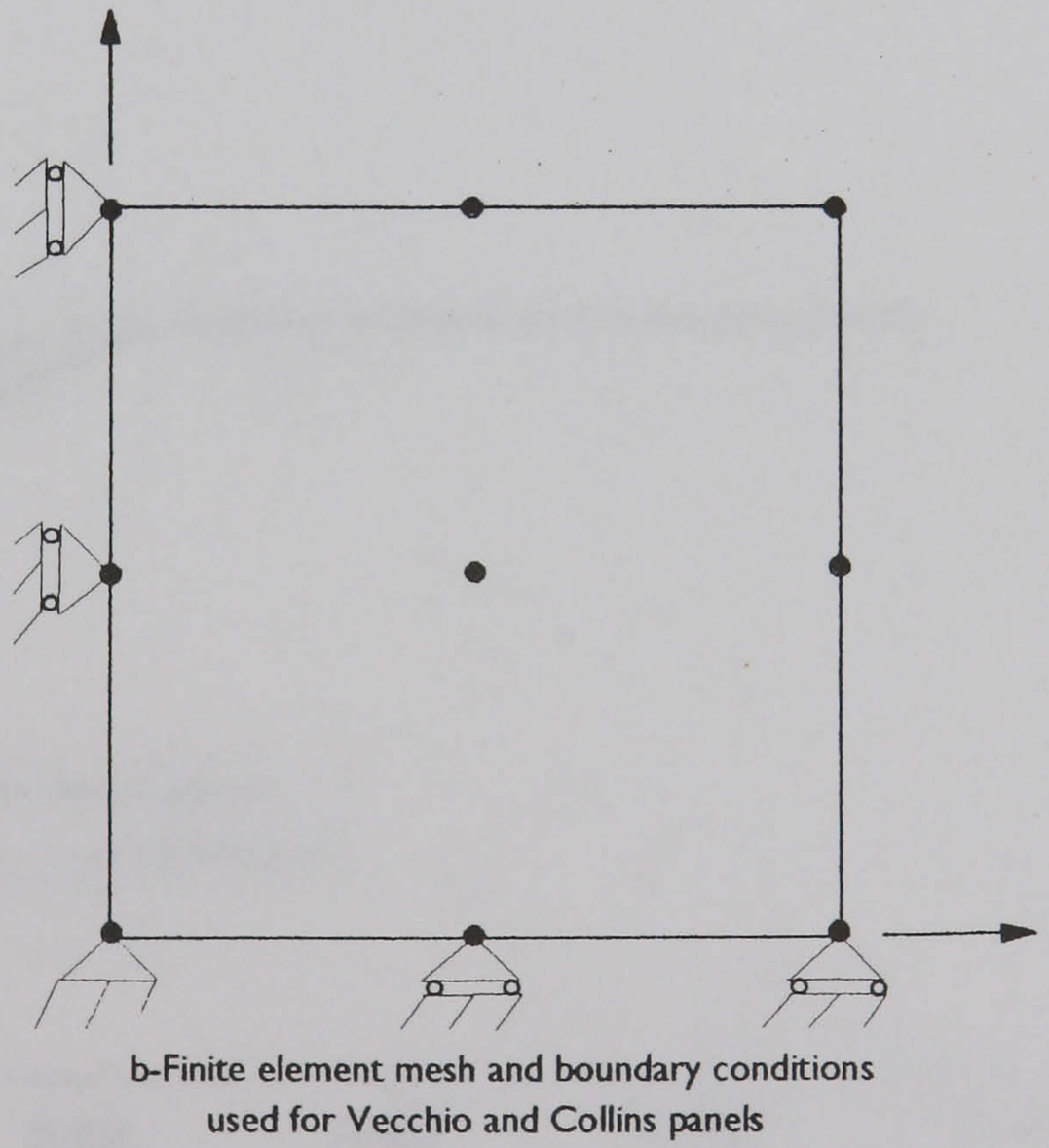

b-Finite element mesh and boundary conditions
used for Vecchio and Collins panels

Fig.5.23- Dimensions, loadings and finite element mesh for Vecchio and Collins panels [12]

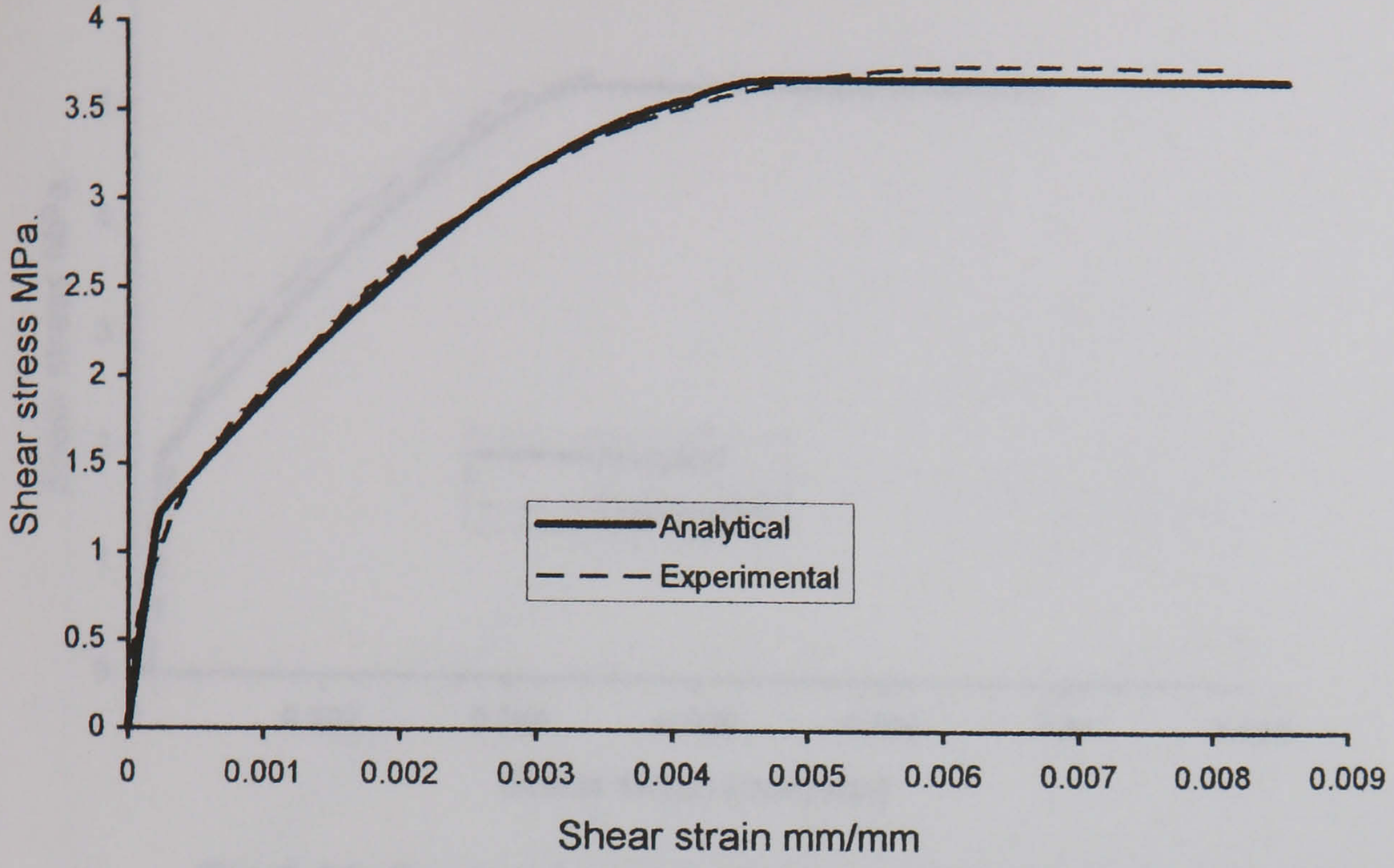

Fig 5.24-Comparison of experimental and analytical results of Vecchio et al. slab [12] No. PV 9.

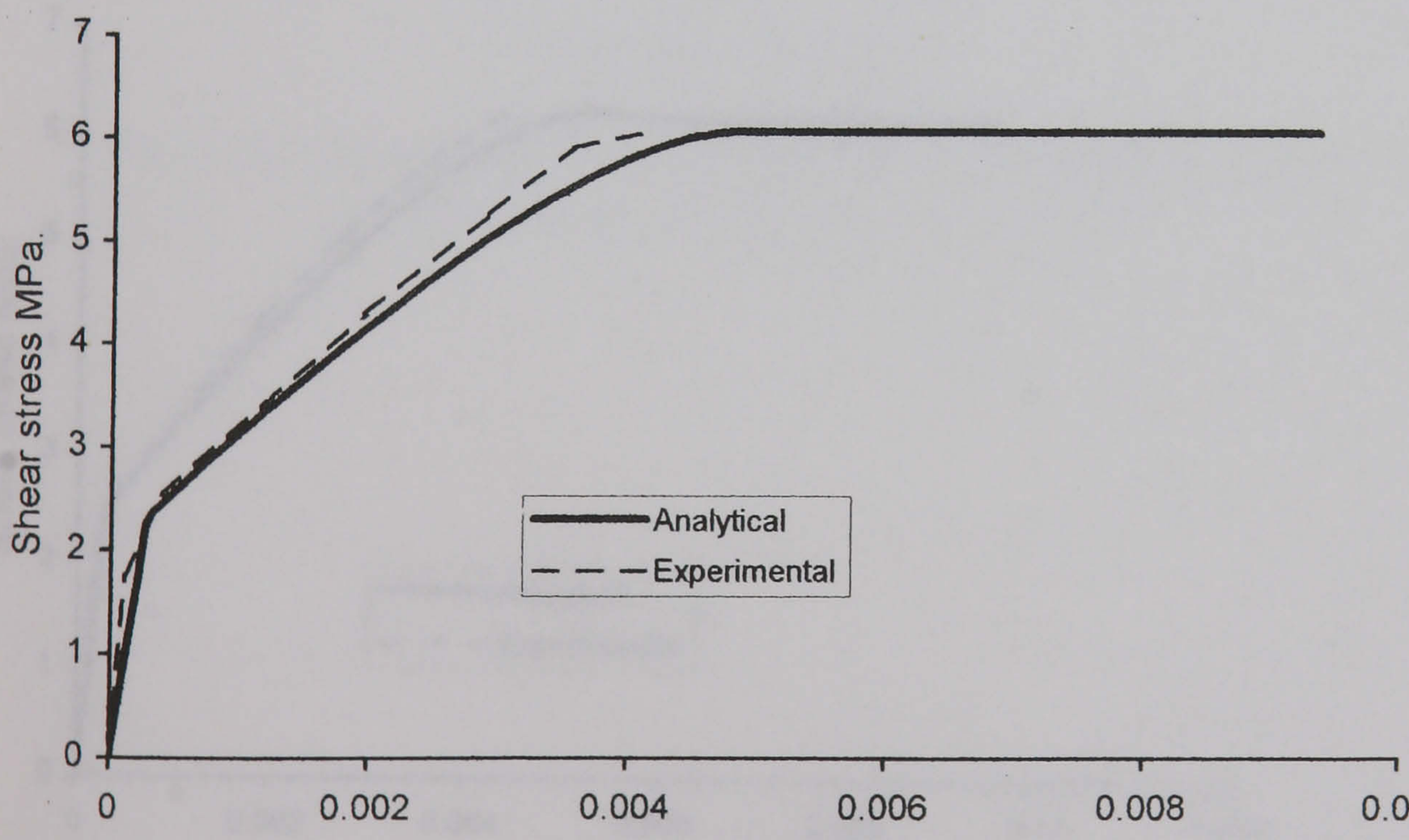

Fig.5.25-Comparison of experimental and analytical results of Vicchio et al. Slab [12] No. PV 22.

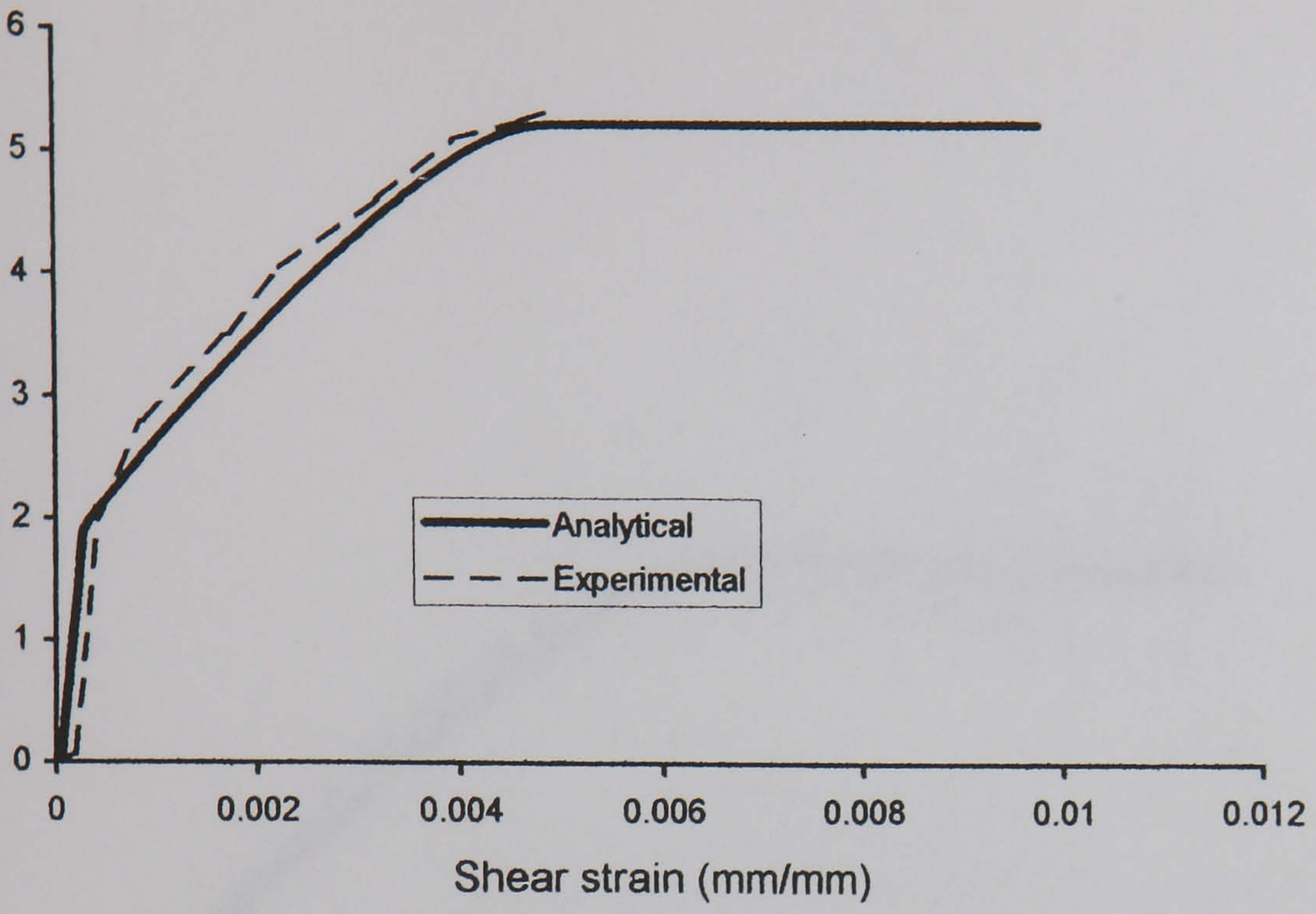

Fig.5.26-Comparison of experimental and analytical results of Vicchio et al. Slab [12] No. PV 26.

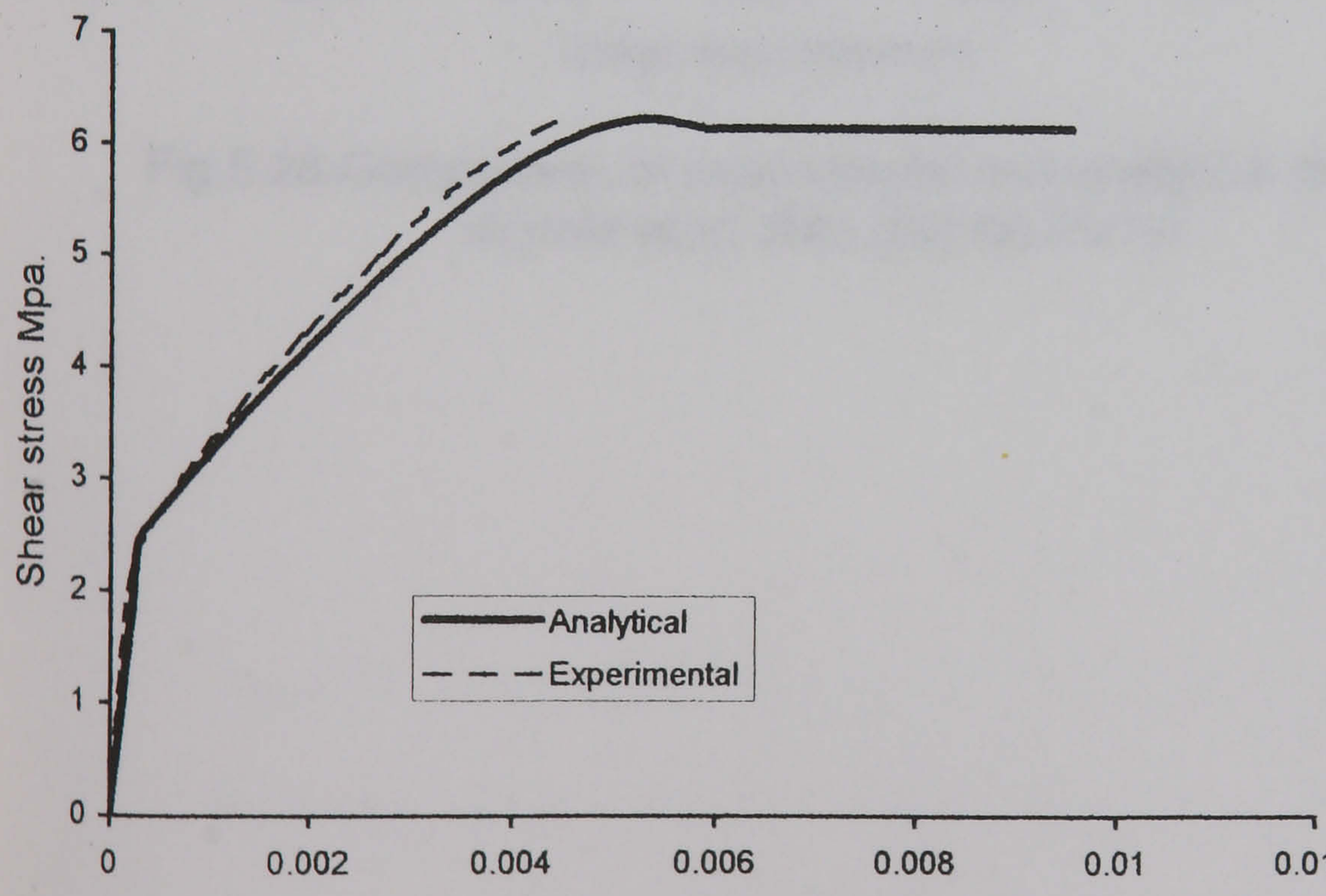

Fig .5.27-Comparison of experimental and analytical results of Vicchio et al. Slab [12] No. PV. 27.

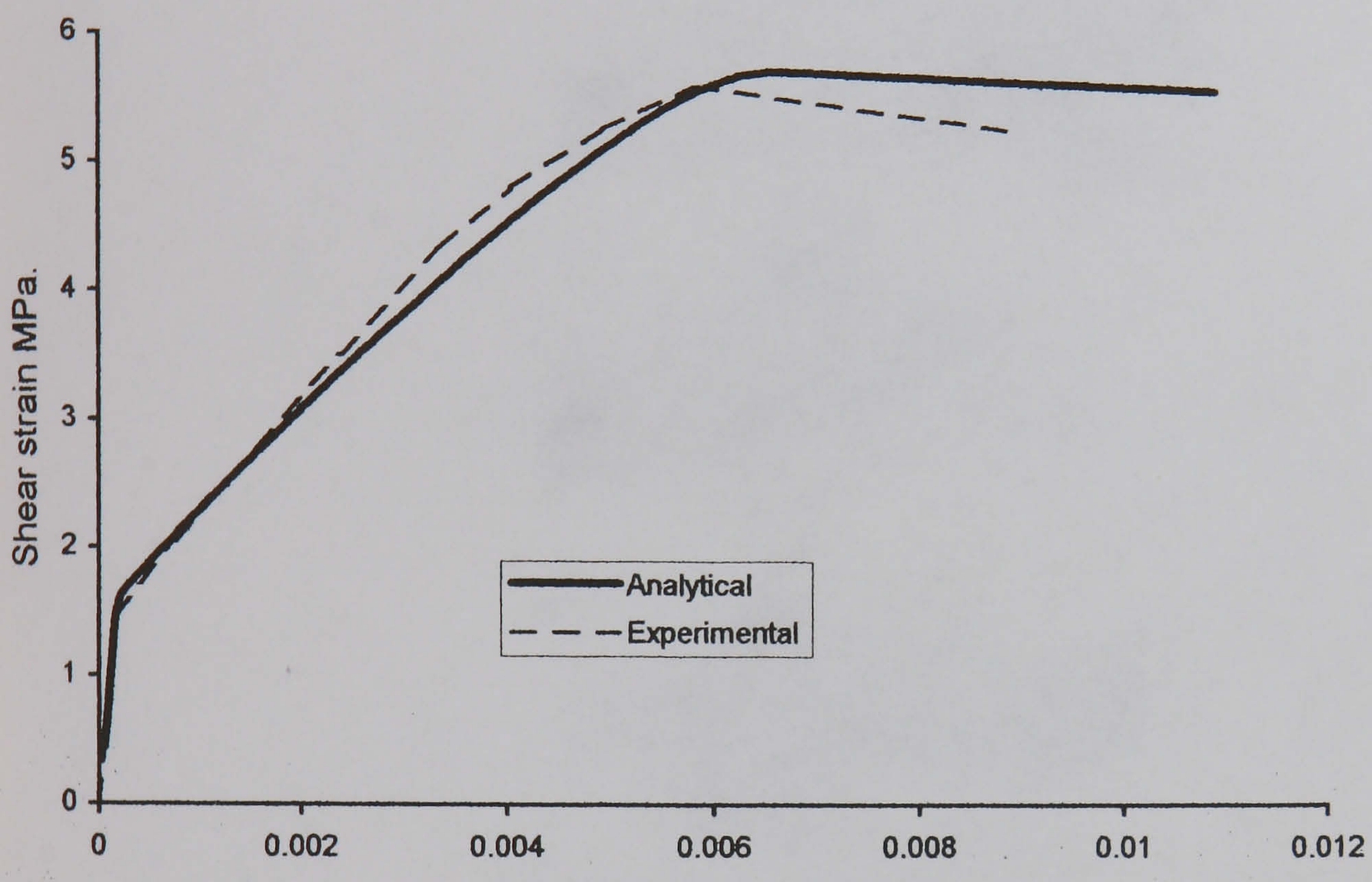

Fig.5.28-Comparison of experimental and analytical results of Vicchio et al. Slab [12] No.PV 28

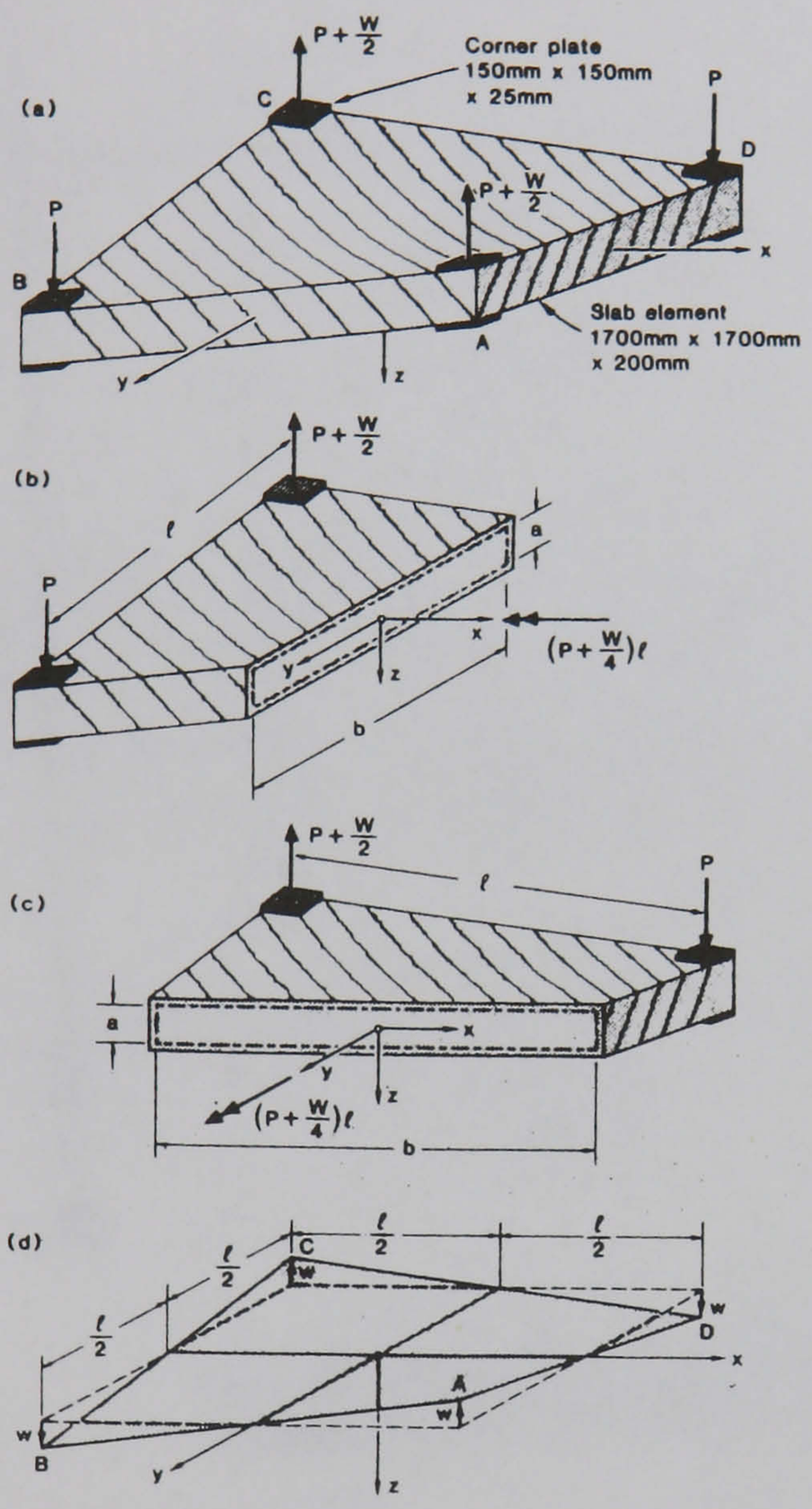

Fig.5.29-Loading and deformation of Marti et al. [13] panels: (a) Applied load, (b) Torsion about x-axis, (c) Torsion about y-axis, (d) Average corner deflection

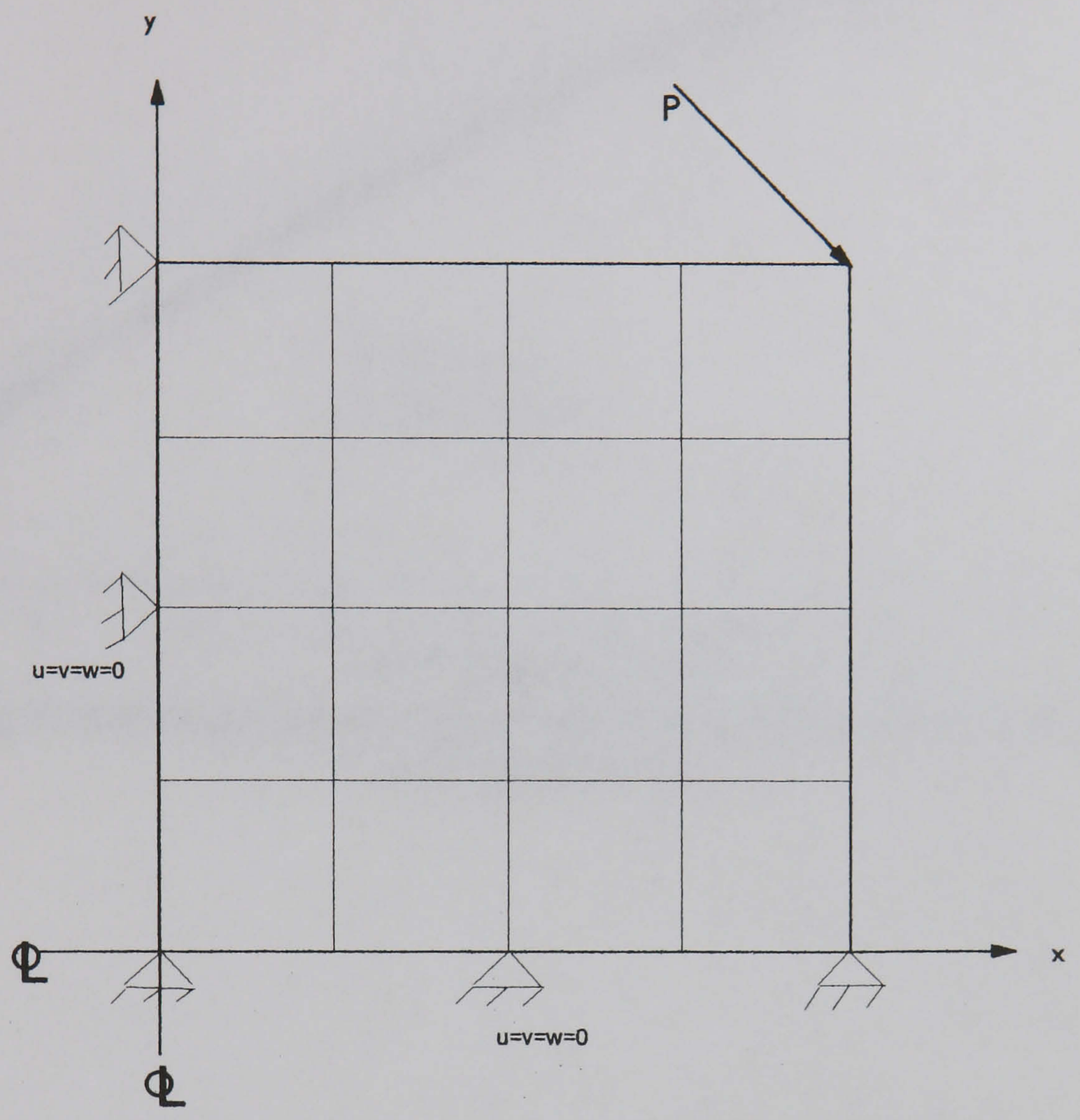

Fig. 5.30-Finite element mesh and the boundary conditions of Marti et al. Panels [13]

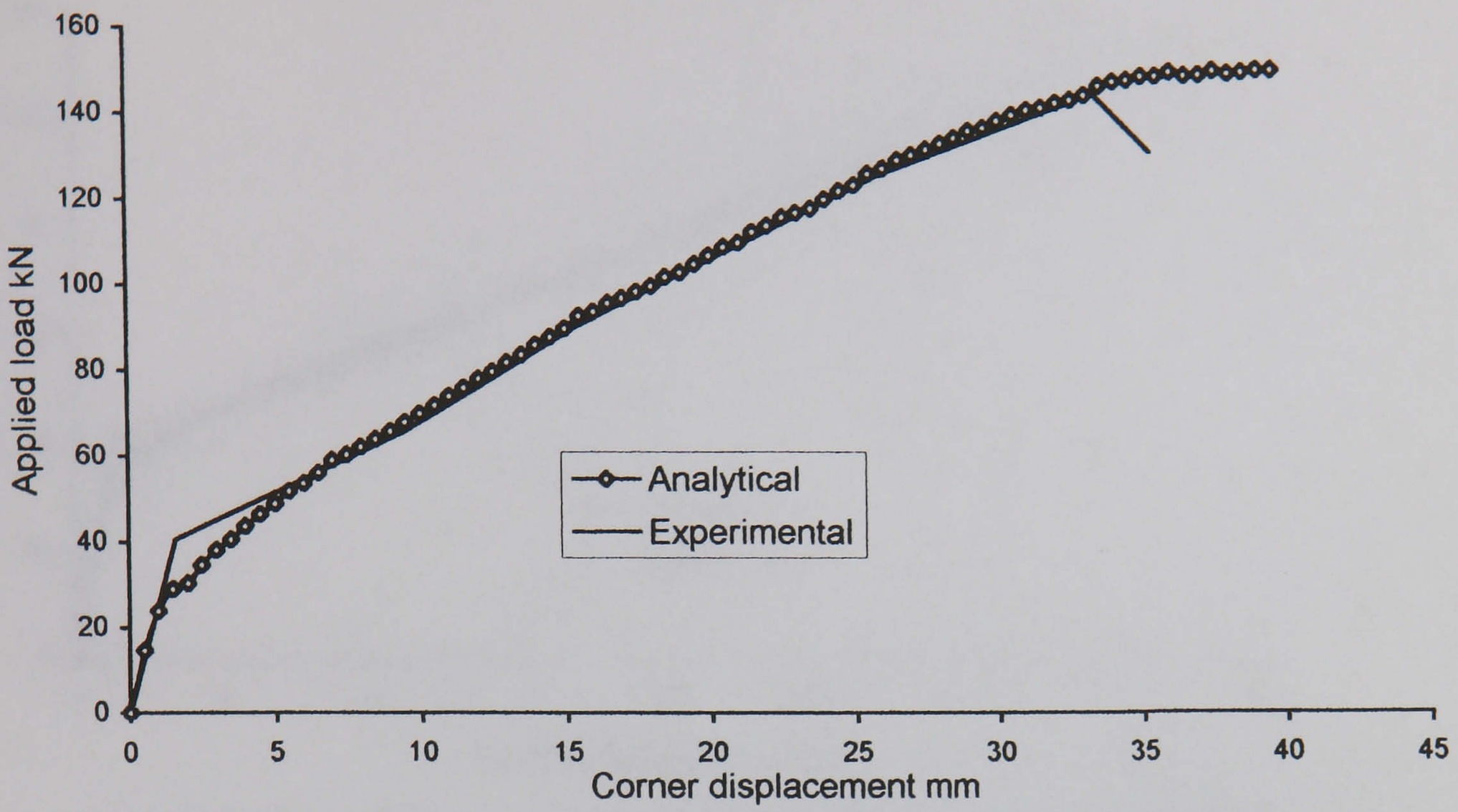

Fig.5.31-Comparison of experimental and analytical results of Marti et al.slab [13] No 2.

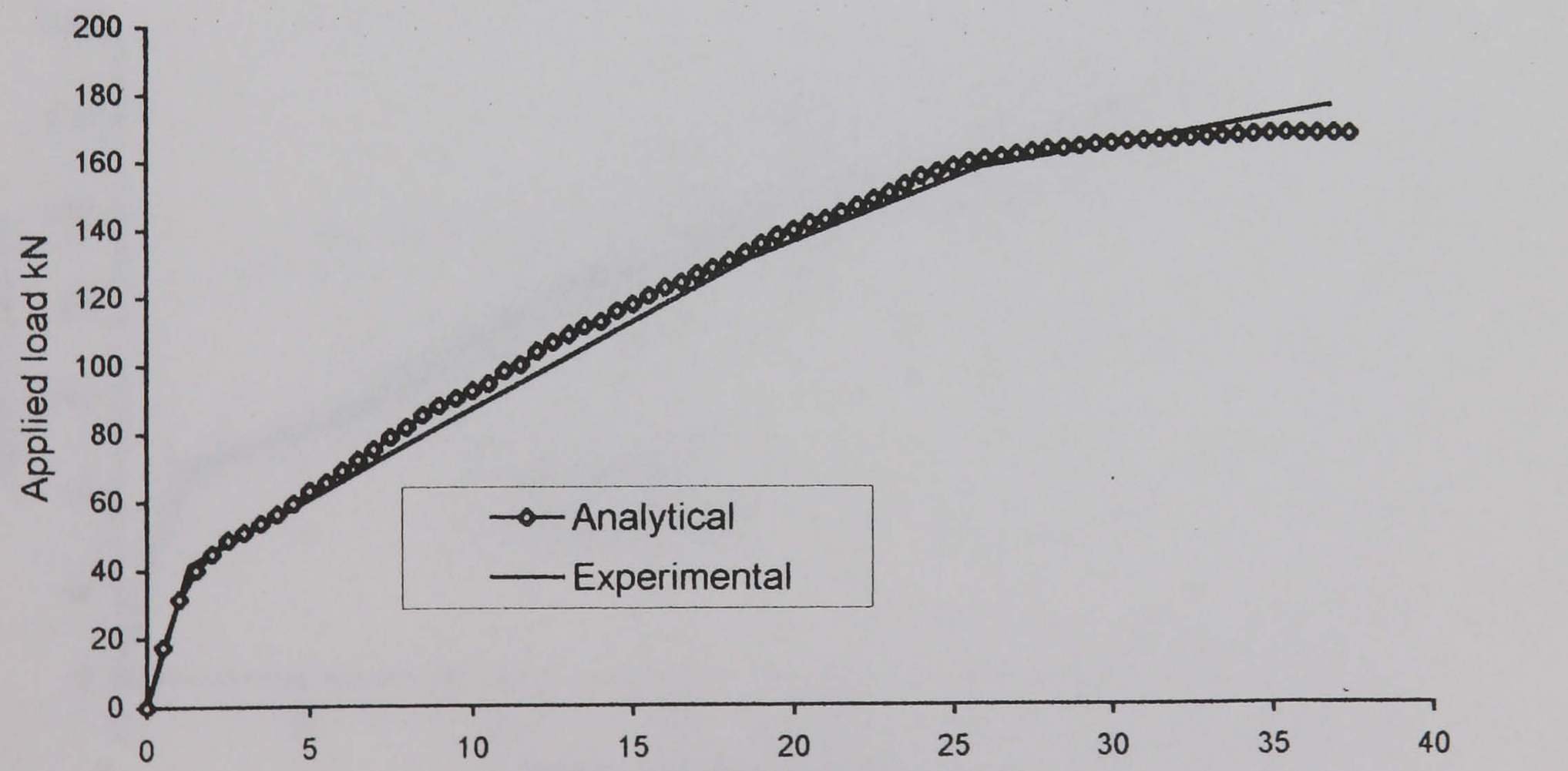

Fig.5.32-Comparison of experimental and analytical results of Marti et al. Slab [13] No. 3

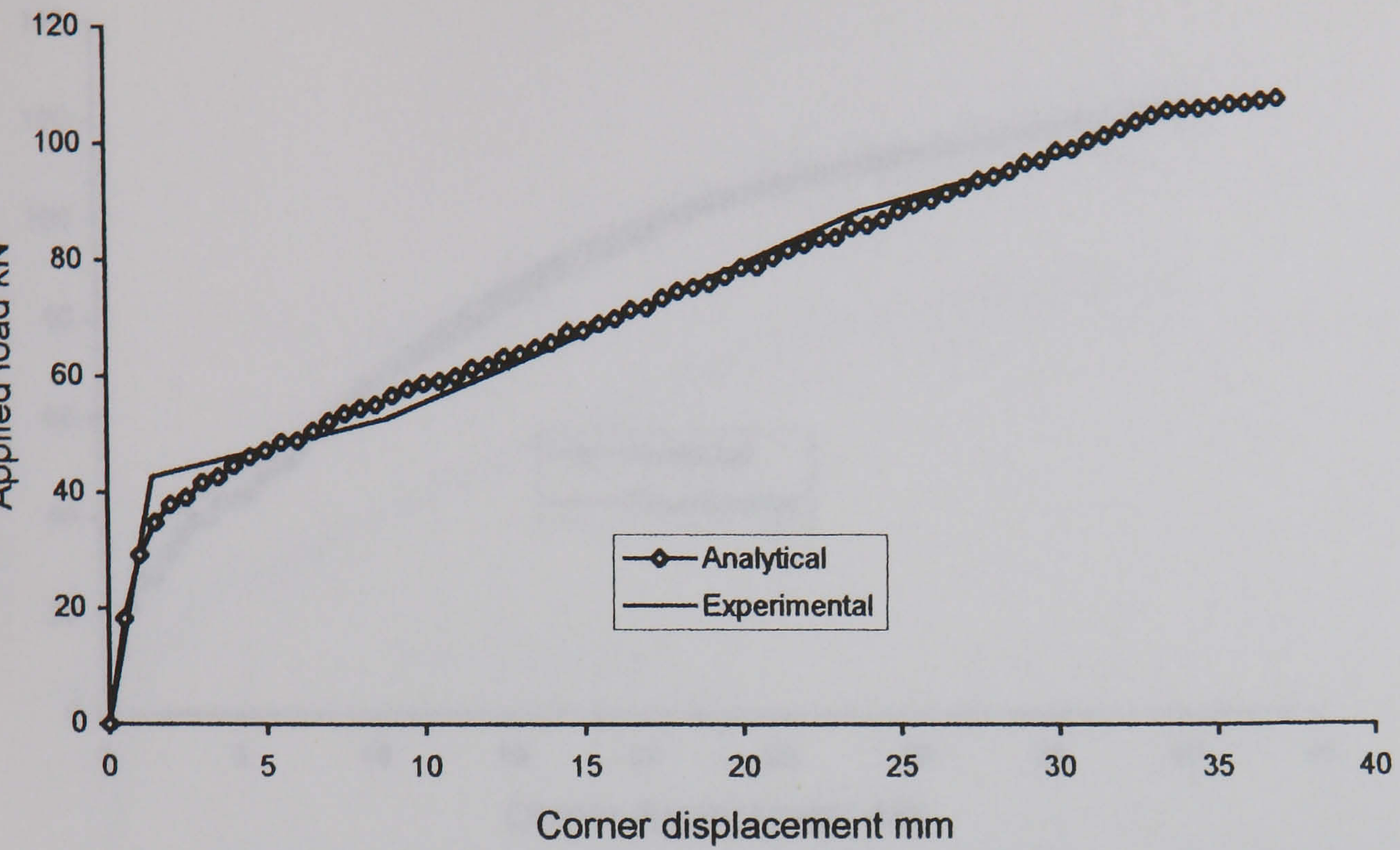

Fig.5.33-Comparison of experimental and analytical results of Marti et al. Slab [13] No. 4.

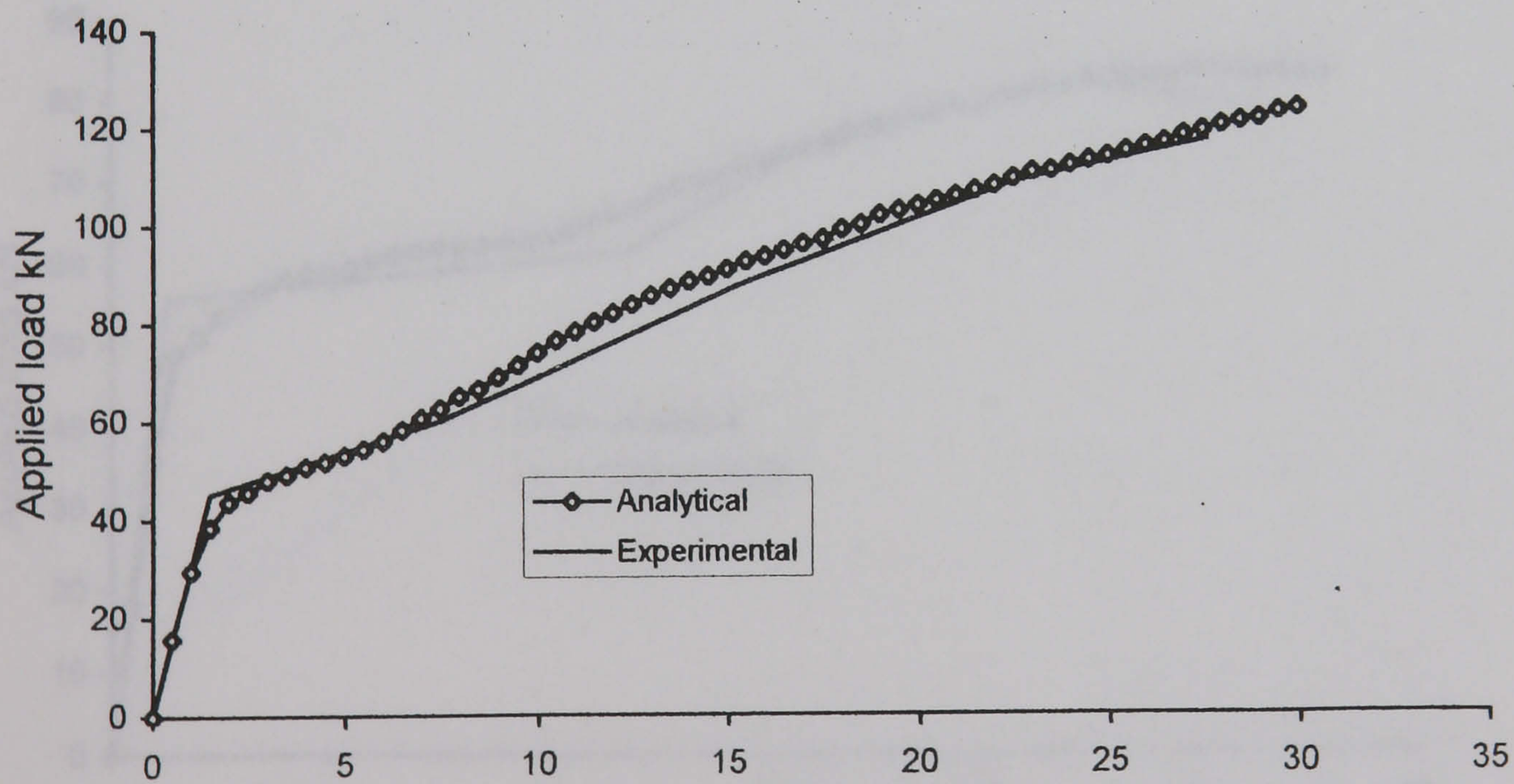

Fig.5.34-Comparison of experimental and analytical results of Marti et al. Slab [13] No. 5.

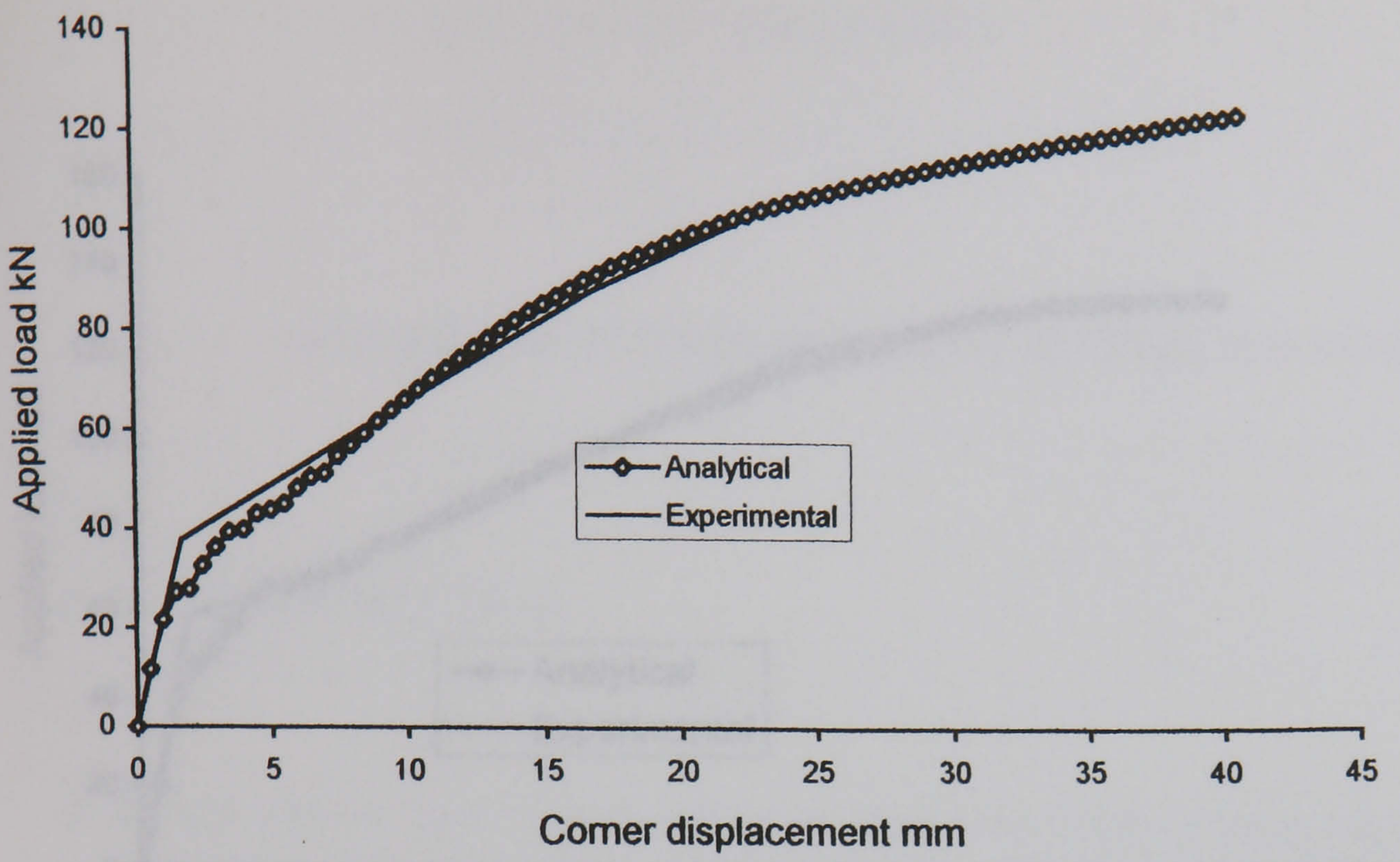

Fig.5.35-Comparison of experimental and analytical results of Marti et al.slab [13] No. 6.

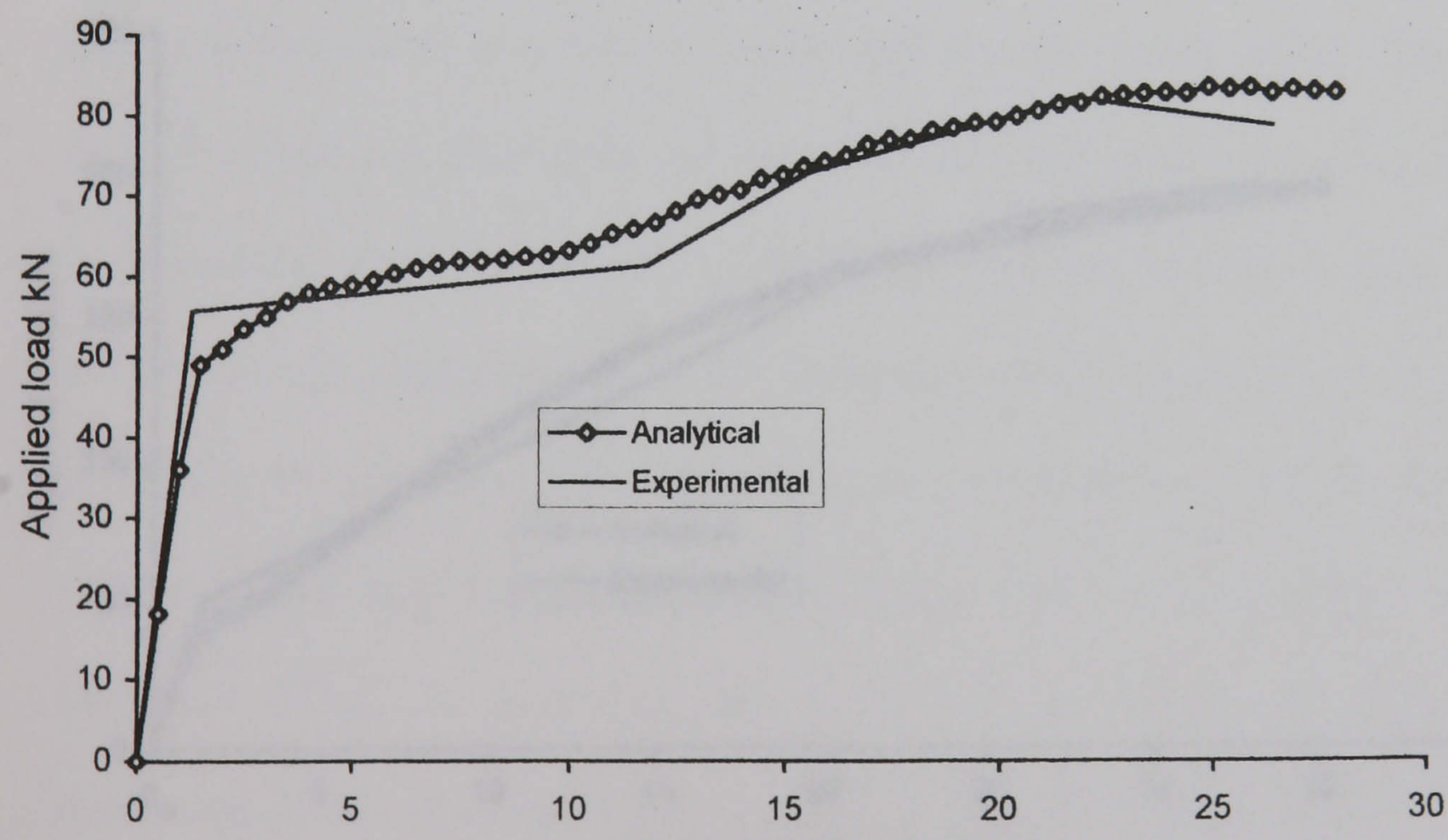

Fig.5.36-Comparison of experimental and analytical results of Marti et al. Slab [13] No. 7.

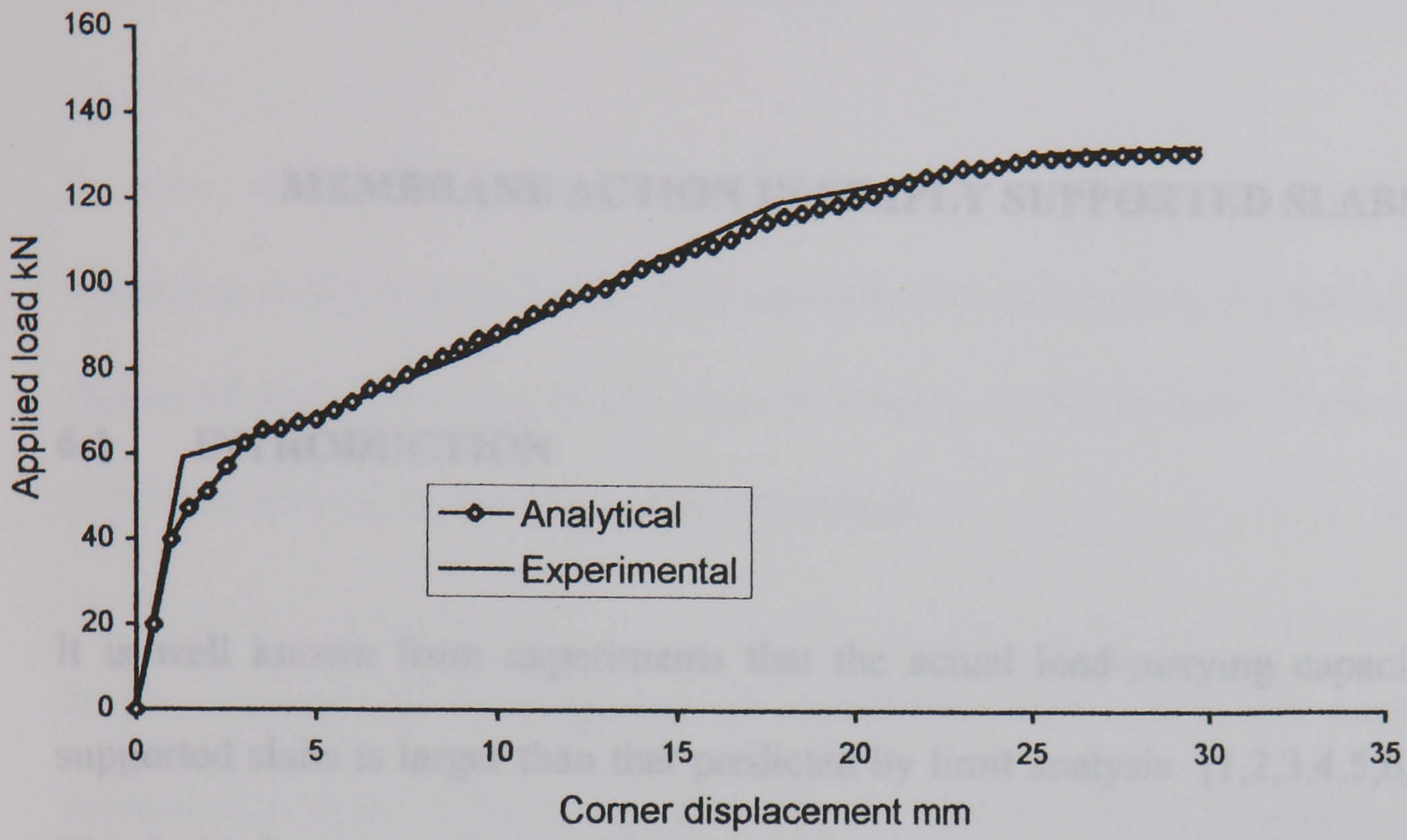

Fig.5.37-Comparison of experimental and analytical results of Marti et al. Slab [13] No. 8.

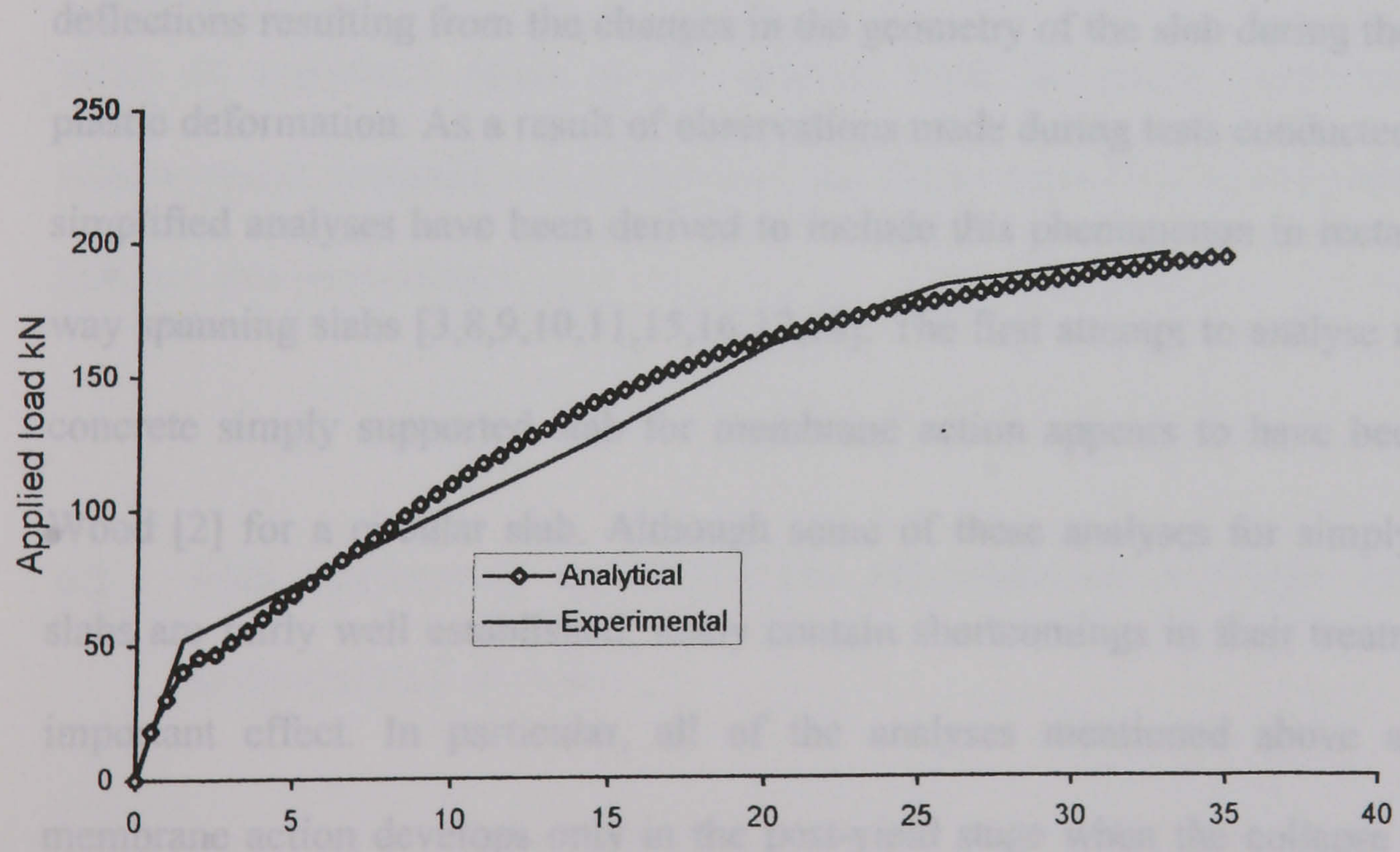

Fig.5.38-Comparison of experimental and analytical results of Marti et al. Slab [13] No. 9.

CHAPTER 6

MEMBRANE ACTION IN SIMPLY SUPPORTED SLABS

6.1 INTRODUCTION

It is well known from experiments that the actual load-carrying capacity of simply supported slabs is larger than that predicted by limit analysis [1,2,3,4,5,6,7,8,9,10,11]. The main factor which can cause an increase of the load of simply supported slabs beyond the plastic collapse load is the membrane action which develops with increasing deflections resulting from the changes in the geometry of the slab during the process of plastic deformation. As a result of observations made during tests conducted, several of simplified analyses have been derived to include this phenomenon in rectangular two-way spanning slabs [3,8,9,10,11,15,16,17,18]. The first attempt to analyse a reinforced concrete simply supported slab for membrane action appears to have been made by Wood [2] for a circular slab. Although some of these analyses for simply supported slabs are fairly well established; many contain shortcomings in their treatment of this important effect. In particular, all of the analyses mentioned above assume that membrane action develops only in the post-yield stage when the collapse mechanism has been formed. In reality, membrane action develops at the onset of cracking, before the collapse mechanism has been formed and before yield of the reinforcement has been reached. Moreover, the theories assumed rigid-plastic material properties and failed to predict the elastic response before failure. Some of the theories that attempt to

determine the complete load-deflection curve [9,11] of simply supported slabs up to failure have neglected membrane forces at low levels of load.

In view of the shortcomings associated with these various simplified methods, numerical methods may be the best approach for determining the behaviour of simply supported slabs from the initial stage of loading up to collapse. Such a possibility is examined here using the finite element method.

In this Chapter an investigation of membrane action effect for simply supported reinforced concrete slabs using finite element analysis will be described. A comparison between the results of the finite element analysis and the results of some of the plastic analyses [2,8] which include the effect of the membrane action are also presented. The effect of membrane action on the ultimate loads for simply supported slabs with reinforcement designed using the Wood and Armer rules [13,14] and yield line theory [12] are also investigated.

6.2 THE GENERAL EFFECTS OF MEMBRANE ACTION ON SIMPLY SUPPORTED SLABS

In order to investigate the effect of membrane action on simply supported reinforced concrete slabs, a 2 m by 2m square 60mm deep slab iso-tropically reinforced at top and bottom similar to that tested by Gohneim[5,6], has been analysed for different reinforcement ratios of 0.5%, 1%, 1.5%, 2%, 2.5% and 3.5%. The material strength

used was 400 MPa. for the steel and 40 MPa. for the concrete. The computer program described in Chapter 3 has been used to analyse the slab up to collapse for the above reinforcement ratios.

The results of the analyses for different reinforcement ratios are shown in Fig.6.1. The reinforcement ratio has no effect up to cracking, which occurred at a load approximately 10.0 kN/m^2, and this is evident from the pre-cracking responses. Increasing the reinforcement ratio increases the load carrying capacity of the slab, as expected.

Fig. 6.2 shows the normalised load-deflection curves with respect to yield line theory collapse load for the above slab with different reinforcement ratios. With low reinforcement ratios the enhancement of the strength of the slab beyond the yield line theory load is more significant. The increase in the strength arises from the tensile membrane action which is induced in the central region of the slab and from the compressive membrane action in the outer region. The introduction of the membrane forces in the slab is the result of the change of geometry of the slab.

Tensile membrane action is more significant in under-reinforced slabs and reduced as the amount of the reinforcement increases in slabs, Fig 6.2. Slabs with a low reinforcement ratio develop proportionally more (tensile) membrane action, which obviously results in a higher enhancement in the load carrying capacity, cases 1-5 Fig.6.2. In case 6 there is no enhancement in the ultimate strength for the slab beyond the yield line theory load; this is because the slab is over-reinforced and failed as a

result of crushing of the concrete rather than yielding of reinforcement, which means that the slab failed before a significant amount of membrane action could develop.

6.3 YIELD CRITERION.

In order to understand the behaviour of reinforced concrete slabs subjected to bending moment and in-plane axial force, the yield criterion for the slab section must be known. Fig.6.3 shows the conditions at yield of a positive-moment section of unit width of slab, iso-tropically reinforced at top and bottom. The stress resultant at the section C_c, T_{st} and T_{sb} is statically equivalent to the membrane force P, acting at mid-depth, and the resisting moment, M, summed about the mid-depth axis. The section is assumed to fail under the action of a bending moment M and the axial force P. Therefore, for a strip of unit width

$$P = T_0 - C_c = T_0 - kf_c' a \qquad 6.1$$

$$\text{or} \qquad a = \frac{(T_0 - P)}{k f_c'} \qquad 6.2$$

$$\text{where} \quad T_0 = T_{st} + T_{sb} \qquad 6.3$$

$$M = kf_c' a(0.5h - 0.5a) - T_{st}(0.5h - d') + T_{sb}(d - 0.5h) \qquad 6.4$$

where T_{st} = tensile force in top steel.

T_{sb} = tensile force in bottom steel.

T_0 = ultimate tensile force in steel.

C_c = compressive force in concrete.

a = depth of the compression block.

$f_c^{'}$ = compressive strength of concrete.

f_y = yield strength of reinforcement.

M = the moment with in-plane axial force.

If M_0 is the moment when $P=0$, then for the slab with 1% of reinforcement described in Section 6.2, the normalised yield criterion with respect to M_0 calculated using the above expressions is shown in Fig.6.4.

6.4 EQUILIBRIUM OF THE MEMBRANE FORCES IN SIMPLY SUPPORTED SLABS

In simply supported slabs the membrane action becomes significant and more important at large deflections. With large deflections at mid-span, the central region of the supported edges tends to move inwards but is restrained from doing so by the adjacent outer regions. This creates a central area of tensile membrane stresses within the slab together with a surrounding ring of compression. Fig. 6.5 illustrates a uniformly loaded simply supported slab undergoing large deflections after the yield line pattern has been formed. In the central region of the slab the cracks will have penetrated through the full depth of the slab. The slab will be in equilibrium under the set of stresses named;

circumferential compressive membrane force and cicumferential and radial tensile membrane force.

In order to follow the development of the tension zone in the centre and the compressive zone in the outer region, the slab described in section 6.2 with a reinforcement ratio of 1%, has been considered. The strain and the stress profiles at points 1, 2 and 3, on the slab, Fig.6.6, obtained from finite element analysis have been investigated. The strain and stress profiles at relative central deflections, $\frac{w_0}{d}$ of 0.25, 0.75, 1.25 and 1.75 Fig.6.7 are shown in Figs. 6.8-6.15. As the deflection increases the geometry of the slab changes; because of this change in geometry the neutral axis rises up towards the top face of the slab at the centre at point 2 and drops down towards the bottom face at the edges, point 1. The movement of the neutral axis creates a zone of tensile stress at the centre surrounded by a compressive zone in the outer region.

At the centre of the slab, point 2, when the deflections becomes 0.25 and 0.75, the neutral axis moves above the central axis of the slab section, which makes the zone of the tensile stresses extend to the top of the slab and the zone of compressive stresses reduces. At relative deflections of 1.25 and 1.75 the tensile stresses almost dominate the upper half of the slab and the zone of the compressive stresses becomes very small in this case the slab cracked right through its depth Figs.6.8-6.9.

At point 1, Figs.6.10-6.13, the compressive stresses increases and extends toward the bottom of the slab with increasing deflections; the major part of the compressive stresses is carried in y-directions.

At the corner at point 3, because of the torsion, the slab is subjected to Compression-tension state of stresses. The centre of the slab is subjected to tensile stresses and the top and bottom faces are subjected to compressive stresses. The compressive stresses reduce with increasing deflections and become zero at sampling point 1,2 and 3 at the top and 7,8 and 9 at the bottom at relative deflection of 1.75 Figs. 6.14-6.15.

6.5 DEVELOPMENT OF MEMBRANE ACTION IN SIMPLY SUPPORTED REINFORCED CONCRETE SLABS.

Slab 2 has also been used to investigate the development of the membrane forces and moments with increasing load. The variation of the membrane forces P_x, P_y and P_{xy} and the variation of the moments M_x and M_y along the central axis of the slab between points 1 and 2, and along the diagonal between the points 2 and 3, Fig.6.6 are investigated at relative central deflections of 0.25, 0.75, 1.25 and 1.75 on the load-deflection curve Fig.6.7.

6.5.1 MEMBRANE FORCES

When the slab deflected the geometry of the slab changed and consequently membrane forces developed in the plane of the slab. The membrane forces P_x and P_y along the central axis and along the diagonal and the membrane shear force P_{xy} along the

diagonal of the slab are normalised with respect to the ultimate tensile force of the reinforcement T_0, and are shown in Figs.6.16-6.19.

From Figs. 6.16-6.18 it can be seen that the membrane forces along the central axis and along the diagonal at the centre of the slab are tensile and they are equal, $\frac{P_x}{T_0} = \frac{P_y}{T_0}$. The membrane forces are increased with increasing deflections and they vary from 0.22 at a relative deflection of 0.25 to 1 at a relative deflection of 1.25 and 1.75. The tensile membrane forces spread and reduce away from the centre of the slab. The length of spread of the tensile membrane action is also increased with increasing deflections. The length of the spread of $\frac{P_x}{T_0}$ and $\frac{P_y}{T_0}$ along the central axis varies between 0.3 L_1 and $0.25\,L_1$ respectively at relative deflection of 0.25 to $0.36\,L_1$ and $0.28\,L_1$ respectively at relative deflection of 1.75. The length of spread of $\frac{P_x}{T_0}$ and $\frac{P_y}{T_0}$ along the diagonal also varies between $0.32\,L_1$ at relative deflection of 0.25 to $0.41\,L_1$ at relative deflection of 1.75. The spread of the tensile membrane forces from the centre of the slab leads to a circular tensile zone at the centre of the slab. Outside the zone the membrane forces change to compression. The depth of the compressive zone is also increased with increasing deflections. Along the central axis the compressive membrane forces $\frac{P_x}{T_0}$ and $\frac{P_y}{T_0}$ varied between 0.15 and 0.25 respectively at relative deflection of 0.25 to 0.77 and 1.8 respectively at relative deflection of 1.75. Along the diagonal the compressive

membrane forces $\frac{P_x}{T_0}$ and $\frac{P_y}{T_0}$ vary between 0.3 at relative deflection of 0.25 to 0.44 at relative deflection of 1.75. At relative deflections of 1.25 and 1.75 the compressive membrane forces are changed to tensile at the corner with a value of 0.25 and 0.35 respectively.

Fig.6.19 shows the variation of the membrane shear force $\frac{P_{xy}}{T_0}$ along the diagonal of the slab; the membrane shear force is zero at the centre and at the corner of the slab and becomes maximum at $0.45\,L_1$ from the centre. The membrane shear force is increased with increasing deflections and varies between 0.12 at relative deflection of 0.25 to 0.475 at relative deflection of 1.75.

Since the slab is symmetrical, the membrane force $\frac{P_x}{T_0}$ is used to study the distribution of the membrane forces in the plane of the slab. The contours of $\frac{P_x}{T_0}$ at relative central deflections of 0.25, 0.75, 1.25 and 1.75, in the plane of the slab, are shown in Figs.6.20-6.23. From the figures, it is clear that the intensity of the tensile membrane force in the centre and the compressive membrane force at the outer region of the slab increase with increasing deflections. The diameter of the tension zone also increases with increasing deflection.

At a relative central deflection of 0.25, Fig. 6.20, all the outer region of the slab is subjected to compression and the centre is subjected to a circular zone of tension of

diameter of $0.5\,L_1$, with maximum tensile force of 20% of the total tensile force in reinforcement. The load at this deflection is approximately half of the yield line theory load, Fig. 6.7, which means that simply supported slabs can develop membrane action right at the onset of cracking before the formation of the collapse mechanism. This result is counter to the assumption of the rigid plastic theories which assume that the tensile membrane action is developed after the yield line theory load is reached.

At a relative deflection of 0.75, which approximately corresponds to 1.20 of yield line theory load, the diameter of the tension zone increased to $0.6\,L_1$ and the tensile membrane force at the centre reaches 60% of the total tensile force in reinforcement. All the outer region of the slab is subjected to compression, Fig.6.21.

At relative deflections of 1.25 and 1.75 which correspond to loads of 1.4 and 1.5 of the yield line theory load respectively, the tensile membrane forces reach purity (100% of the total tensile force in reinforcement, $\frac{P_x}{T_0}$=1), Figs.6.22-6.23. At relative deflection of 1.25 the pure tensile membrane force at the centre of the slab is just a point but at relative deflection of 1.75 the length of the spread of the pure tensile membrane forces is extended to occupy 30% of the slab centre. The diameter of the tension zone also increased to $0.7\,L_1$ and $0.75\,L_1$ at relative deflections of 1.25 and 1.75 respectively. In this case the slab is subjected to a circular tensile zone in the centre surrounded by a circular compressive zone in the outer region. The corners the slab are subjected to tensile membrane force of value of 25% and 50% of the total tensile force in reinforcement at relative deflections of 1.25 and 1.75 respectively, Figs.6.22-6.23.

The contours of membrane shear force $\frac{P_{xy}}{T_0}$ at relative deflection of 1.75 is shown in Fig 6.24. From the figure it can be seen that the membrane shear force is localised in the corners of the slab along the diagonal and is zero at the centre of the slab along x-axis and along y-axis.

The contours of the principal membrane forces and their corresponding directions at relative deflections of 1.25 and 1.75 are shown in Figs.6.25-6.28. It is clear from the figures that the slab is subjected to a ring of radial and circumferential tensile membrane forces at the centre surrounded by a ring of circumferential compressive membrane force in the outer region. This result proves Wood's [2] assumption for simply supported slab at large deflections.

6.5.2 MOMENTS

Figs. 6.29-6.31, shows the moments normalised with respect to the moment when the membrane force is zero, $\frac{M_x}{M_0}$ and $\frac{M_y}{M_0}$, between points 1 and 2 along the centre line and between points 2 and 3 along the diagonal of the slab, Fig.6.6.

From the figures it is clear that the moments at the centre are decreased with increasing deflections as a result of development of tensile membrane action. At a relative deflection of 0.25 the membrane forces become 0.22 and the moments at the centre are

reduced to 0.78. At a relative deflection of 0.75 the membrane force increased to 0.75 and the moment reduced to 0.3 at the centre. At relative deflections greater than the depth of the slab, $\frac{w_0}{d}$=1.25 and 1.75, the pure membrane forces form and the moments are reduced to zero; in this case the load is carried mainly by the reinforcement working as tensile plastic net.

6.6 COMPARISON WITH OTHER THEORETICAL METHODS

For the purpose of comparison, two theoretical methods are chosen. The first one is for a square simply supported slab, proposed by Kemp [8], and the second is for a circular simply supported slab, proposed by Wood [2]. The two methods are based on plastic theory and include the effects of changes in geometry of the slab.

6.6.1 COMPARISON WITH KEMP'S METHOD FOR A SQUARE SLAB.

Kemp [8] follows the same approach for square slab as that proposed by Wood [2] for a circular simply supported slab. The concrete slab was assumed to be iso-tropically reinforced at the bottom face only. To demonstrate the analysis a 4m x 4m x 0.12 m square slab with effective depth of 100mm has been analysed, the material strengths used were 400 MPa. for the steel and 40 MPa. for the concrete.

The yield criterion for the slab section is shown in Fig. 6.32.

6.6.1.1 LOAD DEFLECTION CURVE

The numerical values for the increase in the loads for a given displacement resulting from membrane action using Kemp's theory are calculated in two stages. In the first stage the numerical values are calculated up to deflections less than the deflections at which the pure tensile membrane action forms. In the second stage the numerical values are calculated after the formation of the pure tensile membrane action. The deflection at which a pure tensile membrane action forms was derived by Kemp [8] and is given as $\frac{w_0}{d}=6t$, where t is the ratio of the maximum tensile strength of the reinforcement to the maximum crushing strength of the concrete, $t=\rho\frac{f_y}{f_c'}$

For relative deflections less than the critical value $\frac{w_0}{d}\leq 6t$, the increase in the load above yield line theory collapse load, $\frac{P}{P_y}$, is calculated for a given central deflection, $\frac{w_0}{d}$, from the following equation

$$\frac{P}{P_y}=1+\frac{1}{48t(1-0.75t)}\left(\frac{w_0}{d}\right)^2 \qquad 6.1$$

and after the formation of the pure tensile membrane action, $\frac{w_0}{d}\geq 6t$ the increase in the load is given by

$$\frac{P}{P_y}=1+\frac{0.75t}{(1-0.75t)}\left(\sqrt{\frac{w_0}{d}}\sqrt{\frac{1}{1.5t}}-1\right)^2 \qquad 6.2$$

The increase in the load compared with the collapse load in the above expressions depends only on the relative deflection $\frac{w_0}{d}$, and on the parameter t.

Values of the increase in the load with increasing deflections have been calculated using Kemp's theory and the finite element analysis, for the slab described above with values of t of 0.02 and 0.1. The load-deflection curves obtained are shown in Fig. 6.33. Because of the assumed rigid, perfectly plastic slab behaviour, the load-deflection curves predicted using Kemp's theory show no deflection until the simple yield line theory collapse load is reached. The load-deflection curves predicted using the finite element analysis include the elastic deflections in the un-cracked and cracked state followed by the elasto-plastic deflections as the yield mechanism formed and they merge gradually into the load-deflection curves predicted using Kemp's theory.

The increase in the load caused by membrane action predicted using Kemp's theory is quite small up to the critical deflection stage, $\frac{w_0}{d}\leq 6t$, at which cracking throughout the depth of the slab occurred. The value of this deflection is found to be 0.12 for t = 0.02 and 0.59 for t = 0.1. The percentage increase in the loads compared with yield line theory load at this deflection was found to be 1.1% for t=0.02 and 7% for t=0.1. For deflections greater than this value, the increase in the load becomes more significant and is more pronounced in a slab with a low value of t (or a low percentage of

reinforcement) than in one with a high value of t. At a relative deflection equal to half the depth of the slab, the percentage increase in the load above yield line theory load calculated using Kemp's theory was 13% for $t = 0.02$ and 5% for $t = 0.1$. From the finite element analysis the percentage increase in the load above yield line theory collapse load was 83% for $t = 0.02$ but for $t = 0.1$ the load is equal to yield line theory collapse load. At a relative deflection equal to the slab depth, the percentage increase in the load using Kemp's theory was 52% for $t = 0.02$ and 35% for $t = 0.1$, and from the finite element analysis was 100% for $t = 0.02$ and 35% for $t = 0.1$. At a relative deflection of 2.5 the increase in the load calculated using Kemp's theory and finite element analysis were twice yield line theory collapse load for $t = 0.02$. But for $t = 0.1$, the increase in the load predicted using Kemp's theory was 75% and predicted using finite element analysis is 42%. Generally the load-deflection curves predicted using Kemp's theory and finite element analysis are in good agreement in the case of $t = 0.02$, but in the case of $t = 0.1$ they are in agreement between relative deflections of $\frac{w_0}{d} = 0.5$ to $\frac{w_0}{d} = 1.75$.

It is important to investigate and compare the membrane forces and moments predicted using Kemp's theory and finite element analysis, which causes the increase in the collapse load. For this purpose the slab with $t = 0.1$ is chosen.

6.6.1.2 MEMBRANE FORCES AND MOMENTS

The membrane forces and moments in the x-direction are investigated at relative deflections of $\frac{w_0}{d} = 0.5$, 1.25 and 1.75. The membrane forces are normalised with

respect to the ultimate tensile force in the reinforcement, $\frac{P_x}{T_0}$ and the moments are normalised with respect to moment when membrane forces are zero, $\frac{M_x}{M_0}$ for $t = 0.1$ along the centre line of the slab Fig.6.34, between points 1 and 2 as shown in Figs.6.35-6.40.

At a relative deflection equal to half the depth of the slab, which is below the critical deflection the membrane forces $\frac{P_x}{T_0}$ predicted using Kemp's theory varies linearly along the centre line of the slab and are zero at $0.25L_1$. For the inner half of the slab the membrane force is tensile and equal to 0.7 and in the outer half is compressive and equal to 0.8 at the edge. Compared with finite element results the membrane force is tensile at the centre and compressive in the outer region and they are equal to 0.3 and 0.4 respectively; the membrane forces are zero at $0.275L_1$ Fig.6.35.

At a relative deflection greater than the effective depth of the slab, the slab is cracked throughout its depth and the pure tensile membrane forces occur at the centre and the length of the spread of tensile membrane forces is also increased. At relative deflection of 1.25 the pure tensile membrane forces from Kemp's theory and from finite element analysis occupy about 30% and 20% of the slab centre and the depth of the compressive zone is also increased to 1.1 and 2.35 respectively Fig.6.36. At a relative deflection of 1.75, the pure tensile membrane forces predicted using Kemp's theory and finite element analysis increased to occupy 45% and 25% of the slab centre and the depth of the compressive zone increased to 1.6 and 3 respectively, Fig.6.37.

The moments from finite element analysis and the moments predicted using Kemp's theory are shown in Figs.6.38-6.40.

At a relative deflection of 0.5, the membrane forces developed in the plane of the slab, the moment from finite element analysis reduced to 0.9 and the moment from Kemp's theory results reduced to 0.6 at the centre and increased to1.4 at the edge Fig.6.38.

At a relative deflection of 1.25 and 1.75, because the pure membrane forces occur the moments predicted using the finite element analysis and Kemp's theory reduced to minimum $\frac{M_x}{M_0}$ =0.42, as shown in Figs. 6.39-6.40. The moments at the edge predicted using Kemp's theory were1.45 and 1.6 respectively.

6.6.1.3 DISCUSSION AND CONCLUSION

The membrane forces and moments at the centre of the slab from the finite element analysis in the *x*-direction are generally in good agreement with the predictions of Kemp's theory. In the outer region the compressive membrane forces predicted using Kemp's theory continue in the increase and achieve maximum at the edge; this leads to increase in the moment as the edge approached, which is not true in the case of the simply supported slab. Kemp [8] ignored the membrane forces in the *y*-direction which is not always equal to that one in the *x*-direction, especially in the outer region where the major part of the compressive membrane forces are carried in the *y*-direction.

With reference to results of the membrane forces and the corresponding moments for the slab described above with $t = 0.1$, Figs.6.35-6.40. At a relative deflection of 0.5, the tensile membrane forces developed but their contribution on the load carrying capacity of the slab is not significant. The load predicted using finite element analysis was equal to yield line theory collapse load and the load predicted using Kemp's theory was only 7% higher than the yield line theory collapse load Fig.6.33. At a relative deflection of 1.25 the enhancement of the load above yield line theory load becomes more significant because of the development of the pure membrane action in the plane of the slab; the enhancement predicted using Kemp's theory was 25% and using the finite element analysis was 50%. At relative deflection of 1.75, although the length of the spread on the pure tensile membrane increased the collapse load predicted using the finite element analysis reduced to 48% as a result of the flexural failure of the slab. The enhancement of the collapse load predicted using Kemp's theory was 48% above the yield line theory load at deflection of 1.75 and 75% at deflection of 2.5.

With reference to load-deflection curve predicted using finite element analysis Fig.6.33, the slab cracks at relative deflection of $0.12d$ which corresponds to 0.4 of yield line theory load, the reinforcement yields at relative deflection equal to the depth of the slab, which is corresponds to 1.4 of the yield line theory collapse load and the failure takes place at relative deflection about $1.3d$ by yielding of the reinforcement which corresponds to 1.6 of yield line theory collapse load. In case of the load-deflection curve predicted using Kemp's theory there is no criterion for yielding of the reinforcement or

cracking or crushing of the concrete and the load-deflection curve continues to rise without stopping.

6.6.2 COMPARISON WITH WOOD'S METHOD FOR A CIRCULAR SLAB.

Wood [2] presented an analysis for a circular simply supported slab based on the rigid plastic approach taking into account membrane action caused by the change of the slab geometry. Fig.6.41 shows the circumferential and radial membrane forces and moments, P_θ, P_r, M_θ and M_r respectively, acting on a circular slab element with radius R and inner tensile zone with radius r. A circular slab 4m diameter, effective depth of 100 mm and iso-tropically reinforced with 0.4% of reinforcement at the bottom only has been analysed. The material strengths used were 400 MPa. for the steel and 40 MPa. for the concrete. The yield criterion for the slab with, $t = 0.04$ is shown in Fig. 6.42.

6.6.2.1 LOAD-DEFLECTION CURVE

The typical numerical values for the increase in the load as a result of membrane action using Wood's theory are calculated in two stages in the same way as for Kemp's theory. In the first stage the increase in the load up to deflections less than the deflections at which the pure tensile membrane forms are determined from the following relations

$$\frac{P}{P_y}=1.0+\frac{\mathrm{K}^2}{64\beta}\left(\frac{w_0}{d}\right)^2 \qquad 6.3$$

where K is a constant for the slab section and given by $\frac{\frac{h}{d}}{1-0.75t}$, $\beta=\frac{0.75t}{1-0.75t}$ and h is the slab thickness.

This load goes on rising until a new state of affairs begins with a pure tensile membrane at the centre. This leads to a critical deflection of $\frac{w_0}{d}=2-\frac{4\alpha}{u}$, where $\alpha=\frac{\frac{1}{2}\frac{h}{d}-\frac{3}{2}t}{1-\frac{3}{4}t}$.

When the deflection exceeds the critical deflection, the pure tensile membrane begins and the increase in load is determined from the following relations:

$$\frac{P}{P_y}=1+\frac{1+\frac{1-5\frac{r_1}{R}}{1-\frac{r_1}{R}}\beta}{\left(1+2\frac{r_1}{R}\right)\left(1-\frac{r_1}{R}\right)^2} \qquad 6.4$$

where r_1 is the radius of the spread of the pure tensile membrane action from the centre of the slab. It will be noticed that the increase in the load in equation 6.4 is dependent only on the parameter t and r_1. The corresponding central deflection can be obtained from the following relations

$$\frac{w_0}{d}=\frac{8\frac{\beta}{\mathrm{K}}}{1-\frac{r_1}{R}}+\frac{3}{2\mathrm{K}}\frac{P}{P_y}\frac{r_1^2}{R^2} \qquad 6.5$$

The load-deflection curves normalised with respect to yield line theory collapse load predicted using Wood's theory and finite element analysis for the slab described above are shown in Fig. 6.43. The load-deflection curves are not in agreement with each other. With reference to the Wood's load-deflection curve, the yield line theory type collapse load is controlled at first but after the formation of the pure tensile membrane forces about $\frac{w_0}{d}$=0.119 the load picks up and continues to increase until the failure occurs. When the deflection equals half the effective depth of the slab the pure tensile membrane action from Wood's theory occupies about 35% of the slab radius and enhances the collapse load by about 30% above yield line theory load. At this deflection the increase in the load carrying capacity above the yield line theory load predicted using finite element analysis was 20%.

When the deflection equals the depth of the slab the pure tensile membrane action from Wood's theory occupies half the radius of the slab, the load being nearly twice the yield line theory load. The increase in the load-carrying capacity above yield line theory collapse load predicted using the finite element analysis was half of the increase in the load predicted using Wood's theory at this deflection.

At a relative deflection of 1.5 the pure tensile membrane action from Wood's theory occupies 60% of the slab radius, the load being nearly 150% of the yield line theory

collapse load. At this deflection the finite element analysis predicted the maximum increase in the load-carrying capacity of this slab which is equal to half the enhancement predicted using Wood's theory; after that the slab failed.

It is important to study the membrane action effect, which causes this rise in load and what make the discrepancy between the load-deflection curves, so that the membrane forces and moments are investigated along the radius of the slab.

6.6.2.2 MEMBRANE FORCES AND MOMENTS

The circumferential and radial membrane forces and moments from both Wood's theory and finite element analysis are investigated along the radius of the slab in three selected relative central deflections of 0.5, 1 and 1.5, and they are shown in Figs. 6.44-6.55.

Fig. 6.44 shows the circumferential membrane forces, $\frac{P_\theta}{T_0}$ predicted using both Wood's theory and finite element analysis at relative deflection of 0.5. Also $\frac{P_\theta}{T_0}$ predicted using Wood's theory at relative deflection of 0.199 is shown in the same figure. The membrane forces vary linearly along the radius of the slab and are zero at the mid-point of the radius; for the inner half of the radius they are tensile and for the outer half they are compressive. The pure tensile membrane is just a point at the centre of the slab at this particular deflection, and it spreads outside the centre with increasing deflection. At a relative deflection of 0.5, the overall tensile zone of the membrane forces predicted using Wood's theory and the finite element

analysis was extended to cover a circular zone of radius of 55% of the slab radius. At the centre the pure tensile membrane predicted using Wood's theory occupies 35% of the slab radius, but from the finite element analysis the tensile membrane forces just reached 0.60 of the pure tensile membrane. In the outer region, the membrane forces are changed to compression; Wood's theory gives 2.4 and the present analysis gives 0.75 at the edge of the slab.

With increasing deflections the overall circular zones of the tensile membrane forces increase and the radius of the pure tensile membrane at the centre also increases. The depth of the compressive zone in the outer region also increases with increasing deflections. At relative deflection of 1, the tension zones predicted using Wood's theory and finite element analysis extended to 65% and 60% of the slab radius, and the radius of the pure tensile membrane at the centre extended to 50% and 10% of the slab radius respectively. In the outer region the depth of compressive zones near the edges is also increased; Wood's theory results give 4.2 and the finite element analysis gives 2.2 Fig.6.45. At relative deflection of 1.5, the overall tension zones predicted using Wood's theory and finite element analysis extended to 72% and 62% of the slab radius, and the radius of the pure tensile membrane forces at the centre of the slab extended to 60% and 20% of the slab radius respectively. The depth of the compression zone from Kemp's theory increased to 6 and from finite element analysis increased to 2.8, Fig.6.46.

The circumferential moments predicted using both Wood's theory and finite element analysis at relative deflection of 0.5 are shown in Fig.6.47. Because the membrane forces were induced in the plane of the slab the moments predicted using Wood's theory

and finite element analysis were reduced to 0.42 and 0.7 respectively. In the outer region, because of the compressive membrane forces the moments increase towards the edge of the slab; Wood's theory results gives 2.3 and the finite element analysis gives 1.6. At relative deflections of 1 and 1.5 the moments predicted using Wood's theory and finite element analysis were reduced to minimum at the centre. In the outer region the moments predicted using Wood's theory and finite element analysis increased to 2.85 and 2.3 respectively at relative deflection of 1 and increased to 3.45 and 2.5 respectively at relative deflection of 1.5, Figs.6.48-6.49.

In the radial direction the tensile membrane forces $\frac{P_r}{T_0}$ and the corresponding moments $\frac{M_r}{M_0}$ predicted using Wood's theory and finite element analysis are equal to the circumferential membrane forces $\frac{P_\theta}{T_0}$ and the corresponding moments $\frac{M_\theta}{M_0}$ at the centre of the slab. These radial tensile membrane forces and the corresponding moments are reduced gradually out side the centre of the slab and become zero at the edge. The membrane forces in the radial direction and their corresponding moments at relative deflections of 0.5, 1 and 1.5 are shown in Figs. 6.50-6.55.

6.6.2.3 DISCUSSION AND CONCLUSION

With reference to load-deflection curves Fig.6.43, the curves are not in agreement with each other; this discrepancy is attributed to Wood's assumption of the development of

the pure tensile membrane forces at the centre of the slab at small relative deflection of 0.199 Fig.6.44. This pure tensile membrane force is enough to stiffen up the load-deflection curve and forms a discrepancy between the finite element analysis and Wood's theory results. With regard to the load-deflection curve predicted using finite element analysis the slab cracks at deflection of 0.06*d*, and the reinforcement yields at deflection equal to the depth of the slab which corresponds to 0.41 and 1.5 of yield line theory collapse load respectively. The failure takes place at deflection of 1.45*d*, as a result of yielding of the reinforcement, which corresponds to 1.75 of the yield line theory collapse load. But in the case of the load-deflection curve predicted using Wood's theory there was no evidence of such behaviour of cracking or yielding of reinforcement. The load deflection curve continued to rise without stopping until the tensile membrane forces occupy almost all the slab radius and there are no compressive membrane forces to equilibrate them. In this particular slab, the slab failed when the pure tensile membrane forces occupy about 90% of the slab radius at deflection of 6*d*, which corresponds to 5.5 of yield line theory collapse load.

From the results of the membrane forces and the corresponding moments at relative deflections of 0.5, 1 and 1.5, Figs. 6.44-6.55, the circumferential and radial membrane forces and moments predicted using the finite element analysis after the formation of the pure membrane forces at relative deflections of 1 and 1.5 are in good agreement with those predicted using Wood's theory. At relative deflection of 0.5 there is a difference between the predicted membrane forces at the centre of the slab and their corresponding moments.

From the above results it can be seen that the radial moment at the centre contributes as usual towards carrying the load. But considerable extra strength is now given by the increase of circumferential moment as the edge is approached. The strong compression gives rise to this. The tensile membrane forces at the centre also cause a further rise in load after the formation of the pure tensile membrane forces.

6.7 STUDY OF MEMBRANE ACTION EFFECT ON THE ULTIMATE LOAD OF SIMPLY SUPPORTED SLABS.

In order to study the effect of membrane action on the ultimate load of simply supported slabs, slabs have been designed for ultimate loads on the assumption of a uniformly distributed load, using grade 400 reinforcement and 30 concrete. The reinforcement was designed using two different methods. The first method used the reinforcement design using the ultimate plastic moments calculated from yield line theory [12] using simple straight-line mechanisms. The second method used the reinforcement, which was designed using Wood and Armer rules [13,14] using elastic moment fields. The elastic moment analysis is most conveniently carried out using the finite element method. The moment analysis provides at each point the elastic moments M_x, M_y and M_{xy} which are, respectively, the bending moment about the x-axes, the bending moment about the y-axes and the torsional moment per unit length. The elastic moments are used to calculate the design moments per unit width, M_x^* and M_y^*. The design moments used are given in table 6.1.

For square slab simply supported along all edges and carrying a uniformly distributed load, the Wood and Armer [1,2] design moments coefficients for 16 finite element mesh per quarter Fig.6.56 are given in Table 6.2 at the corners of the elements.

To determine numerically the increase in the collapse load caused by membrane action, the slabs have been analysed up to collapse using the computer program described in Chapter 3 and the predicted collapse loads have been normalised with respect to the original collapse loads from yield line theory and Wood and Armer rules.

6.7.1 STUDY OF SLABS SIMPLY SUPPORTED ALONG ALL EDGES

The investigation of the membrane action effect on the ultimate load of rectangular slabs simply supported along all edges includes the study of three main factors, namely slenderness ratio $\frac{L_1}{d}$, aspect ratio $\frac{L_2}{L_1}$ and the parameter t. where t is the ratio of maximum tensile strength to maximum compressive strength $\rho\frac{f_y}{f_c'}$.

6.7.1.1 EFFECT OF SLENDERNESS RATIO

Two 4 m by 4 m square slabs with different slenderness ratios and different reinforcement ratios are analysed. The slenderness ratios were 40 for slab $S1$, and 25 for the slab $S2$. The results obtained from the analysis are shown in Figs. 6.57-6.58.

For slabs with reinforcement designed using Wood and Armer rules [13,14] for $t = 0.02$ at the centre, the enhancement of the ultimate load for the slab $S1$ was 105% and for the slab $S2$ it was 77%. This enhancement in the ultimate load is decreased gradually with increasing of t at $t = 0.25$ at the centre; the enhancement was 15% for the slab $S1$ and 9% for the slab $S2$.

For slabs with reinforcement designed using plastic moments from yield line theory [12] at $t = 0.02$ the enhancement of the ultimate load for the slab $S1$ was 120% and for the slab $S2$ was 90%. The enhancement in the ultimate load is decreased gradually with increasing of reinforcement ratio until it becomes 23% for the slab $S1$ and17% for the slab $S2$ at $t = 0.25$.

It is clear from the figures that the membrane action has a beneficial effect on the collapse load for simply supported slabs. This effect is more pronounced in thin slabs with a low percentage of reinforcement calculated using yield line theory.

6.7.1.2 EFFECT OF ASPECT RATIO.

To show the effect of membrane action on rectangular slabs, slabs with aspect ratios varied from 1 to 3 have been analysed. All slabs have the same slenderness ratio of 25 and the same t at the slab centre of 0.05.

The numerical results obtained from the analysis are shown in Fig. 6.59. At aspect ratio of 1, the enhancement of the ultimate load for slabs with reinforcement calculated using Wood and Armer rules [13,14] was 56% and for slabs with reinforcement calculated using yield line theory [12] it was 71%. This effect is reduced gradually with increasing of the aspect ratio. At aspect ratio of 2.5, the slab action changed from two-way action to one-way action and the enhancement of the ultimate load remained constant. It is clear from the figure that one-way slabs can develop some amount of membrane action. For slabs with high aspect ratio (one-way slabs), and with reinforcement calculated using Wood and Armer rules [13,14], the enhancement of the ultimate load was 15% and for slabs with reinforcement calculated using yield line theory [12] it was 20%.

It is clear from the numerical results that the membrane action has a beneficial effect on the collapse load for simply supported rectangular slabs. This effect is more pronounced in slabs, with low aspect ratio and with reinforcement calculated using yield line theory.

6.7.2 STUDY OF SLABS SIMPLY SUPPORTED ON FOUR CORNER COLUMNS.

To investigate the effect of membrane action on the ultimate load of slabs simply supported on four columns, slab $S1$, described in Section 6.7.1.1, has been considered, but is in this case simply supported on four columns. The results obtained are shown in Fig.6.60.

It is clear from the figure that for low percentages of reinforcement there is an enhancement of the ultimate load compared with that predicted using yield line theory and Wood and Armer load. For $t = 0.02$ at the centre, the enhancement was 36% corresponding with yield line theory, and 25% corresponding with the Wood and Armer rule. This enhancement reduces gradually as t increases. At $t = 0.2$ and 0.12 at the centre the ultimate collapse loads becomes equal to the yield line theory and Wood and Armer design loads respectively. Where t is greater than 0.2 and 0.12 both methods overestimate the collapse load for the slab.

6.7.3 STUDY OF SLABS SIMPLY SUPPORTED ON TWO ADJACENT EDGES AND ON A COLUMN IN THE OPPOSITE CORNER.

Slab $S1$, which was investigated in Section 6.7.2, is in this case simply supported on two adjacent edges and on a column in the opposite corner. The numerical results obtained from the analysis are shown in Fig. 6.61.

It is clear from the figure that, for low percentage of reinforcement there is an enhancement of the ultimate load compared with that predicted using yield line theory

and Wood and Armer load. Where t = 0.02 at the centre, the enhancement was 52% corresponding with yield line theory and 40% corresponding with Wood and Armer rule. This enhancement reduces gradually as t increases. Where t = 0.25 and 0.17 the ultimate collapse loads become equal to the yield line theory and Wood and Armer design loads respectively. Where t is greater than 0.25 and 0.17 both methods over estimate the collapse load for slabs.

6.8 CONCLUSIONS

An investigation of membrane action using the finite element analysis by including the change of geometry has been carried out for simply supported reinforced concrete slabs. The investigation shows that the increase in the load-carrying capacity above the design load for simply supported slabs is caused by the membrane action which developed in the plane of the slab with increasing deflections. The distribution of the membrane forces is found to be a ring of radial and circumferential tensile membrane forces at the centre surrounded by a ring of circumferential compressive membrane force in the outer region

Comparison between the available plastic methods for membrane action analysis and the finite element analysis has also been carried out for simply supported square and circular slabs. The load-deflection curves predicted using the plastic methods are different from the load-deflection curves predicted using the finite element analysis. This is caused by the assumption of rigid plastic behaviour of theoretical plastic

methods, where the elastic deflections are neglected up to the yield line theory load. However, acceptable agreement was obtained between the finite element analysis and Kemp's [8] theory results for the square slab at post yield line theory load for t =0.02 and between relative deflections of 0.5 to 1.75 at post yield line theory load for t = 0.1

A study of the increase in the ultimate load due to the effect of membrane action in rectangular slabs with different types of simply supports using the reinforcement designed using Wood and Armer rules and yield line theory has also been carried out. The study shows that the percentage increase in the ultimate load is more significant in square slender slabs designed using yield line theory with low value of t and simply supported on four edges.

6.9 REFERENCES

1 Park R. and Gamble W.L., "Reinforced concrete slabs", A Wiley-Interscience Publication, John Wiley and Sons, USA, 1980.

2 Wood R. H., "Plastic and elastic design of slabs and plates", Thames and Hudson. 1961.

3 Park R., "Tensile membrane behaviour of uniformly loaded rectangular reinforced concrete slabs with fully restrained edges", Magazine of Concrete Research, Vol. 16. No. 46. March 1964. pp. 39-44.

4 Taylor R., Maher D. R. H. and Hayes B., "Effect of arrangement of reinforcement on the behaviour of reinforced concrete slabs", Magazine. of Concrete. Research, Vol. 18, No. 55,, June 1966.

5 Ghoneim M. G. and MacGregor J. G., "Tests of reinforced concrete plates under combined in-plane and lateral loads", ACI. Structural Journal, January-February 1994

6 Ghoneim M. G. and MacGregor J. G., "Behaviour of reinforced concrete plates under combined in-plane and lateral loads", ACI. Structural Journal, March-April 1994.

7 Brotchie J. F. and Hooly M. J., "Membrane Action in Slabs", Cracking, Deflection and Ultimate Load of Concrete Slab System, SP-30, ACI. Detroit, 1971, pp. 251-269.

8 Kemp K. O., "Yield of a square reinforced concrete slab on simply supports allowing for membrane action", Structural Engineer. Vol. 45, No. 7, July 1967. pp. 235-240

9 Desayi P. and Kulkarni A. B., "Load deflection behaviour of simply supported rectangular reinforced concrete slabs", Procedure of International Association of Bridge and Structural Engineers 1, P-11/78, February 1978, pp. 1-16.

10 Verreyya V., "Effect of membrane action on yield load of simply supported square slabs with central circular opening", Journal of Institute of Engineers (India), Part CI: Civil Engineers Division, November 1984, Vol. 65, pp. 139-146.

11 Sawzuck A., Winnick L., "Plastic behaviour of simply supported plates at moderately large deflections", International Journal of Solids and Structures, Vol. 1, No. 1, February 1965, pp. 97-111.

12 Johansen K.W., Brudlinieteorier, Gjellerup, Copenhagen, Denmark 1943, English edition: "Yield line theory", Cement and Concrete Association, London 1962, 181p.

13 Wood R. H., "The reinforcement of slabs in accordance with a predetermined field of moments", Concrete, London, Vol. 2, February 1968, pp 69-76.

14 Armer G. S. T., "Discussion on The reinforcement of slabs in accordance with predetermined field of moments", Concrete, London, Vol. 8, August 1968, pp 319-312.

15 Morley C. T., "Yield line theory for reinforced concrete slabs at moderately large deflection", Magazine of Concrete Research, Vol. 19, No 61. December 1967, pp. 211-221.

16 Hayes B., "Allowing of membrane action in the plastic analysis of rectangular reinforced concrete slabs", Magazine of Concrete Research, Vol. 20, No 65, December 1968., pp. 205-211.

17 Taylor R., "A note on a possible basis for a new method of ultimate load design of reinforced concrete slabs", Magazine of Concrete Research". Vol. 17, No 53, December 1965, pp. 183-186.

18 Desayi P., "Simply supported RC skew slabs", International Journal of Structures, Vol. 7. No 79. July-December 1987. pp. 119-139.

Table 6.1- Wood and Armer [1,2] design moment equations.

Moment at bottom	Moment at top
$M_x^*=M_x+\lvert M_{xy}\rvert$ and $M_y^*=M_y+\lvert M_{xy}\rvert$	$M_x^*=M_x-\lvert M_{xy}\rvert$ and $M_y^*=M_y-\lvert M_{xy}\rvert$
if $M_x^*<0$,then $M_x^*=0$ and $M_y^*=M_y+\left\lvert\frac{M_{xy}^2}{M_x}\right\rvert$	if $M_x^*>0$,then $M_x^*=0$ and $M_y^*=M_y-\left\lvert\frac{M_{xy}^2}{M_x}\right\rvert$
if $M_y^*<0$ then, $M_y^*=0$ and $M_x^*=M_x+\left\lvert\frac{M_{xy}^2}{M_y}\right\rvert$	if $M_y^*>0$,then $M_y^*=0$ $M_x^*=M_x-\left\lvert\frac{M_{xy}^2}{M_x}\right\rvert$

Table 6.2 Wood and Armer design moment coefficients for a square slab with 16-element mesh at the corners of the elements.

No	Negative moments coefficients		Positive moments coefficients	
	M_x^*	M_y^*	M_x^*	M_y^*
1	-.4455E-01	-.4455E-01	.4455E-01	.4455E-01
2	-.3865E-01	-.3865E-01	.3865E-01	.3865E-01
3	-.2741E-01	-.2741E-01	.2741E-01	.2741E-01
4	-.1409E-01	-.1409E-01	.1409E-01	.1409E-01
5	.0000E+00	.0000E+00	.0000E+00	.0000E+00
6	-.3865E-01	-.3865E-01	.3865E-01	.3865E-01
7	-.2140E-01	-.2140E-01	.4762E-01	.4762E-01
8	-.3149E-02	-.6003E-02	.4659E-01	.4373E-01
9	.0000E+00	.0000E+00	.3942E-01	.3430E-01
10	.0000E+00	.0000E+00	.2813E-01	.2217E-01

11	-.2741E-01	-.2741E-01	.2741E-01	.2741E-01
12	-.6003E-02	-.3149E-02	.4373E-01	.4659E-01
13	.0000E+00	.0000E+00	.5091E-01	.5091E-01
14	.0000E+00	.0000E+00	.5039E-01	.4718E-01
15	.0000E+00	.0000E+00	.4353E-01	.3904E-01
16	-.1409E-01	-.1409E-01	.1409E-01	.1409E-01
17	.0000E+00	.0000E+00	.3430E-01	.3942E-01
18	.0000E+00	.0000E+00	.4718E-01	.5039E-01
19	.0000E+00	.0000E+00	.5260E-01	.5260E-01
20	.0000E+00	.0000E+00	.5089E-01	.4950E-01
21	.0000E+00	.0000E+00	.0000E+00	.0000E+00
22	.0000E+00	.0000E+00	.2217E-01	.2813E-01
23	.0000E+00	.0000E+00	.3904E-01	.4353E-01
24	.0000E+00	.0000E+00	.4950E-01	.5089E-01
25	.0000E+00	.0000E+00	.5304E-01	.5304E-01

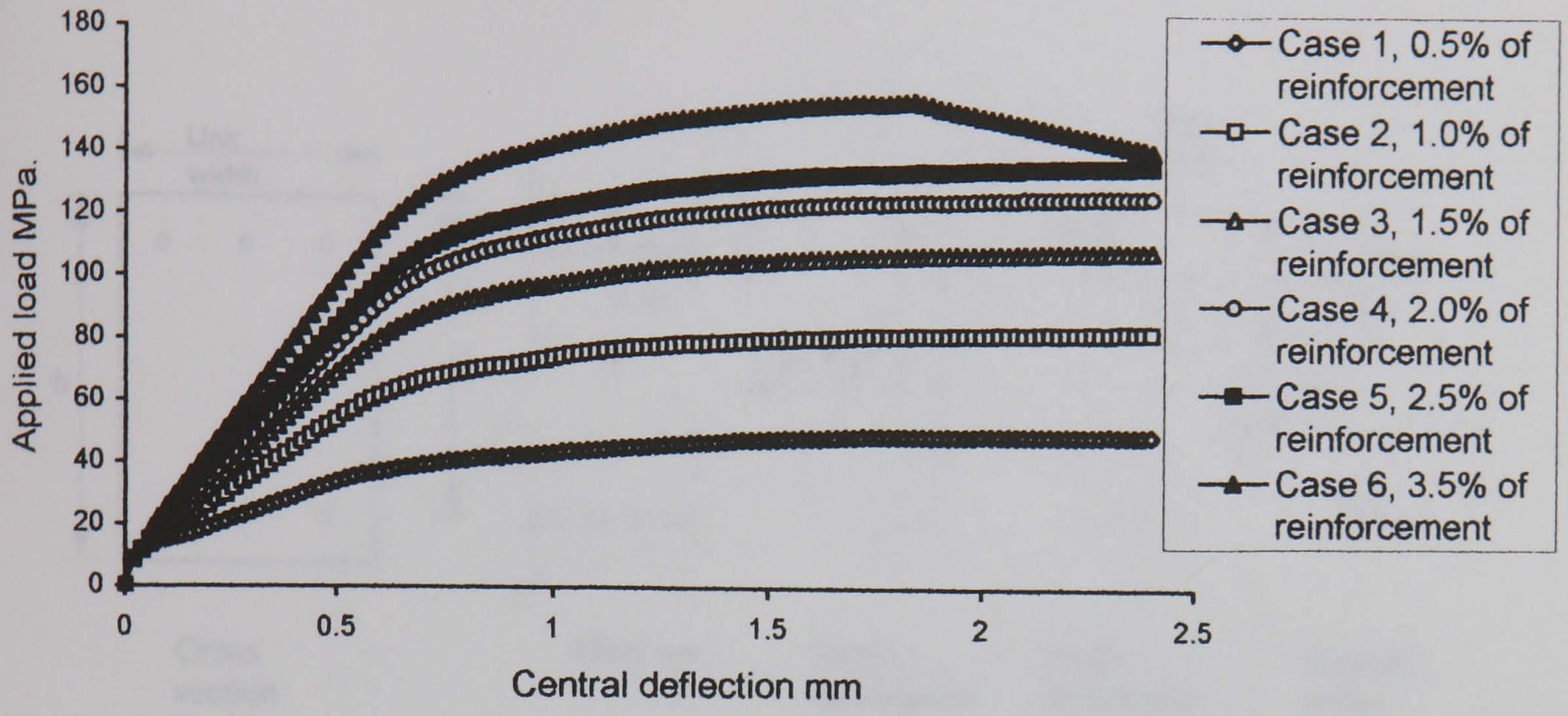

Fig.6.1-Load-deflection curves for simply supported slab with different reinforcement ratios

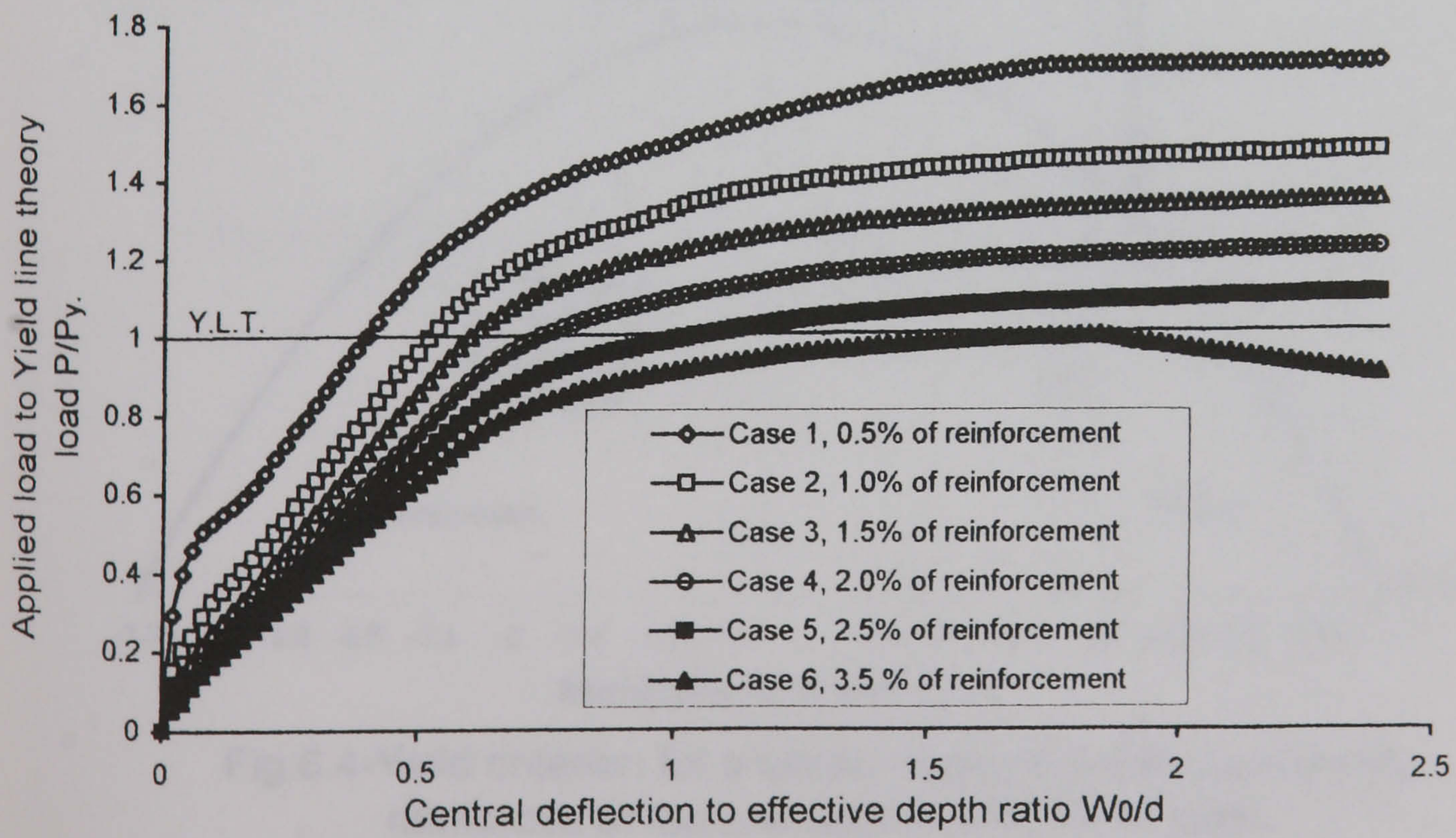

Fig.6.2- Normalised load-deflection curves for simply supported slab with different reinforcement ratios

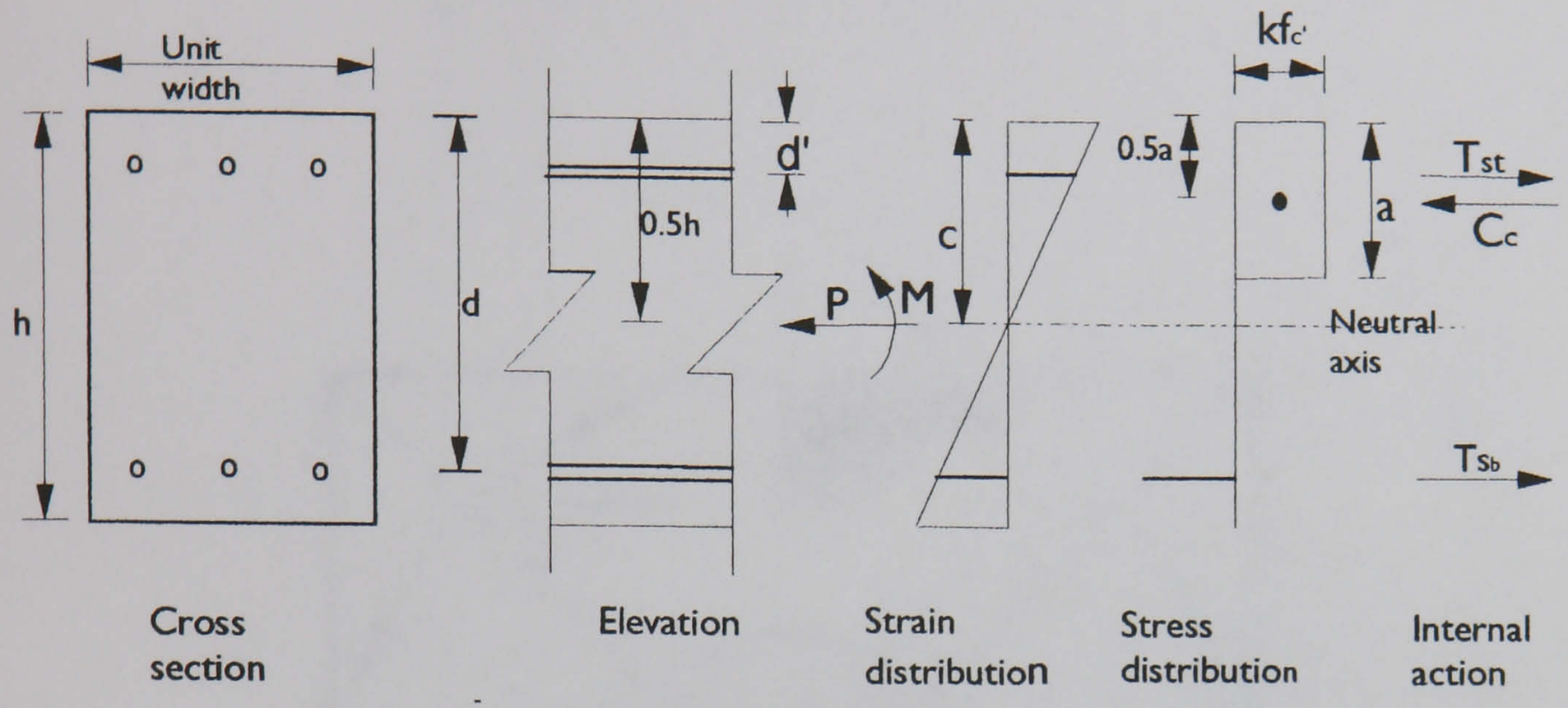

Fig.6.3- Conditions at a positive moment yield section

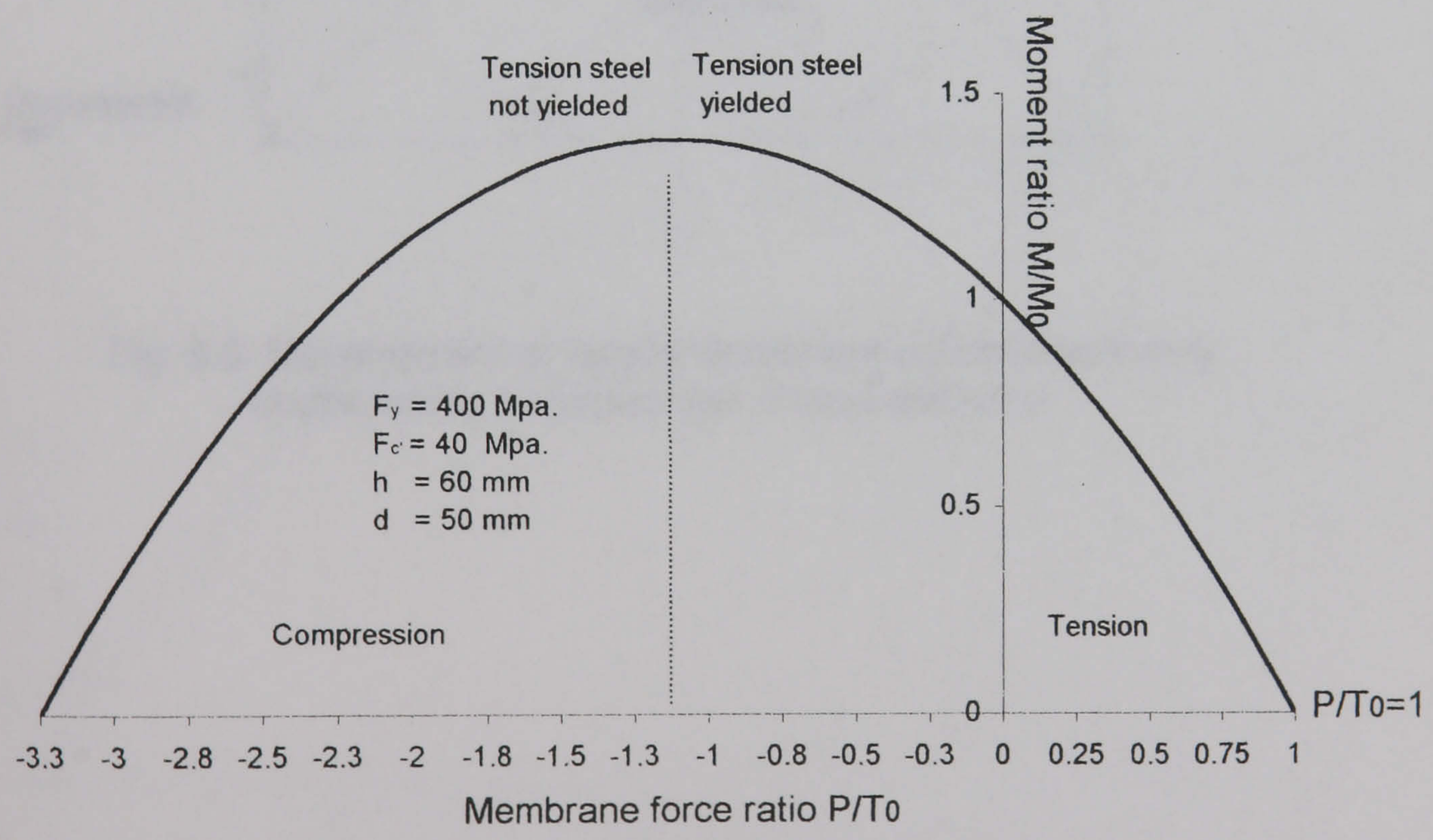

Fig.6.4-Yield criterion for a simply supported slab isotropically reinforced at top and bottom with 1% of steel

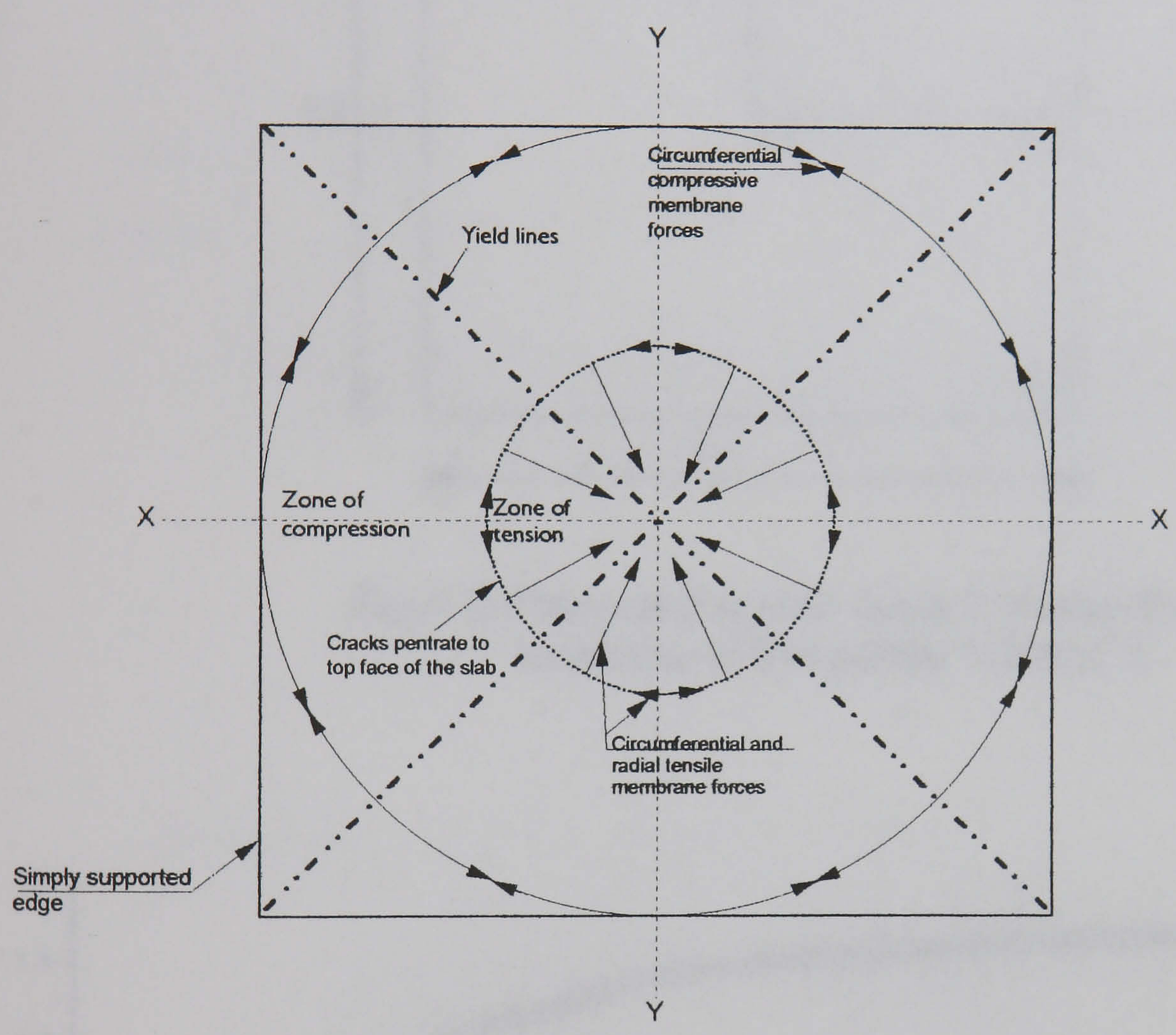

Fig. 6.5- Development of tensile membrane action in uniformly loaded simply supported slab at large deflection.

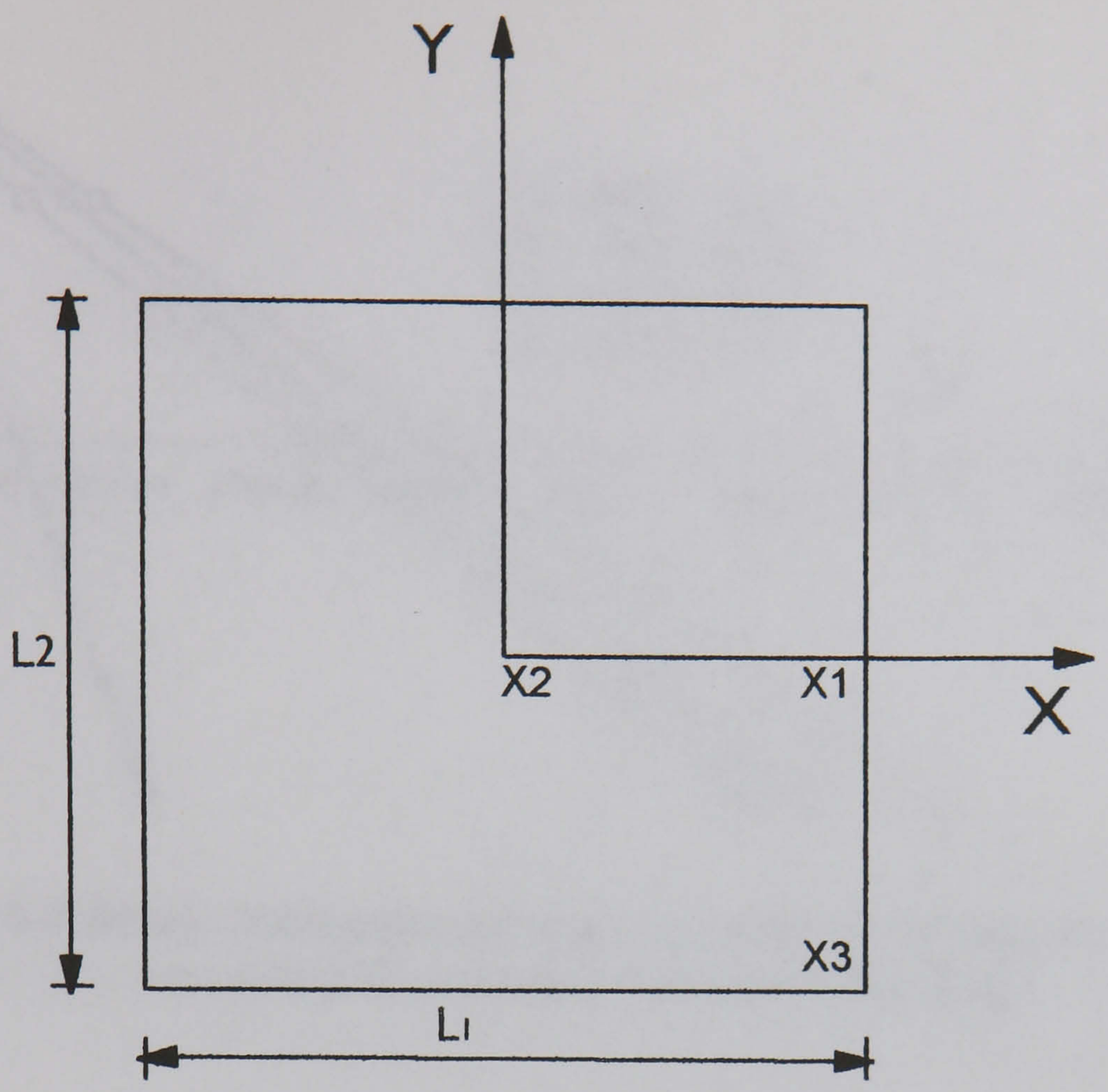

Fig.6.6-Plane of the slab case 2 shows the locations of the points 1,2 and 3

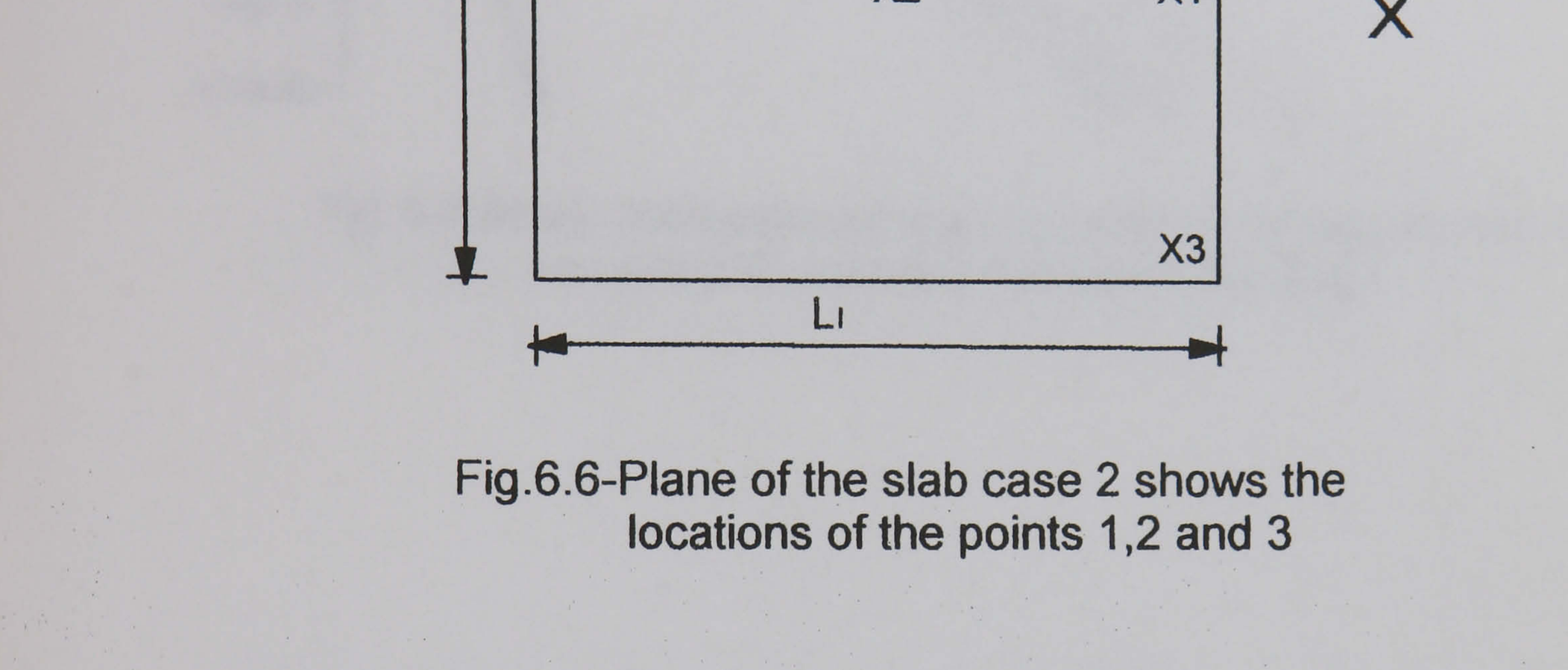

Fig.6.7-Load deflection curve for simply supported slab with reinforcement ratio of 1%

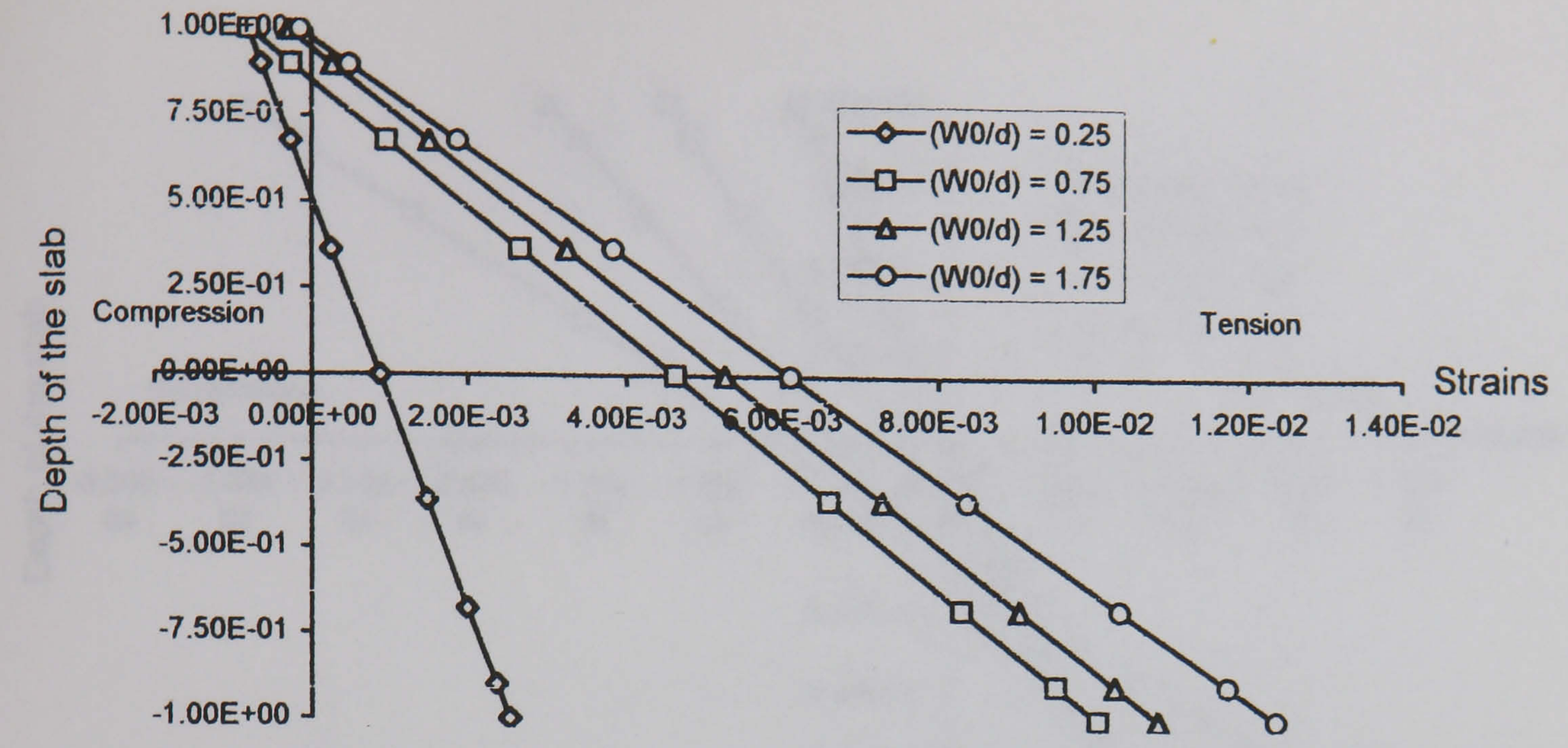

Fig. 6.8-Strain distribution through the depth of the slab at point 2 in x and y-directions at different deflections

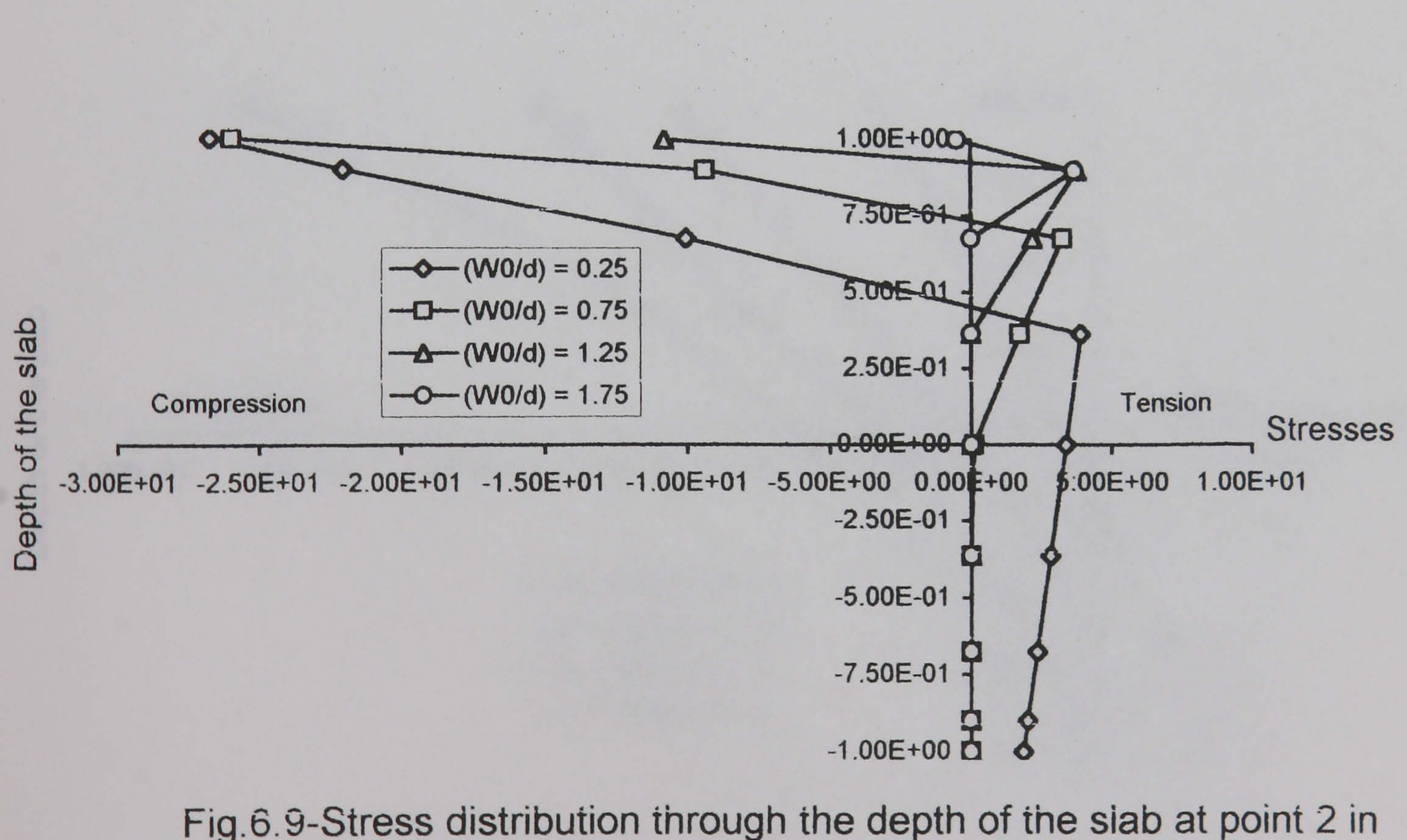

Fig.6.9-Stress distribution through the depth of the slab at point 2 in x and y-directions at different deflections

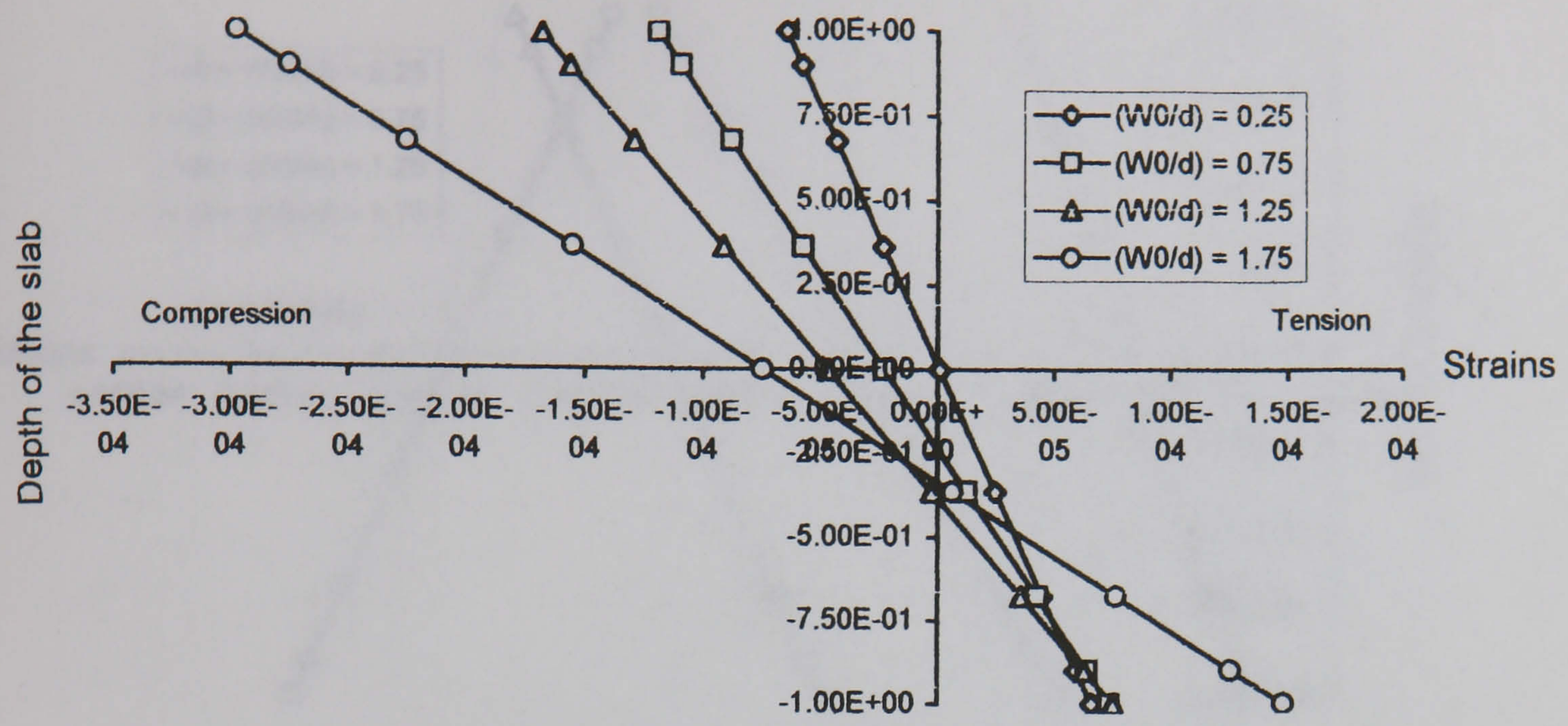

Fig.6.10-Strain distribution through the depth of the slab at point 1 in x-direction at different deflections

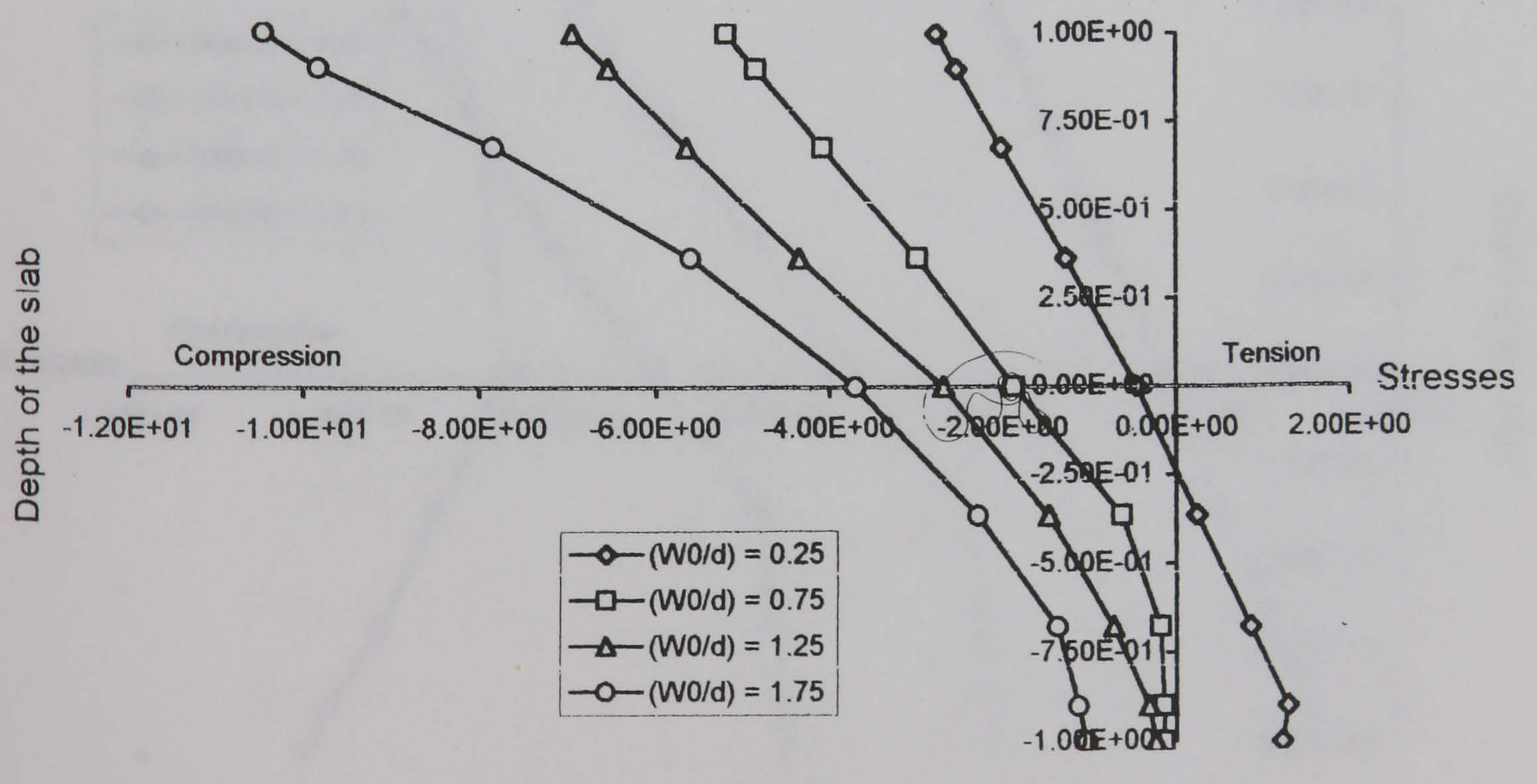

Fig.6.11-Stress distribution through the depth of the slab at point 1 in x-direction at different deflections

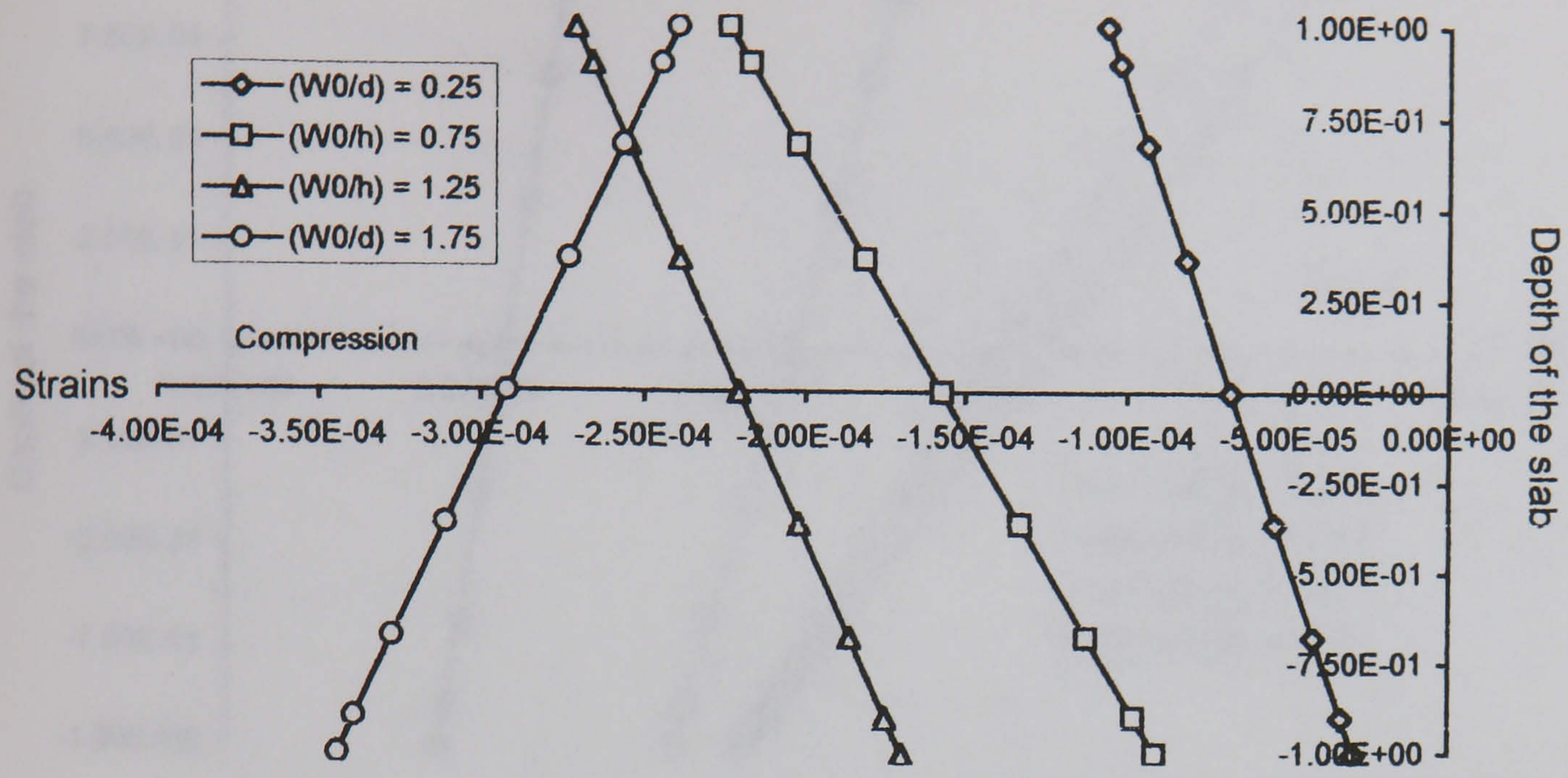

Fig. 6.12-Strain distribution through the depth of the slab at point 1 in y-direction at different deflections

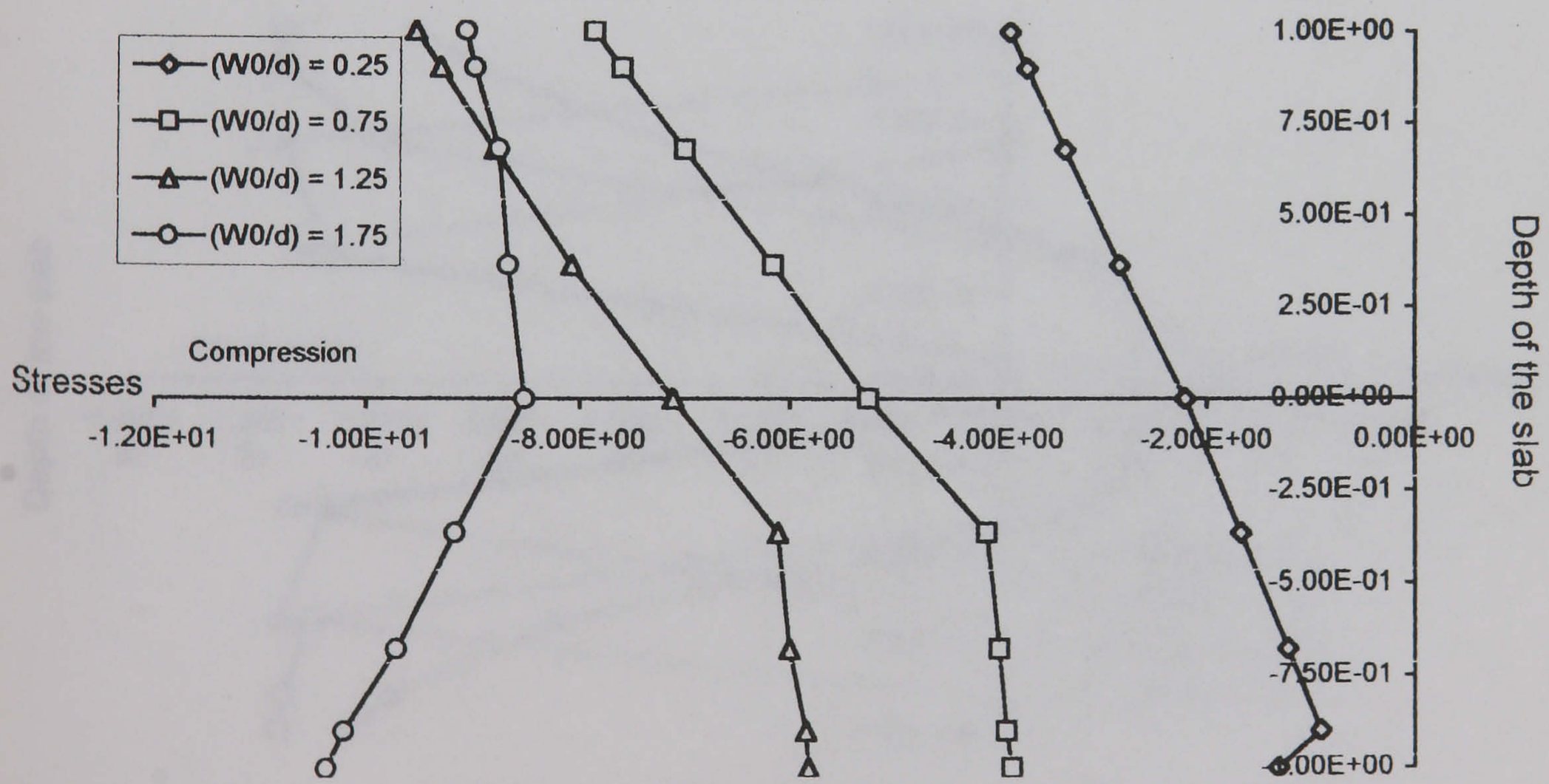

Fig.6.13-Stress distribution through the depth of the slab at point 1 in y-direction at different deflections

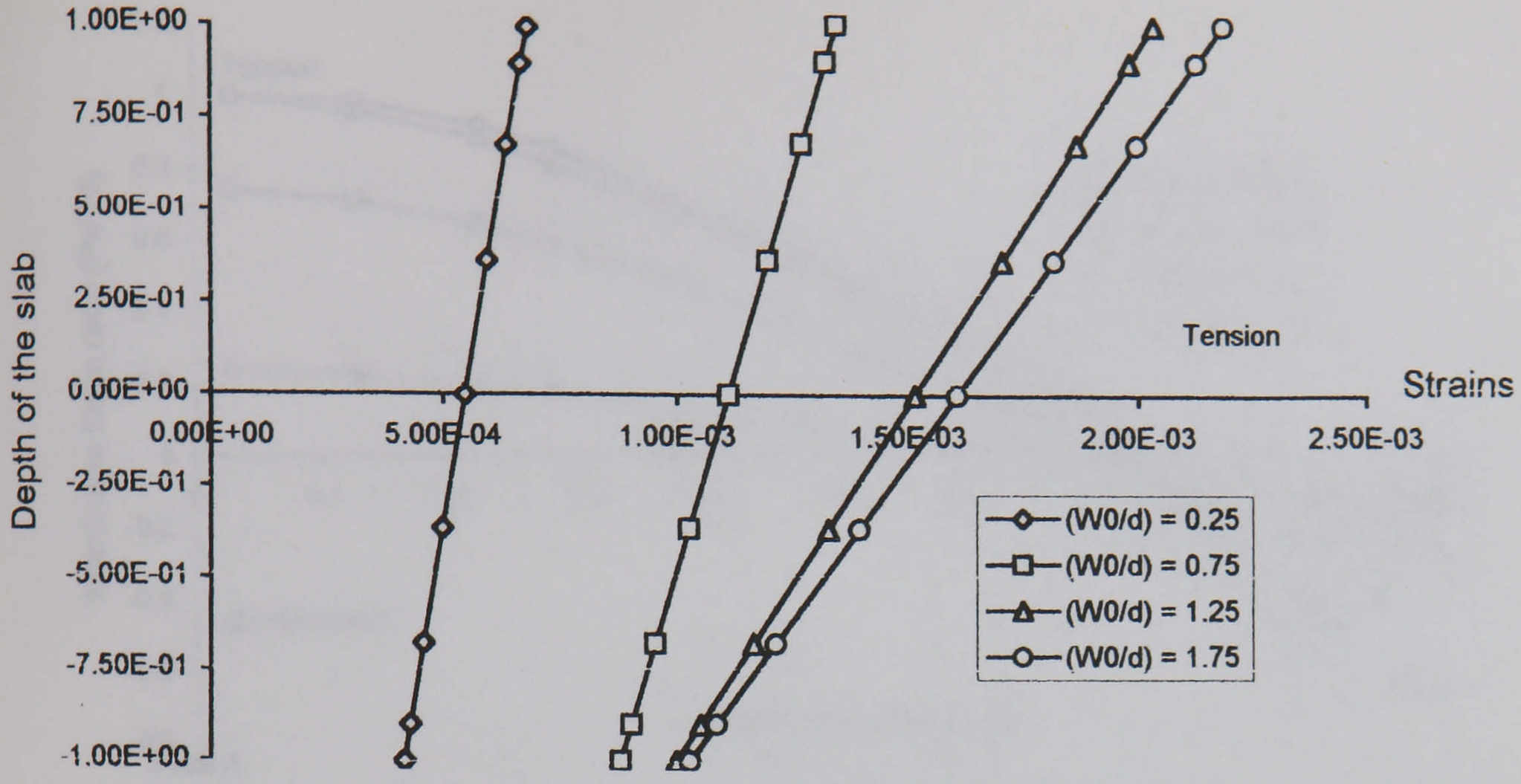

Fig.6.14-Strain distribution through the depth of the slab at point 3 in x and y-direction at different deflections

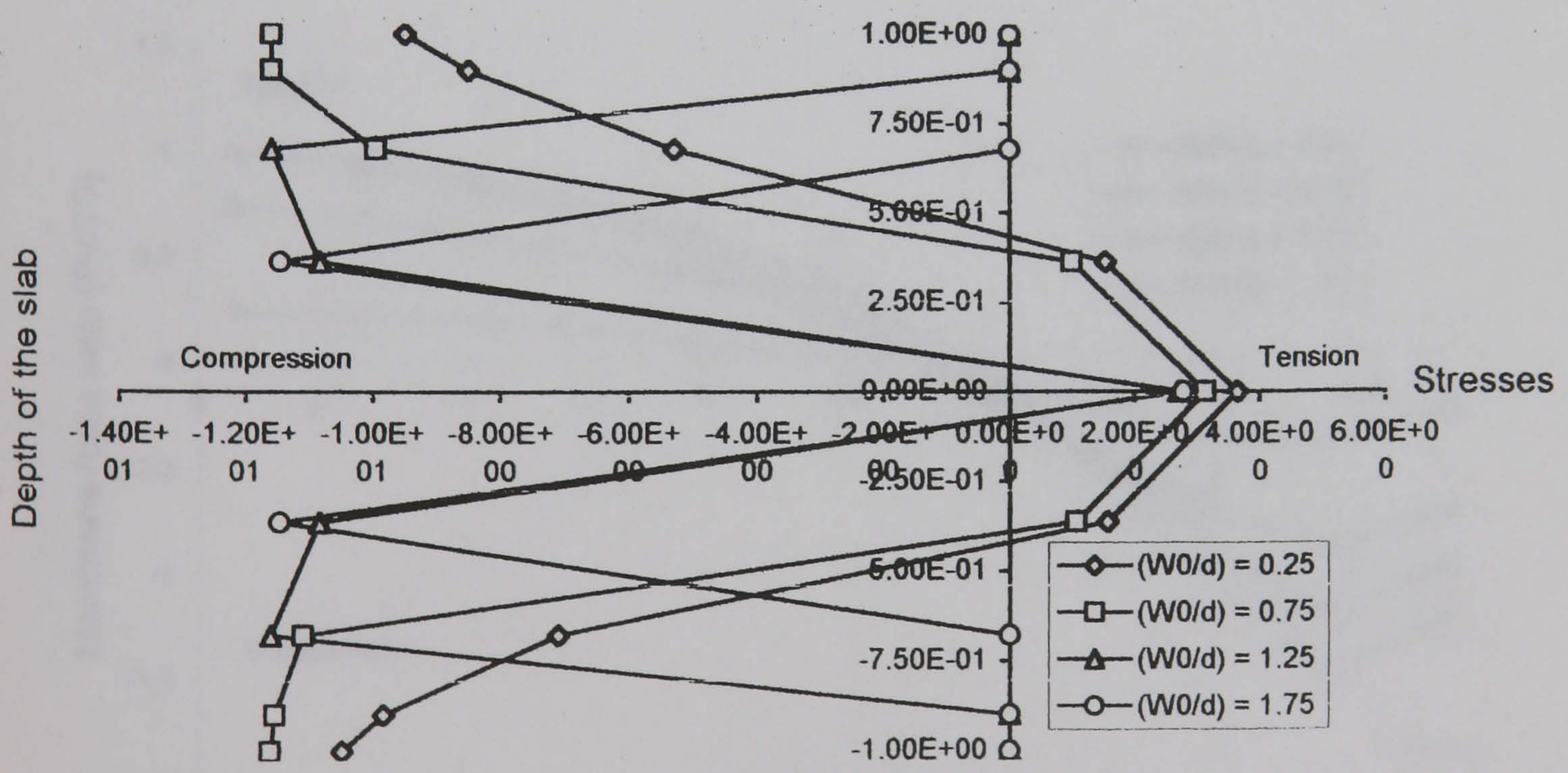

Fig.6.15-Stress distribution through the depth of the slab at point 3 in x and y-direction at different deflections

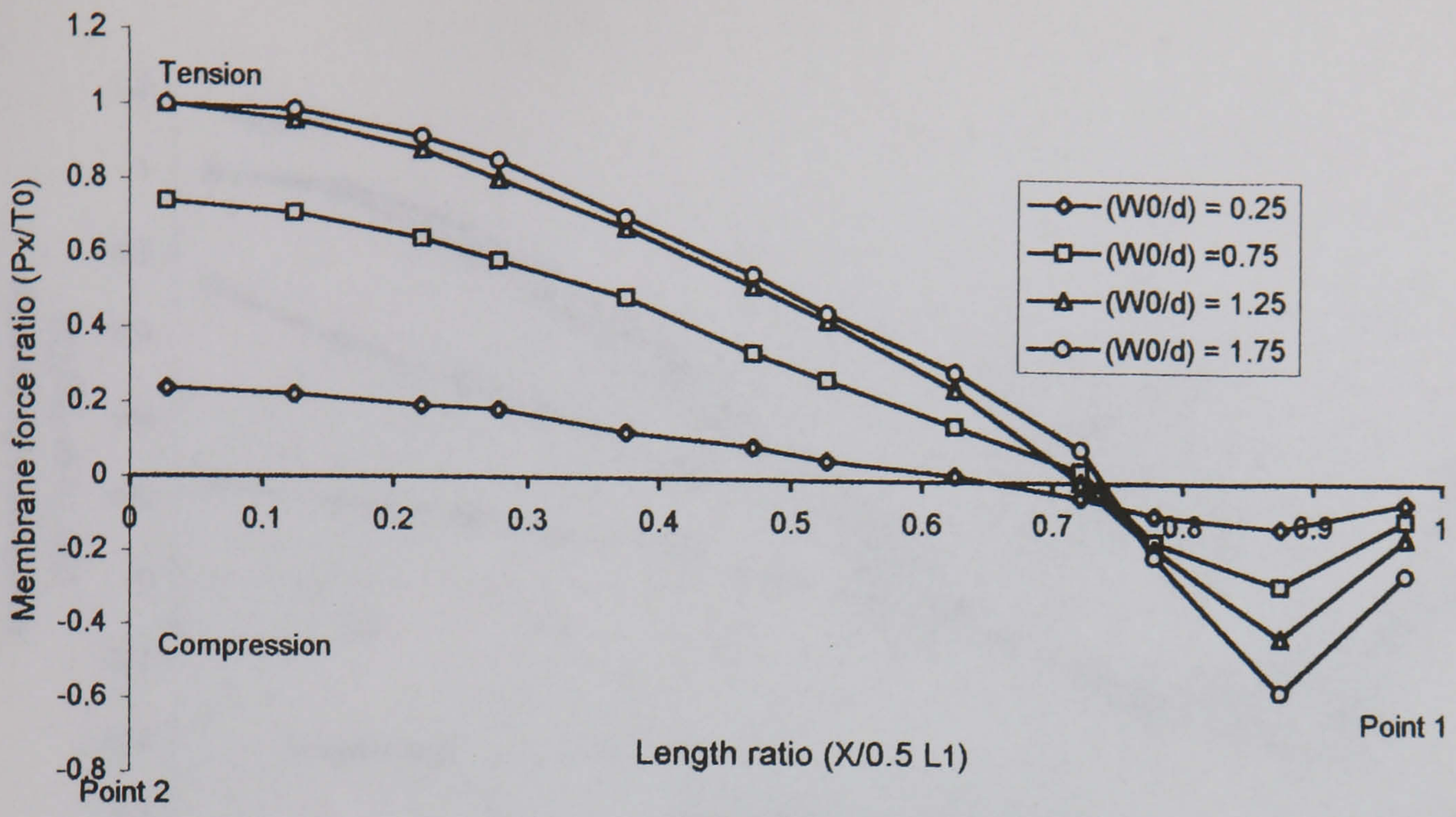

Fig. 6.16-Membrane forces between points 1 and 2 in x-direction at different deflections

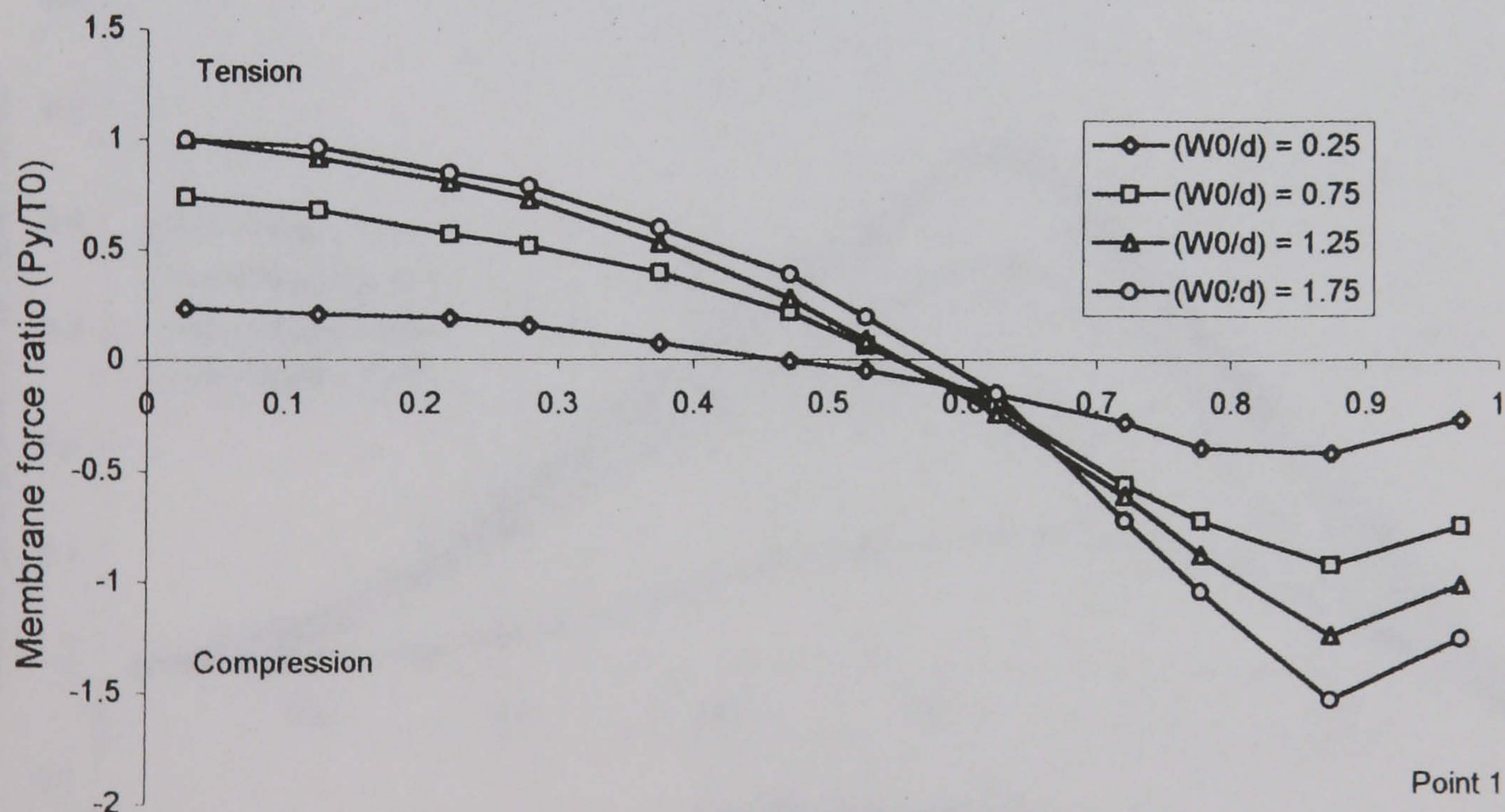

Fig. 6.17-Membrane forces between points 1 and 2 in y-direction at different deflections

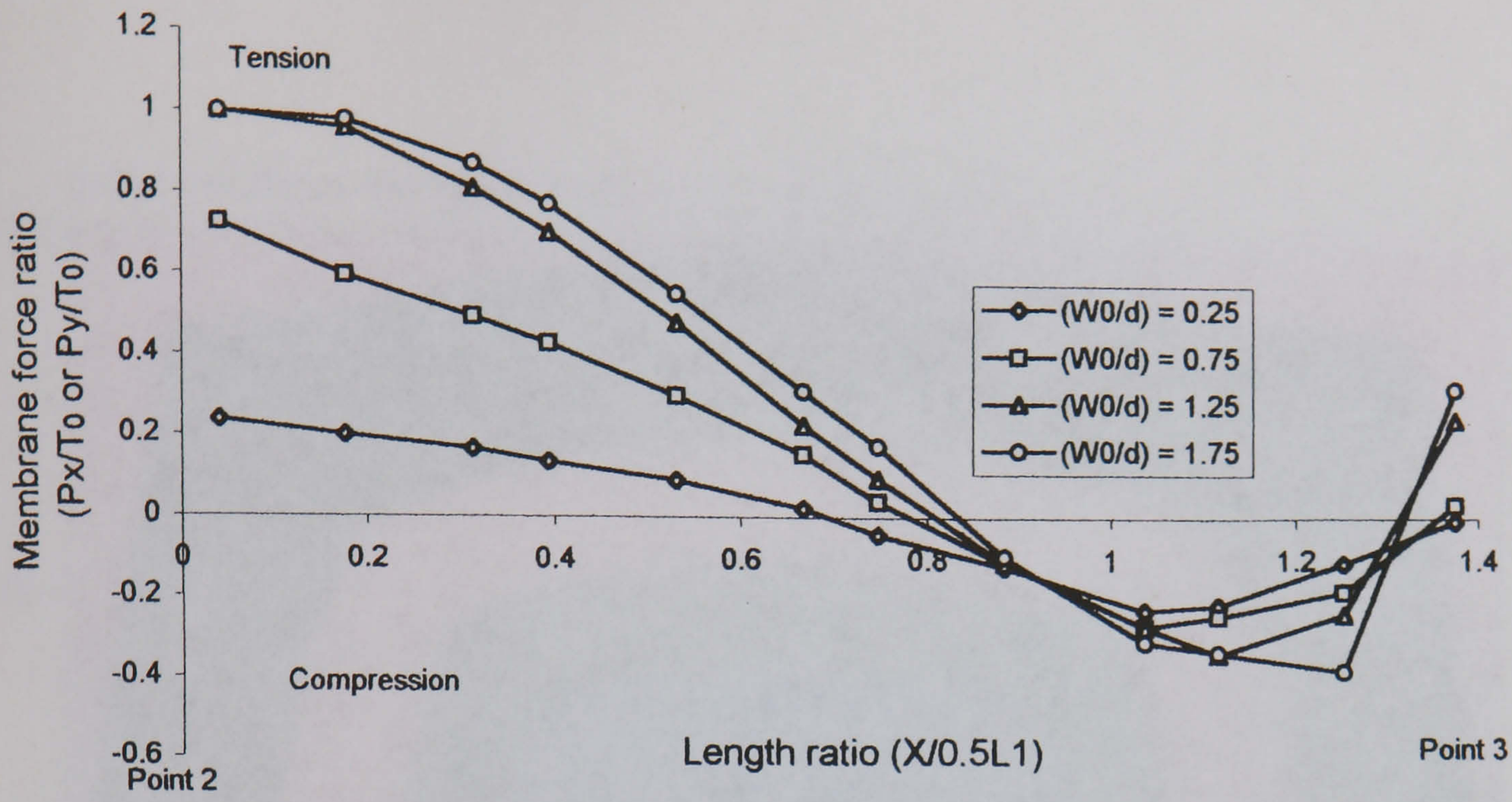

Fig. 6.18-Membrane forces between points 2 and 3 along the diagonal

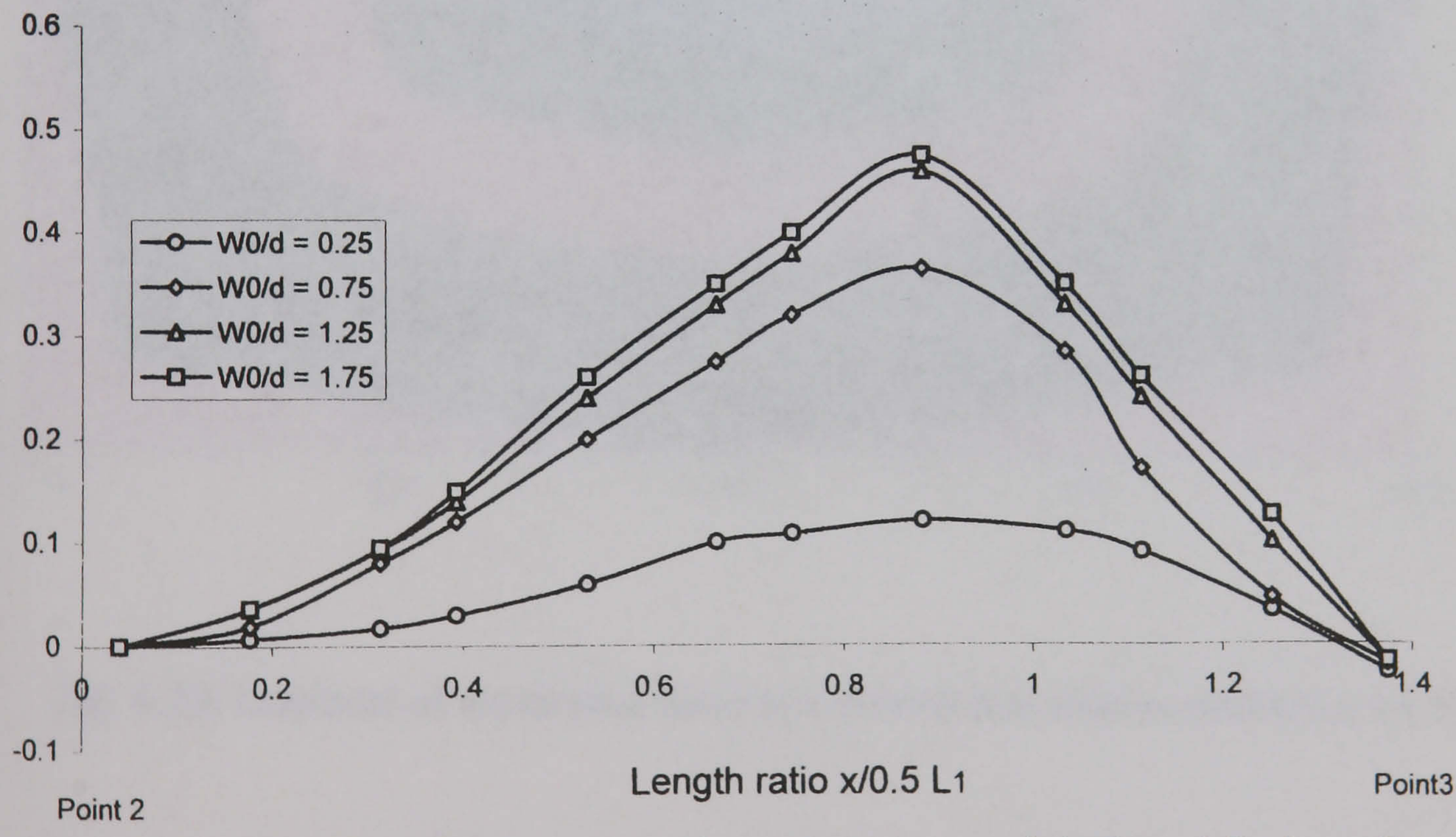

Fig. 6.19- Membrane shear force between points 2 and 3 along the diagonal

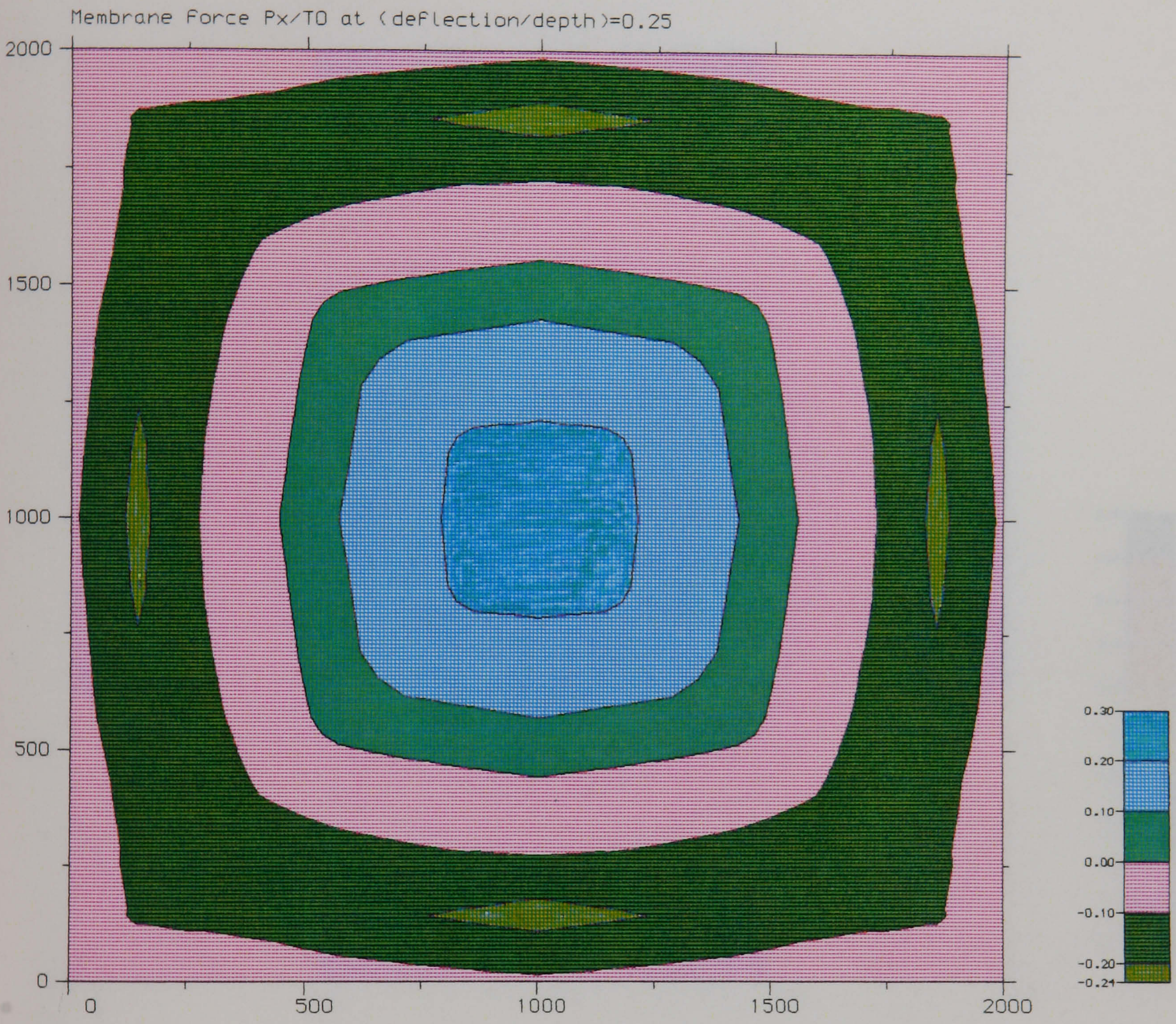

Fig. 6.20- Contours of membrane force in x-direction at relative deflection of 0.25

Fig. 6.21- Contours of membrane force in x-direction at relative deflection of 0.75

Fig. 6.22- Contours of membrane force in x-direction at relative deflection of 1.25

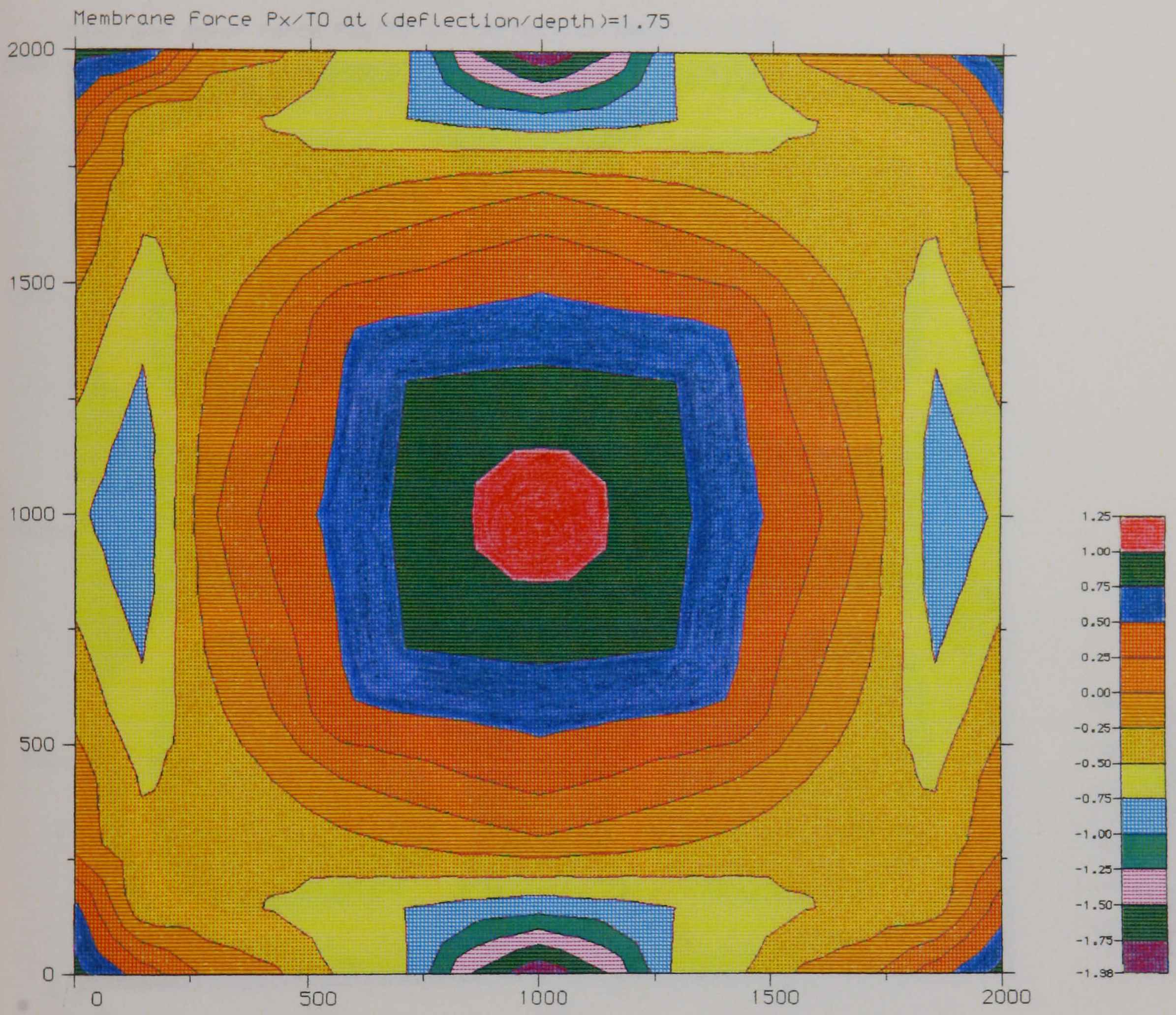

Fig. 6.23- Contours of membrane force in x-direction at relative deflection of 1.75

Fig. 6.24- Contours of membrane shear force at relative deflection of 1.75

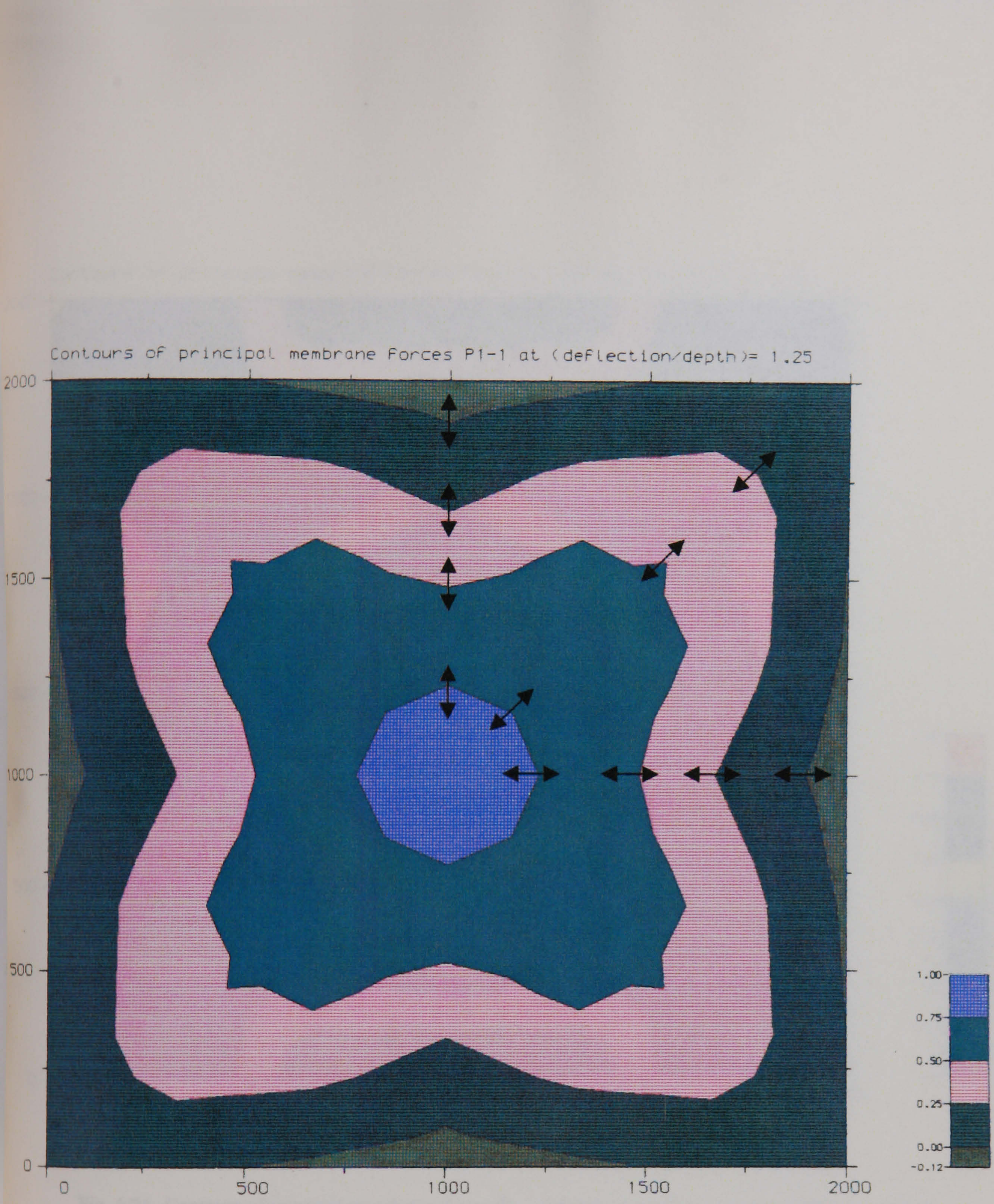

Fig. 6.25- Contours of principal membrane forces P_{1-1} and their directions at relative deflection of 1.25

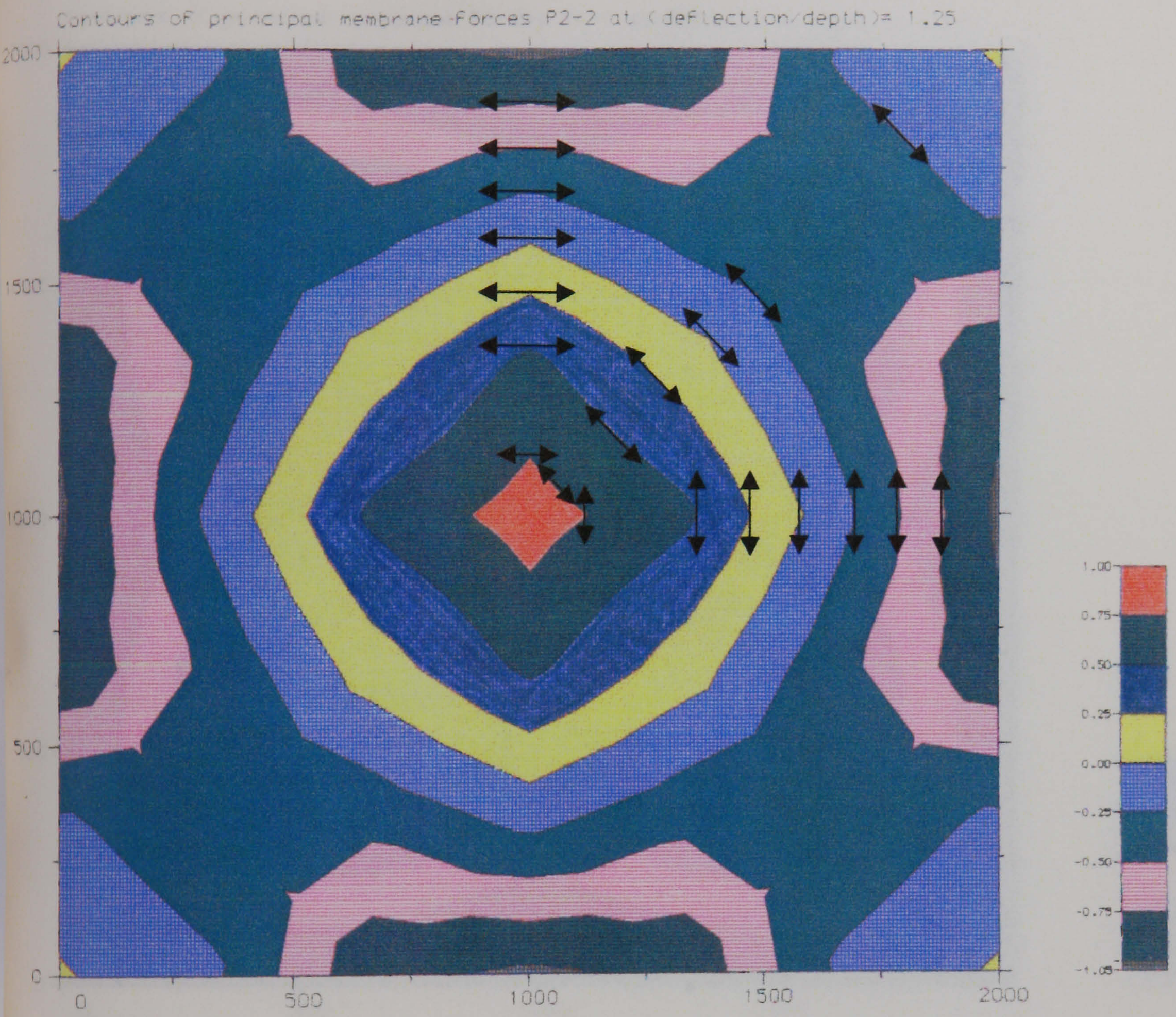

Fig. 6.26- Contours of principal membrane force P_{2-2} and their directions at relative deflection of 1.25

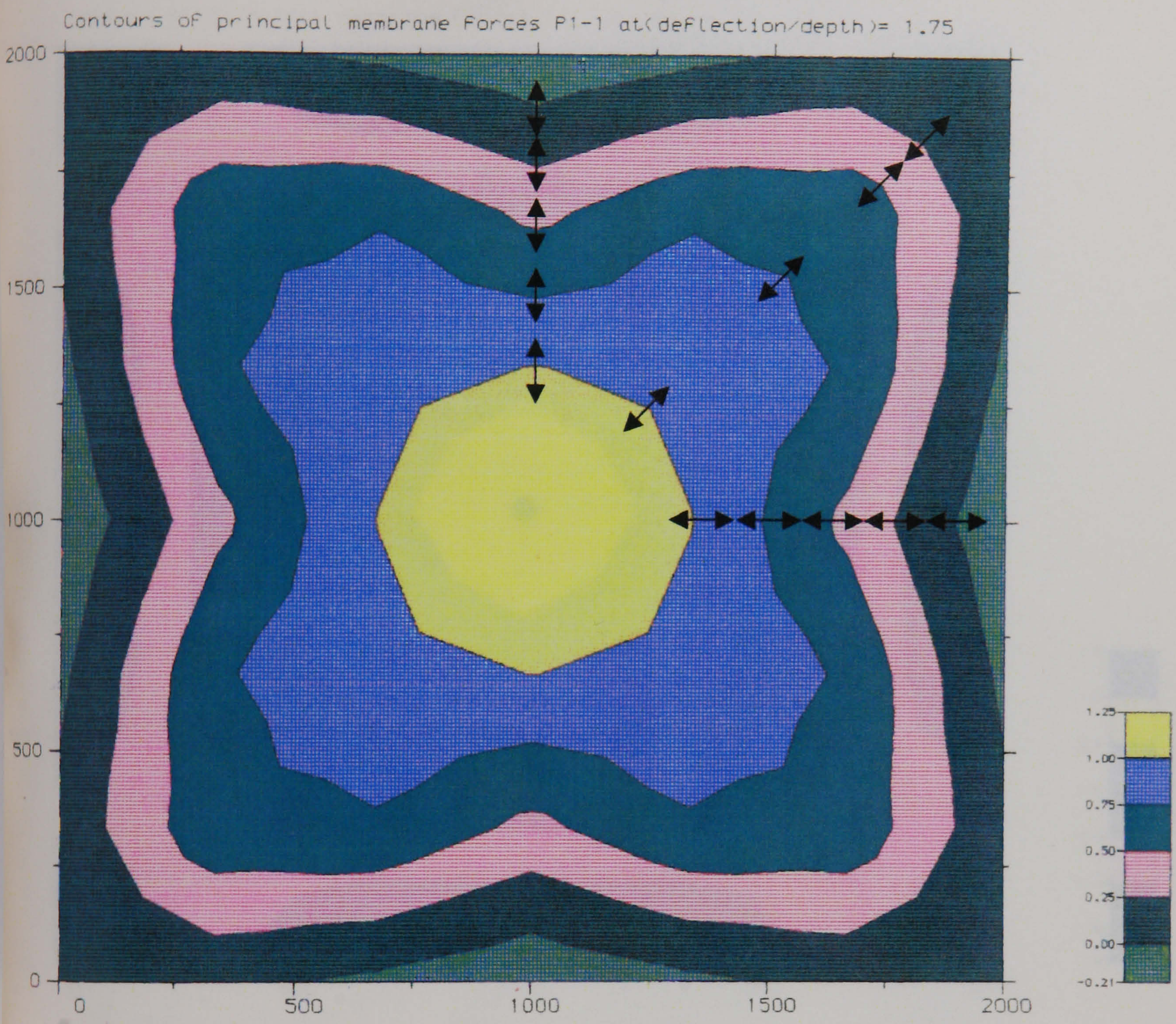

Fig. 6.27- Contours of principal membrane forces P_{1-1} and their directions at relative deflection of 1.75

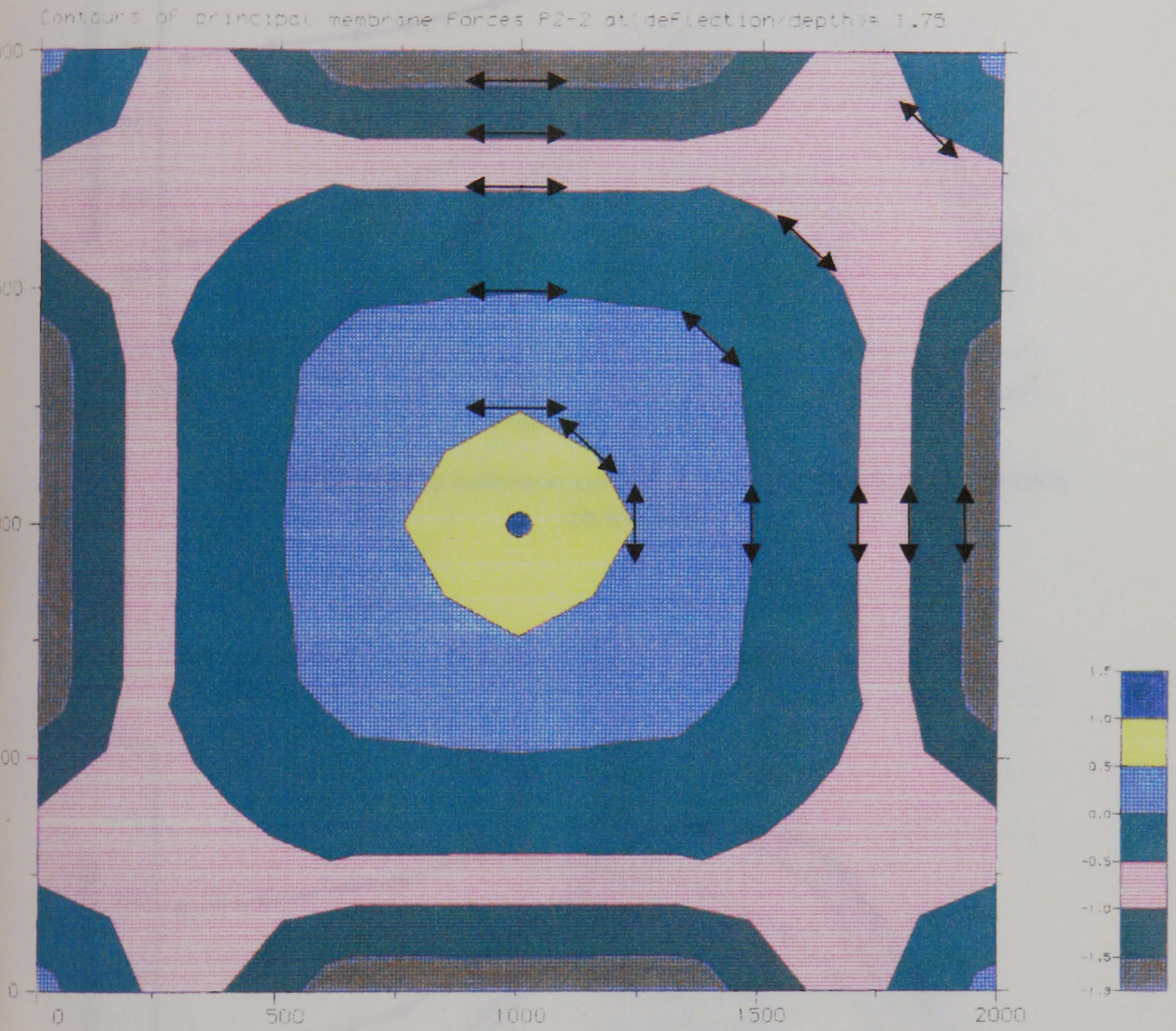

Fig. 6.28- Contours of principal membrane force P_{2-2} and their directions at relative deflection of 1.75

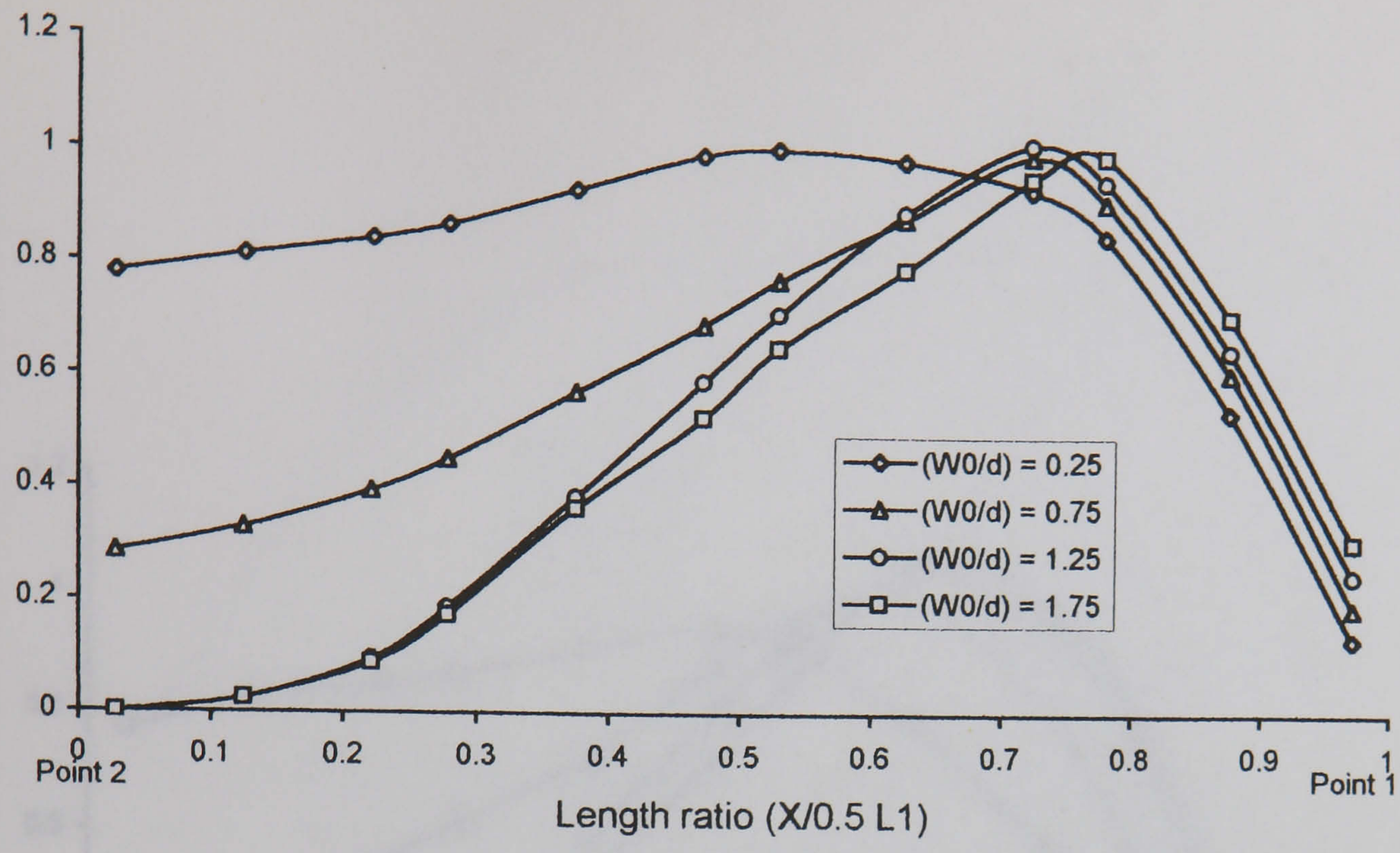

Fig. 6.29-Moments between point 1 and 2 in x-direction at different deflections

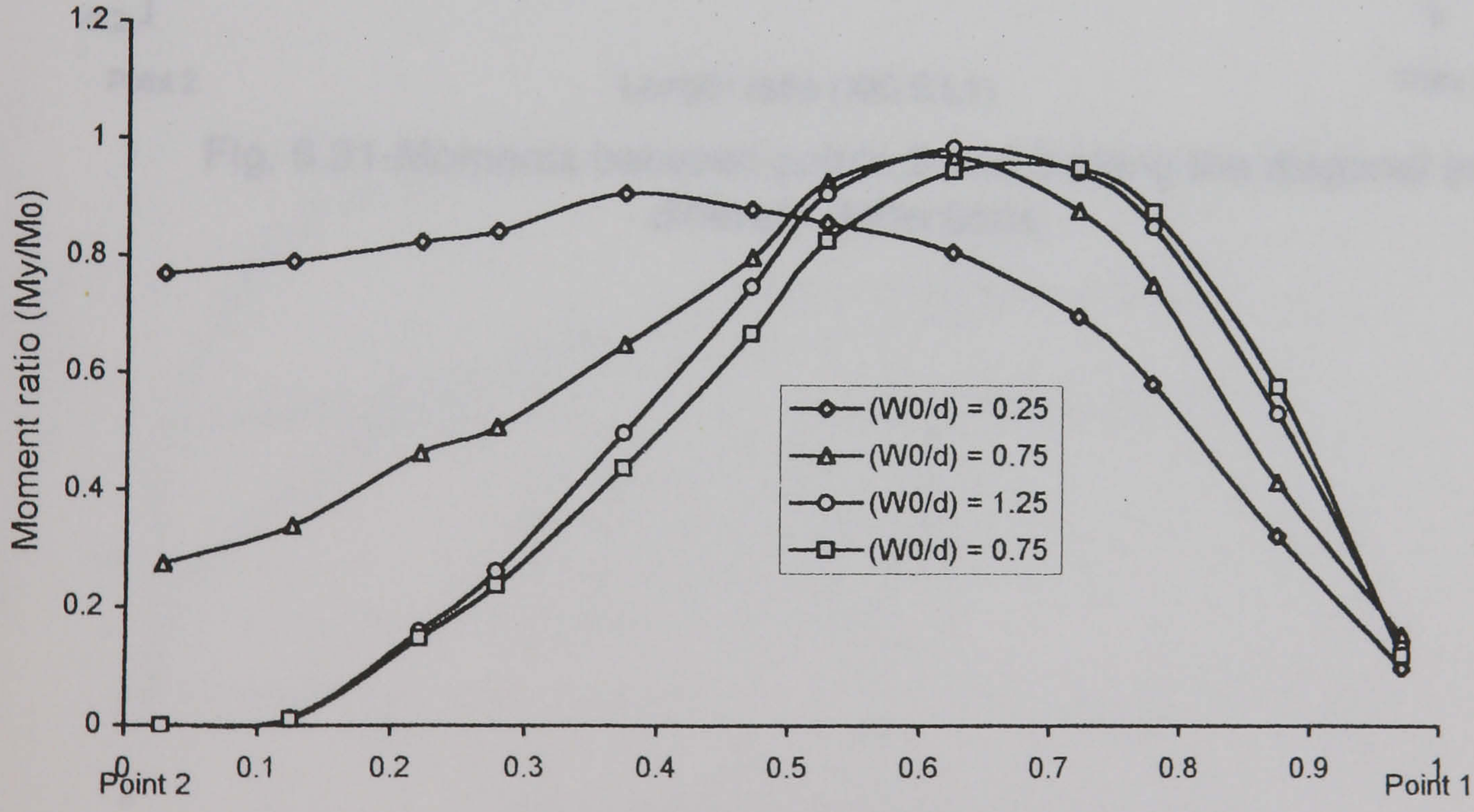

Fig. 6.30-Moments between points 1 and 2 in y-direction at different deflections

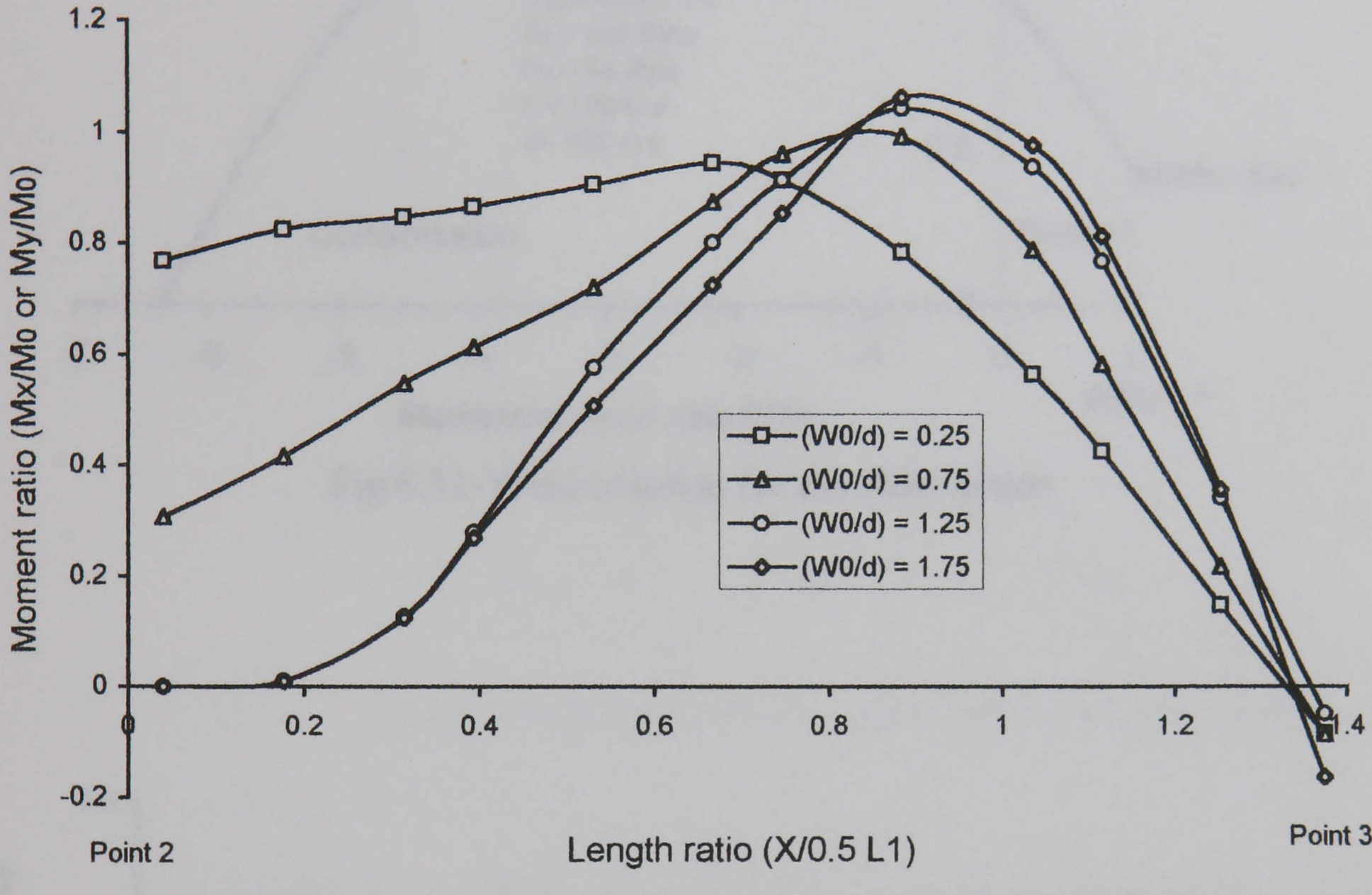

Fig. 6.31-Moments between points 2 and 3 along the diagonal at different deflections

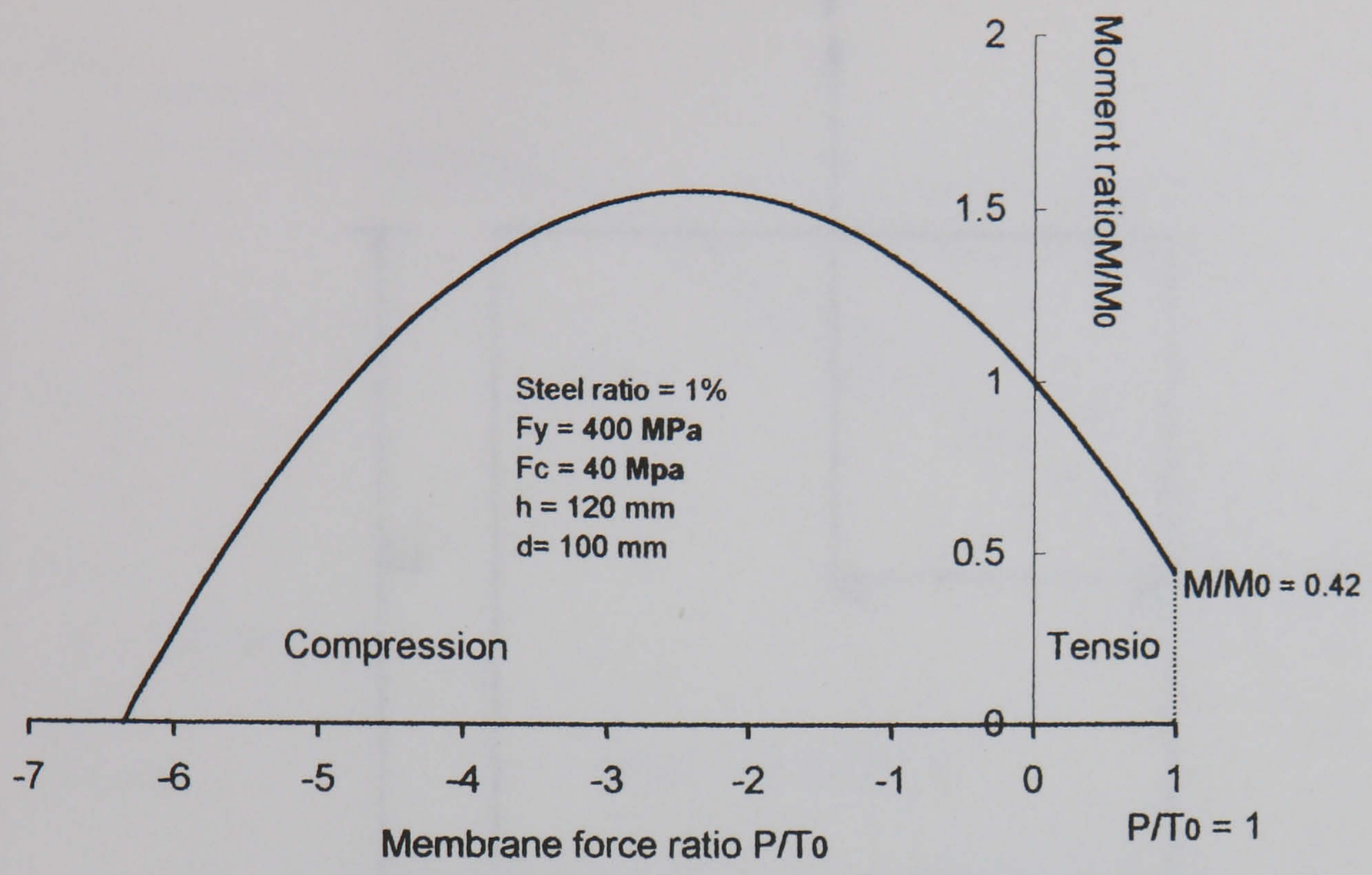

Fig.6.32-Yield criterion for the slab-section

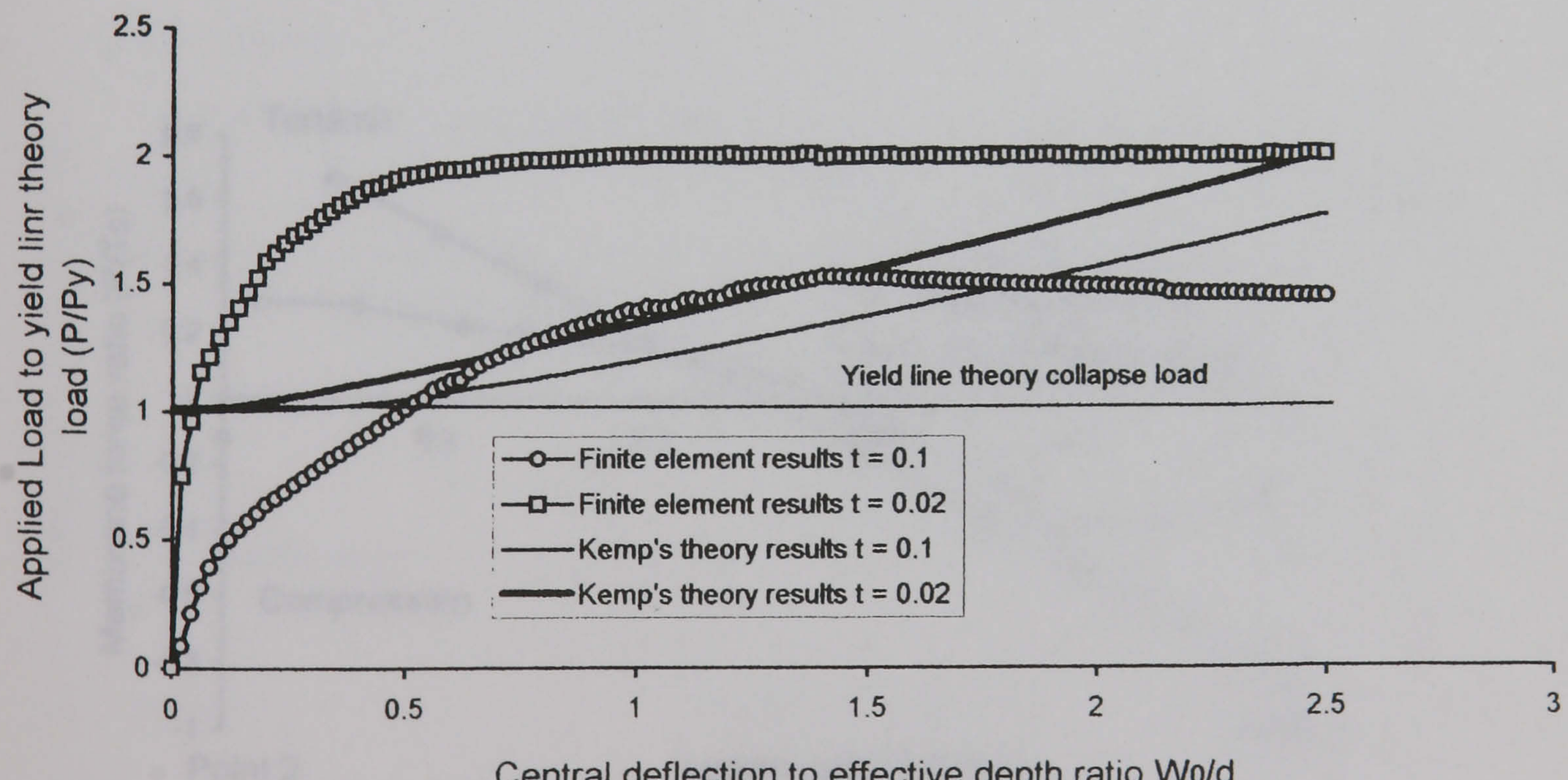

Fig.6.33-Load-deflection curves for simply supported slab with different *t*

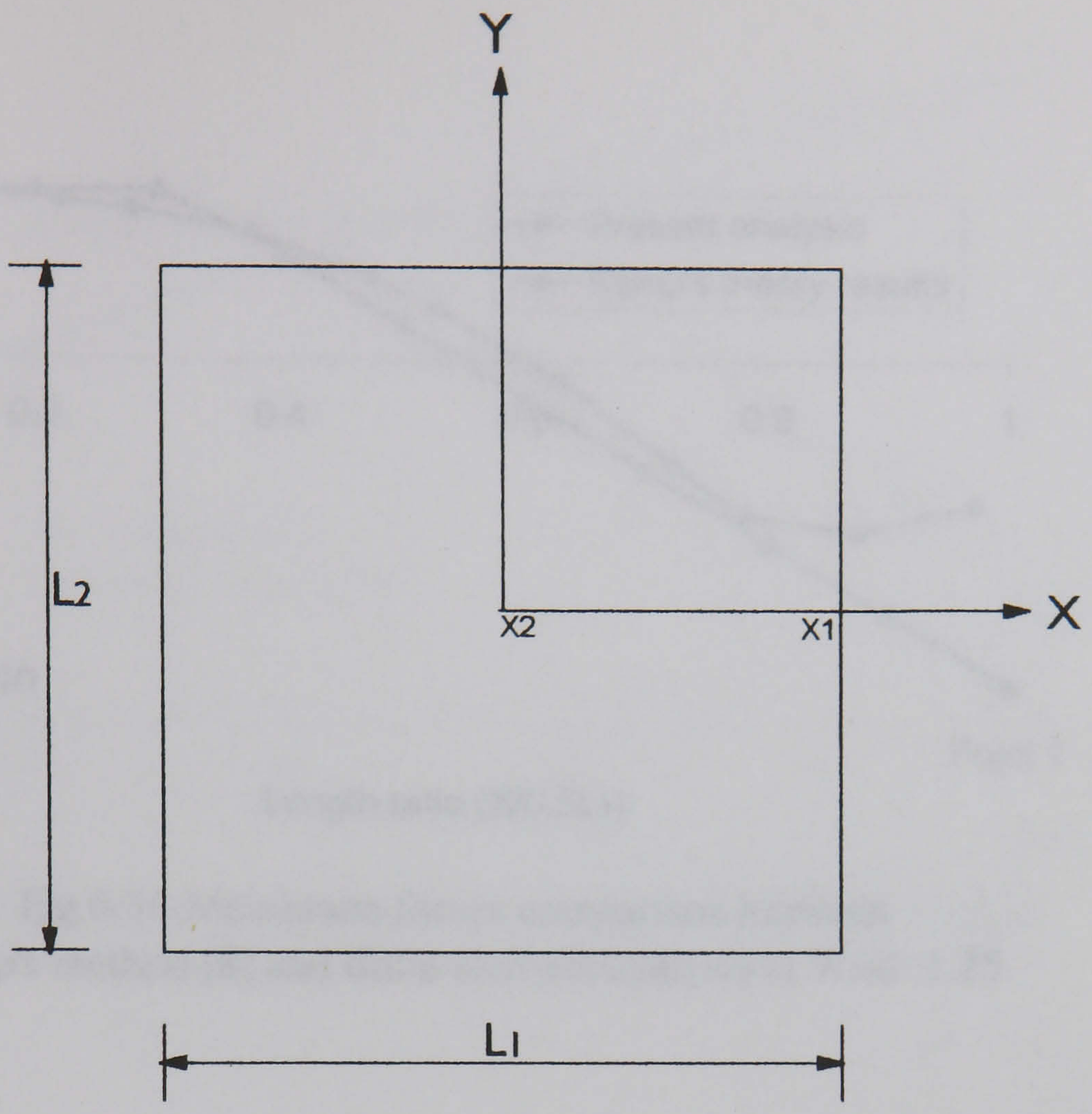

Fig.6.34- Locations of the points 1 and 2 on the plane of the slab

Fig.6.35-Membrane forces comparison betwween
Kemp's method [8] and finite element analysis at $W_0/d = 0.5$

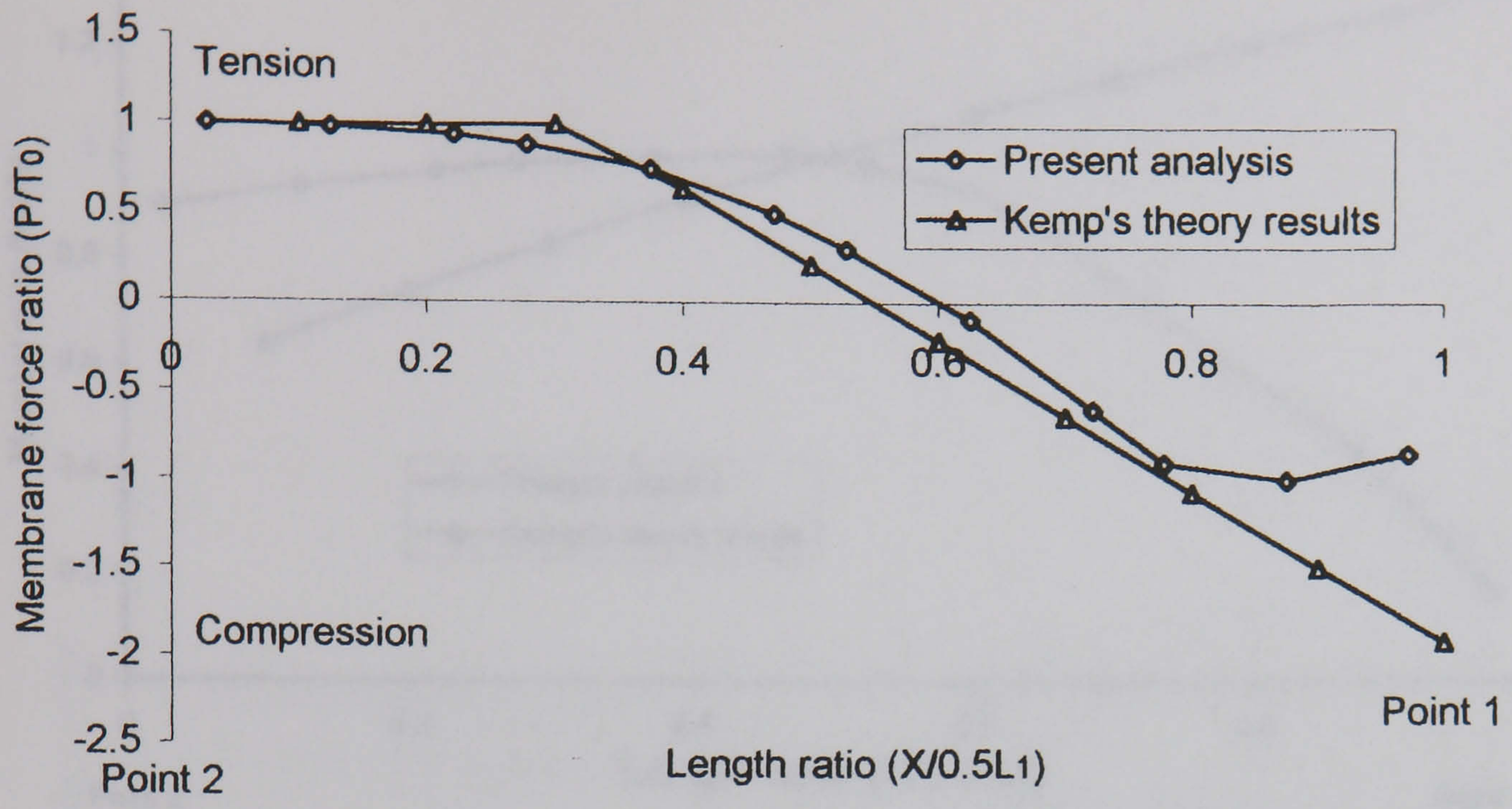

Fig.6.36-Membrane forces comparison between
Kemp's method [8] and finite element analysis at Wo/d=1.25

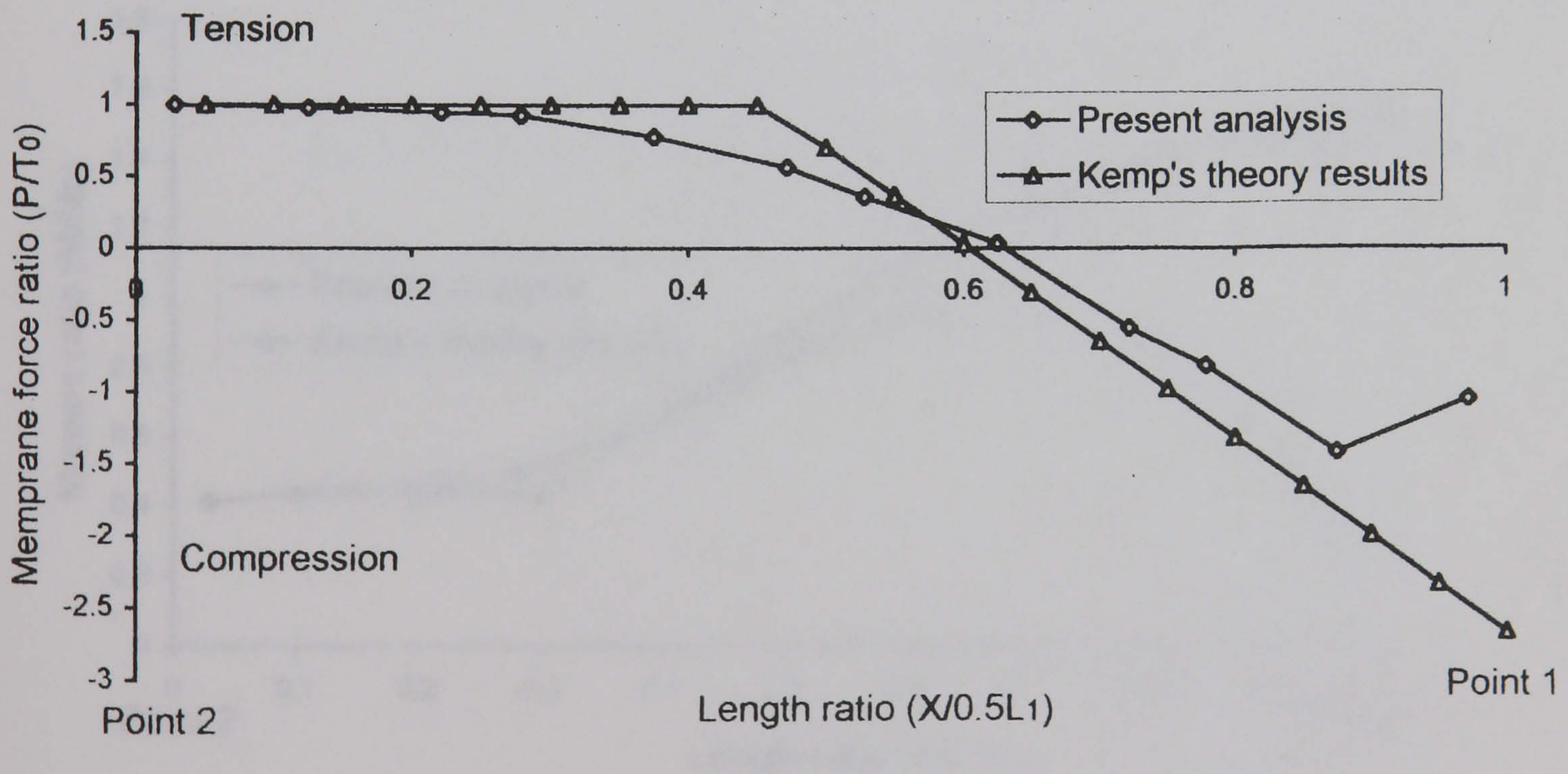

Fig.6.37-Memprane forces comparison between
Kemp's method [8] and finite element analysis at Wo/d=1.75

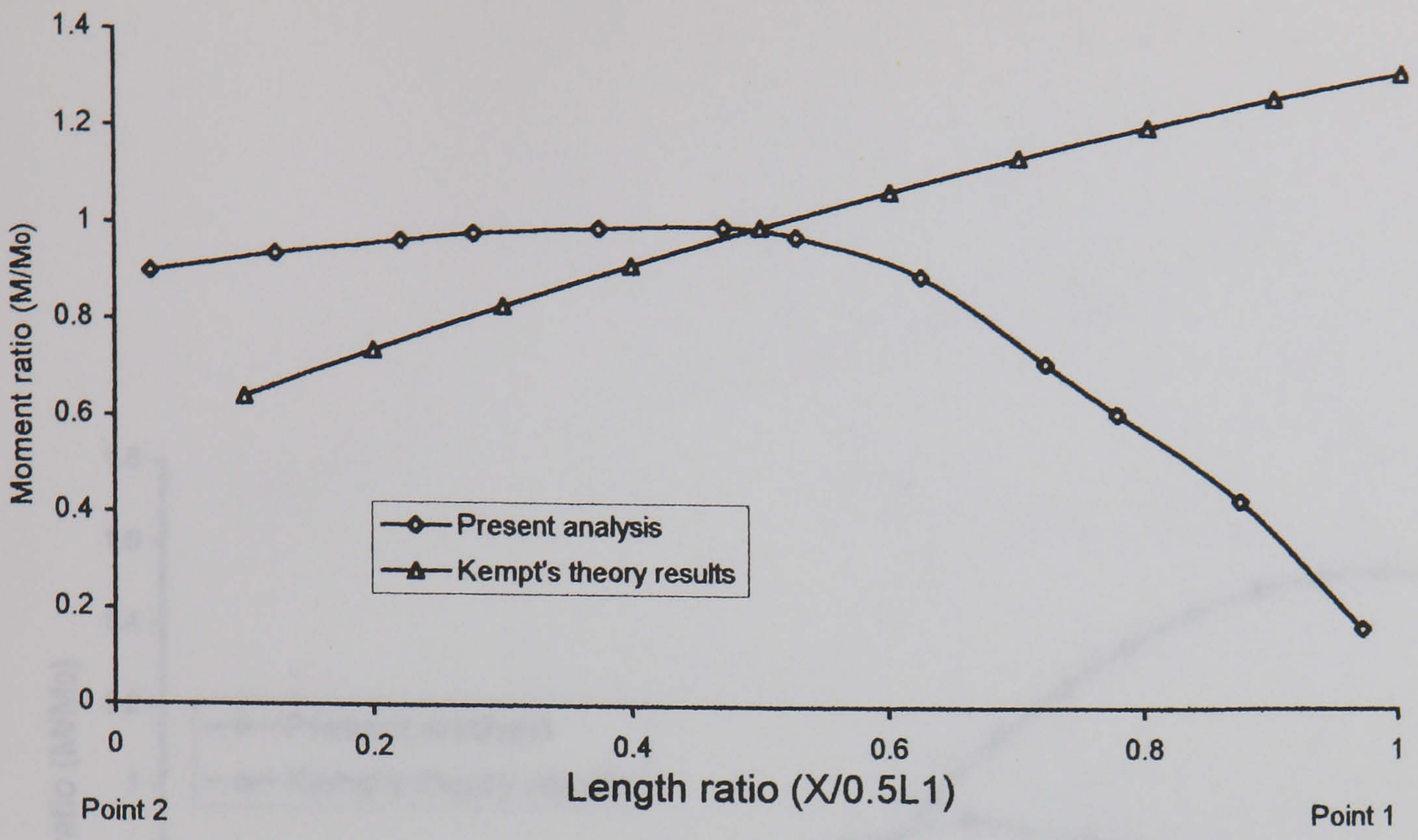

Fig.6.38-Moment comparison between Kemp's method [8] and finite element analysis at $W_0/d = 0.5$

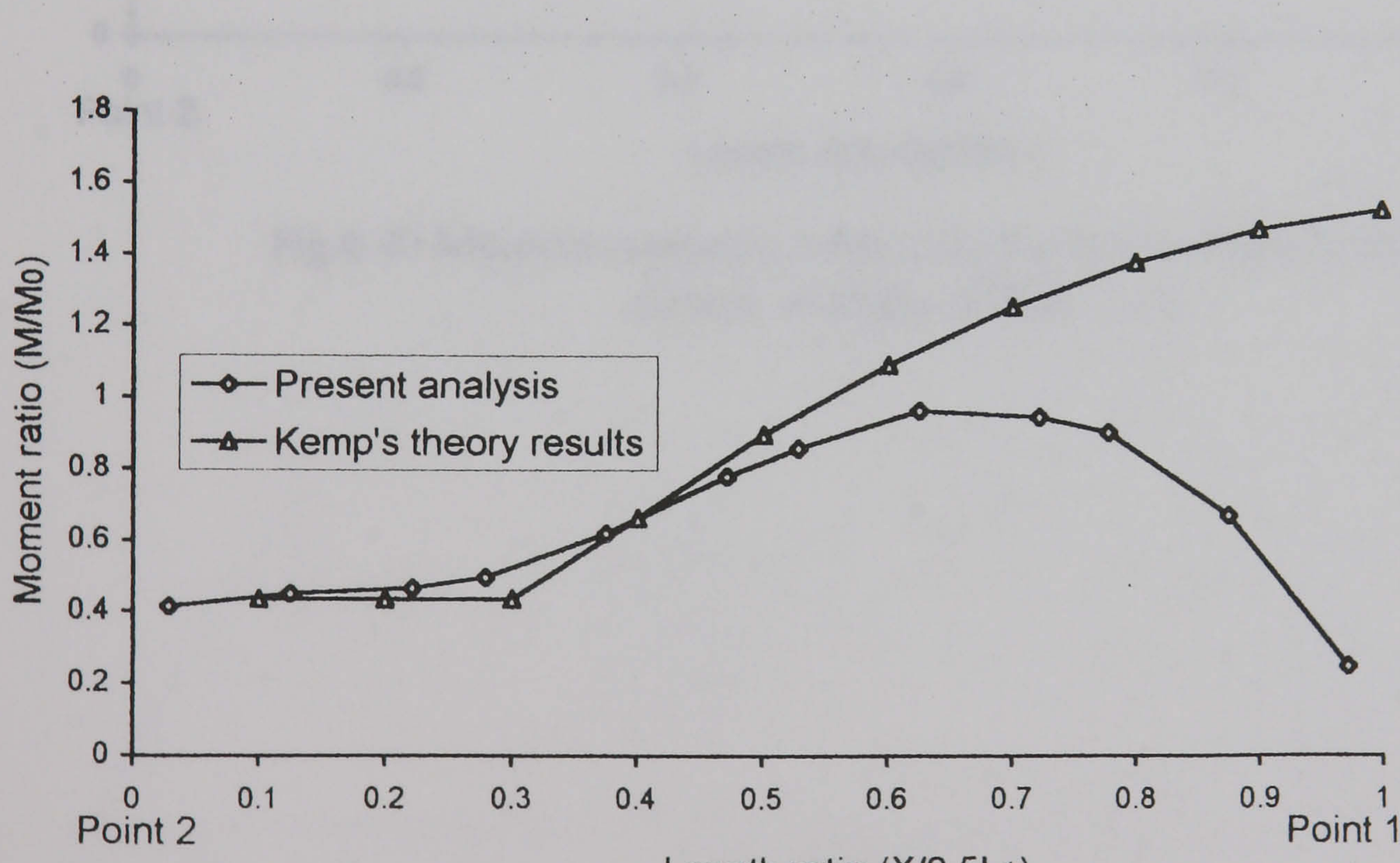

Fig.6.39-Moment comparison between Kemp's method [8] and finite element analysis at $W_0/d = 1.25$

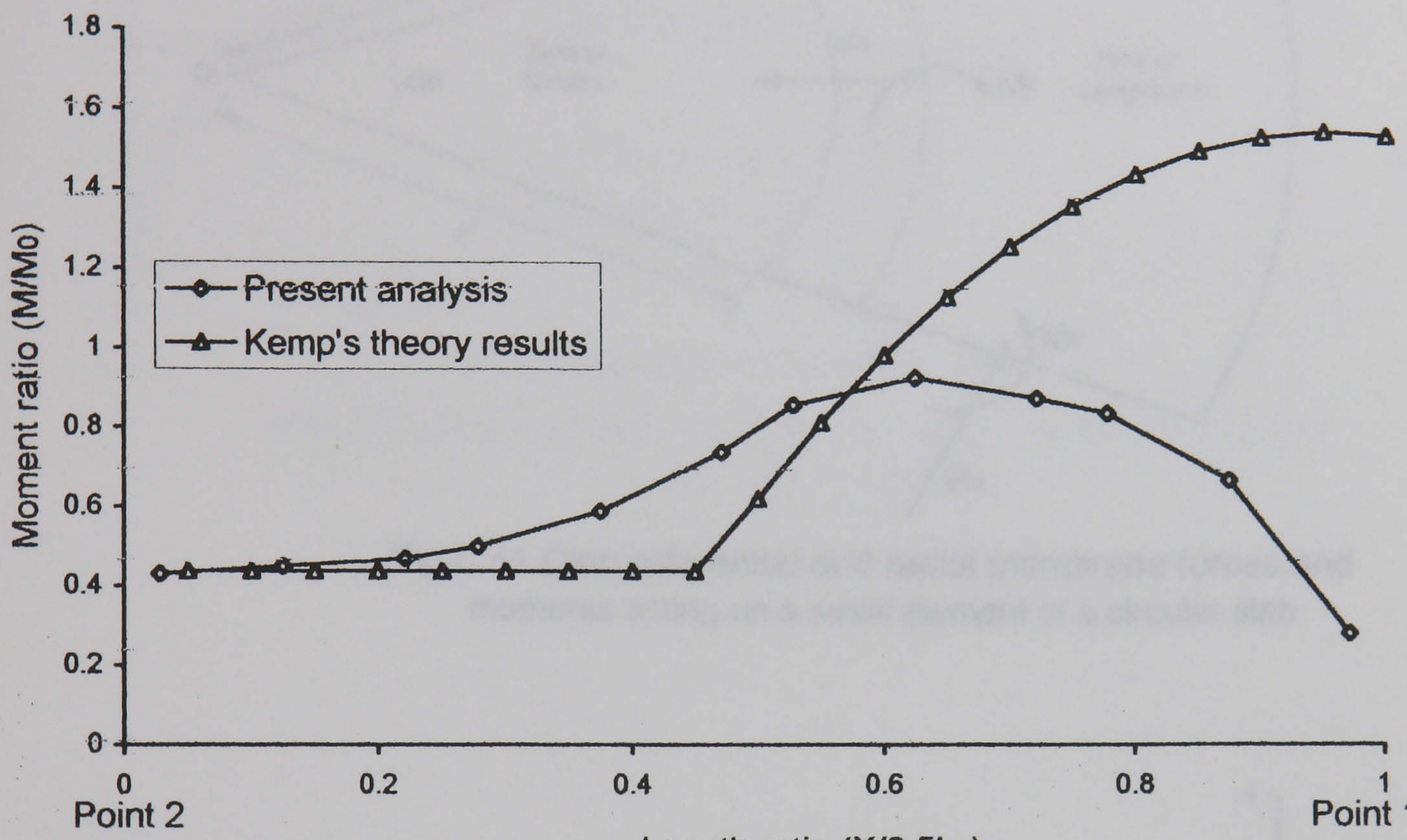

Fig.6.40-Moment comparison between Kemp's method [8] and finite element analysis at $W_0/d=1.75$

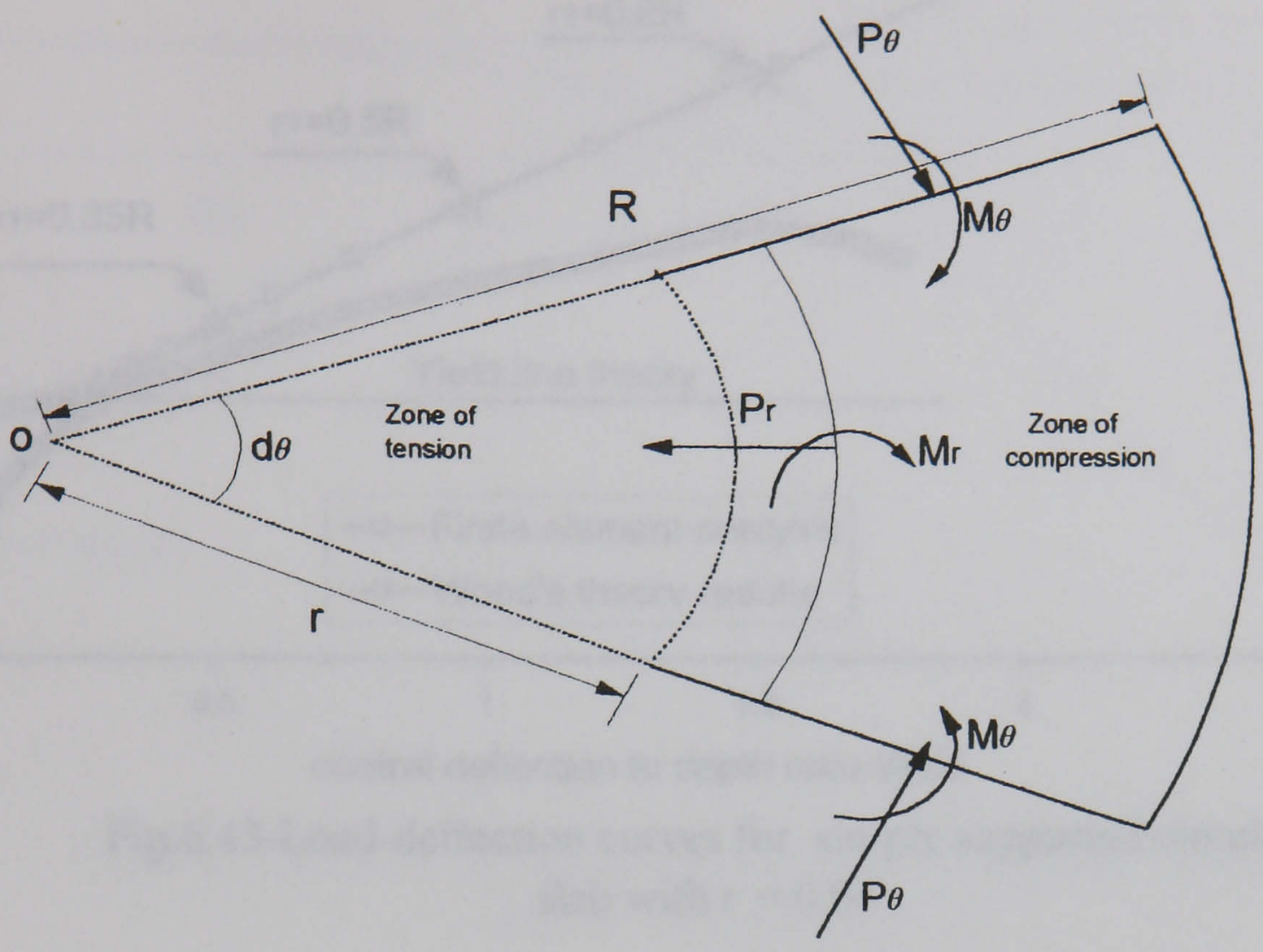

Fig.6.41-Circumferential and radial membrane forces and moments acting on a small element of a circular slab

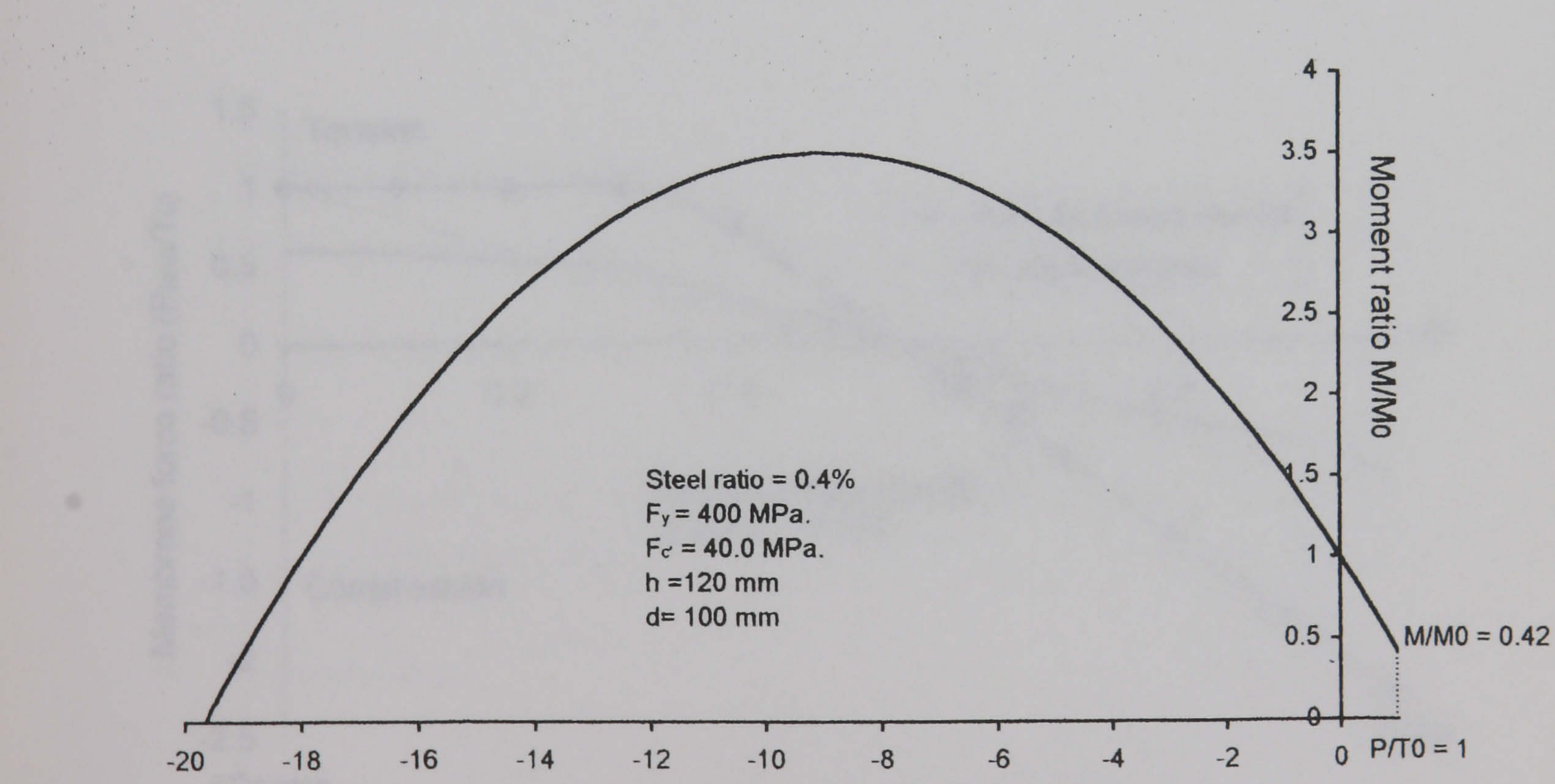

Fig.6.42-Yield criterion for the slab-section

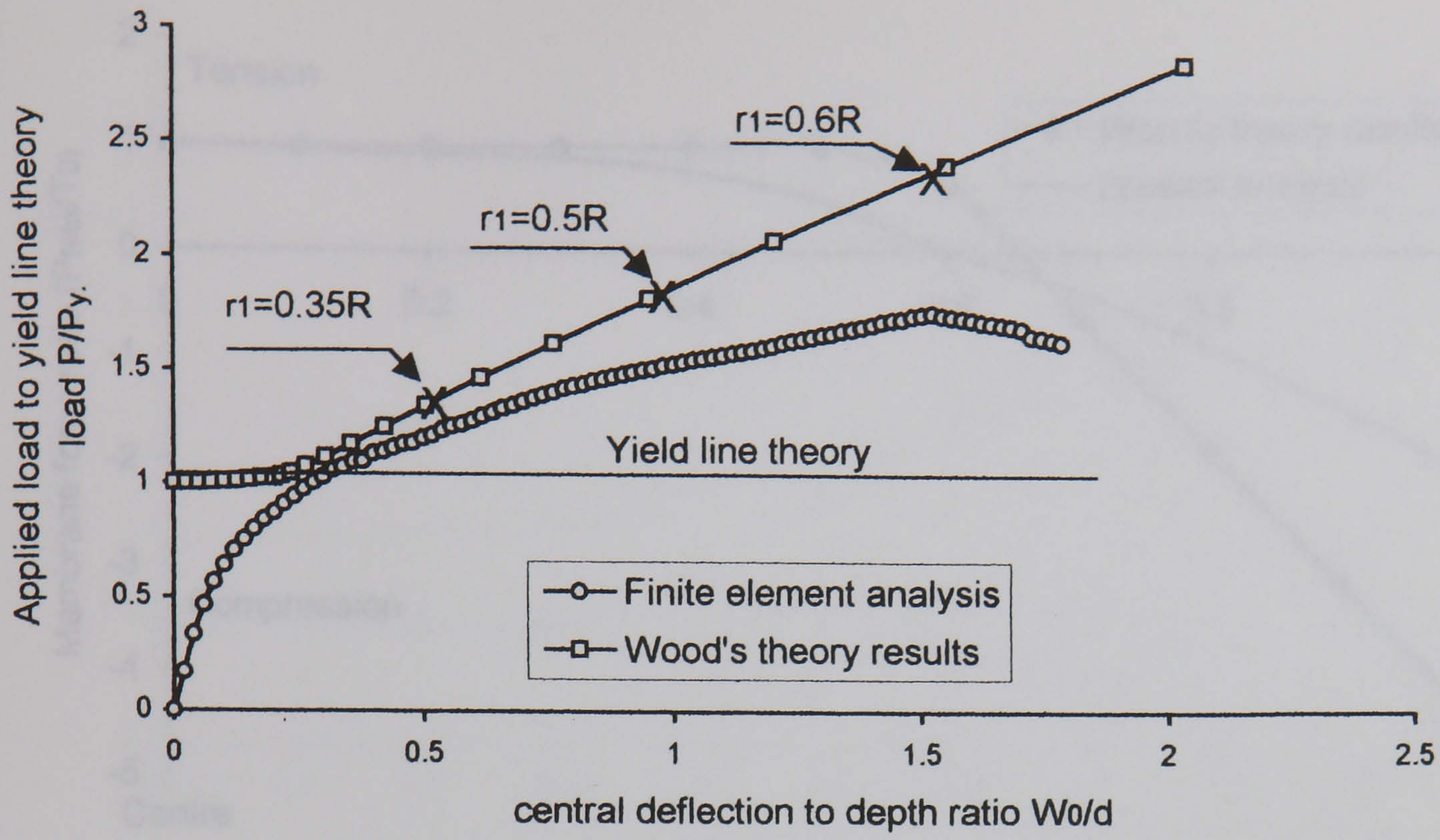

Fig.6.43-Load-deflection curves for simply supported circular slab with $t = 0.04$

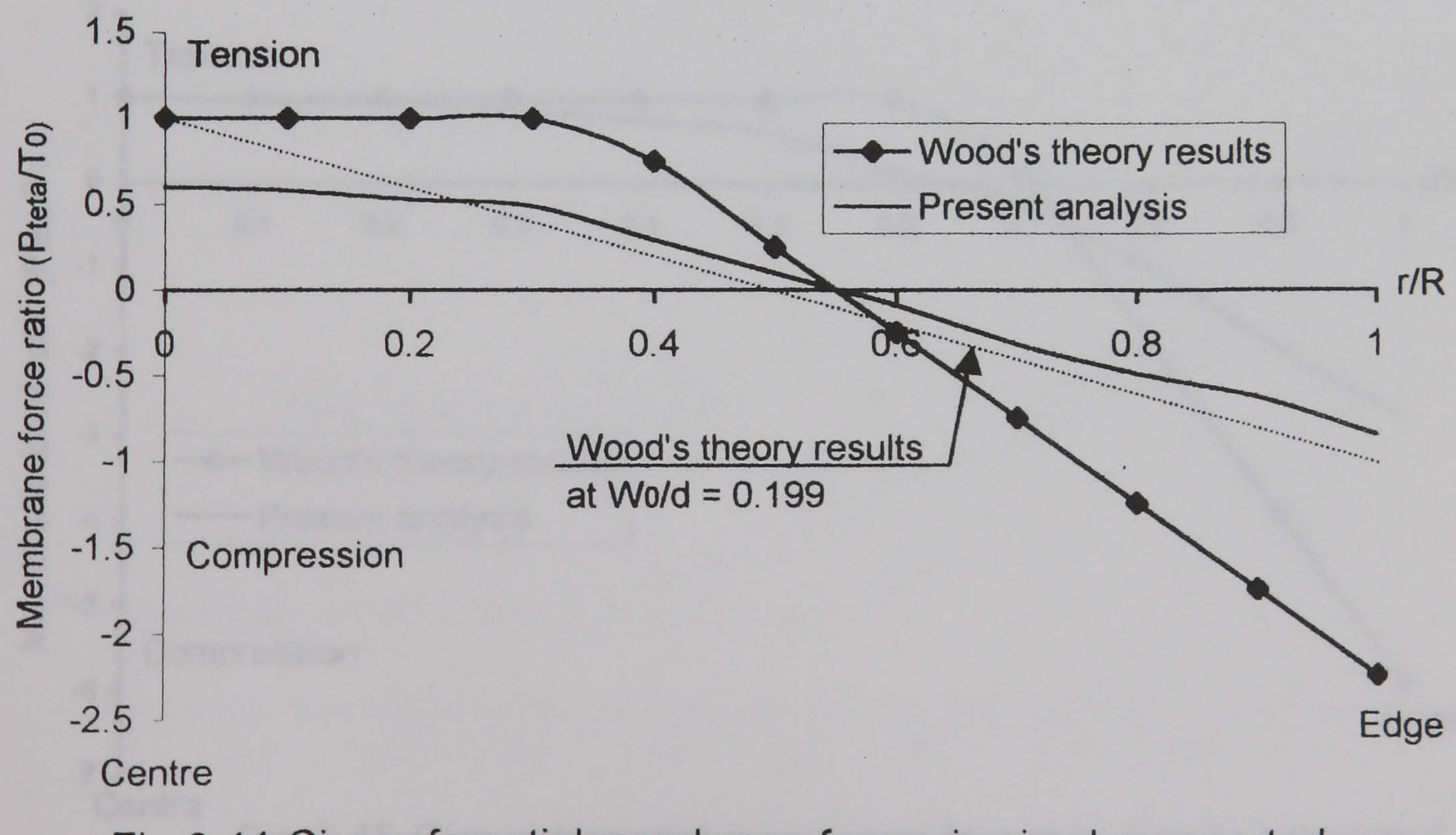

Fig.6.44-Circumferential membrane forces in simply supported circular slab at $W_0/d=0.5$

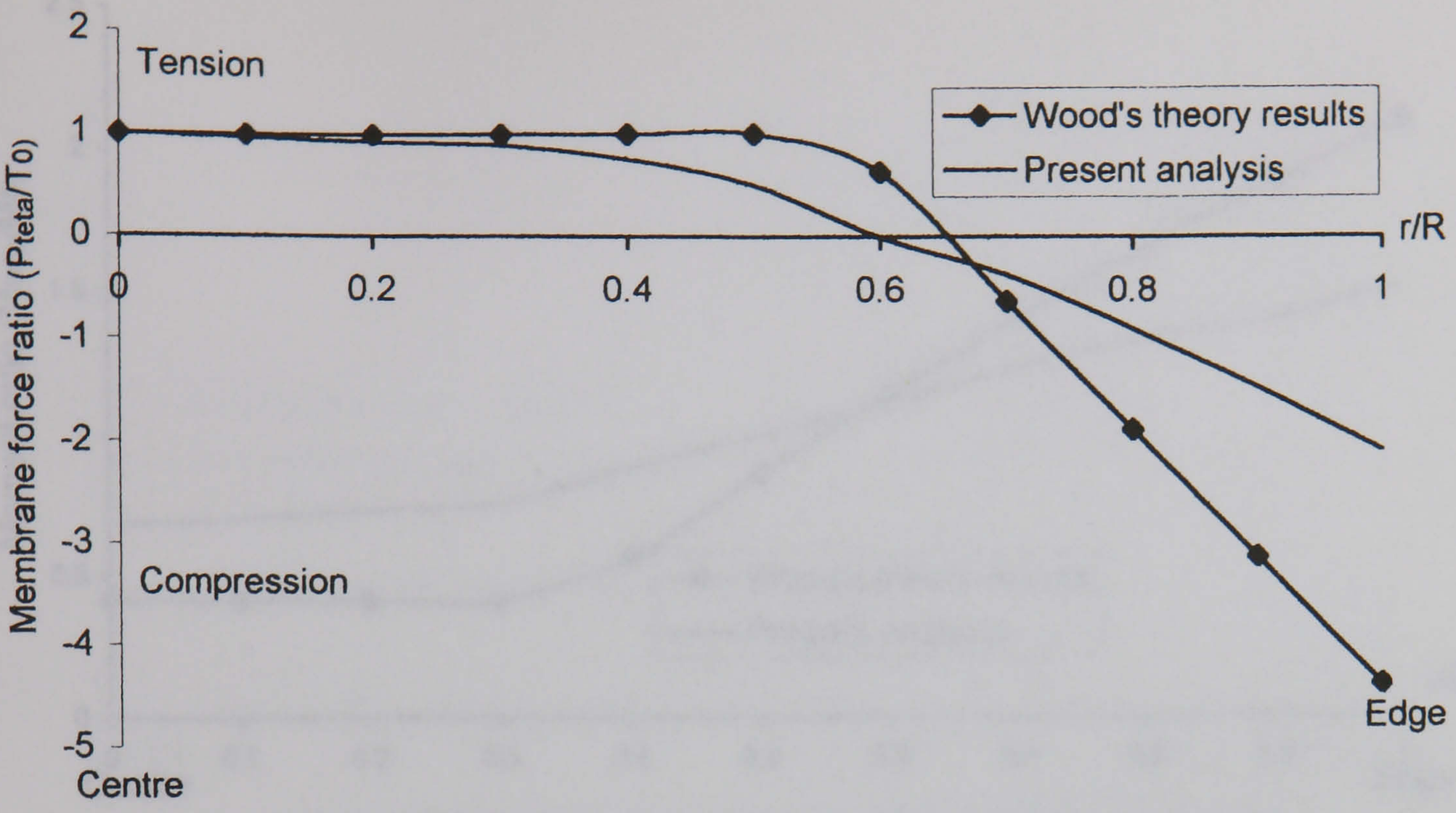

Fig.6.45-Circumferential membrane forces in simply supported circular slab at $W_0/d=1.0$

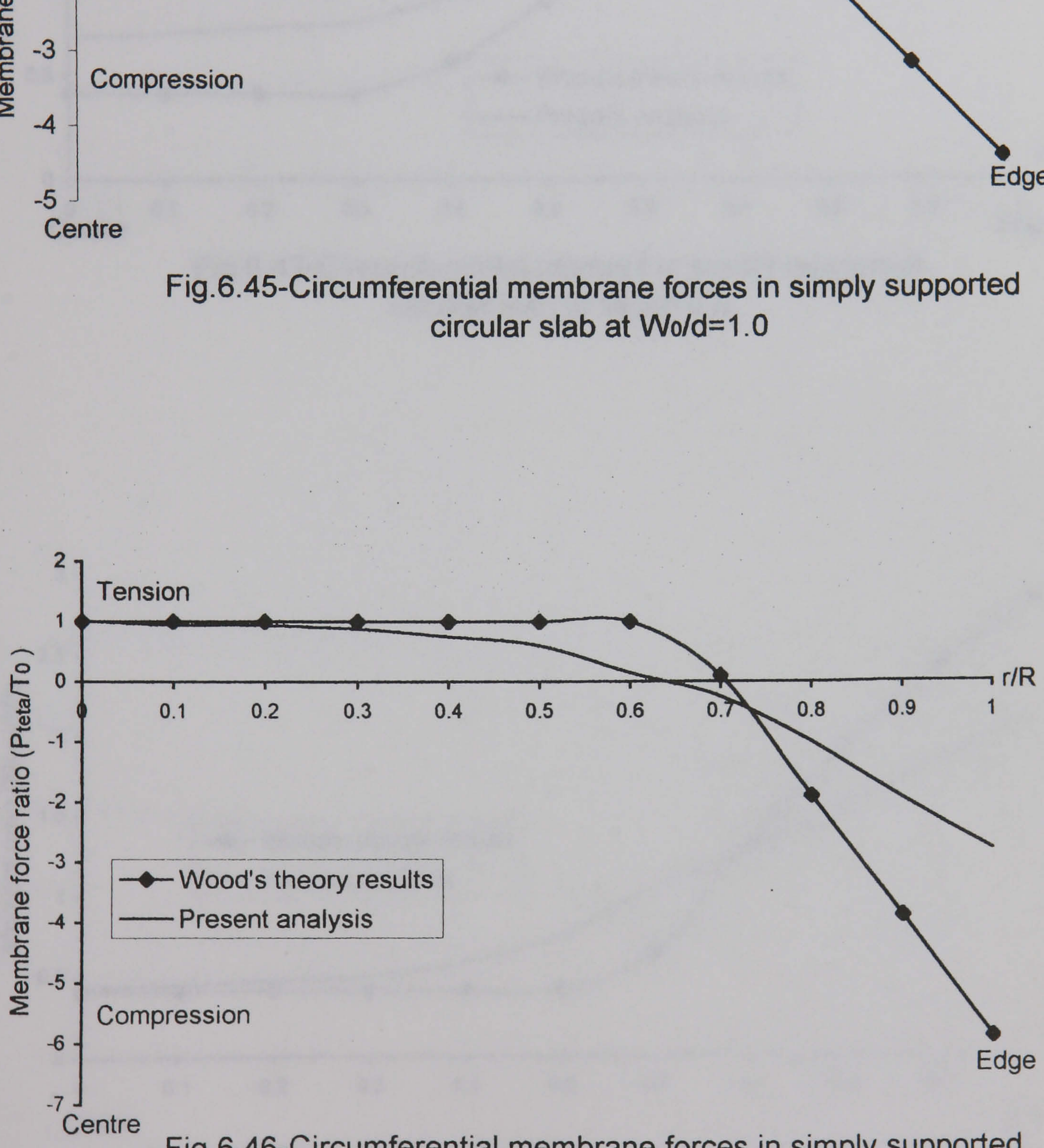

Fig.6.46-Circumferential membrane forces in simply supported circular slab at $W_0/d=1.5$

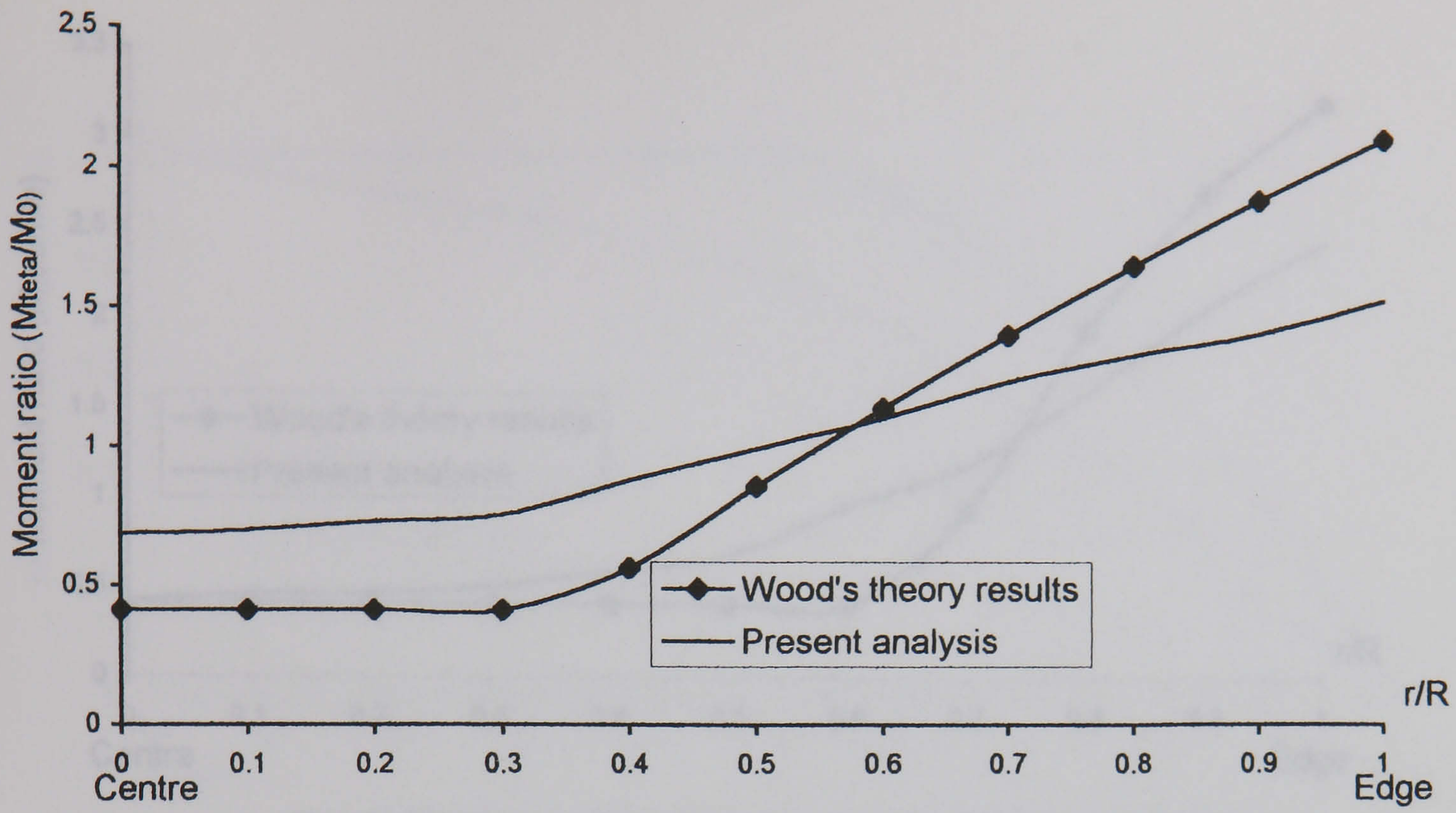

Fig.6.47-Circumferential moment in simply supported circular slab at $W_0/d=0.5$

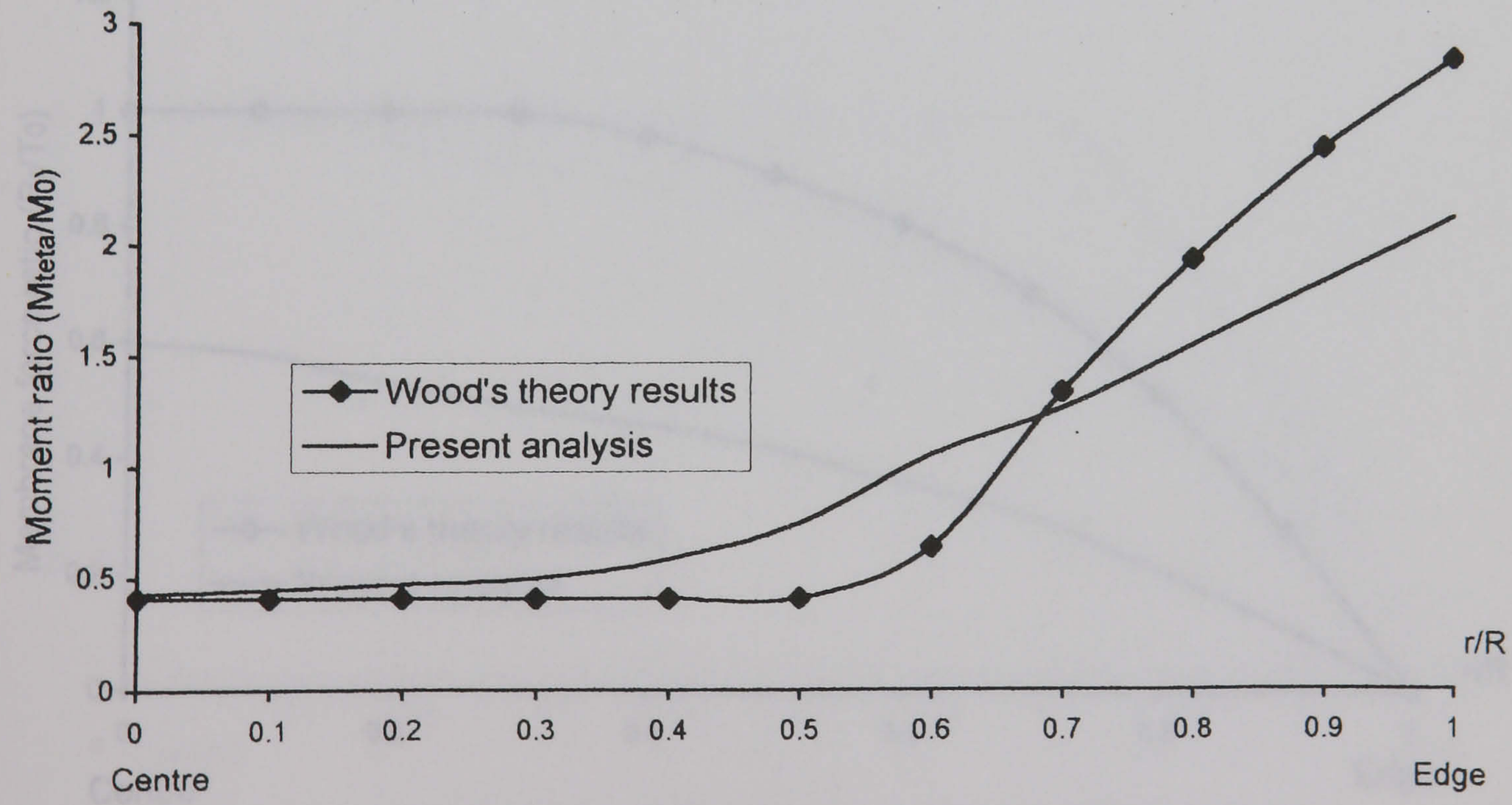

Fig.6.48-Circumferential moment in simply supported circular slab at $W_0/d=1.0$

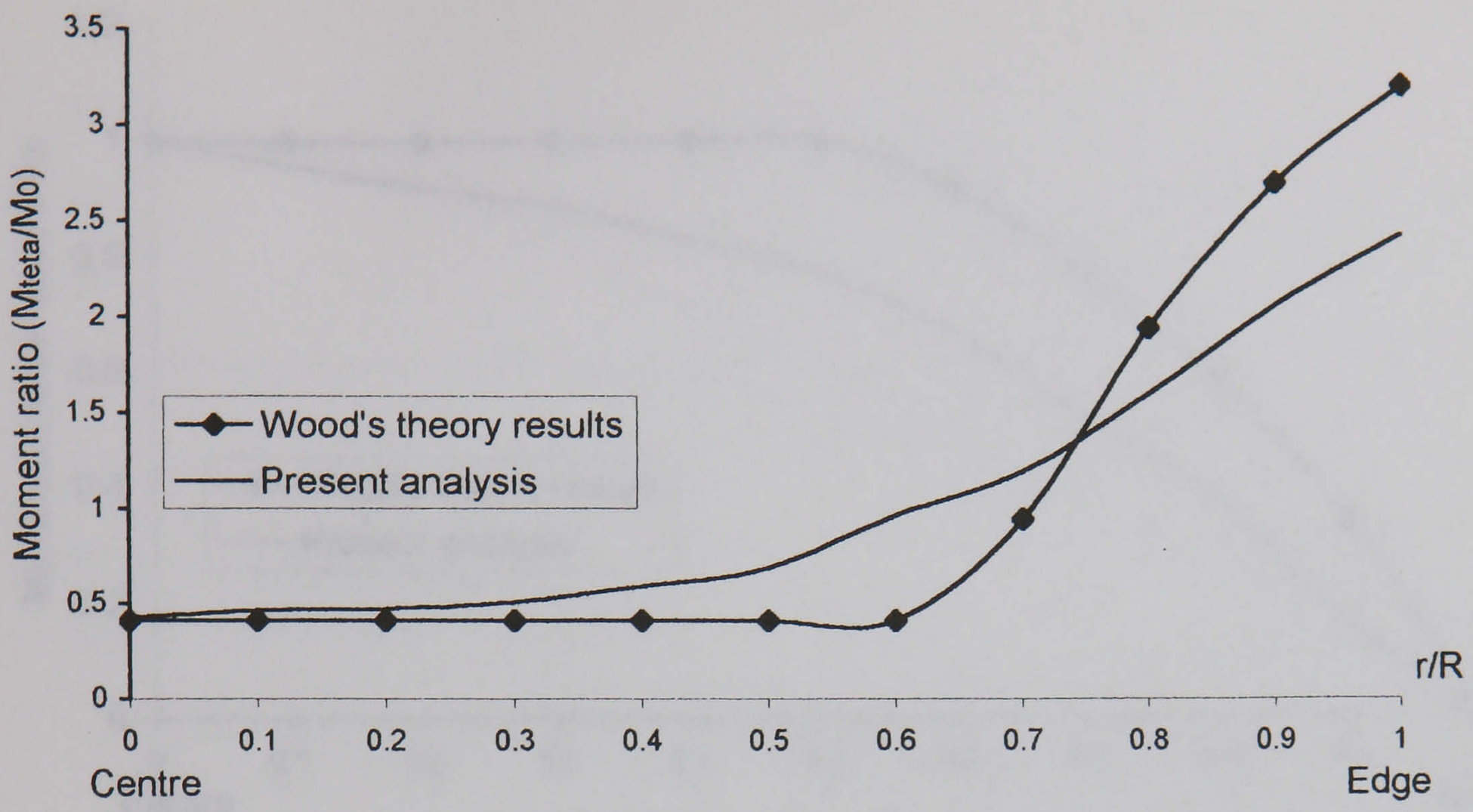

Fig.6.49-Circumferential moment in simply supported circular slab at $w_0/d=1.5$

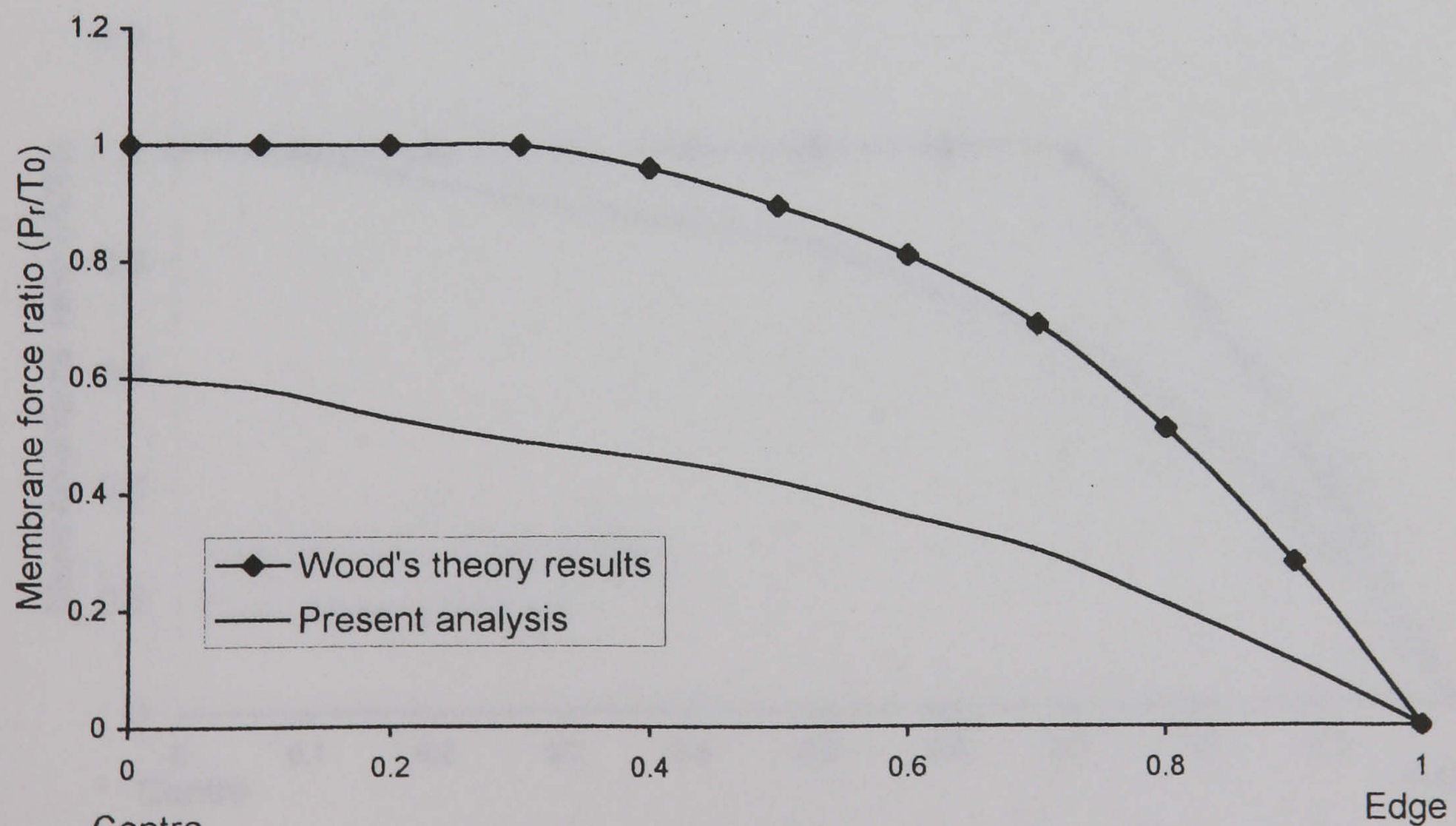

Fig.6.50-Radial membrane forces in simply supported circular slab at $W_0/d=0.5$

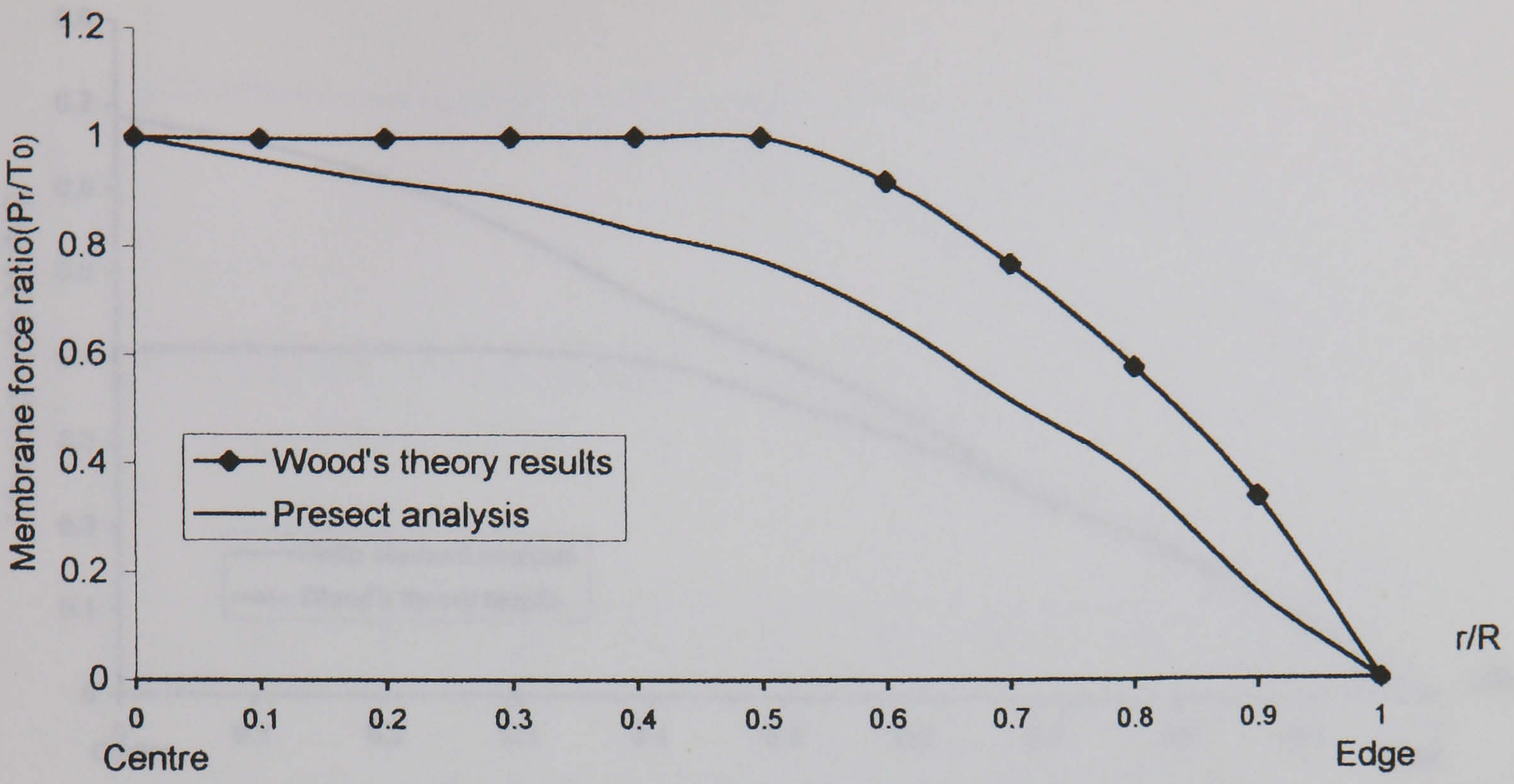

Fig.6.51-Radial membrane forces in simply supported circular slab at $W_0/d=1.0$

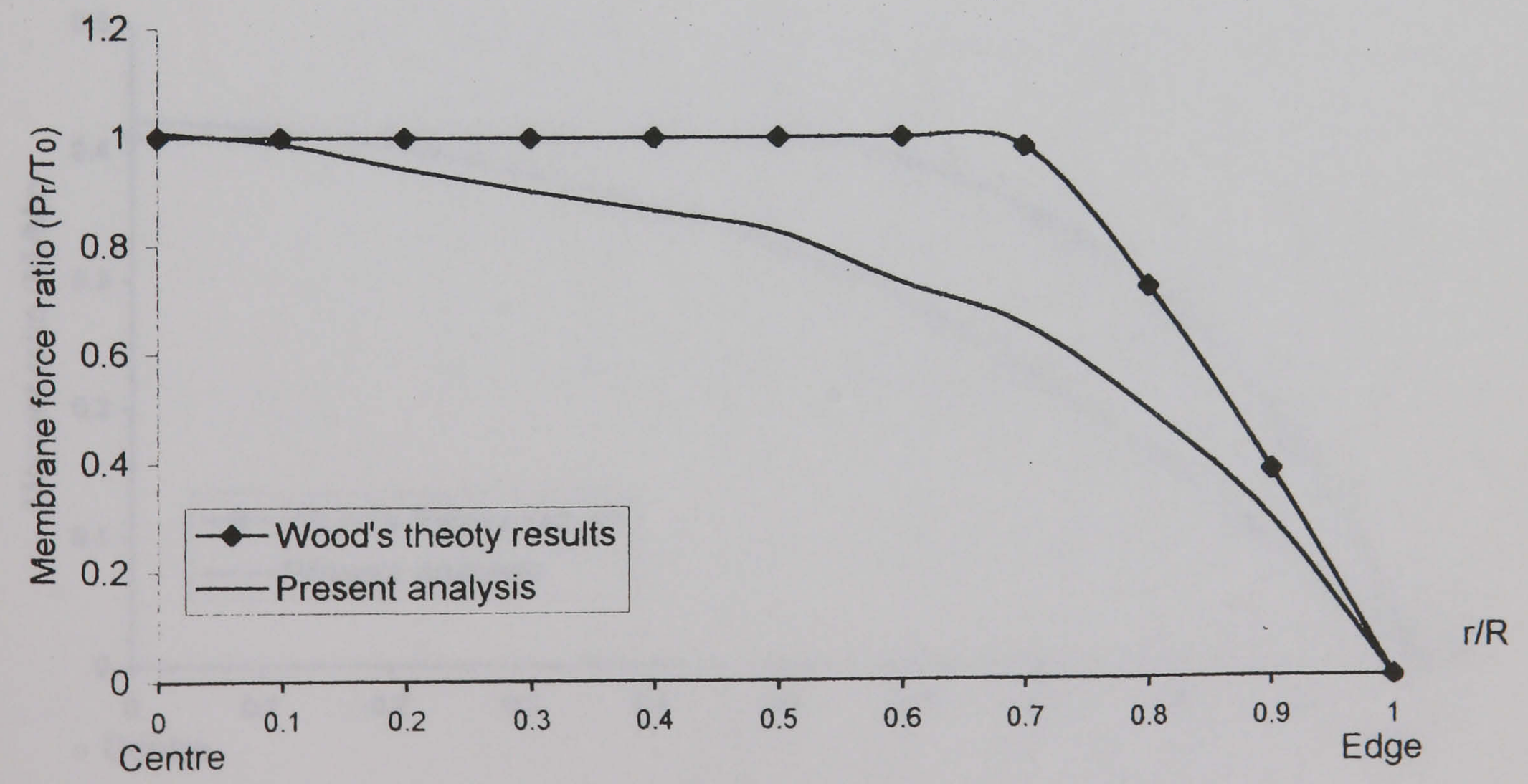

Fig.6.52-Radial membrane forces in simply supported circular slab at $W_0/d=1.5$

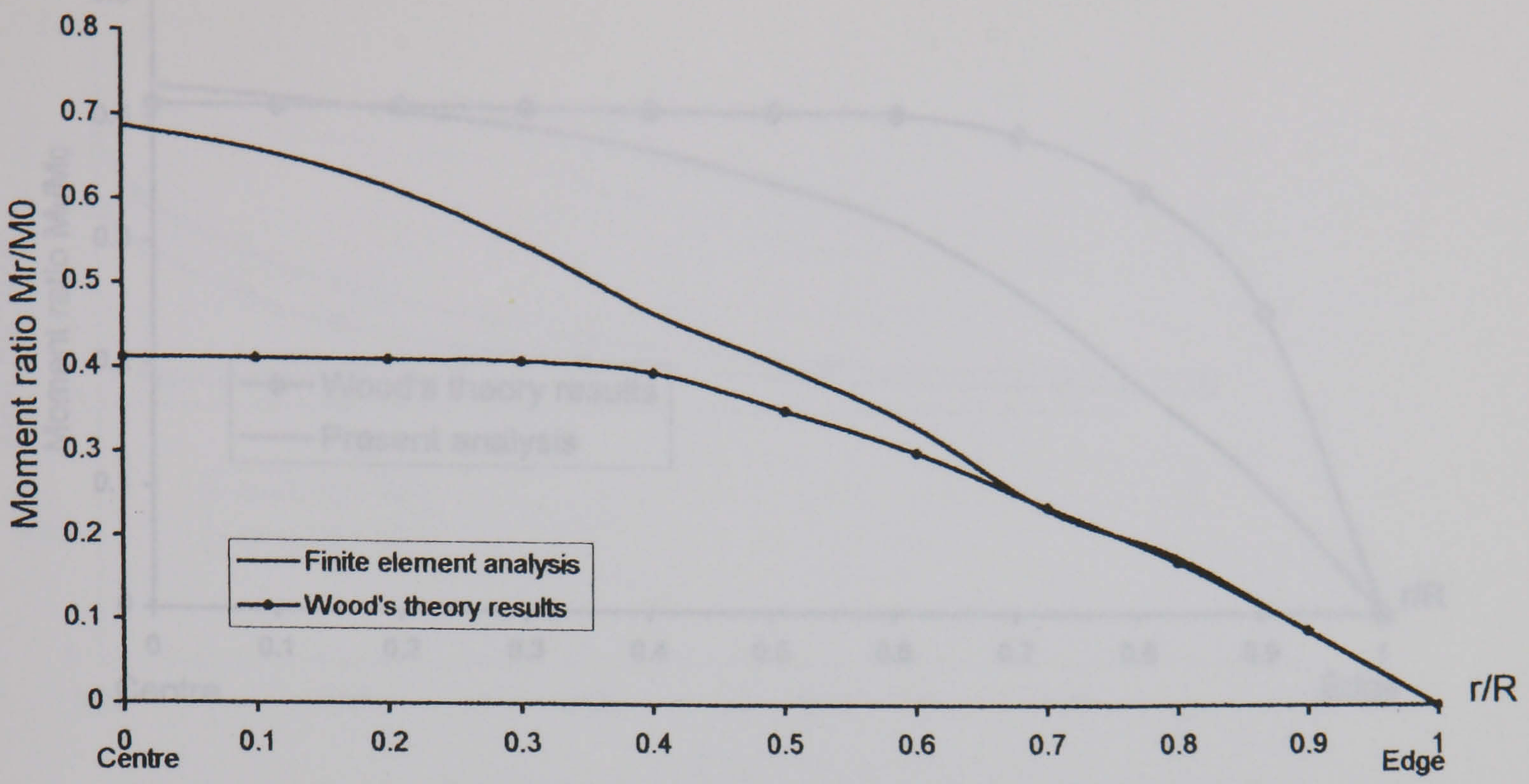

Fig.6.53-Radial moment in simply supported circular slab at W0/h=0.5

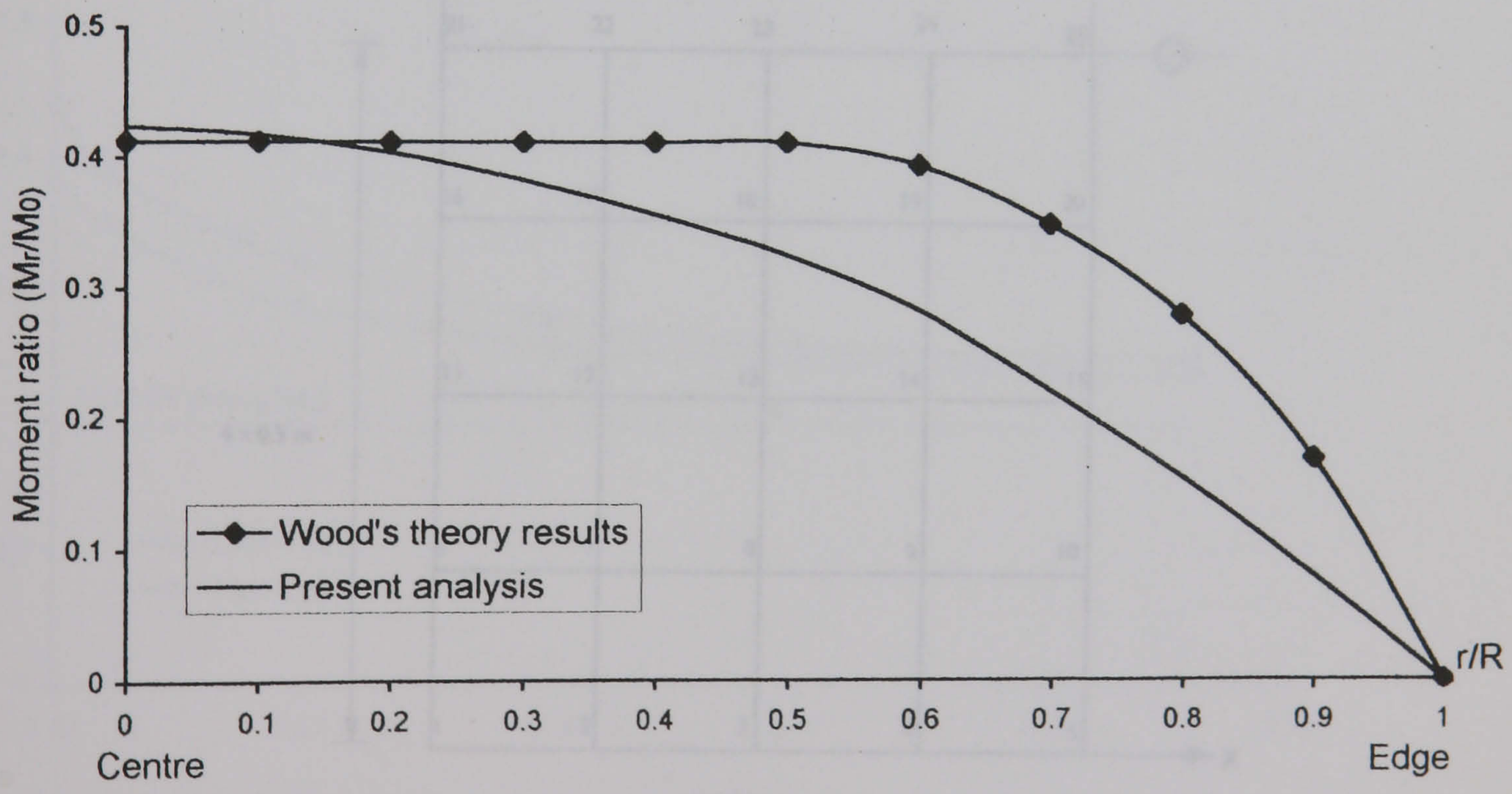

Fig.6.54-Radial moment in simply supported circular slab at W0/d=1.0

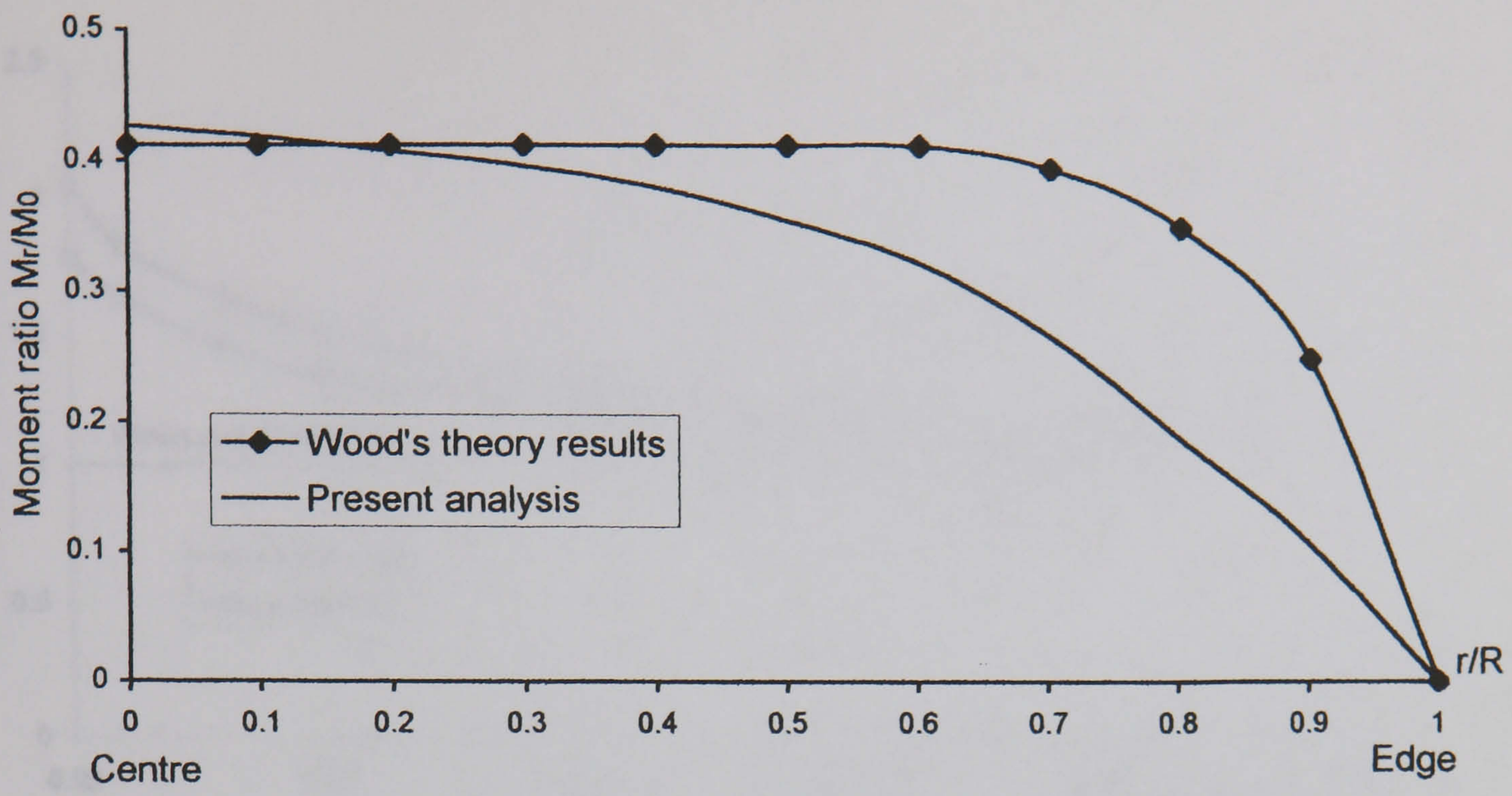

Fig.6.55-Radial moment in simply supported circular slab at W0/d=1.5

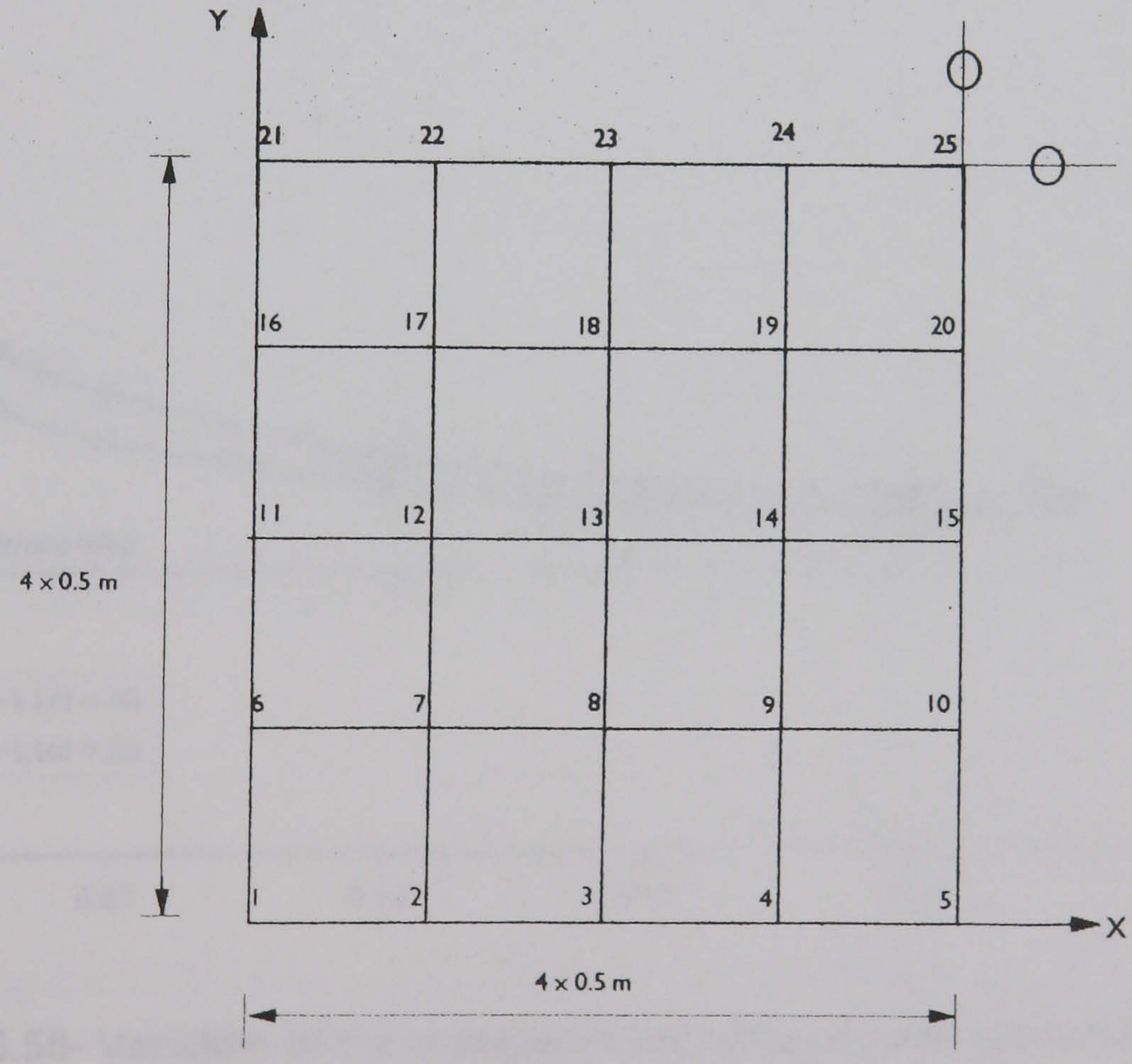

Fig. 6.56- The finite element mesh for the slab

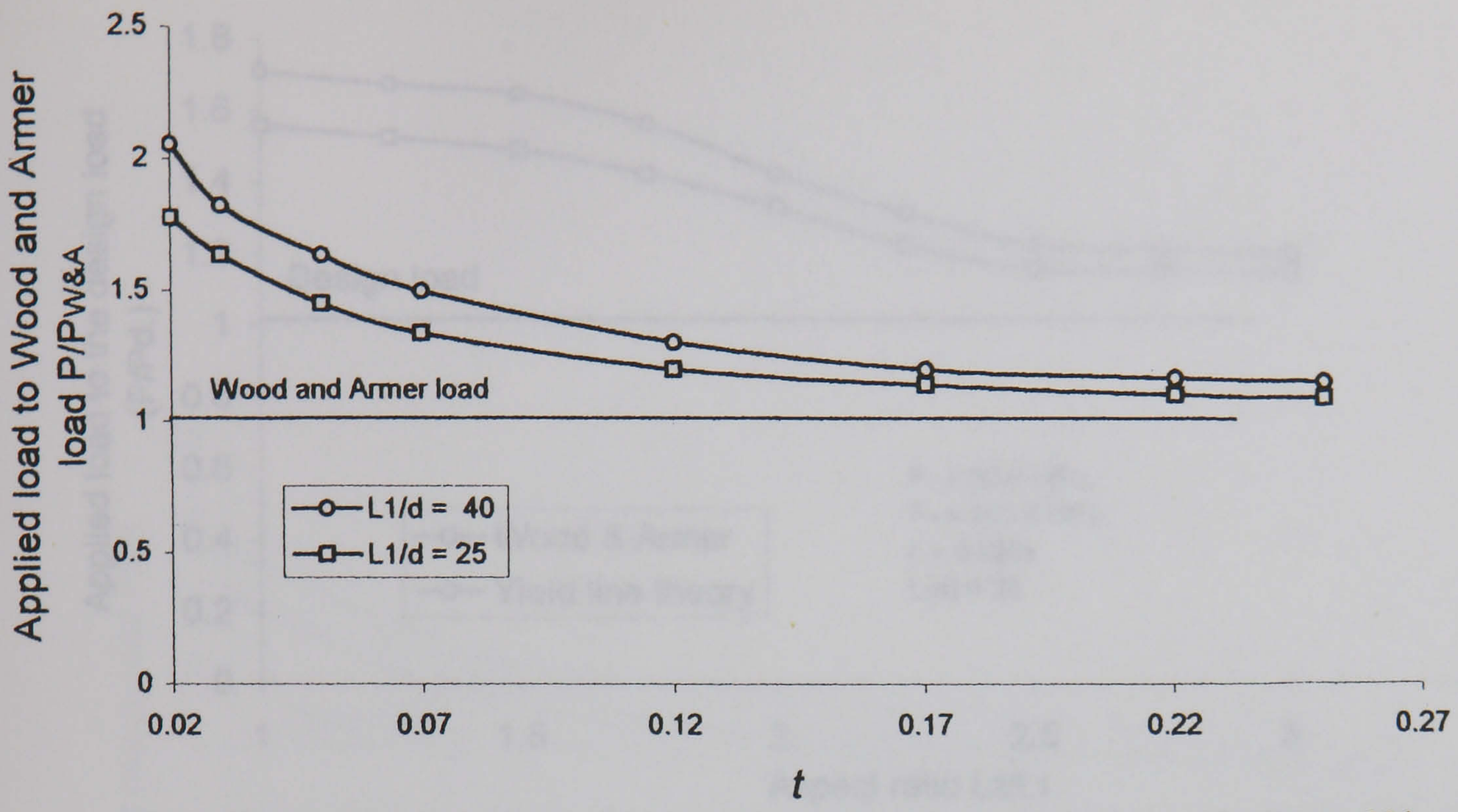

Fig.6.57-Variation of the increase in the ultimate load above Wood and Armer load with increasing t for different slabs

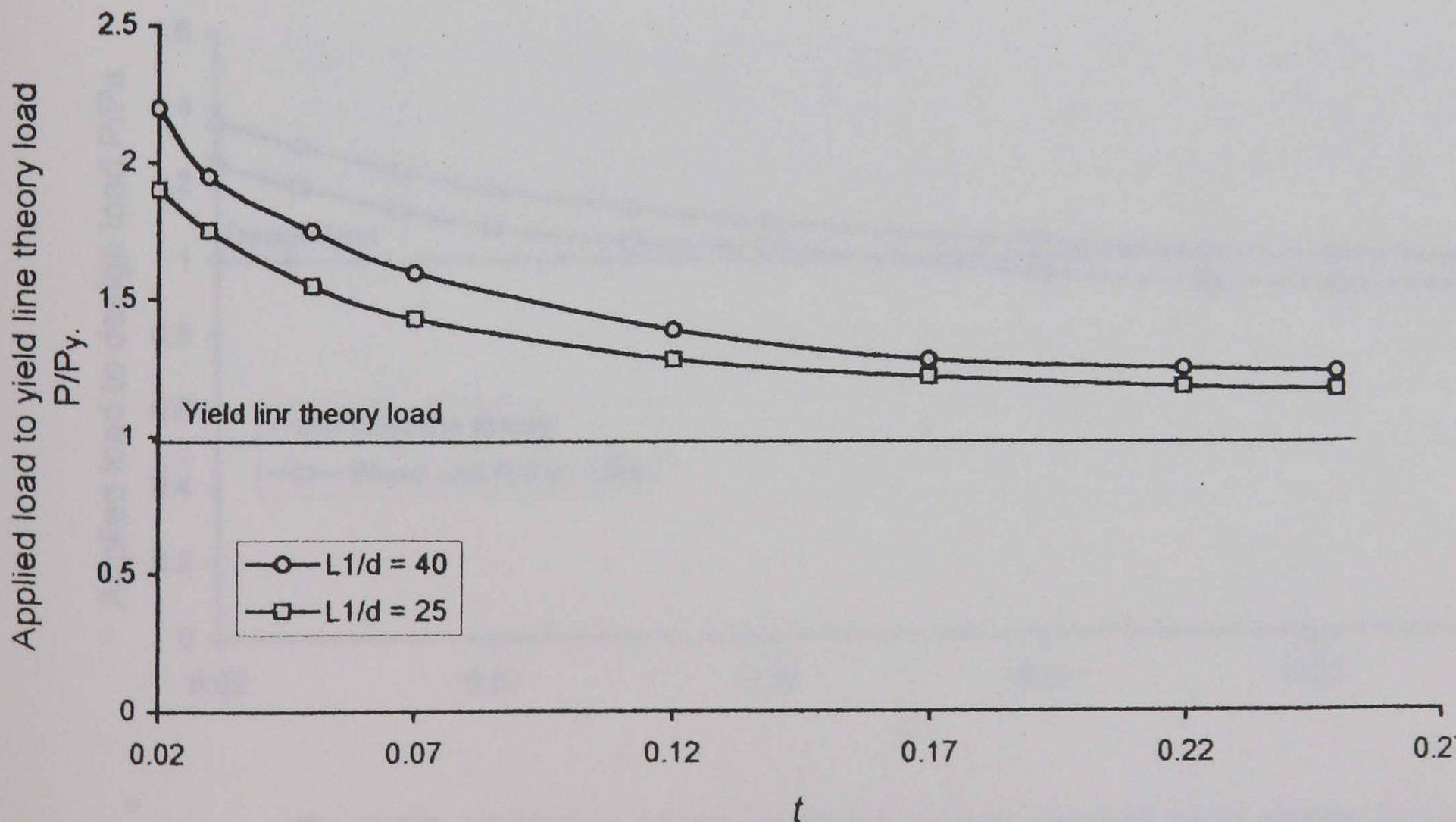

Fig.6.58- Variation of the increase in the ultimate load above yield line theory load with increasing t for different slabs

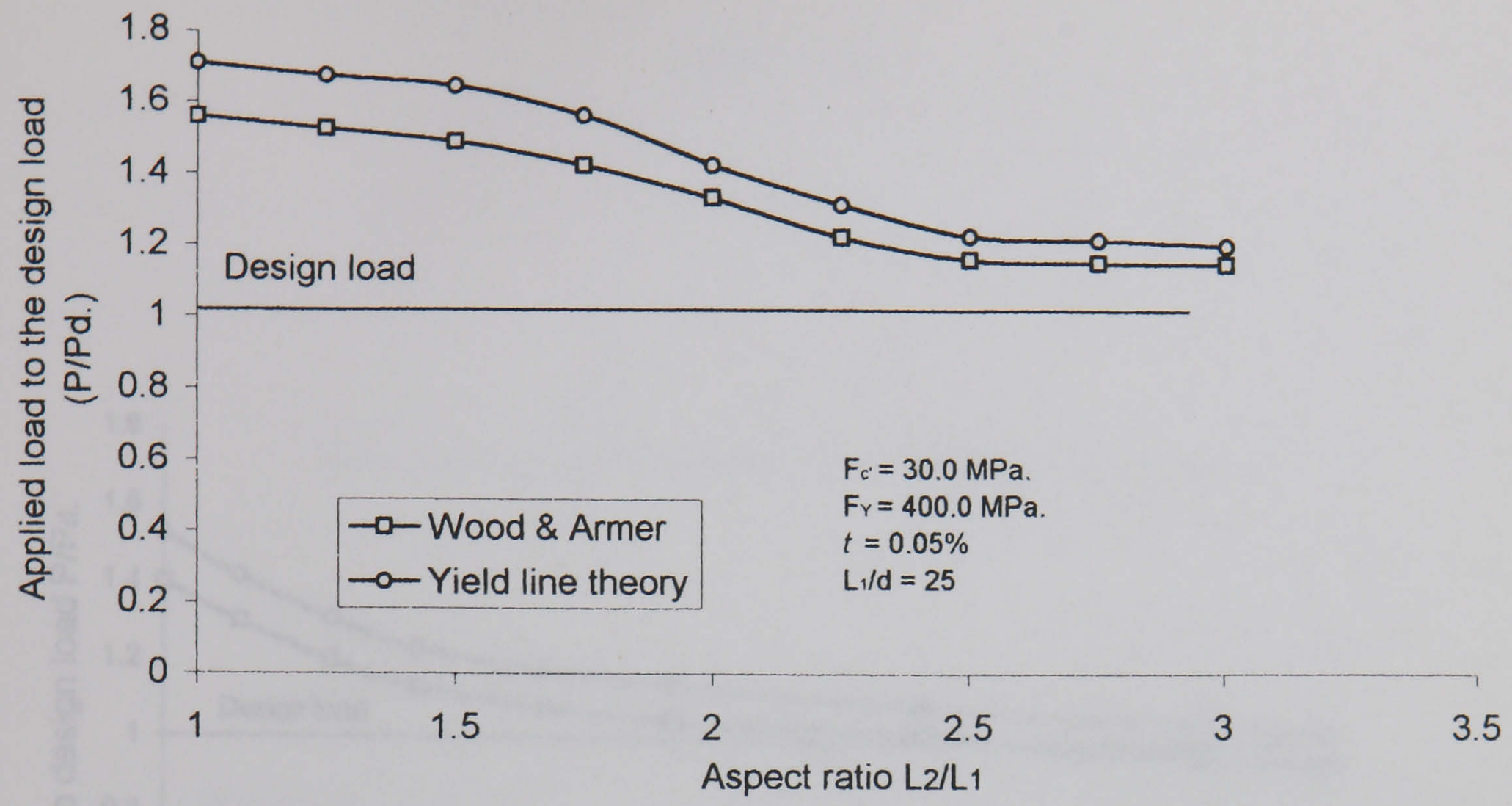

Fig.6.59-Variation of the increase in the ultimate load above the design load with the increase of aspect ratio

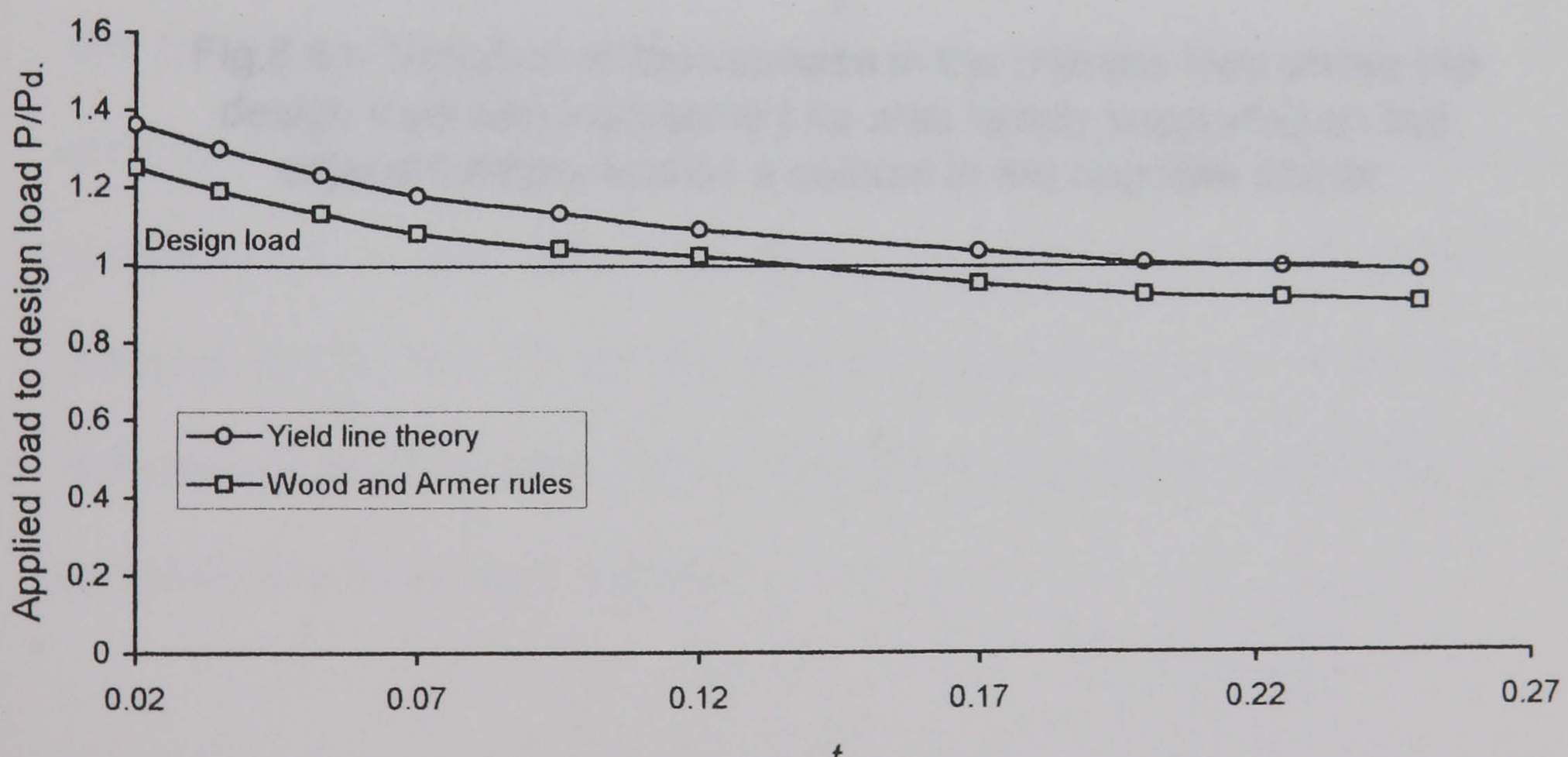

Fig.6.60- Variation of the increase in the ultimate load above the design load with increasing *t* for corner simply supported slab

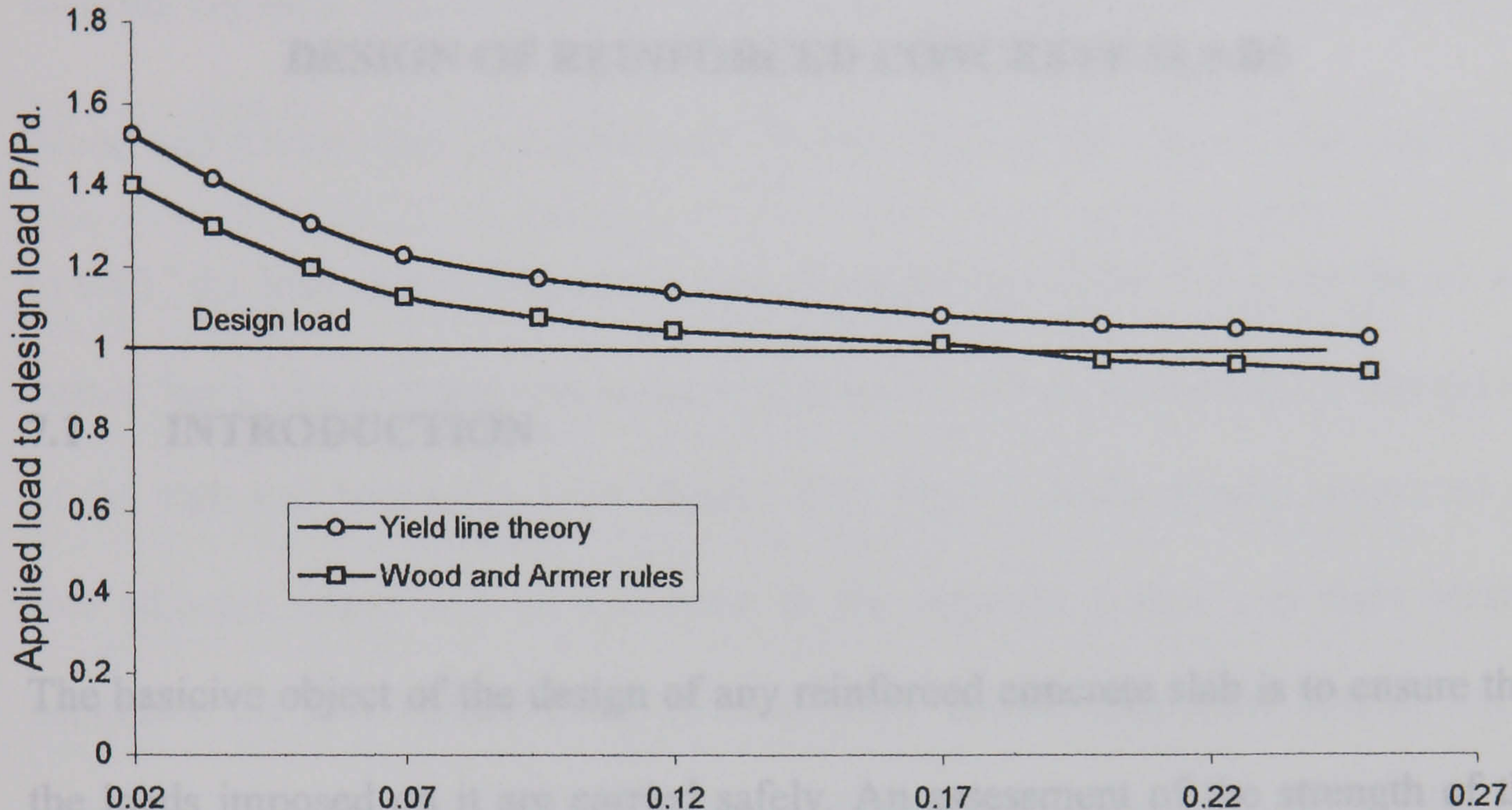

Fig.6.61- Variation of the increase in the ultimate load above the design load with increasing t for slab simply supported on two adjacent edges and on a column in the opposite corner.

CHAPTER 7

DESIGN OF REINFORCED CONCRETE SLABS

7.1 INTRODUCTION

The basicive object of the design of any reinforced concrete slab is to ensure that the loads imposed on it are carried safely. An assessment of the strength of the slab at failure must be complemented by the study of the conditions at the serviceability loads. In the case of reinforced concrete structures, serviceability conditions are mainly those of deflection and crack widths. For a structure designed on the basis of ultimate strength, it is necessary to check that the deflections at working loads of the structure do not exceed the permissible values as specified by an accepted standard.

The Wood and Armer rules [1,2] are one of the most popular design techniques used in the design of bridge decks in the UK. and over the world. These design rules are easy to use and most conveniently carried out using the finite element method. These design rules can produce unsafe results under certain loading conditions like torsion, i.e. an element designed using these rules has a lower

capacity than it is designed for [3]. But studies carried out in Chapter 6 on simply supported slab show that the Wood and Armer rules [1,2] can produce a safe design because of the development of the membrane action in the plane of the slab Fig 7.1. The study shows that membrane action has a beneficial effect on the load-carrying capacity of slabs simply supported on four edges and designed using the Wood and Armer rules. For slabs with $\frac{L_1}{d}$ =40, and t at the centre of the slab equal to 0.02, the load carrying-capacity was increased by 105% above the Wood and Armer load; this increase was reduced gradually with an increasing t at the centre of the slab and becoming 15% where t 0.25 Fig.7.1. Slabs simply supported on two adjacent edges and on a column in the opposite corner and slabs simply supported on four columns can develop some tensile membrane action, which results in an enhancement in the ultimate loads for low reinforcement ratio. But the effect of the membrane action on the ultimate load of such slabs is not significant compared with the slabs simply supported on four edges. Where t equal to 0.02 at the centre of the slab, the percentage increase in the ultimate load above the Wood and Armer load was 40% for slabs simply supported on two adjacent edges and on a column in the opposite corner, and 25% for slabs simply supported on four columns. The Wood and Armer rules overestimated the ultimate loads for such slabs where t above 0.2 and 0.17 respectively, Fig.7.1.

In order to include the membrane action effect in the design of simply supported slabs designed using Wood and Armer rules [1,2], design guidelines for rectangular slabs simply supported on four edges and designed using the Wood and Armer rules [1,2] using elastic moment fields and subjected to uniformly

distributed load will be developed in this Chapter. Design examples will be also presented.

7.2 PRACTICAL SIGNIFICANCE OF MEMBRANE ACTION

To determine the increase in the collapse load caused by membrane action design charts have been developed based on the results of finite element analyses carried out for rectangular simply supported slabs loaded with uniformly distributed load. The reinforcement is designed using the Wood and Armer rules [1,2] and elastic moment fields. The elastic moments are calculated from the Lagrange equation, equation 2.11, using the Fourier series approximation and Navier's method [4]. The Wood and Armer [1,2] design moments are given in Table 7.1.

The variables investigated were the slenderness ratio, $\frac{L_1}{d}$, and the parameter t, where t is equal to the ratio of maximum tensile strength to maximum crushing strength, $\frac{A_s f_y}{d f_c'}$.

The results of the finite element analyses for square slabs with $\frac{L_1}{d}$ of 40 and t parameters varied from 0.02 to 0.27 are shown in Figs. 7.2-7.6; the limitation of deflection [5], Δ, namely l/350 of the span, is also plotted on the figures. This deflection determines the maximum working load, which could be applied to these slabs. From Fig.7.2-7.6 it can be seen that, for the slabs with the same t, the

variations of ρ, $f_c^{'}$ and f_y have little effect on the response if the load is normalised in respect of the Wood and Armer load. Fig. 7.7 shows the load deflection curves for rectangular slab with t = 0.066 and aspect ratios $\frac{L_2}{L_1}$ varying from 1 to 3. It can be seen from the figure that the ultimate load for the rectangular slabs decreases with increasing aspect ratio and becomes unchanged for aspect ratio greater than 2.5.

Design charts have been developed using the finite element analysis for slabs with $\frac{L_1}{d}$ ratios of 40, 35, 30, 25, 20 and 15, and are shown in Figs. 7.8. The design charts give the relationship between the parameter t and the percentage increase in the ultimate load above the Wood and Armer collapse load. Design charts for estimating the working loads for such slabs are also shown in Fig.7.9, based on limitation of deflection, namely l/350. The decrease in the ultimate load with increasing of aspect ratios for the rectangular slabs is also shown in Fig.7.10.

7.3 DESIGN GUIDELINES FOR RECTANGULAR SIMPLY SUPPORTED SLABS DESIGNED USING THE WOOD AND ARMER RULES INCLUDING MEMBRANE ACTION EFFECT.

It has been pointed out in Section 7.1 that the Wood and Armer rules [1,2] produce a safe design for slabs simply supported along all edges because of the development of membrane action. It is therefore the intention of this section to

provide guidelines for the design of simply supported slabs using the Wood and Armer rules, including the effect of membrane action.

The Wood and Armer rules can produce a safe design if the slab satisfies the following conditions.

- The slab is simply supported on four edges.
- The slab is under reinforced.

If the above two conditions are satisfied then the slab can be designed using the following procedure.

1. For a given dimension the slab should be designed for the serviceability limit-state and span to depth ratio should be checked.

2. From the theory of the elastic bending of plates one should calculate the elastic applied bending moments M_x, M_y and the elastic applied twisting moment M_{xy} for a given load, and then one should calculate the design moments M_x^* and M_y^* using the Wood and Armer rules table 7.1.

3. The optimum reinforcement for the slab should be designed using the design moments M_x^* and M_y^*.

4. The parameter t using the reinforcement ratio ρ, at the centre of the slab and the concrete crushing strength $f_c^{'}$ and the steel yield strength f_y should be calculated.

5. Using the slenderness of the slab $\frac{L_1}{d}$, the suitable design charts for ultimate load and for working load from Figs. 7.8 -7.9 should be chosen.

6. From the design charts the load factors according to t should be chosen.

7. From the design chart, Fig.7.10 the load factor for the ultimate load using the aspect ratio of the slab, $\frac{L_1}{L_2}$ should be reduced.

8. The initial design load with the reduced load factor from the design chart should be multiplied to give the ultimate Wood and Armer collapse load and with working load factor should be multiplied to give the maximum working load for the slab.

In order to demonstrate the procedures outlined above, a slab in an office building measuring 5 m x 5 m is simply supported at the edges. The slab is assumed initially to be 200 mm thick. The total dead load including self-weight, screed, finishes, partitions, services etc. is 6.2 kN/m^2 and the imposed load is 2.5

kN/m^2. The slab should be designed using grade 30 concrete and grade 250 reinforcement.

Using load factors 1.4 for dead load and 1.6 for live load, the design load is

1.4 x 6.2 + 1.6 x 2.5 = 12.68 kN/m^2

For cover of 25 mm and 16 mm diameter bars the effective depths are as follows:

For bars in the bottom layer $d = 200 - 25 - 8 = 167$ mm

and for bars in the top layer $d = 200 - 25 - 16\text{-}8 = 151$ mm

To calculate the design moments, a quarter of the slab have been divided into 16 finite element mesh as shown in Fig.7.11. The design moments are calculated at the corners of each element using the Wood and Armer rules and they are given in Table 7.2.

The slab is checked for deflection. The basic span-to-effective depth ratio from table 3.10 in the code [5] is 20. The maximum moment is at the centre of the slab at point 25 and equal to 33.15 $kN\,m/m$.

$$\frac{m}{bd^2} = \frac{33.16\times10^6}{1000\times167^2} = 1.18 \text{ and } f_s = \frac{5\times250}{8} = 156.25.$$

The modification factor for tension steel is $0.55+\frac{477-156.25}{120(0.9+1.18)}=1.83$

Allowable span/d ratio = 20 x 1.83 = 36.7 and actual span/d is 5000/167 = 29.95 mm. The slab is satisfactory with respect to deflections.

The reinforcement ratios are calculated for each element using the optimum moments from table 7.2 and they are given in table 7.3.

The slenderness ratio of the slab $\frac{L_1}{d}$ = 29.95, say 30, and t is calculated using maximum reinforcement ratio in the slab, which is in the bottom at the centre. t = 0.004789 x 250/30 = .03989, say 0.04.

From the design chart, Fig. 7.8-7.9, where t = 0.04 and $\frac{L_1}{d}$ = 30 it can be seen that the percentage increase in the ultimate load above the Wood and Armer collapse load is 60%. Because the slab is square, $\frac{L_1}{L_2}$ = 1 there is no reduction in the ultimate load. Then ultimate Wood and Armer collapse load 1.6 x 12.68 = 20.288 kN/m^2 and the maximum working load is 0.5 x 12.68 = 6.34 kN/m^2

The result of the finite element analysis for the above slab is shown in Fig.7. 12; the maximum working load, which can be carried by the slab, is also shown in the same figure. The working load and the ultimate load calculated using the finite element are in good agreement with the design method.

7.4 CONCLUSION

A design method based on non-linear finite element analysis including the membrane action effect for the design of simply supported rectangular slabs designed using the Wood and Armer [1,2] rules, and elastic moment fields have been provided. Design example to assist the design method has been also provided. Comparison of the design example with non-linear finite element analysis has shown satisfactory results at working load and at ultimate.

7.5 REFERENCES

1. Wood R.H., "The reinforcement of slabs in according with a predetermined field of moments", Concrete, London, Vol. 2, February 1968, pp 69-76.

2. Armer G.S.T., "Discussion on The reinforcement of slabs in accordance with a predetermined field of moments", Concrete, London, Vol. 8, August 1968, pp 319-321.

3. Lodi S.H.,"Reinforced concrete slab elements under bending and twisting moments", PhD. Thesis, Department of Civil and Offshore Engineering, University of Heriot-Watt, December 1997. 228p.

4. Timoshenko S. P. and Krieger W.' "Theory of plates and shells", Second edition, McGraw Hill, Kogakusha, 1959.

5. British Standards Institute, " Code of practice for design of structural use of concrete", BS 8110: Part 1,2:1985.

Table 7.1- Wood and Armer [1,2] design moments

Moment at bottom	Moment at top
$M_x^* = M_x + \lvert M_{xy} \rvert$ and $M_y^* = M_y + \lvert M_{xy} \rvert$	$M_x^* = M_x - \lvert M_{xy} \rvert$ and $M_y^* = M_y - \lvert M_{xy} \rvert$
if $M_x^* < 0$,then $M_x^* = 0$ and $M_y^* = M_y + \left\lvert \frac{M_{xy}^2}{M_x} \right\rvert$	if $M_x^* > 0$,then $M_x^* = 0$ and $M_y^* = M_y - \left\lvert \frac{M_{xy}^2}{M_x} \right\rvert$
if $M_y^* < 0$ then, $M_y^* = 0$ and $M_x^* = M_x + \left\lvert \frac{M_{xy}^2}{M_y} \right\rvert$	if $M_y^* > 0$,then $M_y^* = 0$ $M_x^* = M_x - \left\lvert \frac{M_{xy}^2}{M_x} \right\rvert$

Table 7.2 Design moment at the corners of the different elements for the design example.

No	X	Y	Negative moments		Positive moments	
			M_x^*	M_y^*	M_x^*	M_y^*
1	.0000E+00	.0000E+00	-.2784E+02	-.2784E+02	.2784E+02	.2784E+02
2	.0000E+00	.6250E+00	-.2416E+02	-.2416E+02	.2416E+02	.2416E+02
3	.0000E+00	.1250E+01	-.1713E+02	-.1713E+02	.1713E+02	.1713E+02
4	.0000E+00	.1875E+01	-.8804E+01	-.8804E+01	.8804E+01	.8804E+01
5	.0000E+00	.2500E+01	.0000E+00	.0000E+00	.0000E+00	.0000E+00
6	.6250E+00	.0000E+00	-.2416E+02	-.2416E+02	.2416E+02	.2416E+02
7	.6250E+00	.6250E+00	-.1338E+02	-.1338E+02	.2976E+02	.2976E+02
8	.6250E+00	.1250E+01	-.1968E+01	-.3752E+01	.2912E+02	.2733E+02
9	.6250E+00	.1875E+01	.0000E+00	.0000E+00	.2464E+02	.2143E+02
10	.6250E+00	.2500E+01	.0000E+00	.0000E+00	.1758E+02	.1386E+02
11	.1250E+01	.0000E+00	-.1713E+02	-.1713E+02	.1713E+02	.1713E+02

12	.1250E+01	.6250E+00	-.3752E+01	-.1968E+01	.2733E+02	.2912E+02
13	.1250E+01	.1250E+01	.0000E+00	.0000E+00	.3182E+02	.3182E+02
14	.1250E+01	.1875E+01	.0000E+00	.0000E+00	.3149E+02	.2949E+02
15	.1250E+01	.2500E+01	.0000E+00	.0000E+00	.2720E+02	.2440E+02
16	.1875E+01	.0000E+00	-.8804E+01	-.8804E+01	.8804E+01	.8804E+01
17	.1875E+01	.6250E+00	.0000E+00	.0000E+00	.2143E+02	.2464E+02
18	.1875E+01	.1250E+01	.0000E+00	.0000E+00	.2949E+02	.3149E+02
19	.1875E+01	.1875E+01	.0000E+00	.0000E+00	.3288E+02	.3288E+02
20	.1875E+01	.2500E+01	.0000E+00	.0000E+00	.3181E+02	.3094E+02
21	.2500E+01	.0000E+00	.0000E+00	.0000E+00	.0000E+00	.0000E+00
22	.2500E+01	.6250E+00	.0000E+00	.0000E+00	.1386E+02	.1758E+02
23	.2500E+01	.1250E+01	.0000E+00	.0000E+00	.2440E+02	.2720E+02
24	.2500E+01	.1875E+01	.0000E+00	.0000E+00	.3094E+02	.3181E+02
25	.2500E+01	.2500E+01	.0000E+00	.0000E+00	.3315E+02	.3315E+02

Table 7.3 Reinforcement ratios at the corners of the different elements for the design example.

No	X	Y	Top steel		Bottom steel	
			ρ_x	ρ_y	ρ_x	ρ_y
1	.0000E+00	.0000E+00	.3988E-02	.3988E-02	.3988E-02	.3988E-02
2	.0000E+00	.6250E+00	.3441E-02	.3441E-02	.3441E-02	.3441E-02
3	.0000E+00	.1250E+01	.2414E-02	.2414E-02	.2414E-02	.2414E-02

4	.0000E+00	.1875E+01	.1226E-02	.1226E-02	.1226E-02	.1226E-02
5	.0000E+00	.2500E+01	.0000E+00	.0000E+00	.0000E+00	.0000E+00
6	.6250E+00	.0000E+00	.3441E-02	.3441E-02	.3441E-02	.3441E-02
7	.6250E+00	.6250E+00	.1874E-02	.1874E-02	.4275E-02	.4275E-02
8	.6250E+00	.1250E+01	.2714E-03	.5186E-03	.4179E-02	.3912E-02
9	.6250E+00	.1875E+01	.0000E+00	.0000E+00	.3512E-02	.3040E-02
10	.6250E+00	.2500E+01	.0000E+00	.0000E+00	.2479E-02	.1943E-02
11	.1250E+01	.0000E+00	.2414E-02	.2414E-02	.2414E-02	.2414E-02
12	.1250E+01	.6250E+00	.5186E-03	.2714E-03	.3912E-02	.4179E-02
13	.1250E+01	.1250E+01	.0000E+00	.0000E+00	.4587E-02	.4587E-02
14	.1250E+01	.1875E+01	.0000E+00	.0000E+00	.4537E-02	.4234E-02
15	.1250E+01	.2500E+01	.0000E+00	.0000E+00	.3893E-02	.3476E-02
16	.1875E+01	.0000E+00	.1226E-02	.1226E-02	.1226E-02	.1226E-02
17	.1875E+01	.6250E+00	.0000E+00	.0000E+00	.3040E-02	.3512E-02
18	.1875E+01	.1250E+01	.0000E+00	.0000E+00	.4234E-02	.4537E-02
19	.1875E+01	.1875E+01	.0000E+00	.0000E+00	.4747E-02	.4747E-02
20	.1875E+01	.2500E+01	.0000E+00	.0000E+00	.4585E-02	.4453E-02
21	.2500E+01	.0000E+00	.0000E+00	.0000E+00	.0000E+00	.0000E+00
22	.2500E+01	.6250E+00	.0000E+00	.0000E+00	.1943E-02	.2479E-02
23	.2500E+01	.1250E+01	.0000E+00	.0000E+00	.3476E-02	.3893E-02
24	.2500E+01	.1875E+01	.0000E+00	.0000E+00	.4453E-02	.4585E-02
25	.2500E+01	.2500E+01	.0000E+00	.0000E+00	.4789E-02	.4789E-02

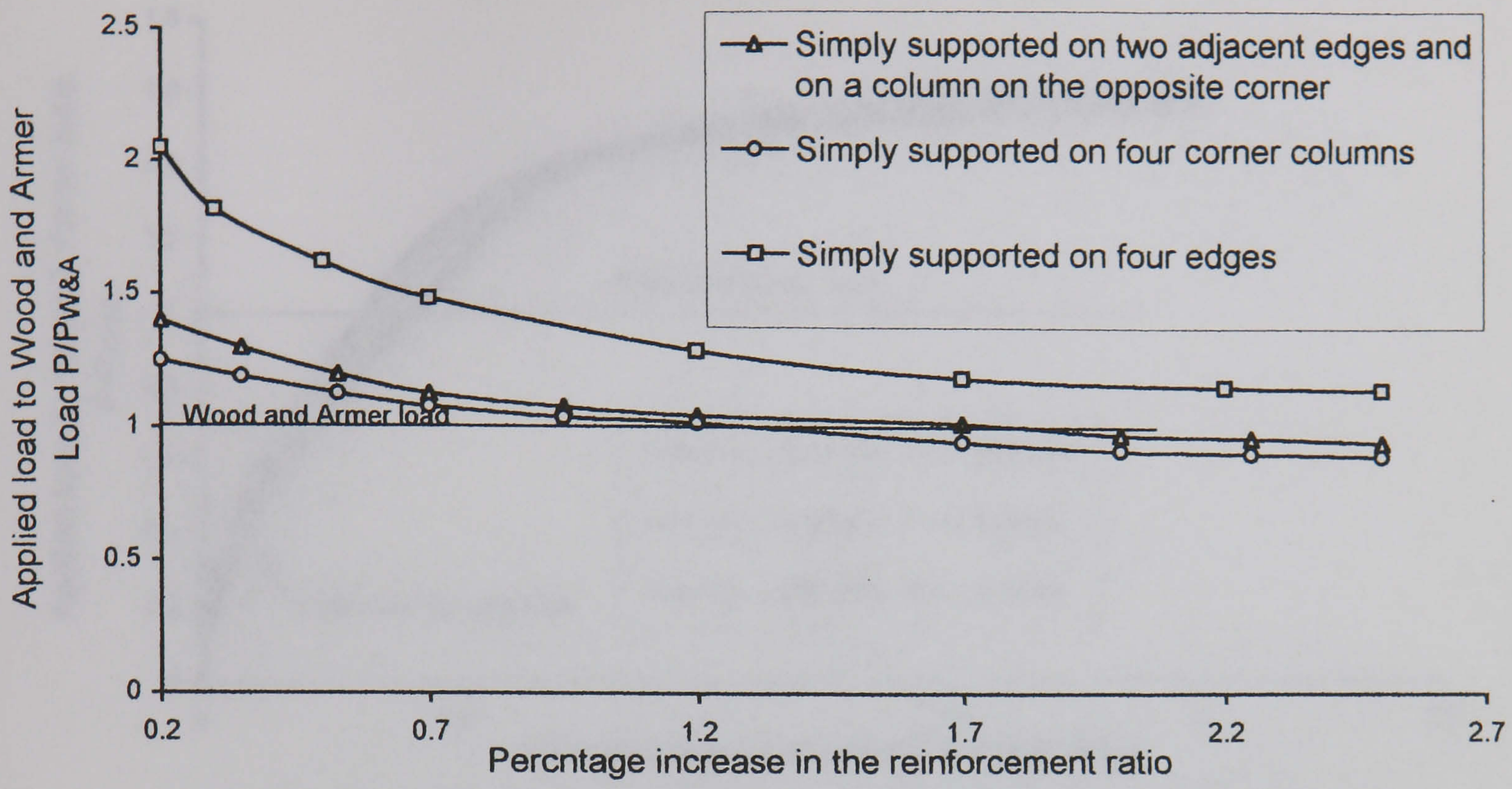

Fig.7.1-Load-deflection curves for slab supported on different simply supports

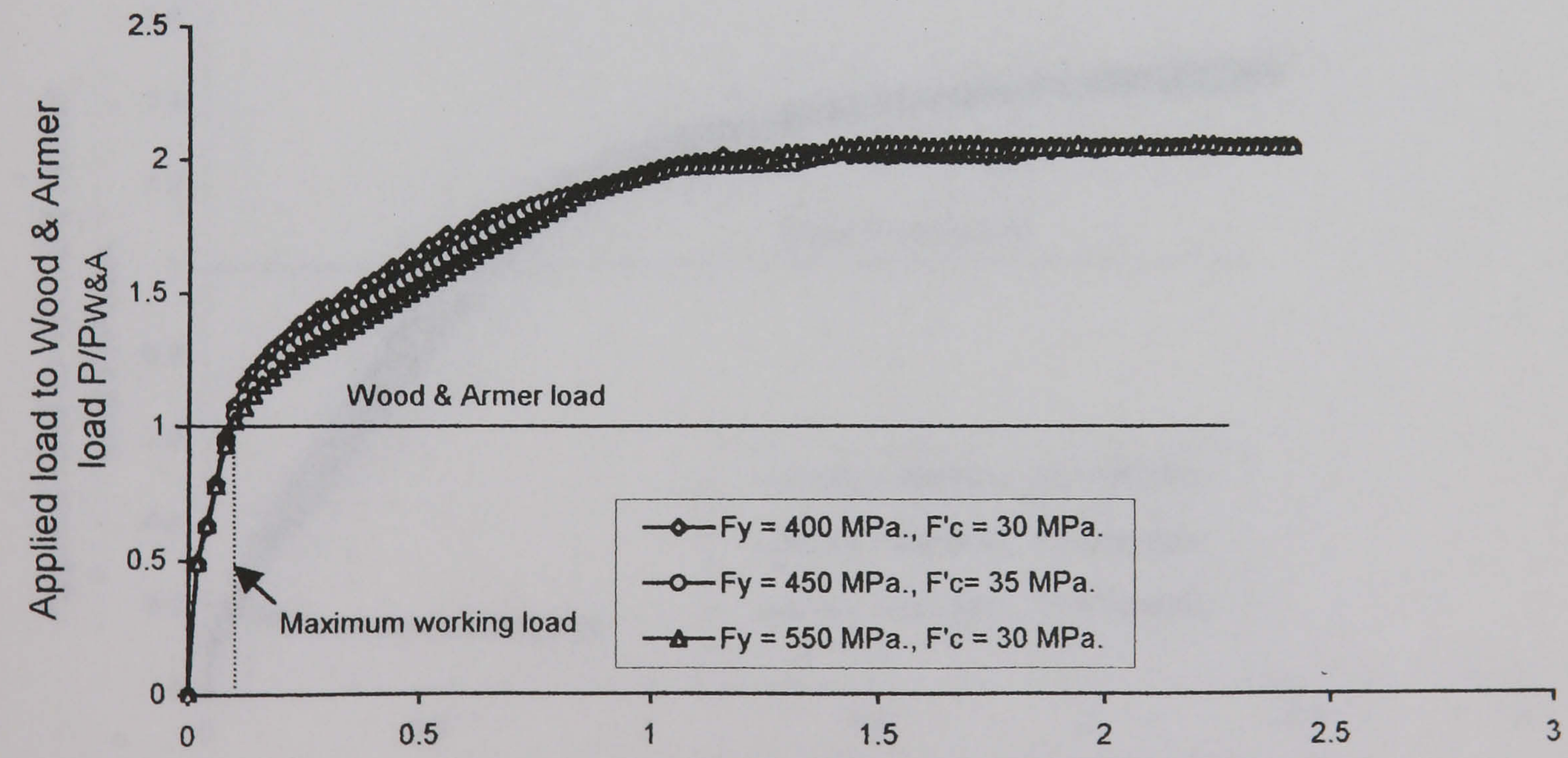

Fig.7.2-Load-deflection curves for simply supported slab with L/d = 40 and t= 0.02666

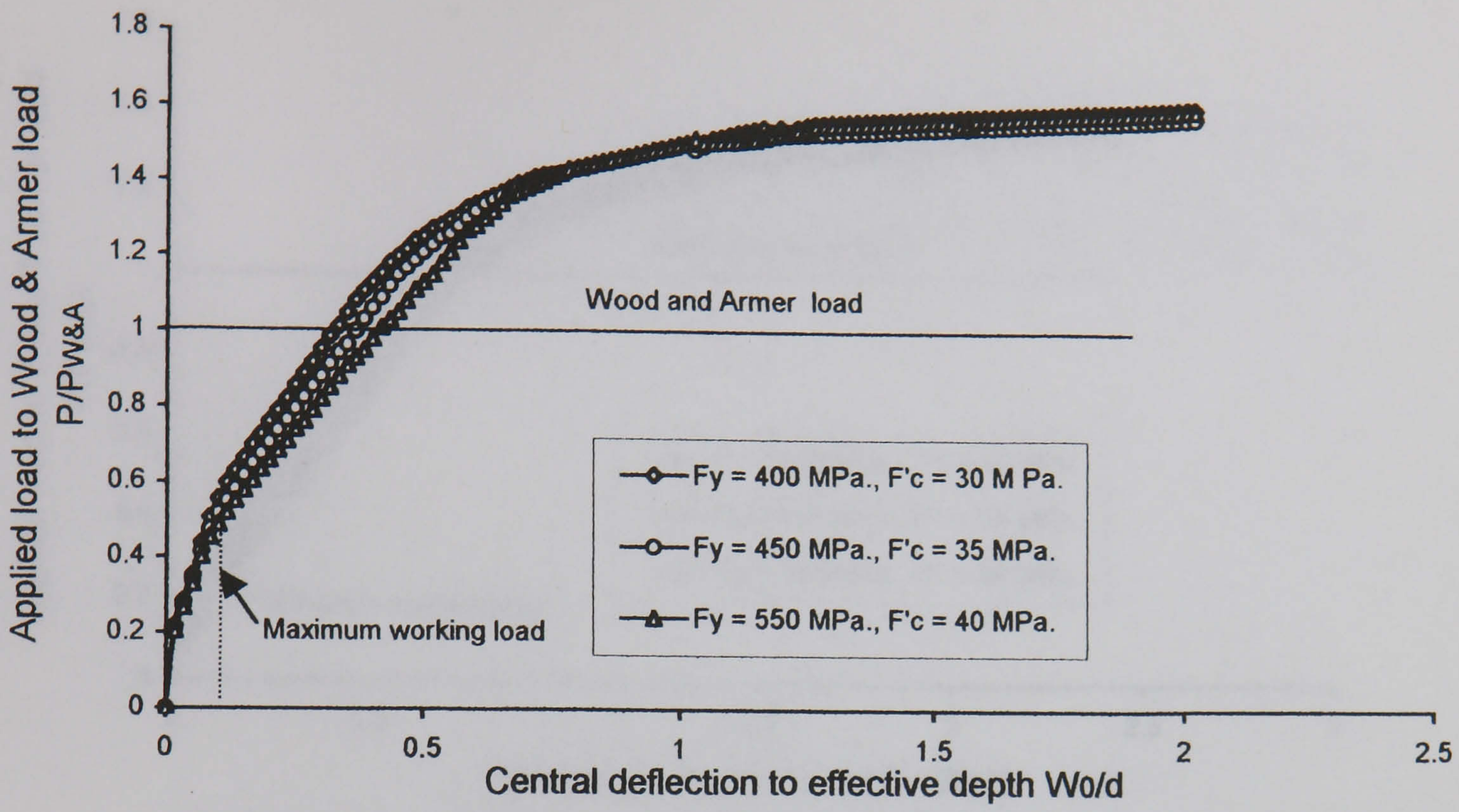

Fig.7.3-Load-deflection curve for simply supported slab with L/d= 40 and t= 0.066

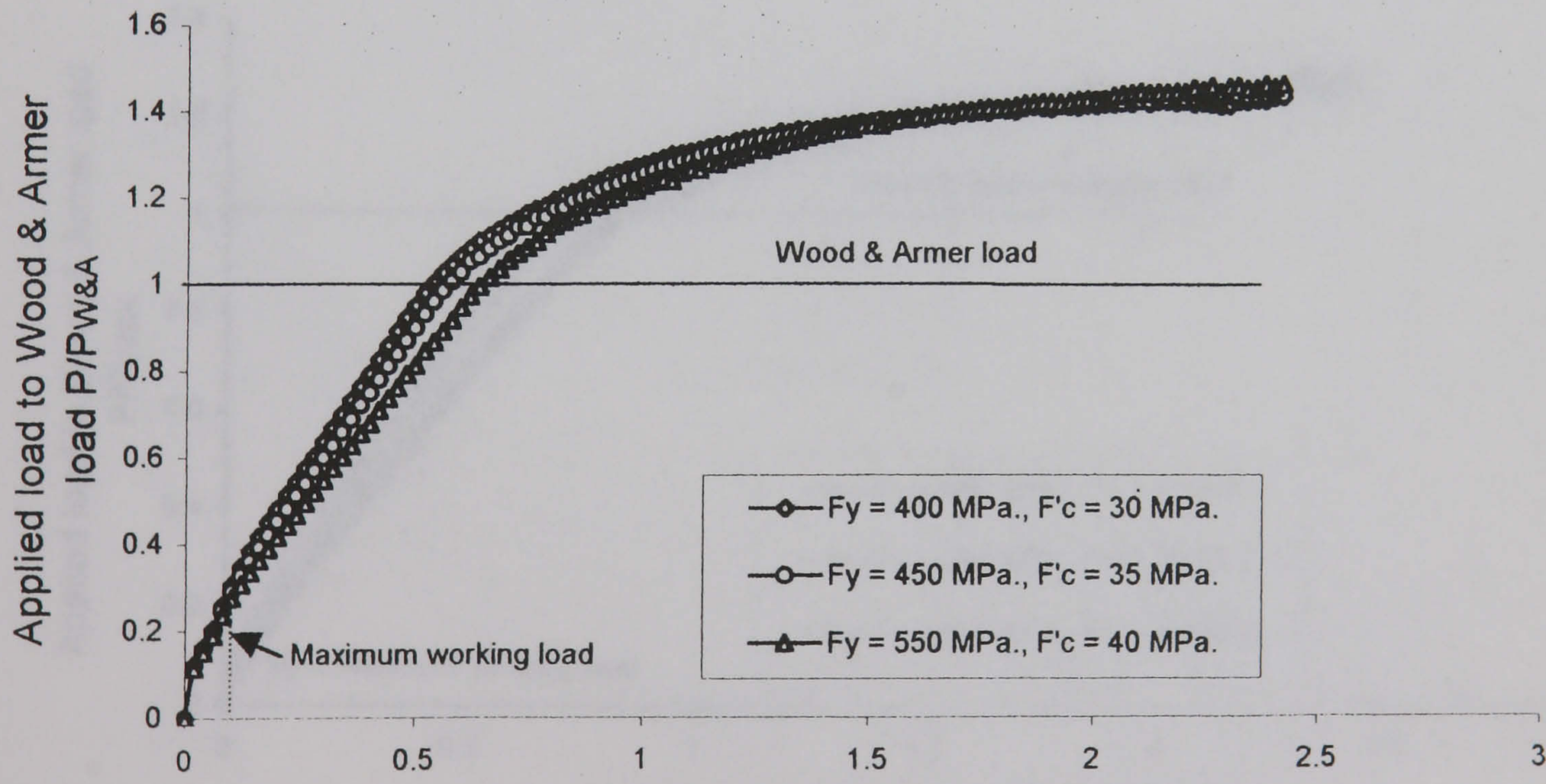

Fig.7.4-Load-deflection curves for simply supported slab L/d=40 and t=0.1333

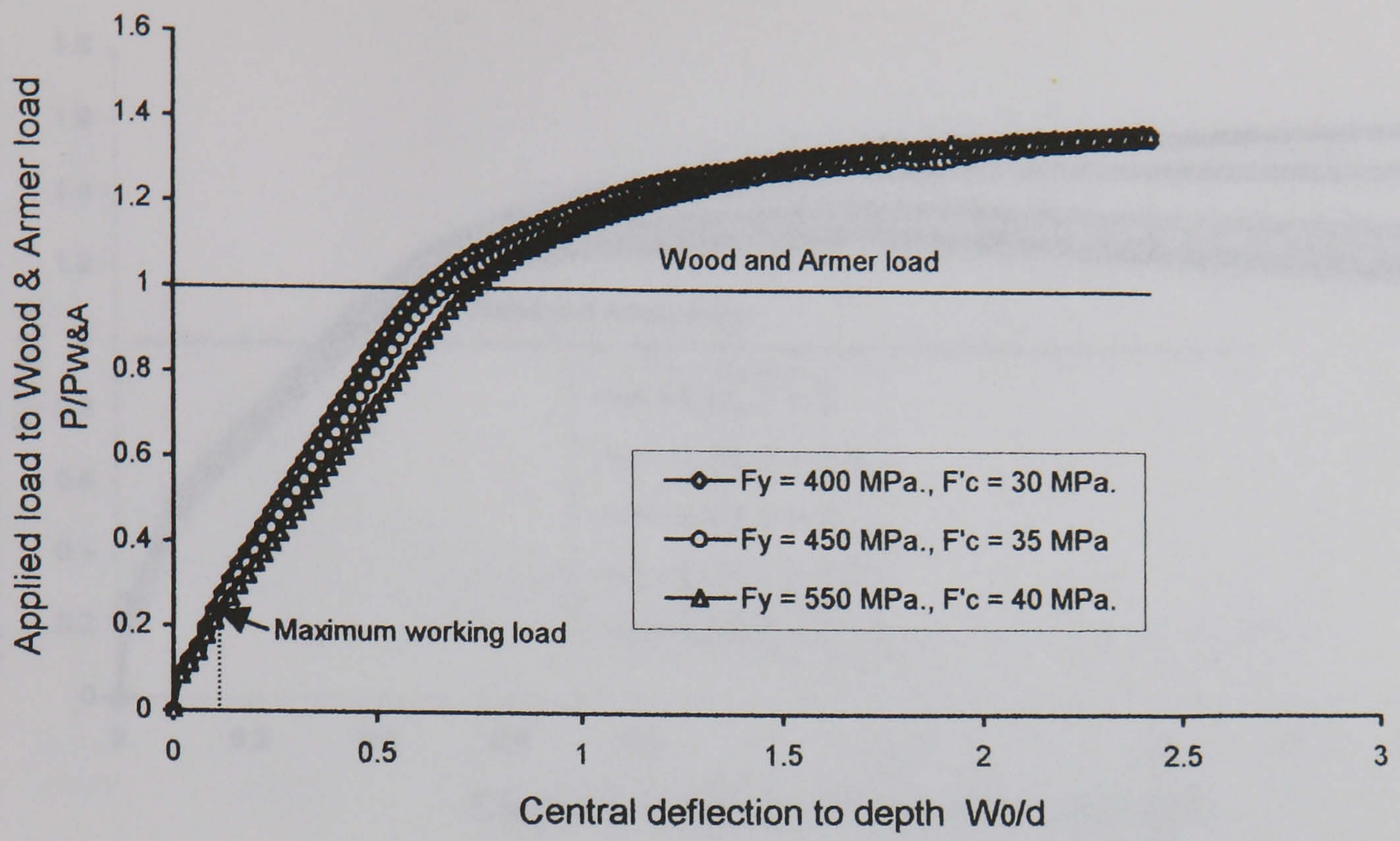

Fig.7.5-Load-deflection curves for simply supported slab with L/d=40 and t=0.2

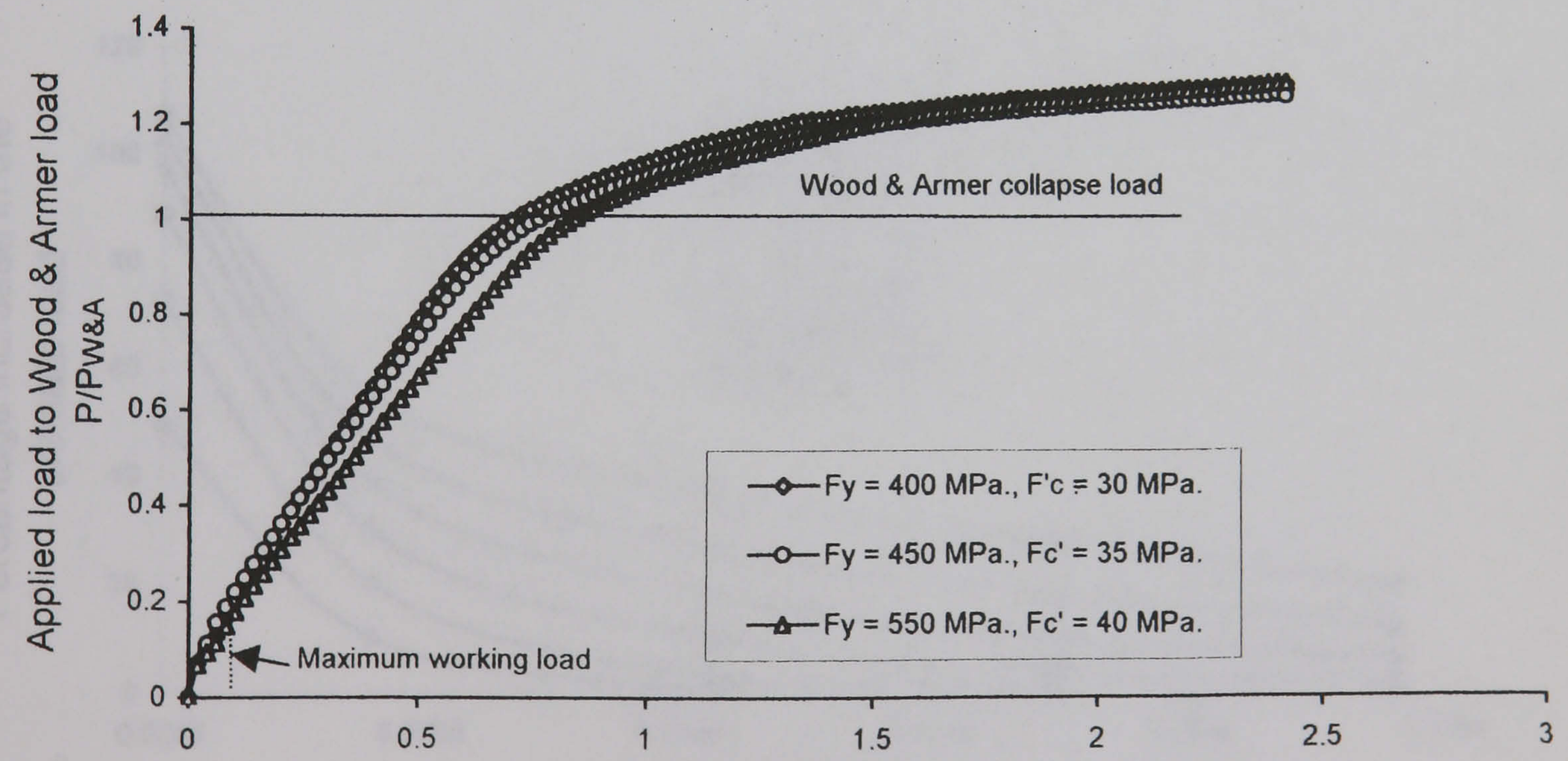

Fig.7.6-Load-deflection curves for simply supported slab with L/d=40and t=0.2666

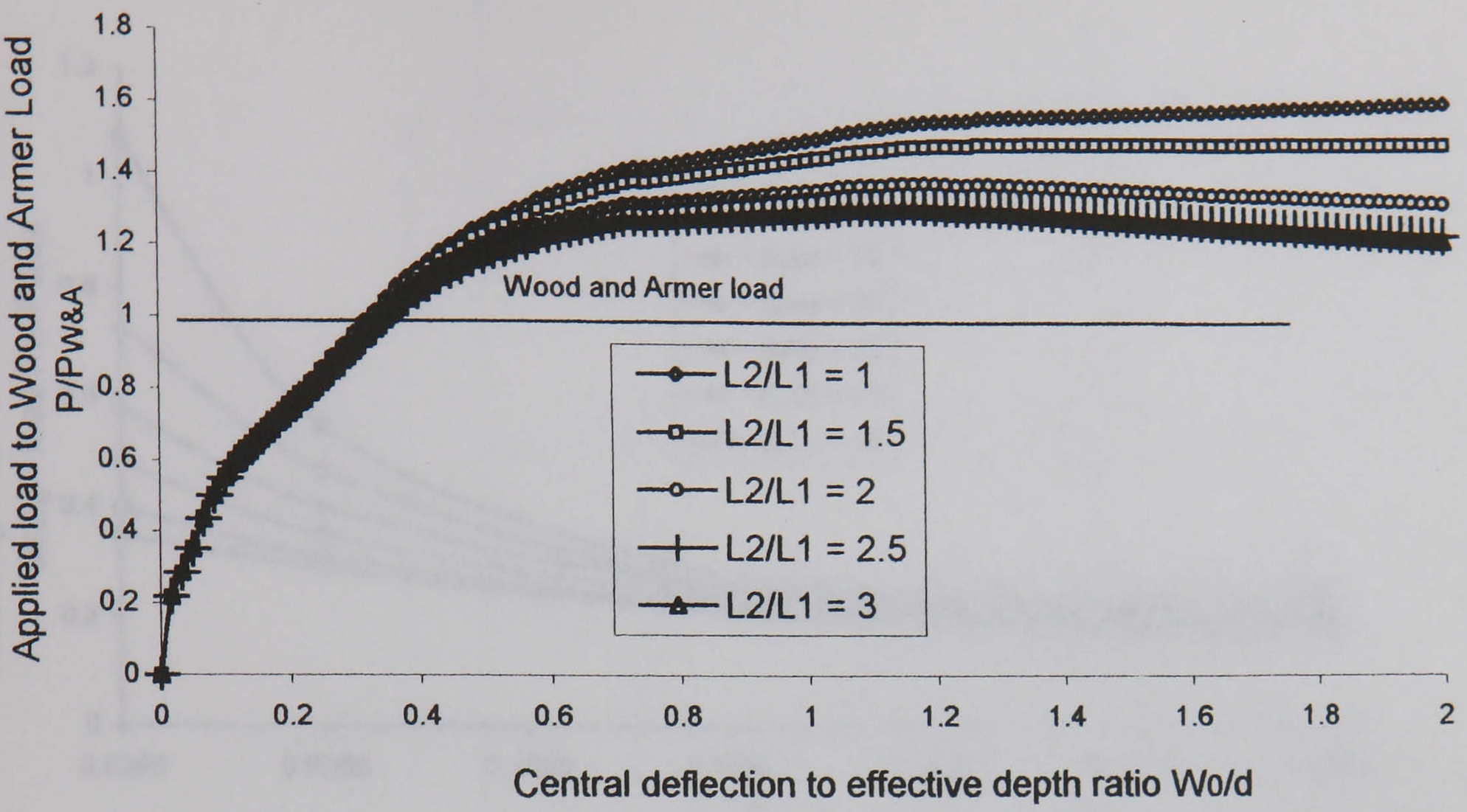

Fig.7.7-Load-deflection curves for slabs with different aspect ratios

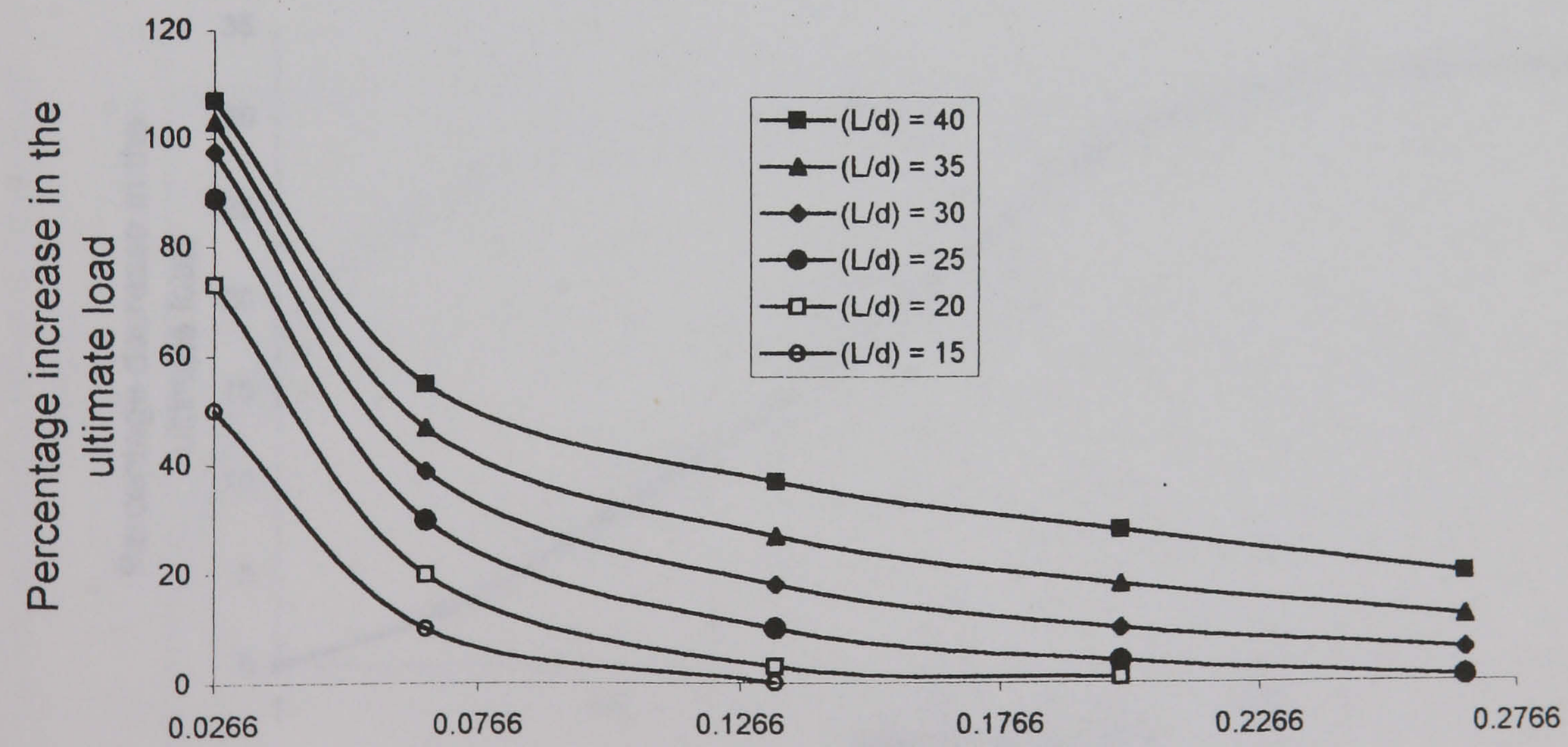

Fig.7.8-Variation of the percentage increase in the ultimate load above Wood & Armer load for simply supported square slabs with variation of the parameter t

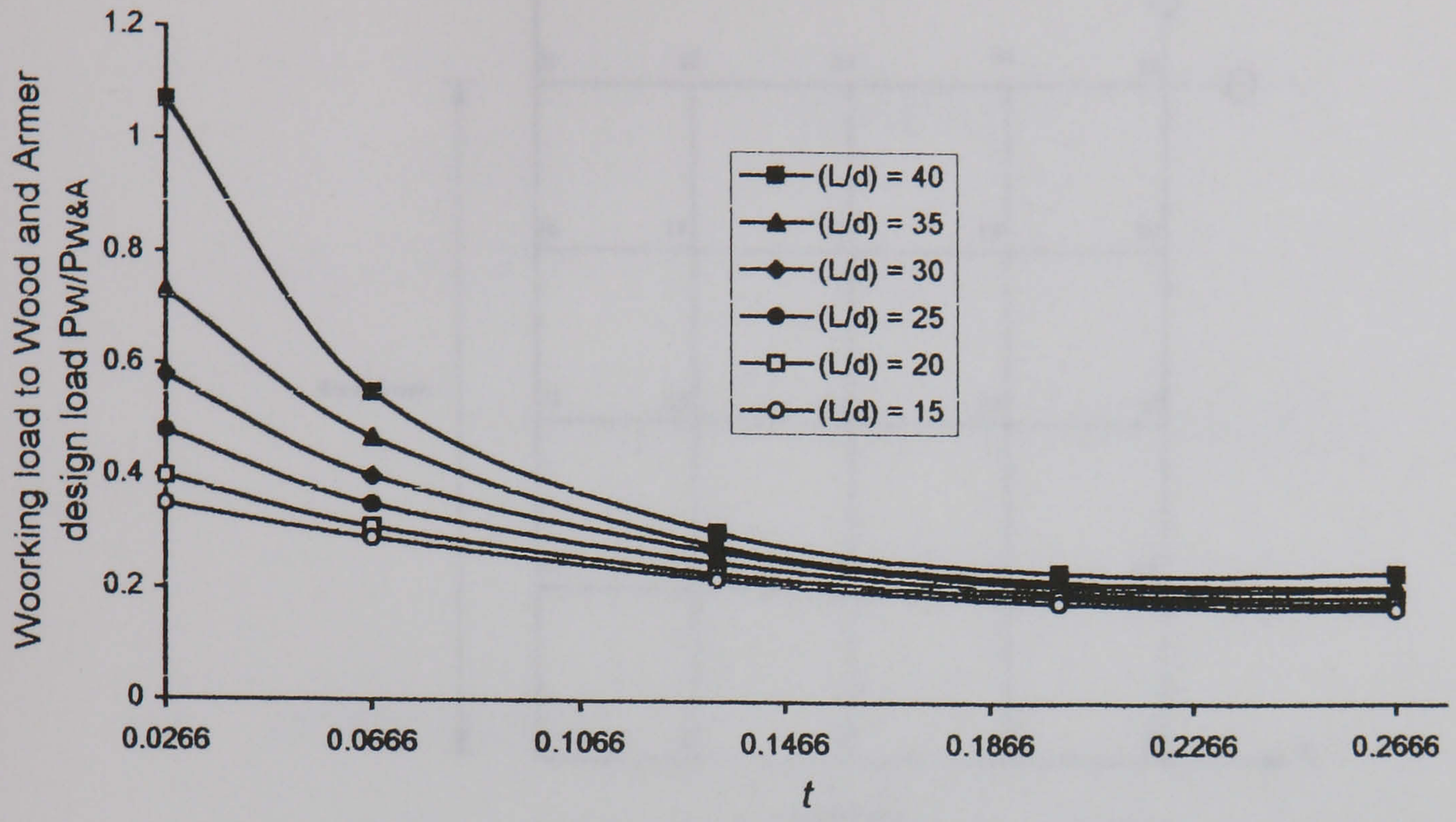

Fig.7.9-Ratio of working load to Wood and Armer design load for simply supported square slab with different t parameters

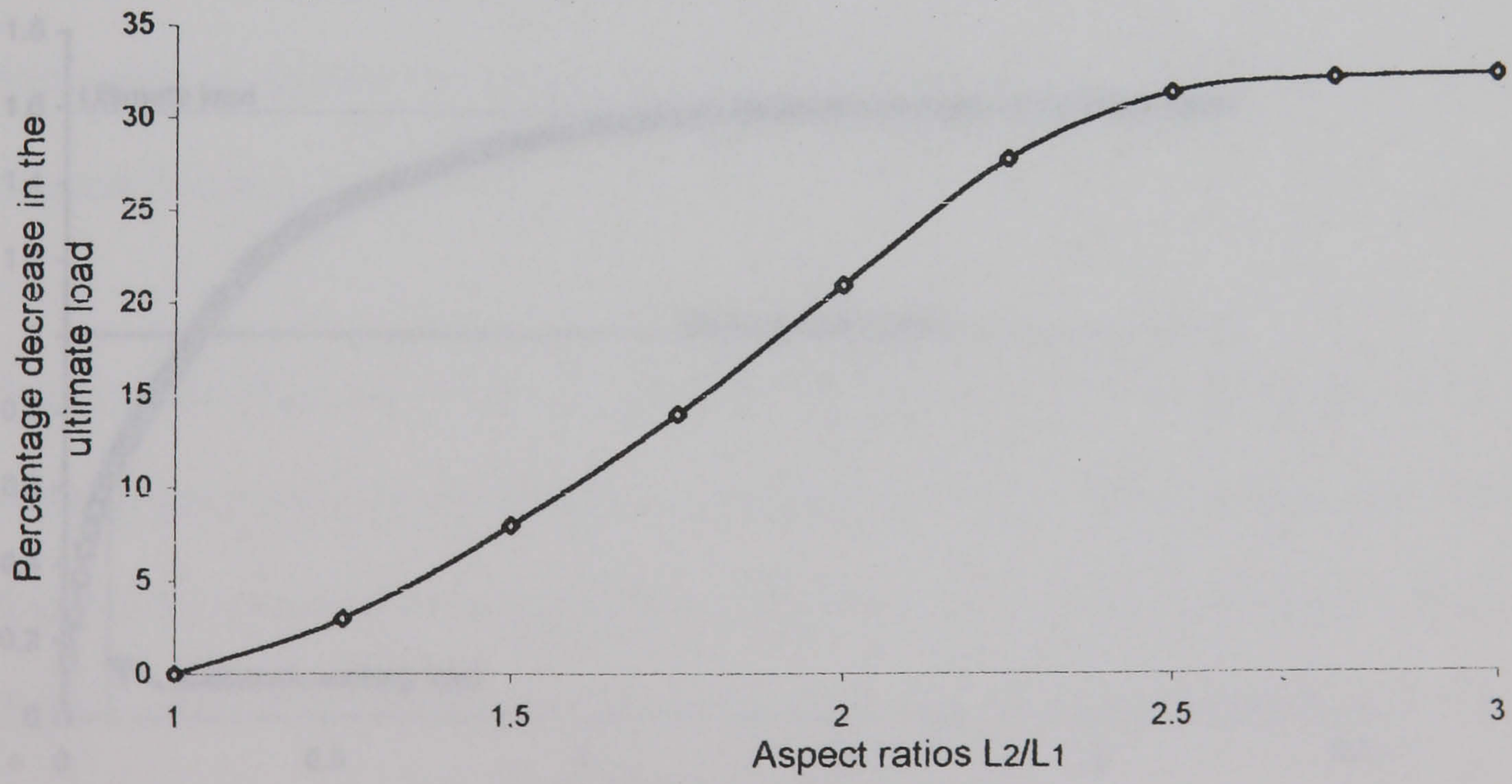

Fig.7.10-Decrease of the ultimate strength with increasing of aspect ratios for rectangular slabs designed using Wood and Armer rules

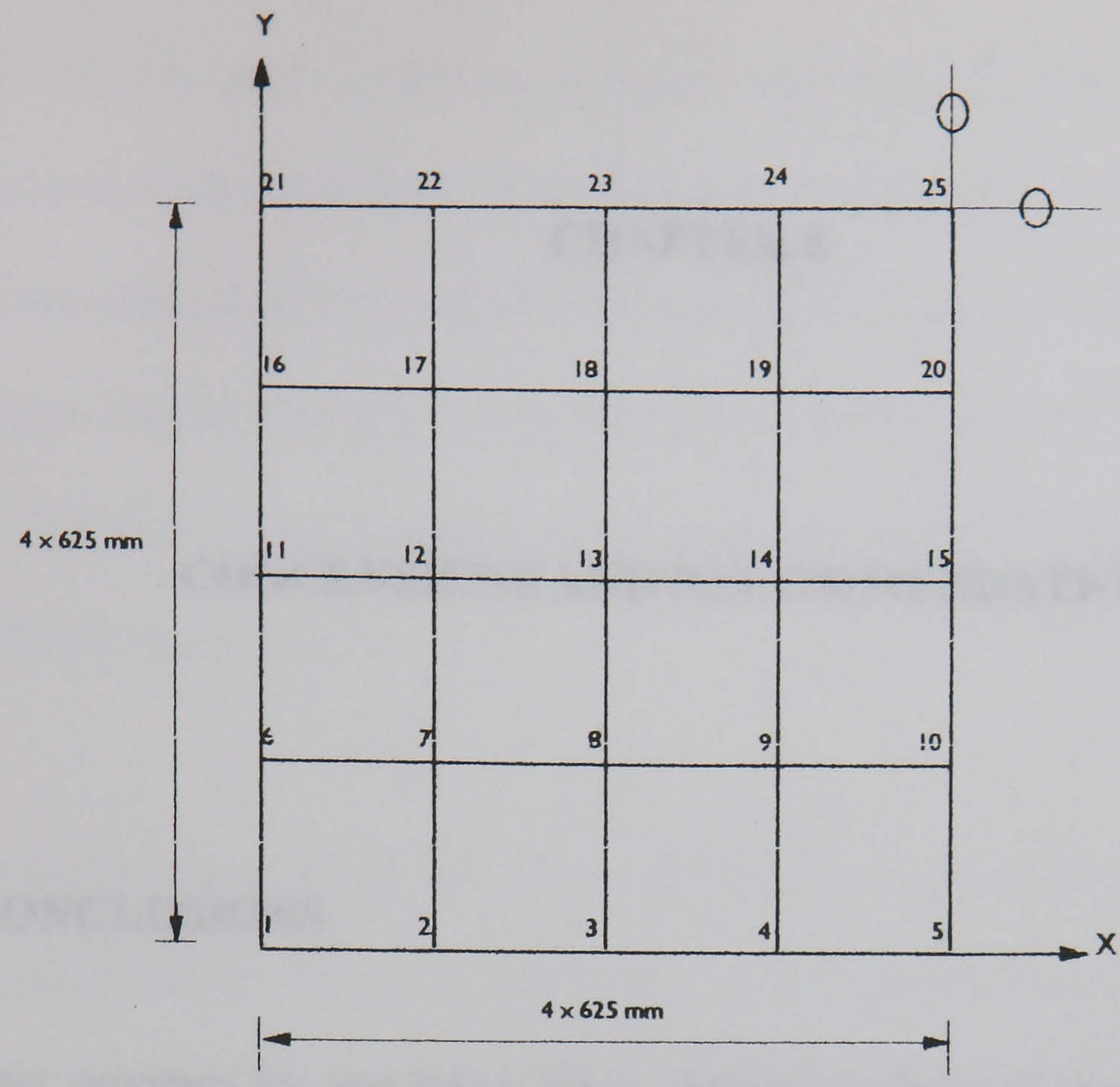

Fig. 7.11- The finite element mesh for the slab

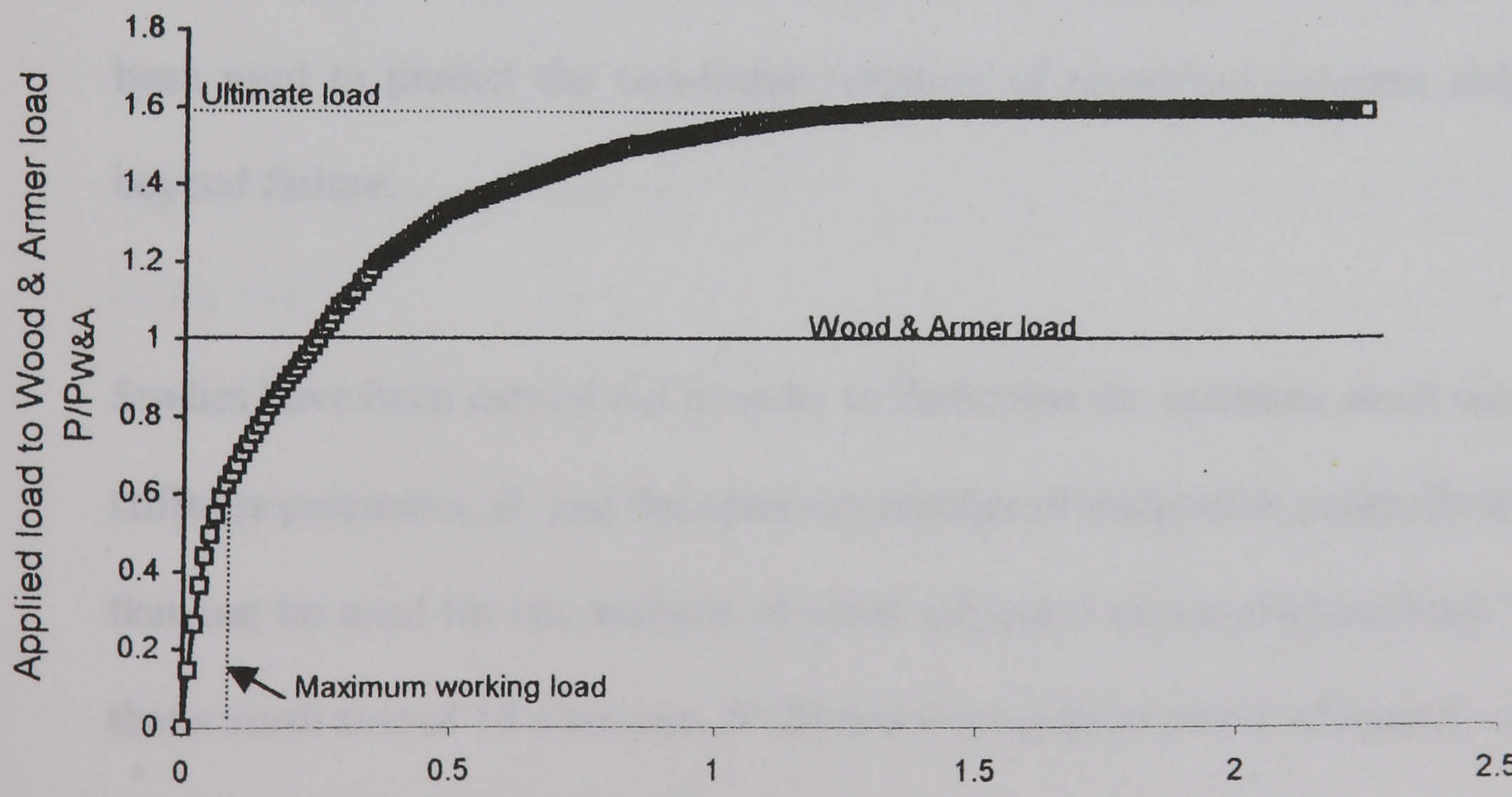

Fig.7.12-Load-deflection curves for simply supported slab designed using the Wood& Armer rules

CHAPTER 8

CONCLUSIONS AND RECOMMENDATIONS

8.1 CONCLUSIONS

A computer program for non-linear finite element analysis of reinforced concrete slabs has been modified in order to use a non-linear stress-strain model for the concrete based on the theory of elasticity. The material model for concrete includes phenomena such as tension stiffening, compression softening and cracking. The computer program has been used to predict the non-linear response of reinforced concrete slabs up to and beyond failure.

Studies have been carried out in order to determine the optimum mesh size, the tension stiffness parameter, B, and the optimum number of integration points through the depth that can be used for the analysis of slabs subjected to out-of-plane load. It was found that a mesh size of 16 elements, B=20 and 9 integration points adequately represents the responses of the slabs analysed.

The program has been validated against several experimental studies. The experimental studies chosen to validate the program had a variety of loading. Nine studies tested

reinforced concrete slabs under out-of-plane uniformly distributed and concentrated loads. One study tested reinforced concrete slabs under combined uniformly distributed in-plane loads and out-of-plane loads, one study tested reinforced concrete slabs under in-plane shear loading and one study test was carried out under bending and twisting moments. The experimental results were compared with the analytical results and a good agreement was obtained.

The program has been used to investigate membrane action in reinforced concrete slabs simply supported along all edges. The tensile membrane action was found to develop in the plane of the slab at the onset of cracking, at loads lower than the yield line theory load. The distribution of the membrane action in the plane of the slab was found to be a circular zone of circumferential and radial tensile membrane forces at the centre equilibrated by a zone of circumferential compressive membrane forces in the outer region. The radius of the spread of the tensile membrane forces and the intensity of the tensile and compressive membrane forces was found to increase with increasing central deflections.

A comparison of the results from the program with the results from the available plastic methods, which include the effect of tensile membrane action, has also been carried out using Kemp's method for a square slab and Wood's method for a circular slab. The load-deflection curves predicted using the plastic methods was found to be different from the load-deflection curves predicted using the proposed computer program at loads lower than the yield line theory load. This is the result from the assumption of rigid plastic behaviour for the theoretical methods, where the deflections are neglected prior

to the yield line theory load. Also the loads predicted using the plastic methods are found to increase with increasing deflections without limitation. In reality the yielding of the reinforcement and the crushing of the concrete will put a limit for this increase in the load with increasing deflections, which is obvious in the case of the load-deflection curves predicted using the finite element method. However, acceptable agreement was obtained for the square slab at post yield line theory load for the low value of t =0.02, where $t=\rho\frac{f_y}{f_c'}$. When t = 0.1 the load-deflection curves are in agreement between relative deflections of 0.5 to 1.75. Kemp's theory for the square slab considers the presence of the membrane forces in one direction only and the result of the comparison between the theory and the computer program in x-direction for the membrane forces was acceptable. However, the result of the comparison for the moments was good in the zone of the tensile membrane forces only. Acceptable agreements were obtained between the finite element results and Wood's theory for the circular slab for the radial and the circumferential membrane forces and moments at relative central deflection to effective depth greater than 0.25.

The program has been used to study the effect of tensile membrane action on the load-carrying capacity of slabs on different simple support conditions, with reinforcement designed using yield line theory and the Wood and Armer rules and subjected to uniformly distributed load. The study shows that the slabs designed using yield line theory and the Wood and Armer rules sustained loads much higher than those predicted using the design methods because of the development of tensile membrane action. The

percentage increase in the load-carrying capacity caused by membrane action was found to be dependent on the slenderness of the slab, aspect ratio of the slab, type of simple supports and the parameter t. A comparison of the percentage increase in the ultimate load above the design load is carried out for slabs on different simple supports, with slenderness ratios of 40 and 25, aspect ratio varied between 1 to 3 and t varied between 0.02 to 0.25. The percentage increase in the ultimate load is found to be more significant for square slender slabs with low value of t, simply supported on four edges and with reinforcement designed using yield line theory. The increase in the ultimate load above the design load for the square slab with slenderness ratio of 40 and with reinforcements designed using yield line theory was found to be between 120% when t = 0.02 and 23% when t = 0.25. This increase in the ultimate load above the design load was reduced by 17% when the Wood and Armer rules were used for the design of the reinforcement. The increase in the ultimate load above the design load is also found to be reduced with decreasing of the slenderness of the slab and with increasing of the aspect ratios. For the above slab the ultimate load was reduced by 38% when the slenderness ratio was 25 and by 33% when the aspect ratio was 3. For square slabs simply supported on four corner columns with slenderness ratio of 40 and with reinforcement designed using yield line theory and Wood and Armer rules, the percentage increase in the ultimate load above design load was found to be 40% and 25% respectively when t = 0.02. Yield line theory and the Wood and Armer rules overestimate the load carrying capacity for the slabs for value of t greater than 0.21 and 0.146 respectively. For square slabs simply supported on two adjacent edges and on a column on the opposite corner with slenderness ratio of 40 and with reinforcement designed using yield line theory and Wood and Armer rules, the percentage increase in

percentage increase in the ultimate load above the design load was found to be 53% and 40% respectively when t = 0.02. Yield line theory and the Wood and Armer rules overestimate the load carrying capacity for the above slabs for a value of t greater than 0.23 and 0.186 respectively. Therefor; there is no doubt about the safety of the design methods because of the development of the membrane action.

Attempts have been made to develop simple design charts and guide-lines by including the tensile membrane action effect for the design of rectangular slabs with reinforcement designed using Wood and Armer rules and simply supported along all edges based on finite element analysis. The design method has been tested using a practical design example and the results of the design method agree with the results of the finite element program. The developed design method could lead to economies in the amount of reinforcement required in some slabs by including the membrane action.

8.2 RECOMMENDATIONS FOR FUTURE RESEARCH

The program could be used to investigate the effects of the presence of the central opening and the central column on the development and distribution of the membrane action in reinforced concrete slabs on simple supports.

The design method developed for rectangular reinforced concrete slabs simply supported along all edges by including tensile membrane action could be extended to cover the circular and skew slabs using the program.

The program could also be used to obtain useful information, which might help in the development of more economic design methods for reinforced concrete restrained slabs by including the effect of the compressive and tensile membrane action.

APPENDIX A

1. USER MANUAL FOR THE FINITE ELEMENT PROGRAM.

1.1 List of all variables, together with their usage is given below.

Card set number.	Indicator.	Description of the indicator.
1.	HEDIN	= title of the problem to be analysed.
2.	ISPEC	= indicator for degree of freedom of the specified displacements after applying the boundary conditions.
	ICONTL	= indicator for load control parameter; 1= load incrementation. 2= displacement incrementation.
	INONLR	= kind of analysis indicator used to specify the analysis; 0= elastic analysis. 1= geometric non-linear analysis. 2= material non-linear analysis. 3= combined geometric and material non-linear analysis.
	INO	= indicator for line search; 0= without line search. 1= with line search.
	IUPDTK	= number of iteration after which the stiffness matrix is updated.
	IMAX	= maximum number of increments.
3.	DUSPEC	= indicator for incremental specified displacement.
	DFACTOR	= indicator for the increase of the incremental specified displacement.
	ALFAD	= displacement convergence tolerance.
	ALFAE	= energy convergence tolerance.
	EPCU	= crushing strain of the concrete.
	EPSC	= peck strain of the concrete.
	ICCN	= indicator for the concrete failure; 1= brittle failure. 2= ductile failure.
	ISTE	= indicator for the strain hardening of the steel model; 1= no strain hardening. 2= with strain hardening.

4.	ESTLL	= models of elasticity of the steel.
	FC	= compressive strength of the concrete.
	FT	= tensile strength of the concrete.
	FY	= yield strength of the reinforcement.
	BETA	= indicator for the tension stiffening parameter. 0= no tension stiffness.
	RFC	= indicator for the discontinuity in the concrete tensile strength after cracking. 1= no discontinuity.
	COFF	= indicator for the compression softening multiplier. 1.2= in case of torsion analysis. 1= in any other case.
	ALFAD1	= displacement convergence tolerance when the iteration exceeded 200.
	ALFAE1	= energy convergence tolerance when the iteration exceeded 200.
5.	ZSTLL	= co-ordinate of top and bottom steel.
6.	TOTNOD	= total number of nodes.
	DIMENSION	= dimensionality of the problem.
7.	NODNUM	= node number.
	DIMEN	= dimension.
8.	ELTYP	= element type.
	TOTELS	=total number of the elements of the type element.
	NODEL	= number of nodes at the element.
	NSTLR	= number of steel layers.
9.	ELNUM	= number of the element.
	STHC	= thickness of the steel layer.
10	E	= models of elasticity of the concrete.
	NU	= Poisson's ratio.
	Z1	= co-ordinate of the bottom of the slab.
	Z2	= co-ordinate of the top of the slab.
11.	DOFNOD	= number of degree of freedom per node.
12.	RESNO	= number of restrained nodes.
13.	RESTR(J)	= condition of restrain on n node.
14.	IPLOD	= indicator for point load.
	IGRAV	= indicator for uniformly distributed load.
	IEDGEX	= indicator for x-edge load.

IEDGEY = indicator for y-edge load.

15. LODNOD = total number of loaded nodes.

16. NODNUM = number of loaded nodes.

17. NULOD = number of loads.

18. UDL(I) = indicator for the load type.

1.2 Data file preparation.

McNeice's slab under central point load is chosen as an example to show the preparation of the data file. The mesh of quarter of the slab is shown in Fig.-A1. The data file is as follows.

```
1  HEDIN
   McNeice's corner supported slab (3x3 finite elements mesh for quarter of the slab),
   the result is shown in Fig. 5.1.
2  ISPEC, ICONTL, INONLR, INO, IUPDTK,IMAX
    1 2 2 1 50 50
3  DUSPEC,DFACTOR,ALFAD,ALFAE,EPCU,EPSC,ICCN,ISTE
    .25 1 0.0009 .0009 -.0035 -.0025 2 2
4  ESTLL, FC, FT,FY,BETA,RFC,COFF,ALFAD1,ALFAE1
    200000 -32.4 3.2 345 30 1 1.2 0.0009 .0009
5  ZSTL(1), ZSTL(2), ZSTL(3), ZSTL(4)
    -11.05 -11.05 11.05 11.05
6  TOTNOD,DIMENSION
    49 2
7  NODNUM,(WORK(J),J=1,DIMEN)
    1 0 0
    2 38.1 0
    3 76.2 0
    4 152.4 0
    5 228.6 0
    6 342.9 0
    7 457.2 0
    8 0 38.1
    9 38.1 38.1
    10 76.2 38.1
    11 152.4 38.1
    12 228.6 38.1
    13 342.9 38.1
    14 457.2 38.1
    15 0 76.2
    16 38.1 76.2
```

17 76.2 76.2
18 152.4 76.2
19 228.6 76.2
20 342.9 76.2
21 457.2 76.2
22 0 152.4
23 38.1 152.4
24 76.2 152.4
25 152.4 152.4
26 228.6 152.4
27 342.9 152.4
28 457.2 152.4
29 0 228.6
30 38.1 228.6
31 76.2 228.6
32 152.4 228.6
3 228.6 228.6
34 342.9 228.6
35 457.2 228.6
36 0 342.9
37 38.1 342.9
38 76.2 342.9
39 152.4 342.9
40 228.6 342.9
41 342.9 342.9
42 457.2 342.9
43 0 457.2
44 38.1 457.2
45 76.2 457.2
46 152.4 457.2
47 228.6 457.2
48 342.9 457.2
49 457.2 457.2

8 ELTYP,TOTELS,NODEL,NSTLR
1 9 9 4

9 ELNUM,(NWORK(J),J=1,NODEL),(STHC(I,J),J=1,NSTLR)
1 1 8 15 16 17 10 3 2 9
0 0 .38 .38
2 3 10 17 18 19 12 5 4 11
0 0 .38 .38
3 5 12 19 20 21 14 7 6 13
0 0 .38 .38
4 15 22 29 30 31 24 17 16 23
0 0 .38 .38
5 17 24 31 32 33 26 19 18 25
0 0 .38 .38
6 19 26 33 34 35 28 21 20 27
0 0 .38 .38

```
    7 29 36 43 44 45 38 31 30 37
    0 0 .38 .38
    8 31 38 45 46 47 40 33 32 39
    0 0 .38 .38
    9 33 40 47 48 49 42 35 34 41
    0 0 .38 .38
10  E,NU,Z1,Z2
    29000 .15 -22.25 22.25
11  DOFNOD
    5
12  RESNOD
    23
13  (RESTR(I,J),J=1,K)
    1 1 2 0 4 5
    2 0 2 0 0 5
    3 0 2 0 0 5
    4 0 2 0 0 5
    5 0 2 0 0 5
    6 0 2 0 0 5
    7 0 2 0 0 5
    8 1 0 0 4 0
    15 1 0 0 4 0
    22 1 0 0 4 0
    29 1 0 0 4 0
    36 1 0 0 4 0
    43 1 0 0 4 0
    49 1 2 3 0 0
    9 1 2 3 0 0
    11 1 2 3 0 0
    13 1 2 3 0 0
    23 1 2 3 0 0
    25 1 2 3 0 0
    27 1 2 3 0 0
    37 1 2 3 0 0
    39 1 2 3 0 0
    41 1 2 3 0 0
14  IPLOD,IGRAV,IEDGEX,IEDGEY
    1 0 0 0
15  LODNOD
    0 0 1
16  NODNUM
    1
17  NULOD
    1 0 0 .25 0 0
18  UDL(I)
    1
    1
```

1.3 Data files for some of the analysed slabs.

1.3.1 Taylor's slab under uniformly distributed load.

Taylor simply supported slab no. 8 (4x4finite elements mesh for quarter of the slab), the result is shown in Fig. 5.15.

```
167 2 2 1 80 80
1 1 0.1 0.1 -.0035 -0.0025 2 2
206910 -38.5 2 375.9 20 .1 1 0.1 0.1
-13.5 -18.3 13.5 18.3
49 2
1 0 0
2 152.5 0
3 305 0
4 457.5 0
5 610 0
6 762.5 0
7 915 0
8 0 152.5
9 152.5 152.5
10 305 152.5
11 457.5 152.5
12 610 152.5
13 762.5 152.5
14 915 152.5
15 0 305
16 152.5 305
17 305 305
18 457.5 305
19 610 305
20 762.5 305
21 915 305
22 0 457.5
23 152.5 457.5
24 305 457.5
25 457.5 457.5
26 610 457.5
27 762.5 457.5
28 915 457.5
29 0 610
30 152.5 610
31 305 610
32 457.5 610
33 610 610
34 762.5 610
35 915 610
36 0 762.5
37 152.5 762.5
```

38 305 762.5
39 457.5 762.5
40 610 762.5
41 762.5 762.5
42 915 762.5
43 0 915
44 152.5 915
45 305 915
46 457.5 915
47 610 915
48 762.5 915
49 915 915
1 9 9 4
1 1 8 15 16 17 10 3 2 9
0 0 .298 .298
2 3 10 17 18 19 12 5 4 11
0 0 .298 .298
3 5 12 19 20 21 14 7 6 13
0 0 .298 .298
4 15 22 29 30 31 24 17 16 23
0 0 .298 .298
5 17 24 31 32 33 26 19 18 25
0 0 .298 .298
6 19 26 33 34 35 28 21 20 27
0 0 .298 .298
7 29 36 43 44 45 38 31 30 37
0 0 .298 .298
8 31 38 45 46 47 40 33 32 39
0 0 .298 .298
9 33 40 47 48 49 42 35 34 41
0 0 .298 .298
32420 0.18 -22.25 22.25
5
33
1 1 2 3 0 0
2 0 0 3 4 0
3 0 0 3 4 0
4 0 0 3 4 0
5 0 0 3 4 0
6 0 0 3 4 0
7 0 0 3 4 0
8 0 0 3 0 5
15 0 0 3 0 5
22 0 0 3 0 5
29 0 0 3 0 5
36 0 0 3 0 5
43 0 0 3 0 5
9 1 2 3 0 0

11 1 2 3 0 0
13 1 2 3 0 0
23 1 2 3 0 0
25 1 2 3 0 0
27 1 2 3 0 0
37 1 2 3 0 0
39 1 2 3 0 0
41 1 2 3 0 0
44 0 2 0 0 5
45 0 2 0 0 5
46 0 2 0 0 5
47 0 2 0 0 5
48 0 2 0 0 5
14 1 0 0 4 0
21 1 0 0 4 0
28 1 0 0 4 0
35 1 0 0 4 0
42 1 0 0 4 0
49 1 2 0 4 5
0 1 0 0
49
1
2
3
4
5
6
7
8
9
10
11
12
13
14
15
16
17
18
19
20
21
22
23
24
25
26
27

28
29
30
31
32
33
34
35
36
37
38
39
40
41
42
43
44
45
46
47
48
49
1

1.3.2 Vecchio and Collins's slab under pure shear.

Vecchio and Collins slab PV 9 (1x1finite elements mesh for quarter of the slab), the result is shown in Fig. 5.24.

```
5 2 2 1 200 200
.05 1 .005 .005 -.0035 -.0025 2 2
200000 -11.6 1.38 455 30 1 1.27 .005 .005
-26 -26 26 26
9 2
1 0 0
2 445 0
3 890 0
4 890 445
5 890 890
6 445 890
7 0 890
8 0 445
9 445 445
1 1 9 4
1 1 8 7 6 5 4 3 2 9
1.25 1.25 1.25 1.25
16227 0.2 -35 35
5
9
```

```
1 1 2 3 4 5
2 0 2 3 4 5
3 0 2 3 4 5
4 0 0 3 4 5
5 0 0 3 4 5
6 0 0 3 4 5
7 0 0 3 4 5
8 0 0 3 4 5
9 1 2 3 0 0
1 0 0 0
1 0 0
7
2 -593.44 0 0 0 0
3 -148.36 0 0 0 0
4 0 593.44 0 0 0
5 148.36 148.36 0 0 0
6 593.44 0 0 0 0
7 148.36 -148.36 0 0 0
8 0 -593.44 0 0 0
1
1
```

1.3.3 Marti's slab under pure twisting.

Marti slab no. 6 (4x4finite elements mesh for quarter of the slab), the result is shown in Fig. 5.35.

```
3 2 3 1 81 81
.5 1 0.009 .009 -.005 -.0025 2 2
200000 -23.3 2 516 10 .6 1.2 0.015 .015
-68 -82 68 82
81 2
1 0 0
2 106.25 0
3 212.5 0
4 318.75 0
5 425 0
6 531.25 0
7 637.5 0
8 743.75 0
9 850 0
10 0 106.25
11 106.25 106.25
12 212.5 106.25
13 318.75 106.25
14 425 106.25
15 531.25 106.25
16 637.5 106.25
17 743.75 106.25
```

18 850 106.25
19 0 212.5
20 106.25 212.5
21 212.5 212.5
22 318.75 212.5
23 425 212.5
24 531.25 212.5
25 637.5 212.5
26 743.75 212.5
27 850 212.5
28 0 318.75
29 106.25 318.75
30 212.5 318.75
31 318.75 318.75
32 425 318.75
33 531.25 318.75
34 637.5 318.75
35 743.75 318.75
36 850 318.75
37 0 425
38 106.25 425
39 212.5 425
40 318.75 425
41 425 425
42 531.25 425
43 637.5 425
44 743.75 425
45 850 425
46 0 531.25
47 106.25 531.25
48 212.5 531.25
49 318.75 531.25
50 425 531.25
51 531.25 531.25
52 637.5 531.25
53 743.75 531.25
54 850 531.25
55 0 637.5
56 106.25 637.5
57 212.5 637.5
58 318.75 637.5
59 425 637.5
60 531.25 637.5
61 637.5 637.5
62 743.75 637.5
63 850 637.5
64 0 743.75
65 106.25 743.75

66 212.5 743.75
67 318.75 743.75
68 425 743.75
69 531.25 743.75
70 637.5 743.75
71 743.75 743.7
72 850 743.75
73 0 850
74 106.25 850
75 212.5 850
76 318.75 850
77 425 850
78 531.25 850
79 637.5 850
80 743.75 850
81 850 850
1 16 9 4
1 1 10 19 20 21 12 3 2 11
2.12 1.06 2.12 1.06
2 3 12 21 22 23 14 5 4 13
2.12 1.06 2.12 1.06
3 5 14 23 24 25 16 7 6 15
2.12 1.06 2.12 1.06
4 7 16 25 26 27 18 9 8 17
2.12 1.06 2.12 1.06
5 19 28 37 38 39 30 21 20 29
2.12 1.06 2.12 1.06
6 21 30 39 40 41 32 23 22 31
2.12 1.06 2.12 1.06
7 23 32 41 42 43 34 25 24 33
2.12 1.06 2.12 1.06
8 25 34 43 44 45 36 27 26 35
2.12 1.06 2.12 1.06
9 37 46 55 56 57 48 39 38 47
2.12 1.06 2.12 1.06
10 39 48 57 58 59 50 41 40 49
2.12 1.06 2.12 1.06
11 41 50 59 60 61 52 43 42 51
2.12 1.06 2.12 1.06
12 43 52 61 62 63 54 45 44 53
2.12 1.06 2.12 1.06
13 55 64 73 74 75 66 57 56 65
2.12 1.06 2.12 1.06
14 57 66 75 76 77 68 59 58 67
2.12 1.06 2.12 1.06
15 59 68 77 78 79 70 61 60 69
2.12 1.06 2.12 1.06
16 61 70 79 80 81 72 63 62 71

```
2.12 1.06 2.12 1.06
22950 0.2 -100 100
5
33
9 1 2 3 0 0
18 1 2 3 0 0
27 1 2 3 0 0
36 1 2 3 0 0
45 1 2 3 0 0
54 1 2 3 0 0
63 1 2 3 0 0
72 1 2 3 0 0
73 1 2 3 0 0
74 1 2 3 0 0
75 1 2 3 0 0
76 1 2 3 0 0
77 1 2 3 0 0
78 1 2 3 0 0
79 1 2 3 0 0
80 1 2 3 0 0
81 1 2 3 0 0
11 1 2 3 0 0
13 1 2 3 0 0
15 1 2 3 0 0
17 1 2 3 0 0
29 1 2 3 0 0
31 1 2 3 0 0
33 1 2 3 0 0
35 1 2 3 0 0
47 1 2 3 0 0
49 1 2 3 0 0
51 1 2 3 0 0
53 1 2 3 0 0
65 1 2 3 0 0
67 1 2 3 0 0
69 1 2 3 0 0
71 1 2 3 0 0
1 0 0 0
0 0 1
1
1 0 0 1 0 0
1
1
```

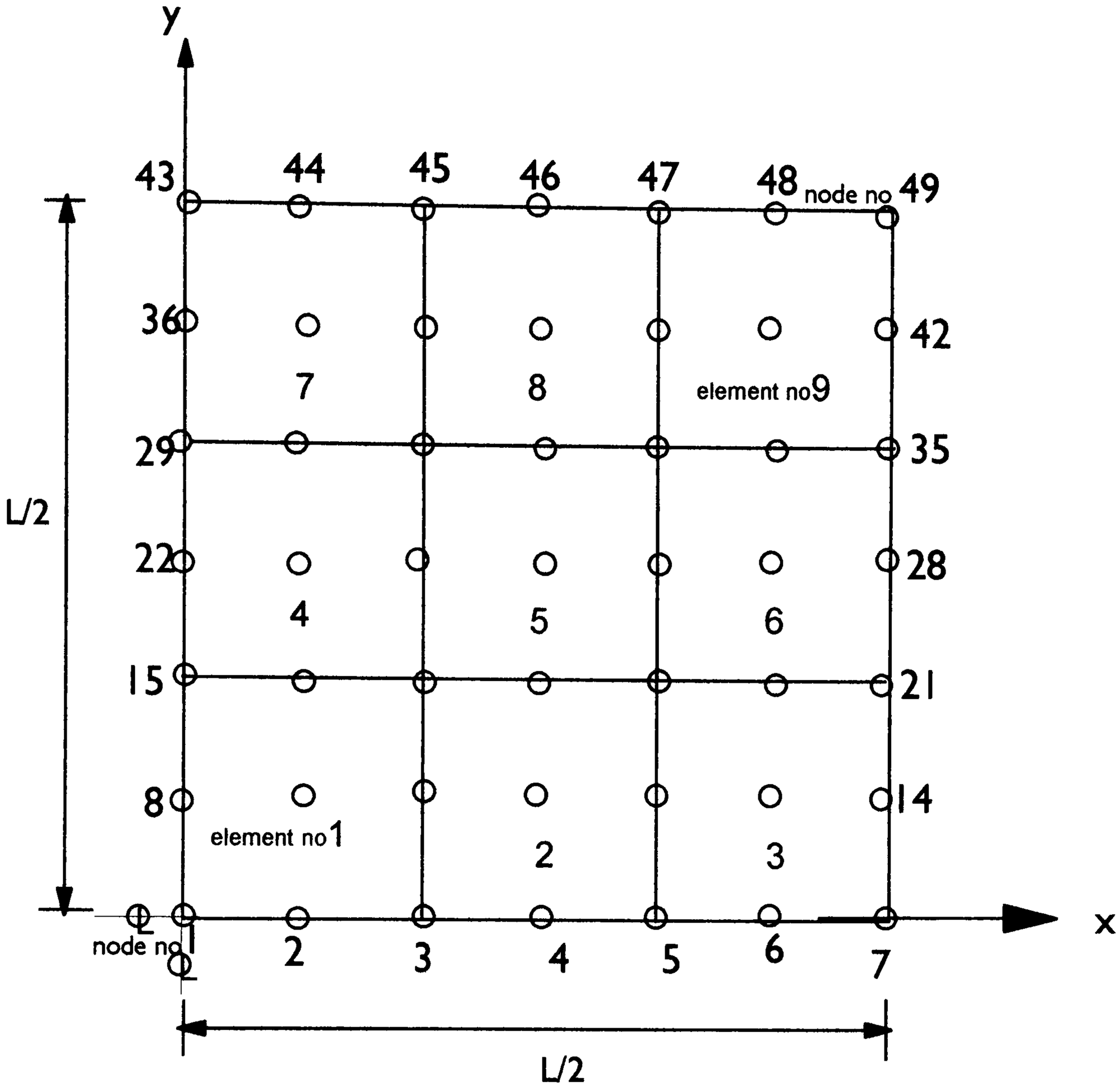

Fig.A1-3x3 Finite element mesh for
Taylor's slab (quarter of the slab)